

**Application of population, physiologically based, and  
semi-physiological pharmacokinetic modeling to  
assess sources of pharmacokinetic variability in  
individual drugs**

Dissertation

zur

Erlangung des Doktorgrades (Dr. rer. nat.)

der

Mathematisch-Naturwissenschaftlichen Fakultät

der

Rheinischen Friedrich-Wilhelms-Universität Bonn

vorgelegt von

**Xia Li**

aus

Shaanxi, China

Bonn, 2020

*Angefertigt mit Genehmigung der Mathematisch-Naturwissenschaftlichen Fakultät der Rheinischen Friedrich-Wilhelms-Universität Bonn*

**1. Gutachter: Prof. Dr. Uwe Fuhr**

**2. Gutachter: Prof. Dr. Ulrich Jaehde**

Tag der mündliche prüfung: 22.05.2020

Erscheinungsjahr: 2020

To my parents and my doctor father

## Publications

This thesis is based on the following four publications:

1. **Xia Li**, Michael Zoller, Uwe Fuhr, Mikayil Huseyn-Zada, Barbara Maier, Michael Vogeser, Johannes Zander, Max Taubert. Ciprofloxacin in critically ill subjects: considering hepatic function, age and sex to choose the optimal dose. *J Antimicrob Chemother* 2018; 74: 682-90. <https://doi.org/10.1093/jac/dky485>
2. **Xia Li**, Sebastian Frechen, Daniel Moj, Thorsten Lehr, Max Taubert, Chih-hsuan Hsin, Gerd Mikus, Pertti J. Neuvonen, Klaus T. Olkkola, Teijo I. Saari, Uwe Fuhr. A Physiologically-based pharmacokinetic model of voriconazole integrating time-dependent inhibition of CYP3A4, genetic polymorphisms of CYP2C19 and predictions of drug-drug interactions. *Clin Pharmacokinetics* (in press). <https://doi.org/10.1007/s40262-019-00856-z>
3. **Xia Li**, Lisa Junge, Max Taubert, Anabelle Dieterich, Dominik Dahlinger, Chris Starke, Sebastian Frechen, Christoph Stelzer, Martina Kinzig, Fritz Sörgel, Ulrich Jaehde, Ulrich Töx, Tobias Goeser, Uwe Fuhr. A novel study design using continuous intravenous and intraduodenal infusions of midazolam and voriconazole for mechanistic quantitative assessment of hepatic and intestinal CYP3A inhibition. *J. Clini. Pharmacol.* (in press). <https://doi.org/10.1002/jcph.1619>
4. Ruijuan Liu<sup>#</sup>, **Xia Li**<sup>#</sup>, Jingyao Wei, Shuaibing Liu, Yuanyuan Chang, Jiali Zhang, Ji Zhang, Xiao Jian Zhang, Uwe Fuhr, Max Taubert, Xin Tian. A single dose of baicalin has no clinically significant effect on the pharmacokinetics of cyclosporine A in healthy Chinese volunteers. *Front Pharmacol* 2019; 10: 518-28. <sup>#</sup>equal contributions <https://doi.org/10.3389/fphar.2019.00518>
5. Malaz Gazzaz, Martina Kinzig, Elke Schaeffeler, Martin Jübner, Chih-hsuan Hsin, **Xia Li**, Max Taubert, Christina Trueck, Juliane Iltgen-Breburda, Daria Kraus, Christian Queckenberg, Marc Stoffel, Matthias Schwab, Fritz Sörgel, Uwe Fuhr. Drinking ethanol has few acute effects on CYP2C9, CYP2C19, NAT2, and P-Glycoprotein activities but somewhat inhibits CYP1A2, CYP2D6, and intestinal CYP3A: So What? *Clin Pharmacol Ther* 2018; 104: 1249–59. <https://doi.org/10.1002/cpt.1083>



## Contribution Report

I declare that, in accordance with the provisions of the doctoral regulations, all the publications included are only used by myself in a dissertation. I would like to declare my contributions to the publications of the projects included in this thesis.

Publication 1: I analyzed the datasets from the clinical trial, developed a population pharmacokinetic model, identified covariates, performed simulations to provide optimal dosing of ciprofloxacin to ICU patients, and finally wrote the manuscript.

Publication 2: I conducted all *in vitro* assays and quantified the samples with LC-MS. I gathered all relevant information from the literature, developed a whole body physiologically based pharmacokinetic model of voriconazole, incorporated time dependent inhibition of CYP3A, performed all the model-based simulations, and wrote the manuscript.

Publication 3: I evaluated the plasma and urine datasets from the clinical trial, developed a novel semi-physiological population pharmacokinetic models for voriconazole, midazolam and its major metabolites, assessed the time course of CYP3A inhibition by voriconazole in liver and small intestine, and finally wrote the manuscript. For this publication, Dr. Lisa Junge who was supervised by the same supervisors is a co-author. In her dissertation with the topic "In silico, in vitro und in vivo Charakterisierung der Hemmung ausgewählter Fremdstoff-metabolisierender Enzyme des Menschen durch Voriconazol" which was awarded with the degree of a "doctor rerum naturalium" of the Faculty of Mathematics and Natural Sciences of the Rheinische Friedrich-Wilhelms-Universität Bonn (2016), she used the same data set. However, at the time of her thesis, Dr. Junge was not yet able to develop a comprehensive and all-embracing model to describe this data. The new and successful evaluation that I developed, also based on work described in publication #2, is the subject of the publication, which therefore is indeed not used in another dissertation.

Publication 4: I analyzed the datasets from the clinical trial, developed a population pharmacokinetics model for cyclosporine A, compared the pharmacokinetics of cyclosporine A during the test and reference periods, and finally wrote the manuscript.

Publication 5: I analyzed the datasets from the clinical trial, developed a population pharmacokinetics model of ethanol, develop a semi-physiological population pharmacokinetic model of midazolam, and wrote the respective parts of the manuscript.

# Contents

<b>1. Introduction.....</b>	<b>1</b>
<b>1.1 Population pharmacokinetic modeling.....</b>	<b>5</b>
1.1.1 Non-linear mixed effects modeling.....	5
1.1.2 Model fitting and parameter estimation.....	7
1.1.3 Model development.....	8
1.1.3.1 Structural model development.....	8
1.1.3.2 Covariate model development.....	8
1.1.3.3 Model evaluation.....	8
1.1.3.3.1 Physiological plausibility.....	9
1.1.3.3.2 OFV.....	9
1.1.3.3.3 The goodness of fit plots.....	9
1.1.3.3.4 $\eta$ -shrinkage check.....	9
1.1.3.3.5 Visual predictive checks.....	9
1.1.3.3.6 Bootstrap statistics.....	10
<b>1.2 Whole-body PBPK modeling.....</b>	<b>11</b>
1.2.1 System-dependent parameters.....	11
1.2.2 Drug-dependent parameters.....	14
1.2.3 Absorption.....	14
1.2.3.1 Absorption models.....	14
1.2.3.1.1 Transit compartment model.....	14
1.2.3.1.2 Weibull absorption model.....	15
1.2.3.1.3 Advanced dissolution, absorption & metabolism.....	15
1.2.3.2 Permeability.....	16
1.2.4 Distribution.....	16
1.2.5 Metabolism.....	17
1.2.5.1 <i>In vitro</i> assay.....	17
1.2.5.2 Extrapolation from <i>in vitro</i> to <i>in vivo</i> .....	17
1.2.5.3 Well-stirred model.....	18
1.2.5.4 Parallel tube model.....	19
1.2.6 Excretion.....	20
<b>1.3 Semi-physiological popPK modeling.....</b>	<b>21</b>
<b>1.4 Study drugs.....</b>	<b>22</b>
1.4.1 Ciprofloxacin.....	22
1.4.1.1 PK of ciprofloxacin.....	22
1.4.1.2 PK/PD relationship of ciprofloxacin.....	23

1.4.1.3 Main considerations .....	23
1.4.2 Voriconazole .....	24
1.4.2.1 PK of voriconazole.....	24
1.4.2.2 PK/PD relationship of voriconazole.....	25
1.4.2.3 Main considerations .....	25
1.4.3 Midazolam.....	27
1.4.3.1 PK of Midazolam .....	27
1.4.3.2 Probe substrate for CYP3A4.....	27
1.4.4 Cyclosporine A.....	28
1.4.4.1 PK of CsA .....	28
1.4.4.2 Main considerations .....	28
1.4.5 Baicalin.....	30
1.4.5.1 PK of baicalin.....	30
1.4.5.2 Main considerations .....	30
1.4.6 Ethanol.....	32
1.4.6.1 PK of ethanol .....	32
1.4.6.2 Main considerations .....	33
<b>2. Aims and objectives.....</b>	<b>34</b>
<b>2.1 The effect of critical illness on ciprofloxacin PK.....</b>	<b>34</b>
<b>2.2 The effect of voriconazole on CYP3A activity .....</b>	<b>34</b>
2.2.1 Using PBPK modeling to understand voriconazol PK and its properties as a perpetrator on drug metabolism via CYP3A and CYP2C19 .....	34
2.2.2 Using semiphysiological PK modeling and the novel study design to quantify the effect of voriconazole on CYP3A activity, and DDIs between voriconazole and midazolam .....	34
<b>2.3 The effect of baicalin co-medication on CsA PK.....</b>	<b>35</b>
<b>2.4 The effect of ethanol on the activity of major drug metabolizing enzymes and transporters .....</b>	<b>35</b>
<b>3. Results.....</b>	<b>36</b>
<b>3.1 The effect of critical illness on ciprofloxacin PK.....</b>	<b>36</b>
<b>3.2 The effect of voriconazole on CYP3A activity .....</b>	<b>36</b>
3.2.1 Using PBPK modeling to understand voriconazol PK and its properties as a perpetrator on drug metabolism via CYP3A and CYP2C19 .....	36
3.2.2 Using semiphysiological PK modeling and the novel study design to quantify the effect of voriconazole on CYP3A activity, and DDIs between voriconazole and midazolam .....	36

<b>3.3 The effect of baicalin co-medication on CsA PK.....</b>	<b>36</b>
<b>3.4 The effect of ethanol on the activity of major drug metabolizing enzymes and transporters .....</b>	<b>37</b>
<b>4. Summary .....</b>	<b>38</b>
<b>4.1 The effect of critical illness on ciprofloxacin PK.....</b>	<b>38</b>
<b>4.2 The effect of voriconazole on CYP3A activity .....</b>	<b>39</b>
4.2.1 Using PBPK modeling to understand voriconazol PK and its properties as a perpetrator on drug metabolism via CYP3A and CYP2C19 .....	39
4.2.2 Using semiphysiological PK modeling and the novel study design to quantify the effect of voriconazole on CYP3A activity, and DDIs between voriconazole and midazolam .....	40
<b>4.3 The effect of baicalin co-medication on CsA PK.....</b>	<b>42</b>
<b>4.4 The effect of ethanol on the activity of major drug metabolizing enzymes and transporters .....</b>	<b>43</b>
<b>4.5 Application of three PK approaches.....</b>	<b>44</b>
<b>5 References .....</b>	<b>46</b>
<b>6 Acknowledgments .....</b>	<b>57</b>
<b>7 Curriculum Vitae.....</b>	<b>58</b>
<b>Abbreviations .....</b>	<b>61</b>
<b>Publications.....</b>	<b>61</b>

# 1. Introduction

Large inter- and intra-individual variability in the response of drugs causes difficulties for clinicians to choose appropriate dosing regimens to target their therapeutic range. While underexposure might cause sub-therapeutic effects, overexposure might lead to adverse effects. Therefore exploring the sources of variability and quantifying the effect of respective covariates are critical for dosing optimization.

The variability in drug response originates in both pharmacokinetics (PK) and pharmacodynamics (PD). PK describes how the body affects a drug, including absorption, distribution, metabolism, and excretion (ADME)<sup>1</sup>. Therefore, factors influencing ADME also result in PK variability, including intrinsic factors, such as age, sex, body weight, genetic polymorphisms of drug metabolizing enzymes and transporters, disease, liver or kidney impairment, as well as extrinsic factors, such as food consumption or co-medication with other drugs. PD explores how a medication affects an organism and explains the relationship between drug concentration at the site of action and the biochemical and physiological effects<sup>2</sup>. PD variability has its origin e.g. in genetic differences in targets, disease status, or interaction with other drugs. The relationship between PK and PD may be described in a chain: The dosing regimen of the drug results in drug concentration-time courses and the varying drug concentrations mediate the fluctuating drug effect; the combination of two relationships produces effect-time profiles, finally resulting in therapeutic outcomes (therapeutic or adverse effects) (**Figure 1**).

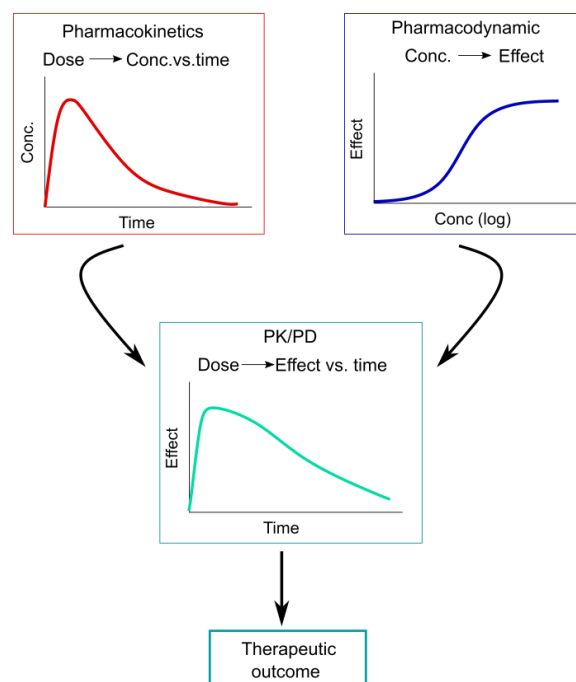


**Figure 1** Synergy of pharmacokinetics and pharmacodynamics (PK/PD) to mediate drug effects.

**Figure 1** indicates that factors influencing PK of a given drug also have an indirect impact on its PD. While the magnitude of an effect on PK is typically higher than the indirect effect on PD, factors influencing PK may still cause clinically relevant effects on therapeutic outcomes, which require to be managed, e.g. by a change in the dosing regimen. Thus, improvement of characterization of the factors contributing to PK variability could assist individualizing and optimizing drug therapy.

There are two conventional ways to analyze a drug's PK, i.e., compartmental and non-compartmental analysis (NCA). The compartmental analysis describes the body by one or more well-mixed compartments, into which the drug is assumed to be kinetically homogeneously distributed<sup>3</sup>. Whereas, NCA requires fewer assumptions and some of the respective parameters may be obtained directly from the raw data, e.g., maximum drug concentration ( $C_{max}$ ), the time taken to reach  $C_{max}$  ( $t_{max}$ ), area under the concentration-time curve (AUC), or by simple calculations, such as terminal half-life ( $t_{1/2}$ ), apparent clearance and volume of distribution (**Figure 2**, left)<sup>4</sup>. These PK parameters can be obtained from each individual profile. The mean and standard deviation of PK parameters derived from each individual profile represent parameter estimates for a typical individual and the respective variability in the population.

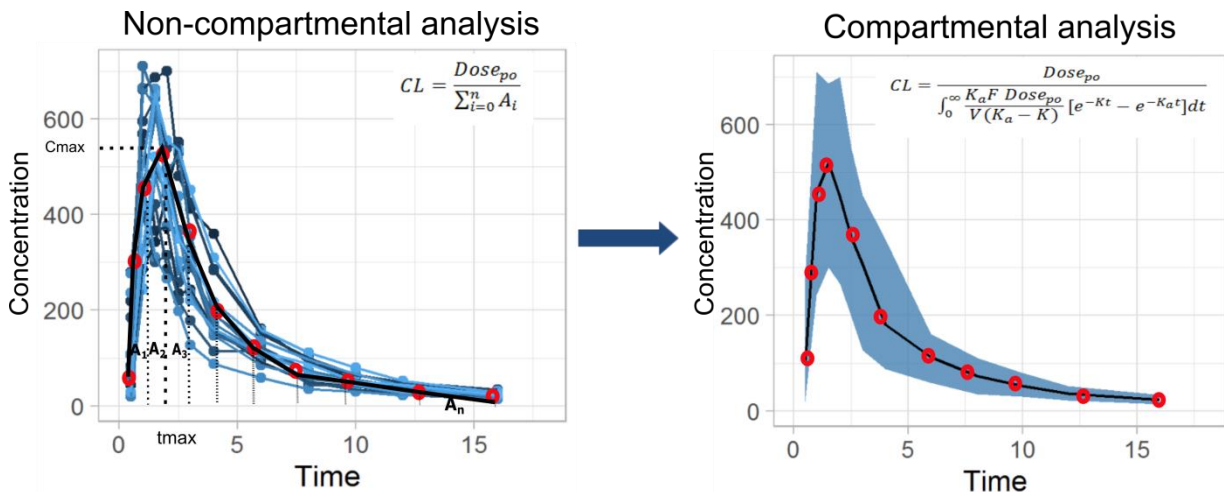


**Figure 2** Pharmacokinetic parameters for each individual obtained by non-compartmental (left) and compartmental analysis (right).  $CL$ , clearance;  $po$ , oral;  $A_i$ , AUC area under the concentration-time curve;  $K_a$ , absorption rate;  $F$ , bioavailability;  $V$ , the volume of distribution;  $K$ , elimination rate.

Compartmental analysis is using a model to describe the concentration-time profile either by the two-stage approach (develop a model by fitting each individual's data separately, and then calculate the mean and standard deviation of PK parameters in the population), or non-linear mixed effect modeling

(develop a model based on all individuals' data and simultaneously estimate the typical value and variance)<sup>5</sup>. For compartmental modeling development, differential equations with PK parameters such as clearance and volume of distribution are implemented into the model to describe the drug transfer between compartments, shown in **Figure 2**, right.

NCA is typically applied to characterize PK parameters within a single study with rich data and to describe exposure of the drug. For multiple studies or sparse sampling techniques, compartmental modeling, especially non-linear mixed effect modeling, is required to analyze a drug's PK, since the two-stage approach may generate biased estimates of interindividual variability.

Whole body physiologically based pharmacokinetic (PBPK) modeling is another type of compartmental modeling approach. As a knowledge-driven approach, PBPK begins with the physiological characteristics of the organism and physicochemical properties of the drug. Whereas, PopPK modeling is a data-driven approach, starting with the observed data and developing models to fit the data. Compartments in popPK modeling (shown in **Figure 3**) do not necessarily have physiological meaning (e.g., the central compartment typically is not identical to the plasma volume). The addition of peripheral compartments to a model is based on the test results for statistical significance showing the additional compartments improve the fit of the model to the data. In contrast, compartments in PBPK represent real solid organs or tissues, and the distribution of the drug into the organ depends on organ blood flow and the respective partition coefficient.

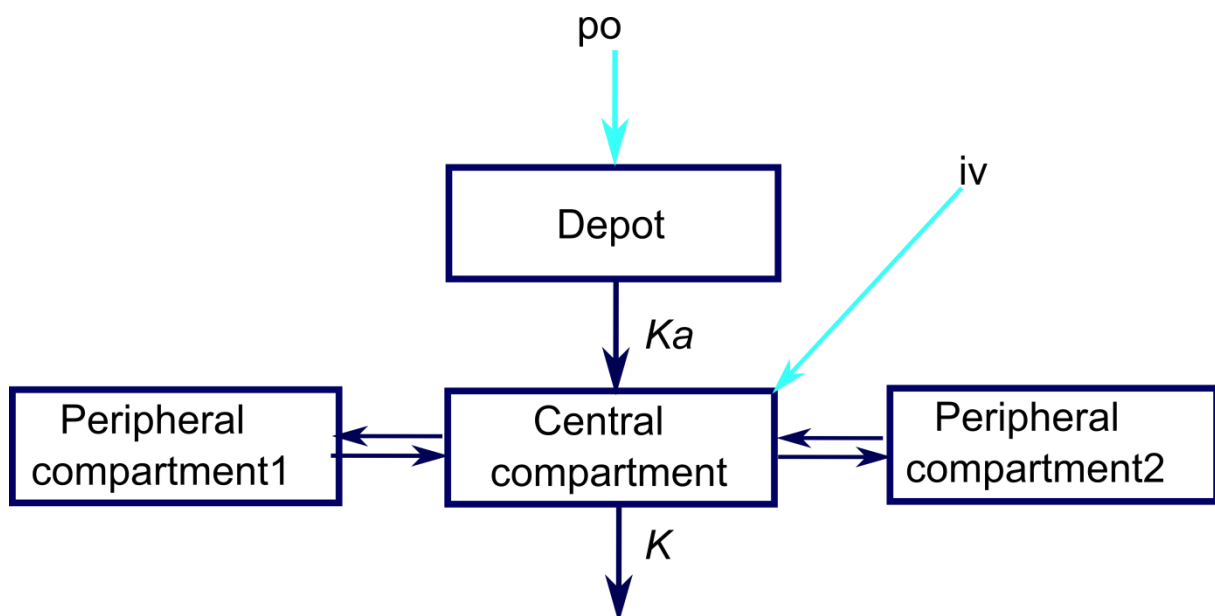


**Figure 3** Structure of typical population pharmacokinetic modeling.  $K_a$ , absorption rate; iv, intravenous; po, oral;  $K$ , elimination rate. Compartments in popPK modeling do not represent physiological organs. The drug is assumed to be homogeneously distributed in the compartments.

PopPK and PBPK modeling are applied in varying situations, although both can be used to understand the PK of a drug and predict the exposure of a drug. Modelers tend to use the best-suited modeling

approach for answering specific questions. For example, popPK modeling is often used to identify and quantify the sources of variability<sup>6</sup>; while PBPK modeling is frequently applied in understanding the metabolism of drugs and mechanistic inhibition or induction by other co-medication as well<sup>7</sup>.



## 1.1 Population pharmacokinetic modeling

PopPK analyzes the PK of drugs at the population level, describing the PK properties of a drug for a typical individual and quantifying and explaining variability in PK among individuals<sup>8,9</sup>. The non-linear mixed effects modeling (NONMEM) is the “gold standard” approach in popPK<sup>10</sup>.

### 1.1.1 Non-linear mixed effects modeling

The NONMEM approach could simultaneously estimate the typical and variance parameters using data from all subjects, combining both fixed and random effects<sup>11</sup>, as shown in **Figure 4**.

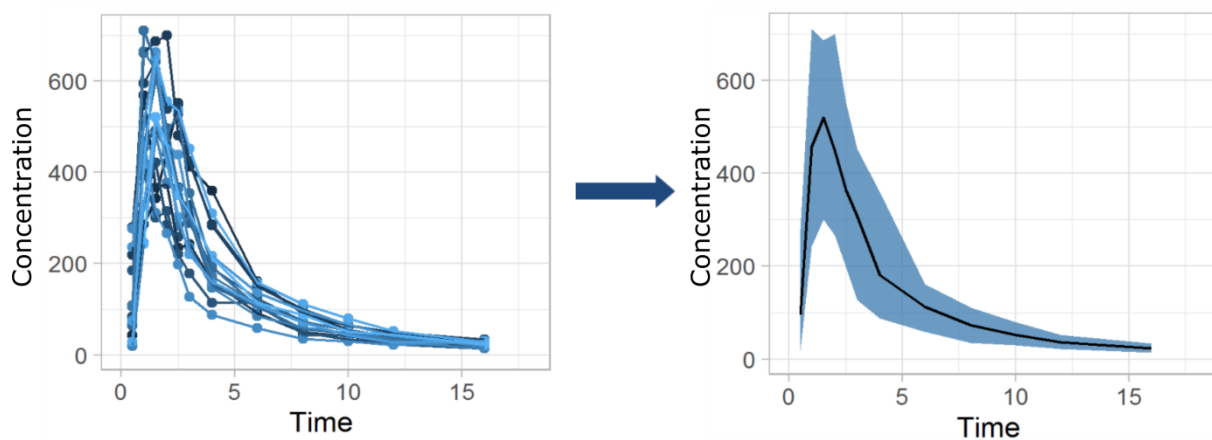


**Figure 4** A non-linear mixed effects model describing the central tendency for a typical individual and the variability for a population. Left, the observed individual concentration-time profiles; Right, the predicted concentration-time profile with an estimate for the typical individual and its variability in the population.

Fixed effects are described as the typical PK parameters, which represent the central tendency in the data, called population predictions (PRED)<sup>9</sup>. In contrast, random effects represent the random variability, quantifying the magnitude of the difference in values of parameters between subjects (defined as IIV) or differences between occasions within a subject (defined as inter-occasion variability (IOV))<sup>3</sup>, as well as differences between the observations and the corresponding individual prediction.

The typical parameter estimates with individual variability (IIV and IOV) could predict individual PK<sup>9</sup>. The IIV can be modeled with an additive function (**Eq.1**) or a constant coefficient of variation (CCV) (**Eq.2**), but the most commonly used is the exponential function (**Eq.3**).

**Eq. 1**  $p_i = \theta + \eta_i$

**Eq. 2**  $p_i = \theta * (1 + \eta_i)$

**Eq. 3**  $p_i = \theta * e^{\eta_i}$

Where  $p_i$  refers to the individual subject parameter;  $\theta$  is the typical value;  $\eta_i$  is the inter-individual variability, assumed to be normally distributed with a mean of zero and a variance of  $\omega^2$  ( $\eta_i \sim N(0, \omega^2)$ ).

Each subject has a unique  $\eta_i$ . The coefficient of variation (CV%) for the parameter is calculated by **Eq. 4**. The additive model (**Eq.1**) has a constant standard deviation, and %CV is smaller when the parameter has a higher value, while CCV model (**Eq.2**) has a constant %CV for all parameter values. The exponential model also has a constant %CV, and the parameter is log-normally distributed, which is used most frequently since it can prevent negative parameter estimates<sup>12</sup>.

**Eq. 4.**  $\%CV = \frac{SD}{mean} * 100$

Where  $CV$  refers to the coefficient of variation;  $SD$  is the standard deviation.

If there is a systematic alteration in the parameter over time, changes in the parameter between different occasions can also be modeled by an occasion-specific effect.

After considering IIV and IOV, the remaining discrepancy between the observed dependent variable (Y) and the corresponding individual prediction (F) is defined as the residual error or residual variability (RV), described by **Eq. 5**<sup>3</sup>. The RV consists of the intra-individual variability, errors in the sample collection, storage, or bioanalytical processes, as well as model misspecification<sup>9</sup>.

**Eq. 5**  $Y - F = ERROR$

The RV is usually introduced by three error models. The proportional residual error is using **Eq. 6**, assuming the error is normally distributed with a mean of zero and variance of  $\sigma_1^2(N(0, \sigma_1^2))$ , but proportional to the magnitude of the prediction. The additive residual error is described by **Eq. 7**, assuming the error is normally distributed with a mean of zero and variance of  $\sigma_2^2(N(0, \sigma_2^2))$ . The combination of both additive and proportional residual error model with **Eq. 8**<sup>13</sup>.

**Eq. 6**  $Y = F * (1 + EPS(1))$

**Eq. 7**  $Y = F + EPS(1)$

**Eq. 8**  $Y = F * (1 + EPS(1)) + EPS(2)$

The total RV as %CV is calculated with **Eq. 9**. The proportional error has a constant %CV, while for the additive error, %CV is greater at a lower concentration, depending on the prediction.

**Eq. 9**  $\%CV = \frac{\sqrt{F^2 * \sigma_1^2 + \sigma_2^2}}{F} * 100$

By integrating both fixed and random residual variability, the individual predicted concentration-time profiles could be calculated with **Eq.10**.

$$\text{Eq.10 } y_{ij} = f(x_{ij}, \theta, \eta_i) * (1 + \varepsilon_{1ij}) + \varepsilon_{2ij}$$

$y_{ij}$  is the  $j^{th}$  dependent variable in  $i^{th}$  individual;  $f$  is a function of the independent variables  $x_{ij}$ , the typical parameter value  $\theta$ , and the inter-individual variability  $\eta_i$ ;  $\varepsilon_{1ij}$  and  $\varepsilon_{2ij}$  represent proportional and additive residual errors, respectively.

### 1.1.2 Model fitting and parameter estimation

The population parameters in the model are estimated by maximizing the likelihood of observing the measures. The likelihood indicates that if the model were true, how likely it is the dependent variables would have been observed based on the current estimated values of the structural and variance parameters<sup>3</sup>, denoted in **Eq. 11**.

$$\text{Eq. 11 } L = \frac{1}{\sqrt{2\pi\sigma^2}} * e^{-\frac{1}{2\sigma^2}*(Y-\hat{Y})^2}$$

Where  $L$  is the likelihood;  $Y$  represents the observed dependent variable;  $\hat{Y}$  refers to the predicted dependent variable based on the model;  $\sigma^2$  is the variance of the model.

For  $n$  observations, the probability is the product of all the individual  $n$  probabilities in **Eq. 12**<sup>3</sup>.

$$\text{Eq. 12 } L = \prod_{i=1}^n \frac{1}{\sqrt{2\pi\sigma_i^2}} * e^{-\frac{1}{2\sigma_i^2}*(Y_i-\hat{Y}_i)^2}$$

Then this can be transformed into **Eq. 13**.

$$\text{Eq. 13 } -2\log(L) = n\log(2\pi) + \sum_{i=1}^n \left[ \log(\sigma_i^2) + \frac{(Y_i-\hat{Y}_i)^2}{\sigma_i^2} \right]$$

The likelihood ratio test is used to assess statistical significance. For model development, one model is often nested in another. We can compare the two models by testing for a significant difference between the two models. The test is based on the ratio of the likelihoods of two models  $L_1/L_2$ .  $-2\log(L_1/L_2)$  follows a  $\chi^2$  distribution with the degrees of freedom being the difference in the number of parameters<sup>14</sup>. Thus,  $-2\log(L_1/L_2)$  is implemented to estimate parameters in NONMEM and defined as the objective function value (OFV). Maximizing likelihood estimation means minimizing OFV. Thus, a lower OFV reflects a better fit. However, the best model is not necessarily the one with the lowest objective function, and other factors should be considered, e.g., biological plausibility and simplicity of the model. For non-nested models, the Akaike Information Criterion (AIC) is used to evaluate which model fits the data best, calculated by **Eq. 14**<sup>15</sup>.

$$\text{Eq. 14 } AIC = 2p - OFV$$

$p$  is the number of parameters.

### 1.1.3 Model development

#### 1.1.3.1 Structural model development

PopPK model is developed according to the work flow shown in **Figure 5**<sup>16</sup>. The structural PK model is developed stepwise, starting with a one-compartment model and typically expanding up to a three-compartment model with linear or nonlinear elimination kinetics. Then the residual error model is tested, including additive, proportional, and combined error models.

Subsequently, IIV is evaluated and implemented on the PK parameters, commonly using an exponential function to maintain positive PK parameter estimates. The correlations among the ETAs ( $\eta_i$ : the inter-individual variability) need to be tested to develop a parsimonious omega structure<sup>16</sup>. Note that an estimate of IIV approaching zero does not mean that there is no IIV for this parameter. Instead, it may suggest that data are not robust enough to obtain an estimate for IIV. When data are sparse at the individual level, the empirical bayes estimates (EBEs) will shrink towards zero (called as  $\eta$ -shrinkage and calculated by  $sh_{\eta} = 1 - \frac{SD(\eta_{EBE})}{\omega}$ )<sup>16,17</sup>. This diagnostic is often applied in PK/PD modeling to evaluate the informativeness of individual predictions (IPRED). If  $\eta$ -shrinkage is above 20%, IPRED shrinks toward the corresponding observations and an overfit occurs<sup>18</sup>.

For inter-occasional variance (IOV), the inclusion depends on the study design features. The occasion is usually defined by period for crossover study.

#### 1.1.3.2 Covariate model development

Covariates should be tested and early integrated as part of the structural model if prior information is available on their influence on the PK of a drug. Otherwise, covariates are recommended to be selected by systematic procedures. There are several covariate selection approaches, including stepwise covariate modeling (SCM)<sup>10</sup>, full fixed effect modeling (FFEM)<sup>19</sup>, full random effects model (FREM)<sup>19</sup>, Wald's approximation to the likelihood ratio test (LRT)<sup>20</sup>, generalized additive modeling (GAM)<sup>21</sup>, least absolute shrinkage and selection operator (Lasso)<sup>22</sup> and so on. Each covariate selection procedure has its own limitations. For example, the most commonly used SCM method includes a forward selection (resulting in a full covariate model) and a backward elimination process (resulting in a final model), which may lead to false-positive selection due to multiple tests, resulting in misleading P-values<sup>23</sup>; or over-estimation of regression coefficients<sup>24</sup> and falsely narrow confidence intervals<sup>25</sup>.

#### 1.1.3.3 Model evaluation

The model is developed based on some assumptions and hypotheses. In general, the final model requires to be evaluated through several diagnostics.

### 1.1.3.3.1 Physiological plausibility

The point estimates of parameters are physiologically and clinically plausible.

### 1.1.3.3.2 OFV

As discussed above, the likelihood-ratio test is usually applied to compare nested models. Since OFV follows a  $\chi^2$  distribution with the number of parameters being the degrees of freedom, the integration of the parameter is determined by the decrease of OFV in **Table 1**<sup>14</sup>. The AIC calculated by **Eq. 14** is used to evaluate non-nested models.

**Table 1** The decrease in OFV required for newly added parameters

$\Delta$ parameter	$\Delta$ OFV	
	p < 0.05	p < 0.01
1	3.84	6.63
2	5.99	9.21
3	7.81	11.34
4	9.49	13.28

### 1.1.3.3.3 The goodness of fit plots

The models are further assessed graphically by the “goodness of fit” plots (GOF), including observed dependent variable versus IPRED and PRED, as well as conditional weighted residuals (CWRES) versus the PRED and time<sup>10</sup>. For a good model, the observations and IPRED or PRED fit each other well, and meantime CWRES are homogeneously scattered around the null ordinates with no obvious trend.

### 1.1.3.3.4 $\eta$ -shrinkage check

$\eta$ -shrinkage requires below 20% to confirm the informativeness of IPRED<sup>18</sup>.

### 1.1.3.3.5 Visual predictive checks

Visual predictive checks (VPC) are conducted to assess predictive performance of the model by simulating a large number of replicates from the original subjects<sup>26</sup>. The median and CIs of the simulated data are plotted against time and compared to observed data. The median predictions depict the trend and the 5<sup>th</sup> and 95<sup>th</sup> percentiles of the simulated predictions show the variability in the population.

### 1.1.3.3.6 Bootstrap statistics

The bootstrap analysis is applied to evaluate the accuracy and precision of the final parameters<sup>27</sup>. Pseudo-replicates are generated by resampling subjects from the original dataset with replacement<sup>28</sup>. Parameters are re-estimated with the new dataset, and resulting parameter distributions are approaching actual distributions. The median is compared to the estimate of the final model from the original dataset. Too large confidence intervals indicate over-parametrization, misspecification, or identifiability problems.

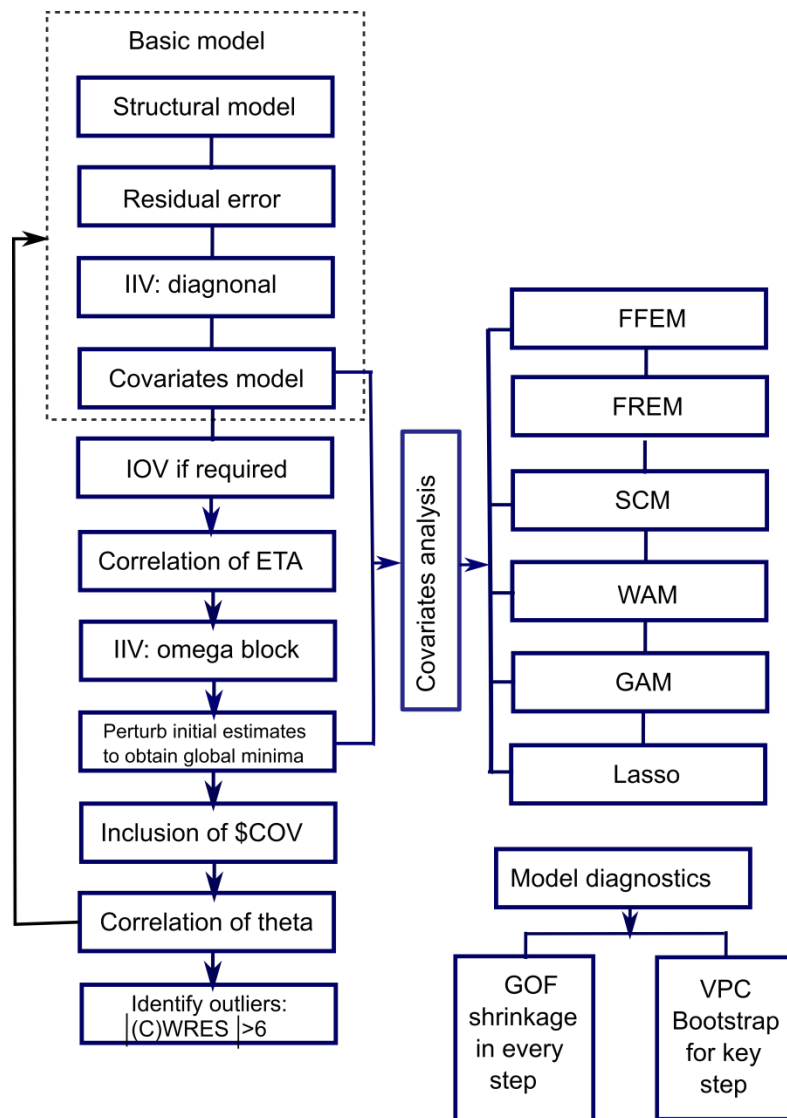


**Figure 5** Population pharmacokinetic modeling working flow<sup>16</sup>. IIV, inter-individual variance; IOV, interoccasional variance; \$COV, covariance step; CWRES, conditional weighted residuals; FFEM, full fixed-effect model; FREM, full random effects model; SCM, stepwise covariates; WAM, Wald's approximation to the likelihood ratio test, GAM, generalized additive modeling, Lasso, least absolute shrinkage and selection operator; GOF, goodness of fit plots; VPC, visual predictive checks.

## 1.2 Whole-body PBPK modeling

PopPK compartmental modeling is a data-driven approach. It is ideal for identifying the sources of inter- and intra-individual variability in the drug exposure, and assessing the relationship between significant covariates and the relevant PK parameters, enabling clinicians to choose an appropriate dosage regimen to target the respective therapeutic range<sup>9</sup>. However, the popPK modeling approach can only provide limited information. For example, the total clearance of a drug can be estimated using the popPK approach, but it is obviously too empirical to decipher the contribution of each metabolic enzyme to total metabolism. In this case, PBPK modeling can be used to help understand the mechanistic basis of drug metabolism, as well as influences caused by the interactions with other drugs<sup>7</sup>.

### 1.2.1 System-dependent parameters

PBPK models consist of a series of anatomical or physiological compartments developed using a mathematical model<sup>7</sup>, as shown in **Figure 6**. Each compartment is defined by the blood flow rate, tissue volume, tissue surface areas, tissue composition, and protein abundance, which are fixed with known/published physiological values<sup>29</sup>. Unlike popPK models, each compartment in PBPK represents a specific organ or tissue, linked by the circulating blood system (i.e., the arterial, venous, and portal vein blood). Typically, a whole-body PBPK model integrates the main organs and tissues, including the stomach, gut, pancreas, spleen, portal vein, gall bladder, liver, kidney, lung, heart, brain, adipose tissue, bone, muscle, and skin<sup>30</sup>. Each tissue is further divided into sub-compartments characterizing the plasma, blood cells, interstitial and intracellular spaces.

The distribution of drugs into PBPK compartments is assumed to follow either perfusion-rate-limited or permeability-rate-limited kinetics. For small lipophilic molecules, they can cross the membrane easily and the tissue blood flow mainly limits the kinetics<sup>31</sup>. At the steady state, the free drug concentration in the tissue equals that in the circulation and the total drug concentration in the tissue is in equilibrium with that in the circulation, determined by tissue to plasma partition coefficient  $K_p$  value. The time to reach equilibrium depends on blood flow rate, tissue volume, and  $K_p$  value<sup>7</sup>.

However, for large polar molecules that have difficulty in penetrating the tissue, the permeability rate across the membrane becomes the limiting process<sup>29</sup>. In this scenario, the specific tissue is assumed to have two compartments, i.e., intracellular and the extracellular space, and the cell membrane acts as a diffusion barrier. The permeability rate constant is assumed to drive the equilibrium across the cell membrane<sup>7</sup>. For some drugs requiring active transport, it also needs to integrate uptake parameters to describe the transport process<sup>32</sup>.

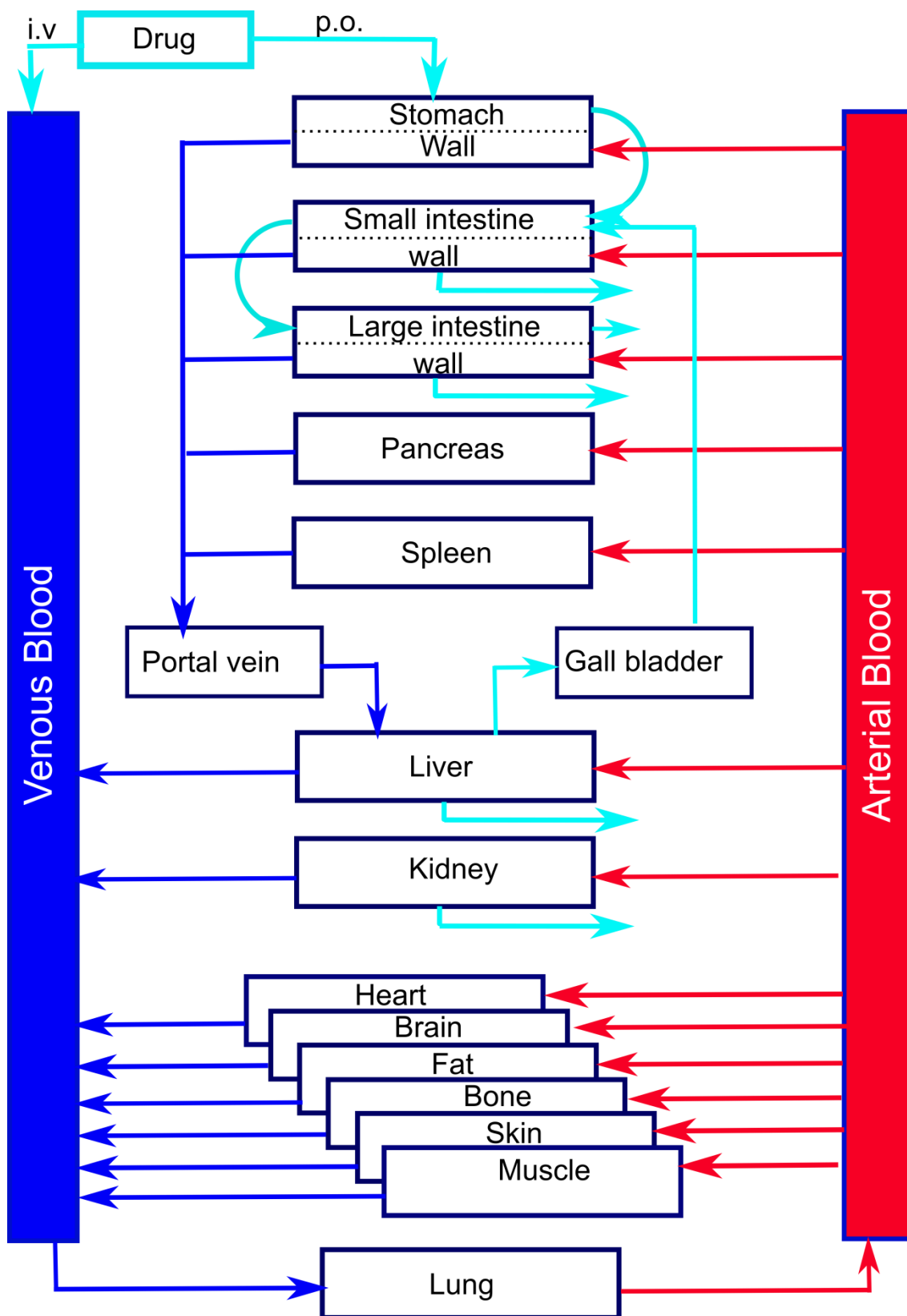


**Figure 6** Structure of a whole body PBPK modeling from PK-SIM®



At steady state, the free drug is equally distributed in the tissue and the circulation, and the aqueous spaces within the tissue, the extracellular space, and the intracellular space are well-mixed. The only reason for alteration in the drug concentration across the organ is elimination and excretion. Therefore, the tissue compartments in PBPK can be classified into two types, i.e., eliminating tissues and non-eliminating tissues<sup>30</sup>. The transfer of drugs between compartments is described using the mass balance differential equations. For non-eliminating tissues, the rate of drug transfer in the tissue is equal to “rate in” minus the “rate out” in **Eq.15**<sup>7</sup>.

$$\text{Eq. 15 } V_T * \frac{dC_T}{dt} = Q_T * C_A - Q_T * C_{v_T}$$

Where  $Q$  is blood flow [L/h],  $C$  is concentration [mg/L],  $V$  is volume [L],  $T$  is tissue,  $A$  is arterial,  $v$  is venous,  $C_{v_T} = \frac{C_T}{Kp/B:P}$ ,  $B:P$  is the ratio of blood versus plasma,  $Kp$  is tissue to plasma partition coefficient of the drug.

For eliminating tissues (e.g., liver and kidney), the rate of clearance is integrated additionally to the “rate out”, shown in **Eq.16**<sup>7</sup>. It is assumed that the free drug concentration at the enzyme/elimination site equals that in the tissue venous blood.

$$\text{Eq. 16 } V_T * \frac{dC_T}{dt} = Q_T * C_A - Q_T * C_{v_T} - CL_{int} * C_{v_{uT}}$$

Where  $CL_{int}$  refers to the intrinsic clearance of the drug [L/h], and  $u$  means unbound drug since enzymes cannot metabolize the bound drug.

From the above differential equations, we can find that the PBPK model consists of both system-dependent parameters (i.e., tissue blood flow rates, tissue volumes) and drug-dependent parameters (i.e., unbound fraction, partition coefficient and intrinsic clearance). The system-dependent parameters differ across species, ethnic groups, and patient subgroups. Commercial PBPK platforms, such as Simcyp Population-Based Simulator (Certara, Sheffield, UK), PK-SIM (Bayer Technology Services, Leverkusen, Germany) and GastroPlus (Simulations Plus, Lancaster, CA), provide the system-dependent physiological parameters for human and most common preclinical species (e.g., mouse, rat, and dog). The specific population groups (such as pediatrics, elderly, pregnancy, kidney/liver dysfunction patients, and obesity) can be integrated into PBPK model with changes in blood flow, abundances of protein, and/or liver/renal function according to physiological and mechanistic features for these special population groups.

A virtual population can be generated based on the information describing demographics, anatomical, and physiological variables using a correlated Monte Carlo approach.<sup>33</sup> The distribution of system parameters for the PBPK model is derived from the distribution of the real population and patients<sup>7</sup>.

## 1.2.2 Drug-dependent parameters

Since system-dependent parameters are usually provided in the software, drug-dependent parameters become the critical parameters for model development. These include physicochemical properties (such as molecular weight, pKa, logP, basic or acidic character), solubility, permeability, ratios of blood-plasma partitioning and protein binding fraction ( $f_u$ ), transporter contribution to drug disposition, and metabolism as e.g. assessed by experiments using liver microsomes or recombinant enzymes (e.g., Michaelis constant  $K_m$  (equal to substrate concentration at which the reaction rate is half-maximal) and maximum catalytic rate constant  $V_{max}$ )<sup>30</sup>. These drug-dependent parameters are usually obtained from *in vitro* assays or sometimes estimated by *in silico* models. These parameters can significantly affect ADME, influencing the exposure of the drug.

## 1.2.3 Absorption

The fraction of an orally administered dose that reaches the systemic circulation is defined as bioavailability, determined by the combined result of gut absorption (influenced by dissolution rate, solubility and permeability), intestinal extraction (dependent on luminal degradation, intestinal secretion or metabolism), and hepatic extraction (determined by hepatic metabolism or biliary excretion), shown in **Eq. 17**<sup>34</sup>.

**Eq. 17**  $F = f_{abs} * f_{gut} * f_{hep}$

Where  $F$  is systemic bioavailability;  $f_{abs}$  is the absorbed fraction of drug in the gastrointestinal tract (GI);  $f_{gut}$  is the fraction of dose escaping gut extraction;  $f_{hep}$  is the fraction of dose escaping hepatic extraction.

For oral administrations, first-order absorption models are usually applied to describe the absorption process. However, drug absorption is complex and sometimes delayed due to a time lag of drug dissolution and transit to the different tissues. Modeling with a simple lag time describes an abrupt switch of the absorption rate at a certain point of time, which may not depict the delayed absorption profiles accurately. Therefore, two models, i.e., transit compartments model and Weibull-type absorption model, are commonly used to mimic the delay.

### 1.2.3.1 Absorption models

#### 1.2.3.1.1 Transit compartment model

Transit compartment models describe the absorption with a chain of pre-systemic compartments, without assigning a physical tissue to each transit compartment, shown in **Figure 7**<sup>35</sup>.

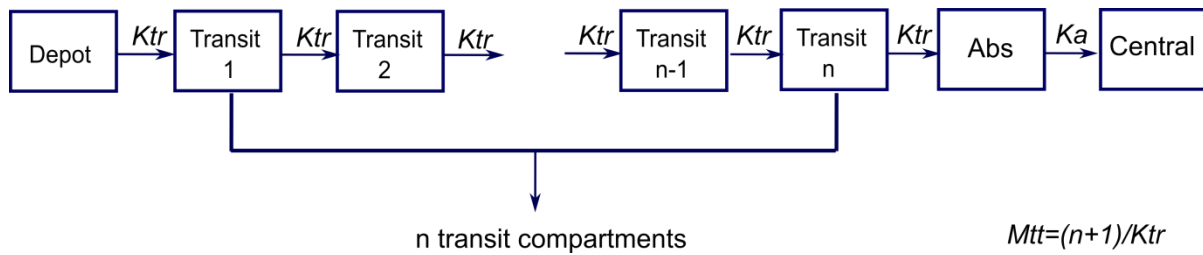


**Figure 7** Scheme of modeling drug absorption through a chain of transit compartments<sup>35</sup>.  $n$  is the number of transit compartments;  $Ktr$  represents the transit rate constant from  $n$ th-1 compartment to the  $n$ th compartment;  $MTT$  is the mean transit time, which means the average time taken by drug molecules traveling from the first transit compartment to the absorption compartment;  $Ka$  is the absorption rate. If over-parameterization is observed,  $Ka$  should be fixed to be equal to  $Ktr$ .

### 1.2.3.1.2 Weibull absorption model

The flexibility of the Weibull function can also be used to empirically describe the variable drug input rates along the GI tract with **Eqs. 18-19**<sup>36</sup>.

**Eq.18**  $f(t, k, \lambda) = 1 - \exp(-(t/\lambda))^k$

**Eq.19**  $\frac{dA(1)}{dt} = -A(1) * \frac{k}{\lambda} \left(\frac{t}{\lambda}\right)^{k-1}$

Where  $\lambda > 0$  is the scale parameter describing the delay;  $k > 0$  is the shape parameter characterizing the steepness of the absorption phase, as either exponential ( $k=1$ ), sigmoid ( $k>1$ ) or parabolic ( $k<1$ ).

### 1.2.3.1.3 Advanced dissolution, absorption & metabolism

Drug absorption is dependent on several physiological and drug-dependent factors, such as gastric emptying, intestinal transit time, intrainestinal pH, fluid volumes, absorption surface, drug stability, solubility, permeability, and so on.

In 2009, Simcyp incorporated an advanced dissolution, absorption and metabolism (ADAM) module in their software<sup>37</sup>. The ADAM model integrates a large number of factors, such as gastric emptying time, intestinal and colonic transit times, enterohepatic recirculation, GI tract surface area, region-specific gut wall permeability, enterocytic blood flow, etc<sup>38</sup>. More importantly, the variability of the pH profile of the GI tract is also introduced into the ADAM model; since the solubility of the drug depends on pH conditions and the dissolution status of the drug may change as it transits through the lumen of the GI tract with a range of pH<sup>37,39</sup>. Therefore, ADAM is considered as a good tool to predict oral drug absorption and bioavailability based on the physiochemical parameters and *in vitro* data.

### 1.2.3.2 Permeability

After being dissolved, a drug can permeate the gut wall either transcellularly or paracellularly. Most drugs depend on the transcellular pathway for absorption. The transcellular specific permeability of the intestinal wall may be calculated based on the drug's lipophilicity and molecular weight within the PK-Sim standard package, or determined by the Caco-2-cell permeability assay.<sup>40</sup> The paracellular pathway is usually not taken into account since this pathway typically has no impact on the accuracy of prediction of the fraction of the dose absorbed in humans.<sup>41</sup> Beyond passive absorption, large and/or hydrophilic molecules with certain specific functional groups may be transported by a carrier protein (transporter) across the enterocyte cell membranes. In this case, a mechanistic membrane transporter model should be integrated into the PBPK model, based on the *in vitro* data.<sup>42</sup>

### 1.2.4 Distribution

Drug distribution into various tissues from the systemic circulation is driven by blood flow rates and permeability, depending on the properties of the drug and the composition of the tissues. The distribution of volumes for different drugs varies, as shown in **Figure 8**.

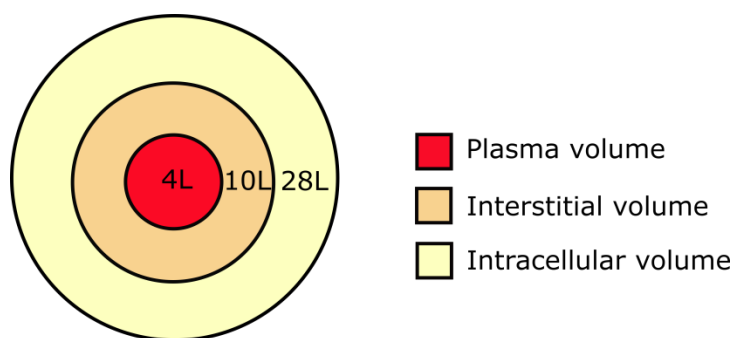


**Figure 8** Physical distribution volumes available to a drug<sup>34</sup>. Large molecules are limited to plasma volume since they cannot pass across the endothelial barrier (distribution volume < 4 L). Small, hydrophilic, and acids drugs tend to distribute in plasma or the interstitial fluids surrounding the tissue cells (distribution volume: 4-14 L), while lipophilic drugs can easily cross the membrane and diffuse into cells (distribution volume: 14-42 L). Lipophilic bases can bind strongly to the tissues, and thus their distribution volume is even greater than total body water (> 42 L)<sup>34</sup>.

The extent of tissue distribution depends on tissue-plasma partition coefficient  $K_p$  and the binding proteins<sup>34</sup>.  $K_p$  is defined as the ratio of the total concentration of drug in the tissue versus plasma at steady state ( $K_p = \frac{C_T}{C_p}$ ). It can be estimated based on the physicochemical data. There are five ways in PK-Sim to calculate the partition coefficients for organs, including the methods according to the PK-Sim standard model, Rodgers&Rowland<sup>43,44,45</sup> Schmitt<sup>46</sup>, Poulin&Theil<sup>47,48,49</sup>, and Berezhkovskiy<sup>50</sup>.

Typically, one of the methods is chosen empirically, i.e. based on the best overlap between observed and predicted concentration-time profiles.

## 1.2.5 Metabolism

Drug metabolism is the main enzymatic biotransformation from the parent drug to metabolites. The rate and extent of metabolism are decisive to describe the PK of a drug. For most drugs, the relevant part of this process usually takes place in the liver or in the intestinal wall. Both hepatocytes and intestinal mucosa cells contain a variety of enzymes that can metabolize the drug by phase I and II metabolism<sup>51</sup>.

### 1.2.5.1 *In vitro* assay

The capacity of an enzyme to catalyze the metabolism of the drug can be explored using *in vitro* systems with recombinant cytochrome P450 (CYP) or UDP-Glucuronosyltransferase (UGT), human liver microsomes, cytosol, or hepatocytes. The metabolism rates are calculated by assessing metabolite formation versus time. Typically, nonlinear regression is then used to fit the Michaelis-Menten equation<sup>52</sup> to the metabolite formation rate versus free parent concentration as described in **Eq.20**.

$$\text{Eq.20 } v = \frac{V_{max} * C_u}{K_M + C_u}$$

Where  $v$  is the metabolite formation rate;  $C_u$  is the unbound drug concentration ( $C_u = C * fu$ );  $V_{max}$  is the maximum velocity of the reaction; and  $K_M$  is the Michaelis-Menten constant, equal to the unbound drug concentration at half of  $V_{max}$ .

The *in vitro* intrinsic metabolic clearance is described by the ratio of  $V_{max}/K_M$  for unsaturated conditions in **Eq.21**.

$$\text{Eq.21 } CL_{int} \approx \frac{V_{max}}{K_M}$$

### 1.2.5.2 Extrapolation from *in vitro* to *in vivo*

The *in vitro* intrinsic clearance  $CL_{int}$  may be extrapolated to *in vivo* by a physiological scaling factor<sup>53</sup> with **Eqs. 22-23**, as shown in **Figure 9**.

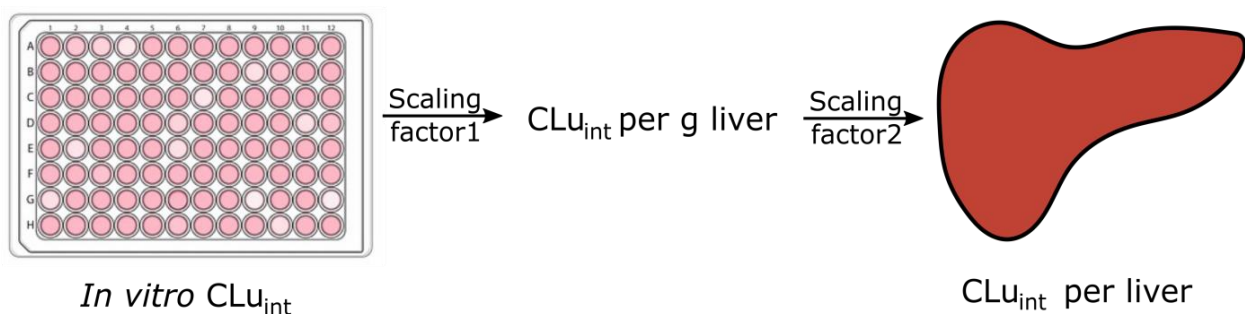


**Figure 9** Scheme of extrapolation *in vitro* results into *in vivo*.  $CLu_{int}$  is the unbound intrinsic clearance

$$\text{Eq.22 } CL_{int} = \left[ \sum_{j=1}^n \left( ISEF_j * rhCL_{int_j} * CYP_j abundance \right) \right] * MPPGL * LW$$

$$\text{Eq.23 } CLu_{int} = \frac{CL_{int}}{f_u}$$

Where  $ISEF_j$  is the intersystem extrapolation factor;  $rhCL_{int_j}$  is the enzyme-specific intrinsic clearance determined within recombinant-based systems ( $\mu\text{L}/\text{min}/\text{pmol}$  CYP enzyme);  $CYP_j abundance$  is the abundance of expression of CYPs in each rhCYP system ( $\text{pmol}/\text{mg}$  protein); MPPGL is the milligrams of microsomal protein per gram of liver ( $\text{mg}/\text{g}$ ); LW is the liver weight ( $\text{kg}$ );  $f_u$  is the fraction unbound;  $CLu_{int}$  is the unbound intrinsic clearance.

### 1.2.5.3 Well-stirred model

The *in vitro* unbound intrinsic clearance  $CLu_{int}$  is introduced into the PBPK model by several models. These models provided a more mechanistic way to extrapolate the *in vitro* to *in vivo*, e.g., “well-stirred” model and “parallel tube” model, shown in **Figures 10, 11**, respectively.

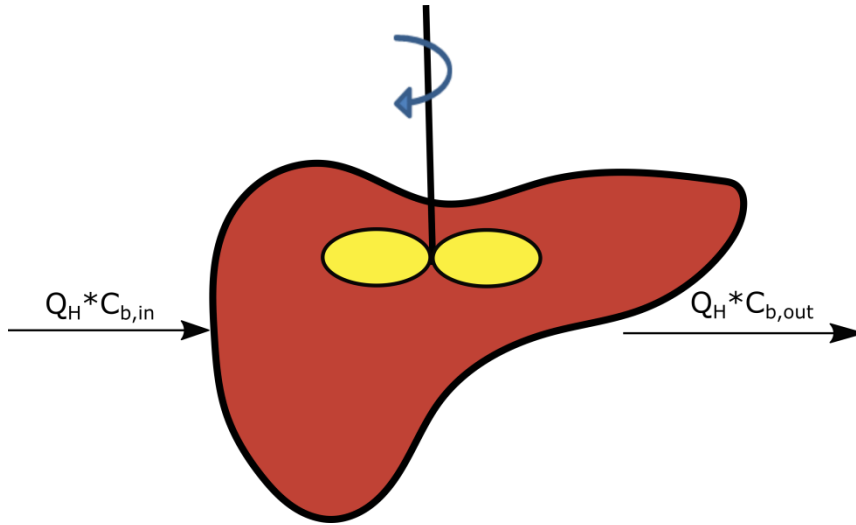


**Figure 10** Assumption of liver well-stirred model.  $Q_H$  is liver blood flow rate;  $C_{b,in}$  and  $C_{b,out}$  is the drug concentration entering into and leaving from the liver.

In the liver, the rate of change of the amount of drug is described by **Eq.24**.

$$\text{Eq.24 } V_H * \frac{dC_H}{dt} = Q_H * C_{b,in} - Q_H * C_{b,out} - CL_{int} * Cu_{cell}$$

Where  $V_H$  is liver volume;  $C_H$  is the total drug concentration in the liver;  $Q_H$  is liver blood flow rate;  $C_{b,in}$  and  $C_{b,out}$  is the drug concentration entering into and leaving from the liver;  $CL_{int}$  is the intrinsic clearance;  $Cu_{cell}$  is the unbound intracellular drug concentration.

The well-stirred model assumes that all aqueous spaces within the blood, interstitial space and intracellular space are well-mixed<sup>54</sup>, described with **Eq. 25**.

$$\mathbf{Eq.25} \quad C_{u_{cell}} = C_{u_{out}} = f_{u_B} * C_{b,out}$$

Where  $C_{u_{out}}$  is the remaining unbound drug concentration;  $f_{u_B}$  is the fraction of unbound concentration in plasma to the whole blood concentration ( $f_{u_B} = \frac{f_u}{c_b/c_p}$ ).

At steady state  $\frac{dC_H}{dt} = 0$ , combining **Eq.24** and **Eq.25** results in **Eq.26**.

$$\mathbf{Eq.26} \quad Q_H * C_{b,in} = Q_H * C_{b,out} + CL_{int} * C_{u_{cell}} = (Q_H + CL_{int} * f_{u_B}) * C_{b,out}$$

Then, the extraction ratio of the liver  $E_H$  is calculated with **Eq.27**.

$$\mathbf{Eq.27} \quad E_H = 1 - \frac{C_{b,out}}{C_{b,in}} = 1 - \frac{Q_H}{Q_H + f_{u_B} * CL_{int}} = \frac{f_{u_B} * CL_{int}}{Q_H + f_{u_B} * CL_{int}}$$

Thus, the total hepatic clearance  $CL_H$  results in **Eq.28**.

$$\mathbf{Eq.28} \quad CL_H = Q_H * E_H = \frac{Q_H * f_{u_B} * CL_{int}}{Q_H + f_{u_B} * CL_{int}}$$

#### 1.2.5.4 Parallel tube model

The “parallel tube” model describes the liver as a series of parallel tubes with enzyme located evenly surrounding the tubes, and at any point along the tube, the drug is distributed in equilibrium between the enzymatic site and tubes<sup>55</sup>, described in **Figure 11** and **Eqs.29-30**.

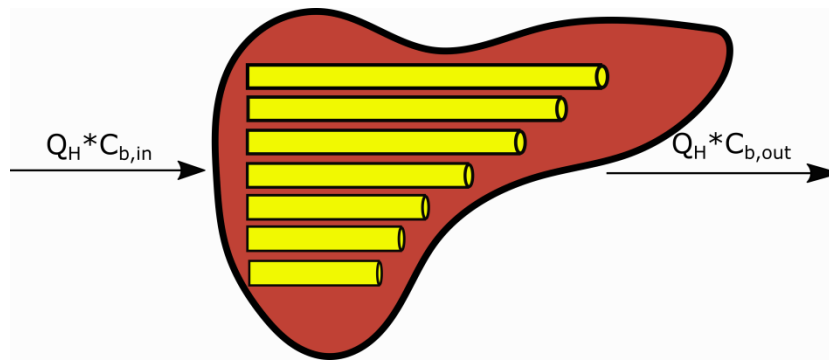


**Figure 11** Parallel tube hepatic elimination model.  $Q_H$  is liver blood flow rate;  $C_{b,in}$  and  $C_{b,out}$  is the drug concentration entering into and leaving from the liver.

$$\mathbf{Eq.29} \quad CL_H = Q_H * (1 - e^{-f_{u_B} * \frac{CL_{int}}{Q_H}})$$

$$\mathbf{Eq.30} \quad E_H = 1 - e^{-f_{u_B} * CL_{int} / Q_H}$$

Where  $CL_H$  is the total hepatic clearance;  $Q_H$  is liver blood flow rate;  $f_{u_B}$  is the fraction of unbound concentration in plasma to the whole blood concentration ( $f_{u_B} = \frac{f_u}{C_b/C_p}$ );  $f_u$  is the unbound fraction;  $C_b$  is the drug concentration in the blood;  $C_p$  is the drug concentration in the plasma;  $CL_{u_{int}}$  is the unbound intrinsic clearance;  $E_H$  is the extraction ratio of the liver.

### 1.2.6 Excretion

For hydrophilic drugs, the compound could be excreted renally as the parent drug. The fraction of the dose excreted in the urine is calculated by **Eq.31**.

$$\text{Eq.31 } f_e = \frac{A_{unchanged}}{dose} = \frac{CL_R}{CL}$$

Where  $A_{unchanged}$  is the amount of unchanged drug excreted in the urine;  $CL_R$  is renal clearance;  $CL$  is the total clearance of drug metabolism and renal clearance.

Thus, the renal clearance  $CL_R$  could be calculated by **Eq.32**.

$$\text{Eq.32 } CL_R = \frac{A_{unchange}}{AUC}$$

Renal elimination of a drug is determined by glomerular filtration, active tubular secretion, and tubular reabsorption. Lipophilic drugs are quickly reabsorbed, while hydrophilic drugs are readily excreted through the kidney. All these three processes can be integrated into a PBPK model to describe renal drug clearance.



### 1.3 Semi-physiological popPK modeling

PBPK can provide total variability for the observed PK data, which are actually the combined results from inter-individual variability (IIV) for each key process or parameter. To investigate the variability from the specific process, a semi-physiological population modelling approach is a good option, which can not only quantify IIV of the key parameters and provide a mechanistic model at the population level, but also explore drug metabolism in the local tissues or organs.

The semi-physiological popPK modeling approach is both knowledge- and data- driven, depending on physiological parameters (e.g., blood flow for specific organs), physicochemical properties of drugs (e.g., unbound fraction, blood versus plasma ratio, permeability), as well as drug concentration-time datasets<sup>56</sup>. Semi-physiological popPK model usually consists of conventional distributional compartments (central and peripheral compartments) and additional specific organ compartments (e.g., gut lumen, gut wall, portal vein, liver, kidney, or tumor).

Compared to popPK, the advantage of the semi-physiological model is that it can explore the contribution of the physiological process to the PK of drugs, and more importantly, predict the local tissue concentration and the therapeutic effect or toxicity directly at the tissue sites.

In comparison to PBPK, the semi-physiological popPK modeling is much simpler and only incorporates the desired tissue compartment into the model without requiring other additional organs. Furthermore, it can apply stochastic methods to provide predictions of population variability and evaluate sources of inter- and intra-individual variability.

The disadvantage of the semi-physiological modeling approach is the extensive workload and the requirement of individual datasets for drug concentrations. Another concern about the semi-physiological modeling is that this approach is based on several assumptions of underlying processes, and it requires fixing certain parameters to arbitrary values, which may result in a scaling effect of other parameters or even lead to model misspecification.

## 1.4 Study drugs

### 1.4.1 Ciprofloxacin

The chemical name of ciprofloxacin is 1-cyclopropyl-6-fluoro-1,4-dihydro-4-oxo-7-(1-piperazinyl)-3-quinolin carboxylic acid (**Figure 12**). Belonging to the group of fluoroquinolones, it functions by inhibiting the ligase activity of the type II topoisomerases, gyrase and topoisomerase IV, thereby inhibiting bacterial DNA replication, transcription, repair, and recombination<sup>57</sup>. Ciprofloxacin is commonly used in the treatment of severe infections since it is a broad spectrum antibacterial drug to most Gram-negative bacteria, especially *Pseudomonas aeruginosa*<sup>58</sup>. It is generally applied in the therapy of urinary tract infections, sexually transmitted diseases, skin and bone infections, GI infections caused by a multiresistant organism, lower respiratory tract infections, febrile neutropenia (combined with antibiotics against Gram-positive bacteria), intra-abdominal infections (combined with an anti-anaerobic agent) and malignant external otitis<sup>59</sup>.



**Figure 12** Chemical structure of ciprofloxacin

#### 1.4.1.1 PK of ciprofloxacin

After oral administration, ciprofloxacin is absorbed rapidly to reach the peak serum concentration ( $C_{max}$ ) within 1 to 2 hours<sup>57,60,61</sup>. The bioavailability of oral ciprofloxacin is approximately 70%<sup>62</sup>. Binding of ciprofloxacin to serum proteins is 20 to 40%<sup>63</sup>. The volume of distribution is reported from 122 to 350 L at steady-state after oral or intravenous dosing<sup>57,64</sup>.

The PK of ciprofloxacin has a linear relationship between serum concentrations and doses administered either orally and intravenously up to doses of 250 mg<sup>65,66</sup>. For healthy subjects, renal clearance, including glomerular filtration and tubular secretion, accounts for approximately 66% of total serum clearance. The rest is eliminated through metabolic degradation, biliary excretion, and transluminal secretion across the enteric mucosa<sup>57,67,68</sup>. The terminal half-life  $t_{1/2}$  is about 3 to 4 hours<sup>66</sup>.

### 1.4.1.2 PK/PD relationship of ciprofloxacin

For antibiotics, three established PK/PD indexes were defined: the ratio of AUC over 24 h at steady-state versus the minimum inhibitory concentration MIC ( $AUC_{0-24}/MIC$ ),  $C_{max}$  divided by the MIC ( $C_{max}/MIC$ ), the cumulative percentage of a 24 h period that the drug concentration exceeds the MIC at steady-state PK conditions ( $T > MIC$ )<sup>69</sup>.

Like other fluoroquinolones, ciprofloxacin has concentration-dependent bactericidal activity. The value of 125 for the ratio of  $AUC_{0-24}/MIC$  has considered being minimally effective and a value of above 250 shows increased *in vivo* bactericidal rates and a shorter time to bactericidal eradication<sup>70</sup>.

### 1.4.1.3 Main considerations

Significant adverse effects associated with ciprofloxacin are seldom with the overall worldwide incidence of 5-10%<sup>71</sup>. The most commonly reported adverse reactions are usually mild to moderate, involving gastrointestinal tract (nausea, vomiting, and diarrhea), metabolic or nutritional disorders<sup>57</sup>.

When ciprofloxacin is applied in critically ill patients, underexposure is the primary concern. In clinical practice, a dose reduction is recommended in patients with renal insufficiency<sup>57,67,68</sup>. However, the relationship between measured creatinine clearance and ciprofloxacin is poor for patients with renal dysfunction<sup>72</sup>. In this case, non-renal elimination pathways might compensate for the elimination of ciprofloxacin<sup>67,68</sup>. In clinical practice, dosing reduction of ciprofloxacin only depends on creatinine clearance / estimated glomerular filtration rate<sup>73</sup>, ignoring non-renal pathways. This procedure might lead to under-exposure and thus to exposing patients at risk of treatment failure. Therefore, it is vital to identify valid predictors of ciprofloxacin PK concerning kidney and liver function of patients and to assess the need for dose reductions in isolated/combined kidney and liver dysfunction in critically ill patients.

## 1.4.2 Voriconazole

The chemical name of voriconazole is (2~{R},3~{S})-2-(2,4-difluorophenyl)-3-(5-fluoropyrimidin-4-yl)-1-(1,2,4-triazol-1-yl)butan-2-ol (**Figure 13**). As a second-generation triazole antifungal agent, it inhibits the cytochrome P450 enzyme 14- $\alpha$ -sterol demethylase (CYP51), to disrupt the fungal membrane and prevent fungal growth<sup>74</sup>. Voriconazole has excellent activity against a wide range of clinically relevant fungal pathogens, including the most commonly occurring species of the genera *Aspergillus* and *Candida*, and several important emerging fungi, such as *Scedosporium* and *Fusarium* species<sup>75,76</sup>. Voriconazole is widely used for the treatment and prophylaxis of a variety of invasive fungal diseases (IFDs) and is considered as a first-line treatment against invasive aspergillosis and infections due to *Candida krusei*<sup>77,78</sup>. It is more effective and has fewer adverse effects than amphotericin B to treat aspergillosis<sup>76</sup>. Furthermore, since voriconazole could cross the blood-brain barrier, it is recommended for patients with central nervous system IFDs<sup>79-81</sup>.



**Figure 13** Chemical structure of voriconazole

### 1.4.2.1 PK of voriconazole

Both intravenous and oral formulations of voriconazole are used in clinical practice. For oral administration, voriconazole is absorbed rapidly within two hours<sup>82,83</sup>. Protein binding is approximately 58% independent of dose or plasma concentrations<sup>75</sup>. The volume of distribution is reported to range from 140 to 322 L<sup>84</sup>. The bioavailability of this drug is dependent on the dose. At therapeutic oral doses, the bioavailability is around 90%, allowing switching between oral and intravenous administration when clinically appropriate<sup>85,86</sup>. At low oral doses (50 mg), the first-pass metabolism is high, and bioavailability is only around 39%<sup>87</sup>. Voriconazole's nonlinear PK with dose- and time-dependence is reported to be relevant to its saturable metabolism<sup>87</sup> and the auto-inhibition on its metabolic enzyme CYP3A4<sup>88</sup>.

Voriconazole is extensively metabolized via CYP2C19 and 3A4<sup>89</sup>, and slightly by CYP2C9 and flavin-containing monooxygenase<sup>90</sup>, with less than 6% being excreted renally as the parent drug<sup>91,92</sup>. After oral or intravenous administration of multiple radiolabeled doses, approximately 80-83% of the radioactivity is recovered in urine, almost all of this as metabolites, and less than 20% is excreted in the faeces<sup>75,84</sup>.

#### 1.4.2.2 PK/PD relationship of voriconazole

Voriconazole exhibits time-dependent fungistatic activity against *Candida* species and time-dependent slow fungicidal activity against *Aspergillus* species.<sup>84</sup> Dose fractionation studies in animals demonstrated the AUC/MIC ratio as the PK/PD parameter which was most predictive of efficacy (correlation coefficient  $r^2$  for AUC/MIC=82%, for  $C_{max}/MIC=63%$ , for  $T>MIC=75%$ )<sup>84,93</sup>. A voriconazole free drug  $fAUC/MIC$  value higher than 25 and a  $fC_{min}/MIC$  value above one is recommended for adjusted dosage regimens as a strategy to increase clinical response rates, particularly among patients with a failed clinical response to current standard therapy<sup>94</sup>.

#### 1.4.2.3 Main considerations

In the clinical practice for the treatment of invasive aspergillosis, the loading dose of voriconazole is 6 mg/kg twice daily, and the maintenance dose is 4mg/kg twice daily or 200 mg twice daily<sup>95</sup>. However, since voriconazole exhibits nonlinear PK with large inter- and intra-individual variability<sup>84,85</sup>, it causes difficulties for clinicians to choose appropriate dosing regimens to target its narrow therapeutic range, especially in the case of high doses in severe infections, or for long-term treatments.<sup>96</sup> Underexposure of voriconazole may decrease efficacy, whereas overexposure increases the risk mainly for neural and hepatic toxicity<sup>97,98</sup>. Therefore, it is crucial to explore the metabolism of voriconazole and to better understand the nonlinear PK of voriconazole. Meanwhile, quantifying the sources of variability is also important to be considered to predict PK of voriconazole.

The main metabolic enzyme for voriconazole is CYP2C19. Therefore, CYP2C19 genetic polymorphisms may cause large IIV of voriconazole exposure. It is reported that 3-fold higher  $C_{max}$  values and 2- to 5-fold higher AUC values are present in poor metabolizers (PMs) compared to those in normal CYP2C19 metabolizers (NMs) or rapid metabolizers (RMs)<sup>96,99,100</sup>. CYP2C19 gene test is beneficial to the patient before initiating voriconazole, especially for Asian people. Because the prevalence of CYP2C19 PM is 8.4% in Asian, which is higher than Caucasians (4.0%) and Africa (5.2%), exposing Asian patients at a higher potential of voriconazole overdose and toxicity<sup>101</sup>. The most common side effects are a visual disturbance, neurological/psychiatric disorder, hepatotoxicity, GI symptoms, and skin disorders<sup>95</sup>.

Furthermore, voriconazole is also extensively metabolized via CYP3A4, and meanwhile, this drug also inhibits CYP3A. Therefore, the CYP3A4-mediated interactions should be carefully taken into

account, including interactions with CYP3A4 inhibitors<sup>102</sup>, CYP3A4 inducers<sup>103</sup>, or CYP3A4 probe substrates<sup>104</sup>.

### 1.4.3 Midazolam

The chemical name of midazolam is 8-chloro-6-(2-fluorophenyl)-1-methyl-4-H-imidazo[1,5-a][1,4] benzodiazepine (**Figure 14**). Midazolam is a well-established probe substrate for the *in vivo* assessment of CYP3A activity. In this thesis, we use midazolam to evaluate the inhibition of perpetrator drugs (ethanol and voriconazole) on CYP3A at gut wall and liver.

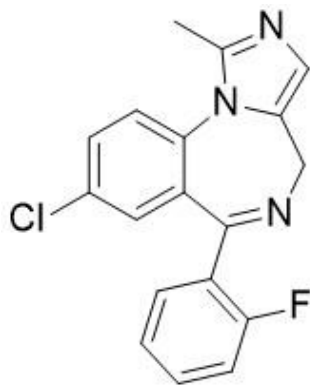


**Figure 14** Chemical structure of midazolam

#### 1.4.3.1 PK of Midazolam

After oral administration, midazolam is rapidly absorbed<sup>107</sup>. Plasma protein binding is 96-98%, and the volume of distribution ranges from 49 to 84 L at steady state<sup>108</sup>. Midazolam is extensively metabolized by CYP3A, which are mainly expressed in mature enterocytes of the gut wall and centrilobular hepatocytes in humans<sup>109-111</sup>. Therefore, the bioavailability of midazolam is low, ranging from 30 to 50% due to the pronounced first-pass metabolism<sup>108,112</sup>. The elimination half-life is 1.5 to 2.5 hours. The metabolism of midazolam is mainly (60-80%) via 1'-hydroxylation<sup>107</sup> and, to a lesser extent (5%), by 4-hydroxylation, followed by urinary excretion as 1'-O-glucuronide derivative<sup>113-116</sup>. Direct midazolam N-glucuronidation via uridine 5'-diphospho-glucuronosyltransferase family 1 member A4 (UGT1A4) accounts for less than 2 % of midazolam elimination<sup>117</sup>.

#### 1.4.3.2 Probe substrate for CYP3A4

Midazolam is an ideal probe substrate for the *in vivo* assessment of CYP3A activity recommended by the FDA and EMA<sup>105,106</sup>. The PK of midazolam shows dose linearity within a single dose range of 0.075-7.5 mg, indicating no saturation of the enzyme<sup>104,108,118-120</sup>. The assessment of perpetrator drug effects on CYP3A4 activity in both the gut wall and liver requires dissection of any impact on the two sites. Although it is not possible to directly measure intestinal metabolism of midazolam, it can be estimated by models (PBPK or semi-physiological and PBPK models) based on clinical studies with both oral and intravenous administration, which is described in detail in the thesis.

### 1.4.4 Cyclosporine A

The chemical name of cyclosporine A (CsA) is cyclo-(L-Alanyl-D-alanyl-N-methyl-L-leucyl-N-methyl-L-leucyl-N-methyl-L-valyl-3-hydroxy-N,4-dimethyl-L-2-amino-6-octenoyl-L-a-amino-buteryl-N-methylglycyl-N-methyl-L-leucyl-L-valyl-N-methyl-L-leucyl) (**Figure 15**). It is an immunosuppressant drug widely used since the early 1980s as first-line therapy to prevent the rejection of transplanted solid organs and hematopoietic stem cell transplantation<sup>121</sup>.

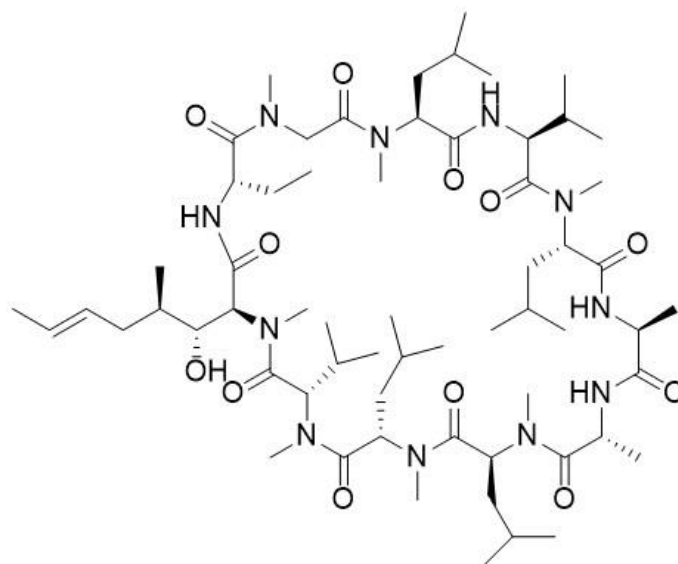


**Figure 15** Chemical structure of Cyclosporine A

#### 1.4.4.1 PK of CsA

After oral administration, CsA is incompletely absorbed from the GI tract. Absorption is highly variable and depends on CsA preparation, food intake, co-medication, type of transplanted organ, or amount of bile in the gut<sup>122</sup>. CsA is a lipophilic molecule, and its distribution mainly depends on biological carriers such as lipoproteins and erythrocytes in the blood (approximate 14-58% of CsA bound to erythrocytes, and 9-21% bound to lipoproteins)<sup>122</sup>. The steady-state volume of distribution of CsA is reported to range from 210 to 350 L<sup>123</sup>.

CsA is extensively metabolized by CYP3A in the liver, to a lesser degree in the intestinal wall, and subject to efflux from renal tubular and other cells via P-gp<sup>124</sup>. The terminal elimination half-life highly varies and ranges from 5 to 18 h<sup>123</sup>. The major excretion route of CsA is via the bile, mainly as metabolites of the drug. Renal excretion accounts for only 6% of the dose administered.<sup>123,125</sup>

#### 1.4.4.2 Main considerations

Therapeutic drug monitoring for CsA is essential since it has a narrow therapeutic range and large inter-individual PK variability<sup>126</sup>. Underexposure might cause graft-versus-host disease and acute rejection episodes, while overexposure might result in toxicity<sup>127</sup>.



Factors affecting the metabolism of CsA include liver disease, age, and DDIs during transplantation, especially in the case when co-administered with CYP3A or P-gp perpetrators<sup>125</sup>. For example, concomitant administration of ketoconazole elevated CsA concentrations several-fold<sup>128,129</sup>. Imatinib, a potent inhibitor of CYP3A4 and P-gP, could approximately double CsA exposure<sup>130</sup>. Therefore, clinicians should be very cautious with regard to DDIs between CsA and CYP3A or P-gp inhibitors.

### 1.4.5 Baicalin

Baicalin, baicalein 7-O-glucuronide (**Figure 16**), is the main bioactive compound from *Scutellaria baicalensis*<sup>131</sup>. It is widely applied in traditional Chinese medicine for the treatment of inflammation, hepatitis, various infections, and tumors<sup>132,133,134,135</sup>. Baicalin capsules (250 mg per capsule, approval no. H20158009) were approved in 2005 by the state food and drug administration of China as adjuvant therapy of hepatitis (2 capsules 3 times a day). Baicalin and its aglycone baicalein having anti-inflammatory and antioxidant properties might benefit organ transplant patients treated with CsA<sup>136,137</sup>.

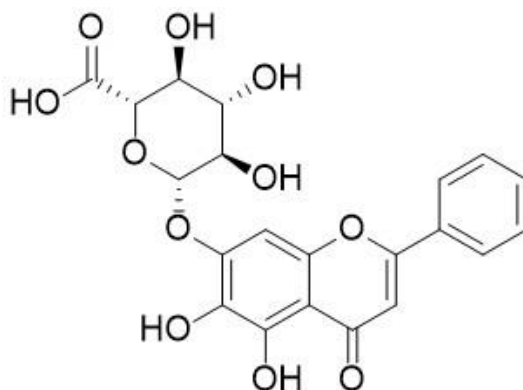


**Figure 16** Chemical structure of Baicalin

#### 1.4.5.1 PK of baicalin

After oral administration, baicalin is readily hydrolyzed to its aglycone baicalein by  $\beta$ -glucuronidase derived from intestinal bacteria<sup>138</sup>. Compared to baicalin, baicalein is better absorbed in the GI<sup>139,140</sup>. However, baicalein is again conjugated to baicalin by UGT in the gut wall and liver<sup>141</sup>. Baicalin has a high protein binding of 86-92%<sup>142</sup> while baicalein had a moderate affinity. Thus, the conversion from baicalin into baicalein can influence its distribution<sup>143</sup>.

Baicalin has a short elimination half-life ( $6.36 \pm 5.85$  h) and undergoes extensive metabolism<sup>144</sup>. The metabolism of baicalin is mainly located in the intestinal tract, liver, and kidney, resulting in several metabolites, including baicalein, baicalein 6-O- $\beta$ -D-glucopyranuronoside, and baicalein 6,7-di-O- $\beta$ -glucopyranuronoside<sup>145,142</sup>.

#### 1.4.5.2 Main considerations

Several lines of evidence indicate that baicalin might cause DDIs in humans, especially DDIs with CYP3A and P-gp substrates; indeed, baicalein exhibits inhibition on CYP3A and P-gp in rats<sup>146,147</sup>. Intravenous administration of high baicalin doses (0.23-0.90 g/kg) to rats decreased the clearance of midazolam by up to 43 %<sup>148</sup>. Neither a single nor multiple intravenous doses of baicalin affected the PK of CsA in rats<sup>149</sup>. However, oral administration significantly decreased  $C_{max}$  and  $AUC_{0-\infty}$  of CsA<sup>149</sup>.

This suggests that baicalin might have an effect on intestinal absorption and/or secretion of CsA. Further study revealed that after multiple oral doses of baicalin treatment, the expression of P-gp of rats increased in the intestine, but was not changed in the liver<sup>149</sup>. Therefore, a possible DDI between CsA and baicalin needs to be further investigated.

## 1.4.6 Ethanol

### 1.4.6.1 PK of ethanol

According to WHO estimates, beverages containing ethanol are consumed by more than half of the population aged 15 years or older worldwide<sup>150</sup>. However, there is large variability in absorption, distribution, metabolism, and elimination of ethanol among the populations<sup>151</sup>.

The absorption rate of ethanol depends on drinking patterns (bolus or repetitive drinking), the concentration of ethanol, gastric emptying and especially on fed or fasted state of the individual<sup>152,153</sup>. Peak ethanol blood concentration is higher after a single dose than after several smaller doses. Since ethanol crosses membranes by passive diffusion, a higher concentration of ethanol in beverages results in a greater concentration gradient, driving more rapid absorption<sup>154</sup>. However, results from another study questioned this theory, in which blood alcohol concentration (BAC) curves were not much different when 0.75 g/kg ethanol was consumed on an empty stomach as 4, 8, 20, and 44% v/v dilutions with water<sup>153</sup>. Another important factor is the emptying rate of the stomach. Therefore, factors influencing stomach emptying such as food, drugs, smoking cigarettes, stress etc. also affect the rate of absorption of ethanol<sup>153,155</sup>.

The distribution of ethanol is closely related to the amount of water in the body, with sex- and age-related differences<sup>156</sup>. The distribution volume of ethanol is about 0.6 L/kg for women and 0.7 L/kg for men<sup>157,158</sup>. Ethanol does not bind to plasma proteins. The concentration of ethanol in the tissue depends on the relative water content of the tissue and quickly reaches equilibrium with the plasma concentration<sup>151</sup>.

Most of the ingested ethanol (90-98%) is removed from the body by oxidative metabolism<sup>153</sup>. Ethanol metabolism occurs primarily in the liver by a successive oxidation pathway, first to form acetaldehyde and then acetate (in **Figure 17**)<sup>154</sup>. The remaining fraction of the dose administered (2-8%) is excreted unchanged via kidney, lung, and skin<sup>159</sup>. The conversion of ethanol into acetaldehyde is mainly mediated by cytosolic alcohol dehydrogenases (ADH), limiting the rate of oxidization. The  $K_m$  values of most ADH isozymes are low (0.05-0.1 g/L), and ADH is saturated after the first couple of drinks<sup>151,153</sup>. Thus, at high ethanol concentrations, the elimination process follows zero-order kinetics at maximum velocity, also denoted as Michaelis-Menten kinetics<sup>151</sup>.

Also, CYP2E1 contributes to the metabolism of ethanol with a higher  $K_m$  of ethanol (0.6-0.8 g/L) and becomes more important after moderate to heavy drinking<sup>160</sup>. CYP2E1 is inducible after periods of heavy drinking over weeks or months<sup>160,161</sup>.

Several factors influence the elimination of ethanol, including sex, age, genetic polymorphism of ADH, biological rhythms, chronic alcohol exposure, or co-medication with other drugs (e.g., ADH inhibitors)<sup>154</sup>.

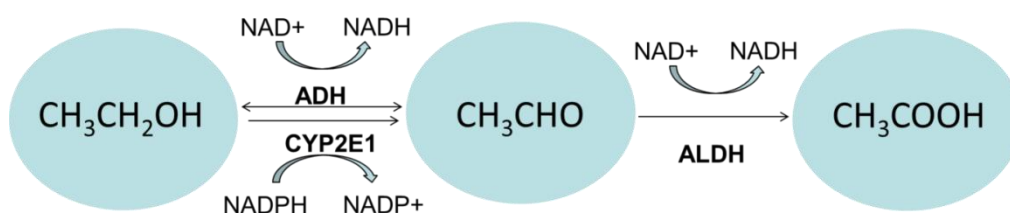


**Figure 17** General pathway for the metabolism of ethanol.  $\text{CH}_3\text{CH}_2\text{OH}$  is ethanol;  $\text{CH}_3\text{CHO}$  is acetaldehyde;  $\text{CH}_3\text{COOH}$  is acetate; ADH is alcohol dehydrogenase; ALDH is the aldehyde dehydrogenase;  $\text{NAD}^+$  is nicotinamide adenine dinucleotide. Ethanol is metabolized into acetaldehyde by alcohol dehydrogenase and CYP2E1. Acetaldehyde is further metabolized into acetate by aldehyde dehydrogenase. The metabolic pathway involves nicotinamide adenine dinucleotide as a carrier of electrons.

#### 1.4.6.2 Main considerations

Ethanol affects the activity of drug-metabolizing enzymes, including CYPs or drug transporters. This may cause DDIs between ethanol and other medications<sup>162,163</sup>. Clinical trials of the effect of ethanol on human CYP were mainly conducted for CYP2E1. After acute ethanol consumption, the activity of CYP2E1 dramatically decreased by 93.2%<sup>164</sup>; while it was significantly induced 2-fold after chronic consumption<sup>165,166</sup>, probably related to a decelerated CYP2E1 degradation<sup>167</sup>.

*In vitro* studies on the effect of ethanol on CYPs were mainly carried out to identify appropriate solvents for substrates and inhibitors of *in vitro* assays to assess CYP activity and gave controversial results<sup>168-170</sup>. These results indicate that ethanol may change drug metabolism *in vitro* by several mechanisms, including enzyme inhibition and degradation<sup>170</sup>. Therefore, it is crucial to systematically evaluate the effect of acute alcohol consumption on the activity of important drug-metabolizing enzymes and transporters *in vivo*.

## **2. Aims and objectives**

The overarching objective of the thesis was to assess important sources of PK variability using appropriate modeling approaches such as popPK modeling, PBPK modeling, and semi-physiological popPK modeling. This was exemplified in several individual drugs. For these, the effect of relevant covariates on its PK was quantified. Finally, the appropriate models were used to predict the consequences of any changes in such covariates.

### **2.1 The effect of critical illness on ciprofloxacin PK**

The study aim was to 1) develop a popPK model of ciprofloxacin in critically ill patients; 2) identify the covariates and quantify their contribution to PK variability; 3) based on identified indicators, calculate the probability of anti-infective target attainment (AUC/MIC) and the probability of exceeding toxicity AUC limits; 4) to assess the rationale for ciprofloxacin dosing regimen adjustments for patients with isolated and combined hepatic and renal insufficiency.

### **2.2 The effect of voriconazole on CYP3A activity**

The aims were to understand the nonlinear PK of voriconazole with dose- and time-dependence, search for the reasons behind nonlinear PK, explore primary sources of the large inter- and intra-individual PK variability of voriconazole, develop an appropriate model to describe *in vivo* PK data, and perform model-based simulations to predict appropriate dosing regimens for voriconazole.

#### **2.2.1 Using PBPK modeling to understand voriconazole PK and its properties as a perpetrator on drug metabolism via CYP3A and CYP2C19**

This study aimed to 1) investigate the metabolism of voriconazole in detail to understand dose- and time-dependent alterations in the PK of the drug; 2) provide a whole-body PBPK model as the basis for safe and effective use of voriconazole according to CYP2C19 genotype; 3) assess the dynamic inhibition of CYP3A4 by voriconazole in liver and small intestine; 4) predict DDIs between voriconazole and other CYP3A4 probe substrates.

#### **2.2.2 Using semiphysiological PK modeling and the novel study design to quantify the effect of voriconazole on CYP3A activity, and DDIs between voriconazole and midazolam**

This DDI study between voriconazole and midazolam was performed to 1) investigate the dynamic inhibition of voriconazole on CYP3A at the respective enzyme sites; 2) quantify the variability of active CYP3A in the liver and gut wall; 3) to investigate a novel study design for the assessment of DDIs caused by CYP3A inhibition.

### **2.3 The effect of baicalin co-medication on CsA PK**

CsA is susceptible to DDIs since it is metabolized mainly by CYP3A and it is a substrate of P-glycoprotein. Baicalin's main metabolite baicalein can inhibit CYP3A and P-gP. This study was carried out to investigate the effect of baicalin on CsA PK and to explore the safety co-administration of CsA and baicalin in humans.

### **2.4 The effect of ethanol on the activity of major drug metabolizing enzymes and transporters**

This project was mainly carried out to evaluate the effect of acute alcohol consumption on the activity of CYP1A2, CYP2C9, CYP2C19, CYP2D6, intestinal CYP3A4, hepatic CYP3A4, NAT2, as well as on the drug transporter p-glycoprotein. Within this project, popPK modeling was used to describe the PK of ethanol and to describe the effect of ethanol on intestinal and hepatic CYP3A activity.

## 3. Results

### 3.1 The effect of critical illness on ciprofloxacin PK

Xia Li, Michael Zoller, Uwe Fuhr, Mikayil Huseyn-Zada, Barbara Maier, Michael Vogeser, Johannes Zander, Max Taubert. Ciprofloxacin in critically ill subjects: considering hepatic function, age and sex to choose the optimal dose. *J Antimicrob Chemother* 2018; 74:682-90.

<https://doi.org/10.1093/jac/dky485>

### 3.2 The effect of voriconazole on CYP3A activity

#### 3.2.1 Using PBPK modeling to understand voriconazol PK and its properties as a perpetrator on drug metabolism via CYP3A and CYP2C19

Xia Li, Sebastian Frechen, Daniel Moj, Thorsten Lehr, Max Taubert, Chih-hsuan Hsin, Gerd Mikus, Pertti J. Neuvonen, Klaus T. Olkkola, Teijo I. Saari, Uwe Fuhr. A Physiologically-based pharmacokinetic model of voriconazole integrating time-dependent inhibition of CYP3A4, genetic polymorphisms of CYP2C19 and predictions of drug-drug interactions. *Clin Pharmacokinetics* (in press) <https://doi.org/10.1007/s40262-019-00856-z>

#### 3.2.2 Using semiphysiological PK modeling and the novel study design to quantify the effect of voriconazole on CYP3A activity, and DDIs between voriconazole and midazolam

Xia Li, Lisa Junge, Max Taubert, Anabelle Dieterich, Dominik Dahlinger, Chris Starke, Sebastian Frechen, Christoph Stelzer, Martina Kinzig, Fritz Sörgel, Ulrich Jaehde, Ulrich Töx, Tobias Goeser, Uwe Fuhr. A novel study design using continuous intravenous and intraduodenal infusions of midazolam and voriconazole for mechanistic quantitative assessment of hepatic and intestinal CYP3A inhibition. *J. Clini. Pharmacol.* (in press). <https://doi.org/10.1002/jcph.1619>

### 3.3 The effect of baicalin co-medication on CsA PK

Ruijuan Liu<sup>#</sup>, Xia Li<sup>#</sup>, Jingyao Wei, Shuaibing Liu, Yuanyuan Chang, Jiali Zhang, Ji Zhang, Xiao Jian Zhang, Uwe Fuhr, Max Taubert, Xin Tian. A single dose of baicalin has no clinically significant effect on the pharmacokinetics of cyclosporine A in healthy Chinese volunteers. *Front Pharmacol* 2019; 10: 518-19. <sup>#</sup>equal contributions <https://doi.org/10.3389/fphar.2019.00518>



### **3.4 The effect of ethanol on the activity of major drug metabolizing enzymes and transporters**

Malaz Gazzaz, Martina Kinzig, Elke Schaeffeler, Martin Jübner, Chih-hsuan Hsin, **Xia Li**, Max Taubert, Christina Trueck, Juliane Iltgen-Breburda, Daria Kraus, Christian Queckenberg, Marc Stoffel, Matthias Schwab, Fritz Sörgel, Uwe Fuhr. Drinking ethanol has few acute effects on CYP2C9, CYP2C19, NAT2, and P-Glycoprotein activities but somewhat inhibits CYP1A2, CYP2D6, and intestinal CYP3A: So What? *Clin Pharmacol Ther* 2018; 104: 1249–59. <https://doi.org/10.1002/cpt.1083> (My contribution to the project includes developing and describing the models of ethanol and midazolam)

## 4. Summary

### 4.1 The effect of critical illness on ciprofloxacin PK

Ciprofloxacin is an important antibiotic in the treatment of severe infections. Pathophysiological changes often result in altered PK of ciprofloxacin in critically ill patients. We aimed to assess the rationale for ciprofloxacin dosing regimen adjustments for isolated and combined hepatic and renal in critically ill patients. Therefore, ciprofloxacin PK was investigated in 15 critically ill patients with severe infections. 400 mg ciprofloxacin was administered intravenously twice daily for four days, and blood samples were collected at multiple time points for four days, resulting in 444 quantifiable serum concentrations of ciprofloxacin.

Based on the dataset, a popPK model was developed. A two-compartment model with linear elimination described the PK of ciprofloxacin best (central volume V1: 24.2-33.5 L for day 1 to 4; peripheral volume V2: 83.2 L; clearance CL: 16.2-20.9 L/h for day 1 to 4; and inter-compartmental clearance Q: 71.2 L/h). Systematic changes of CL and V1 from day 1 to 4 were identified, indicating alterations of the PK of ciprofloxacin throughout the treatment course. Covariates regarding kidney and liver dysfunction were tested, resulting in a final covariate model comprising age, sex, and total plasma bilirubin, which in total explained 60% of IIV.

The probability of exceeding the AUC limit of 250 mg·h/L depending on age, sex, and bilirubin for a daily dose of 800 and 1200 mg were evaluated. Females were at higher risk, especially at older age with elevated bilirubin. For daily doses of 1200 mg, the risk of AUC > 250 mg·h/L for females at age 65 years with bilirubin 4 mg/dL was about 20%, while the risk for male subjects at age 60 years with bilirubin 10 mg/dL was below 1%. Given a daily dose of 800 mg, the risk of exceeding the AUC limit was only slightly elevated for male subjects while it was increased to about 20% for female subjects at the age of 80 years with a bilirubin concentration of 5 mg/dL.

Appropriate target attainment (AUC/MIC > 125) was also evaluated for the covariates identified. For male subjects at an age below 50 years with normal bilirubin, a dose increase to 1200 (800) mg/day was needed, given an MIC of 0.25 (0.125) mg/L, while given a MIC of 0.5 mg/L, sufficient AUC/MIC ratios were only observed with 1200 mg per day and an age of at least 65 years or elevated bilirubin concentrations. For female subjects at an age below 55 years with normal bilirubin, an increase to 1200 (800) mg/day would be needed given a MIC of 0.5 (0.25) mg/L.

Thus, total bilirubin, age, and sex might be important parameters facilitating the choice of an appropriate dose of ciprofloxacin in critically ill patients. A dose reduction based on creatinine clearance is not supported while a decrease to 400 mg seems reasonable for female patients with higher age and considerably increased bilirubin if MIC values of the causative strains are  $\leq 0.25$  mg/L.

## 4.2 The effect of voriconazole on CYP3A activity

### 4.2.1 Using PBPK modeling to understand voriconazole PK and its properties as a perpetrator on drug metabolism via CYP3A and CYP2C19

The nonlinear PK of voriconazole with large inter- and intra-individual variability causes difficulties for clinicians to select appropriate dosing. We conducted *in vitro* assays to search for the reasons behind nonlinear PK. Then, a whole-body PBPK model was developed based on the *in vitro* assay and on *in vivo* data, considering genetic polymorphisms of CYP2C19.

The IC<sub>50</sub> shift assay showed that voriconazole had time-dependent inhibition (TDI) on CYP3A4 with a 16 fold shift in the absence and presence of NADPH. The further inactivation kinetic assay gave a  $K_I$  (the inhibition concentration when reaching half of  $k_{inact}$ ) of 9.33 (95% CIs: 2.56-34.0)  $\mu\text{M}$  and a  $k_{inact}$  (maximum inactivation rate constant) of 0.0428 (95% CIs: 0.0171-0.107)  $\text{min}^{-1}$  for CYP3A4, supporting TDI to be introduced into the PBPK model. However, the input of  $k_{inact}$  of 0.0428  $\text{min}^{-1}$  led to an overestimation of midazolam exposure for DDI studies. Therefore,  $k_{inact}$  was optimized as 0.015  $\text{min}^{-1}$  in the PBPK model based on the concentration-time profiles from the clinical trial with multiple intravenous dosing of voriconazole. Moreover, genetic polymorphisms of CYP2C19 were integrated into a model for RMs (rapid metabolizers), NMs (normal metabolizers), IM (intermediate metabolizers) or PM (poor metabolizers) with the reference CYP2C19 expression values of 0.79, 0.76, 0.40, and 0.01  $\mu\text{mol}$  CYP2C19 per L of liver tissue, respectively<sup>171</sup>.

The *in vitro* results as well as *in vivo* datasets from clinical trials supported the development of a whole-body PBPK model of voriconazole. The PBPK model evaluation demonstrated a good performance of the model, with 71% of predicted/observed aggregate AUC ratios and all aggregate C<sub>max</sub> ratios from 28 evaluation datasets being within a 0.5- to 2-fold range. For those studies reporting CYP2C19 genotype, 89% of aggregate AUC ratios and all aggregate C<sub>max</sub> ratios were inside a 0.5- to 2-fold range of 44 test datasets. The results of model-based simulation showed that the standard maintenance dose of 200 mg voriconazole BID (twice daily) oral dosing is sufficient for CYP2C19 IMs (intermediate metabolizers: \*1/\*2, \*1/\*3, \*2/\*17, and \*2/\*2/\*17) to reach the tentative therapeutic range of >1-2 mg/L to <5-6 mg/L for C<sub>trough</sub> (trough concentrations for multiple dosings), while 400 mg might be more suitable for RMs (rapid metabolizers: \*1/\*17, \*17/\*17) and NMs (normal metabolizers, \*1/\*1). When the model was integrated with independently developed CYP3A4 substrate models (midazolam and alfentanil), the observed AUC change of substrates by voriconazole was inside the 90% confidence interval (CI) of the predicted AUC change, indicating that CYP3A4 inhibition was appropriately incorporated into the voriconazole model.

Therefore, the PBPK model developed here could support individual dose adjustment of voriconazole according to genetic polymorphisms of CYP2C19 as well as DDI risk management between voriconazole and CYP3A4 probe substrates.

## 4.2.2 Using semiphysiological PK modeling and the novel study design to quantify the effect of voriconazole on CYP3A activity, and DDIs between voriconazole and midazolam

A limitation to quantify the DDI mediated by CYP3A inhibition is that the extent of inhibition observed is usually an average of continuously changing inhibition caused by the dynamic alteration of concentrations of both substrate and inhibitor, and the changing contributions from the two main expression sites of CYP3A, i.e., gut wall and liver. It is difficult to capture the time course of inhibition using standard DDI studies.

Therefore, a novel study design was applied in six healthy participants to characterize the time course and extent of inhibition of hepatic and intestinal CYP3A enzymes. It was an open-label, change-over, randomized four-period study. Subject received a continuous intraduodenal or intravenous infusion of the CYP3A substrate midazolam at a constant rate for 24 hours (0.26 mg/h). This was combined with intraduodenal or intravenous infusion of the CYP3A inhibitor voriconazole, administered at scheduled rates of 7.5 and 15 mg/h from 8 to 16 and 16 to 24 hours, respectively, after the start of MDZ infusion. Plasma and urine concentrations of VRZ, MDZ and its major metabolites, were quantified by LC-MS/MS.

Previously published popPK models were not suitable to describe the data. Integration of mechanism-based inactivation of the metabolizing enzymes into the model ( $k_{inact}$ : 2.83 h<sup>-1</sup>;  $K_I$ : 9.33 μM) could describe the PK of voriconazole well. By introducing competitive inhibition of voriconazole on midazolam metabolism (the inhibition constant  $K_{i,MDZ}$  for primary hydroxylation: 0.586 μM;  $K_{i,1'-OH-MDZ}$  and  $K_{i,4-OH-MDZ}$  for secondary glucuronidation: 1.13 and 0.356 μM), the concentration-time profiles of midazolam and its metabolites were captured appropriately. The model provides estimates of local concentrations of substrate and inhibitor at both of the CYP3A expression sites, thus enabling to describe the temporal course of the respective extent of inhibition and to predict the exposure of CYP3A substrates when co-administered with voriconazole.

The combination of intravenous and intestinal infusions turned out to be suitable to investigate the systemic and pre-systemic CYP3A metabolism, enabling to identify the contribution of hepatic and intestinal metabolism<sup>172</sup>. Our results confirmed that no saturation of MDZ metabolism by CYP3A occurred. In our evaluation, midazolam total hepatic clearance of 19.8 l/h was similar to the published values (19.4-31.4 l/h) after intravenous administration<sup>107,173-175</sup>. The sum of estimated midazolam hepatic and intestinal clearance of 24.1 l/h is consistent with the reported total clearance of 22.8-39.8 L/h after oral administration<sup>173,176,177</sup>. The bioavailability of midazolam (30.8%) was in a good agreement with reported values (30-50%)<sup>108</sup>. For voriconazole, the peculiar way of administration was relevant for its PK behaviour. The bioavailability of voriconazole in the present study (18.7%) was much lower than the value reported for therapeutic doses (82.6%)<sup>178</sup>. One possible reason is that the

enzymes mediating voriconazole metabolism were saturated at therapeutic doses but not at the low dose/dose rate used in the present study, which is supported by reports on a dose-dependent bioavailability of VRZ<sup>87</sup>. Auto-inhibition of voriconazole at high doses might also contribute to the discrepancy in bioavailability. Daily chronic voriconazole doses used in DDI studies were typically in the range of 200 to 800 mg<sup>104,179</sup>, while in the present study the doses and input rates of voriconazole were low since we aimed at investigating a gradual response rather than maximal inhibition. In addition, we used two different input rates to achieve two different intestinal/ hepatic concentrations of VRZ, which is the minimum to assess the concentration dependency of the extent of inhibition.

The results of the present pilot study suggest that the combination of intravenous and intra-duodenal infusions of inhibitors and substrates has the potential to provide a more accurate assessment of DDIs occurring in both gut wall and liver. Using this approach, a detailed description of the inhibitory effects of VRZ on MDZ metabolism at the hepatic and intestinal CYP3A expression sites was possible, including the time course of inhibition and respective sources of inter-individual variability. The model may be helpful to assess the potential of VRZ to cause DDIs with other CYP3A substrates. Further studies with lower complexity (inhibitors without mechanism-based inhibition; single inhibitor infusion rate per study period) and a larger sample size are required to further evaluate this approach.

### 4.3 The effect of baicalin co-medication on CsA PK

CsA is a first-line immunosuppressant therapy used following organ and stem cell transplantation. Co-administration of CsA and baicalin might affect CsA PK since CsA is metabolized mainly by CYP3A and is a substrate of P-glycoprotein, while baicalin's main metabolite baicalein inhibits CYP3A and P-gP. Therefore, the effect of baicalein on CsA PK was investigated in a clinical study in 16 healthy volunteers. Since this is the first clinical study to investigate the effect of baicalin on CsA PK in humans, a single dose was given considering safety reasons. Subjects received a single 200 mg oral CsA dose alone in the reference period and combination with 500 mg baicalein in the test period. PK of CsA was analyzed using both non-compartmental analysis (NCA) and the popPK approach. For the NCA assessment, treatments were compared by the standard bioequivalence method.

90 % CIs of AUC and  $C_{max}$  test-to-reference ratios were within the bioequivalence boundaries of 80-125%. For the popPK analysis, a two-compartment model (clearance [CL]: 62.8 L/h, central [Vc] and peripheral [Vp] volume of distribution: 254L and 388L, Q: 23.6 L/h) with transit compartments to describe absorption (absorption rate [Ka]: 12.4 h<sup>-1</sup>, number of transit compartments [N]: 20) best described CsA concentrations. Except for Ka and Q, the 95% CIs of the factor "baicalin co-treatment" on the parameters were inside the 0.8-1.25 range, indicating that baicalin did not have an effect on the exposure to CsA to a clinically relevant extent. For Ka and Q, the CIs included unity but exceeded the range, reflecting pronounced IIV.

Therefore, no relevant effect of baicalin co-administration on CsA PK was identified and both treatments were well tolerated.

#### **4.4 The effect of ethanol on the activity of major drug metabolizing enzymes and transporters**

High ethanol concentrations were reported to have effects on the activity of several CYP450 enzymes *in vitro*, while *in vivo* data on ethanol-drug interactions are sparse. Therefore, the study was performed to quantify the effect of acute ethanol exposure (initial blood concentrations 0.7 g/L) on major drug metabolizing enzymes CYP1A2, CYP2C9, CYP2C19, CYP2D6, CYP3A, NAT2, and P-glycoprotein.

Eight women and eight men participated in a randomized crossover study with six doses of administration of either vodka or water. A loading dose of ethanol (males, 0.76 g/kg; female, 0.65 g/kg) was given 2 hours before administration of oral probe drugs and maintenance ethanol doses (males, 0.30 g/kg; female, 0.26 g/kg) were given every 4 hours in the test period. Water was given in the reference period instead of ethanol. Enzyme/transporter activity was assessed by a cocktail of probe substrates, including caffeine (CYP1A2/NAT2), tolbutamide (CYP2C9), omeprazole (CYP2C19), dextromethorphan (CYP2D6), midazolam (CYP3A), and digoxin (P-glycoprotein). In both periods, the cocktail of oral probe drugs was administered 2 hours after the first ethanol dose, and midazolam was intravenously injected 2 hours after cocktail administration.

The PK of ethanol was appropriately described by a one-compartment model with an additive error. The body weight has a significant exponential relationship to the volume of distribution, and males have a 40% lower maximal ethanol metabolism capacity compared to females.

To separately evaluate the contribution of both intestinal and hepatic CYP3A to midazolam metabolism, a semi-physiological population PK model was developed for plasma concentrations of midazolam and 1'-hydroymidazolam. Then, the assessment of the effect of ethanol on midazolam metabolism at both sites resulted in that ethanol reduced intestinal midazolam extraction to be 0.77-fold (90% CI 0.69–0.86) but had no significant effect on midazolam hepatic clearance. Thus, a high ethanol exposure when occurring during treatment with drugs having extensive first-pass metabolism by CYP3A may occasionally cause a relevant increase in drug exposure.

The effects of ethanol exposure on other drug metabolizing enzymes and transporters were summarized in the last paper of the result part.

## 4.5 Application of three PK approaches

PBPK and popPK modeling are conventional approaches to assess the PK of a drug. Semi-physiological popPK modeling is an intermediate approach.

One of the advantages of PopPK is that it can be used to test hypotheses on the sources of PK variability due to intrinsic factors (e.g., age, weight, gender, and genotype) and extrinsic factors (e.g., co-medication with other drugs). In the ciprofloxacin project, covariates, such as age, sex, and total bilirubin plasma concentrations were identified as significant covariates by the popPK approach, which in total explained 60% of IIV. Of course, bilirubin is not a direct source of ciprofloxacin PK variability, but an apparently suitable indicator for liver function. PopPK can describe the relationship between drug clearance and organ function based on empirical observations and available parameters to describe organ function, rather than based on theoretical knowledge of the mechanisms for drug clearance. Therefore, to extrapolate the results from popPK models with confidence, the relationship must be physiologically reasonable and consistent with our understanding of the mechanisms. As an advantage, popPK can quantify individual variability in PK parameters and residual variability. This enables to predict the probability of target attainment or toxicity in a population based on drug exposure.

PBPK is frequently applied in drug discovery and development from the early stages with limited data to the late stage with more data available to make decisions on candidate selection, to support the selection of the first-in-human dose, to assess the DDI potential of investigational drugs, to support the design of clinical trials involving DDIs, to decide on inclusion/exclusion criteria for studies with drug metabolized by polymorphic enzymes, or provide exposure predictions in special populations.<sup>180–183</sup> In contrast to popPK, PBPK can predict local drug concentrations in each organ and support PD analysis. Also, PBPK software platforms, like PK-Sim, contain a library of different species (i.e., human, monkey, beagle, dog, minipig, rat, mouse)<sup>180</sup>, making it possible to extrapolate information obtained in animals to humans to assist first human dose selection. Furthermore, PBPK software also provide databases on different ethnic populations (e.g., European, Asian, Black American, Mexican American, White American) to allow to extend results to other populations based on relevant physiological differences<sup>184</sup>. PBPK is even helpful to assess exposure in children, in pregnancy and in preterm infants, which is beneficial for these populations with limited data from clinical trials due to ethic issues<sup>185–187</sup>. Most importantly, the PBPK approach can support IVIVE. In the voriconazole project, the time-dependent inhibition of voriconazole on CYP3A was identified from *in vitro* assays but was later incorporated into the PBPK model to describe the *in vivo* profiles of voriconazole.

The semi-physiological popPK modeling combines the essential elements of both approaches. The semi-physiological popPK approach can reduce model complexity and meanwhile still allow the inclusion of mechanistic elements<sup>188,189</sup>. Semi-physiological popPK models can not only estimate PK



parameters including population variability based on experimentally obtained concentration datasets, but the models can also take advantage of its mechanistic structure, thus allowing local tissue drug concentration to be predicted. Therefore, the efficacy and toxicity of a drug can be directly linked to the relevant tissue concentration prediction, which is quite useful in the case of CYP3A inhibition<sup>190</sup>, as shown here for the DDIs between voriconazole and midazolam or the effect of ethanol on the PK of midazolam. Furthermore, the semi-physiological model can inform and support the design of prospective clinical DDI studies even when *in vivo* data are limited because this approach can take advantage of the physiological structure and extrapolate *in vitro* data to *in vivo* to provide predictions for the clinical effect.

In conclusion, all three approaches have powerful descriptive and predictive abilities and can support decision-making during drug development. In the case of voriconazole presented here, even a combination of models was required to improve the understanding of the properties of the drug. Without the development of the PBPK model of voriconazole which provided the appropriate mechanistic components, the development of a semi-physiological model with the additional options has not been possible. The selection of the most suitable of the modeling approaches ultimately depends on the specific questions to be answered and the type of data available.

## 5 References

1. Nelson E. Kinetics of drug absorption, distribution, metabolism, and excretion. *J Pharm Sci* 1961; **50**: 181–92.
2. Sandritter TL, McLaughlin M, Artman M, *et al.* The interplay between pharmacokinetics and pharmacodynamics. *Pediatr Rev* 2017; **38**: 195–206.
3. Mould DR, Upton RN. Basic concepts in population modeling, simulation, and model-based drug development. *CPT pharmacometrics Syst Pharmacol* 2012; **1**: e6.
4. Gabrielsson J, Weiner D. Non-compartmental Analysis. In: *Methods in molecular biology (Clifton, N.J.)*. Vol 929., 2012; 377–89.
5. Sheiner LB, Beal SL. Evaluation of methods for estimating population pharmacokinetic parameters. I. Michaelis-menten model: Routine clinical pharmacokinetic data. *J Pharmacokinet Biopharm* 1980; **8**: 553–71.
6. Charles B. Population pharmacokinetics: an overview. *Aust Prescr* 2014; **37**: 210–3.
7. Jones H, Rowland-Yeo K. Basic concepts in physiologically based pharmacokinetic modeling in drug discovery and development. *CPT pharmacometrics Syst Pharmacol* 2013; **2**: e63.
8. U.S. Food and Drug Administration. *Population Pharmacokinetics Guidance for Industry draft guidance*. 2019.
9. Mould DR, Upton RN. Basic concepts in population modeling, simulation, and model-based drug development-part 2: introduction to pharmacokinetic modeling methods. *CPT pharmacometrics Syst Pharmacol* 2013; **2**: e38.
10. Keizer RJ, Karlsson MO, Hooker A. Modeling and simulation workbench for NONMEM: tutorial on Pirana, PsN, and Xpose. *CPT pharmacometrics Syst Pharmacol* 2013; **2**: e50.
11. Olofsen E, Dinges DF, Van Dongen HPA. Nonlinear Mixed-Effects Modeling: Individualization and Prediction. *Aviat Space Environ Med* 2004; **75**: A134-40.
12. Wright PMC. Population based pharmacokinetic analysis: why do we need it; what is it; and what has it told us about anaesthetics? *Br J Anaesth* 1998; **80**: 488–501.
13. Proost JH. Combined proportional and additive residual error models in population pharmacokinetic modelling. *Eur J Pharm Sci* 2017; **109**: S78–82.
14. Wählby U, Jonsson EN, Karlsson MO. Assessment of actual significance levels for covariate effects in NONMEM. *J Pharmacokinet Pharmacodyn* 2001; **28**: 231–52.
15. Olofsen E, Dahan A. Using Akaike’s information theoretic criterion in mixed-effects modeling of pharmacokinetic data: a simulation study. *F1000Research* 2013; **2**: 71.
16. Byon W, Smith MK, Chan P, *et al.* Establishing best practices and guidance in population modeling: an experience with an internal population pharmacokinetic analysis guidance. *CPT Pharmacometrics Syst Pharmacol* 2013; **2**: e51.
17. Savic RM, Karlsson MO. Importance of shrinkage in empirical bayes estimates for diagnostics: problems and solutions. *AAPS J* 2009; **11**: 558–69.
18. Karlsson MO, Savic RM. Diagnosing model diagnostics. *Clin Pharmacol Ther* 2007; **82**: 17–20.
19. Karlsson MO. A full model approach based on the covariance matrix of parameters and covariates. In: *AAPS*. Vol 20., 2004; 207–53.
20. Kowalski KG, Hutmacher MM. Efficient screening of covariates in population models using Wald’s approximation to the likelihood ratio test. *J Pharmacokinet Pharmacodyn* 2001; **28**: 253–75.

21. Mandema JW, Verotta D, Sheiner LB. Building population pharmacokinetic-pharmacodynamic models. I. Models for covariate effects. *J Pharmacokinet Biopharm* 1992; **20**: 511–28.
22. Ribbing J, Nyberg J, Caster O, *et al.* The lasso—a novel method for predictive covariate model building in nonlinear mixed effects models. *J Pharmacokinet Pharmacodyn* 2007; **34**: 485–517.
23. Whittingham, Mark J. Stephens, Philip A. Bradbury, Richard Freckleton RP. Why do we still use stepwise modelling in ecology and behaviour? *J Anim Ecol* 2006; **75**: 1182–9.
24. Steyerberg EW, Eijkemans MJC, Habbema JDF. Stepwise selection in small data sets: a simulation study of bias in logistic regression analysis. *J Clin Epidemiol* 1999; **52**: 935–42.
25. Gastonguay MR. Full covariate models as an alternative to methods relying on statistical significance for inferences about covariate effects: a review of methodology and 42 case studies. In: *AAPS.*, 2004; W4354.
26. Post TM, Freijer JI, Ploeger BA, *et al.* Extensions to the visual predictive check to facilitate model performance evaluation. *J Pharmacokinet Pharmacodyn* 2008; **35**: 185–202.
27. Ette EI. Stability and Performance of a Population Pharmacokinetic Model. *J Clin Pharmacol* 1997; **37**: 486–95.
28. Parke J, Holford NHG, Charles BG. A procedure for generating bootstrap samples for the validation of nonlinear mixed-effects population models. *Comput Methods Programs Biomed* 1999; **59**: 19–29.
29. Kuepfer L, Niederalt C, Wendl T, *et al.* Applied concepts in PBPK modeling: how to build a PBPK/PD model. *CPT pharmacometrics Syst Pharmacol* 2016; **5**: 516–31.
30. Zhuang X, Lu C. PBPK modeling and simulation in drug research and development. *Acta Pharm Sin B* 2016; **6**: 430–40.
31. Jones HM, Gardner IB, Watson KJ. Modelling and PBPK simulation in drug discovery. *AAPS J* 2009; **11**: 155–66.
32. Hanke N, Frechen S, Moj D, *et al.* PBPK models for CYP3A4 and P-gp DDI prediction: a modeling network of rifampicin, itraconazole, clarithromycin, midazolam, alfentanil, and digoxin. *CPT Pharmacometrics Syst Pharmacol* 2018; **7**: 647–59.
33. Jamei M, Dickinson GL, Rostami-Hodjegan A. A framework for assessing inter-individual variability in pharmacokinetics using virtual human populations and integrating general knowledge of physical chemistry, biology, anatomy, physiology and genetics: A tale of “bottom-up” vs “top-down” recognition of covariates. *Drug Metab Pharmacokinet* 2009; **24**: 53–75.
34. Peters SA. *Physiologically-based pharmacokinetic (PBPK) modeling and simulations*. Hoboken, NJ, USA: John Wiley & Sons, Inc.; 2012.
35. Savic RM, Jonker DM, Kerbusch T, *et al.* Implementation of a transit compartment model for describing drug absorption in pharmacokinetic studies. *J Pharmacokinet Pharmacodyn* 2007; **34**: 711–26.
36. Rietbrock S, Merz PG, Fuhr U, *et al.* Absorption behavior of sulphiride described using Weibull functions. *Int J Clin Pharmacol Ther* 1995; **33**: 299–303.
37. Jamei M, Turner D, Yang J, *et al.* Population-based mechanistic prediction of oral drug absorption. *AAPS J* 2009; **11**: 225–37.
38. S. Darwich A, Neuhoff S, Jamei M, *et al.* Interplay of Metabolism and Transport in Determining Oral Drug Absorption and Gut Wall Metabolism: A Simulation Assessment Using the Advanced Dissolution, Absorption, Metabolism (ADAM) Model. *Curr Drug Metab* 2011; **11**: 716–29.

39. Vertzoni M, Augustijns P, Grimm M, *et al.* Impact of regional differences along the gastrointestinal tract of healthy adults on oral drug absorption: An UNGAP review. *Eur J Pharm Sci* 2019; **134**: 153–75.
40. van Breemen RB, Li Y. Caco-2 cell permeability assays to measure drug absorption. *Expert Opin Drug Metab Toxicol* 2005; **1**: 175–85.
41. Thelen K, Coboeken K, Willmann S, *et al.* Evolution of a detailed physiological model to simulate the gastrointestinal transit and absorption process in humans, Part 1: Oral solutions. *J Pharm Sci* 2011; **100**: 5324–45.
42. Moj D, Hanke N, Britz H, *et al.* Clarithromycin, midazolam, and digoxin: application of PBPK modeling to gain new insights into drug-drug interactions and co-medication Regimens. *AAPS J* 2017; **19**: 298–312.
43. Rodgers T, Leahy D, Rowland M. Physiologically based pharmacokinetic modeling 1: predicting the tissue distribution of moderate-to-strong bases. *J Pharm Sci* 2005; **94**: 1259–76.
44. Rodgers T, Rowland M. Mechanistic approaches to volume of distribution predictions: understanding the processes. *Pharm Res* 2007; **24**: 918–33.
45. Rodgers T, Leahy D, Rowland M. Tissue distribution of basic drugs: accounting for enantiomeric, compound and regional differences amongst beta-blocking drugs in rat. *J Pharm Sci* 2005; **94**: 1237–48.
46. Schmitt W. General approach for the calculation of tissue to plasma partition coefficients. *Toxicol Vitro* 2008; **22**: 457–67.
47. Poulin P, Theil F. A priori prediction of tissue:plasma partition coefficients of drugs to facilitate the use of physiologically-based pharmacokinetic models in drug discovery. *J Pharm Sci* 2000; **89**: 16–35.
48. Poulin P, Theil F-P. Prediction of pharmacokinetics prior to in vivo studies. II. generic physiologically based pharmacokinetic models of drug disposition. *J Pharm Sci* 2002; **91**: 1358–70.
49. Poulin P, Theil F-P. Prediction of pharmacokinetics prior to in vivo studies. 1. Mechanism-based prediction of volume of distribution. *J Pharm Sci* 2002; **91**: 129–56.
50. Berezhkovskiy LM. Volume of distribution at steady state for a linear pharmacokinetic system with peripheral elimination. *J Pharm Sci* 2004; **93**: 1628–40.
51. Iyanagi T. Molecular mechanism of phase I and phase II drug-metabolizing enzymes: implications for detoxification. *Int Rev Cytol* 2007; **260**: 35–112.
52. Michaelis L, Menten ML, Johnson KA, *et al.* The original Michaelis constant: translation of the 1913 Michaelis-Menten paper. *Biochemistry* 2011; **50**: 8264–9.
53. Barter ZE, Bayliss MK, Beaune PH, *et al.* Scaling factors for the extrapolation of in vivo metabolic drug clearance from in vitro data: reaching a consensus on values of human microsomal protein and hepatocellularity per gram of liver. *Curr Drug Metab* 2007; **8**: 33–45.
54. Rowland M, Benet LZ, Graham GG. Clearance concepts in pharmacokinetics. *J Pharmacokinetic Biopharm* 1973; **1**: 123–36.
55. Pang KS, Rowland M. Hepatic clearance of drugs. I. Theoretical considerations of a “well-stirred” model and a “parallel tube” model. Influence of hepatic blood flow, plasma and blood cell binding, and the hepatocellular enzymatic activity on hepatic drug clearance. *J Pharmacokinetic Biopharm* 1977; **5**: 625–53.
56. Frechen S, Junge L, Saari TI, *et al.* A semiphysiological population pharmacokinetic model for dynamic inhibition of liver and gut wall cytochrome P450 3A by voriconazole. *Clin Pharmacokinetic* 2013; **52**: 763–81.

57. Vance-Bryan K, Guay DRP, Rotschafer JC. Clinical pharmacokinetics of ciprofloxacin. *Clin Pharmacokinet* 1990; **19**: 434–61.
58. Zelenitsky S, Ariano R, Harding G, *et al.* Evaluating ciprofloxacin dosing for *Pseudomonas aeruginosa* infection by using clinical outcome-based Monte Carlo simulations. *Antimicrob Agents Chemother* 2005; **49**: 4009–14.
59. Davis R, Markham A, Balfour JA. Ciprofloxacin. *Drugs* 1996; **51**: 1019–74.
60. Lubasch A, Keller I, Borner K, *et al.* Comparative pharmacokinetics of ciprofloxacin, gatifloxacin, grepafloxacin, levofloxacin, trovafloxacin, and moxifloxacin after single oral administration in healthy volunteers. *Antimicrob Agents Chemother* 2000; **44**: 2600–3.
61. Bergan T, Delin C, Johansen S, *et al.* Pharmacokinetics of ciprofloxacin and effect of repeated dosage on salivary and fecal microflora. *Antimicrob Agents Chemother* 1986; **29**: 298–302.
62. Drusano GL, Standiford HC, Plaisance K, *et al.* Absolute oral bioavailability of ciprofloxacin. *Antimicrob Agents Chemother* 1986; **30**: 444–6.
63. Bayer Pharmaceuticals Corporation. *CIPRO*® (*ciprofloxacin hydrochloride*) Tablets. 2004.
64. Lettieri JT, Rogge MC, Kaiser L, *et al.* Pharmacokinetic profiles of ciprofloxacin after single intravenous and oral doses. *Antimicrob Agents Chemother* 1992; **36**: 993–6.
65. Bergan T, Thorsteinsson SB, Solberg R, *et al.* Pharmacokinetics of ciprofloxacin: intravenous and increasing oral doses. *Am J Med* 1987; **82**: 97–102.
66. Bergan T, Thorsteinsson SB, Kolstad IM, *et al.* Pharmacokinetics of ciprofloxacin after intravenous and increasing oral doses. *Eur J Clin Microbiol* 1986; **5**: 187–92.
67. Viell B, Krause B, Schaaf S, *et al.* Transintestinal elimination of ciprofloxacin in humans- Concomitant assessment of its metabolites in serum, ileum and colon. *Infection* 1992; **20**: 324–7.
68. Rohwedder RW, Bergan T, Thorsteinsson SB, *et al.* Transintestinal elimination of ciprofloxacin. *Diagn Microbiol Infect Dis* **13**: 127–33.
69. Nielsen EI, Cars O, Friberg LE. Pharmacokinetic/pharmacodynamic (PK/PD) indices of antibiotics predicted by a semimechanistic PKPD model: a step toward model-based dose optimization. *Antimicrob Agents Chemother* 2011; **55**: 4619–30.
70. Forrest A, Nix DE, Ballow CH, *et al.* Pharmacodynamics of intravenous ciprofloxacin in seriously ill patients. *Antimicrob Agents Chemother* 1993; **37**: 1073–81.
71. Campoli-Richards DM, Monk JP, Price A, *et al.* Ciprofloxacin. *Drugs* 1988; **35**: 373–447.
72. Khachman D, Conil J, Georges B, *et al.* Optimizing ciprofloxacin dosing in intensive care unit patients through the use of population pharmacokinetic-pharmacodynamic analysis and Monte Carlo simulations. *J Antimicrob Chemother* 2011; **66**: 1798–809.
73. U.S. Food and Drug Administration. *Center for drug evaluation and research approval package for: application number: NDA 21-554 ciprofloxacin extended-release tablets* ([https://www.accessdata.fda.gov/drugsatfda\\_docs/nda/2003/021554Orig1s000Approv.pdf](https://www.accessdata.fda.gov/drugsatfda_docs/nda/2003/021554Orig1s000Approv.pdf)). 2003.
74. Ghannoum MA, Rice LB. Antifungal agents: mode of action, mechanisms of resistance, and correlation of these mechanisms with bacterial resistance. *Clin Microbiol Rev* 1999; **12**: 501–17.
75. Pfizer. *VFEND*® I.V. (*voriconazole*) for Injection *VFEND*® Tablets [https://www.accessdata.fda.gov/drugsatfda\\_docs/label/2010/021266s032lbl.pdf](https://www.accessdata.fda.gov/drugsatfda_docs/label/2010/021266s032lbl.pdf). 2010.
76. Sandherr M, Maschmeyer G. Pharmacology and metabolism of voriconazole and Posaconazole in the treatment of invasive aspergillosis: review of the literature. *Eur J Med Res* 2011; **16**: 139–44.
77. Patterson TF, Thompson GR, Denning DW, *et al.* Practice guidelines for the diagnosis and

- management of aspergillosis: 2016 update by the infectious diseases society of America. *Clin Infect Dis* 2016; **63**: e1–60.
78. Pappas PG, Kauffman CA, Andes DR, *et al.* Clinical practice guideline for the management of Candidiasis: 2016 update by the infectious diseases society of America. *Clin Infect Dis* 2015; **62**: e1–50.
79. Schwartz S, Thiel E. Cerebral aspergillosis: tissue penetration is the key. *Med Mycol* 2009; **47**: S387–93.
80. Schwartz S, Thiel E. Poster Sessions I and II , Interdisciplinary Workshop, Satellite Symposia I-IV. *Ann Hematol* 2004; **83**: S13–58.
81. Stiefel M, Reiß T, Staeger MS, *et al.* Successful treatment with voriconazole of Aspergillus brain abscess in a boy with medulloblastoma. *Pediatr Blood Cancer* 2007; **49**: 203–7.
82. Purkins L, Wood N, Greenhalgh K, *et al.* Voriconazole, a novel wide-spectrum triazole: oral pharmacokinetics and safety. *Br J Clin Pharmacol* 2003; **56 Suppl 1**: 10–6.
83. Levêque D, Nivoix Y, Jehl F, *et al.* Clinical pharmacokinetics of voriconazole. *Int J Antimicrob Agents* 2006; **27**: 274–84.
84. Theuretzbacher U, Ihle F, Derendorf H. Pharmacokinetic/pharmacodynamic profile of voriconazole. *Clin Pharmacokinet* 2006; **45**: 649–63.
85. Purkins L, Wood N, Ghahramani P, *et al.* Pharmacokinetics and safety of voriconazole following intravenous- to oral-dose escalation regimens. *Antimicrob Agents Chemother* 2002; **46**: 2546–53.
86. Mori M, Kobayashi R, Kato K, *et al.* Pharmacokinetics and safety of voriconazole intravenous-to-oral switch regimens in immunocompromised Japanese pediatric patients. *Antimicrob Agents Chemother* 2015; **59**: 1004–13.
87. Hohmann N, Kocheise F, Carls A, *et al.* Dose-dependent bioavailability and CYP3A Inhibition contribute to non-linear pharmacokinetics of voriconazole. *Clin Pharmacokinet* 2016; **55**: 1535–45.
88. Li X, Frechen S, Moj D, *et al.* A Physiologically-Based Pharmacokinetic Model of Voriconazole Integrating Time-dependent Inhibition of CYP3A4, Genetic Polymorphisms of CYP2C19 and Predictions of Drug-Drug Interactions. *Clin Pharmacokinet* 2019: in press.
89. Hyland R, Jones BC, Smith DA. Identification of the cytochrome P450 enzymes involved in the N-oxidation of voriconazole. *Drug Metab Dispos* 2003; **31**: 540–7.
90. Yanni SB, Annaert PP, Augustijns P, *et al.* Role of flavin-containing monooxygenase in oxidative metabolism of voriconazole by human liver microsomes. *Drug Metab Dispos* 2008; **36**: 1119–25.
91. Hohmann N, Kreuter R, Blank A, *et al.* Autoinhibitory properties of the parent but not of the N-oxide metabolite contribute to infusion rate-dependent voriconazole pharmacokinetics. *Br J Clin Pharmacol* 2017; **83**: 1954–65.
92. Roffey SJ, Cole S, Comby P, *et al.* The disposition of voriconazole in mouse, rat, rabbit, guinea pig, dog, and human. *Drug Metab Dispos* 2003; **31**: 731–41.
93. Andes D, Marchillo K, Stamstad T, *et al.* In vivo pharmacokinetics and pharmacodynamics of a new triazole, voriconazole, in a murine candidiasis model. *Antimicrob Agents Chemother* 2003; **47**: 3165–9.
94. Wang T, Xie J, Wang Y, *et al.* Pharmacokinetic and pharmacodynamic properties of oral voriconazole in patients with invasive fungal infections. *Pharmacother J Hum Pharmacol Drug Ther* 2015; **35**: 797–804.
95. Pfizer Canada Inc. VFEND® voriconazole tablets 50 mg and 200 mg for injection 200 mg / vial (10 mg/mL when reconstituted) powder for oral suspension 3 g / bottle (40 mg/mL when reconstituted)

submission control No: 187649. Kirkland, Quebec; 2016.

96. Owusu Obeng A, Egelund EF, Alsultan A, *et al.* CYP2C19 polymorphisms and therapeutic drug monitoring of voriconazole: are we ready for clinical implementation of pharmacogenomics? *Pharmacotherapy* 2014; **34**: 703–18.
97. Pascual A, Calandra T, Bolay S, *et al.* Voriconazole therapeutic drug monitoring in patients with invasive mycoses improves efficacy and safety outcomes. *Clin Infect Dis* 2008; **46**: 201–11.
98. Jin H, Wang T, Falcione BA, *et al.* Trough concentration of voriconazole and its relationship with efficacy and safety: a systematic review and meta-analysis. *J Antimicrob Chemother* 2016; **71**: 1772–85.
99. Lee S, Kim B-H, Nam W-S, *et al.* Effect of CYP2C19 polymorphism on the pharmacokinetics of voriconazole after single and multiple doses in healthy volunteers. *J Clin Pharmacol* 2012; **52**: 195–203.
100. Weiss J, ten Hoevel MM, Burhenne J, *et al.* CYP2C19 genotype is a major factor contributing to the highly variable pharmacokinetics of voriconazole. *J Clin Pharmacol* 2009; **49**: 196–204.
101. Martis S, Peter I, Hulot J-S, *et al.* Multi-ethnic distribution of clinically relevant CYP2C genotypes and haplotypes. *Pharmacogenomics J* 2013; **13**: 369–77.
102. Damle B, Varma M V, Wood N. Pharmacokinetics of voriconazole administered concomitantly with fluconazole and population-based simulation for sequential use. *Antimicrob Agents Chemother* 2011; **55**: 5172–7.
103. Damle B, LaBadie R, Crownover P, *et al.* Pharmacokinetic interactions of efavirenz and voriconazole in healthy volunteers. *Br J Clin Pharmacol* 2008; **65**: 523–30.
104. Saari TI, Laine K, Leino K, *et al.* Effect of voriconazole on the pharmacokinetics and pharmacodynamics of intravenous and oral midazolam. *Clin Pharmacol Ther* 2006; **79**: 362–70.
105. U.S. Food and Drug Administration. *Clinical drug interaction studies-study design, data analysis, and clinical implications guidance for industry*. <https://www.fda.gov/regulatory-information/search-fda-guidance-documents/clinical-drug-interaction-studies-study-design-data-analysis-and-clini>. 2017.
106. European Medicines Agency. *Guideline on the investigation of drug interactions 21 June 2012 CPMP/EWP/560/95/Rev. 1 Corr. 2\*\** [https://www.ema.europa.eu/en/documents/scientific-guideline/guideline-investigation-drug-interactions\\_en.pdf](https://www.ema.europa.eu/en/documents/scientific-guideline/guideline-investigation-drug-interactions_en.pdf). 2012.
107. Heizmann P, Eckert M, Ziegler WH. Pharmacokinetics and bioavailability of midazolam in man. *Br J Clin Pharmacol* 1983; **16**: Suppl 1: 43S-49S.
108. Fuhr U, Hsin C, Li X, *et al.* Assessment of pharmacokinetic drug-drug interactions in humans: in vivo probe substrates for drug metabolism and drug transport revisited. *Annu Rev Pharmacol Toxicol* 2019; **59**: 507–36.
109. Peters SA, Jones CR, Ungell A-L, *et al.* Predicting drug extraction in the human gut wall: assessing contributions from drug metabolizing enzymes and transporter proteins using preclinical models. *Clin Pharmacokinet* 2016; **55**: 673–96.
110. Yokose T, Doy M, Taniguchi T, *et al.* Immunohistochemical study of cytochrome P450 2C and 3A in human non-neoplastic and neoplastic tissues. *Virchows Arch* 1999; **434**: 401–11.
111. Palmer CN, Coates PJ, Davies SE, *et al.* Localization of cytochrome P-450 gene expression in normal and diseased human liver by in situ hybridization of wax-embedded archival material. *Hepatology* 1992; **16**: 682–7.
112. Thummel KE, O’Shea D, Paine MF, *et al.* Oral first-pass elimination of midazolam involves both gastrointestinal and hepatic CYP3A-mediated metabolism. *Clin Pharmacol Ther* 1996; **59**: 491–502.

113. Nguyen HQ, Kimoto E, Callegari E, *et al.* Mechanistic modeling to predict midazolam metabolite exposure from in vitro data. *Drug Metab Dispos* 2016; **44**: 781–91.
114. Floyd MD, Gervasini G, Masica AL, *et al.* Genotype-phenotype associations for common CYP3A4 and CYP3A5 variants in the basal and induced metabolism of midazolam in European- and African-American men and women. *Pharmacogenetics* 2003; **13**: 595–606.
115. Vossen M, Sevestre M, Niederalt C, *et al.* Dynamically simulating the interaction of midazolam and the CYP3A4 inhibitor itraconazole using individual coupled whole-body physiologically-based pharmacokinetic (WB-PBPK) models. *Theor Biol Med Model* 2007; **4**: 1–15.
116. Kabi F. *Midazolam injection, USP Rx only*  
[https://www.accessdata.fda.gov/drugsatfda\\_docs/label/2017/208878Orig1s000lbl.pdf](https://www.accessdata.fda.gov/drugsatfda_docs/label/2017/208878Orig1s000lbl.pdf). 2017.
117. Hyland R, Osborne T, Payne A, *et al.* In vitro and in vivo glucuronidation of midazolam in humans. *Br J Clin Pharmacol* 2009; **67**: 445–54.
118. Eap C, Buclin T, Cucchia G, *et al.* Oral administration of a low dose of midazolam (75microg) as an in vivo probe for CYP3A activity. *Eur J Clin Pharmacol* 2004; **60**: 237–46.
119. Lappin G, Kuhnz W, Jochemsen R, *et al.* Use of microdosing to predict pharmacokinetics at the therapeutic dose: Experience with 5 drugs. *Clin Pharmacol Ther* 2006; **80**: 203–15.
120. Gorski JC, Jones DR, Haehner-Daniels BD, *et al.* The contribution of intestinal and hepatic CYP3A to the interaction between midazolam and clarithromycin. *Clin Pharmacol Ther* 1998; **64**: 133–43.
121. Colombo D, Ammirati E. Cyclosporine in transplantation - a history of converging timelines. *J Biol Regul Homeost Agents* **25**: 493–504.
122. Fahr A. Cyclosporin Clinical Pharmacokinetics. *Clin Pharmacokinet* 1993; **24**: 472–95.
123. U S Food and Drug Administration. *NEORAL® soft gelatin capsules (cyclosporine capsules, USP) modified NEORAL® oral solution (cyclosporine oral solution, USP) modified*.
124. Hebert M. Contributions of hepatic and intestinal metabolism and P-glycoprotein to cyclosporine and tacrolimus oral drug delivery. *Adv Drug Deliv Rev* 1997; **27**: 201–14.
125. Ptachcinski RJ, Venkataramanan R, Burckart GJ. Clinical pharmacokinetics of cyclosporin. *Clin Pharmacokinet* 1986; **11**: 107–32.
126. Morris RG. Cyclosporin therapeutic drug monitoring-an established service revisited. *Clin Biochem Rev* 2003; **24**: 33–46.
127. Rogosheske JR, Fargen AD, DeFor TE, *et al.* Higher therapeutic CsA levels early post transplantation reduce risk of acute GVHD and improves survival. *Bone Marrow Transplant* 2014; **49**: 122–5.
128. Albengres E, Tillement JP. Cyclosporin and ketoconazole, drug interaction or therapeutic association? *Int J Clin Pharmacol Ther Toxicol* 1992; **30**: 555–70.
129. Keogh A, Spratt P, McCosker C, *et al.* Ketoconazole to reduce the need for cyclosporine after cardiac transplantation. *N Engl J Med* 1995; **333**: 628–34.
130. Atiq F, Broers AEC, Andrews LM, *et al.* A clinically relevant pharmacokinetic interaction between cyclosporine and imatinib. *Eur J Clin Pharmacol* 2016; **72**: 719–23.
131. Shi H, Ren K, Lv B, *et al.* Baicalin from *Scutellaria baicalensis* blocks respiratory syncytial virus (RSV) infection and reduces inflammatory cell infiltration and lung injury in mice. *Sci Rep* 2016; **6**: 35851.
132. Xi Y, Wu M, Li H, *et al.* Baicalin attenuates high fat diet-induced obesity and liver dysfunction: dose-response and potential role of CaMKK $\beta$ /AMPK/ACC pathway. *Cell Physiol Biochem* 2015; **35**:



2349–59.

133. Zhao W, Liu L, Wang Y, *et al.* Effects of a combination of puerarin, baicalin and berberine on the expression of proliferator-activated receptor- $\gamma$  and insulin receptor in a rat model of nonalcoholic fatty liver disease. *Exp Ther Med* 2016; **11**: 183–90.

134. Ming J, Zhuoneng L, Guangxun Z. Protective role of flavonoid baicalin from *Scutellaria baicalensis* in periodontal disease pathogenesis: A literature review. *Complement Ther Med* 2018; **38**: 11–8.

135. Gong W, Zhao Z, Liu B, *et al.* Exploring the chemopreventive properties and perspectives of baicalin and its aglycone baicalein in solid tumors. *Eur J Med Chem* 2017; **126**: 844–52.

136. Shieh DE, Liu LT, Lin CC. Antioxidant and free radical scavenging effects of baicalein, baicalin and wogonin. *Anticancer Res* 2000; **20**: 2861–5.

137. Dinda B, Dinda S, DasSharma S, *et al.* Therapeutic potentials of baicalin and its aglycone, baicalein against inflammatory disorders. *Eur J Med Chem* 2017; **131**: 68–80.

138. Akao T, Kawabata K, Yanagisawa E, *et al.* Baicalin, the predominant flavone glucuronide of *scutellariae radix*, is absorbed from the rat gastrointestinal tract as the aglycone and restored to its original form. *J Pharm Pharmacol* 2000; **52**: 1563–8.

139. Kalapos-Kovács B, Magda B, Jani M, *et al.* Multiple ABC transporters efflux baicalin. *Phyther Res* 2015; **29**: 1987–90.

140. Taiming L, Xuehua J. Investigation of the absorption mechanisms of baicalin and baicalein in rats. *J Pharm Sci* 2006; **95**: 1326–33.

141. Zhang L, Li C, Lin G, *et al.* Hepatic metabolism and disposition of baicalein via the coupling of conjugation enzymes and transporters-in vitro and in vivo evidences. *AAPS J* 2011; **13**: 378–89.

142. Tang Y, Zhu H, Zhang Y, *et al.* Determination of human plasma protein binding of baicalin by ultrafiltration and high-performance liquid chromatography. *Biomed Chromatogr* 2006; **20**: 1116–9.

143. Huang T, Liu Y, Zhang C. Pharmacokinetics and bioavailability enhancement of baicalin: a review. *Eur J Drug Metab Pharmacokinet* 2018; **44**: 159–68.

144. Noh K, Kang Y, Nepal M, *et al.* Role of intestinal microbiota in baicalin-induced drug interaction and its pharmacokinetics. *Molecules* 2016; **21**: 337–49.

145. Wang Y, Yang J, Li X, *et al.* The metabolism of baicalin in rat and the biological activities of the metabolites. *Evidence-Based Complement Altern Med* 2012; **2012**: 1–6.

146. Morisaki T, Hou X-L, Takahashi K, *et al.* Baicalin pharmacokinetic profile of absorption process using novel in-vitro model: cytochrome P450 3A4-induced Caco-2 cell monolayers combined with rat intestinal rinse fluids. *J Pharm Pharmacol* 2013; **65**: 1526–35.

147. Miao Q, Wang Z, Zhang Y, *et al.* In vitro potential modulation of baicalin and baicalein on P-glycoprotein activity and expression in Caco-2 cells and rat gut sacs. *Pharm Biol* 2016; **54**: 1548–56.

148. Tian X, Cheng Z-Y, Jin H, *et al.* Inhibitory effects of baicalin on the expression and activity of CYP3A induce the pharmacokinetic changes of midazolam in Rats. *Evid Based Complement Alternat Med* 2013; **2013**: 179643.

149. Tian X, Chang Y, Wei J, *et al.* Baicalin reduces ciclosporin bioavailability by inducing intestinal p-glycoprotein in rats. *J Pharm Pharmacol* 2019; **71**: 788–96.

150. WHO. Harmful use of alcohol kills more than 3 million people each year, most of them men. 2018.

151. Norberg A, Jones AW, Hahn RG, *et al.* Role of variability in explaining ethanol pharmacokinetics. *Clin Pharmacokinet* 2003; **42**: 1–31.

152. Dubowski KM. Absorption, distribution and elimination of alcohol: highway safety aspects. *J Stud Alcohol Suppl* 1985; **10**: 98–108.
153. Jones AW. Pharmacokinetics of Ethanol-Issues of Forensic Importance Toxicity of cocaethylene View project. *Forensic Sci Rev* 2011; **23**: 91–136.
154. Cederbaum AI. Alcohol metabolism. *Clin Liver Dis* 2012; **16**: 667–85.
155. Wilkinson PK, Sedman AJ, Sakmar E, *et al*. Pharmacokinetics of ethanol after oral administration in the fasting state. *J Pharmacokinet Biopharm* 1977; **5**: 207–24.
156. Cowan JM, Weathermon A, McCutcheon JR, *et al*. Determination of volume of distribution for ethanol in male and female subjects. *J Anal Toxicol* 1996; **20**: 287–90.
157. Kwo PY, Ramchandani VA, O'Connor S, *et al*. Gender differences in alcohol metabolism: relationship to liver volume and effect of adjusting for body mass. *Gastroenterology* 1998; **115**: 1552–7.
158. Marshall AW, Kingstone D, Boss M, *et al*. Ethanol elimination in males and females: relationship to menstrual cycle and body composition. *Hepatology* 2007; **3**: 701–6.
159. Jones AW. Urine as a biological specimen for forensic analysis of alcohol and variability in the urine-to-blood relationship. *Toxicol Rev* 2006; **25**: 15–35.
160. Jones AW. Alcohol, its absorption, distribution, metabolism, and excretion in the body and pharmacokinetic calculations. *Wiley Interdiscip Rev Forensic Sci* 2019; **1**: e1340.
161. Tsutsumi M, Lasker JM, Takahashi T, *et al*. In Vivo Induction of Hepatic P4502E1 by Ethanol: Role of Increased Enzyme Synthesis. *Arch Biochem Biophys* 1993; **304**: 209–18.
162. Johnson BA, Seneviratne C. Alcohol–medical drug interactions. *Handb Clin Neurol* 2014; **125**: 543–59.
163. Chan L-N, Anderson GD. Pharmacokinetic and pharmacodynamic drug interactions with ethanol (alcohol). *Clin Pharmacokinet* 2014; **53**: 1115–36.
164. Loizou GD, Cocker J. The effects of alcohol and diallyl sulphide on CYP2E1 activity in humans: a phenotyping study using chlorzoxazone. *Hum Exp Toxicol* 2001; **20**: 321–7.
165. Oneta CM, Lieber CS, Li J, *et al*. Dynamics of cytochrome P4502E1 activity in man: induction by ethanol and disappearance during withdrawal phase. *J Hepatol* 2002; **36**: 47–52.
166. Girre C, Lucas D, Hispard E, *et al*. Assessment of cytochrome P4502E1 induction in alcoholic patients by chlorzoxazone pharmacokinetics. *Biochem Pharmacol* 1994; **47**: 1503–8.
167. Zhukov A, Ingelman-Sundberg M. Relationship between cytochrome P450 catalytic cycling and stability: fast degradation of ethanol-inducible cytochrome P450 2E1 (CYP2E1) in hepatoma cells is abolished by inactivation of its electron donor NADPH-cytochrome P450 reductase. *Biochem J* 1999; **340 ( Pt 2)**: 453–8.
168. Busby WF, Ackermann JM, Crespi CL. Effect of methanol, ethanol, dimethyl sulfoxide, and acetonitrile on in vitro activities of cDNA-expressed human cytochromes P-450. *Drug Metab Dispos* 1999; **27**: 246–9.
169. Gonzalez-Perez V, Connolly EA, Bridges AS, *et al*. Impact of organic solvents on cytochrome P450 probe reactions: filling the gap with (S)-warfarin and midazolam hydroxylation. *Drug Metab Dispos* 2012; **40**: 2136–42.
170. Rokitta D, Pfeiffer K, Streich C, *et al*. The effect of organic solvents on enzyme kinetic parameters of human CYP3A4 and CYP1A2 in vitro. *Toxicol Mech Methods* 2013; **23**: 576–83.
171. Shirasaka Y, Chaudhry AS, McDonald M, *et al*. Interindividual variability of CYP2C19-catalyzed drug metabolism due to differences in gene diplotypes and cytochrome P450 oxidoreductase

content. *Pharmacogenomics J* 2016; **16**: 375–87.

172. Hohmann N, Kocheise F, Carls A, *et al.* Midazolam microdose to determine systemic and pre-systemic metabolic CYP3A activity in humans. *Br J Clin Pharmacol* 2015; **79**: 278–85.

173. Mandona JW, Tuk B, van Steveninck AL, *et al.* Pharmacokinetic-pharmacodynamic modeling of the central nervous system effects of midazolam and its main metabolite  $\alpha$ -hydroxymidazolam in healthy volunteers. *Clin Pharmacol Ther* 1992; **51**: 715–28.

174. Clausen T, Wolff J, Hansen P, *et al.* Pharmacokinetics of midazolam and alpha-hydroxymidazolam following rectal and intravenous administration. *Br J Clin Pharmacol* 1988; **25**: 457–63.

175. Pentikainen PJ, Valisalmi L, Himberg JJ, *et al.* Pharmacokinetics of midazolam following intravenous and oral administration in patients with chronic liver disease and in healthy subjects. *J Clin Pharmacol* 1989; **29**: 272–7.

176. van Rongen A, Kervezee L, Brill M, *et al.* Population pharmacokinetic model characterizing 24-hour variation in the pharmacokinetics of oral and intravenous midazolam in healthy volunteers. *CPT pharmacometrics Syst Pharmacol* 2015; **4**: 454–64.

177. Anderson BJ, Larsson P. A maturation model for midazolam clearance. *Pediatr Anesth* 2011; **21**: 302–8.

178. Scholz I, Oberwittler H, Riedel K-D, *et al.* Pharmacokinetics, metabolism and bioavailability of the triazole antifungal agent voriconazole in relation to CYP2C19 genotype. *Br J Clin Pharmacol* 2009; **68**: 906–15.

179. Shi H-Y, Yan J, Zhu W-H, *et al.* Effects of erythromycin on voriconazole pharmacokinetics and association with CYP2C19 polymorphism. *Eur J Clin Pharmacol* 2010; **66**: 1131–6.

180. Sinha VK, Snoeys J, Osselaer N Van, *et al.* From preclinical to human - prediction of oral absorption and drug-drug interaction potential using physiologically based pharmacokinetic (PBPK) modeling approach in an industrial setting: a workflow by using case example. *Biopharm Drug Dispos* 2012; **33**: 111–21.

181. Chen Y, Jin JY, Mukadam S, *et al.* Application of IVIVE and PBPK modeling in prospective prediction of clinical pharmacokinetics: strategy and approach during the drug discovery phase with four case studies. *Biopharm Drug Dispos* 2012; **33**: 85–98.

182. De Buck SS, Sinha VK, Fenu LA, *et al.* Prediction of human pharmacokinetics using physiologically based modeling: a retrospective analysis of 26 clinically tested drugs. *Drug Metab Dispos* 2007; **35**: 1766–80.

183. Edginton AN, Willmann S. Physiology-based simulations of a pathological condition. *Clin Pharmacokinet* 2008; **47**: 743–52.

184. Zurlinden TJ, Reisfeld B. Characterizing the effects of race/ethnicity on acetaminophen pharmacokinetics using physiologically based pharmacokinetic modeling. *Eur J Drug Metab Pharmacokinet* 2017; **42**: 143–53.

185. Gaohua L, Abduljalil K, Jamei M, *et al.* A pregnancy physiologically based pharmacokinetic (p-PBPK) model for disposition of drugs metabolized by CYP1A2, CYP2D6 and CYP3A4. *Br J Clin Pharmacol* 2012; **74**: 873–85.

186. Michelet R, Bocxlaer J Van, Vermeulen A. PBPK in preterm and term neonates: a Review. *Curr Pharm Des* 2018; **23**: 5943–54.

187. Claassen K, Thelen K, Coboeken K, *et al.* Development of a physiologically-based pharmacokinetic model for preterm neonates: evaluation with in vivo data. *Curr Pharm Des* 2015; **21**: 5688–98.

188. Quinney SK, Zhang X, Luckisiri A, *et al.* Physiologically based pharmacokinetic model of

mechanism-based inhibition of CYP3A by clarithromycin. *Drug Metab Dispos* 2010; **38**: 241–8.

189. Zhang X, Quinney SK, Gorski JC, *et al.* Semiphysiologically based pharmacokinetic models for the inhibition of midazolam clearance by diltiazem and its major metabolite. *Drug Metab Dispos* 2009; **37**: 1587–97.

190. Gazzaz M, Kinzig M, Schaeffeler E, *et al.* Drinking ethanol has few acute effects on CYP2C9, CYP2C19, NAT2, and P-glycoprotein activities but somewhat inhibits CYP1A2, CYP2D6, and intestinal CYP3A: so what? *Clin Pharmacol Ther* 2018; **104**: 1249–59.

## 6 Acknowledgments

I would like to express my sincere gratitude to my parents. They always support and care for me with unconditional love. When my father was diagnosed as cancer with limited days, he even insisted me to spend time and effort on my study, rather than accompany him for the following days. He was afraid to interrupt my studies, so he did not tell me his pain and sickness until his last day. This is my biggest regret in my life. I will always do my best to make him proud in heaven.

I greatly appreciate my doctor father, Prof. Dr. Uwe Fuhr. He accepted me when I changed my subjects from the pharmaceutical technology area to pharmacometrics without any modeling and simulation skills. He provides support whenever I have difficulties in working and life. I appreciate him for leading me to the fascinating world for clinical pharmacology and gave me inspiration, patience, and brilliant ideas. When I was stuck by the hurdle stackle, he convinced me and encouraged me that I can manage in solving the problems. He also gave me the independence to create and test my ideas. After my father passed by, he treats me like his daughter and gives me feel at home. I really thank Oma Gisela and Opa Hermann for giving me a family love and support me to survive in a difficult time. I feel so lucky to have grandparents here in Germany.

Prof. Ulrich Jaehde helped me become a student of the University of Bonn, and for providing his advice and thoughts throughout the work presented in this thesis.

My colleagues Max Taubert and Chih-hsuan Hsin were excellent colleagues and friends. Max Taubert's talent in pharmacometrics contributed greatly to my study. Whenever I met technique problems, he always provided excellent support and guided me to find solutions. Chih-hsuan Hsin spoke the same language as me and made me feel at home. We together shared happiness and sorrow and gave encouragment to each other. She also assisted me a lot when I started *in vitro* assay. My other colleagues, Usman Arshad, Sami Ullah, Malaz Gazzaz, thanks a lot for the enjoyable time, and friendship.

I also thank Prof. Thorsten Lehr and Daniel Moj at Saarland University. They first introduced me to PBPK modeling, taught me how to use PK-Sim, and provided great suggestions to improve my project and manuscript.

I appreciate to China Scholarship Council to provide me the financial support during the study.

## 7 Curriculum Vitae

### Personal information

### University education

2015.10-present	Ph.D. in Pharmacometrics, Department I of Pharmacology, University Hospital of Cologne (supervisor: Prof.Dr.med. Uwe Fuhr)
2014.10-2015.09	Pharmaceutical technology, Department of Pharmacy, Free University of Berlin (supervisor: Prof.Dr.Rainer Müller)
2011.09-2014.06	M.Sc in Pharmaceutical Chemistry, Department of Pharmacy, Soochow University
2007.09-2011.06	B.Sc in pharmacy, Department of Pharmacy, Soochow University

### Software expertises and skills

PopPK	NONMEM, PsN, Xpose & Pirana, WinNonlin
PBPK	PK-SIM, MoBi, Simcyp
Simulation	R, Simulx
Programming	Visual Basic

### Research Publications (Selected)

1. **Li X**, Zoller M, Fuhr U, *et al.* Ciprofloxacin in critically ill subjects: considering hepatic function, age and sex to choose the optimal dose. *J Antimicrob Chemother* 2018; **74**: 682-690. <https://doi.org/10.1093/jac/dky485>
2. **Li X**, Frechen S, Moj D, *et al.* A Physiologically-based pharmacokinetic model of voriconazole integrating time-dependent inhibition of CYP3A4, genetic polymorphisms of CYP2C19 and predictions of drug-drug interactions. *Clin Pharmacokinetics* (in press) <https://doi.org/10.1007/s40262-019-00856-z>
3. **Li X**, Junge L, Taubert M, *et al.* A novel study design using continuous intravenous and intraduodenal infusions of midazolam and voriconazole for mechanistic quantitative assessment of hepatic and intestinal CYP3A inhibition. *J. Clini. Pharmacol.* (in press). <https://doi.org/10.1002/jcph.1619>
4. Liu R<sup>#</sup>, **Li X**<sup>#</sup>, Wei Y, *et al.* A single dose of baicalin has no clinically significant effect on the pharmacokinetics of cyclosporine A in healthy Chinese volunteers. *Front Pharmacol* 2019; **10**: 518. <sup>#</sup>equal contributions <https://doi.org/10.3389/fphar.2019.00518>
5. Fuhr U, Hsin C, **Li X**, *et al.* Assessment of pharmacokinetic drug-drug interactions in Humans: in Vivo

- probe substrates for drug metabolism and drug transport revisited. *Annu Rev Pharmacol Toxicol* 2019; **59**: 507–36. <https://doi.org/10.1146/annurev-pharmtox-010818-021909>
6. Gazzaz M, Kinzig M, Schaeffeler E, *et al.* Drinking ethanol has few acute effects on CYP2C9, CYP2C19, NAT2, and P-Glycoprotein activities but somewhat inhibits CYP1A2, CYP2D6, and intestinal CYP3A: So What? *Clin Pharmacol Ther* 2018; **104**: 1249–59. <https://doi.org/10.1002/cpt.1083>
  7. **Li X**, Zhao J, Peng C, *et al.* Cytotoxic triterpenoid glycosides from the roots of *Camellia oleifera*. *Planta Med* 2014; **80**: 590–8. <http://dx.doi.org/10.1055/s-0034-1368428>
  8. **Li X**, Zhao J, Yang M, *et al.* Physalins and withanolides from the fruits of *Physalis alkekengi* L. var. *franchetii* (Mast.) Makino and the inhibitory activities against human tumor cells. *Phytochem Lett* 2014; **10**: 95–100. <https://doi.org/10.1016/j.phytol.2014.08.004>
  9. **Li X**, Zhao J, Li X, *et al.* New Triterpenoid glycosides from the roots of *Camellia oleifera* Abel. *Helv Chim Acta* 2015; **98**: 496–508. <https://doi.org/10.1002/hlca.201400208>
  10. Wu J<sup>#</sup>, **Li X**<sup>#</sup>, Zhao J, *et al.* Anti-inflammatory and cytotoxic withanolides from *Physalis minima*. *Phytochemistry* 2018; **155**: 164–70. <sup>#</sup>equal contributions <https://doi.org/10.1016/j.phytochem.2018.08.009>
  11. Yang P, **Li X**, Liu Y-L, *et al.* Two triterpenoid glycosides from the roots of *Camellia oleifera* and their cytotoxic activity. *J Asian Nat Prod Res* 2015; **17**: 800–7. <https://doi.org/10.1080/10286020.2015.1004630>

### Patents (n=8)

A new antitumor compound extracted from *Camellia oleifera* with its preparation method and antitumor activity  
 ZL 201410044618.8, issued country: China, Licensing:2016.03.23;  
 ZL 201410044619.2, issued country: China, Licensing:2016.01.13;  
 ZL 201410044617.3, issued country: China, Licensing:2016.01.20;  
 ZL 201410044676.0, issued country: China, Licensing:2016.08.17;  
 ZL 201410044523.6, issued country: China, Licensing:2016.08.17;  
 ZL 201410044521.7, issued country: China, Licensing:2016.05.25;  
 ZL 201410043589.3, issued country: China, Licensing:2016.03.02;  
 ZL 201410044524.0, issued country: China, Licensing:2016.01.20.

### Conference poster presentations

- 1 **Li X**, Frechen S, Moj D, *et al.* A physiologically-Based Pharmacokinetic Model of Voriconazole. *PAGE* 2019, abstract 8995, ISSN 1871-6032. <https://www.page-meeting.org/default.asp?abstract=8995>
- 2 **Li X**, Zander J, Fuhr U, *et al.* Population pharmacokinetics of ciprofloxacin in critically ill patients-a covariate analysis. *PAGE* 2018, abstract 8594, ISSN 1871-6032. <https://www.page-meeting.org/default.asp?abstract=8594>

- 3 **Li X**, Taubert M, Tian Y, *et al.* Population pharmacokinetics of multiple oral doses of alcohol in humans. *PAGE* 2016, abstract 5864, ISSN1871-6032. <https://www.page-meeting.org/default.asp?abstract=5864>
- 4 **Li X**, Staufenbiel S, Keck C. et al. Betulin formulated as smartCrystals® for increasing dermal bioavailability *Jahrestagung der Gesellschaft für Dermopharmazie* (GD), 2015, 14-15.  
[http://www.gd-online.de/german/veranstalt/images2015/19.GD\\_JT\\_2015\\_Abstracts\\_Poster\\_all.pdf](http://www.gd-online.de/german/veranstalt/images2015/19.GD_JT_2015_Abstracts_Poster_all.pdf)



## Abbreviations

<b>ADAM</b>	Advanced dissolution, absorption and metabolism
<b>ADME</b>	Absorption, distribution, metabolism and elimination
<b>ADH</b>	Alcohol dehydrogenases
<b>ALDH</b>	Aldehyde dehydrogenase
<b>AIC</b>	Akaike Information Criterion
<b>AUC</b>	Area under the curve
<b>A<sub>unchanged</sub></b>	Amount of unchanged drug excreted in the urine
<b>BAC</b>	Blood alcohol concentration
<b>BID</b>	Twice daily
<b>B:P</b>	Ratio of blood versus plasma
<b>C</b>	Concentration
<b>CCV</b>	Constant coefficient of variation
<b>CI</b>	Confidence interval
<b>CL</b>	Clearance
<b>CL<sub>H</sub></b>	Hepatic clearance
<b>CL<sub>u<sub>int</sub></sub></b>	Unbound intrinsic clearance
<b>CL<sub>int</sub></b>	Intrinsic clearance
<b>CL<sub>R</sub></b>	Renal clearance
<b>C<sub>max</sub></b>	Maximum plasma concentration
<b>CsA</b>	Cyclosporine A
<b>\$COV</b>	Covariance step
<b>C<sub>trough</sub></b>	Trough concentrations for multiple dosings
<b>C<sub>T</sub></b>	Tissue drug concentration
<b>C<sub>p</sub></b>	Plasma drug concentration
<b>CV</b>	Coefficient of variation
<b>CWRES</b>	Conditional weighted residuals
<b>CYP</b>	Cytochrome P450
<b>DDI</b>	Drug drug interaction
<b>DV</b>	Dependent variable
<b>EBEs</b>	Empirical bayes estimates
<b>E<sub>H</sub></b>	Hepatic extraction ratio
<b>EMs</b>	Extensive metabolizers
<b>EMA</b>	European Medicines Agency
<b>FDA</b>	U.S. Food and Drug Administration

<b>FFEM</b>	Full fixed effect modeling
<b>FREM</b>	Full random effects model
<b>F</b>	Bioavailability
<b>fu</b>	Unbound fraction
<b>fu<sub>B</sub></b>	fraction of unbound concentration in plasma to the whole blood concentration
<b>GAM</b>	Generalized additive modeling
<b>GI</b>	Gastrointestinal
<b>GOF</b>	Goodness of fit plots
<b>H</b>	Hepatic
<b>IIV</b>	Inter-individual variability
<b>IMs</b>	Intermediate metabolizers
<b>IFDs</b>	Invasive fungal diseases
<b>IOV</b>	Inter-occasion variability
<b>IPRED</b>	Individual predictions
<b>iv</b>	Intravenous
<b>IVIVE</b>	In vitro-in vivo extrapolation
<b>K</b>	Elimination rate
<b>K<sub>a</sub></b>	Absorption rate
<b>K<sub>i</sub></b>	Reversible inhibition constant
<b>K<sub>I</sub></b>	The inhibition concentration when reaching half of $k_{inact}$
<b>k<sub>inact</sub></b>	Maximum inactivation rate constant
<b>K<sub>m</sub></b>	Michaelis constant, equal to substrate concentration at which the reaction rate is half-maximal
<b>K<sub>p</sub></b>	Tissue to plasma partition coefficient
<b>K<sub>tr</sub></b>	A transit rate constant from nth-1 compartment to the n <sup>th</sup> compartment
<b>L</b>	Likelihood
<b>Lasso</b>	Least absolute shrinkage and selection operator
<b>LRT</b>	Likelihood ratio test
<b>MIC</b>	Minimum inhibitory concentration
<b>MTT</b>	Mean transit time
<b>NAD<sup>+</sup></b>	Nicotinamide adenine dinucleotide
<b>NCA</b>	Non-compartmental analysis
<b>NMs</b>	Normal metabolizers
<b>NONMEM</b>	Non-linear mixed effects modeling
<b>OFV</b>	Objective function value

<b>PBPK</b>	Physiologically based pharmacokinetics
<b>PD</b>	Pharmacodynamics
<b>PMs</b>	Poor metabolizers
<b>PK</b>	Pharmacokinetics
<b>PK/PD</b>	Pharmacokinetics and pharmacodynamics
<b>po</b>	Oral
<b>PopPK</b>	Population pharmacokinetics
<b>PRED</b>	Population predictions
<b>Q</b>	Blood flow
<b>Q<sub>H</sub></b>	Hepatic blood flow
<b>RMs</b>	Rapid metabolizers
<b>RV</b>	Residual variability
<b>SCM</b>	Stepwise covariate modeling
<b>SD</b>	Standard deviation
<b>t<sub>1/2</sub></b>	Elimination half-life
<b>t<sub>max</sub></b>	Time when concentration reaches the maximum
<b>UGT</b>	UDP-Glucuronosyltransferase
<b>V</b>	Volume of distribution
<b>V<sub>c</sub></b>	The central volume of distribution
<b>V<sub>max</sub></b>	The maximum catalytic rate constant
<b>V<sub>p</sub></b>	The peripheral volume of distribution
<b>VPC</b>	Visual predictive checks
<b>WAM</b>	Wald's approximation to the likelihood ratio test,

## Ciprofloxacin in critically ill subjects: considering hepatic function, age and sex to choose the optimal dose

Xia Li<sup>1</sup>†, Michael Zoller<sup>2</sup>‡, Uwe Fuhr<sup>1</sup>, Mikayil Huseyn-Zada<sup>2</sup>, Barbara Maier<sup>3</sup>, Michael Vogeser<sup>3</sup>, Johannes Zander<sup>3</sup>‡ and Max Taubert<sup>1</sup>‡\*

<sup>1</sup>Department I of Pharmacology, Clinical Pharmacology, Cologne University Hospital, Cologne, Germany; <sup>2</sup>Department of Anesthesiology, Hospital of the Ludwig-Maximilians-University of Munich, Munich, Germany; <sup>3</sup>Institute of Laboratory Medicine, Hospital of the Ludwig-Maximilians-University of Munich, Munich, Germany

\*Corresponding author. Department I of Pharmacology, Center for Pharmacology, Clinical Pharmacology Unit, University Hospital Cologne (AöR), Gleueler Straße 24, 50931 Köln, Germany. Tel: +49-(0)-221-478-86716; Fax: +49-(0)-221-478-7011; E-mail: max.taubert@uk-koeln.de

ORCID: [orcid.org/0000-0001-8925-7782](https://orcid.org/0000-0001-8925-7782)

†Both authors contributed equally.

‡Both authors contributed equally.

Received 9 May 2018; returned 7 August 2018; revised 24 October 2018; accepted 5 November 2018

**Background:** Pathophysiological changes often result in altered pharmacokinetics of ciprofloxacin in critically ill patients. Although ciprofloxacin clearance ( $CL_{CIP}$ ) substantially depends on kidney function in healthy volunteers, its relationship to measured creatinine clearance ( $CL_{CRM}$ ) is weak in critically ill patients.

**Objectives:** To assess the need for dose reductions in isolated or combined kidney and liver dysfunction in critically ill patients and to re-evaluate relationships between kidney parameters, demographics and ciprofloxacin pharmacokinetics.

**Methods:** A population pharmacokinetic model was developed based on 444 ciprofloxacin serum concentrations from 15 critically ill patients with severe infections.  $CL_{CIP}$  relationships to parameters reflecting hepatic function,  $CL_{CRM}$ , Cockcroft–Gault creatinine clearance ( $CL_{CRCG}$ ), serum creatinine, sex, weight and age were explored. A simulation study was conducted to integrate knowledge from the new and previously published models.

**Results:** Total bilirubin was identified as a hepatic parameter with a clear relationship to  $CL_{CIP}$ . A significant relationship between  $CL_{CIP}$  and  $CL_{CRCG}$  could be attributed to age and sex only.  $CL_{CIP}$  was not associated with  $CL_{CRM}$ . The predicted risk of potential overexposure ( $AUC > 250$  mg·h/L) was low even with 1200 mg/day ciprofloxacin daily for patients with reduced  $CL_{CRCG}$  ( $< 30$  mL/min: risk of 0.7%), while the risk was remarkably higher in elderly female patients with elevated bilirubin (risk of about 20% for 65-year-old women with total bilirubin of 4 mg/dL).

**Conclusions:** Bilirubin, age and sex should be considered to assess the need for dose reductions. For MICs  $\leq 0.25$  mg/L, it might be appropriate to reduce the dose to 400 mg/day for elderly female subjects with high bilirubin.

### Introduction

Ciprofloxacin is an important drug in the treatment of severe infections due to its activity against a wide range of Gram-negative bacteria, including *Pseudomonas aeruginosa*.<sup>1</sup> Since glomerular filtration and tubular secretion account for approximately two-thirds of ciprofloxacin clearance ( $CL_{CIP}$ ), a dose reduction is recommended in patients with impaired renal function.<sup>2–4</sup> However, pharmacokinetic studies in critically ill patients have revealed that the relationship between measured creatinine clearance ( $CL_{CRM}$ , calculated from serum creatinine and urine samples) and  $CL_{CIP}$

might be poor.<sup>5</sup> Therefore, non-renal elimination pathways, including hepatic metabolism, biliary excretion and transmembrane secretion across the enteric mucosa,<sup>3,4</sup> seem to contribute substantially to the elimination of ciprofloxacin. Dose reductions in patients with impaired renal, but intact non-renal elimination might therefore lead to underexposure<sup>6</sup> and considering hepatic function for dose adjustments might be beneficial. However, no appropriate hepatic covariate related to  $CL_{CIP}$  has been identified yet. In contrast to  $CL_{CRM}$ , a close relationship between Cockcroft–Gault  $CL_{CR}$ <sup>7</sup> ( $CL_{CRCG}$ ) and  $CL_{CIP}$  has been reported.<sup>5,8</sup> In critically ill subjects with unstable kidney function,  $CL_{CRCG}$  only marginally

reflects the true creatinine kinetics,<sup>9</sup> which challenges its use in ICU patients. Since the Cockcroft–Gault equation comprises weight, age, sex and serum creatinine concentration, it might also represent non-renal processes that are related to these components. Indeed, a relationship with  $CL_{CIP}$  has been reported for all components of the Cockcroft–Gault equation separately.<sup>10–12</sup> Additionally, changes in muscle mass and liver function have been shown to affect the Cockcroft–Gault equation.<sup>13,14</sup> Identifying the components of the Cockcroft–Gault equation most relevant to ciprofloxacin pharmacokinetics might be beneficial to further assess dose adjustments in specific patient groups. The aim of our evaluation was to assess the rationale for ciprofloxacin dosing regimen adjustments given isolated and combined hepatic and renal impairment by identifying hepatic covariates and investigating the relationship between  $CL_{CRM}$ ,  $CL_{CRCG}$ , the single components of the Cockcroft–Gault equation and ciprofloxacin pharmacokinetics in critically ill subjects.

## Patients and methods

### Patients

This clinical study was carried out on a group of 15 critically ill patients (study group) in the ICU of the Department of Anesthesiology, University Hospital of Munich, Munich, Germany. For inclusion/exclusion criteria, please refer to Clinicaltrials.gov (NCT01793012). All patients were treated with ciprofloxacin due to suspected infection; 14 out of 15 patients met the criteria<sup>15</sup> of sepsis and septic shock. Covariate characteristics from a similar but independent group of patients from the same cohort study treated with other antibiotic substances (simulation group) was used for simulations. This simulation group was chosen since it was larger in size and thus reflected the distribution of covariate values in critically ill subjects more closely. The characteristics of the study group and the simulation group are shown in Table 1.

### Ethics

Written informed consent was obtained from all patients or their legal representatives. The study was approved by the Ethics Committee of the Ludwig-Maximilians-University of Munich (approval number 428-12) and carried out in accordance with all relevant regulations and the principles of the Declaration of Helsinki.

### Study design

This was a prospective observational single-centre cohort study. Ciprofloxacin (400 mg) was administered intravenously twice daily by 30 min infusions. Six, eight and one patients received one, two and three ciprofloxacin infusions, respectively, prior to the first study day, i.e. before taking the first pharmacokinetic sample; the respective timings were recorded. Blood samples were collected extensively at multiple timepoints (predose, 0.25, 0.5, 1.5, 4 and 7.25 h post-dose; 12 and 16 h if a dose was left out) over four consecutive study days. Exact sampling times were recorded by the medical staff. Four hundred and forty-four quantifiable serum concentrations of ciprofloxacin were available [median (range), 32 (17–33) samples per patient; 187, 98, 91 and 68 samples on study days 1, 2, 3 and 4, respectively].  $CL_{CRM}$  was determined based on urine collections over 24 h. Clinical chemistry and haematology parameters were measured once per day.

### Analytical method

After immediate transport to the Institute of Laboratory Medicine, University of Munich, blood samples were centrifuged (3000 g, 10 min),

aliquotted into polypropylene tubes and stored at  $-80^{\circ}\text{C}$ . After thawing, total serum ciprofloxacin concentrations were finally determined using an isotope dilution UPLC-MS/MS method. The calibration curve was linear ( $r^2 > 0.99$ ) with a lower limit of quantification of 0.05 mg/L. Mean inaccuracy was within  $\pm 4.0\%$  and intra- and inter-day coefficients of variation were  $\leq 7.25\%$ . Please refer to Zander et al.<sup>16</sup> for further information.

## Population pharmacokinetic analysis and simulation study

The further evaluation consisted of the development of a population pharmacokinetic model and a subsequent simulation study incorporating previously published models.

### Basic population pharmacokinetic analysis

A population pharmacokinetic non-linear mixed-effects model was built with NONMEM 7.4.1 (Icon Development Solutions, Ellicott City, MD, USA). Data visualization was performed using R 3.4.2 (R Foundation for Statistical Computing, Vienna, Austria) and model diagnostics were conducted using XPOSE 4.5.0.<sup>17</sup> Perl-speaks-NONMEM<sup>18</sup> (PsN) served as an application programming interface. The structural pharmacokinetic model was developed stepwise, starting with a one-compartment model with linear elimination kinetics. Up to three compartments were evaluated. Inter-individual (IIV) and inter-occasion (IOV) variability were tested and additive, proportional and combined error models were evaluated. Model choices were based on the objective function value (OFV), with a change by 6.64 points being considered as statistically significant with  $P < 0.01$ , sufficient model stability as indicated by parameter CIs obtained from bootstrap statistics with 1000 samples,<sup>19</sup> and visual predictive checks.<sup>20</sup>

### Covariate model development

Covariates were evaluated with respect to  $CL_{CIP}$  since it is the only parameter determining target attainment in terms of AUC-to-MIC ratios (AUC/MIC) at steady-state.<sup>1</sup> To assess the relationship between  $CL_{CIP}$  and liver function, a set of five hepatic parameters (ALT, anti-thrombin, total bilirubin, cholinesterase and factor V) was chosen. The role of parameters related to kidney function was evaluated in two steps: first,  $CL_{CRCG}$  and  $CL_{CRM}$  were evaluated; then the single components of the Cockcroft–Gault equation (body weight, serum creatinine, age and sex) were evaluated separately. The final covariate model comprised hepatic parameters and components of the Cockcroft–Gault equation that fulfilled the following two criteria. The first criterion (significance criterion) was a decrease in OFV by  $\geq 6.63$  points when introducing the respective covariate into the basic model (i.e. without other covariates). Although the significance criterion is well-established,<sup>21</sup> it does not enable assessment of whether a relationship between a pharmacokinetic parameter and a covariate is stable over multiple study days. Statistical significance might, for example, originate from a strong relationship on a single study day that is not apparent on the other study days. Additionally, the significance criterion assumes that the OFV follows a  $\chi^2$  distribution.<sup>21</sup> A second criterion (stability criterion) was therefore used to ascertain that relationships were stable throughout at least two study days. To be considered stable, 95% parameter CIs obtained for study days 1 to 4 must not cover zero (i.e. no effect) on at least two out of four days<sup>19</sup> and the sign of the respective point estimate must not change throughout the respective study days. CIs were based on bootstrap statistics with 1000 samples.

## Pharmacokinetic/pharmacodynamic simulation study

### Criteria for adequate ciprofloxacin treatment

For total ciprofloxacin concentrations, an AUC/MIC ratio  $\geq 125$  was chosen as the primary target for PTA calculations since it is related to a high probability of clinical/microbiological cure for Gram-negative bacteria.<sup>22</sup>

**Table 1.** Clinical and demographic characteristics of patient groups

Patient group (model)	Own study group (model A)	Simulation group (joint simulation)	Group 1 (model B)	Group 1 (model C)	Group 2 (model D)
Model type	pop PK	simulation	pop PK	PBPK	pop PK
Type of patients	ICU patients	ICU patients	ICU patients		ICU patients
Serum concentrations (n)	444	NA	588		210
Number of patients (sex)	8 (f), 7 (m)	71 (f), 95 (m)	27 (f), 75 (m)		13 (f), 27 (m)
Age (years)	49 (23–79)	58 (22–94)	62 (18–92)		70 ± 9 <sup>a</sup>
Total body weight (kg)	69 (40–80)	75 (40–150)	76 (38–120)		65 ± 17.2 <sup>a</sup>
Serum creatinine (µmol/L)	109 (44–239)	106 (27–539)	81 (35–446)		66 (24–683)
CL <sub>CRM</sub> (mL/min)	45 (5–251)	59 (1.5–511)	78 (5–205)		61 (7–177)
CL <sub>CR</sub> Cockcroft–Gault (mL/min)	56 (13–204)	64 (13–255)	89 (15–342)		NR
AST (U/L)	46 (20–678)	46 (20–678)	42 (13–2533)		27 (4–112)
ALT (U/L)	29 (4–552)	35 (4–2521)	48 (10–674)		39 (13–268)
Total bilirubin (mg/dL)	1.8 (0.2–19.5)	1 (0.2–38)	NR		NR
Haemoglobin (g/dL)	9.1 (6.7–12.0)	9.8 (7.5–16.1)	9.5 (7–15)		NR
Haematocrit (%)	27 (22–33)	29 (21–50)	29 (22–64)		NR
Serum albumin (g/dL)	2.2 (1.4–3.4)	2.7 (1.8–4.3)	NR		3 (2.6–3.9)
APACHE II	27 (15–48)	26 (6–51)	NR		18 ± 5 <sup>a</sup>
SAPS II	NR	NR	48 (13–102)		NR
SOFA	12 (3–23)	11 (1–24)	NR		NR

Values shown are median (range). pop PK, population pharmacokinetic model; PBPK, physiologically based pharmacokinetic model; NR, not reported; NA, not applicable; f, female; m, male; SAPS II, Simplified Acute Physiology Score II.

<sup>a</sup>Mean ± SD, median and range were not reported.

An AUC/MIC ratio  $\geq 250$  was defined as the secondary target since it is linked to a shortened time to bacterial eradication.<sup>22</sup> A PTA of at least 90% was considered appropriate.

Although no applicable data on pharmacokinetic thresholds related to ciprofloxacin toxicity are available, upper AUC limits were defined based on the following reasoning. Typical side effects, such as chondropathy, are considered class effects, while the risk of side effects differs remarkably between different fluoroquinolones.<sup>23</sup> Differences in the risk of side effects have mainly been attributed to varying systemic exposure of different fluoroquinolones, proposing that excessive AUCs are linked to increased toxicity.<sup>23</sup> Based on an AUC/MIC goal of 250 mg/L and an MIC of 0.5 mg/L, which represents the zone of intermediate susceptibility in non-species-related breakpoints and the threshold for susceptibility for *P. aeruginosa*,<sup>24</sup> a minimum AUC of 125 mg·h/L would be needed. Attaining markedly higher AUCs is not necessary in terms of efficacy while they might come at an increased risk of adverse effects. Thus, an upper AUC limit of 250 mg·h/L, representing twice (safety margin) the intended AUC given an MIC of 0.5 mg/L, was defined. This does not necessarily reflect toxic exposure since no information on toxicokinetic/toxicodynamic parameters is available. It seems reasonable, however, to adjust dosing regimens such that the intended AUC/MIC ratio is achieved while controlling for the risk of attaining unnecessarily high AUCs. The exceeding of an AUC limit of 125 mg·h/L was additionally evaluated to assess the impact of different AUC limits.

### Evaluation of excessive AUCs depending on CL<sub>CRGG</sub>

In case the newly developed covariate model did not feature CL<sub>CRGG</sub> or serum creatinine, further simulations were carried out to assess the probability of attaining excessive AUCs based on previously published models. So far, it has been customary to base predictions on single population pharmacokinetic models. However, each published model provides valuable information and should ideally be incorporated in simulation studies. This possibly attenuates the disadvantages of limited sample sizes in pharmacokinetic

studies and might reduce the overall bias of predictions. Therefore, this simulation was jointly based on three published models comprising serum creatinine or CL<sub>CRGG</sub>.<sup>5,25,26</sup> The three previously published models were chosen such that patient groups were similar, model validation was sufficient<sup>27</sup> and all necessary information (pharmacokinetic parameters, standard errors) was available. Patient characteristics of all employed models are summarized in Table 1 and the evaluated models are further described in Tables S1 and S2 (available as Supplementary data at JAC Online). For further technical details, please refer to the Supplementary Methods.

## Results

### Population pharmacokinetic model

#### Base model

A two-compartment model with linear elimination and a combined error model appropriately described the pharmacokinetics of ciprofloxacin. IIV (IOV) was estimated on CL and central V ( $V_1$ ), leading to a significant drop in OFV by 654.4 (668.0) and 66.5 (20.7) points, respectively. Systematic changes of CL and  $V_1$  from day 1 to 4 were observed, suggesting alterations of the pharmacokinetics of ciprofloxacin throughout the treatment course. Estimating CL and  $V_1$  for each day separately improved the model significantly [OFV reduced by 19.4 points, IOV of CL ( $V_1$ ) dropped to 18% (25%)] and revealed that CL increased throughout the treatment course [16.2 L/h on day 1, 20.9 L/h on day 4, inter-individual coefficient of variation (CV) 19%].  $V_1$  ranged from 24.2 to 33.5 L (CV 52%) (Table 2).

#### Covariate analysis

An overview of the covariate evaluation is provided in Table 3. Among the evaluated liver parameters, only bilirubin had a clear



relationship with  $CL_{CIP}$  throughout the treatment course (Figure S1) and improved the model significantly (Table 3).  $CL_{CIP}$  decreased with increasing bilirubin serum concentrations. Anti-thrombin and factor V also improved the model significantly, but their relationship with  $CL_{CIP}$  was not stable.  $CL_{CRM}$  did not improve the model significantly while  $CL_{CRCG}$  exhibited a stable relationship with  $CL_{CIP}$  throughout all four study days and improved the model significantly (Figure S2). When each component of  $CL_{CRCG}$  was evaluated separately, age and sex had a clear relationship with  $CL_{CIP}$  (Figure S3) and improved the model significantly while no consistent relationship was found with serum creatinine and body weight (Figures S2 and S3). Thus, a final covariate model (model A) comprising age, sex and bilirubin resulted (Figure 1), which in total explained 60% of IIV. Model A is shown in Equation 1, the final covariate equation for predicting  $CL_{CIP}$  (L/h), where bili is the total serum bilirubin concentration (mg/dL), age is in years, and for sex, 0 = male and 1 = female. Based on parameter point estimates; for bootstrap statistics please refer to Table 2. Model diagnostics for the final model are shown in Figures S4 and S5.

$$CL = 16.3 \times [1 + (49 - age) \times 0.0153] \times [1 - 0.432 \times sex] \times \left[ \frac{bili}{1.85} \right]^{-0.241} \quad (1)$$

### Simulation study

An evaluation of the relationship between  $CL_{CRCG}$  and the probability of attaining excessive AUCs was not feasible with the newly developed model (model A). Therefore, the relationship with  $CL_{CRCG}$  was explored based on a joint evaluation of previously published models comprising  $CL_{CRCG}$  or serum creatinine covariates (creatinine model, based on models B–D) and the relationship to bilirubin, age and sex was evaluated based on the newly developed covariate model (model A). Weighting factors of 13%, 19% and 68% were calculated for the models B, C and D. Model-related uncertainties in predicted AUCs were low (SD of AUC  $\leq 1.4\%$ ), while the inter-study variability was distinctly larger (SD of AUC  $\leq 17\%$ ). For model A, evaluations were based on the CL estimate on day 1.

#### Percentage of patients exceeding the upper AUC limit

Given a dose of 1200 mg/day, the AUC limit (AUC > 250 mg·h/L) was exceeded in 0.3% of subjects with  $CL_{CRCG} > 30$  mL/min and in 0.7% of subjects with  $CL_{CRCG} \leq 30$  mL/min (creatinine model, Figure S6). In contrast to marginal differences among  $CL_{CRCG}$  groups, pronounced differences were apparent for certain combinations of age, sex and bilirubin (model A, Figure 2, bottom). Female subjects were at higher risk of attaining excessive AUCs especially at older ages. Given a daily dose of 1200 mg, the risk was increased in elderly female subjects with elevated bilirubin concentrations (e.g. risk of AUC > 250 mg·h/L of about 20% for females with age 65 years and bilirubin 4 mg/dL). In contrast, excessive AUCs were attained in male subjects receiving 1200 mg/day only at high age, e.g. risk of <1% at age 60 years and bilirubin 10 mg/dL. For daily doses of 800 mg, the risk of exceeding the AUC limit was only slightly elevated for male subjects while it was increased to about 20% for female subjects with an age of 80 years and a bilirubin concentration of 5 mg/dL (Figure 2, top). With a daily dose of 400 mg, the AUC limit was exceeded in almost no subjects (less than 0.1%). When decreasing the AUC limit to 125 mg·h/L

**Table 2.** Pharmacokinetic parameter estimates of the newly developed population pharmacokinetic model of ciprofloxacin (model A)

Parameter (unit)	Median	95% CI
Fixed effects		
$CL_{day1}$ (L/h)	16.2	(13.4–19.7)
$CL_{day2}$ (L/h)	17.4	(14.0–20.1)
$CL_{day3}$ (L/h)	20.1	(16.6–23.8)
$CL_{day4}$ (L/h)	20.9	(17.8–25.8)
$V_{1, day1}$ (L)	24.2	(13.9–36.4)
$V_{1, day2}$ (L)	32.9	(21.1–44.2)
$V_{1, day3}$ (L)	29.3	(18.0–42.9)
$V_{1, day4}$ (L)	33.5	(21.3–48.8)
$V_2$ (L)	83.2	(74.1–94.8)
$Q_{PER}$ (L/h)	71.2	(46.2–93.9)
$\theta_1$ (age)	0.0156	(0.002–0.0208)
$\theta_2$ (sex)	−0.413	(−0.559 to −0.214)
$\theta_3$ (bilirubin)	−0.250	(−0.374 to −0.138)
Random effects		
IIV CL (CV%)	18.7	(7.18–27.7)
IIV $V_1$ (CV%)	51.5	(27.2–88.8)
IOV CL (CV%)	15.9	(9.6–21.9)
IOV $V_1$ (CV%)	23.3	(6.62–38.4)
Residual error		
PRV (CV%)	18.3	(16.4–20.1)
ARV (CV%)	11.4	(3.86–15.7)

The estimates are from bootstrap statistics of the final model. CL and  $V_1$  (central V), both estimated separately on study days 1 to 4.  $V_2$ , peripheral V;  $Q_{PER}$ , inter-compartmental CL;  $\theta_1$  (age), effect of age on CL;  $\theta_2$  (bilirubin), effect of bilirubin on CL;  $\theta_3$  (sex), effect of sex on CL; PRV, proportional residual variability; ARV, additive residual variability.

and given a dose of 1200 mg/day, differences between  $CL_{CRCG}$  groups were slightly more pronounced (16.3% with  $CL_{CRCG} \leq 30$  mL/min versus 7.6% with  $CL_{CRCG} > 30$ ) and female (male) subjects had an increased risk of excess at middle age with normal (elevated) bilirubin concentrations (e.g. risk of 40% for females with age 52 years and normal bilirubin and for males with age 52 years and bilirubin 10 mg/dL).

#### PTA

PTAs based on the newly developed model A for the entire population are shown in Figure 3. No appropriate target attainment (AUC/MIC > 125) resulted for MICs of  $\geq 1$  mg/L. Daily doses of 1200 mg yielded a PTA of 83% for an MIC of 0.5 mg/L while a daily dose of 800 mg/day was sufficient to attain a PTA of at least 90% for an MIC of 0.25 mg/L and 400 mg/day was adequate for an MIC of 0.125 mg/L in the entire population. However, model A indicated that an appropriate target attainment (AUC/MIC > 125) depended on sex, age and bilirubin in the following manner (Figure S7). For male subjects, an increase to 1200 (800) mg/day was needed (PTA > 90%) given an MIC of 0.25 (0.125) mg/L if age was below about 50 years and bilirubin was normal, while sufficient AUC/MIC ratios given an MIC of 0.5 mg/L were only observed with 1200 mg per day and an age of at least 65 years or elevated bilirubin concentrations. For female subjects, an increase to 1200 (800) mg/day

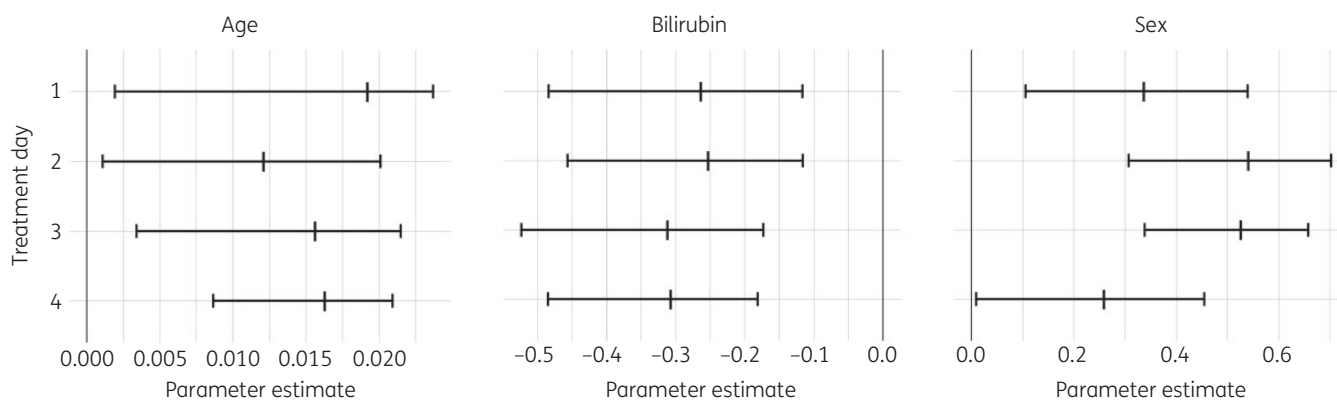


**Figure 1.** CIs and medians of estimates of covariate parameters (model A). 95% CIs (bars) and medians (vertical lines) of estimated covariate parameters for age, bilirubin and sex based on a bootstrap with 1000 samples for study days 1 to 4, respectively.

**Table 3.** Results of covariate evaluation

Covariate	dOFV	Significance	Stability	Inclusion criteria met?
Parameters related to kidney function				
CL <sub>CRM</sub>	-2.9	-	-	no
CL <sub>CRCG</sub>	-9.3	+	+	yes
age	-7.4	+	+	yes
sex	-12.3	+	+	yes
body weight	-5.8	-	-	no
serum creatinine concentration	-5.4	-	-	no
Parameters related to liver function				
anti-thrombin	-15.3	+	-	no
total bilirubin	-12.2	+	+	yes
factor V	-10.0	+	-	no
ALT	-8.4	+	-	no
cholinesterase	-7.5	+	-	no

Change in OFV (dOFV) following the separate introduction of covariates of interest to the base model as well as the stability of the covariate relationship. A covariate was considered stable if (i) the respective parameter CI did not cover zero on two out of four study days and (ii) the sign of the respective point estimate did not change (stability criterion). Changes in OFV of at least 6.64 points were considered significant (significance criterion). Inclusion criteria for further evaluation were both a significant change in OFV and a stable relationship. + = yes, - = no.

was only needed given an MIC of 0.5 (0.25) mg/L if age was below about 55 years and bilirubin was normal.

## Discussion

Total bilirubin was identified as a potential indicator of hepatic function with a significant and consistent relationship with CL<sub>CIP</sub>. No link between CL<sub>CRM</sub> and CL<sub>CIP</sub> could be confirmed, questioning a substantial influence of kidney function on ciprofloxacin exposure in critically ill patients. Indeed, age and sex were the only components of the Cockcroft–Gault equation with a clear relationship to CL<sub>CIP</sub>. Predicted excess of high AUCs was relatively low for patients with low CL<sub>CRCG</sub> while a combination of high age and increased bilirubin was linked to a high probability of potential overexposure, especially in women.

Concerns have been raised over recommendations to reduce ciprofloxacin doses in the presence of impaired kidney function<sup>6</sup> since underexposure with an increased risk of therapeutic failure

might result. Our evaluation confirms that general dose reductions are neither supported for low predicted nor CL<sub>CRM</sub> values in critically ill patients. In contrast, a drastically increased risk of high AUCs in patients with a combination of older age and elevated bilirubin concentrations suggests that dose reductions might be suitable in such patients. To diminish the risk of potential overexposure, a standard dose of 800 mg per day seems appropriate in older female subjects with moderately elevated bilirubin while a decrease to 400 mg per day might be needed in females with a combination of very old age and highly elevated bilirubin (Figure 2, top). This is largely compatible with the goal of attaining sufficient PTAs since doses of 800 or 1200 mg per day (MIC of 0.25 or 0.5 mg/L) were only needed for younger women (age below about 60 years) with normal bilirubin (Figure S7). Isolated increases in bilirubin in young women do not apparently pose the need for dose reductions while age is a more pronounced isolated risk factor. In men administered 800 mg of ciprofloxacin per day, potential toxic concentrations were rarely observed (Figure 2, top).



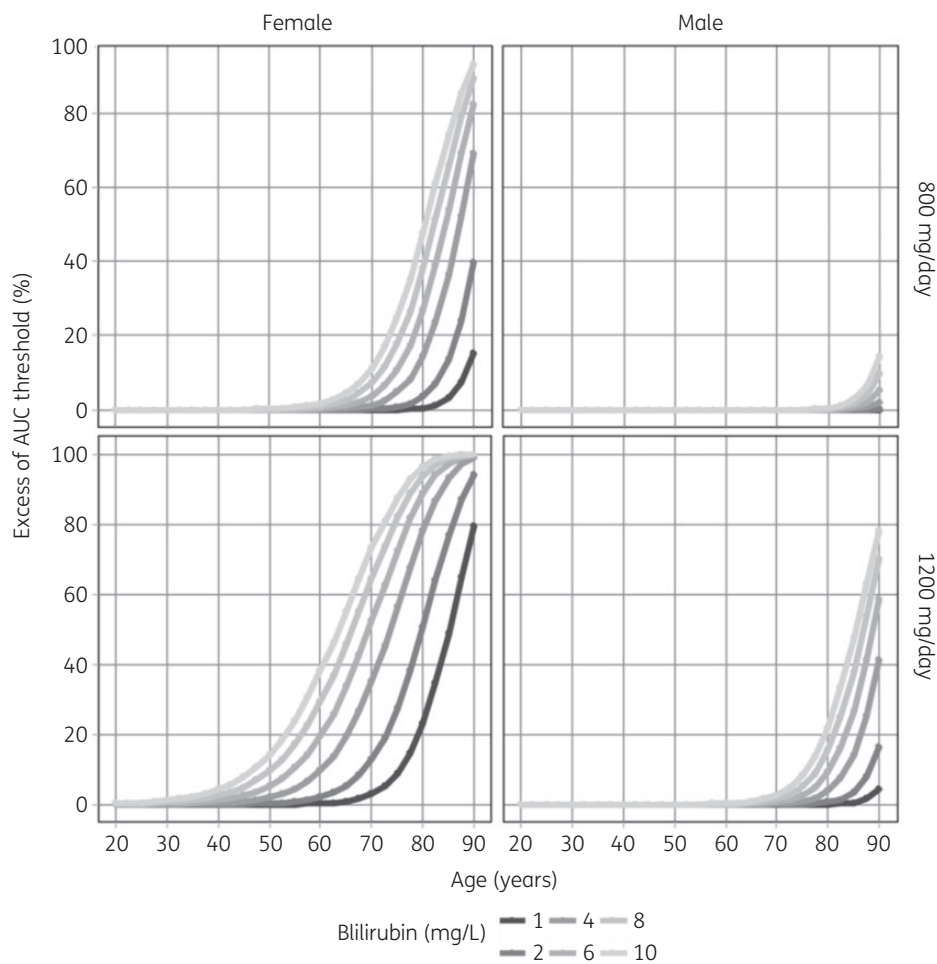


**Figure 2.** Probability of exceeding AUC limits depending on age, sex and bilirubin for a daily dose of 800 and 1200 mg ciprofloxacin (model A). Probability of exceeding the AUC limit of 250 mg·h/L depending on age, total bilirubin and sex (female: left side, male: right side) for 800 (top) and 1200 (bottom) mg ciprofloxacin per day. AUC excess represents the probability of exceeding the AUC limit given a certain covariate constellation.

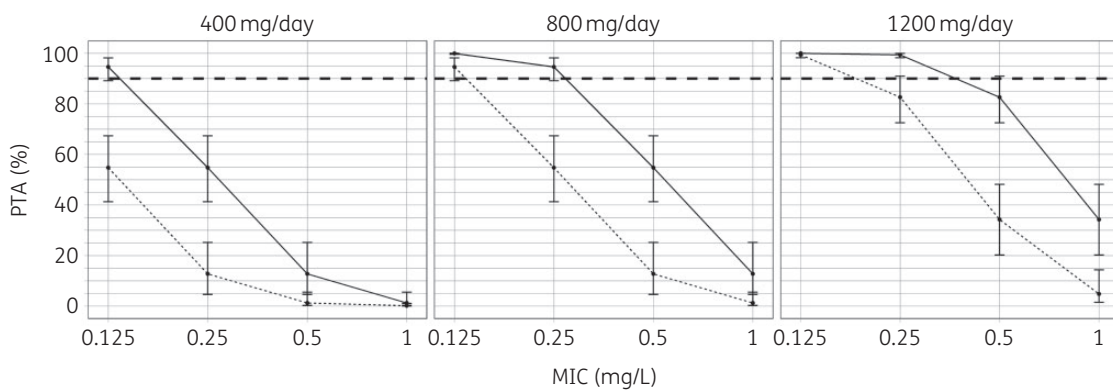


**Figure 3.** PTA based on the newly developed model A. PTAs for daily doses of 400, 800 and 1200 mg ciprofloxacin per day and MICs of 0.125, 0.25, 0.5 and 1 mg/L based on the newly developed model. Solid (dashed) lines reflect an AUC/MIC target of 125 h (250 h). Dots represent means and bars represent 90% CIs of PTAs. The long-dashed line indicates the target PTA of 90%.

In healthy volunteers, the hepatic route accounts for ~20% of ciprofloxacin elimination,<sup>28</sup> which has mostly been neglected in previous models of ciprofloxacin pharmacokinetics. However, hepatic elimination might represent a notable compensatory pathway

preventing drug accumulation in the case of renal failure<sup>29,30</sup> and its contribution might be substantial in critically ill subjects. Indeed, studies on critically ill patients indicate that dose reductions might be needed only in the presence of combined kidney and liver

dysfunction. For example, Jones *et al.*<sup>6</sup> reported increased ciprofloxacin concentrations in eight patients with renal impairment and intra-abdominal disease while no dose reduction in isolated kidney or hepatic dysfunction was supported. Increased bilirubin concentrations can result from many disorders, such as haemolysis, disorders of haem synthesis, hereditary diseases, impaired biliary secretion and intestinal disorders.<sup>31</sup> However, the fact that several other liver parameters were at least moderately related to CL indicates that liver function might be predominantly responsible for this correlation. Since organ hypoperfusion is expected in patients with sepsis and shock, it is also possible that elevated bilirubin concentrations partially reflect insufficient perfusion and a resulting liver dysfunction, which is also often observed in critically ill subjects.<sup>32</sup> Indeed, hyperbilirubinaemia has been shown to be associated with increased mortality and risk of multiple organ failure. Bilirubin might therefore not only specifically reflect pharmacokinetic changes associated with hepatic impairment, but multiple organ dysfunction resulting from hypoperfusion. Further studies might differentiate between indirect and direct bilirubin, which might provide further information on mechanisms underlying the identified relationship to CL<sub>CIP</sub>.

The absence of a relevant relationship between CL<sub>CRM</sub> and CL<sub>CIP</sub> has been shown previously<sup>5,8,26</sup> and might be a consequence of the compensatory elimination via other routes. In general, CL<sub>CRM</sub> is considered the best measure of CL<sub>CR</sub> in ICU patients, who are prone to rapid changes in creatinine kinetics.<sup>33</sup> Following a change in kidney function, several days might be needed for creatinine serum concentrations to attain steady-state,<sup>34</sup> and changes in muscle mass<sup>35</sup> and V values occur frequently in critically ill subjects.<sup>36</sup> Therefore, using the Cockcroft–Gault equation to predict CL<sub>CR</sub> should be avoided in such patients.<sup>9</sup> Khachmann *et al.*<sup>5</sup> introduced CL<sub>CRCG</sub> into a ciprofloxacin model despite no significant relationship between CL<sub>CRM</sub> and CL<sub>CIP</sub>, arguing that the single components of the Cockcroft–Gault equation might have been relevant. In fact, we found no relationship between serum creatinine or body weight and CL<sub>CIP</sub> in our patient collective. Age and sex might also reflect active tubular secretion, which plays a significant role in ciprofloxacin elimination but only a minor role in creatinine elimination.<sup>12,37,38</sup> However, active tubular secretion and glomerular filtration are expected to jointly decrease in the presence of impaired kidney function. Additionally, CL<sub>NR</sub> might be related to age and sex.<sup>12,38,39</sup> Previous studies revealed a lower CL in elderly versus young patients<sup>11</sup> and trough concentrations of ciprofloxacin were shown to be related to age rather than CL<sub>CR</sub>.<sup>40</sup> Finally, age might also reflect changes in body composition and reduced functional reserves.<sup>41,42</sup> A relationship between sex and CL<sub>CIP</sub> in healthy volunteers has previously been reported by Overholser *et al.*<sup>12</sup> Interestingly, the total CL but not the CL<sub>R</sub> of ciprofloxacin significantly differed between male and female subjects. Thus, sex differences were attributed to non-renal elimination, possibly due to differences in efflux transporter activity. Further studies are needed to elucidate whether doses should be adapted based on sex.

In our evaluation, the CL<sub>CIP</sub> on the first study day was comparable to the other evaluated models (point estimate 13.5, 18 and 17.8 L/h, respectively, compared with 16.3 L/h in our model). This was about half of the CL in healthy volunteers,<sup>43</sup> which might have been a result of renal and/or hepatic dysfunction.<sup>44,45</sup> Despite the small number of subjects, the evaluated dataset provided valuable information by enabling assessment of pharmacokinetics throughout four treatment

days. This enabled assessment of systematic changes in pharmacokinetics over time. Indeed, ciprofloxacin doses would need to be increased by about 30% if the CL rises from 16.2 L/h (day 1) to 20.9 L/h (day 4) to attain the same PTA. Although it is probably the exposure to antibiotics during the first hours that is particularly critical for the therapeutic outcome,<sup>46</sup> changes in target attainment might be important for prolonged infections that demand a long-term sufficient exposure to antibiotics. When considering the presented evaluation of potential overexposure, it should be noted that results might change significantly if further information on parameters related to toxicity becomes available. For example, trough and maximum attained concentrations were not part of this evaluation and the chosen AUC limit of 250 mg·h/L is high compared with typically achieved AUCs.<sup>47</sup> However, defining lower AUC limits would have conflicted with the intended AUC/MIC ratio of 250 given an MIC of 0.5 mg/dL, which is the susceptibility breakpoint for *Pseudomonas* spp. according to EUCAST. Finally, conclusions would not change significantly when lowering the AUC limit to 125 mg·h/L.

The main limitation of our study was the limited number of patients evaluated, which reduced the power to identify covariate relationships. Therefore, it was not feasible to extensively evaluate other potentially relevant covariates, such as disease severity scores. Additionally, measurements of ciprofloxacin in urine were not available, which would have provided further information on the renal elimination of ciprofloxacin. Furthermore, ethnicities between the jointly evaluated models were heterogeneous. However, patient characteristics and model parameter estimates were similar between the evaluated models, precluding major pharmacokinetic differences between patient groups.

## Conclusions

Total bilirubin, age and sex might be important parameters facilitating the choice of appropriate dose of ciprofloxacin in ICU patients. A dose reduction based on CL<sub>CR</sub> is not supported while a reduction to 400 mg per day seems reasonable for female subjects with higher age and highly increased bilirubin if MIC values for the causative strains are  $\leq 0.25$  mg/L.

## Funding

This study was supported by internal funding. X. L. obtained financial support provided by the China Scholarship Council during her PhD studies (scholarship number 201406920024).

## Transparency declarations

None to declare.

## Supplementary data

Supplementary Methods, Figures S1 to S7 and Tables S1 and S2 are available as Supplementary data at JAC Online.

## References

- Zelenitsky S, Ariano R, Harding G *et al.* Evaluating ciprofloxacin dosing for *Pseudomonas aeruginosa* infection by using clinical outcome-based Monte Carlo simulations. *Antimicrob Agents Chemother* 2005; **49**: 4009–14.

- 2 Vance-Bryan K, Guay DRP, Rotschafer JC. Clinical pharmacokinetics of ciprofloxacin. *Clin Pharmacokinet* 1990; **19**: 434–61.
- 3 Viell B, Krause B, Schaaf S et al. Transintestinal elimination of ciprofloxacin in humans—concomitant assessment of its metabolites in serum, ileum and colon. *Infection* 1992; **20**: 324–7.
- 4 Rohwedder RW, Bergan T, Thorsteinsson SB et al. Transintestinal elimination of ciprofloxacin. *Diagn Microbiol Infect Dis* **13**: 127–33.
- 5 Khachman D, Conil J, Georges B et al. Optimizing ciprofloxacin dosing in intensive care unit patients through the use of population pharmacokinetic-pharmacodynamic analysis and Monte Carlo simulations. *J Antimicrob Chemother* 2011; **66**: 1798–809.
- 6 Jones EM, McMullin CM, Hedges AJ et al. The pharmacokinetics of intravenous ciprofloxacin 400 mg 12 hourly in patients with severe sepsis: the effect of renal function and intra-abdominal disease. *J Antimicrob Chemother* 1997; **40**: 121–4.
- 7 Cockcroft DW, Gault H. Prediction of creatinine clearance from serum creatinine. *Nephron* 1976; **16**: 31–41.
- 8 Cios A, Wyska E, Szymura-Oleksiak J et al. Population pharmacokinetic analysis of ciprofloxacin in the elderly patients with lower respiratory tract infections. *Exp Gerontol* 2014; **57**: 107–13.
- 9 Bouchard J, Macedo E, Soroko S et al. Comparison of methods for estimating glomerular filtration rate in critically ill patients with acute kidney injury. *Nephrol Dial Transplant* 2010; **25**: 102–7.
- 10 Forrest A, Ballow CH, Nix DE et al. Development of a population pharmacokinetic model and optimal sampling strategies for intravenous ciprofloxacin. *Antimicrob Agents Chemother* 1993; **37**: 1065–72.
- 11 Nord CE, Norby SR. Changing trends in antibiotic therapy: role of ciprofloxacin. *Scand J Infect Dis* 1988; **20**: 1–128.
- 12 Overholser BR, Kays MB, Forrest A et al. Sex-related differences in the pharmacokinetics of oral ciprofloxacin. *J Clin Pharmacol* 2004; **44**: 1012–22.
- 13 Poggio ED, Nef PC, Wang X et al. Performance of the Cockcroft–Gault and modification of diet in renal disease equations in estimating GFR in ill hospitalized patients. *Am J Kidney Dis* 2005; **46**: 242–52.
- 14 MacAulay J, Thompson K, Kiberd BA et al. Serum creatinine in patients with advanced liver disease is of limited value for identification of moderate renal dysfunction: are the equations for estimating renal function better? *Can J Gastroenterol* 2006; **20**: 521–6.
- 15 Dellinger RP, Levy MM, Rhodes A et al. Surviving sepsis campaign: international guidelines for management of severe sepsis and septic shock, 2012. *Intensive Care Med* 2013; **39**: 165–228.
- 16 Zander J, Maier B, Suhr A et al. Quantification of piperacillin, tazobactam, cefepime, meropenem, ciprofloxacin and linezolid in serum using an isotope dilution UHPLC-MS/MS method with semi-automated sample preparation. *Clin Chem Lab Med* 2015; **53**: 781–91.
- 17 Jonsson EN, Karlsson MO. Xpose—an S-PLUS based population pharmacokinetic/pharmacodynamic model building aid for NONMEM. *Comput Methods Programs Biomed* 1998; **58**: 51–64.
- 18 Lindbom L, Ribbing J, Jonsson EN. Perl-speaks-NONMEM (PsN)—a Perl module for NONMEM related programming. *Comput Methods Programs Biomed* 2004; **75**: 85–94.
- 19 Ravva P, Gastonguay MR, Tensfeldt TG et al. Population pharmacokinetic analysis of varenicline in adult smokers. *Br J Clin Pharmacol* 2009; **68**: 669–81.
- 20 Bergstrand M, Hooker AC, Wallin JE et al. Prediction-corrected visual predictive checks for diagnosing nonlinear mixed-effects models. *AAPS J* 2011; **13**: 143–51.
- 21 Wahlby U, Jonsson EN, Karlsson MO. Assessment of actual significance levels for covariate effects in NONMEM. *J Pharmacokinet Pharmacodyn* 2001; **28**: 231–52.
- 22 Forrest A, Nix DE, Ballow CH et al. Pharmacodynamics of intravenous ciprofloxacin in seriously ill patients. *Antimicrob Agents Chemother* 1993; **37**: 1073–81.
- 23 Stahlmann R. Clinical toxicological aspects of fluoroquinolones. *Toxicol Lett* 2002; **127**: 269–77.
- 24 European Committee on Antimicrobial Susceptibility Testing. Data from the EUCAST MIC Distribution Website. <https://mic.eucast.org/>.
- 25 Sadiq MW, Nielsen EI, Khachman D et al. A whole-body physiologically based pharmacokinetic (WB-PBPK) model of ciprofloxacin: a step towards predicting bacterial killing at sites of infection. *J Pharmacokinet Pharmacodyn* 2017; **44**: 69–79.
- 26 Gai X, Shen N, He B et al. [Population pharmacokinetics of ciprofloxacin in Chinese elderly patients with lower respiratory tract infection]. *Zhonghua Yi Xue Za Zhi* 2015; **95**: 1581–5.
- 27 Brendel K, Dartois C, Comets E et al. Are population pharmacokinetic and/or pharmacodynamic models adequately evaluated? *Clin Pharmacokinet* 2007; **46**: 221–34.
- 28 Spooner AM, Deegan C, D’Arcy DM et al. An evaluation of ciprofloxacin pharmacokinetics in critically ill patients undergoing continuous veno-venous haemodiafiltration. *BMC Clin Pharmacol* 2011; **11**: 11–20.
- 29 Pea F, Poz D, Viale P et al. Which reliable pharmacodynamic breakpoint should be advised for ciprofloxacin monotherapy in the hospital setting? A TDM-based retrospective perspective. *J Antimicrob Chemother* 2006; **58**: 380–6.
- 30 Nouaille-Degorce B, Veau C, Dautrey S et al. Influence of renal failure on ciprofloxacin pharmacokinetics in rats. *Antimicrob Agents Chemother* 1998; **42**: 289–92.
- 31 Fevery J. Bilirubin in clinical practice: a review. *Liver Int* 2008; **28**: 592–605.
- 32 Pierrakos C, Velissaris D, Felleiter P et al. Increased mortality in critically ill patients with mild or moderate hyperbilirubinemia. *J Crit Care* 2017; **40**: 31–5.
- 33 Sunder S, Jayaraman R, Mahapatra HS et al. Estimation of renal function in the intensive care unit: the covert concepts brought to light. *J Intensive Care* 2014; **2**: 31–8.
- 34 Waikar SS, Bonventre JV. Creatinine kinetics and the definition of acute kidney injury. *J Am Soc Nephrol* 2009; **20**: 672–9.
- 35 Baxmann AC, Ahmed MS, Marques NC et al. Influence of muscle mass and physical activity on serum and urinary creatinine and serum cystatin C. *Clin J Am Soc Nephrol* 2008; **3**: 348–54.
- 36 Swaminathan R, Ho CS, Chu LM et al. Serum creatinine and fat-free mass (lean body mass). *Clin Chem* 1986; **32**: 371–3.
- 37 FDA. Center for Drug Evaluation and Research Approval Package for: Application Number: NDA 21-554 Ciprofloxacin Extended-release Tablets. 2003. [https://www.accessdata.fda.gov/drugsatfda\\_docs/nda/2003/021554Orig1s000Appov.pdf](https://www.accessdata.fda.gov/drugsatfda_docs/nda/2003/021554Orig1s000Appov.pdf).
- 38 Schmucker DL. Age-related changes in liver structure and function: implications for disease? *Exp Gerontol* 2005; **40**: 650–9.
- 39 Durnas C, Loi C-M, Cusack BJ. Hepatic drug metabolism and aging. *Clin Pharmacokinet* 1990; **19**: 359–89.
- 40 Paladino JA, Forrest A, Wilton JH. Predictors of trough concentrations of oral ciprofloxacin. *Pharmacotherapy* 1993; **13**: 504–7.
- 41 Fried LP, Ferrucci L, Darer J et al. Untangling the concepts of disability, frailty, and comorbidity: implications for improved targeting and care. *Journals Gerontol Ser A Biol Sci Med Sci* 2004; **59**: M255–63.
- 42 Evans WJ, Campbell WW. Sarcopenia and age-related changes in body composition and functional capacity. *J Nutr* 1993; **123**: 465–8.
- 43 Lettieri JT, Rogge MC, Kaiser L et al. Pharmacokinetic profiles of ciprofloxacin after single intravenous and oral doses. *Antimicrob Agents Chemother* 1992; **36**: 993–6.
- 44 Rolando N, Wade J, Davalos M et al. The systemic inflammatory response syndrome in acute liver failure. *Hepatology* 2000; **32**: 734–9.

**45** Morgan ET. Impact of infectious and inflammatory disease on cytochrome P450-mediated drug metabolism and pharmacokinetics. *Clin Pharmacol Ther* 2009; **85**: 434–8.

**46** Martinez MN, Papich MG, Drusano GL. Dosing regimen matters: the importance of early intervention and rapid attainment of the pharmacokinetic/

pharmacodynamic target. *Antimicrob Agents Chemother* 2012; **56**: 2795–805.

**47** Shah A, Lettieri J, Nix D et al. Pharmacokinetics of high-dose intravenous ciprofloxacin in young and elderly and in male and female subjects. *Antimicrob Agents Chemother* 1995; **39**: 1003–6.

**Ciprofloxacin in critically ill subjects: considering hepatic function,  
age and sex to choose the optimal dose**

**(Supplementary document)**

**Xia LI<sup>1#</sup>, Michael ZOLLER<sup>2#</sup>, Uwe FUHR<sup>1</sup>, Mikayil HUSEYN\_ZADA<sup>2</sup>, Barbara MAIER<sup>3</sup>, Michael VOGESER<sup>3</sup>, Johannes ZANDER<sup>3+</sup>, Max TAUBERT<sup>1+\*</sup>**

1 Department I of Pharmacology, Clinical Pharmacology, Cologne University Hospital, Cologne, Germany;

2 Department of Anesthesiology, Hospital of the Ludwig-Maximilians-University of Munich, Munich, Germany;

3 Institute of Laboratory Medicine, Hospital of the Ludwig-Maximilians-University of Munich, Munich, Germany.

# Both authors contributed equally

+ Both authors contributed equally

**\*Corresponding Author**

Max Taubert

Department I of Pharmacology, Center for Pharmacology, Clinical Pharmacology Unit

University Hospital Cologne (AöR)

Gleueler Straße 24, 50931 Köln, Germany

Email: max.taubert@uk-koeln.de

Tel: +49-(0)-221-478-86716

Fax: +49-(0)-221-478-7011

**Table S1. Parameter estimates as employed in the simulation study**

Parameter	Model A	Model B	Model C	Model D
TVCL (L/h)	16.3 (9%)	18 (5%)	13.5 (14%)	17.8 (6%)
IIV <sub>CL</sub>	0.0489 (54%)	0.169 (23%)	0.273 (9%)	0.0562 (28%)
CRCL <sub>CG</sub>	n.a.	0.42 (45%)	0.674(26%)	n.a.
CR	n.a.	n.a.	n.a.	0.00125 (3%)
age	0.0153 (38%)	n.a.	n.a.	n.a.
bilirubin	-0.241 (20%)	n.a.	n.a.	n.a.
sex	-0.431 (18%)	n.a.	n.a.	n.a.

**Table S1.** Point estimates (relative standard errors) of the newly developed model A and the reported models B to D. TVCL, typical value of ciprofloxacin clearance; IIV<sub>CL</sub>, inter-individual variability of clearance; covariate parameter estimates related to Cockcroft-Gault creatinine clearance (CRCL<sub>CG</sub>), serum creatinine (CR), age, total bilirubin and sex. n.a., not applicable, indicates that the respective parameters were not part of the model.

**Table S2. Covariate model equations used in the simulation study**

Model	Equation
A	$CL = 16.3 * [1 + (49 - age) * 0.0153] * [1 - 0.431 * sex] * [bili/1.85]^{-0.241}$
B	$CL = 18 * (CRCL_{CG}/91.7)^{0.42}$
C	$CL = 13.5 + 0.039 * CRCL_{CG} * (1 + 0.674)$
D	$CL = 17.8 * [1 - (88.4 * CR - 67) * 0.00125]$

**Table S2.** Covariate models for predicting ciprofloxacin clearance (CL) (L/h) from models A, B, C and D as used in the simulation study; based on Cockcroft-Gault creatinine clearance (CRCL<sub>CG</sub>, mL/min), serum creatinine concentration (CR, mg/dL), age (age, years), sex (sex, 0 = male, 1 = female), and total bilirubin concentration (bili, mg/dL). Utilized parameter estimates correspond to Table S1.

**Figure S1. Confidence intervals and medians of parameter estimates of alanine aminotransferase, anti-thrombin, bilirubin, cholinesterase, and factor V as additive covariates for ciprofloxacin clearance**

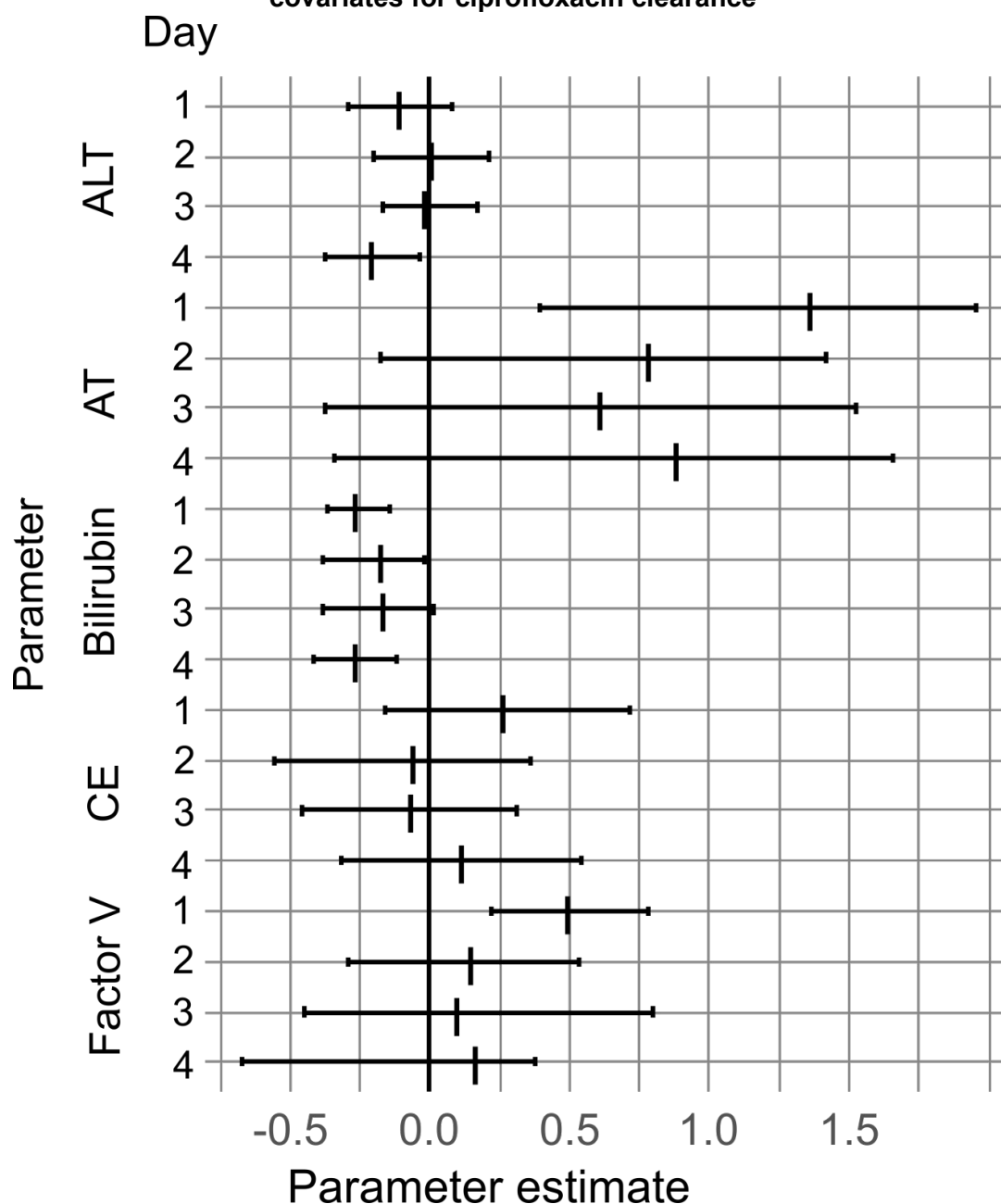


**Figure S1** 95% confidence intervals and medians of estimated covariate parameters reflecting liver function (bars indicate CI, vertical lines indicate medians) from bootstrap results in the covariate evaluation (also see Figure 1). Parameter estimates for alanine aminotransferase concentration (ALT), anti-thrombin concentration (AT), total bilirubin concentration (BILI), cholinesterase concentration (CE), and factor V concentration. A value of zero indicates “no effect”.

**Figure S2. Confidence intervals and medians of parameter estimates of CRCL<sub>CG</sub>, measured creatinine clearance, and creatinine as additive covariates for ciprofloxacin clearance**

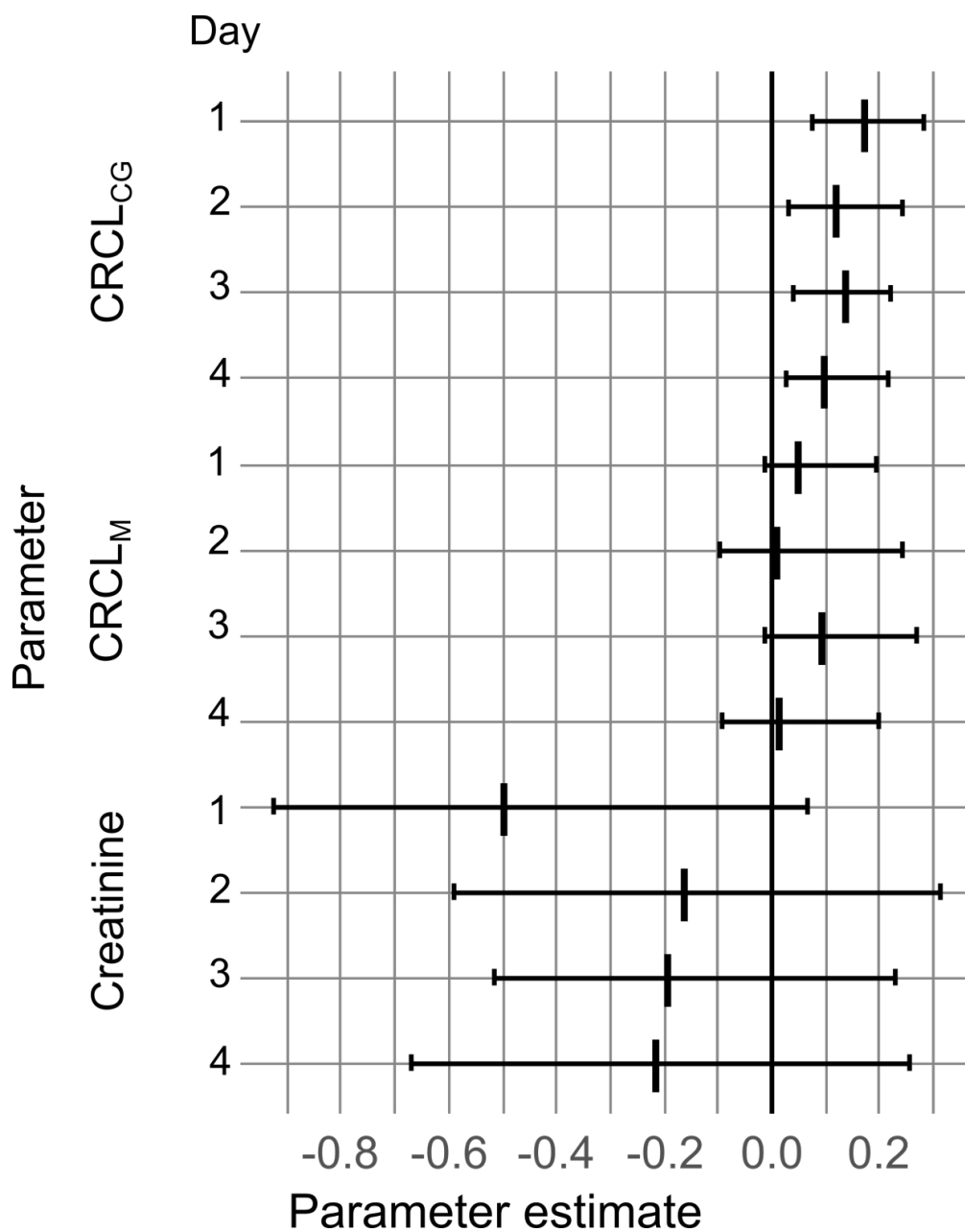


**Figure S2** 95% confidence intervals and medians of estimated covariate parameters reflecting kidney function (bars indicate CI, vertical lines indicate medians) from bootstrap results in the covariate evaluation (also see Figure 1). Parameter estimates for creatinine clearance predicted by Cockcroft-Gault equation (CRCL<sub>CG</sub>), measured creatinine clearance (CRCL<sub>M</sub>), and serum creatinine concentration (Creatinine). A value of zero indicates “no effect”.



**Figure S3. Confidence intervals and medians of parameter estimates of age, sex and weight as covariates for ciprofloxacin clearance**

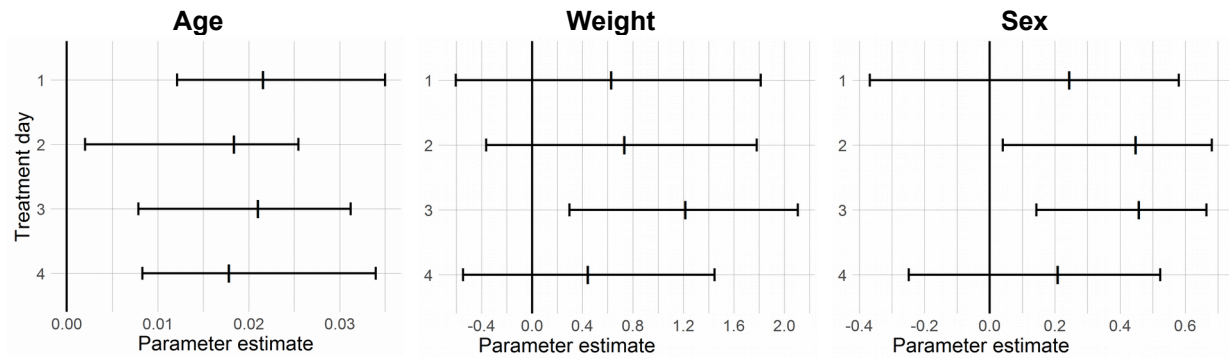


**Figure S3** 95% confidence intervals and medians of estimated covariate parameters (bars indicate CI, vertical lines indicate medians) from 1000 bootstrap results in the covariate evaluation (also see Figure 1). Parameter estimates for age, weight and sex. A value of zero indicates “no effect”.

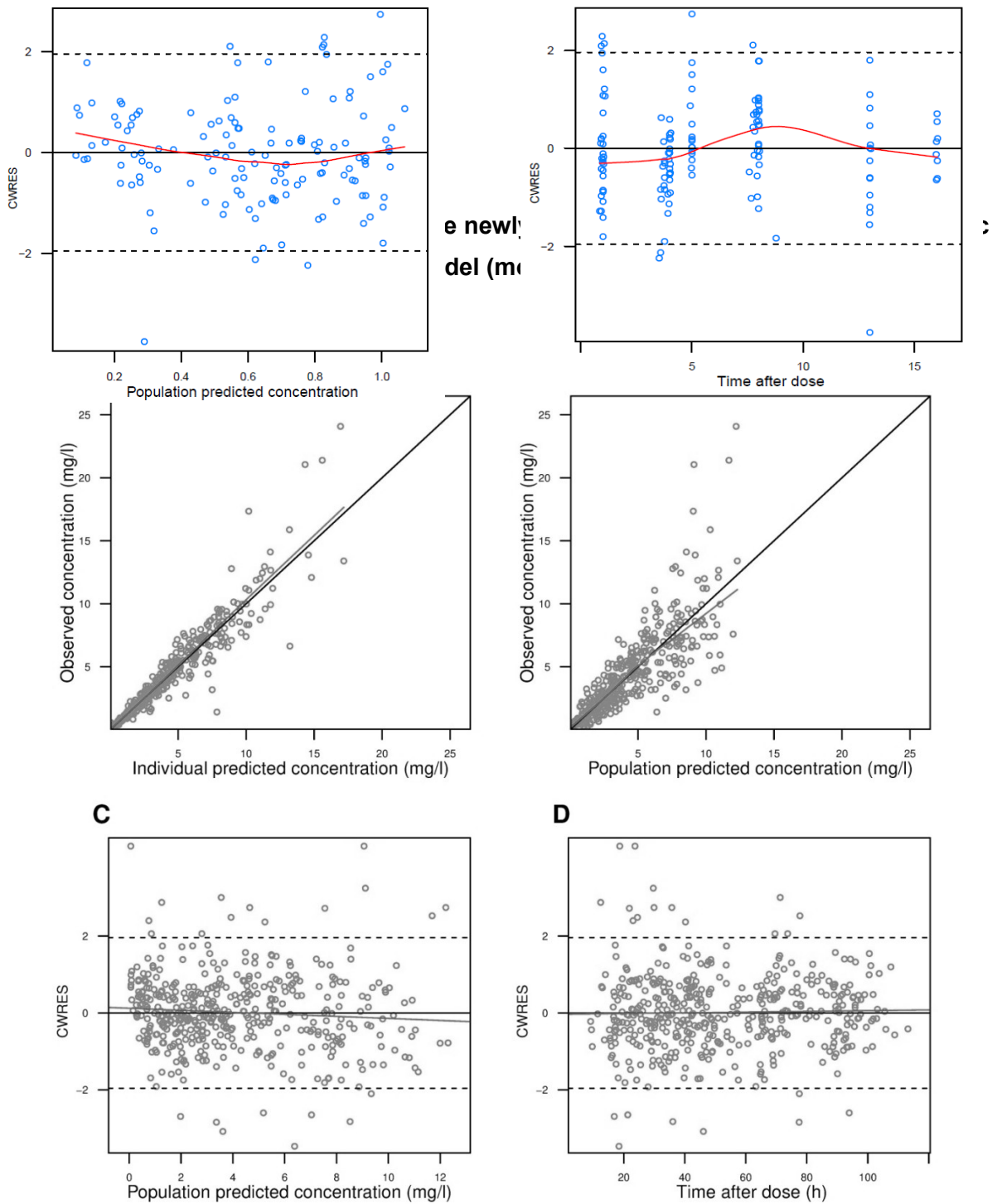


**Figure S4** Goodness-of-fit plots. Observed serum ciprofloxacin concentrations versus individual predictions (A) and population predictions (B) as obtained from the final pharmacokinetic model (model A). Conditional weighted residuals (CWRES) versus population predicted serum ciprofloxacin concentrations (C) and versus time after the first dose (D).

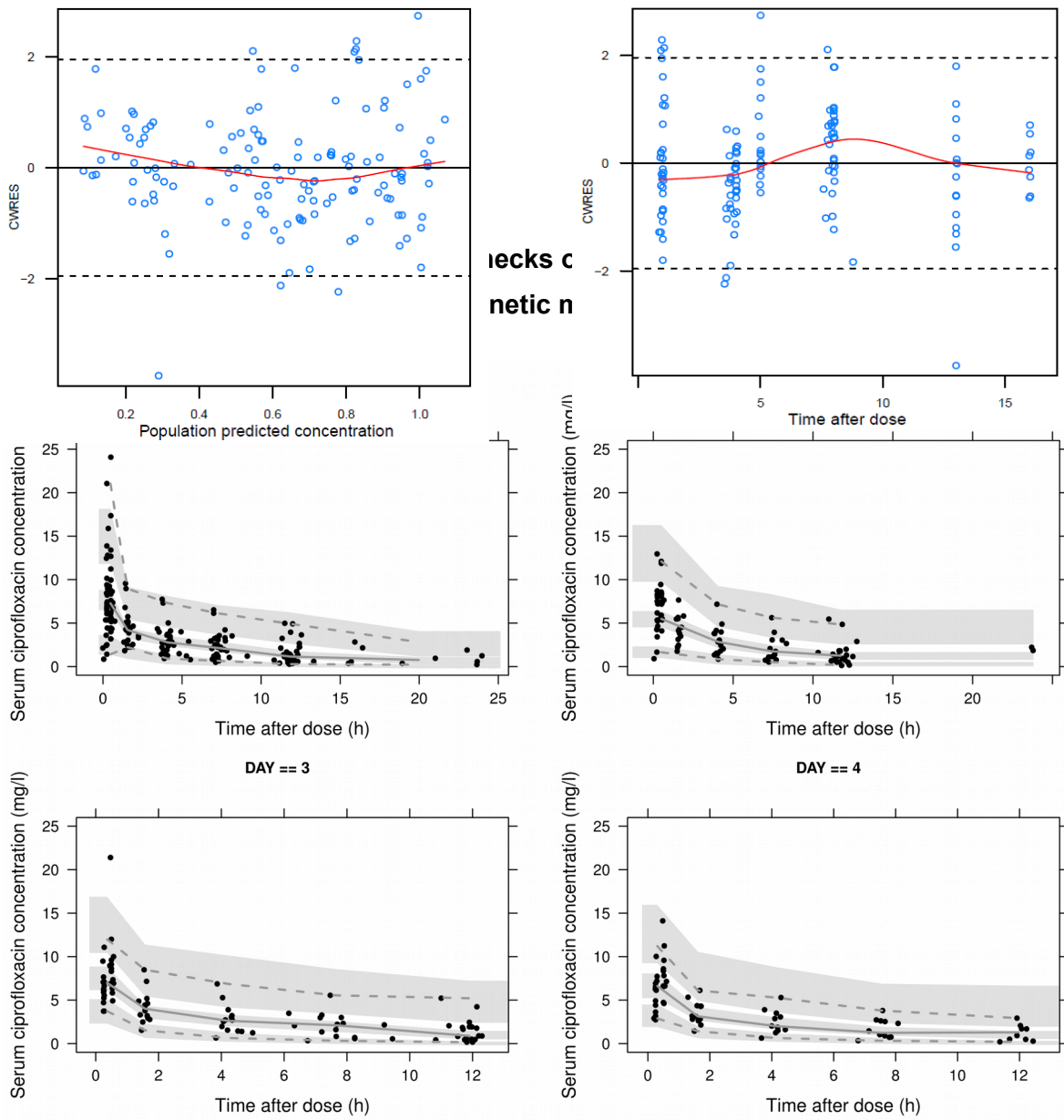


**Figure S5** Visual predictive checks of the final model stratified by treatment day (DAY 1 to 4). Black dots represent observed concentrations. The solid line represents the median observed serum concentrations while 2.5<sup>th</sup> and 97.5<sup>th</sup> percentiles of the data are represented by dashed lines. Shaded areas indicate 95% intervals simulated from the model.

**Figure S6. Probability of exceeding AUC limits stratified by estimated creatinine clearance (Cockcroft-Gault) for a daily dose of 1200 mg**

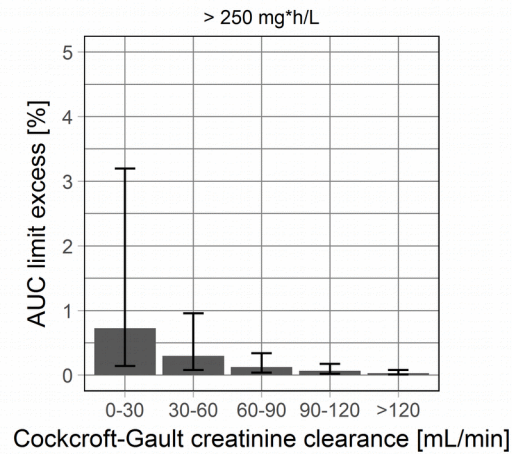


**Figure S6** Probability of exceeding an AUC limit of 250 mg\*h/L, stratified by Cockcroft-Gault creatinine clearance values. Simulation results from the creatinine model, i.e. the joint model based on previously published models B, C and D. Error bars represent 90% CIs.

**Figure S7. PTAs stratified by age, bilirubin and gender**

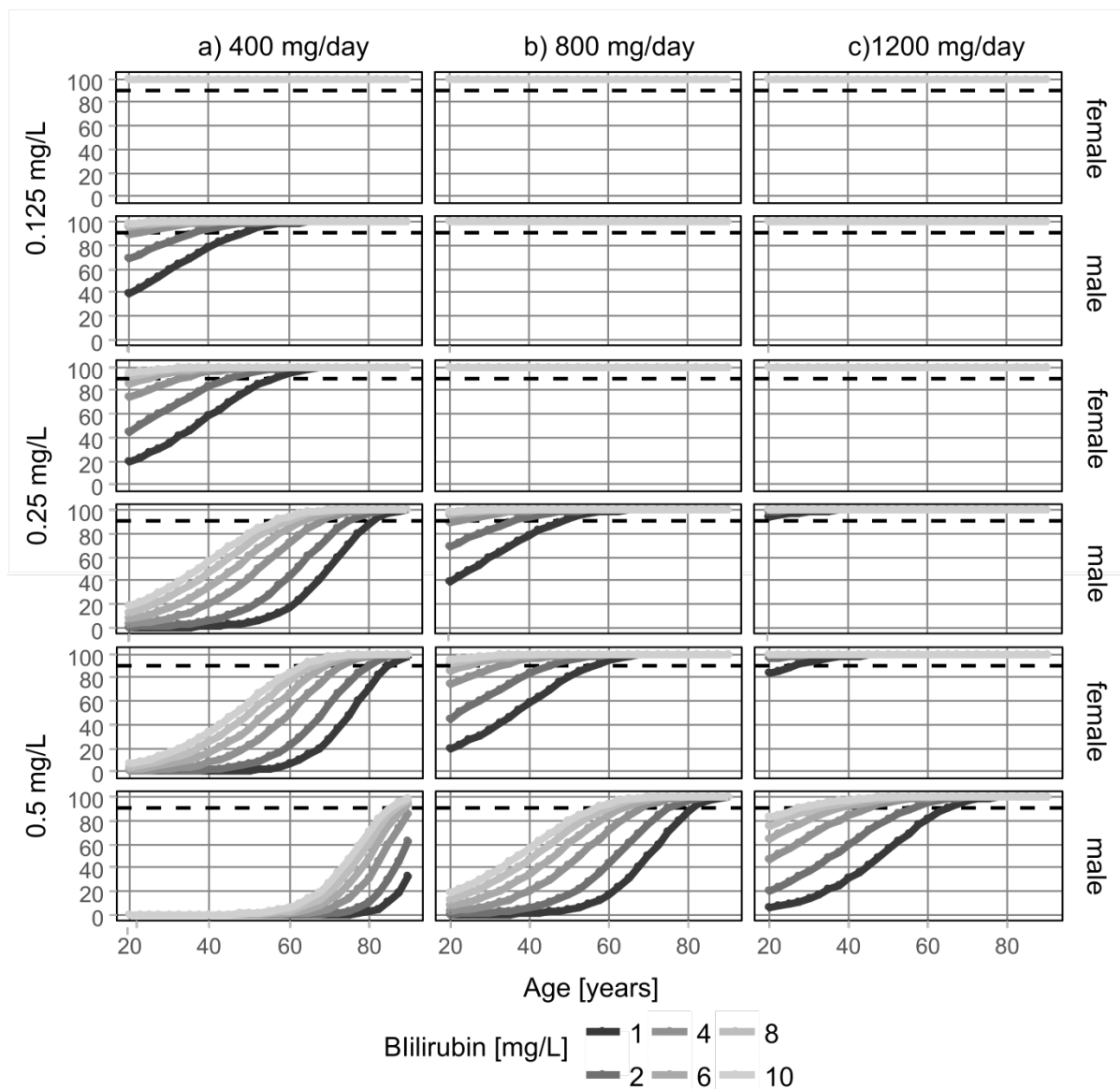


**Figure S7** Probability of target attainment ( $AUC/MIC > 125h$ ) for daily doses of 400 (a), 800 (b) and 1200 (c) mg/day of ciprofloxacin depending on age total bilirubin concentration and sex for an MIC of 0.125 (top), 0.25 (middle) and 0.5 (bottom) mg/L. The dashed line indicates the target PTA of 90%. Simulations are based on model A.

## Supplementary Methods. Description of the weighting method for the joint evaluation.

When integrating several models into a joint evaluation, a procedure for weighting the contribution of each model to the joint result is needed. A customary approach to weight the contribution in meta-analysis is to use the inverse of the respective standard error.<sup>1</sup> However, standard errors are usually not reported for the quantities of interest, such as AUC/MIC ratios or PTAs. Since we were interested in steady state AUC/MIC ratios (**Eq. S1**), which are the basis of ciprofloxacin PTAs, the standard errors of AUC/MIC ratios on a log-scale were approximated by sampling model parameters from normal distributions using published model parameter point estimates and standard errors and repeatedly generating AUC/MIC ratios. This sampling procedure is similar to the approach suggested by Colin et al.,<sup>2</sup> but differs in that parameters were assumed to be independent. The assumption of independence was necessary since parameter covariances are usually not reported. To account for the influence of covariates, the obtained standard errors were averaged over covariate data from subjects of the simulation group (see **Table 1**), therefore reflecting the uncertainty in predictions for a typical population of critically ill subjects. The contribution of each model to the joint evaluation was then weighted by the inverse of the respective average standard error (weighted average, **Eq. S2**). All sampling steps were demanded to have a relative sampling error  $\leq 1\%$ , which was assessed by 100-fold re-sampling. Finally, confidence intervals of weighted averages were approximated by repeatedly ( $n = 1,000$ ) sampling model parameters and calculating the resulting PTAs and weighted averages.

$$\text{(Eq. S1)} \quad AUC_{ss} = \frac{dose}{CL}$$

Equation S1. Steady state AUC ( $AUC_{ss}$ ), determined by the daily dose and clearance (CL).

$$\text{(Eq. S2)} \quad w_i = v_i / \sum_{j=1}^n v_j$$

Equation S2. The contribution of model  $i$  to the joint result is calculated based on the average AUC standard error on a log-scale ( $v_i$ ), relative to the sum of AUC standard errors of all models.

1. Cochran WG. The combination of estimates from different experiments. *Biometrics* 1954; **10**: 101–29.

2. Colin P, Eleveld DJ, Jonckheere S, et al. What about confidence intervals? A word of caution when interpreting PTA simulations. *J Antimicrob Chemother* 2016; **71**: 2502–8.



# A Physiologically Based Pharmacokinetic Model of Voriconazole Integrating Time-Dependent Inhibition of CYP3A4, Genetic Polymorphisms of CYP2C19 and Predictions of Drug–Drug Interactions

Xia Li<sup>1</sup> · Sebastian Frechen<sup>2</sup> · Daniel Moj<sup>3</sup> · Thorsten Lehr<sup>3</sup> · Max Taubert<sup>1</sup> · Chih-hsuan Hsin<sup>1</sup> · Gerd Mikus<sup>4</sup> · Pertti J. Neuvonen<sup>5</sup> · Klaus T. Oikola<sup>6</sup> · Teijo I. Saari<sup>7</sup> · Uwe Fuhr<sup>1</sup>

© Springer Nature Switzerland AG 2019

## Abstract

**Background** Voriconazole, a first-line antifungal drug, exhibits nonlinear pharmacokinetics (PK), together with large interindividual variability but a narrow therapeutic range, and markedly inhibits cytochrome P450 (CYP) 3A4 in vivo. This causes difficulties in selecting appropriate dosing regimens of voriconazole and coadministered CYP3A4 substrates.

**Objective** This study aimed to investigate the metabolism of voriconazole in detail to better understand dose- and time-dependent alterations in the PK of the drug, to provide the model basis for safe and effective use according to CYP2C19 genotype, and to assess the potential of voriconazole to cause drug–drug interactions (DDIs) with CYP3A4 substrates in more detail.

**Methods** In vitro assays were carried out to explore time-dependent inhibition (TDI) of CYP3A4 by voriconazole. These results were combined with 93 published concentration–time datasets of voriconazole from clinical trials in healthy volunteers to develop a whole-body physiologically based PK (PBPK) model in PK-Sim<sup>®</sup>. The model was evaluated quantitatively with the predicted/observed ratio of the area under the plasma concentration–time curve (AUC), maximum concentration ( $C_{\max}$ ), and trough concentrations for multiple dosings ( $C_{\text{trough}}$ ), the geometric mean fold error, as well as visually with the comparison of predicted with observed concentration–time datasets over the full range of recommended intravenous and oral dosing regimens.

**Results** The result of the half maximal inhibitory concentration ( $IC_{50}$ ) shift assay indicated that voriconazole causes TDI of CYP3A4. The PBPK model evaluation demonstrated a good performance of the model, with 71% of predicted/observed aggregate AUC ratios and all aggregate  $C_{\max}$  ratios from 28 evaluation datasets being within a 0.5- to 2-fold range. For those studies reporting CYP2C19 genotype, 89% of aggregate AUC ratios and all aggregate  $C_{\max}$  ratios were inside a 0.5- to 2-fold range of 44 test datasets. The results of model-based simulations showed that the standard oral maintenance dose of voriconazole 200 mg twice daily would be sufficient for CYP2C19 intermediate metabolizers (IMs; \*1/\*2, \*1/\*3, \*2/\*17, and \*2/\*2/\*17) to reach the tentative therapeutic range of > 1–2 mg/L to < 5–6 mg/L for  $C_{\text{trough}}$ , while 400 mg twice daily might be more suitable for rapid metabolizers (RMs; \*1/\*17, \*17/\*17) and normal metabolizers (NMs; \*1/\*1). When the model was integrated with independently developed CYP3A4 substrate models (midazolam and alfentanil), the observed AUC change of substrates by voriconazole was inside the 90% confidence interval of the predicted AUC change, indicating that CYP3A4 inhibition was appropriately incorporated into the voriconazole model.

**Conclusions** Both the in vitro assay and model-based simulations support TDI of CYP3A4 by voriconazole as a pivotal characteristic of this drug's PK. The PBPK model developed here could support individual dose adjustment of voriconazole according to genetic polymorphisms of CYP2C19, and DDI risk management. The applicability of modeling results for patients remains to be confirmed in future studies.

---

**Electronic supplementary material** The online version of this article (<https://doi.org/10.1007/s40262-019-00856-z>) contains supplementary material, which is available to authorized users.

Extended author information available on the last page of the article

## Key Points

A whole-body physiologically based pharmacokinetic (PBPK) model of voriconazole incorporating time-dependent inhibition (TDI), specifically mechanism-based inhibition (MBI) of cytochrome P450 (CYP) 3A4, was successfully developed to accurately capture the time- and dose-dependent alterations of voriconazole PK for different CYP2C19 genotypes.

Model-based simulations could (1) elaborate potential exposure-equivalent dosing regimens for CYP2C19 genotype groups; (2) assess the dynamic inhibition of CYP3A4 by voriconazole in the liver and small intestine; and (3) predict DDIs between voriconazole and other CYP3A4 substrates.

## 1 Introduction

Voriconazole is an essential drug in the treatment of severe fungal infections due to its activity against a wide range of clinically relevant fungal pathogens, including the most commonly occurring species of the genera *Aspergillus* and *Candida*, and some emerging fungi, such as *Scedosporium* and *Fusarium* species [1]. Moreover, voriconazole is well-established as first-line therapy for patients with invasive aspergillosis [2–4]. However, the drug exhibits nonlinear PK with large interindividual and intraindividual variability [5, 6], which causes difficulties for clinicians when choosing appropriate dosing regimens to target its narrow therapeutic range, especially in the case of high doses in severe infections, or for long-term treatments [7].

While underexposure of voriconazole may decrease efficacy, overexposure increases the risk primarily for neural and hepatic toxicity [8, 9]. Until now, no universally applicable therapeutic range has been established. In 2013, two Japanese societies recommended voriconazole trough concentrations for multiple dosings ( $C_{\text{trough}}$ ) of 1–2 mg/L to 4–5 mg/L [10], while in 2014 the British Society for Medical Mycology recommended  $C_{\text{trough}}$  of 1 mg/L to 4–6 mg/L [11]. In 2017, according to the Third Fungal Diagnosis and Management of *Aspergillus* diseases Clinical Guideline, a  $C_{\text{trough}}$  range of 1–5.5 mg/L was considered adequate for most patients with voriconazole prophylaxis or treatment, while the recommended range for patients with severe infections was 2–6 mg/L [4]. In 2018, the Chinese Pharmacological Society recommended a range of 0.5–5 mg/L [12]. Thus, in the present project, we selected lower and upper  $C_{\text{trough}}$  of > 1–2 mg/L and < 5–6 mg/L, respectively.

Voriconazole is extensively metabolized via the cytochrome P450 (CYP) enzymes CYP2C19 and CYP3A4 [13], slightly by CYP2C9 and flavin-containing monooxygenase (FMO) [14], while < 2% is excreted renally as the parent drug [15–17]. The main metabolite in plasma was reported as voriconazole N-oxide, accounting for 72% of circulating metabolites [1]. However, Geist et al. found that voriconazole N-oxide and its conjugates excreted in urine within 12 h postdose during steady-state only accounted for 1% of the dose, while excretion of other metabolites, i.e. dihydroxy fluoropyrimidine–voriconazole and hydroxy fluoropyrimidine–voriconazole, together with their conjugates, accounted for 14% and 3% of the dose, respectively [17]. This was in agreement with another study where the major metabolite excreted in urine over 96 h was dihydroxy fluoropyrimidine–voriconazole, accounting for 13% of the dose of voriconazole [18]. Therefore, it seems reasonable to also consider dihydroxy-fluoropyrimidine voriconazole and hydroxy-fluoropyrimidine voriconazole as major metabolites of voriconazole, although both have low plasma concentrations due to their high renal clearances, which was reported to be approximately 150- and 55-fold higher, respectively, than that of voriconazole N-oxide [17]. However, two other groups found that the main metabolite of voriconazole excreted in urine within 48 h after administration was voriconazole N-oxide, accounting for 10–21% of the dose [15, 16]. The discrepancies between the studies may be explained by the respective length of urine collection periods, together with the different elimination half-life of the metabolites and a potential time-dependent inhibition (TDI) of CYP3A4. Thus, both fluoropyrimidine hydroxylation and N-oxidation pathways were considered as the main metabolic pathways, mainly mediated by CYP3A4 and CYP2C19, as shown in Fig. 1.

Genetic polymorphisms of CYP2C19 are a major source for interindividual variability, as reflected by threefold higher maximum concentration ( $C_{\text{max}}$ ) values and two- to fivefold higher area under the plasma concentration–time curve (AUC) values in CYP2C19 poor metabolizers (PMs) compared with those in normal metabolizers (NMs) or rapid metabolizers (RMs) [7, 19, 20].

Furthermore, voriconazole is also an inhibitor of CYP3A4 and CYP2C19 [21]. In vitro, voriconazole inhibition constant ( $K_i$ ) for the competitive inhibition of CYP3A4-mediated metabolism of midazolam was reported to range from 0.15 to 0.66  $\mu\text{M}$  [21, 22], indicating potent inhibition. In agreement with the in vitro results, the AUC of midazolam was considerably increased to 940% and 353% by oral and intravenous coadministration of therapeutic doses of voriconazole in vivo, respectively [23]. Furthermore, voriconazole was reported to mediate ‘autoinhibition’ of



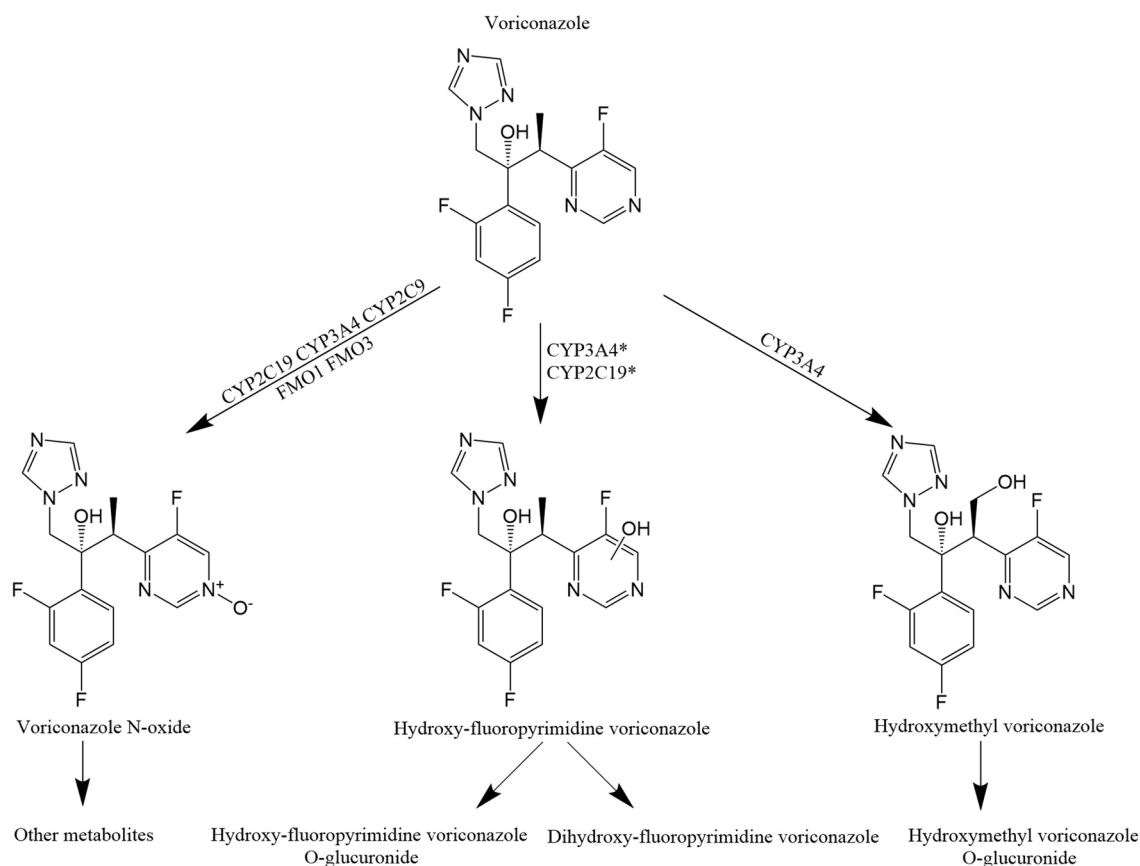


**Fig. 1** Metabolic pathway for voriconazole. \*Indirect evidence from different CYP2C19 genotype groups [18]. CYP cytochrome P450, FMO flavin-containing monooxygenase

CYP3A4 activity in vivo [15, 24]. In addition, to properly describe the respective processes concerning enzyme inhibition by voriconazole in vivo, ‘TDI’ and ‘autoinhibition’, respectively, of voriconazole were integrated into the non-linear mixed-effects models reported by Friberg et al. and Kim et al., respectively [25, 26].

Therefore, we investigated the inhibition of voriconazole and its metabolite voriconazole N-oxide on CYP3A4 and CYP2C19 in vitro. Based on the in vitro assay results, a whole-body physiologically based pharmacokinetic (PBPK) model of voriconazole incorporating CYP3A4 TDI was then developed to describe dose- and time-dependent PK in the different CYP2C19 genotypes. Finally, model-based simulations were carried out to (1) elaborate potentially exposure-equivalent dosing regimens for CYP2C19 genotype groups; (2) assess the dynamic inhibition of CYP3A4 by voriconazole in the liver and small intestine; and (3) further evaluate drug–drug interactions (DDIs) between voriconazole and other CYP3A4 probe substrates. An early stage of this work has been presented at the Population Approach Group in Europe conference [27].

## 2 Methods

### 2.1 In Vitro Assay for Inhibition of Cytochrome P450 (CYP) CYP2C19 and CYP3A4

The in vitro assay for inhibition of human CYP2C19 and CYP3A4 by voriconazole and its metabolite voriconazole N-oxide, together with the respective measurements and data analysis, were carried out according to the methods described in the electronic supplementary materials (ESM).

### 2.2 Model Development

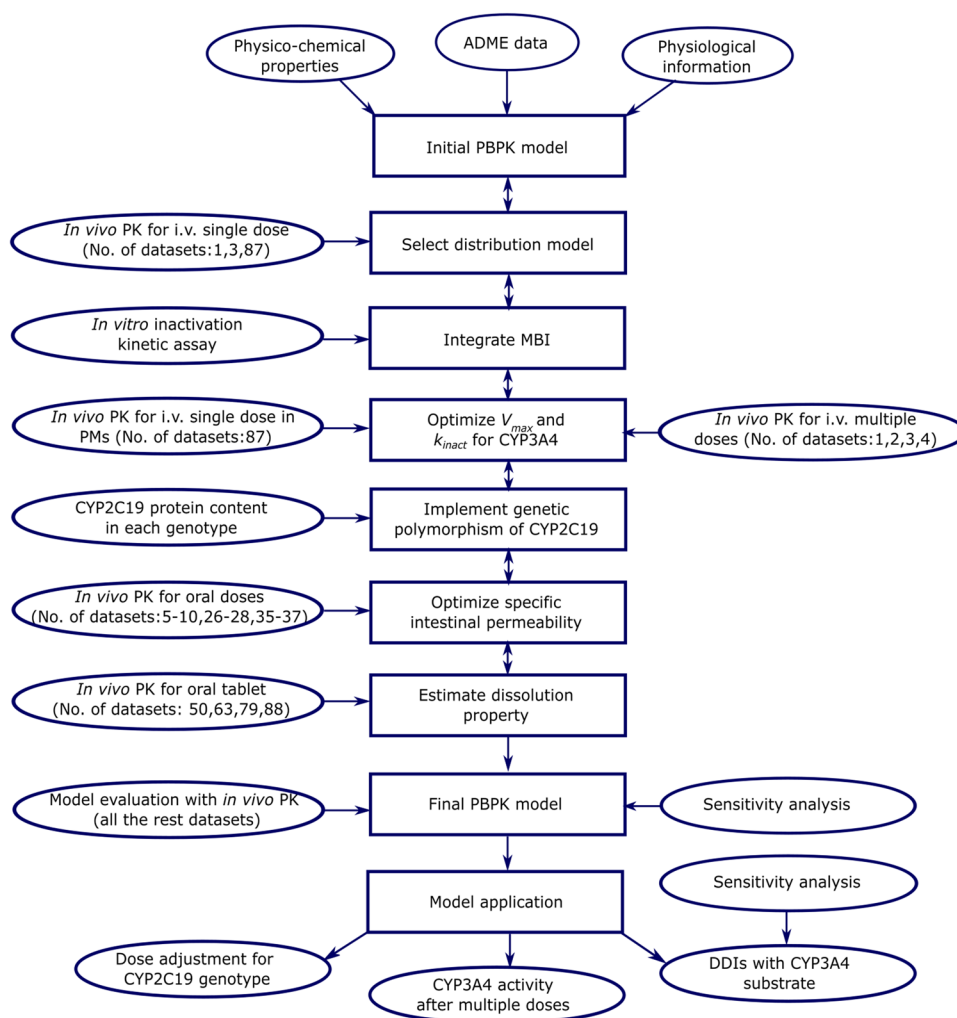
The PBPK model for voriconazole was developed by combining bottom-up and top-down approaches. An extensive literature search was performed to obtain (a) drug physicochemical properties; (b) PK parameters describing absorption, distribution, metabolism and excretion processes; and (c) clinical studies of intravenous and oral administration of voriconazole to healthy subjects with different dosing regimens. The clinical studies were screened and selected according to the following criteria: (1) intravenous or oral

administration of voriconazole; (2) healthy volunteers; (3) plasma concentration–time datasets of voriconazole were available; and (4) articles published in English. The training dataset for model development was selected based on (1) the information required for each step of model development; (2) the parameters need to be optimized; (3) the number of studies available; and (4) the informative content of datasets for individual studies (genotype groups, dosing regimens, and routes of administration), as shown in Fig. 2. Except datasets required and used for model development, all the remaining clinical trial datasets were utilized for model evaluation. The contribution of training datasets containing aggregate data from each clinical study was weighted equally to enable incorporation of some clinical studies that provided important information but did not report standard deviation (SD) or another measure of variability. Individual concentration–time datasets were pooled according to genotype groups, with the contribution of each individual dataset being weighted equally.

The modeling software PK-Sim<sup>®</sup> (version 7.3.0, part of the Open Systems Pharmacology (OSP) suite) was used for model development, which consists of a system- and drug-dependent component. System-dependent physiological parameters (organ volumes, blood flow rates, hematocrit, etc.) were provided in PK-Sim<sup>®</sup> with the small molecule model [28–30]. Demographic characteristics of subjects were taken from each clinical study. Drug-specific physicochemical properties were obtained from the literature. Organ–plasma partition coefficients were determined using the Poulin and Theil method based on both the literature [31] and the best overlap between observed and predicted concentration–time datasets.

The workflow of model development is presented in Fig. 2. For model development, the simplifying assumption was made that the metabolism of voriconazole is mediated exclusively by CYP3A4 and CYP2C19; the minor contributions of CYP2C9, FMOs, and unchanged renal elimination of voriconazole were neglected [13, 16]. Tissue

**Fig. 2** Workflow of voriconazole PBPK model development and evaluation. The PK datasets used to select the distribution model were also utilized to optimize  $V_{max}$  and  $k_{inact}$  for CYP3A4. There were 21 PK datasets for model development and 72 for model evaluation in total. *ADME* absorption, distribution, metabolism, elimination, *PK* pharmacokinetics, *TDI* time-dependent inhibition, *PMs* poor metabolizers, *DDIs* drug–drug interactions, *PBPK* physiologically based pharmacokinetic, *CYP* cytochrome P450,  $V_{max}$  maximum velocity,  $k_{inact}$  maximum inactivation rate constant



expression distribution of enzymes was provided by the PK-Sim<sup>®</sup> expression database based on reverse transcription-polymerase chain reaction (RT-PCR) profiles [32], together with the reference value of 4.32  $\mu\text{mol}$  CYP3A4 and 0.76  $\mu\text{mol}$  CYP2C19 per liter of liver tissue [33]. The relative CYP2C19 expression for different genotypes was obtained based on the CYP2C19 protein content ratio in genotype-defined pooled human liver microsomes [34]. The metabolism process of voriconazole was described using Michaelis–Menten kinetics [35]. As reported by Damle et al. [31],  $K_m$  for CYP3A4 and CYP2C19 was set to 15 and 3.5  $\mu\text{M}$ , respectively, and maximum velocity ( $V_{\text{max}}$ ) for CYP2C19 was fixed to 1.19 pmol/min/pmol.  $V_{\text{max}}$  for CYP3A4 was optimized based on the concentration–time datasets in CYP2C19 PMs [18], with the assumption that only CYP3A4 contributes to the metabolism of voriconazole in PMs. TDI was integrated into the model assuming that it reflects mechanism-based inhibition (MBI), with Eq. S4 in the ESM based on the in vitro inactivity assay results of  $K_I$  (the inhibition concentration when reaching half of  $k_{\text{inact}}$ ). The other parameter  $k_{\text{inact}}$  (maximum inactivation rate constant) was optimized based on concentration–time curves after multiple intravenous administrations [36], since the in vitro derived  $k_{\text{inact}}$  parameter value led to an overprediction of midazolam AUCs when evaluating the voriconazole–midazolam DDI studies.

The specific intestinal permeability was optimized based on the studies, including both intravenous and oral administration of voriconazole [6, 37, 38]. The dissolution of the formulation was assumed to follow a Weibull function and was estimated based on the concentration–time datasets after oral administration [18].

### 2.3 Model Evaluation

Model-based stochastic simulations were created for visual comparison with the observed concentration–time datasets of voriconazole in different CYP2C19 genotype groups. For clinical trials not reporting CYP2C19 genotype information, the population was assumed to be NM as this genotype is the most common 2C19 polymorphism prevalent in more than 64% of White, African American, Hispanic, and Ashkenazi populations [39]. To compare the variability of observed and simulated PK datasets, 68% population prediction intervals (approximately mean  $\pm$  SD in case of assumed normal distribution) were plotted if the observed concentration–time datasets were reported as mean ( $\pm$  SD), while 95% population prediction intervals were described when all individual concentration–time datasets were available [40]. The visual criteria for a good model performance were that 95% population prediction intervals should cover the observed individual plasma concentration–time datasets, or that the observed aggregate plasma concentration–time datasets

should be inside the 68% population prediction intervals. Predicted AUC,  $C_{\text{max}}$ , and  $C_{\text{trough}}$  values were compared with observed values via goodness-of-fit plots.

The quantitative evaluation criterion for a good model performance was that the ratios of predicted to observed AUC,  $C_{\text{max}}$ , and  $C_{\text{trough}}$  should be within 0.5- to 2.0-fold limits, as shown in Tables 1 and 2, and Table S4 in the ESM. As a quantitative summary of the predictive performance of the model, the geometric mean fold error (GMFE) was calculated using Eq. (1) [41].

$$\text{GMFE} = 10^{(\sum |\log_{10}(\text{pred } P/\text{obs } P)|)/n}, \quad (1)$$

where GMFE is the geometric mean fold error of all AUC,  $C_{\text{max}}$ , or  $C_{\text{trough}}$  predictions from the respective model, pred  $P$  is the predicted parameter (AUC,  $C_{\text{max}}$ , or  $C_{\text{trough}}$ ), obs  $P$  is the observed parameter (AUC,  $C_{\text{max}}$ , or  $C_{\text{trough}}$ ), and  $n$  is the number of studies.

### 2.4 Drug–Drug Interactions with Other CYP3A4 Substrates

Published PBPK models of the CYP3A4 probe substrates midazolam or alfentanil were integrated with the model of voriconazole to assess the inhibitory effects of voriconazole on CYP3A4 in vivo and to verify the inhibition model of voriconazole [41]. The DDI modeling performance was evaluated by both visual comparison of predicted versus observed probe substrate PK datasets, and by calculation of DDI AUC ratios and  $C_{\text{max}}$  ratios according to Eqs. (2) and (3).

$$\text{DDI AUC ratio} = \frac{\text{AUC}_{\text{treatment}}}{\text{AUC}_{\text{reference}}}, \quad (2)$$

$$\text{DDI } C_{\text{max}} \text{ ratio} = \frac{C_{\text{max treatment}}}{C_{\text{max reference}}}, \quad (3)$$

where AUC (or  $C_{\text{max}}$ ) treatment is the AUC (or  $C_{\text{max}}$ ) of victim drug with voriconazole co-treatment, and AUC (or  $C_{\text{max}}$ ) reference is the AUC (or  $C_{\text{max}}$ ) for victim drug administration alone.

### 2.5 Sensitivity Analysis

According to Eq. (4), the ratio of the relative change of AUC during a dosing interval ( $\text{AUC}_{\tau}$ ) versus the relative alteration of the evaluated parameter was calculated at steady state after the standard therapeutic multiple dosings of voriconazole by oral administration. The sensitivity analysis was also conducted for the DDI between voriconazole and midazolam. Parameters selected for the sensitivity analysis fulfilled one of the following criteria [41]: (1) optimized; (2)

**Table 1** Clinical studies without information on the CYP2C19 genotype used for voriconazole model development and evaluation

Dose (mg)	Route	n	Male (%)	Age (years)	Weight (kg)	Use of dataset	Pred AUC (mg*h/L)	Obs AUC (mg*h/L)	Pred/Obs AUC	Pred C <sub>max</sub> (mg/L)	Obs C <sub>max</sub> (mg/L)	Pred/Obs C <sub>max</sub>	References	No. of data-sets
3/kg, qd D1	IV (1 h)	9	100	24 (20–31)	72 (60–87)	D/A	7.90	5.22	1.51	2.45	2.14	1.14	[36]	1
3/kg, bid D3–11.5 (3/kg, qd D1)	IV (1 h)	9	100	24 (20–31)	72 (60–87)	D/A	16.7	16.5	1.01	3.54	3.62	0.98	[36]	2
6/kg, bid D1	IV (1 h)	9	100	28 (19–41)	73 (66–80)	D/A	16.2	13.2	1.23	5.12	4.70	1.09	[36]	3
3/kg, bid D2–9.5 (6/kg, bid D1)	IV (1 h)	9	100	28 (19–41)	73 (66–80)	D/A	15.2	13.3	1.14	3.39	3.06	1.11	[36]	4
3/kg, bid D2–7 (6/kg bid D1)	IV (1 h)	14	100	26.5±1.48*	78.7±1.93*	D/A	17.3	13.9	1.24	3.64	3.00	1.21	[6]	5
200, bid D8–13.5 (6/kg, bid D1; 3/kg, bid D2–7)	PO (–)	14	100	26.5±1.48*	78.7±1.93*	D/A	13.7	9.77	1.40	2.17	1.89	1.15	[6]	6
4/kg, bid D2–7 (6/kg bid D1)	IV (1 h)	7	100	24.7±2.37*	73.2±2.12*	D/A	34.4	29.5	1.17	5.82	5.40	1.08	[6]	7
300, bid D8–13.5 (6/kg bid D1; 4/kg, bid D2–7)	PO (–)	7	100	24.7±2.37*	73.2±2.12*	D/A	20.6	30.9	0.67	2.95	4.84	0.61	[6]	8
5/kg, bid D2–7 (6/kg bid D1)	IV (1 h)	14	100	26.5±1.48*	78.7±1.93*	D/A	44.5	43.4	1.03	7.46	7.18	1.04	[6]	9
400, bid D8–13.5 (6/kg bid D1; 5/kg, bid D2–7)	PO (–)	14	100	26.5±1.48*	78.7±1.93*	D/A	31.8	37.6	0.85	4.48	5.27	0.85	[6]	10
100, sig	IV (4 h)	20	95	32 (23–52)	80.8±11.8*	E/A	3.25	2.63 <sup>a</sup>	1.24	0.51	0.48	1.06	[15]	11
400, sig	IV (2 h)	20	95	32 (23–52)	80.8±11.8*	E/A	16.5	21.1 <sup>a</sup>	0.78	3.14	3.73	0.84	[15]	12
400, sig	IV (4 h)	20	95	32 (23–52)	80.8±11.8*	E/A	16.1	18.8 <sup>a</sup>	0.86	2.23	2.67	0.84	[15]	13
400, sig	IV (6 h)	20	95	32 (23–52)	80.8±11.8*	E/A	15.9	17.6 <sup>a</sup>	0.90	1.81	1.83	0.99	[15]	14
200, sig	IV (1.5)	52	100	26.9±4.9*	70.7±7.8*	E/A	7.53	8.13 <sup>a,♦</sup>	0.93	1.91	2.14 <sup>♦</sup>	0.89	[46]	15

Table 1 (continued)

Dose (mg)	Route	n	Male (%)	Age (years)	Weight (kg)	Use of dataset	Pred AUC (mg*h/L)	Obs AUC (mg*h/L)	Pred/Obs AUC	Pred C <sub>max</sub> (mg/L)	Obs C <sub>max</sub> (mg/L)	Pred/Obs C <sub>max</sub>	References	No. of data-sets
1.5/kg, qd D1	PO (-)	11	100	27 (20–45)	73 (60–90)	E/A	2.67	0.88	<b>3.03</b>	0.62	0.364	1.70	[47]	16
1.5/kg, tid D3–11.5 (1.5/kg, qd D1)	PO (-)	11	100	27 (20–45)	73 (60–90)	E/A	6.48	3.79	1.71	1.34	1.11	1.21	[47]	17
2/kg, qd D1	PO (-)	8	100	26 (20–36)	74 (66–89)	E/A	4.07	1.18	<b>3.45</b>	0.85	0.485	1.75	[47]	18
2/kg, bid D3–11.5 (2/kg, qd D1)	PO (-)	8	100	26 (20–36)	74 (66–89)	E/A	9.52	4.30	<b>2.21</b>	1.61	1.01	1.59	[47]	19
2/kg, qd D1	PO (-)	8	100	31 (21–44)	74 (64–87)	E/A	3.46	1.44	<b>2.40</b>	0.82	0.646	1.27	[47]	20
2/kg, tid D3–11.5 (2/kg, qd d1)	po(-)	8	100	31 (21–44)	74 (64–87)	E/A	9.23	9.04	1.02	1.88	2.18	0.86	[47]	21
3/kg, qd D1	PO (-)	8	100	25 (18–30)	73 (61–87)	E/A	5.65	3.15	1.79	1.22	1.19	1.03	[47]	22
3/kg, bid D3–11.5 (3/kg, qd D1)	PO (-)	8	100	25 (18–30)	73 (61–87)	E/A	15.4	11.2	1.38	2.50	2.36	1.06	[47]	23
4/kg, qd D1	PO (-)	8	100	25 (20–37)	74 (66–94)	E/A	7.67	5.90	1.30	1.35	1.57	0.86	[47]	24
4/kg, qd D3–11.5 (4/kg, qd D1)	PO (-)	8	100	25 (20–37)	74 (66–94)	E/A	14.3	13.2	1.08	1.98	2.07	0.96	[47]	25
200, bid D1–6.5	PO (-)	9	100	22 (19–25)	74 (67–91)	D/A	14.4	12.9	1.12	2.40	2.24	1.07	[37]	26
200, bid D1	PO (cap)	6	100	29 (23–36)	74 (67–82)	D/A	4.58	3.14	1.46	1.23	0.96	1.28	[38]	27
200, bid D2–6.5 (200, bid D1)	PO (cap)	6	100	29 (23–36)	74 (67–82)	D/A	12.0	12.5 <sup>a</sup>	0.96	2.20	2.04	1.08	[38]	28
400, qd D1	PO (-)	18	100	26 (20–40)	75 (66–92)	E/A	9.22	9.31	0.99	1.92	2.31	0.83	[48]	29
200, bid D2–9.5 (400, qd D1)	PO (-)	18	100	26 (20–40)	75 (66–92)	E/A	12.5	11.2	1.12	2.23	2.08	1.07	[48]	30

**Table 1** (continued)

Dose (mg)	Route	n	Male (%)	Age (years)	Weight (kg)	Use of dataset	Pred AUC (mg*h/L)	Obs AUC (mg*h/L)	Pred/Obs AUC	Pred C <sub>max</sub> (mg/L)	Obs C <sub>max</sub> (mg/L)	Pred/Obs C <sub>max</sub>	References	No. of data-sets
200, bid D2-4 (400, bid D1)	PO (-)	12	-	18-50	>40	E/A	12.4	15.2 <sup>a</sup> ♦	0.82	2.23	2.60♦	0.86	[49]	31
200, bid D22-24 (400, bid D21)	PO (-)	12	-	18-50	>40	E/A	12.0	13.6 <sup>a</sup> ♦	0.88	2.21	2.50♦	0.88	[49]	32
200, bid D2-2.5 (400, bid D1)	PO (tab)	13	100	31 (19-52)	78 (62-88)	E/A	13.0	26.5 <sup>a</sup> ♦	<b>0.49</b>	2.24	3.60♦	0.62	[50]	33
200, bid D2-2.5 (400, bid D1)	PO (tab)	16	100	40 (26-54)	80 (65-95)	E/A	13.1	26.8 <sup>a</sup> ♦	<b>0.49</b>	2.24	3.36♦	0.67	[50]	34
200, bid D1-6.5	PO (tab)	10	100	25 (20-30)	73 (62-85)	D/A	13.1	10.5	1.25	2.32	1.87	1.24	[51]	35
200, bid D1-6.5	PO (-)	12	100	29 (21-39)	75 (67-82)	D/A	12.1	13.6	0.89	2.19	2.25	0.97	[52]	36
200, bid D1-6.5	PO (-)	11	100	29 (20-42)	77 (61-91)	D/A	12.0	9.42	1.27	2.16	2.00	1.08	[53]	37
200, bid D2-3.5 (400, bid D1)	PO (-)	14	0	35 (19-51)	74 (52-87)	E/A	13.5	17.6 <sup>a</sup>	0.77	2.32	2.80	0.83	[54]	38
200, bid D2-2.5 (400, bid D1)	PO (tab)	16	100	34 (20-48)	79 (59-92)	E/A	13.0	26.3 <sup>a</sup> ♦	<b>0.49</b>	2.22	3.06♦	0.73	[55]	39
200, bid D2-3.5 (400, bid D1)	PO (-)	16	0	26 (19-36)	-	E/A	18.5	14.9♦	1.24	2.91	2.64♦	1.10	[56]	40
200, bid D2-3.5 (400, bid D1)	PO (-)	16	100	30 (20-42)	-	E/A	12.6	24.0♦	0.53	2.10	2.74♦	0.77	[57]	41

Table 1 (continued)

Dose (mg)	Route	<i>n</i>	Male (%)	Age (years)	Weight (kg)	Use of dataset	Pred AUC (mg*h/L)	Obs AUC (mg*h/L)	Pred/Obs AUC	Pred $C_{max}$ (mg/L)	Obs $C_{max}$ (mg/L)	Pred/Obs $C_{max}$	References	No. of datasets
200, bid D2–6.5 (400, bid D1)	PO (tab)	20	50	28 (20–43)	–	E/A	12.9	11.2	1.15	2.33	2.37	0.98	[58]	42
200, bid D2–7.5 (400, bid D1)	PO (–)	14	100	29 (18–45)	–	E/A	14.6	14.7 <sup>a,♦</sup>	0.99	2.47	2.87 <sup>♦</sup>	0.86	[59]	43
200, bid D2–3.5 (400, bid D1)	PO (–)	18	100	28 (20–40)	–	E/A	13.2	29.9 <sup>b,♦</sup>	<b>0.44</b>	2.25	3.96 <sup>♦</sup>	0.57	[60]	44
								GMFE (range)	1.39 (0.44–3.45)			1.20 (0.57–1.75)		
								Pred/Obs within twofold	36/44			44/44		

AUC values are reported as  $AUC_{\tau}$  unless otherwise specified

Observed aggregate values are reported as geometric mean if not specified otherwise

The ratios of predicted versus observed AUC and  $C_{max}$  outside the 0.5- to 2.0-fold limits are shown in bold

/kg per kilogram of body weight, *D* day of treatment according to the numbering in the reference, *sig* single dose, *qd* once daily, *bid* twice daily, *tid* three times daily, *IV* intravenously, *PO* orally, *E* datasets for model evaluation, *D* dataset for model development, *A* aggregate datasets, *tab* tablet, *cap* capsule, *Obs* observed aggregate value from the literature, *Pred* predicted value based on the model, *GMFE* geometric mean fold error, *CYP* cytochrome P450, *AUC* area under the concentration–time curve, – indicates not available, ♦ indicates arithmetic mean, \* indicates standard error

<sup>a</sup> $AUC_{obs}$

<sup>b</sup>AUC at steady state

**Table 2** Clinical studies with information on the CYP2C19 genotype used for voriconazole model development and evaluation

CYP2C19 genotype	Dose (mg)	Route	n	Male (%)	Age (years)	Weight (kg)	Use of dataset	Pred AUC (mg*h/L)	Obs AUC (mg*h/L)	Pred/Obs AUC	Pred C <sub>max</sub> (mg/L)	Obs C <sub>max</sub> (mg/L)	Pred/Obs C <sub>max</sub>	References	No. of datasets
RM (*1/*17, *17/*17)	50, sig	IV (2 h)	8	63	30 (24–53)	71 (55–96)	E/I	1.66	1.02	1.63	0.39	0.320	1.22	[24]	45
	50, sig	PO (tab)	8	63	30 (24–53)	71 (55–96)	E/I	1.08	0.40	<b>2.70</b>	0.27	0.167	1.62	[24]	46
	400, sig	IV (2 h)	7	71	30 (24–53)	73 (58–96)	E/I	17.5	16.5	1.06	3.49	3.29	1.06	[24]	47
	400, sig	PO (tab)	7	71	30 (24–53)	73 (58–96)	E/I	9.37	15.3	0.61	1.6	3.21	0.50	[24]	48
	400, sig	IV (2 h)	6	67	25 (23–28)	75 (61–93)	E/I	17.4	18.8	0.93	3.56	4.05	0.88	[18]	49
	400, sig	PO (tab)	6	67	25 (23–28)	75 (61–93)	D/I	10.3	13.6	0.76	1.66	2.90	0.57	[18]	50
	200, sig	PO (tab)	4	100	21 ± 2*	–	E/A	6.07	3.39	1.79	1.22	1.15	1.06	[61]	51
	400, sig	PO (cap)	3	0	29 (24–37)	69 (64–74)	E/I	13.9	15.9	0.87	1.83	2.97	0.62	[62]	52
	400, sig	PO (tab)	5	100	26 (24–31)	80 (71–87)	E/I	11.2	11.6	0.97	1.79	2.22	0.81	[63]	53
	400, sig	PO (cap)	8	100	27 (24–37)	–	E/A	12.0 <sup>a</sup>	13.3 <sup>a</sup>	0.90	1.69	2.16	0.78	[20]	54
								GMFE (range)		1.36 (0.61–2.70)			1.37 (0.50–1.62)		
NM (*1/*1)	50, sig	IV (2 h)	4	100	35 (24–46)	77 (65–86)	E/I	1.69	1.24	1.36	0.38	0.345	1.10	[24]	55
	50, sig	PO (tab)	3	100	35 (24–46)	77 (65–86)	E/I	1.12	0.53	<b>2.11</b>	0.27	0.167	1.62	[24]	56
	400, sig	IV (2 h)	4	100	35 (24–46)	77 (65–86)	E/I	18.1	21.4	0.85	3.33	3.61	0.92	[24]	57
	400, sig	PO (tab)	3	100	35 (24–46)	77 (65–86)	E/I	11.2	13.6	0.82	1.79	2.21	0.81	[24]	58
	200, sig	IV (1 h)	6	100	26.7 ± 2.9*	71.2 ± 4.3*	E/A	9.03 <sup>a</sup>	6.51 <sup>a</sup>	1.39	2.48	2.74	0.91	[19]	59
	200, qd D1	PO (–)	6	100	26.7 ± 2.9*	71.2 ± 4.3*	E/A	6.16 <sup>b</sup>	4.64 <sup>b</sup>	1.33	1.24	2.32	0.53	[19]	60
	200, bid D2–7 (200, qd D1)	PO (–)	6	100	26.7 ± 2.9*	71.2 ± 4.3*	E/A	16.4 <sup>b</sup>	19.3 <sup>b</sup>	0.85	2.41	3.21	0.75	[19]	61
	400, sig	IV (2 h)	2	50	31 (24–38)	76 (69–83)	E/I	19.9	18.8	1.06	3.28	4.05	0.81	[18]	62
	400, sig	PO (tab)	2	50	31 (24–38)	76 (69–83)	D/I	13.4	13.6	0.99	1.87	2.90	0.64	[18]	63
	200, sig	PO (tab)	7	100	22 ± 1.5*	59.4 ± 6.2*	E/A	6.04	5.16 <sup>♥</sup>	1.17	1.41	1.45 <sup>♥</sup>	0.97	[64]	64
	200, sig	PO (tab)	8	100	21 ± 2*	–	E/A	6.97	6.18	1.13	1.46	1.65	0.88	[61]	65
	200, bid D2–2.5 (400, bid D1)	PO (–)	24	83	27 (18–45)	69 (49–103)	E/A	13.9 <sup>b</sup>	12.9 <sup>b,♦</sup>	1.08	2.32	3.01 <sup>♦</sup>	0.77	[65]	66
	200, bid D2–3.5 (400, bid D1)	PO (–)	8	100	29 (22–43)	70 (56–77)	E/A	17.9 <sup>c</sup>	31.0 <sup>c,♦</sup>	0.58	2.75	4.02 <sup>♦</sup>	0.68	[31]	67
	400, sig	PO (tab)	4	100	25 (22–31)	78 (70–88)	E/I	11.5	16.9	0.68	1.69	3.11	0.54	[63]	68
400, sig	PO (cap)	5	100	28 (25–31)	78 (71–85)	E/I	12.0	15.9	0.75	1.69	2.97	0.57	[62]	69	



Table 2 (continued)

CYP2C19 genotype	Dose (mg)	Route	n	Male (%)	Age (years)	Weight (kg)	Use of dataset	Pred AUC (mg*h/L)	Obs AUC (mg*h/L)	Pred/Obs AUC	Pred C <sub>max</sub> (mg/L)	Obs C <sub>max</sub> (mg/L)	Pred/Obs C <sub>max</sub>	References	No. of datasets
	400, sig	PO (cap)	9	100	27 (22–31)	–	E/A	9.82 <sup>a</sup>	16.4 <sup>a</sup>	0.60	1.59	3.10	0.51	[20]	70
									GMFE (range)	1.31 (0.58–2.11)			1.38 (0.51–1.62)		
IM (*1/*2,*1/*3,*2/*17, *2/*2/*17)	50, sig	IV (2 h)	4	75	30 (25–34)	71 (56–78)	E/I	1.86	1.13	1.65	0.42	0.32	1.31	[24]	71
	50, sig	PO (tab)	4	75	30 (25–34)	71 (56–78)	E/I	1.29	0.58	<b>2.22</b>	0.31	0.22	1.41	[24]	72
	400, sig	IV (2 h)	4	75	30 (25–34)	71 (56–78)	E/I	22.8	25.0	0.91	3.70	3.82	0.97	[24]	73
	400, sig	PO (tab)	4	75	30 (25–34)	71 (56–78)	E/I	14.2	23.2	0.61	2.14	3.32	0.64	[24]	74
	200, sig	IV (1 h)	6	100	24.7±2.7*	74.2±7.3*	E/A	9.96 <sup>a</sup>	10.1 <sup>a</sup>	0.99	2.45	3.36	0.73	[19]	75
	200, qd D1	PO (–)	6	100	24.7±2.7*	74.2±7.3*	E/A	7.07 <sup>b</sup>	7.02 <sup>b</sup>	1.01	1.22	1.81	0.67	[19]	76
	200, bid D2–7 (200, qd D1)	PO (–)	6	100	24.7±2.7*	74.2±7.3*	E/A	29.7	42.4 <sup>b</sup>	0.70	3.50	5.78	0.61	[19]	77
	400, sig	IV (2 h)	8	63	26 (24–32)	76 (65–103)	E/I	22.9	37.4	0.61	3.53	4.33	0.82	[18]	78
	400, sig	PO (tab)	8	63	26 (24–32)	76 (65–103)	D/I	14.9	30.9	<b>0.48</b>	1.89	3.28	0.58	[18]	79
	400, sig	PO (tab)	5	100	27 (26–31)	80 (68–93)	E/I	12.8	22.2	0.58	1.79	3.15	0.57	[63]	80
PM (*2/*2, *2/*3,*3/*3)	400, sig	PO (cap)	8	78	26 (22–33)	76 (62–84)	E/I	15.6	20.7	0.75	1.83	2.85	0.64	[62]	81
	400, sig	PO (cap)	14	100	26 (22–33)	–	E/A	13.2 <sup>a</sup>	25.7 <sup>a</sup>	0.51	1.77	2.84	0.62	[20]	82
									GMFE (range)	1.51 (0.48–2.22)			1.46 (0.57–1.41)		
	50, bid D2–2.5 (100, bid D1)	PO	8	100	29 (24–45)	76 (68–102)	E/A	5.07 <sup>b</sup>	6.00 <sup>b,♦</sup>	0.85	0.72	0.760 <sup>♦</sup>	0.95	[65]	83
	200, sig	IV (1 h)	6	100	27.3±3.6*	68.9±3.5*	E/A	14.3 <sup>a</sup>	20.5 <sup>a</sup>	0.70	2.71	2.92	0.93	[19]	84
	200, qd D1	PO (–)	6	100	27.3±3.6*	68.9±3.5*	E/A	9.23 <sup>b</sup>	9.25 <sup>b</sup>	1.00	1.35	2.41	0.56	[19]	85
	200, bid D2–7 (200, qd D1)	PO	6	100	27.3±3.6*	68.9±3.5*	E/A	122 <sup>b</sup>	58.7 <sup>b</sup>	<b>2.08</b>	12.1	7.21	1.68	[19]	86
	400, sig	IV (2 h)	4	50	30 (20–37)	69 (58–79)	D/I	38.8	44.4	0.87	3.94	4.30	0.92	[18]	87
	400, sig	PO (tab)	4	50	30 (20–37)	69 (58–79)	D/I	25.2	41.6	0.61	2.08	3.91	0.53	[18]	88
	400, sig	PO (tab)	4	33	29 (19–37)	67 (47–85)	E/I	30.2	42.4	0.71	2.19	3.24	0.68	[62]	89
200, sig	PO (tab)	7	100	21.6±2.2*	58.4±8.1*	E/A	11.7	17.2 <sup>♥</sup>	0.68	1.7	1.36 <sup>♥</sup>	1.25	[64]	90	

**Table 2** (continued)

CYP2C19 genotype	Dose (mg)	Route	n	Male (%)	Age (years)	Weight (kg)	Use of dataset	Pred AUC (mg*h/L)	Obs AUC (mg*h/L)	Pred/Obs AUC	Pred C <sub>max</sub> (mg/L)	Obs C <sub>max</sub> (mg/L)	Pred/Obs C <sub>max</sub>	References	No. of datasets
	200, sig	PO (tab)	8	100	21 ± 2*	–	E/A	11.3	16.3	0.69	1.63	1.89	0.86	[61]	91
	200, bid	PO (–)	8	100	29 (22–43)	70 (56–77)	E/A	79.9 <sup>c</sup>	77.1 <sup>c,♦</sup>	1.04	8.76	10.9 <sup>♦</sup>	0.80	[31]	92
	D2–3.5 (400, bid D1)														
	400, sig	PO (cap)	4	100	31 (19–37)	–	E	25.0 <sup>a</sup>	45.7 <sup>a</sup>	0.55	2.26	3.13	0.72	[20]	93
									GMFE (range)	1.39 (0.55–2.08)			1.34 (0.53–1.68)		
									GMFE (range)	1.39 (0.48–2.70)			1.39 (0.50–1.68)		
									Pred/Obs within twofold	44/49			49/49		

AUC values are reported as AUC<sub>obs</sub> unless otherwise specified

Observed aggregate values are reported as arithmetic mean unless otherwise specified

*D* day of treatment according to the numbering in the reference, *sig* single dose, *qd* once daily, *bid* twice daily, *IV* intravenously, *PO* orally, *E* datasets for model evaluation, *D* datasets for model development, *I* individual datasets, *A* aggregate datasets, *tab* tablet, *cap* capsule, *Obs* observed aggregate value from the literature, *Pred* predicted value based on the model, *GMFE* geometric mean fold error, *RM* rapid metabolizers, *NM* normal metabolizers, *IM* intermediate metabolizers, *PM* poor metabolizers, *CYP* cytochrome P450, *AUC* area under the concentration–time curve, *C<sub>max</sub>* maximum concentration, – indicates not available, ♦ indicates geometric mean, ♥ indicates median, \* indicates standard deviation

The ratios of predicted versus observed AUC and C<sub>max</sub> outside the 0.5- to 2.0-fold limits are shown in bold

<sup>a</sup>AUC<sub>∞</sub>

<sup>b</sup>AUC<sub>τ</sub>

<sup>c</sup>AUC<sub>12</sub>

related to optimized parameters; (3) a strong influence on calculation methods used in the model; and (4) significant impact in the model.

$$S = \frac{\Delta AUC}{AUC} \div \frac{\Delta p}{p}, \quad (4)$$

where  $S$  is the sensitivity of AUC to the evaluated parameter,  $\Delta AUC$  is the change of AUC,  $AUC$  is the AUC with the initial value,  $\Delta p$  is the change of the assessed parameter value, and  $p$  is the parameter with the initial value. A sensitivity value of +1.0 means that a 10% change in the examined parameter causes a 10% alteration of the predicted  $AUC_{\tau}$ .

In addition, we evaluated the uncertainty of inhibitory parameters  $K_I$  and  $k_{inact}$  by Monte Carlo simulations. First, 1000 pairs of  $K_I$  and  $k_{inact}$  values were randomly sampled based on the normal distribution of  $k_{inact}$  of [point estimate and 95% confidence interval (CI)] 0.015 (0.011–0.019)  $\text{min}^{-1}$  and the log normal distribution of  $K_I$  of 9.33 (2.56–34.0)  $\mu\text{M}$ ; these 1000 pairs of parameters were then entered into the model to perform simulations of AUC and  $C_{max}$ . Two scenarios were simulated. Scenario A was oral treatment of voriconazole 400 mg twice daily on the first day followed by 200 mg twice daily for 2 weeks, which was considered to be sufficient to achieve steady-state.  $AUC_{\text{last-1\_last}}$  and  $C_{max}$  values of the last dosing interval were simulated. Scenario B was oral treatment of voriconazole 400 mg twice daily on the first day followed by 200 mg twice daily on the second day, and oral coadministration of midazolam 7.5 mg with the last dose of voriconazole.  $AUC_{\text{last}}$  and  $C_{max}$  values of voriconazole and midazolam for the last dose were simulated.

## 2.6 Virtual Population Characteristics

Based on the demographic characteristics from each clinical trial, virtual populations of 100 individuals were generated to quantitatively assess the variability of the predicted concentration–time datasets from the respective clinical trials. Information on age, body weight, body height and proportion of female participants was integrated into the software for each clinical trial. The default population variabilities for enzyme expression in PK-Sim<sup>®</sup> were used.

## 2.7 Model Applications

First, model-based simulations were performed according to the dosing regimens of the clinical trials in Table 1 to compare the predicted versus observed data, capturing the nonlinear PK of voriconazole including dose- and time-dependence. Second, different CYP2C19 genotype groups, i.e. RMs, NMs, intermediate metabolizers (IMs) and PMs were simulated respectively to depict the effect of genetic

polymorphisms of CYP2C19 on the metabolism of voriconazole in Table 2. Based on the PBPK model, we then explored the performance of various maintenance doses in different CYP2C19 genotype groups (RMs, NMs, and IMs). Virtual populations of 1000 individuals were generated based on the summary demographic characteristics from all clinical trials. The simulated dosing regimens were 400 mg twice daily on the first day, followed by 100–400 mg twice daily on the following days for 2 weeks, which was considered to be sufficient to achieve steady-state. The trough plasma concentration sample was simulated to be taken prior to the last dose. The probability of target attainment and of reaching potentially toxic  $C_{trough}$  values was calculated based on two different definitions of therapeutic ranges to reflect the heterogeneity of guidelines. Thus, a therapeutic target of  $C_{trough}$  at least 1 or 2 mg/L and at most 5 or 6 mg/L was defined. Third, the time course of active CYP3A4 content in both the liver and small intestine during voriconazole treatment was simulated based on the most frequent oral therapeutic dosing regimen of voriconazole, i.e. 400 mg twice daily on the first day and then 200 mg twice daily on the following days. Fourth, by connecting the PBPK models of midazolam (or alfentanil) and voriconazole, DDI models between voriconazole and the victim drugs were set up (see Table 3).

## 3 Results

### 3.1 In Vitro Assays

The results of the half maximal inhibitory concentration ( $IC_{50}$ ) shift assays indicated that voriconazole caused TDI on CYP3A4, with a 16-fold difference in the absence and presence of nicotinamide adenine dinucleotide phosphate (NADPH) (see Table 4), supporting TDI to be introduced into the PBPK model. In contrast, inhibition of CYP2C19 was only within a two/threefold range of  $IC_{50}$  shift and was therefore considered as negligible during model development. The inactivation kinetic assay gave a  $K_I$  of 9.33 (95% CI 2.56–34.0)  $\mu\text{M}$  and a  $k_{inact}$  of 0.0428 (95% CI 0.0171–0.107)  $\text{min}^{-1}$  for CYP3A4, which were used for the parameterization in the PBPK model (see Table 5).

### 3.2 Model Development and Evaluation

#### 3.2.1 Clinical Studies

Among all 93 concentration–time datasets of voriconazole from clinical trials, 21 were used for the model development and 72 were used for model evaluation (see Tables 1 and 2). The participants were all healthy volunteers, with an age range of 18–53 years and a body weight of 47–103 kg. CYP2C19 genotypes included 62 RMs (\*1/\*17, \*17/\*17),

**Table 3** DDI study dosing regimens, populations, and predicted and observed AUC and  $C_{max}$  ratios

Perpetrator (mg)	Victim	<i>n</i>	Male (%)	Age (years)	Weight (kg)	Use of dataset	Pred AUC ratio with/without VRZ (90% CI)	Obs AUC ratio with/without VRZ (90% CI)	Pred AUC ratio/Obs AUC ratio	Pred $C_{max}$ ratio with/without VRZ (90% CI)	Obs $C_{max}$ ratio with/without VRZ (90% CI)	Pred $C_{max}$ ratio/Obs $C_{max}$ ratio	References
Voriconazole 400 bid D1, 200 bid D2, PO	Alfentanil 0.02 mg/kg, IV	12	58	19–31	65–105	E/A	3.41 (1.69–5.28)	3.97 (3.39–4.66) <sup>a</sup>	0.86	–	–	–	[66]
Voriconazole 400 bid D1, 200 bid D2, PO	Midazolam 0.05 mg/kg, IV	10	100	19–26	65–100	E/I	3.95 (1.96–6.41)	3.61 (3.20–4.08) <sup>b</sup>	1.09	–	–	–	[23]
Voriconazole 400 bid D1, 200 bid D2, PO	7.5 mg, PO	10	100	19–26	65–100	E/I	7.51 (2.83–12.0)	9.85 (8.23–11.8) <sup>b</sup>	0.76	2.44 (1.90–3.44)	3.56 (2.85–4.44) <sup>b</sup>	0.69	[23]

Observed aggregated values are reported as geometric mean unless otherwise specified

VRZ voriconazole, *D* day of treatment according to the numbering in the reference, *bid* twice daily, *E* datasets for model evaluation, *I* individual datasets, *A* aggregate datasets, *IV* intravenously, *PO* orally, *Obs* observed aggregated value from the literature, *Pred* predicted value based on the model, *CI* confidence interval, *AUC* area under the concentration–time curve,  $C_{max}$  maximum concentration, *DDI* drug–drug interaction, – indicates not available

<sup>a</sup>AUC<sub>10</sub>

<sup>b</sup>AUC<sub>∞</sub>

**Table 4**  $IC_{50}$ ,  $IC_{50}$  shift,  $K_i$  assay results (point estimates with 95% confidence intervals)

Enzyme	Inhibitor	$IC_{50}$ ( $\mu$ M)	$K_i$ ( $\mu$ M)	$IC_{50}$ ( $\mu$ M)		$IC_{50}$ shift (fold difference)
				Without NADPH	With NADPH	
CYP3A4 (midazolam)	VRZ	6.04 (3.41–10.7)	0.470 (0.344–0.636)	48.7 (18.5–128)	3.00 (0.465–19.3)	16
	VRZ N-oxide	3.52 (2.08–5.95)	0.894 (0.650–1.22)	32.3 (21.1–49.4)	5.24 (0.814–33.7)	6
CYP2C19 (mephenytoin)	VRZ	17.1 (11.7–25.0)	1.08 (0.815–1.43)	47.6 (8.47–267)	24.1 (17.6–33.0)	2
	VRZ N-oxide	119 (49.0–289)	9.00 (6.94–11.7)	145 (71.6–295)	44.0 (26.8–72.4)	3
CYP2C19 (omeprazole)	VRZ	5.29 (3.98–7.02)	1.26 (0.839–1.82)	17.9 (11.9–27.1)	5.46 (1.10–27.0)	3
	VRZ N-oxide	40.4 (5.78–282)	7.43 (5.58–9.80)	121 (72.0–202)	21.0 (12.6–34.8)	6

The inactivity pre-incubation time was 30 min and the secondary activity incubation time was 10 min

VRZ voriconazole,  $K_i$  inhibition constant,  $IC_{50}$  half maximal inhibitory concentration of the inhibitor, NADPH nicotinamide adenine dinucleotide phosphate, CYP cytochrome P450

**Table 5** TDI  $K_i/k_{inact}$  assay conditions and results (point estimates with 95% confidence intervals)

Enzyme	Substrate	Voriconazole concentrations ( $\mu$ M)	Duration of pre-incubation (min)	Incubation time (min)	$K_i$ ( $\mu$ M)	$k_{inact}$ ( $\text{min}^{-1}$ )	$k_{inact}/K_i$ (mL/min/ $\mu$ mol)
CYP3A4	Midazolam	0, 4, 12, 40, 120, 400	0, 1, 3, 6, 12, 18, 24, 30	10	9.33 (2.56–34.0)	0.0428 (0.0171–0.107)	0.00459

$K_i$  inhibition concentration when reaching half of  $k_{inact}$ ,  $k_{inact}$  maximum inactivation rate constant, TDI time-dependent inhibition, CYP cytochrome P450

101 NMs (\*1/\*1), 77 IMs (\*1/\*2, \*1/\*3, \*2/\*17, \*2/\*2/\*17), and 65 PMs (\*2/\*2, \*2/\*3, \*3/\*3) (see Table 2). Administration protocols included both oral and intravenous routes, both single and multiple doses, and individual doses ranging from 1.5 to 6 mg/kg and from 50 to 400 mg.

### 3.2.2 Model Development

The input parameters describing the PBPK model of voriconazole are listed in Table 6.  $V_{max}$  for CYP3A4 was originally fixed to 0.31 pmol/min/pmol according to the reported value by Damle et al. [31]. However, simulations resulted in a more than twofold overprediction for AUC for low doses of voriconazole. The reasons for overprediction of AUC were explored. Simultaneous and separate optimization of  $V_{max}$  for CYP3A4 and CYP2C19 showed that the optimized value for CYP2C19 was approaching the value reported, while for CYP3A4, the optimized value was far higher than the reported value. A possible reason was that the reported value for CYP3A4 was obtained without consideration of TDI on CYP3A4, which might lead to underestimation of  $V_{max}$ . Furthermore, the subjects in the clinical studies belonged to different CYP2C19 genotypes, which provided the possibility to optimize the  $V_{max}$  of CYP3A4. Therefore, this parameter was optimized as 2.12 pmol/min/pmol based on the concentration–time datasets of CYP2C19 PMs with intravenous administration [18], assuming that only CYP3A4 mediated the metabolism of voriconazole in PMs due to the deficiency of CYP2C19. For other genotypes,

both CYP2C19 and CYP3A4 contributed to the metabolism of voriconazole. The different CYP2C19 genotypes were integrated into the model for RMs, NMs, IMs or PMs, with the reference CYP2C19 expression values of 0.79, 0.76, 0.40 and 0.01  $\mu$ mol/L, respectively [34]. Therefore, in the absence of evidence for another root cause of AUC overprediction, TDI of CYP3A4 by voriconazole was introduced into the model, assuming that it reflects MBI, with Eq. S4 in the ESM based on the in vitro inactivation kinetic parameter  $K_i$  of 9.33  $\mu$ M. When the in vitro  $k_{inact}$  of 0.0428  $\text{min}^{-1}$  served as the model input, the predicted concentration–time datasets of midazolam in DDI with co-treatment of voriconazole were overestimated. Therefore,  $k_{inact}$  was finally optimized as 0.015  $\text{min}^{-1}$  based on the concentration–time datasets with multiple intravenous dosing of voriconazole [36].

### 3.2.3 Model Evaluation

The predicted PK results for the respective clinical trials in comparison with the observed aggregate values are presented in Tables 1 and 2, together with administration protocols and subjects' details. Prediction performance of the model was quantitatively evaluated by the ratios of predicted versus observed aggregate AUC and  $C_{max}$  values, with calculated GMFEs being shown in Tables 1 and 2. Among the 28 test datasets for subjects with unspecified genotype, 71% of predicted/observed aggregate AUC ratios and all aggregate  $C_{max}$  ratios were within the 0.5- to 2.0-fold limits (Table 1). Taking the genotype of CYP2C19 into consideration, from

**Table 6** Physicochemical and PK parameters of the voriconazole PBPK model

Parameter	Units	Value used in the voriconazole model	Source of values	Description
MW	g/mol	349.3	349.3	Molecular weight
fu	%	42 [1, 31, 67, 68]	42 [1, 31, 67, 68]	Fraction unbound
log <i>P</i>		1.8 [31, 68]	1.75 [69], 1.65*, 1.8 [31, 68], 2.56 [67]	Lipophilicity
pKa		1.60 (base) [70]	1.60 [70], 1.76 [31, 67, 68], 12.71 (acidic)*, 2.27 (basic)*	Acid dissociation constant
Solubility (pH)	mg/mL	3.2 (1.0) [70], 2.7 (1.2) [71], 0.1 (7.0)*	0.2 [68], 0.0978*, 3.2 (1.0) [70], 2.7 (1.2) [71]	Solubility
Specific intestinal permeability	cm/s	$2.71 \times 10^{-4}$	Optimized, $2.81 \times 10^{-5}$ [31]	Normalized to surface area
Partition coefficients		Poulin and Theil [31, 67]	Poulin and Theil [31, 67]	Organ-plasma partition coefficients
Cellular permeabilities		PK-Sim standard	–	Permeation across cell membranes
CYP3A4 <i>K<sub>m</sub></i>	μmol/L	15 [31]	15 [31], 11 [31], $16 \pm 10$ [72], $11 \pm 3$ [72], 235 [13], $834.7 \pm 182.2$ [68]	Substrate concentration at which the reaction rate is half-maximal
CYP3A4 <i>k<sub>cat</sub></i>	min <sup>-1</sup>	2.12	Optimized, 0.31 [31], 0.1 [31], $32.2 \pm 28.4$ [68], $0.05 \pm 0.01$ [72], $0.10 \pm 0.01$ [72], 0.14 [13]	CYP3A4 catalytic rate constant <sup>#</sup>
CYP2C19 <i>K<sub>m</sub></i>	μmol/L	3.5 [31]	3.5 [31], $9.3 \pm 3.6$ [68], $14 \pm 6$ [72], 3.5 [13]	Substrate concentration at which the reaction rate is half-maximal <sup>#</sup>
CYP2C19 <i>k<sub>cat</sub></i>	min <sup>-1</sup>	1.19 [31]	1.19 [31], $40 \pm 13.9$ [68], $0.22 \pm 0.02$ [72], 0.39 [13]	CYP2C19 catalytic rate constant <sup>#</sup>
GFR fraction		1	–	Fraction of filtered drug reaching the urine
CYP3A4 <i>K<sub>I</sub></i>	μmol/L	9.33	In vitro result from this study	The inhibitor concentration when reaching half of <i>k<sub>inact</sub></i>
CYP3A4 <i>k<sub>inact</sub></i>	min <sup>-1</sup>	0.015	Optimized from in vitro results from this study (0.04)	The maximum inactivation rate constant
<i>D<sub>T,50</sub></i> for tablet	min	30	Optimized	Dissolution time when 50% of the substance dissolved
Shape factor for tablet		1.29	Optimized	Dissolution shape parameter for Weibull function

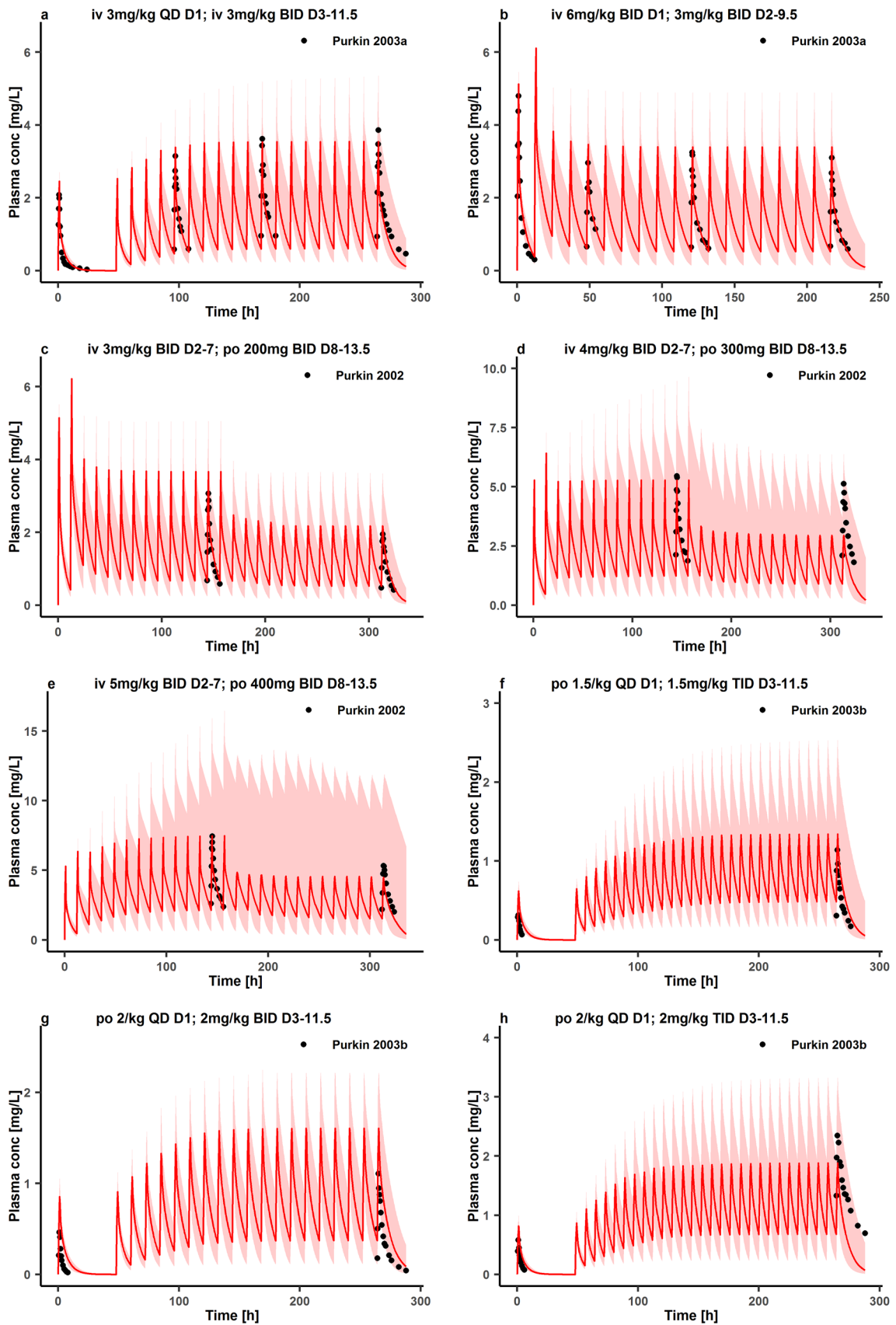
CYP cytochrome P450 (CYP3A4 *k<sub>cat</sub>* 2.12 min<sup>-1</sup> was optimized), GFR glomerular filtration rate, PK pharmacokinetics, PBPK physiologically based pharmacokinetic, PK pharmacokinetic, – indicates not available

\*Drug bank; all three reported solubility values were used for interpolation

<sup>#</sup>Values apply for global voriconazole metabolism via this enzyme irrespective of the metabolic pathway; specific intestinal permeability  $2.71 \times 10^{-4}$  cm/s was optimized

44 test datasets, 89% of aggregate AUC ratios and all aggregate *C<sub>max</sub>* ratios were within 0.5- to 2.0-fold (Table 2). In addition, 85% of predicted/observed aggregate *C<sub>trough</sub>* ratios from clinical trials after multiple administration were within the 0.5- to 2.0-fold range (Table S4 in the ESM). The performance of the model was visualized by comparing predicted and observed concentration–time datasets, as shown in Figs. 3 and 4, and in Figs. S1, S2 and S4–7 in the ESM. The model-based simulations for multiple doses captured the dose- and time-dependent nonlinear PK of voriconazole well (Fig. 3, and Figs. S1, S4, and S7 in the ESM). Although the

**Fig. 3** Prediction performance of the voriconazole PBPK model on aggregate plasma concentrations for multiple doses. Observed aggregate data reported in the literature are shown as a dot, triangle, square, cross, or crossed square [6, 36–38, 47–60]; population simulation medians are shown as lines; and the shaded areas illustrate the 68% population prediction intervals. Details of dosing regimens, study populations, and predicted versus observed PK parameters are summarized in Table 1. *D* day of treatment according to the numbering in the reference, *qd* once daily, *bid* twice daily, *tid* three times daily, *IV* intravenously, *PO* orally, *Plasma conc* voriconazole plasma concentration, *PBPK* physiologically based pharmacokinetic, *PK* pharmacokinetic





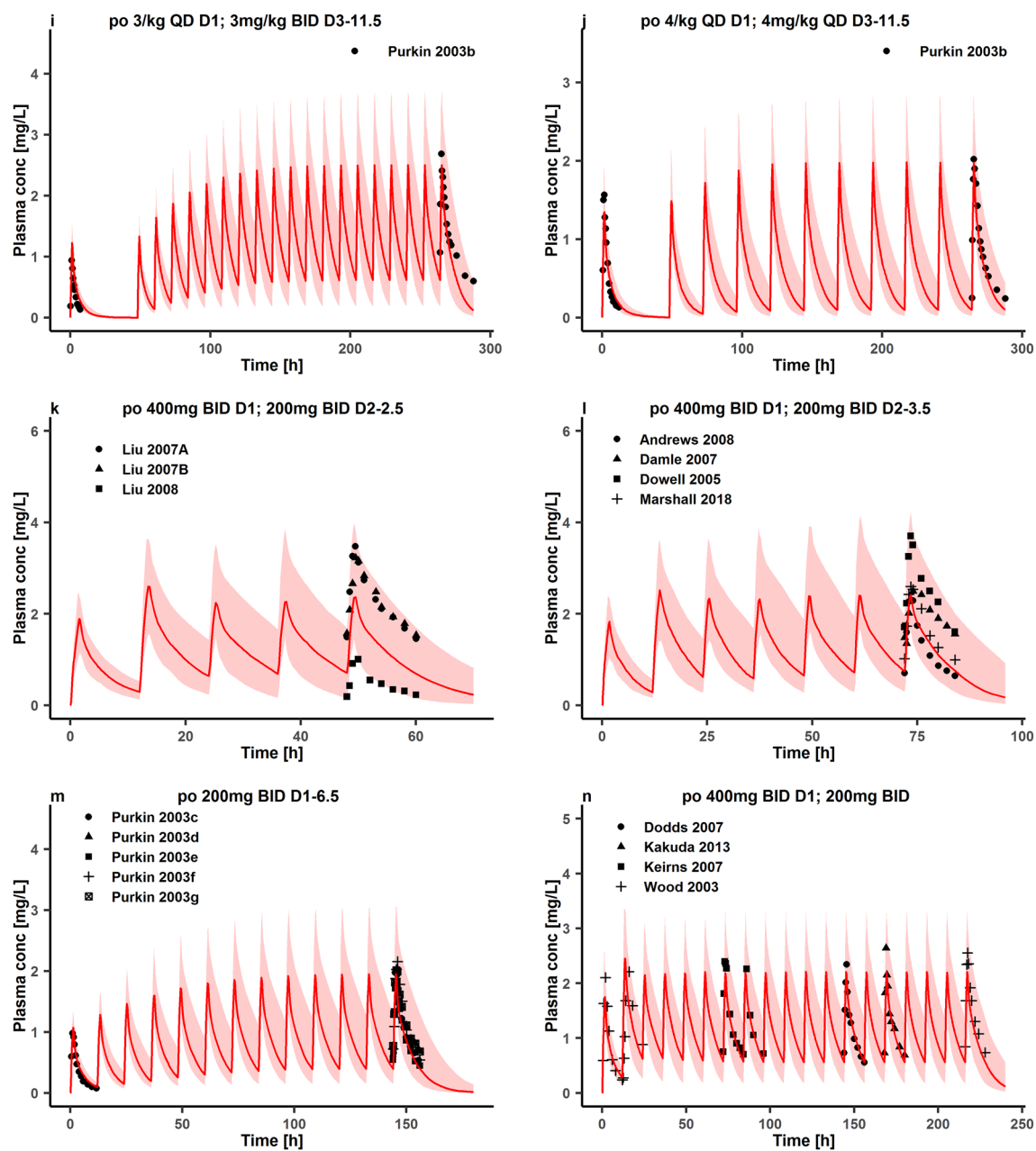
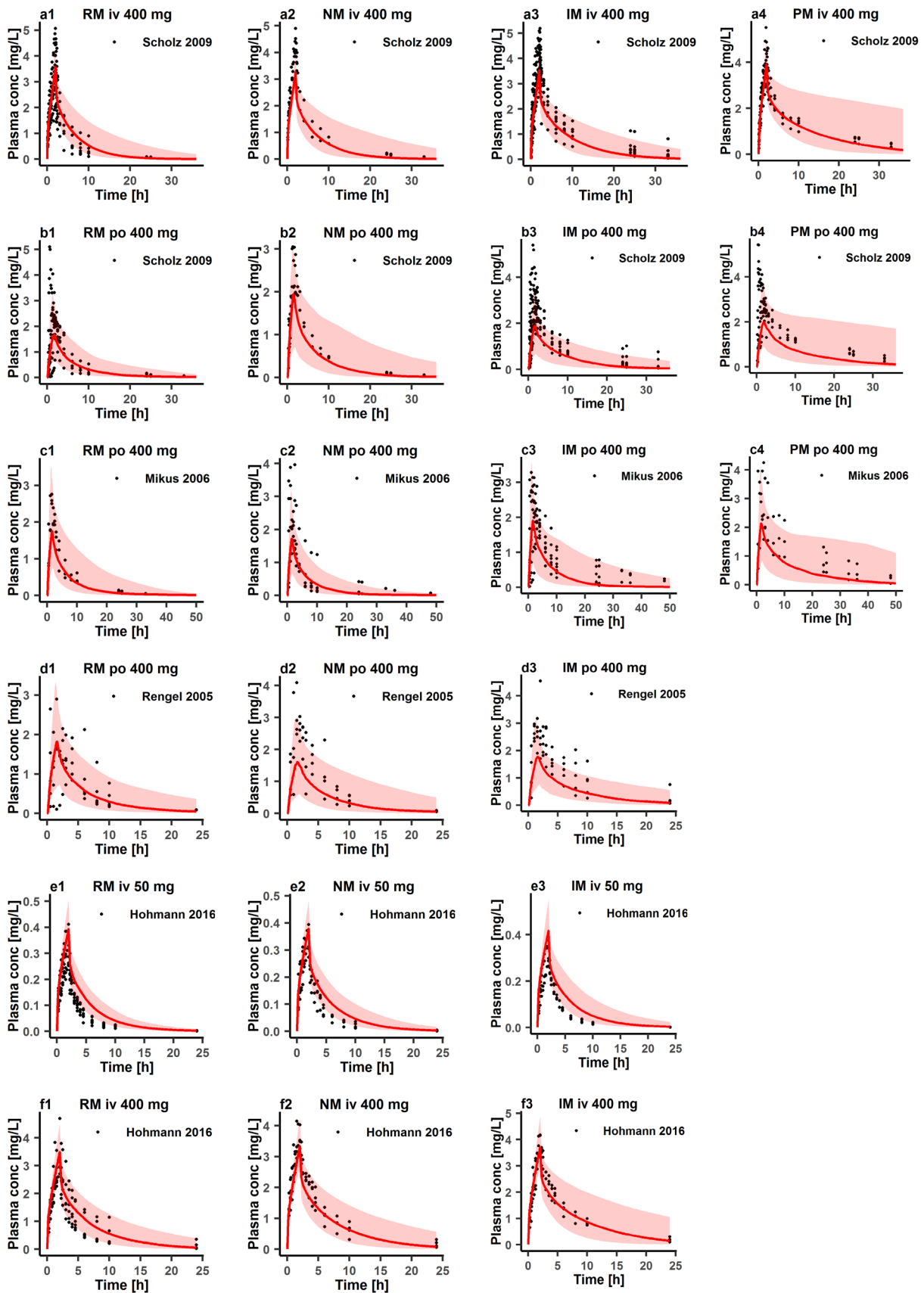


Fig. 3 (continued)

population predictions for low doses (i.e. 50 mg) reflected overestimation compared with the observed individual data, for the therapeutic dose of 400 mg the 95% prediction interval covered the variability of the observed individual data sufficiently (Fig. 4, and Fig. S5 in the ESM), indicating that simulations grouped by different CYP2C19 genotype were suitable to describe the effect of genetic polymorphisms of CYP2C19 on the metabolism of voriconazole. This was confirmed by the population predictions of observed aggregate concentration–time datasets for both single and multiple doses in different CYP2C19 genotype groups, despite

Fig. 4 Prediction performance of the voriconazole PBPK model on individual plasma concentrations in different CYP2C19 genotype groups for a single dose. Observed individual data reported in the literature are shown as dots [18, 24, 62, 63]; population simulation medians are shown as lines; and the shaded areas illustrate the 95% population prediction intervals. Details of dosing regimens, study populations, and predicted versus observed PK parameters are summarized in Table 2. *IV* intravenously, *PO* oral, *Plasma conc* voriconazole plasma concentration, *RM* rapid metabolizers, *NM* normal metabolizers, *IM* intermediate metabolizers, *PM* poor metabolizers, *Rengel* Rengelshausen, *PBPK* physiologically based pharmacokinetic, *PK* pharmacokinetic, *CYP* cytochrome P450





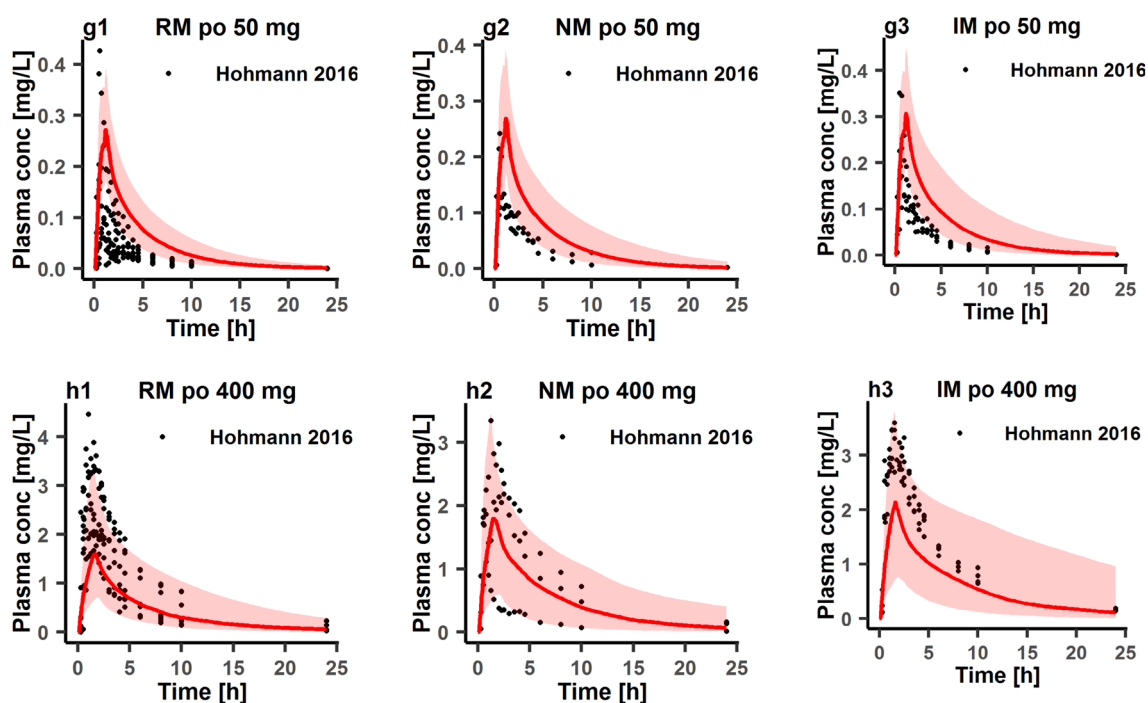


Fig. 4 (continued)

an overprediction of exposure for multiple doses in PMs (Figs. S2 and S7 in the ESM). Furthermore, plotting predicted versus observed AUC,  $C_{\max}$  and  $C_{\text{trough}}$  from all the clinical studies confirmed a good fit of the final PBPK model of voriconazole for most clinical trials (Fig. 5), while some overprediction of AUC values was present for low doses.

### 3.3 Sensitivity Analysis

A sensitivity analysis was performed based on the simulation of the therapeutic multiple oral dosing regimen (i.e. 400 mg twice daily on the first day and then 200 mg twice daily on the following days until reaching steady-state) to assess the impact of the parameters on the model. The voriconazole model was most sensitive to CYP2C19  $k_{\text{cat}}$ ,  $K_m$ , and fraction unbound values (all taken from the literature), with sensitivity values ranging from  $-1.08$  to  $0.75$  (Fig. S3a in the ESM). Analysis of the parameters for voriconazole/midazolam DDI models on the  $\text{AUC}_{\text{last}}$  of midazolam showed that sensitivity was most pronounced for midazolam lipophilicity, CYP3A4  $k_{\text{inact}}$  and  $K_I$  with the sensitivity values beyond  $-1.0$  or  $1.0$  (Fig. S3b in the ESM).

The assessment of the uncertainty of inhibitory parameters  $K_I$  and  $k_{\text{inact}}$  in scenario A showed that simulated  $\text{AUC}_{\text{tlast-1\_tlast}}$  of voriconazole was (point estimate and 90% CI)  $12.6$  ( $7.77$ – $16.4$ )  $\text{mg/L}\cdot\text{h}$  and  $C_{\max}$  was  $2.61$  ( $2.02$ – $3.01$ )  $\text{mg/L}$ , corresponding to a 90% CI of  $61.6$ – $130\%$  of the point estimate for  $\text{AUC}_{\text{tlast-1\_tlast}}$  and  $77.4$ – $115\%$  for

$C_{\max}$ . The simulation of scenario B resulted in voriconazole  $\text{AUC}_{\text{last}}$  values of  $14.1$  ( $7.67$ – $22.3$ )  $\text{mg/L}\cdot\text{h}$  and  $C_{\max}$  values of  $2.46$  ( $1.86$ – $3.05$ )  $\text{mg/L}$ ; and midazolam  $\text{AUC}_{\text{last}}$  values of  $0.753$  ( $0.227$ – $1.84$ )  $\text{mg/L}\cdot\text{h}$  and  $C_{\max}$  values of  $0.121$  ( $0.0751$ – $0.149$ )  $\text{mg/L}$ . This corresponded to relative 90% CIs for voriconazole  $\text{AUC}_{\text{last}}$  of  $54.4$ – $158\%$  and  $C_{\max}$  of  $75.6$ – $124\%$ ; and for midazolam  $\text{AUC}_{\text{last}}$  of  $30.3$ – $244\%$  and  $C_{\max}$  of  $62.1$ – $123\%$  of the respective point estimates.

### 3.4 Model Application

#### 3.4.1 Suitable Maintenance Doses in CYP2C19 Genotype Groups

A separate simulation of specific CYP2C19 genotype groups could reasonably describe both observed individual and aggregate concentration–time datasets for either a single dose or multiple doses, as assessed by the respective criteria (Table 2 and Fig. 3, and Figs. S2, S5, and S7 in the ESM). Therefore, model-based simulations were carried out to explore the performance of voriconazole maintenance doses for different CYP2C19 genotypes (Fig. 8). The standard dosage (oral 400 mg twice daily on the first day and 200 mg twice daily for the following days) was confirmed to be appropriate for IMs, while for RMs and NMs, the 200 mg maintenance dose provided an insufficient exposure, with a probability of target attainment of  $<30\%$ . The results of model-based simulations showed that doubling

**Fig. 5** Goodness-of-fit plot of the PBPK model of voriconazole. Predicted versus observed aggregate AUC (**a**),  $C_{max}$  (**b**), and  $C_{trough}$  (**c**) of voriconazole from all clinical studies. The identity line and 0.5- to 2.0-fold acceptance limits are shown as solid and dashed lines, respectively. Different colors represent different clinical trials. “\*” after the study name shows that different genotype groups are displayed in the study. *PBPK* physiologically based pharmacokinetic, *AUC* area under the concentration–time curve,  $C_{max}$  maximum concentration,  $C_{trough}$  trough concentration

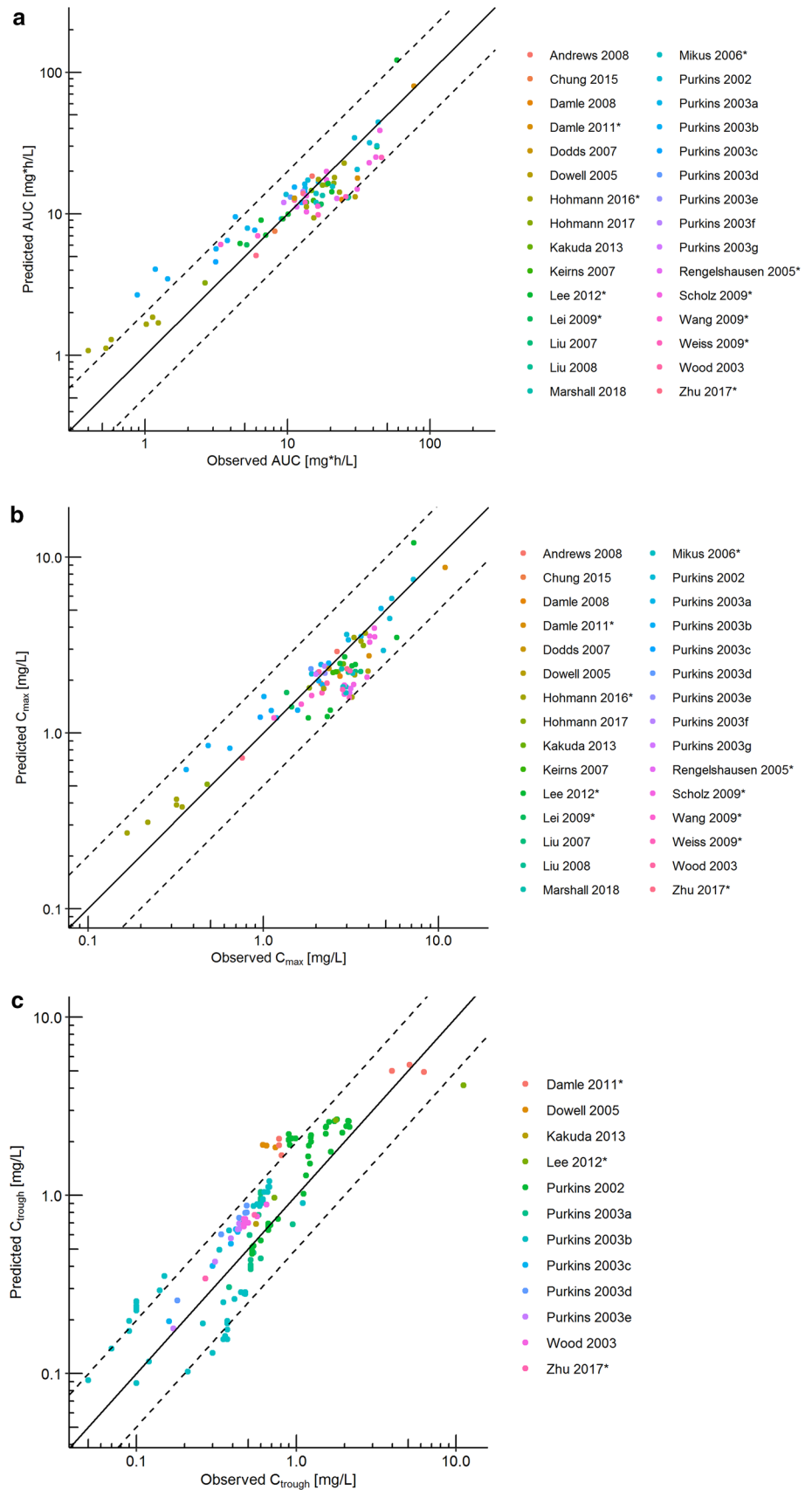
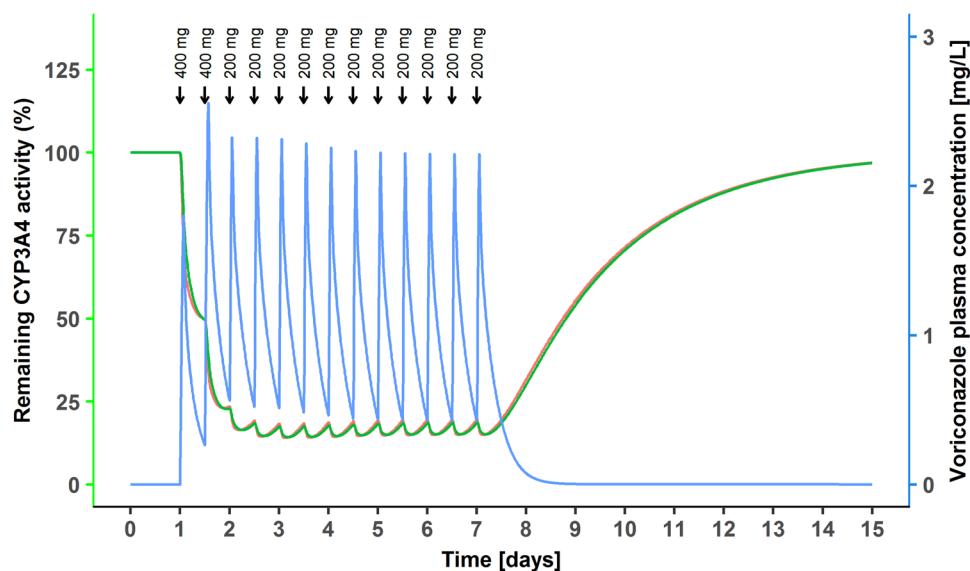


**Fig. 6** Effect of therapeutic multiple oral dosings of voriconazole on hepatic and small intestinal CYP3A activity. Predicted change of relative hepatic (green line) and small intestinal (red line) CYP3A activity over time after therapeutic multiple oral dosings of voriconazole. The blue line represents voriconazole plasma concentration, and arrows indicate dosing events of a standard therapeutic dosing schedule for oral voriconazole. CYP cytochrome P450



the maintenance dose for RMs and NMs could increase the probability of target attainment twofold while maintaining a probability of reaching toxic concentrations below 20%. The less reliable prediction for multiple doses in PMs precludes the suggestion of an appropriate maintenance dose regimen in PMs, although it clearly shows that the 200 mg twice daily dose is too high.

### 3.4.2 Inhibition of CYP3A4 by Voriconazole

The time courses of CYP3A4 activity in both the liver and small intestine were assessed during long-term voriconazole treatment. The maximum inhibition was reached at 51.2 h in the liver and 52.5 h in the small intestine (Fig. 6), resulting from the combination of the physiological CYP3A4 turnover and TDI (in our model, MBI) of CYP3A4 (Eq. S4 in the ESM). The CYP3A activity was predicted to recover 90% of its baseline 5 days after the last voriconazole dose.

### 3.4.3 Drug–Drug Interaction Modeling

The CYP3A4 inhibition model of voriconazole was further applied to the DDI between CYP3A4 probe substrates as victims (midazolam and alfentanil) and voriconazole as the perpetrator. Figure 7, and Fig. S8 in the ESM, demonstrate the good performance of DDI PBPK models for voriconazole and the two probe substrates. The observed AUC change of substrates during co-treatment with voriconazole was inside the 90% CI of the predicted AUC change. For alfentanil, the predicted/observed DDI AUC ratio of alfentanil was 0.86, indicating that this inhibition model was appropriate (Table 3). The inhibition model was further confirmed to be suitable by the predicted/observed midazolam DDI

AUC ratios of 1.09 and 0.76, respectively, for intravenous and oral administration of midazolam (Table 3).

## 4 Discussion

A whole-body PBPK model of voriconazole integrating TDI of CYP3A4 has been successfully developed. Model-based simulations of voriconazole plasma concentrations were in good agreement with observations from clinical studies with both intravenous and oral administration of a wide range of single and multiple doses. The model was also appropriate to predict voriconazole plasma concentrations for individual CYP2C19 genotype groups and the extent of DDIs with the CYP3A4 probe substrates midazolam and alfentanil caused by voriconazole.

Several lines of evidence supported that the incorporation of TDI should be considered to accurately describe the PK of voriconazole. First, Mikus and colleagues proposed that ‘autoinhibition’ of CYP3A was the key to explaining the observed dose nonlinearity of voriconazole elimination after administration of 50 and 400 mg in healthy volunteers [15, 24]. Second, time-dependent disproportionately increasing exposure of voriconazole was found in vivo after multiple doses, e.g. AUC for multiple intravenous administration (3 mg kg<sup>-1</sup> over 1 h once on the first day and twice daily on the following days) on the fifth day of treatment was more than twofold higher than the predicted value based on the results for the first dose under the assumption of dose-linearity, and continued to increase until the 12th-day doses [36]. Third, both Friberg et al. and Kim et al. integrated ‘time-dependent inhibition’ or ‘autoinhibition’ in their models to describe the respective processes regarding enzyme inhibition by voriconazole in vivo [25, 26]. Fourth, our

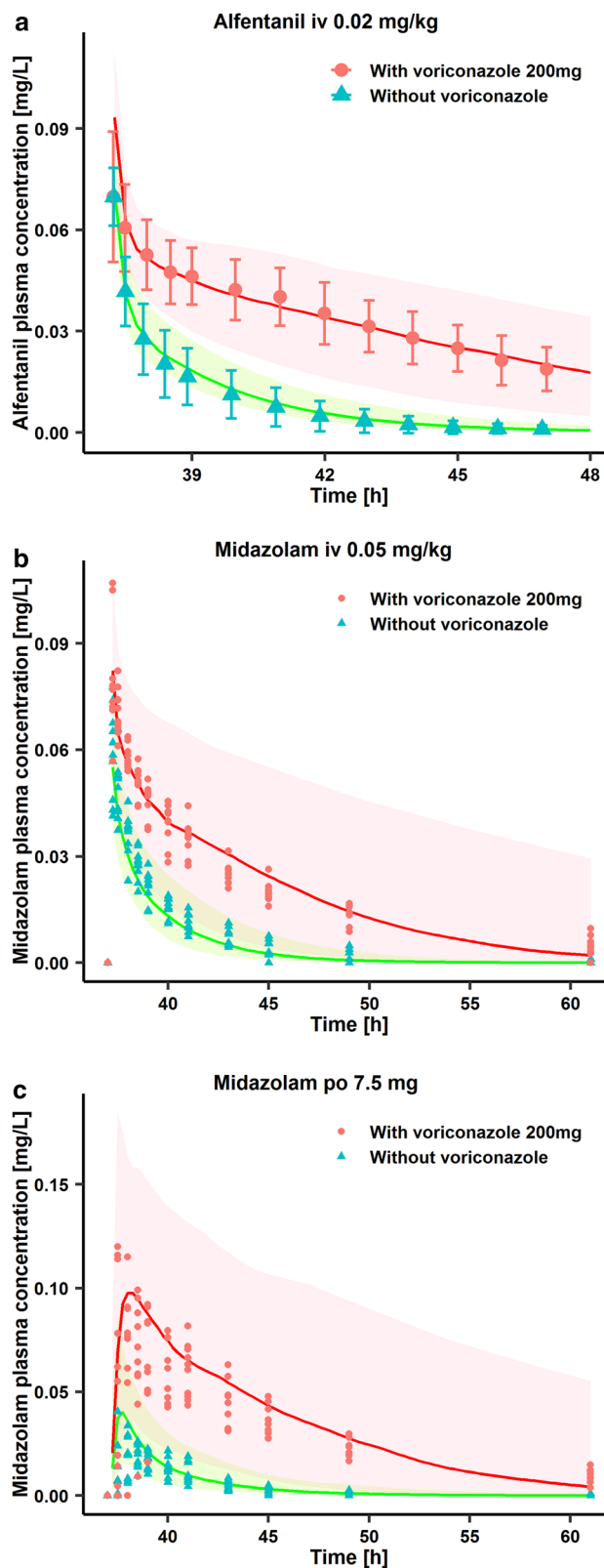
**Fig. 7** Prediction performance of voriconazole PBPK model in DDIs with CYP3A4 probe substrates. The voriconazole model integrated with the models of CYP3A4 probe substrates predicted inhibitory effects of voriconazole on CYP3A4 in vivo. Population predictions of **a** alfentanil or **b**, **c** midazolam plasma concentration–time datasets, with and without voriconazole treatment, were compared with observed data shown as green triangles (control), red dots (voriconazole coadministration) or symbols  $\pm$ SD [23, 66]. Population simulation medians are shown as green lines (control) or red lines (voriconazole coadministration), and the shaded areas illustrate the respective **a** 68% and **b**, **c** 95% population prediction intervals. Details of dosing regimens, study populations, and predicted and observed DDI AUC ratios and  $C_{max}$  ratios are summarized in Table 3. *IV* intravenously, *PO* orally, *PBPK* physiologically based pharmacokinetic, *DDI* drug–drug interactions, *CYP* cytochrome P450, *SD* standard deviation, *AUC* area under the plasma concentration–time curve,  $C_{max}$  maximum concentration

in vitro assays clearly showed a pronounced  $IC_{50}$  shift from 48.7 to 3  $\mu$ M, verifying TDI of CYP3A4 by voriconazole (Table 4). Indeed, incorporation of TDI (assuming MBI) into the PBPK model turned out to be essential to predict the dose- and time-dependent PK nonlinearity of voriconazole.

Beyond TDI, reversible inhibition of CYP3A4 and CYP2C19 by voriconazole was also explored. Our in vitro assay resulted in a competitive inhibition of CYP3A4  $K_i$  of 0.47 (95% CI 0.344–0.636)  $\mu$ M, which is in agreement with the results from other studies, e.g. competitive inhibition ( $K_i=0.66$   $\mu$ M) and noncompetitive inhibition ( $K_i=2.97$   $\mu$ M) in one study [21], and solely competitive inhibition ( $K_i=0.15$   $\mu$ M) in another study [22]. However, in vivo evaluation of DDIs between voriconazole and midazolam indicated that assumption of a simple competitive inhibition only was explicitly not sufficient in vivo [42]. A TDI model of CYP3A was discussed in the previous research but was not incorporated due to a lack of in vitro data to support it. At that time, a hypothetical extra effect compartment was introduced to describe a time delay [42]. Thus, we conducted an in vitro assay to explore TDI of voriconazole on CYP3A4 to fully understand the metabolism of voriconazole.

Furthermore, our in vitro assay showed competitive inhibition of voriconazole on CYP2C19 with  $K_i$  values of 1.08 (95% CI 0.815–1.43)  $\mu$ M and 1.26 (95% CI 0.839–1.82)  $\mu$ M using omeprazole and mephenytoin as substrates, respectively (see Table 4), which could provide some evidence for DDIs between voriconazole and CYP2C19 probe substrates (e.g. omeprazole and mephenytoin). In vivo, voriconazole was reported to increase the  $C_{max}$  and  $AUC_{\tau}$  of omeprazole by 116% and 280% [43], respectively. However, detailed in vivo data were not available, which limited the evaluation of the PBPK DDI models between voriconazole and CYP2C19 substrates, which is one of the limitations of our PBPK model.

Beyond the effects of the parent drug, the inhibition of voriconazole N-oxide on CYP3A4 and CYP2C19 was also investigated. Although voriconazole N-oxide exhibited



reversible inhibition on both enzymes, the effects were weaker with  $K_i$  0.894 (95% CI 0.650–1.22) and 9.00 (95% CI 6.94–11.7)  $\mu$ M, respectively (see Table 4). Additionally,



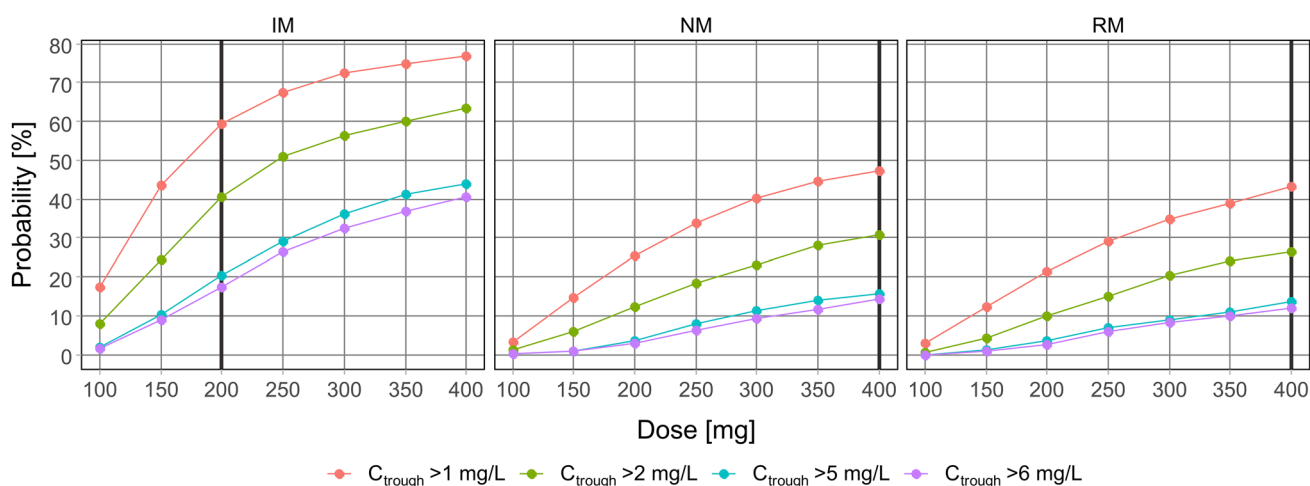


**Fig. 8** Probability of target attainment for therapeutic and toxic  $C_{trough}$  in different CYP2C19 genotype groups for long-term dosing. The simulated dosing regimens were 400 mg bid on the first day, followed by 100–400 mg bid on the following days for 2 weeks. The final trough plasma concentration sample was simulated to be taken prior to the last dose. Red and green lines represent the probability of therapeutic target attainment based on  $C_{trough}$  above 1 mg/L and above

2 mg/L, respectively. Blue and purple lines show the probability of toxicity target attainment based on  $C_{trough}$  above 5 mg/L and above 6 mg/L, respectively. Black lines show the optimal dose for each genotype group. *IM* intermediate metabolizers, *NM* normal metabolizers, *RM* rapid metabolizers,  $C_{trough}$  trough concentration, *CYP* cytochrome P450, *bid* twice daily

at therapeutic voriconazole doses, plasma concentrations of voriconazole N-oxide typically reach only about one-third compared with that of its parent drug [17]. Thus, the inhibition by voriconazole N-oxide would be much less than that of the parent drug and was considered negligible during PBPK model development.

The advantages of the PBPK model approach presented here becomes evident when compared with an empirical population PK model. PBPK models can provide a more precise mechanistic picture of inhibition processes. Based on the developed PBPK model, it was feasible to describe the time course of inhibition of CYP3A4 during and after voriconazole treatment by taking into account the dynamic nature of the inhibition process, with a clear differentiation between liver and small intestinal enzyme activity (Fig. 6). Furthermore, this PBPK model could be applied to predict the effect of voriconazole dosing schemes on other CYP3A4 substrate drugs, and to thus manage respective clinical DDIs. This was verified by the observation that the prediction of DDIs was mostly appropriate for oral and intravenous midazolam, as well as for alfentanil (Fig. 7, and Fig. S8 in the ESM), both being established CYP3A4 probe substrates [44].

For a thorough understanding of voriconazole PK, CYP2C19 genotype groups were another important factor during model development since the wide interindividual variability mainly results from differences in enzyme activity between CYP2C19 genotypes. Therefore, suitable maintenance doses for the CYP2C19 genotype groups (RMs, NMs, and IMs) were suggested based on simulations. For

PMs, the search for a dose to provide an appropriate exposure was less reliable due to the limited performance of the model for multiple doses in this genotype group. With TDI on CYP3A4 activity and deficiency of CYP2C19, voriconazole would accumulate in PMs and might reach extremely high concentrations after multiple administrations. However, the observations from one study showed that the increase of voriconazole concentrations in PMs after multiple doses was less than predicted (Fig. S2f in the ESM) [19], indicating that other elimination pathways may compensate and thus attenuate drug accumulation in the body. However, for PMs, the experimental data to quantitatively describe voriconazole PK in individuals were sparse, limiting the integration of more complex pathways.

Although the presented model performed well with respect to both single and multiple doses and in most CYP2C19 genotype groups (RMs, NMs, and IMs), it has several limitations. First is the assumption that only CYP3A4 and CYP2C19 mediate primary metabolism and elimination of voriconazole. This assumption may result in overestimation of the role of CYP3A4 and CYP2C19 activity; however, the consequence of ignoring FMO and CYP2C9 should be acceptable in most CYP2C19 genotypes (RMs, NMs, and IMs).  $K_m$  values for FMO1 and FMO3 are in the millimolar range (about 3 mM) [14], which is far beyond the concentrations reached in vivo. A contribution of CYP2C9 was identified in only one paper [13] with a small  $V_{max}$  value, which was not confirmed in other in vitro assays [13, 45]. Renal excretion of unchanged voriconazole is <2%, and primary metabolism by glucuronidation is also negligible [17].

Thus, it is reasonable to simplify the primary metabolism of voriconazole as depending on CYP3A4 and CYP2C19 only. In addition, the fact that our model was able to properly describe most published data supports the pivotal role of CYP3A4 and CYP2C19 for overall voriconazole elimination. Another limitation is that the minor inhibitory effect of voriconazole N-oxide observed *in vitro*, as well as possible effects of other voriconazole metabolites, were not taken into account. In addition, we did not attempt to simultaneously describe the concentration–time datasets of voriconazole N-oxide and other metabolites (hydroxy-fluoropyrimidine voriconazole and dihydroxy-fluoropyrimidine voriconazole) reported in a few published studies to limit the complexity of the model and to limit the number of assumptions required. The third limitation was that during model development, datasets with low voriconazole doses, e.g. 50 mg, were not successfully integrated into the model. When extrapolating the model predictions to low dosages, the simulation showed some overprediction of voriconazole concentrations; however, such low doses are not clinically relevant. Fourth, based on the datasets of healthy volunteers, the model-based simulations provided suggestions for an appropriate dosage for CYP2C19 genotype subgroup (see Fig. 8). However, the applicability of modeling results for patients needs to be confirmed in future studies. Currently, therapeutic drug monitoring for voriconazole would be preferred for all patient subgroups to guarantee proper voriconazole concentrations in each patient. Fifth, while an all-embracing assessment of all uncertainties of input parameters on various potential model outcomes was not feasible, we performed an assessment of the uncertainty of the key parameters, i.e.  $K_1$  and  $k_{\text{inact}}$ . While the 90% CI of the resulting distribution for the exposure of voriconazole itself was within the 0.5- to 2-fold range of its median in the model, the respective simulated 90% CI for midazolam exposure slightly exceeded a twofold deviation from the median. However, in light of the observed high variability in exposure changes of midazolam when coadministered with voriconazole, we concluded that the uncertainty of the inhibitory parameters is acceptable in our model, in particular given the fact that a potential covariance of  $K_1$  and  $k_{\text{inact}}$  was neglected for parameter sampling. On the other hand, the need to optimize the experimentally obtained  $k_{\text{inact}}$  based on clinical data may also reflect the limitations of our *in vitro* experiments to quantitatively predict enzyme inhibition *in vivo*.

Although the current model successfully described the complex metabolism of voriconazole, we suggest to further verify the model by additional *in vitro* studies (e.g. elucidating the exact mechanism of TDI on CYP3A4) and clinical studies (e.g. studies quantifying the metabolites of voriconazole, i.e. voriconazole N-oxide, hydroxy-fluoropyrimidine voriconazole, and dihydroxy-fluoropyrimidine voriconazole in plasma/urine/feces; studies in PMs with low multiple

doses; and DDI studies between CYP3A4 substrates and voriconazole, including quantification of its metabolites and different routes of administration of both substrates and voriconazole).

## 5 Conclusions

TDI of CYP3A4 by voriconazole is an important PK characteristic of the drug and needs to be taken into account, along with the CYP2C19 genotype, to properly predict the exposure of voriconazole. By incorporating these elements, a PBPK model of voriconazole was developed that could accurately capture the time- and dose-dependent alterations of voriconazole PK, as well as DDIs caused by voriconazole inhibitory effects on CYP3A4. This model could support individual dose optimization of voriconazole, as well as DDI risk management. It will be provided as a public tool in the OSP repository (<http://www.open-systems-pharmacology.org/>) to assess the DDI potential of investigational drugs, support the design of clinical trials, or to expand the model for predictions in special populations.

## Compliance with Ethical Standards

**Funding** XL obtained financial support provided by the China Scholarship Council during the study and during manuscript preparation (No. 201406920024). TIS obtained a governmental research grant (#13821) from the Hospital District of South-West Finland to support his work.

**Conflict of interest** Sebastian Frechen is an employee and potential shareholder of Bayer AG, Leverkusen, Germany. Xia Li, Daniel Moj, Thorsten Lehr, Max Taubert, Chih-hsuan Hsin, Gerd Mikus, Pertti J. Neuvonen, Klaus T. Olkkola, Teijo I. Saari, and Uwe Fuhr have no conflicts of interest to declare.

## References


1. US FDA. Pfizer Label: voriconazole for injection, tablets, oral suspension: LAB-0271-12. US FDA; 2005.
2. Herbrecht R, Denning DW, Patterson TF, Bennett JE, Greene RE, Oestmann J-W, et al. Voriconazole versus amphotericin B for primary therapy of invasive aspergillosis. *N Engl J Med.* 2002;347:408–15.
3. Misch EA, Safdar N. Updated guidelines for the diagnosis and management of aspergillosis. *J Thorac Dis.* 2016;8:E1771–6.
4. Ullmann AJ, Aguado JM, Arikan-Akdagli S, Denning DW, Groll AH, Lagrou K, et al. Diagnosis and management of Aspergillus diseases: executive summary of the 2017 ESCMID-ECMM-ERS guideline. *Clin Microbiol Infect.* 2018;24:e1–38.
5. Theuretzbacher U, Ihle F, Derendorf H. Pharmacokinetic/pharmacodynamic profile of voriconazole. *Clin Pharmacokinet.* 2006;45:649–63.
6. Purkins L, Wood N, Ghahramani P, Greenhalgh K, Allen MJ, Kleiner D. Pharmacokinetics and safety of voriconazole following intravenous- to oral-dose escalation regimens. *Antimicrob Agents Chemother.* 2002;46:2546–53.

7. Owusu Obeng A, Egelund EF, Alsultan A, Peloquin CA, Johnson JA. CYP2C19 polymorphisms and therapeutic drug monitoring of voriconazole: are we ready for clinical implementation of pharmacogenomics? *Pharmacotherapy*. 2014;34:703–18.
8. Pascual A, Calandra T, Bolay S, Buclin T, Bille J, Marchetti O. Voriconazole therapeutic drug monitoring in patients with invasive mycoses improves efficacy and safety outcomes. *Clin Infect Dis*. 2008;46:201–11.
9. Jin H, Wang T, Falcione BA, Olsen KM, Chen K, Tang H, et al. Trough concentration of voriconazole and its relationship with efficacy and safety: a systematic review and meta-analysis. *J Antimicrob Chemother*. 2016;71:1772–85.
10. Hamada Y, Tokimatsu I, Mikamo H, Kimura M, Seki M, Takakura S, et al. Practice guidelines for therapeutic drug monitoring of voriconazole: a consensus review of the Japanese Society of Chemotherapy and the Japanese Society of Therapeutic Drug Monitoring. *J Infect Chemother*. 2013;19:381–92.
11. Ashbee HR, Barnes RA, Johnson EM, Richardson MD, Gorton R, Hope WW. Therapeutic drug monitoring (TDM) of antifungal agents: guidelines from the British Society for Medical Mycology. *J Antimicrob Chemother*. 2014;69:1162–76.
12. Chen K, Zhang X, Ke X, Du G, Yang K, Zhai S. Individualized medication of voriconazole: a practice guideline of the division of therapeutic drug monitoring. *Chinese Pharmacological Society. Ther Drug Monit*. 2018;40:663–74.
13. Hyland R, Jones BC, Smith DA. Identification of the cytochrome P450 enzymes involved in the N-oxidation of voriconazole. *Drug Metab Dispos*. 2003;31:540–7.
14. Yanni SB, Annaert PP, Augustijns P, Bridges A, Gao Y, Benjamin DK, et al. Role of flavin-containing monooxygenase in oxidative metabolism of voriconazole by human liver microsomes. *Drug Metab Dispos*. 2008;36:1119–25.
15. Hohmann N, Kreuter R, Blank A, Weiss J, Burhenne J, Haefeli WE, et al. Autoinhibitory properties of the parent but not of the N-oxide metabolite contribute to infusion rate-dependent voriconazole pharmacokinetics. *Br J Clin Pharmacol*. 2017;83:1954–65.
16. Roffey SJ, Cole S, Comby P, Gibson D, Jezequel SG, Nedderman ANR, et al. The disposition of voriconazole in mouse, rat, rabbit, guinea pig, dog, and human. *Drug Metab Dispos*. 2003;31:731–41.
17. Geist MJP, Egerer G, Burhenne J, Riedel K-D, Weiss J, Mikus G. Steady-state pharmacokinetics and metabolism of voriconazole in patients. *J Antimicrob Chemother*. 2013;68:2592–9.
18. Scholz I, Oberwittler H, Riedel K-D, Burhenne J, Weiss J, Haefeli WE, et al. Pharmacokinetics, metabolism and bioavailability of the triazole antifungal agent voriconazole in relation to CYP2C19 genotype. *Br J Clin Pharmacol*. 2009;68:906–15.
19. Lee S, Kim B-H, Nam W-S, Yoon SH, Cho J-Y, Shin S-G, et al. Effect of CYP2C19 polymorphism on the pharmacokinetics of voriconazole after single and multiple doses in healthy volunteers. *J Clin Pharmacol*. 2012;52:195–203.
20. Weiss J, ten Hoevel MM, Burhenne J, Walter-Sack I, Hoffmann MM, Rengelshausen J, et al. CYP2C19 genotype is a major factor contributing to the highly variable pharmacokinetics of voriconazole. *J Clin Pharmacol*. 2009;49:196–204.
21. Jeong S, Nguyen PD, Desta Z. Comprehensive in vitro analysis of voriconazole inhibition of eight cytochrome P450 (CYP) enzymes: major effect on CYPs 2B6, 2C9, 2C19, and 3A. *Antimicrob Agents Chemother*. 2009;53:541–51.
22. Yamazaki H, Nakamoto M, Shimizu M, Murayama N, Niwa T. Potential impact of cytochrome P450 3A5 in human liver on drug interactions with triazoles. *Br J Clin Pharmacol*. 2010;69:593–7.
23. Saari TI, Laine K, Leino K, Valtonen M, Neuvonen PJ, Olkkola KT. Effect of voriconazole on the pharmacokinetics and pharmacodynamics of intravenous and oral midazolam. *Clin Pharmacol Ther*. 2006;79:362–70.
24. Hohmann N, Kocheise F, Carls A, Burhenne J, Weiss J, Haefeli WE, et al. Dose-dependent bioavailability and CYP3A inhibition contribute to non-linear pharmacokinetics of voriconazole. *Clin Pharmacokinet*. 2016;55:1535–45.
25. Friberg LE, Ravva P, Karlsson MO, Liu P. Integrated population pharmacokinetic analysis of voriconazole in children, adolescents, and adults. *Antimicrob Agents Chemother*. 2012;56:3032–42.
26. Kim Y, Rhee S-J, Park WB, Yu K-S, Jang I-J, Lee S. A personalized CYP2C19 phenotype-guided dosing regimen of voriconazole using a population pharmacokinetic analysis. *J Clin Med*. 2019;8:227–41.
27. Li X, Frechen S, Moj D, Taubert M, Hsin C, Mikus G, et al. A physiologically-based pharmacokinetic model of voriconazole (abstract no. 8995). *Population Approach Group in Europe*; 2019. ISSN 1871-6032.
28. Davies B, Morris T. Physiological parameters in laboratory animals and humans. *Pharm Res*. 1993;10:1093–5.
29. Edginton AN, Schmitt W, Willmann S. Development and evaluation of a generic physiologically based pharmacokinetic model for children. *Clin Pharmacokinet*. 2006;45:1013–34.
30. Mordenti J. Man versus beast: pharmacokinetic scaling in mammals. *J Pharm Sci*. 1986;75:1028–40.
31. Damle B, Varma MV, Wood N. Pharmacokinetics of voriconazole administered concomitantly with fluconazole and population-based simulation for sequential use. *Antimicrob Agents Chemother*. 2011;55:5172–7.
32. Meyer M, Schneckener S, Ludewig B, Kuepfer L, Lippert J, Weinstein S. Using expression data for quantification of active processes in physiologically based pharmacokinetic modeling. *Drug Metab Dispos*. 2012;40:892–901.
33. Rodrigues AD. Integrated cytochrome P450 reaction phenotyping: attempting to bridge the gap between cDNA-expressed cytochromes P450 and native human liver microsomes. *Biochem Pharmacol*. 1999;57:465–80.
34. Shirasaka Y, Chaudhry AS, McDonald M, Prasad B, Wong T, Calamia JC, et al. Interindividual variability of CYP2C19-catalyzed drug metabolism due to differences in gene diplotypes and cytochrome P450 oxidoreductase content. *Pharmacogenomics J*. 2016;16:375–87.
35. Michaelis L, Menten ML, Johnson KA, Goody RS. The original Michaelis constant: translation of the 1913 Michaelis–Menten paper. *Biochemistry*. 2011;50:8264–9.
36. Purkins L, Wood N, Greenhalgh K, Eve MD, Oliver SD, Nichols D. The pharmacokinetics and safety of intravenous voriconazole—a novel wide-spectrum antifungal agent. *Br J Clin Pharmacol*. 2003;56:2–9.
37. Purkins L, Wood N, Kleinermans D, Love ER. No clinically significant pharmacokinetic interactions between voriconazole and indinavir in healthy volunteers. *Br J Clin Pharmacol*. 2003;56(Suppl 1):62–8.
38. Purkins L, Wood N, Kleinermans D, Greenhalgh K, Nichols D. Effect of food on the pharmacokinetics of multiple-dose oral voriconazole. *Br J Clin Pharmacol*. 2003;56:17–23.
39. Strom CM, Goos D, Crossley B, Zhang K, Buller-Burkle A, Jarvis M, et al. Testing for variants in CYP2C19: population frequencies and testing experience in a clinical laboratory. *Genet Med*. 2012;14:95–100.
40. European Medicines Agency. Guideline on the reporting of physiologically based pharmacokinetic (PBPK) modelling and simulation. EMA/CHMP/458101/2016. EMA; 2018.
41. Hanke N, Frechen S, Moj D, Britz H, Eissing T, Wendl T, et al. PBPK models for CYP3A4 and P-gp DDI prediction: a modeling network of rifampicin, itraconazole, clarithromycin, midazolam, alfentanil, and digoxin. *CPT Pharmacomet Syst Pharmacol*. 2018;7:647–59.



42. Frechen S, Junge L, Saari TI, Suleiman AA, Rokitta D, Neuvonen PJ, et al. A semiphysiological population pharmacokinetic model for dynamic inhibition of liver and gut wall cytochrome P450 3A by voriconazole. *Clin Pharmacokinet*. 2013;52:763–81.
43. Donnelly JP, De Pauw BE. Voriconazole—a new therapeutic agent with an extended spectrum of antifungal activity. *Clin Microbiol Infect*. 2004;10:107–17.
44. Fuhr U, Hsin C, Li X, Jabrane W, Sörgel F. Assessment of pharmacokinetic drug-drug interactions in humans: in vivo probe substrates for drug metabolism and drug transport revisited. *Annu Rev Pharmacol Toxicol*. 2019;59:507–36.
45. Schulz J, Kluwe F, Mikus G, Michelet R, Kloft C. Novel insights into the complex pharmacokinetics of voriconazole: a review of its metabolism. *Drug Metab Rev*. 2019;51:247–65.
46. Chung H, Lee H, Han H, An H, Lim KS, Lee Y, et al. A pharmacokinetic comparison of two voriconazole formulations and the effect of CYP2C19 polymorphism on their pharmacokinetic profiles. *Drug Des Dev Ther*. 2015;9:2609–16.
47. Purkins L, Wood N, Greenhalgh K, Allen MJ, Oliver SD. Voriconazole, a novel wide-spectrum triazole: oral pharmacokinetics and safety. *Br J Clin Pharmacol*. 2003;56(Suppl 1):10–6.
48. Wood N, Tan K, Purkins L, Layton G, Hamlin J, Kleinerms D, et al. Effect of omeprazole on the steady-state pharmacokinetics of voriconazole. *Br J Clin Pharmacol*. 2003;56(Suppl 1):56–61.
49. Keirns J, Sawamoto T, Holum M, Buell D, Wisemandle W, Alak A. Steady-state pharmacokinetics of micafungin and voriconazole after separate and concomitant dosing in healthy adults. *Antimicrob Agents Chemother*. 2007;51:787–90.
50. Liu P, Foster G, Gandelman K, LaBadie RR, Allison MJ, Gutierrez MJ, et al. Steady-state pharmacokinetic and safety profiles of voriconazole and ritonavir in healthy male subjects. *Antimicrob Agents Chemother*. 2007;51:3617–26.
51. Purkins L, Wood N, Ghahramani P, Kleinerms D, Layton G, Nichols D. No clinically significant effect of erythromycin or azithromycin on the pharmacokinetics of voriconazole in healthy male volunteers. *Br J Clin Pharmacol*. 2003;56:30–6.
52. Purkins L, Wood N, Kleinerms D, Nichols D. Histamine H<sub>2</sub>-receptor antagonists have no clinically significant effect on the steady-state pharmacokinetics of voriconazole. *Br J Clin Pharmacol*. 2003;56(Suppl 1):51–5.
53. Purkins L, Wood N, Ghahramani P, Love ER, Eve MD, Fielding A. Coadministration of voriconazole and phenytoin: pharmacokinetic interaction, safety, and toleration. *Br J Clin Pharmacol*. 2003;56(Suppl 1):37–44.
54. Marshall WL, McCrea JB, Macha S, Menzel K, Liu F, van Schanke A, et al. Pharmacokinetics and tolerability of letermovir coadministered with azole antifungals (posaconazole or voriconazole) in healthy subjects. *J Clin Pharmacol*. 2018;58:897–904.
55. Liu P, Foster G, LaBadie RR, Gutierrez MJ, Sharma A. Pharmacokinetic interaction between voriconazole and efavirenz at steady state in healthy male subjects. *J Clin Pharmacol*. 2008;48:73–84.
56. Andrews E, Damle BD, Fang A, Foster G, Crownover P, LaBadie R, et al. Pharmacokinetics and tolerability of voriconazole and a combination oral contraceptive co-administered in healthy female subjects. *Br J Clin Pharmacol*. 2008;65:531–9.
57. Damle B, LaBadie R, Crownover P, Glue P. Pharmacokinetic interactions of efavirenz and voriconazole in healthy volunteers. *Br J Clin Pharmacol*. 2008;65:523–30.
58. Dodds Ashley ES, Zaas AK, Fang AF, Damle B, Perfect JR. Comparative pharmacokinetics of voriconazole administered orally as either crushed or whole tablets. *Antimicrob Agents Chemother*. 2007;51:877–80.
59. Kakuda TN, Van Solingen-Ristea R, Aharchi F, De Smedt G, Witek J, Nijs S, et al. Pharmacokinetics and short-term safety of etravirine in combination with fluconazole or voriconazole in HIV-negative volunteers. *J Clin Pharmacol*. 2013;53:41–50.
60. Dowell JA, Schranz J, Baruch A, Foster G. Safety and pharmacokinetics of coadministered voriconazole and anidulafungin. *J Clin Pharmacol*. 2005;45:1373–82.
61. Wang G, Lei H, Li Z, Tan Z, Guo D, Fan L, et al. The CYP2C19 ultra-rapid metabolizer genotype influences the pharmacokinetics of voriconazole in healthy male volunteers. *Eur J Clin Pharmacol*. 2009;65:281–5.
62. Mikus G, Schöwel V, Drzewinska M, Rengelshausen J, Ding R, Riedel KD, et al. Potent cytochrome P450 2C19 genotype-related interaction between voriconazole and the cytochrome P450 3A4 inhibitor ritonavir. *Clin Pharmacol Ther*. 2006;80:126–35.
63. Rengelshausen J, Banfield M, Riedel K, Burhenne J, Weiss J, Thomsen T, et al. Opposite effects of short-term and long-term St John's wort intake on voriconazole pharmacokinetics. *Clin Pharmacol Ther*. 2005;78:25–33.
64. Lei H-P, Wang G, Wang L-S, Ou-yang D, Chen H, Li Q, et al. Lack of effect of ginkgo biloba on voriconazole pharmacokinetics in Chinese volunteers identified as CYP2C19 poor and extensive metabolizers. *Ann Pharmacother*. 2009;43:726–31.
65. Zhu L, Brüggemann RJ, Uy J, Colbers A, Hruska MW, Chung E, et al. CYP2C19 genotype-dependent pharmacokinetic drug interaction between voriconazole and ritonavir-boosted atazanavir in healthy subjects. *J Clin Pharmacol*. 2017;57:235–46.
66. Saari TI, Laine K, Leino K, Valtonen M, Neuvonen PJ, Olkkola KT. Voriconazole, but not terbinafine, markedly reduces alfentanil clearance and prolongs its half-life. *Clin Pharmacol Ther*. 2006;80:502–8.
67. Zane NR, Thakker DR. A physiologically based pharmacokinetic model for voriconazole disposition predicts intestinal first-pass metabolism in children. *Clin Pharmacokinet*. 2014;53(12):1171–82.
68. Qi F, Zhu L, Li N, Ge T, Xu G, Liao S. Influence of different proton pump inhibitors on the pharmacokinetics of voriconazole. *Int J Antimicrob Agents*. 2017;49(4):403–9.
69. Pfizer. Vfend: voriconazole for IV infusion safety data sheet. 2018. [https://pfe-pfizercom-prod.s3.amazonaws.com/products/material\\_safety\\_data/voriconazole\\_IV\\_infusion\\_22-mar-2018.pdf](https://pfe-pfizercom-prod.s3.amazonaws.com/products/material_safety_data/voriconazole_IV_infusion_22-mar-2018.pdf).
70. Pfizer Canada Inc. VFEND® voriconazole tablets 50 mg and 200 mg for injection 200 mg / vial (10 mg/mL when reconstituted) powder for oral suspension 3 g / bottle (40 mg/mL when reconstituted) submission control No: 196793. Kirkland, Quebec; 2016. [https://www.pfizer.ca/sites/default/files/201710/VFEND\\_PM\\_E\\_196793\\_23Sept2016.pdf](https://www.pfizer.ca/sites/default/files/201710/VFEND_PM_E_196793_23Sept2016.pdf).
71. Scientific Discussion-VFEND Procedure No. EMEA/H/C/387/X/09. [London]: London; 2004. [https://www.ema.europa.eu/en/documents/scientific-discussion-variation/vfend-h-c-387-x-0009-epar-scientific-discussion-extension\\_en.pdf](https://www.ema.europa.eu/en/documents/scientific-discussion-variation/vfend-h-c-387-x-0009-epar-scientific-discussion-extension_en.pdf).
72. Murayama N, Imai N, Nakane T, Shimizu M, Yamazaki H. Roles of CYP3A4 and CYP2C19 in methyl hydroxylated and N-oxidized metabolite formation from voriconazole, a new antifungal agent, in human liver microsomes. *Biochem Pharmacol*. 2007;73:2020–6.

## Affiliations

Xia Li<sup>1</sup>  · Sebastian Frechen<sup>2</sup> · Daniel Moj<sup>3</sup> · Thorsten Lehr<sup>3</sup> · Max Taubert<sup>1</sup> · Chih-hsuan Hsin<sup>1</sup> · Gerd Mikus<sup>4</sup> · Pertti J. Neuvonen<sup>5</sup> · Klaus T. Olkkola<sup>6</sup> · Teijo I. Saari<sup>7</sup> · Uwe Fuhr<sup>1</sup> 

✉ Uwe Fuhr  
uwe.fuhr@uk-koeln.de

<sup>1</sup> Department I of Pharmacology, Center for Pharmacology, Faculty of Medicine and University Hospital Cologne, University of Cologne, Gleueler Straße 24, 50931 Cologne, Germany

<sup>2</sup> Clinical Pharmacometrics, Bayer AG, Leverkusen, Germany

<sup>3</sup> Department of Pharmacy, Clinical Pharmacy, Saarland University, Saarbrücken, Germany

<sup>4</sup> Department of Clinical Pharmacology and Pharmacoepidemiology, University of Heidelberg, Heidelberg, Germany

<sup>5</sup> Department of Clinical Pharmacology, University of Helsinki and Helsinki University Hospital, Helsinki, Finland

<sup>6</sup> Department of Anaesthesiology, Intensive Care and Pain Medicine, University of Helsinki and Helsinki University Hospital, Helsinki, Finland

<sup>7</sup> Department of Anaesthesiology and Intensive Care, University of Turku and Turku University Hospital Turku, Turku, Finland

# **A Physiologically-Based Pharmacokinetic Model of Voriconazole Integrating Time-dependent Inhibition of CYP3A4, Genetic Polymorphisms of CYP2C19 and Predictions of Drug-Drug Interactions**

## **Supplementary document**

**Xia Li<sup>1</sup>, Sebastian Frechen<sup>2</sup>, Daniel Moj<sup>3</sup>, Thorsten Lehr<sup>3</sup>, Max Taubert<sup>1</sup>, Chih-hsuan Hsin<sup>1</sup>, Gerd Mikus<sup>4</sup>, Pertti J. Neuvonen<sup>5</sup>, Klaus T. Olkkola<sup>6</sup>, Teijo I. Saari<sup>7</sup>, Uwe Fuhr<sup>1</sup>**

1 University of Cologne, Faculty of Medicine and University Hospital Cologne, Center for Pharmacology, Department I of Pharmacology; Cologne, Germany;

2 Clinical Pharmacometrics, Bayer AG; Leverkusen, Germany;

3 Department of Pharmacy, Clinical Pharmacy, Saarland University; Saarbrücken, Germany;

4 Department of Clinical Pharmacology and Pharmacoepidemiology, University of Heidelberg; Heidelberg, Germany;

5 Department of Clinical Pharmacology, University of Helsinki and Helsinki University Hospital; Helsinki, Finland;

6 Department of Anaesthesiology, Intensive Care and Pain Medicine, University of Helsinki and Helsinki University Hospital, Helsinki, Finland;

7 Department of Anaesthesiology and Intensive Care, University of Turku and Turku University Hospital; Turku, Finland.

## **Corresponding author:**

Univ.-Prof. Dr. med. Uwe Fuhr

University of Cologne, Faculty of Medicine and University Hospital Cologne, Center for Pharmacology, Department I of Pharmacology; Gleueler Straße 24, 50931 Cologne, Germany

Email: [uwe.fuhr@uk-koeln.de](mailto:uwe.fuhr@uk-koeln.de)

Tel: +49-(0)-221-478-6672 (office), -5230 (direct line)

Fax: +49-(0)-221-478-7011

**Table of contents**

<b>1. METHODS</b>	<b>3</b>
1.1 <i>In vitro</i> assay for inhibition of CYP2C19 and CYP3A4 by voriconazole and its metabolite voriconazole-N-oxide	3
1.2 Time-dependent inhibition in the PBPK model	5
<b>2. RESULTS</b>	
Duration of incubation	6
<b>3. TABLES</b>	<b>7</b>
Table S1. Incubation conditions and $K_m$ results	7
Table S2. Incubation conditions and results for inhibition assay	7
Table S3. LC-MS/MS conditions	7
Table S4. Trough concentrations of voriconazole for multiple doses from clinical trials used for model evaluation	8
<b>4. FIGURES</b>	<b>12</b>
Figure S1 Prediction performance of voriconazole PBPK model on aggregate plasma concentrations for a single intravenous dose	12
Figure S2 Prediction performance of voriconazole PBPK model on aggregate plasma concentrations in different CYP2C19 genotype groups	13
Figure S3 Sensitivity analysis of voriconazole PBPK model	15
Figure S4 Prediction performance of voriconazole PBPK model on aggregate plasma concentrations for multiple doses (semi-logarithmic scale)	16
Figure S5 Prediction performance of voriconazole PBPK model on individual plasma concentrations in different CYP2C19 genotype groups for a single dose (semi-logarithmic scale)	18
Figure S6 Prediction performance of voriconazole PBPK model on aggregate plasma concentrations for a single intravenous dose (semi-logarithmic scale)	21
Figure S7 Prediction performance of voriconazole PBPK model on aggregate plasma concentrations in different CYP2C19 genotype groups (semi-logarithmic scale)	22
Figure S8 Prediction performance of voriconazole PBPK model in DDI with CYP3A4 probe substrates (semi-logarithmic scale)	25
<b>5. REFERENCE</b>	<b>26</b>

## 1 METHODS

### 1.1 *In vitro* assay for inhibition of CYP2C19 and CYP3A4 by voriconazole and its metabolite voriconazole-N-oxide

#### 1.1.1 Chemicals

Voriconazole, 1'-hydroxy-midazolam, and labetalol hydrochloride were purchased from Sigma-Aldrich (St Louis, MO, USA). Voriconazole N-oxide, (S)-mephenytoin, and (S)-4'-hydroxy-mephenytoin were obtained from Toronto Research Chemicals (North York, ON, Canada). Midazolam hydrochloride was bought from Rotexmedica GmbH Arzneimittelwerk (Trittau, SH, Germany). All chemicals and solvents were high-performance liquid chromatography (HPLC) grade. Human recombinant CYP3A4 and CYP2C19, human cytochrome P450 oxidoreductase and cytochrome b5, and the NADPH regenerating system were acquired from Corning Life Sciences (Tewksbury, MA, USA).

#### 1.1.2 General incubation conditions

According to the validated assays reported [1,2], incubations were carried out in 96-well polypropylene reaction plates on a heating block (ThermoStat plus, Eppendorf, Hamburg, Germany) at 37°C. The incubation solution contained 0.1 M phosphate buffer (pH 7.4), recombinant CYP3A4 (or CYP2C19), NADPH-regenerating system including NADP<sup>+</sup> (1.3 mM), glucose-6-phosphate (3.3 mM), glucose-6-phosphate-dehydrogenase (0.4 U/ml), magnesium chloride (3.3 mM), and substrates and /or inhibitors as applicable. Solvent (acetonitrile) concentration in the incubation solution was less than 2 % (v/v). The reactions were commenced by the addition of the NADPH regenerating system (5 µl) to a final incubation volume of 100 µl and terminated by adding 100 µl ice-cold acetonitrile. Thereafter, samples were centrifuged for 10 min at 16100 x g force. Finally, 100 µl of the supernatant was collected and mixed with 125 µl labetalol internal standard solution (1.83 µM aqueous solution) for LC-MS/MS analysis.  $K_m/V_{max}$  and  $IC_{50}$  assays were carried out in triplicate.  $K_i$  assays and time-dependent inhibition (TDI) assays ( $IC_{50}$  shift and  $K_I/k_{inact}$ ) were carried out in duplicate due to the large number of samples and the space limits of 96-well plates.

#### 1.1.3 Determination of $K_m$ values

To optimize substrate concentrations for the subsequent inhibition assays,  $K_m$  values were determined by incubating a range of substrate concentrations. First, based on the enzyme concentration recommended in literature [1], the recombinant enzyme at the protein concentration, as shown in **Table S1** was mixed with buffer and warmed up to 37°C. Then aliquots of the mixture (90 µl) were pipetted into each well of a 96-well plate on a heating block at 37°C, followed by adding 5 µl containing a range of six substrate concentrations. Two negative control samples were incubated in parallel, i.e., one without NADPH-regenerating system and one without enzyme.

#### 1.1.4 Determination of incubation time

The suitable duration of incubations was determined using linearity experiments measuring the formation of the major metabolites of the probe substrates versus incubation time (0-30 min). Substrate concentrations in these experiments were around  $K_m$ , as shown in **Table S2**.

### 1.1.5 Determination of IC<sub>50</sub> values

Reversible inhibition of voriconazole and voriconazole N-oxide on CYP3A4 and 2C19 were tested by IC<sub>50</sub> and  $K_i$  assays. IC<sub>50</sub> assays were carried out by incubating with a range of inhibitor concentrations (voriconazole or voriconazole N-oxide: 0  $\mu$ M and 1.2-400  $\mu$ M), together with the substrate (at concentrations around  $K_m$ ), enzyme and NADPH as shown in **Table S2**.

### 1.1.6 Determination of $K_i$ values

Based on the results from  $K_m$  and IC<sub>50</sub> determinations, we selected a range of substrate concentrations (shown in **Table S2**) and inhibitor concentrations (0 and about 0.25\*IC<sub>50</sub>, 0.5\*IC<sub>50</sub>, 1\*IC<sub>50</sub>, 2.5\*IC<sub>50</sub>, 5\*IC<sub>50</sub>, 10\*IC<sub>50</sub>) for the reversible inhibition  $K_i$  assay. Enzyme concentrations in the  $K_i$  assay were the same as in the IC<sub>50</sub> assay.

### 1.1.7 TDI to determinate IC<sub>50</sub> shift

To explore TDI of voriconazole and voriconazole N-oxide, IC<sub>50</sub> shift assays were carried out. These assays consisted of two periods, i.e., pre-incubation of inhibitor and enzyme for 30 min in the absence and presence of NADPH, respectively, followed by the substrate incubation period to measure remaining enzyme activity. In the first period, a range of concentrations of voriconazole (or voriconazole N-oxide) covering 0 and 0.1-fold to 10-fold IC<sub>50</sub> (see **Table S2**) were pre-incubated with recombinant CYP3A4 (or CYP2C19) at 37°C. Vehicle controls were included to account for any nonspecific decrease in enzyme activity during the incubation. For the second incubation period, the samples were diluted 10-fold for CYP3A4 and 5-fold for CYP2C19 prior to addition of the probe substrate (at concentrations around  $K_m$ ) to reduce the concentration of inhibitor and thereby to minimize its direct inhibitory effects. To have sufficient enzyme activity to be quantified after this dilution step, pre-incubations were carried out with 10-fold (for CYP3A4) and 5-fold (for CYP2C19) higher enzyme concentrations, aimed to be diluted accordingly in the second period.

### 1.1.8 TDI to determinate $K_I$ and $k_{inact}$

TDI was characterized additionally by the  $K_I/k_{inact}$  assay on CYP3A4. It was carried out in a similar way as the IC<sub>50</sub> shift assay. First, a range of concentrations of voriconazole (0, 4, 12, 40, 120, and 400  $\mu$ M) were pre-incubated with recombinant CYP3A4 and NADPH at 37°C. Then, at 0, 1, 3, 6, 12, 18, 24, 30 min, the preincubation samples were diluted 10-fold in the secondary incubation with midazolam (at a concentration around 10 fold  $K_m$ ) for 10 min.

### 1.1.9 Quantification of metabolites

The metabolites were quantified by LC-MS/MS with labetalol (1.83  $\mu$ M) as internal standard using an API 5000 with QJET™ Ion Guide (AB SCIEX, Concord, Ontario, Canada), a binary Agilent 1200 pump, an Agilent 1260 Infinity standard autosampler (Agilent Technologies Inc., Santa Clara, CA, USA) and Analyst software version 1.6.2 (AB SCIEX, Concord, Ontario, Canada). 20  $\mu$ L of sample was injected into a Nucleodur C18 Isis column (125 mm  $\times$  2 mm, 3  $\mu$ M) (Macherey-Nagel, Dueren, NW, Germany), eluted with the mobile phase consisting of: water with 0.1% formic acid (solvent A) and acetonitrile with 0.1% formic acid (solvent B) at a flow rate of 400  $\mu$ L/min. The column temperature was maintained at 40°C. The calibration standards and quality control samples were prepared by adding 10  $\mu$ L of the appropriate combined working solution to 90  $\mu$ L of 0.1 M phosphate buffer, then mixing with 100  $\mu$ L of acetonitrile. 100  $\mu$ L of the solution was then collected and spiked with 125  $\mu$ L

of aqueous IS working solution (1.83  $\mu\text{M}$  labetalol) and transferred to glass vials for LC-MS/MS analysis. The solvent concentration in calibration standards and quality control samples were the same as in the measured samples. Although calibration standards and quality control samples did not contain enzyme preparations, the protein effect could be considered as negligible due to the low respective protein concentration in incubation around 7 mg/L (as compared to about 70000 mg/L in human plasma). The analytical method was validated according to the European Medicines Agency guideline “Bioanalytical method validation, EMEA/CHMP/EWP/192217/2009 Rev. 1” [3]. Intra-day coefficients of variation were lower than 11.04% regarding relative standard deviation for the lowest quality control samples. The mean inaccuracy was lower than 5.27%. LC/MS/MS parameters, solvent gradient, and standard curve ranges are listed in **Table S3**. The lower limits of quantification for 1'-hydroxymidazolam, 4'-hydroxymephenytoin, and 5'-hydroxyomeprazole were 0.0111, 0.0111, and 0.0815  $\mu\text{M}$ , respectively.

### 1.1.10 Data analysis of *in vitro* assay

All *in vitro* assay datasets were analyzed using GraphPad Prism 7 (GraphPad, La Jolla, CA, USA) [4]. Point estimates with 95% confidence intervals (CIs) were estimated based on the single assay with triplicates.  $\text{IC}_{50}$  values were determined by regression analysis using the logarithm of inhibitor concentrations versus the percentage of the remaining enzyme activity after incubation. The data were fit to a standard sigmoidal curve.  $\text{IC}_{50}$  shift values were calculated as the ratio of the  $\text{IC}_{50}$  value acquired after pre-incubation for 30 min in the absence versus presence of NADPH.

For  $K_I/k_{inact}$  assays, the natural logarithm of percentage remaining activity of enzyme after the pre-incubation time was calculated by **Eq. S1** [5]. Plotting the value obtained by **Eq. S1** against the preincubation time resulted in a line and the negative slope of the line was defined as  $k_{obs}$ . Each inhibitor concentration produced the respective  $k_{obs}$ . Non-linear analysis for  $k_{obs}$  and respective inhibitor concentrations resulted in a Michaelis-Menten model to provide  $K_I$  and  $k_{inact}$  value according to **Eq. S2** [1].

$$\text{Eq.S1 } \ln \text{ of percentage remaining activity} = \ln \left( \frac{\text{activity with inhibitor treatment}_t}{\text{activity with vehicle}_t} \times 100 \right)$$

$$\text{Eq.S2 } k_{obs} = k_{obs|I=0} + \frac{k_{inact} * [I]}{K_I + [I]}$$

[I]: inhibitor concentration ( $\mu\text{M}$ );  $k_{obs}$ : inactivation rate constant at specific inhibitor concentration ( $\text{min}^{-1}$ );  $k_{obs|I=0}$ : inactivation rate constant in the absence of inhibitor ( $\text{min}^{-1}$ );  $k_{inact}$ : maximum time-dependent inactivation rate constant ( $\text{min}^{-1}$ );  $K_I$ : the inhibitor concentration when  $k_{obs}$  reaches half times of  $k_{inact}$  ( $\mu\text{M}$ ).

## 1.2 TDI incorporated as mechanism-based inactivation in the PBPK model

At the steady state and in the absence of an inhibitor, the amount of enzyme *in vivo* is constant at its expression site. The synthesis of CYP3A4 in the liver was calculated to be 0.08  $\mu\text{mol/L/h}$  with **Eq.S3** based on the reference

enzyme concentration of 4.32  $\mu\text{mol}$  CYP3A4/L liver tissue and the degradation  $K_{deg}$  of 0.019  $\text{hour}^{-1}$  in the liver (default value in PK-Sim®).

$$\text{Eq. S3 } R_0 = K_{deg} \times E_0$$

$R_0$ : zero-order synthesis rate of enzyme;  $E_0$ : the original amount of active enzyme;  $K_{deg}$ : first-order degradation rate of the enzyme.

However, in the presence of the inhibitor, enzyme degradation is accelerated. The rate of alteration of the enzyme is described by **Eq. S4**.

$$\text{Eq. S4 } \frac{dE_{(t)}}{dt} = R_0 - K_{deg} \times E_{(t)} - \frac{k_{inact} \times [I]}{K_I + [I]} \times E_{(t)}$$

$E_{(t)}$ : amount of active enzyme present at time  $t$ ;  $K_I$ : dissociation rate constant, obtained from *in vitro* experiments;  $k_{inact}$ : maximum inactivation rate constant, obtained from *in vitro* experiments and subsequently optimized based on multiple intravenous administration PK datasets.

## 2 RESULT DETAILS NOT REPORTED IN THE MAIN MANUSCRIPT

### 2.1 Duration of incubation

The formation of 1'-OH-midazolam was linear for the incubation of midazolam with CYP3A4 during 15 minutes, while the formation of 5-OH-omeprazole was linear for at least 20 minutes for the incubation of omeprazole with CYP2C19. Finally, 8 min was selected as the incubation time for CYP3A4, 20 min as the incubation time for CYP2C19 with omeprazole and 10 min with S-mephenytoin (in **Table S1**). We did not test S-mephenytoin separately but assumed sufficient metabolic stability of CYP2C19 based on the omeprazole experiment and on published data [5].



**Table S1. Incubation conditions and  $K_m$  results**

Enzyme	Substrate	Incubation time	Protein concentration	$K_m$	$V_{max}$
		<i>min</i>	<i>pmol/ml</i>	$\mu M$	<i>pmol/pmol P450/min</i>
CYP3A4	Midazolam	8	0.875	0.733(0.570-0.940)	25.1(23.4-26.9)
CYP2C19	S-Mephenytoin	10	4	23.0(19.0-27.9)	19.3(18.1-20.6)
CYP2C19	Omeprazole	20	4	2.26(1.63-3.11)	6.47(5.93-7.05)

$V_{max}$ : maximum reaction velocity;  $K_m$ : the substrate concentration at which the reaction rate is half of  $V_{max}$ .

**Table S2. Incubation conditions and results for inhibition assay**

Enzyme	Substrate	Protein concentration <sup>a</sup>	Substrate conc. range <sup>b</sup> used for $K_m$ , $V_{max}$ determination	Substrate conc. range <sup>c</sup> used for $K_i$ determination	Substrate conc. used for $IC_{50}$ , $IC_{50}$ shift determination	Substrate concentration used for $K_i$ , $k_{inact}$ determination
		<i>pmol/ml</i>	$\mu M$	$\mu M$	$\mu M$	$\mu M$
CYP3A4	Midazolam	8.75→0.875	0.156-10	0.3-10	0.73	7.3
CYP2C19	S-Mephenytoin	20→4	2.5-160	3-120	12	-
CYP2C19	Omeprazole	20→4	0.625-40	0.75-22.6	2.26	-

<sup>a</sup> Denotes protein concentrations used in the inactivation pre-incubations and after dilution in the activity incubations.

<sup>b</sup> Concentration range used to determine  $K_m$  and  $V_{max}$  values with six substrate concentrations evenly log-spaced over the range.

<sup>c</sup> Concentration range used to determine  $K_i$  values with six substrate concentrations evenly log-spaced over the range.

$V_{max}$ : maximum reaction velocity;  $K_m$ : the substrate concentration at which the reaction rate is half of  $V_{max}$ ;  $K_i$ : inhibitor constant;  $IC_{50}$ : half maximal inhibitory concentration of inhibitor;  $K_i$ : the inhibitor concentration when  $k_{obs}$  reaches half of  $k_{inact}$ ;  $k_{inact}$ : maximum time-dependent inactivation rate constant.

**Table S3. LC-MS/MS conditions**

Analyte	Mass transition	Standard curve range	Mode	CE	DP	LC gradient
		$\mu M$		<i>eV</i>	<i>eV</i>	<i>%B (min)</i>
1'-Hydroxmidazolam	341→324	0.0111-2.70	Positive	31	116	10(0)→10(1)→90(3)
4'-Hydroxymephenytoin	235→150	0.0111-2.70	Positive	29	121	→90(5)→10(5.1)→10(7)
5'-Hydroxyomeprazole	362→214	0.0815-1.98	Positive	19	116	

Solvent A was 0.1% formic acid in water; solvent B was 0.1% formic acid in acetonitrile.

CE, collision energy; DP, declustering potential; LC, liquid chromatography.

**Table S4 Trough concentrations of voriconazole for multiple doses from clinical trials used for model evaluation**

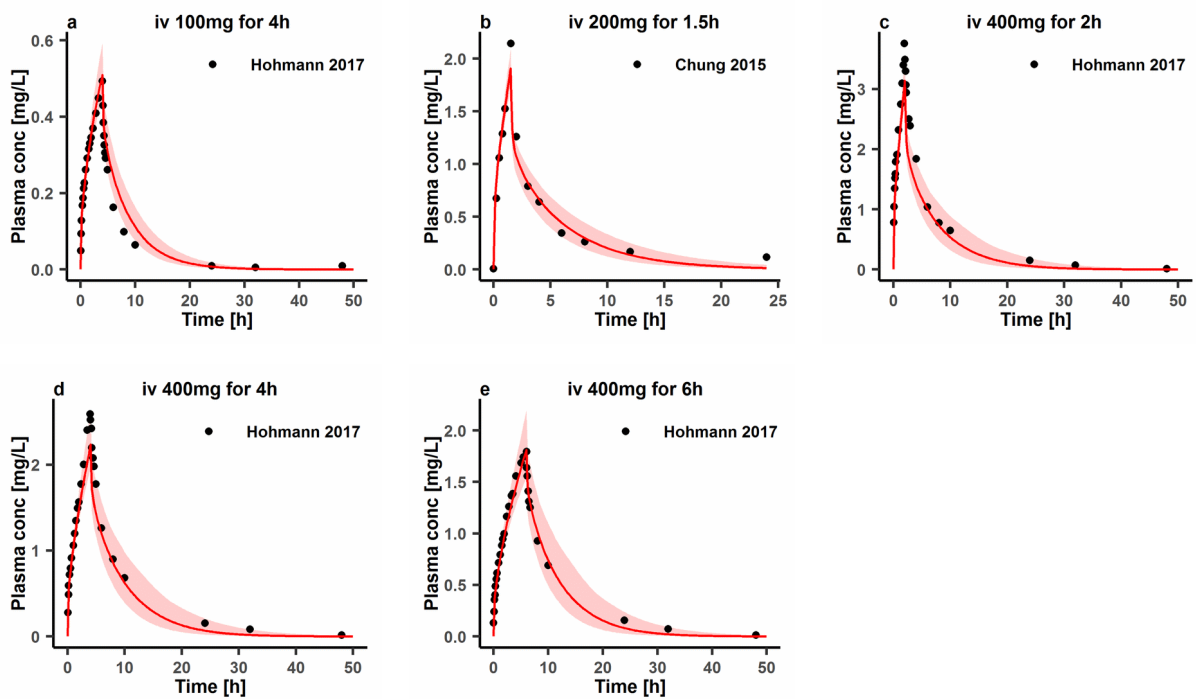
Dose [mg]	Route	Day	Pred C <sub>trough</sub> [mg/L]	Obs C <sub>trough</sub> [mg/L]	Pred/Obs C <sub>trough</sub>	Ref.
3/kg,QD,D1; 3/kg,BID D3-11.5	iv(1h)	3	0.38	0.30	1.25	[6]
3/kg,QD,D1; 3/kg,BID D3-11.5	iv(1h)	4	0.51	0.60	0.85	[6]
3/kg,QD,D1; 3/kg,BID D3-11.5	iv(1h)	5	0.58	0.77	0.75	[6]
3/kg,QD,D1; 3/kg,BID D3-11.5	iv(1h)	6	0.59	0.89	0.66	[6]
3/kg,QD,D1; 3/kg,BID D3-11.5	iv(1h)	7	0.60	0.96	0.63	[6]
3/kg,QD,D1; 3/kg,BID D3-11.5	iv(1h)	8	0.60	1.02	0.59	[6]
3/kg,QD,D1; 3/kg,BID D3-11.5	iv(1h)	9	0.60	1.04	0.57	[6]
3/kg,QD,D1; 3/kg,BID D3-11.5	iv(1h)	10	0.60	1.03	0.58	[6]
3/kg,QD,D1; 3/kg,BID D3-11.5	iv(1h)	11	0.60	0.94	0.64	[6]
6 /kg, BID,D1; 3 /kg,BID D2-9.5	iv(1h)	2	0.95	0.69*	1.38	[6]
6 /kg, BID,D1; 3 /kg,BID D2-9.5	iv(1h)	3	0.60	0.44*	1.36	[6]
6 /kg, BID,D1; 3 /kg,BID D2-9.5	iv(1h)	4	0.54	0.48*	1.13	[6]
6 /kg, BID,D1; 3 /kg,BID D2-9.5	iv(1h)	5	0.52	0.43*	1.20	[6]
6 /kg, BID,D1; 3 /kg,BID D2-9.5	iv(1h)	6	0.52	0.39*	1.35	[6]
6 /kg, BID,D1; 3 /kg,BID D2-9.5	iv(1h)	7	0.52	0.40*	1.32	[6]
6 /kg, BID,D1; 3 /kg,BID D2-9.5	iv(1h)	8	0.52	0.41*	1.28	[6]
6 /kg, BID,D1; 3 /kg,BID D2-9.5	iv(1h)	9	0.52	0.40*	1.31	[6]
6 /kg, BID,D1; 3 /kg,BID D2-9.5	iv(1h)	9.5	0.52	0.41*	1.28	[6]
3 /kg,BID,D2-7; 200,BID D8-13.5 (6 /kg, BID,D1)	iv(1h),po(-)	2	1.10	0.91	1.21	[7]
3 /kg,BID,D2-7; 200,BID D8-13.5 (6 /kg, BID,D1)	iv(1h),po(-)	3	0.77	0.74	1.05	[7]
3 /kg,BID,D2-7; 200,BID D8-13.5 (6 /kg, BID,D1)	iv(1h),po(-)	4	0.69	0.68	1.01	[7]
3 /kg,BID,D2-7; 200,BID D8-13.5 (6 /kg, BID,D1)	iv(1h),po(-)	5	0.67	0.66	1.01	[7]
3 /kg,BID,D2-7; 200,BID D8-13.5 (6 /kg, BID,D1)	iv(1h),po(-)	6	0.67	0.68	0.99	[7]
3 /kg,BID,D2-7; 200,BID D8-13.5 (6 /kg, BID,D1)	iv(1h),po(-)	7	0.67	0.69	0.97	[7]
3 /kg,BID,D2-7; 200,BID D8-13.5 (6 /kg, BID,D1)	iv(1h),po(-)	8	0.67	0.64	1.05	[7]
3 /kg,BID,D2-7; 200,BID D8-13.5 (6 /kg, BID,D1)	iv(1h),po(-)	9	0.60	0.56	1.08	[7]
3 /kg,BID,D2-7; 200,BID D8-13.5 (6 /kg, BID,D1)	iv(1h),po(-)	10	0.54	0.52	1.04	[7]
3 /kg,BID,D2-7; 200,BID D8-13.5 (6 /kg, BID,D1)	iv(1h),po(-)	11	0.53	0.51	1.04	[7]
3 /kg,BID,D2-7; 200,BID D8-13.5 (6 /kg, BID,D1)	iv(1h),po(-)	12	0.53	0.49	1.08	[7]
3 /kg,BID,D2-7; 200,BID D8-13.5 (6 /kg, BID,D1)	iv(1h),po(-)	13	0.53	0.49	1.08	[7]
3 /kg,BID,D2-7; 200,BID D8-13.5 (6 /kg, BID,D1)	iv(1h),po(-)	13.5	0.53	0.47	1.13	[7]
4 /kg,BID,D2-7; 300,BID D8-13.5 (6 /kg, BID,D1)	iv(1h),po(-)	2	1.15	1.29	0.89	[7]
4 /kg,BID,D2-7; 300,BID D8-13.5 (6 /kg, BID,D1)	iv(1h),po(-)	3	1.19	1.65	0.72	[7]
4 /kg,BID,D2-7; 300,BID D8-13.5 (6 /kg, BID,D1)	iv(1h),po(-)	4	1.20	1.90	0.63	[7]
4 /kg,BID,D2-7; 300,BID D8-13.5 (6 /kg, BID,D1)	iv(1h),po(-)	5	1.22	1.51	0.81	[7]
4 /kg,BID,D2-7; 300,BID D8-13.5 (6 /kg, BID,D1)	iv(1h),po(-)	6	1.23	2.12	0.58	[7]
4 /kg,BID,D2-7; 300,BID D8-13.5 (6 /kg, BID,D1)	iv(1h),po(-)	7	1.24	2.18	0.57	[7]
4 /kg,BID,D2-7; 300,BID D8-13.5 (6 /kg, BID,D1)	iv(1h),po(-)	8	1.24	2.00	0.62	[7]

4 /kg,BID,D2-7; 300,BID D8-13.5 (6 /kg, BID,D1)	iv(1h),po(-)	9	0.99	2.08	<b>0.48</b>	[7]
4 /kg,BID,D2-7; 300,BID D8-13.5 (6 /kg, BID,D1)	iv(1h),po(-)	10	0.94	2.08	<b>0.45</b>	[7]
4 /kg,BID,D2-7; 300,BID D8-13.5 (6 /kg, BID,D1)	iv(1h),po(-)	11	0.91	1.92	<b>0.47</b>	[7]
4 /kg,BID,D2-7; 300,BID D8-13.5 (6 /kg, BID,D1)	iv(1h),po(-)	12	0.90	2.03	<b>0.44</b>	[7]
4 /kg,BID,D2-7; 300,BID D8-13.5 (6 /kg, BID,D1)	iv(1h),po(-)	13	0.90	2.20	<b>0.41</b>	[7]
4 /kg,BID,D2-7; 300,BID D8-13.5 (6 /kg, BID,D1)	iv(1h),po(-)	13.5	0.90	2.06	<b>0.44</b>	[7]
5 /kg,BID,D2-7; 400,BID D8-13.5 (6 /kg, BID,D1)	iv(1h),po(-)	2	1.11	1.02	1.09	[7]
5 /kg,BID,D2-7; 400,BID D8-13.5 (6 /kg, BID,D1)	iv(1h),po(-)	3	1.65	1.76	0.94	[7]
5 /kg,BID,D2-7; 400,BID D8-13.5 (6 /kg, BID,D1)	iv(1h),po(-)	4	1.94	2.24	0.86	[7]
5 /kg,BID,D2-7; 400,BID D8-13.5 (6 /kg, BID,D1)	iv(1h),po(-)	5	2.06	2.44	0.84	[7]
5 /kg,BID,D2-7; 400,BID D8-13.5 (6 /kg, BID,D1)	iv(1h),po(-)	6	2.11	2.62	0.81	[7]
5 /kg,BID,D2-7; 400,BID D8-13.5 (6 /kg, BID,D1)	iv(1h),po(-)	7	2.13	2.60	0.82	[7]
5 /kg,BID,D2-7; 400,BID D8-13.5 (6 /kg, BID,D1)	iv(1h),po(-)	8	2.15	2.42	0.89	[7]
5 /kg,BID,D2-7; 400,BID D8-13.5 (6 /kg, BID,D1)	iv(1h),po(-)	9	1.80	2.67	0.68	[7]
5 /kg,BID,D2-7; 400,BID D8-13.5 (6 /kg, BID,D1)	iv(1h),po(-)	10	1.73	2.60	0.66	[7]
5 /kg,BID,D2-7; 400,BID D8-13.5 (6 /kg, BID,D1)	iv(1h),po(-)	11	1.60	2.58	0.62	[7]
5 /kg,BID,D2-7; 400,BID D8-13.5 (6 /kg, BID,D1)	iv(1h),po(-)	12	1.54	2.43	0.63	[7]
5 /kg,BID,D2-7; 400,BID D8-13.5 (6 /kg, BID,D1)	iv(1h),po(-)	13	1.53	2.41	0.63	[7]
5 /kg,BID,D2-7; 400,BID D8-13.5 (6 /kg, BID,D1)	iv(1h),po(-)	13.5	1.53	2.22	0.69	[7]
1.5/kg,QD D1; 1.5/kg,TID D3-11.5	po(-)	3	0.12	0.12	1.03	[8]
1.5/kg,QD D1; 1.5/kg,TID D3-11.5	po(-)	4	0.26	0.19	1.36	[8]
1.5/kg,QD D1; 1.5/kg,TID D3-11.5	po(-)	5	0.35	0.25	1.40	[8]
1.5/kg,QD D1; 1.5/kg,TID D3-11.5	po(-)	6	0.41	0.26	1.57	[8]
1.5/kg,QD D1; 1.5/kg,TID D3-11.5	po(-)	7	0.45	0.29	1.57	[8]
1.5/kg,QD D1; 1.5/kg,TID D3-11.5	po(-)	8	0.47	0.28	1.66	[8]
1.5/kg,QD D1; 1.5/kg,TID D3-11.5	po(-)	9	0.48	0.28	1.72	[8]
1.5/kg,QD D1; 1.5/kg,TID D3-11.5	po(-)	10	0.48	0.28	1.70	[8]
1.5/kg,QD D1; 1.5/kg,TID D3-11.5	po(-)	11	0.48	0.29	1.68	[8]
2/kg,QD D1; 2 /kg,BID D3-11.5	po(-)	3	0.10	0.09	1.13	[8]
2/kg,QD D1; 2 /kg,BID D3-11.5	po(-)	4	0.21	0.10	<b>2.05</b>	[8]
2/kg,QD D1; 2 /kg,BID D3-11.5	po(-)	5	0.30	0.13	<b>2.30</b>	[8]
2/kg,QD D1; 2 /kg,BID D3-11.5	po(-)	6	0.35	0.16	<b>2.25</b>	[8]
2/kg,QD D1; 2 /kg,BID D3-11.5	po(-)	7	0.36	0.16	<b>2.22</b>	[8]
2/kg,QD D1; 2 /kg,BID D3-11.5	po(-)	8	0.37	0.16	<b>2.38</b>	[8]
2/kg,QD D1; 2 /kg,BID D3-11.5	po(-)	9	0.37	0.19	1.94	[8]
2/kg,QD D1; 2 /kg,BID D3-11.5	po(-)	10	0.37	0.20	1.87	[8]
2/kg,QD D1; 2 /kg,BID D3-11.5	po(-)	11	0.37	0.18	<b>2.10</b>	[8]
2/kg,QD D1; 2 /kg,TID D3-11.5	po(-)	3	0.15	0.35	<b>0.43</b>	[8]
2/kg,QD D1; 2 /kg,TID D3-11.5	po(-)	4	0.38	0.64	0.60	[8]
2/kg,QD D1; 2 /kg,TID D3-11.5	po(-)	5	0.54	0.87	0.62	[8]
2/kg,QD D1; 2 /kg,TID D3-11.5	po(-)	6	0.63	1.04	0.60	[8]
2/kg,QD D1; 2 /kg,TID D3-11.5	po(-)	7	0.66	1.04	0.63	[8]

2/kg,QD D1; 2 /kg,TID D3-11.5	po(-)	8	0.67	1.11	0.60	[8]
2/kg,QD D1; 2 /kg,TID D3-11.5	po(-)	9	0.68	1.12	0.61	[8]
2/kg,QD D1; 2 /kg,TID D3-11.5	po(-)	10	0.68	1.20	0.57	[8]
2/kg,QD D1; 2 /kg,TID D3-11.5	po(-)	11	0.68	1.20	0.57	[8]
3/kg,QD D1; 3 /kg,BID D3-11.5	po(-)	3	0.14	0.29	0.48	[8]
3/kg,QD D1; 3 /kg,BID D3-11.5	po(-)	4	0.33	0.49	0.67	[8]
3/kg,QD D1; 3 /kg,BID D3-11.5	po(-)	5	0.47	0.71	0.67	[8]
3/kg,QD D1; 3 /kg,BID D3-11.5	po(-)	6	0.57	0.89	0.64	[8]
3/kg,QD D1; 3 /kg,BID D3-11.5	po(-)	7	0.59	0.87	0.68	[8]
3/kg,QD D1; 3 /kg,BID D3-11.5	po(-)	8	0.61	0.90	0.68	[8]
3/kg,QD D1; 3 /kg,BID D3-11.5	po(-)	9	0.62	0.95	0.65	[8]
3/kg,QD D1; 3 /kg,BID D3-11.5	po(-)	10	0.62	0.95	0.65	[8]
3/kg,QD D1; 3 /kg,BID D3-11.5	po(-)	11	0.62	0.94	0.66	[8]
4/kg,QD D1; 4/kg,QD D3-11.5	po(-)	3	0.05	0.09	0.54	[8]
4/kg,QD D1; 4/kg,QD D3-11.5	po(-)	4	0.07	0.14	0.51	[8]
4/kg,QD D1; 4/kg,QD D3-11.5	po(-)	5	0.09	0.17	0.52	[8]
4/kg,QD D1; 4/kg,QD D3-11.5	po(-)	6	0.09	0.20	<b>0.46</b>	[8]
4/kg,QD D1; 4/kg,QD D3-11.5	po(-)	7	0.10	0.23	<b>0.43</b>	[8]
4/kg,QD D1; 4/kg,QD D3-11.5	po(-)	8	0.10	0.25	<b>0.40</b>	[8]
4/kg,QD D1; 4/kg,QD D3-11.5	po(-)	9	0.10	0.25	<b>0.39</b>	[8]
4/kg,QD D1; 4/kg,QD D3-11.5	po(-)	10	0.10	0.24	<b>0.42</b>	[8]
4/kg,QD D1; 4/kg,QD D3-11.5	po(-)	11	0.10	0.23	<b>0.44</b>	[8]
200,BID D1-6.5	po(cap)	2	0.16	0.20	0.81	[9]
200,BID D1-6.5	po(cap)	3	0.3	0.40	0.75	[9]
200,BID D1-6.5	po(cap)	4	0.39	0.53	0.73	[9]
200,BID D1-6.5	po(cap)	5	0.42	0.64	0.65	[9]
200,BID D1-6.5	po(cap)	6	0.43	0.63	0.68	[9]
200,BID D1-6.5	po(cap)	6.5	0.43	0.62	0.69	[9]
200,BID D1-6.5	po(tab)	2	0.18	0.26	0.70	[10]
200,BID D1-6.5	po(tab)	3	0.34	0.60	0.56	[10]
200,BID D1-6.5	po(tab)	4	0.44	0.75	0.59	[10]
200,BID D1-6.5	po(tab)	5	0.48	0.80	0.60	[10]
200,BID D1-6.5	po(tab)	6	0.49	0.80	0.61	[10]
200,BID D1-6.5	po(tab)	6.5	0.49	0.88	0.56	[10]
200,BID D1-6.5	po(-)	2	0.17	0.18	0.95	[11]
200,BID D1-6.5	po(-)	3	0.31	0.42	0.73	[11]
200,BID D1-6.5	po(-)	4	0.39	0.57	0.68	[11]
200,BID D1-6.5	po(-)	5	0.43	0.64	0.67	[11]
200,BID D1-6.5	po(-)	6	0.44	0.69	0.63	[11]
200,BID D1-6.5	po(-)	6.5	0.44	0.65	0.68	[11]
400,BID D1; 200,BID D2-9.5	po(-)	2	0.65	0.89	0.73	[12]
400,BID D1; 200,BID D2-9.5	po(-)	3	0.57	0.76	0.75	[12]
400,BID D1; 200,BID D2-9.5	po(-)	4	0.5	0.70	0.71	[12]
400,BID D1; 200,BID D2-9.5	po(-)	5	0.48	0.74	0.65	[12]
400,BID D1; 200,BID D2-9.5	po(-)	6	0.47	0.69	0.68	[12]
400,BID D1; 200,BID D2-9.5	po(-)	7	0.47	0.67	0.70	[12]
400,BID D1; 200,BID D2-9.5	po(-)	8	0.47	0.73	0.64	[12]
400,BID D1; 200,BID D2-9.5	po(-)	9	0.47	0.73	0.64	[12]
400,BID D1; 200,BID D2-9.5	po(-)	9.5	0.47	0.74	0.64	[12]
400,BID D1; 200,BID D2-3.5	po(-)	2	0.62	1.92	<b>0.32</b>	[13]
400,BID D1; 200,BID D2-3.5	po(-)	3	0.65	1.90	<b>0.34</b>	[13]
400,BID D1; 200,BID D2-3.5	po(-)	3.5	0.74	1.86	<b>0.40</b>	[13]
400,BID D1; 200,BID D2-7.5	po(-)	7.5	0.56	0.69	0.81	[14]

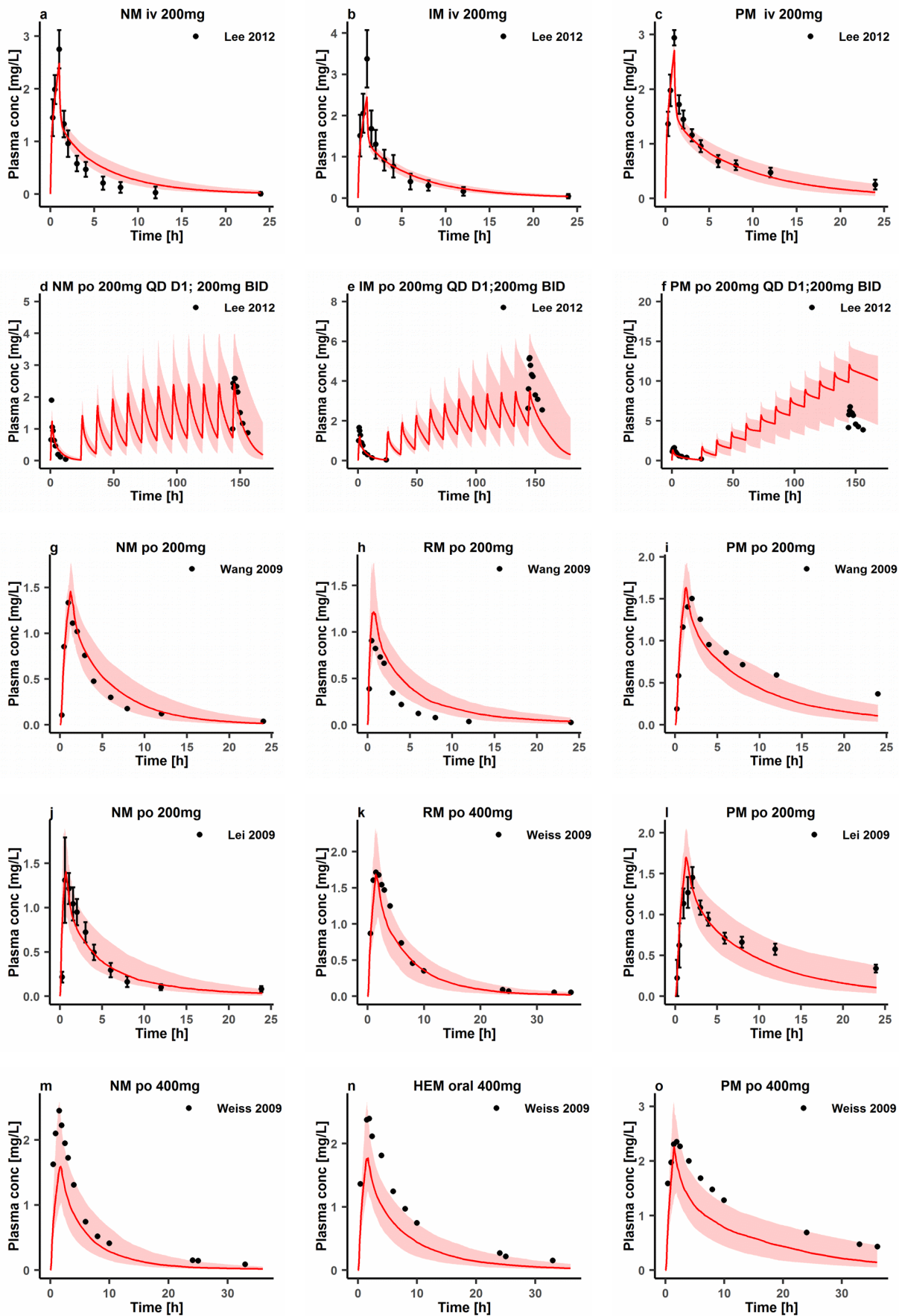
400,BID D1; 200,BID D2-2.5	po(-)	2.5	0.55	0.78*	0.71	[15]
100,BID D1; 50, BID D2-2.5	po(-)	2.5	0.27	0.34*	0.79	[15]
200,QD; 200,BID D2-7	po(-)	6	0.73	0.97	0.75	[16]
200,QD; 200,BID D2-7	po(-)	6	1.77	2.64	0.67	[16]
200,QD; 200,BID D2-7	po(-)	6	11.15	4.14	2.69	[16]
400,BID D1; 200,BID D2-3.5	po(-)	2	0.81	1.68	0.48	[17]
400,BID D1; 200,BID D2-3.5	po(-)	2.5	0.78	1.91	0.41	[17]
400,BID D1; 200,BID D2-3.5	po(-)	3	0.78	2.07	0.38	[17]
400,BID D1; 200,BID D2-3.5	po(-)	2	3.96	4.99	0.79	[17]
400,BID D1; 200,BID D2-3.5	po(-)	2.5	5.13	5.39	0.95	[17]
400,BID D1; 200,BID D2-3.5	po(-)	3	6.3	4.92	1.28	[17]
GMFE(range)						1.55(0.32-2.69)
Pred/Obs within 2-fold						122/144

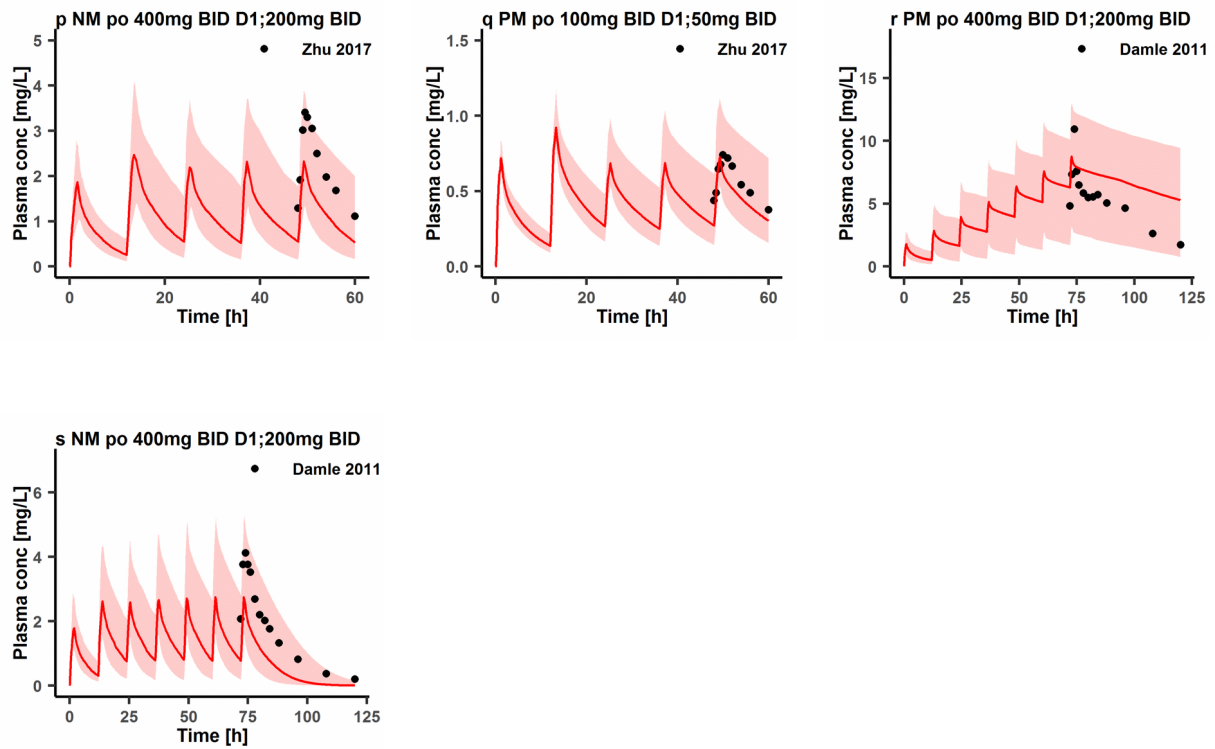
Observed aggregate values are reported as arithmetic mean if not specified otherwise, ♦: geometric mean; /kg: per kg of body weight; D: day of treatment according to the numbering in the reference; SIG: single dose, QD: once daily, BID: twice daily, TID: three times daily; iv: intravenously, po: orally; tab: tablet, cap: capsule;  $C_{trough}$ : trough concentration; Obs: observed aggregate value from literature, Pred: predicted value based on the model; GMFE: geometric mean fold error. The ratios of predicted versus observed  $C_{trough}$  outside 0.5- to 2.0-fold limits were printed in bold.

**Figure S1 Prediction performance of voriconazole PBPK model on aggregate plasma concentrations for a single intravenous dose**

Observed aggregate data reported in the literature are shown as dots [18,19]. Population simulation medians are shown as lines; the shaded areas illustrate the 68% population prediction intervals. Details of dosing regimens, study populations, predicted versus observed PK parameters are summarized in **Table 1**. iv: intravenously; Plasma conc: plasma concentration.

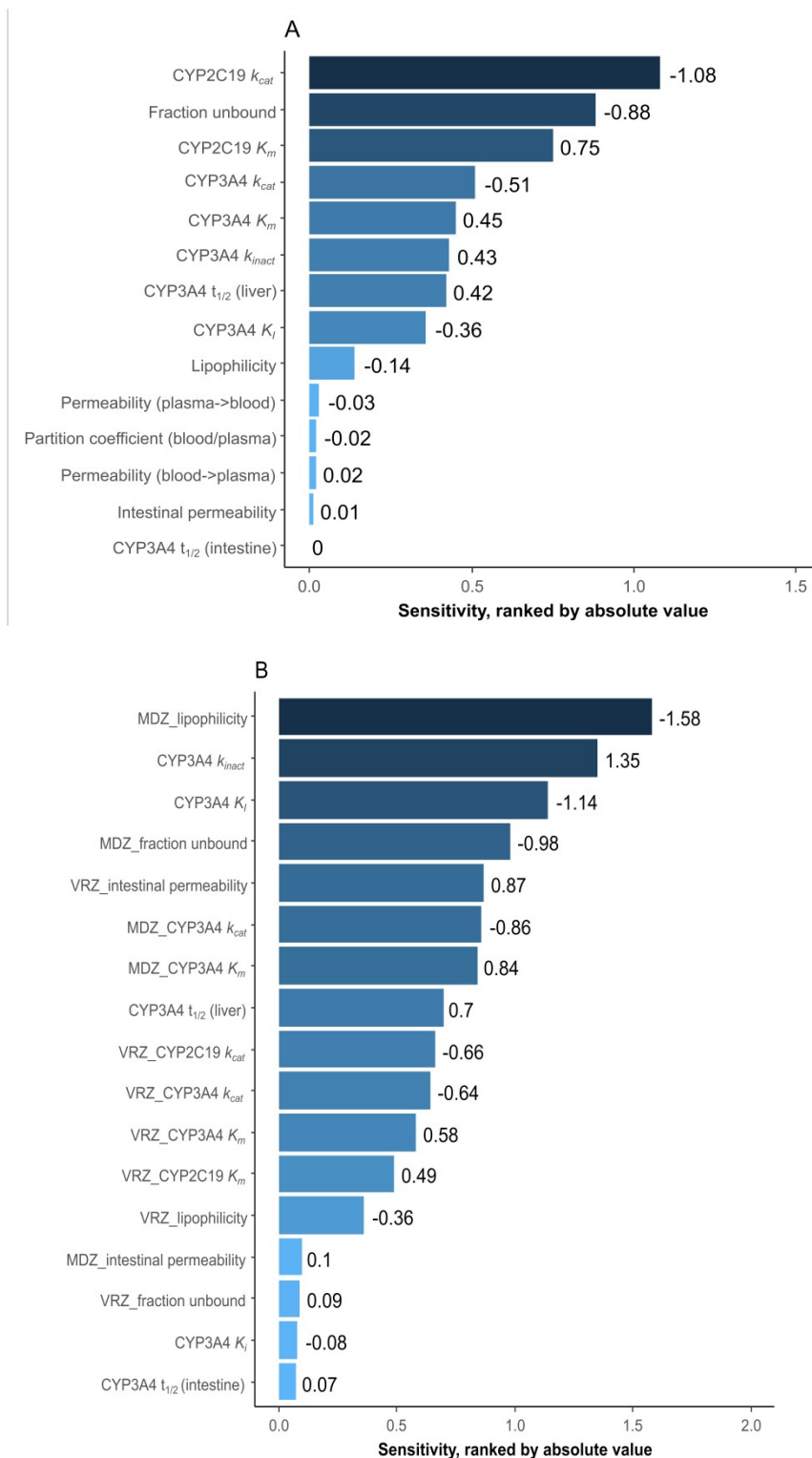
**Figure S2 Prediction performance of voriconazole PBPK model on aggregate plasma concentrations in different CYP2C19 genotype groups**





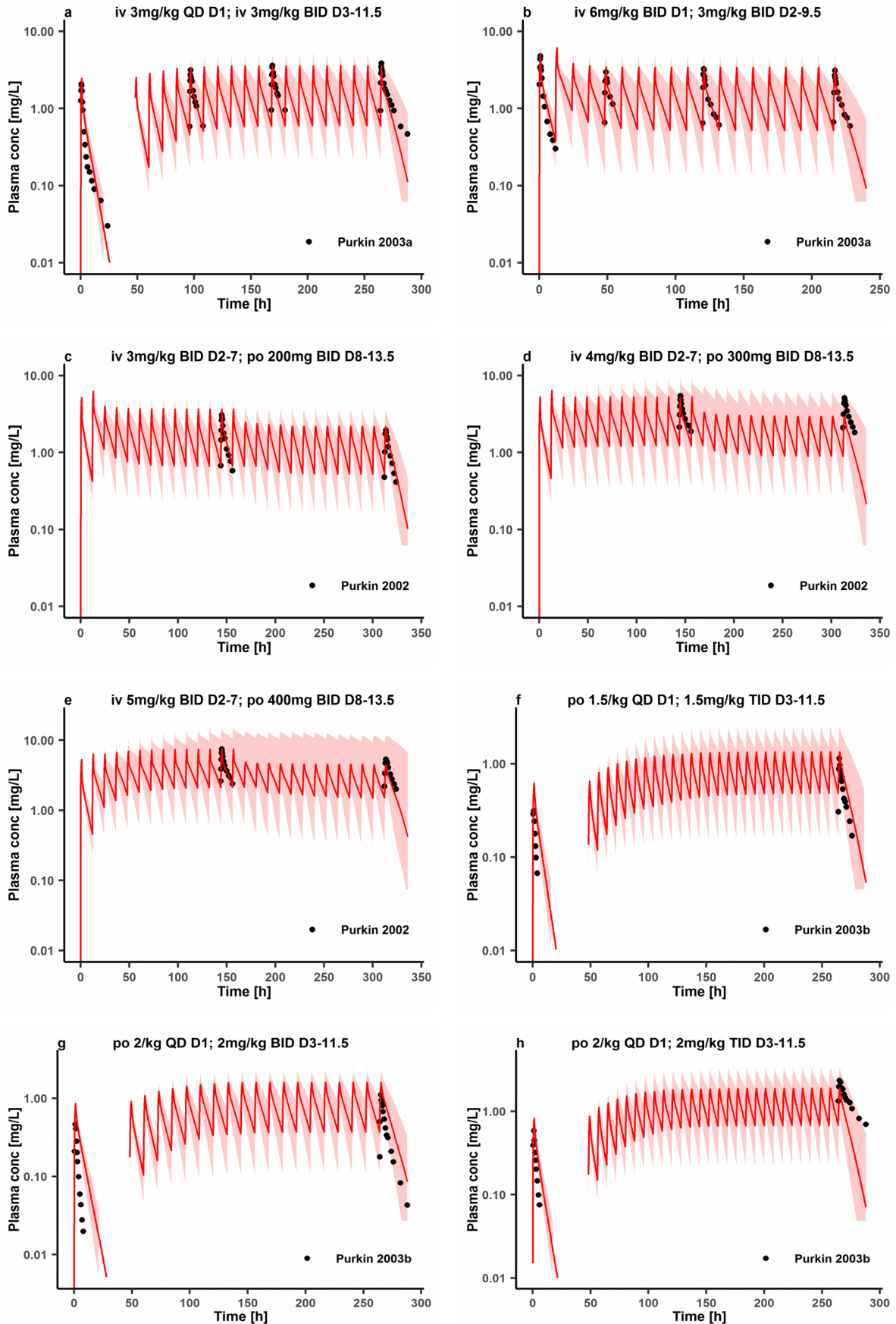
Observed aggregate data reported in the literature are shown as dots or dots  $\pm$  SD [16,17,20–23]. Population simulation medians are shown as lines; the shaded areas illustrate the 68% population prediction intervals. Details of dosing regimens, study populations, predicted versus observed PK parameters are summarized in **Table 2**. D: day of treatment according to the numbering in the reference; QD: once daily, BID: twice daily; iv: intravenously, po: oral; Plasma conc: plasma concentration; RM: rapid metabolizers, NM: normal metabolizers, IM: intermediate metabolizers, PM: poor metabolizers.

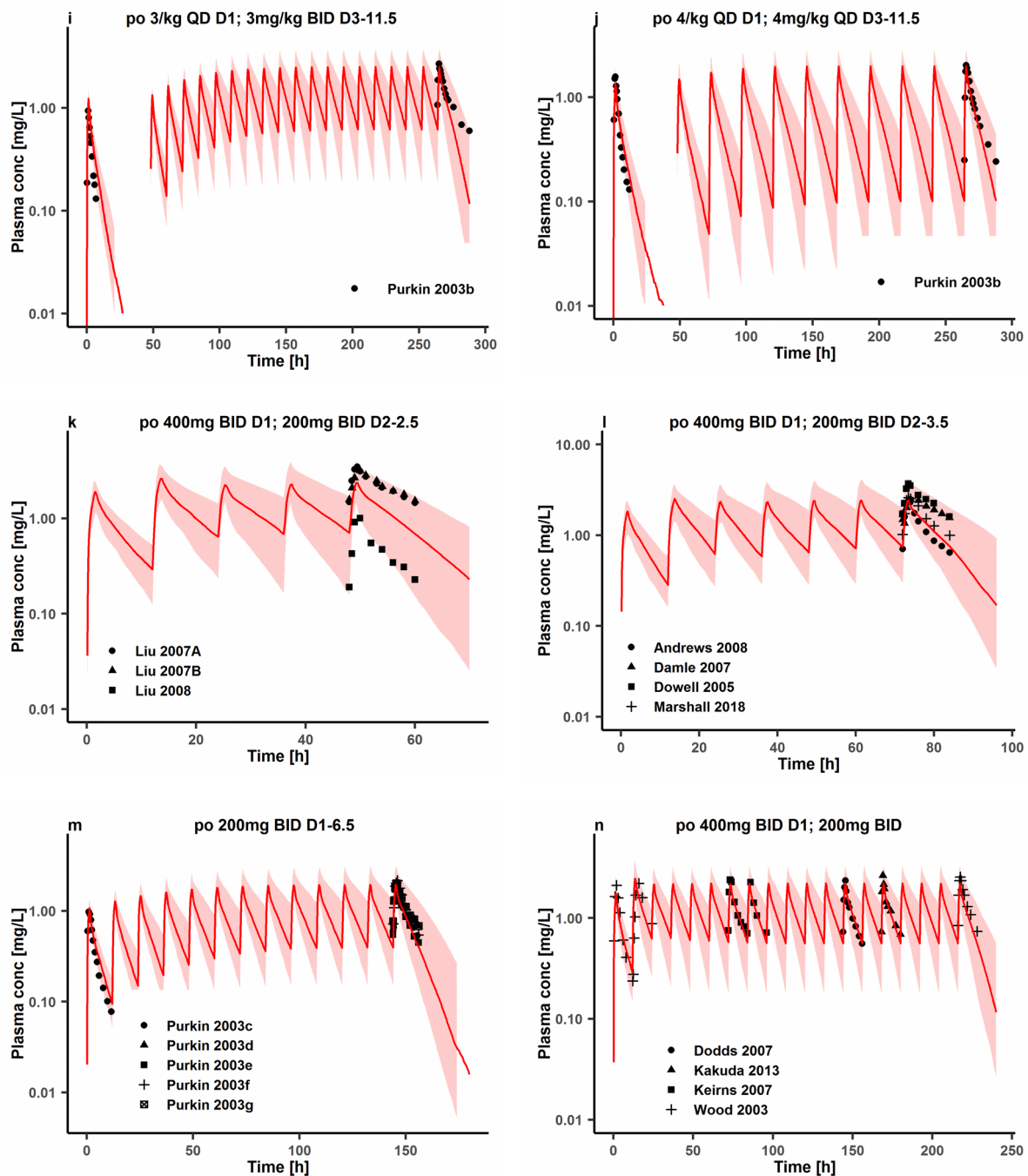


**Figure S3 Sensitivity analysis of voriconazole PBPK model**

The sensitivity of the model to single parameters measured as the change of A) the simulated AUC of voriconazole under steady-state conditions of a 400 mg twice daily on the first day and then 200 mg twice daily on the following day's oral voriconazole regimen in CYP2C19 EMs; B) the simulated AUC of midazolam after oral treatment of voriconazole 400 mg twice daily on the first day and 200 mg twice daily on the second day, and the oral co-administration of 7.5 mg midazolam during the last dose of voriconazole. A sensitivity value of + 1.0 signifies that a 10% increase of the examined parameter causes a 10% increase of the simulated AUC. MDZ: midazolam, VRZ: voriconazole,  $t_{1/2}$ : half-life. The parameters were defined in **Table 6**.

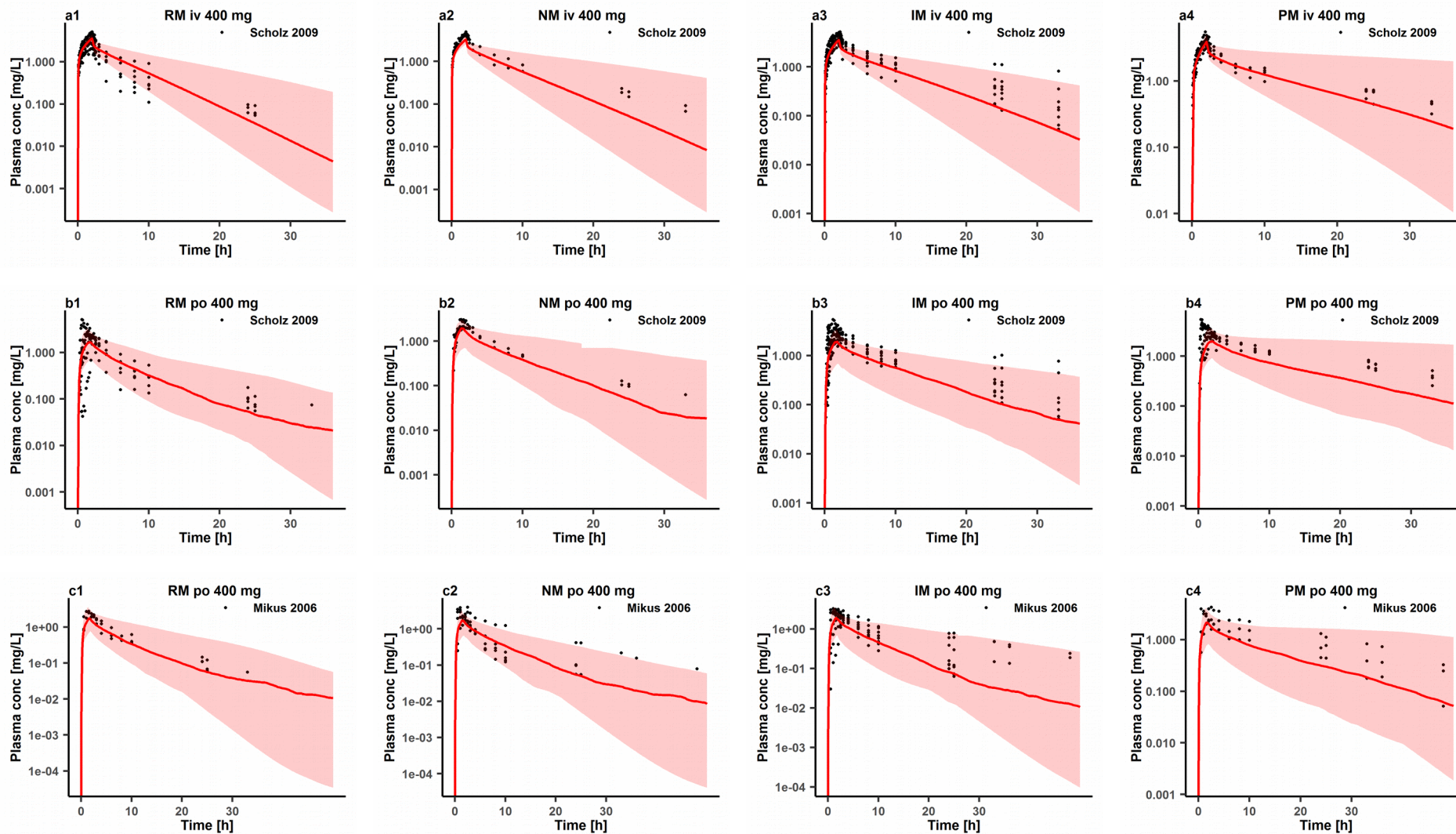
**Figure S4 Prediction performance of voriconazole PBPK model on aggregate plasma concentrations for multiple doses (semi-logarithmic scale)**

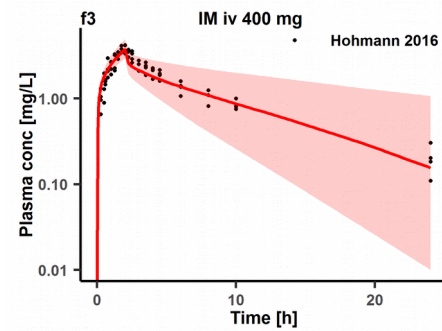
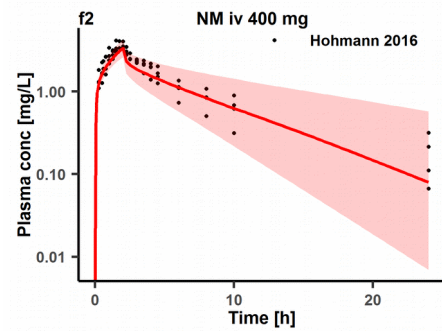
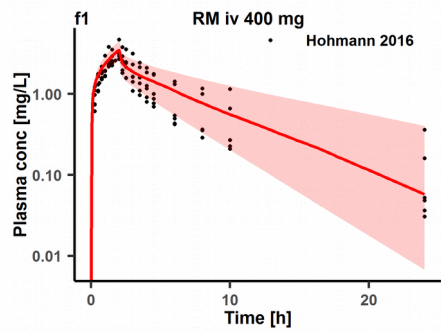
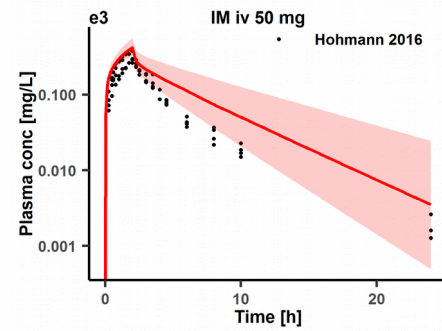
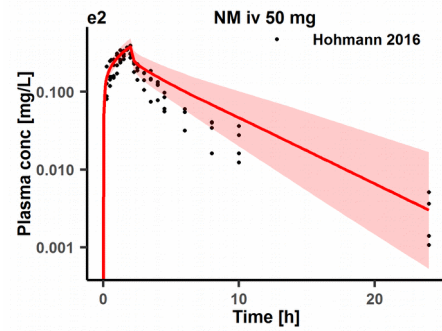
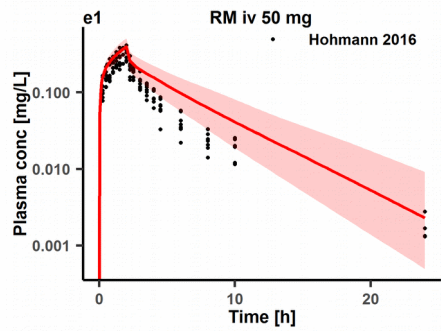
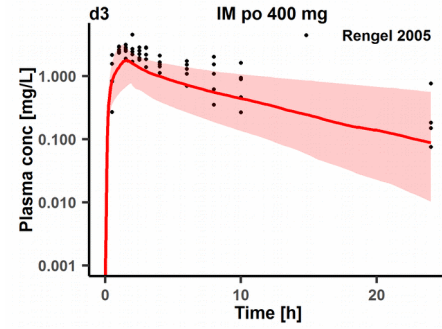
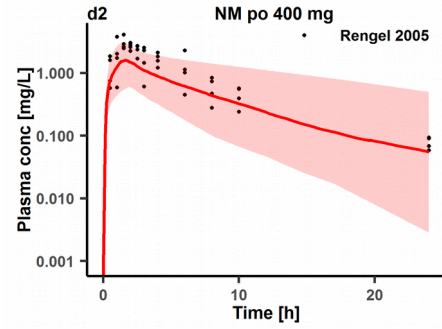
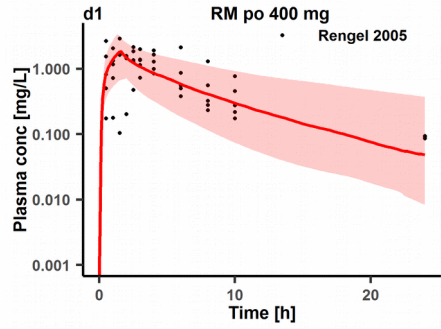




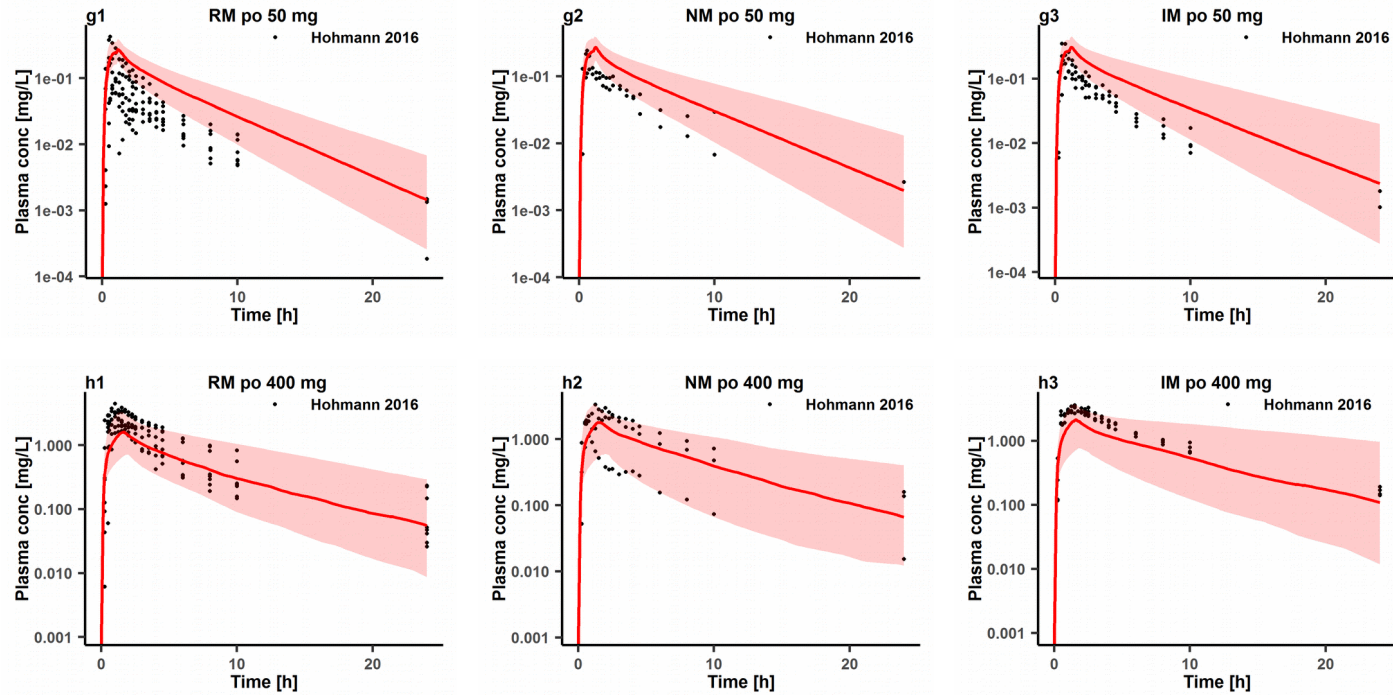
Observed aggregate data reported in the literature are shown as dots, triangles, square, cross, or crossed square [6–14,25–33]. Population simulation medians are shown as lines; the shaded areas illustrate the 68% population prediction intervals. Details of dosing regimens, study populations, predicted versus observed PK parameters are summarized in **Table 1**. D: day of treatment according to the numbering in the reference; QD: once daily, BID: twice daily, TID: three times daily; iv: intravenously, po: oral; Plasma conc: plasma concentration.

**Figure S5 Prediction performance of voriconazole PBPK model on individual plasma concentrations in different CYP2C19 genotype groups for a single dose (semi-logarithmic scale)**

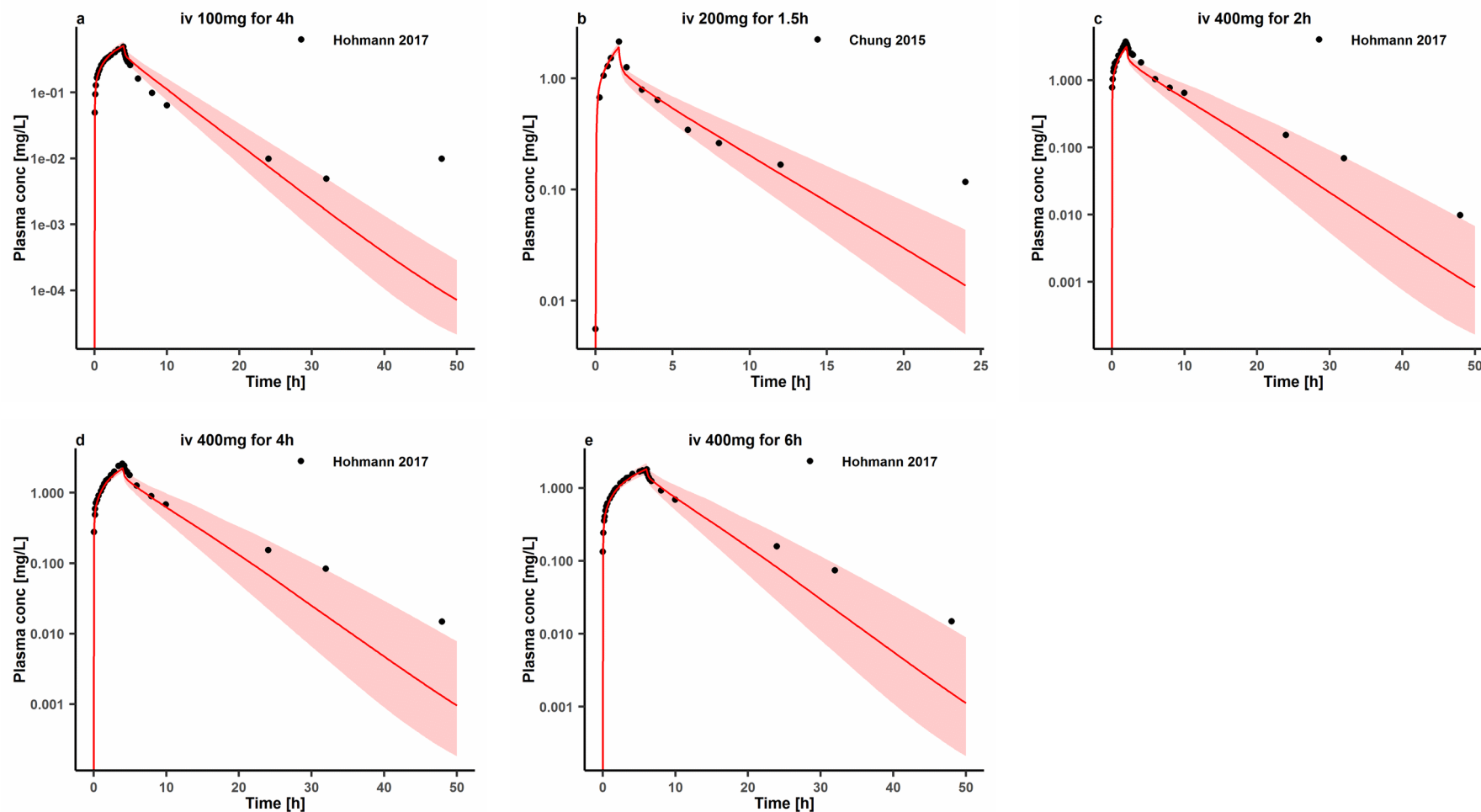




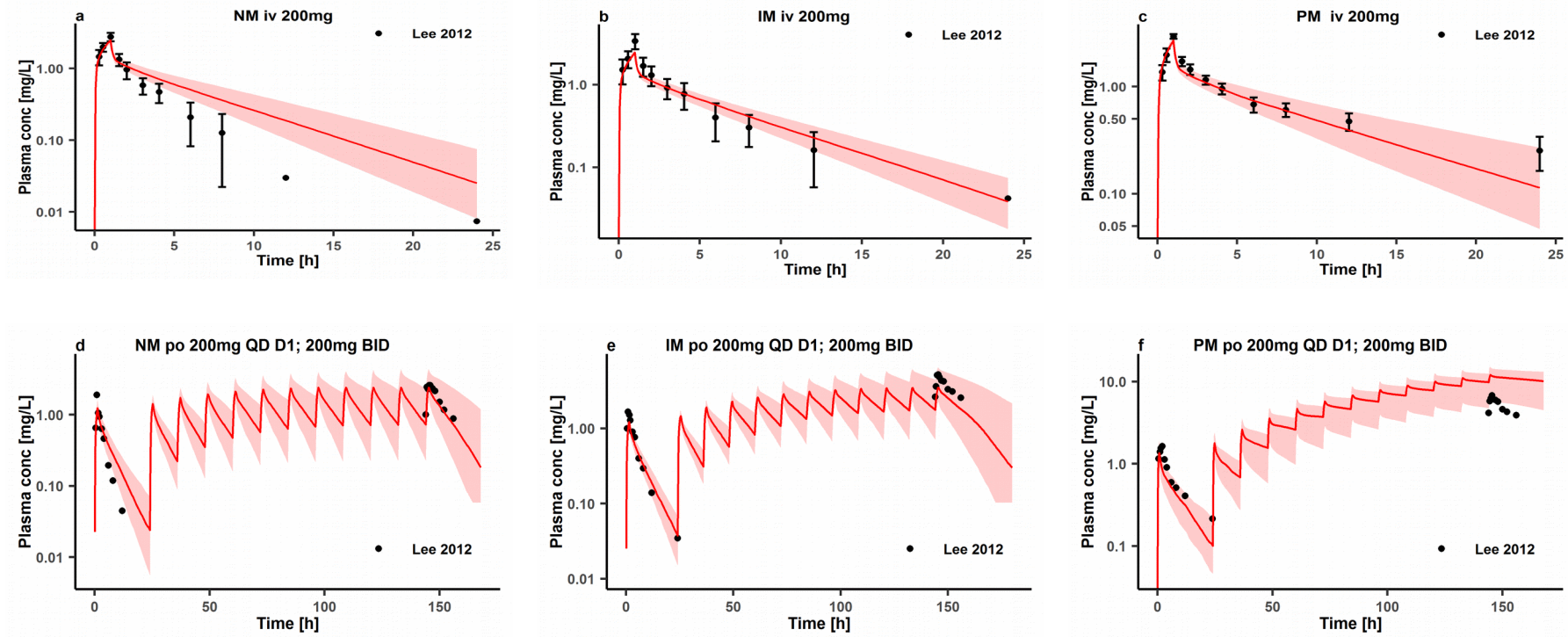




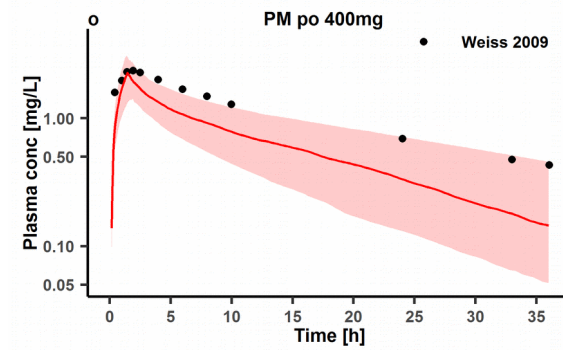
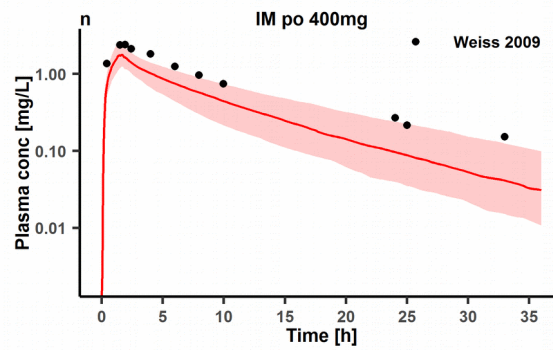
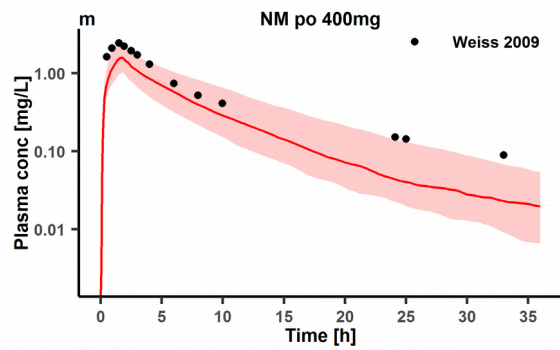
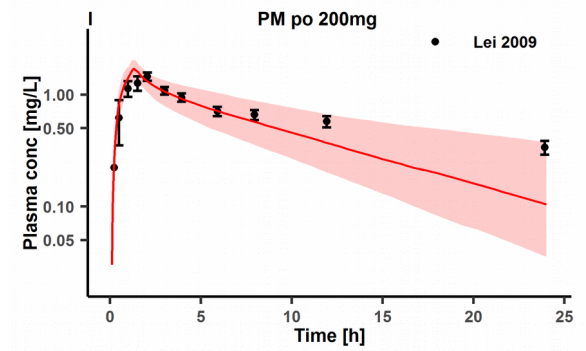
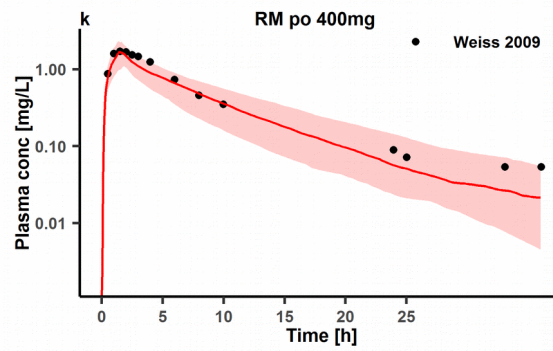
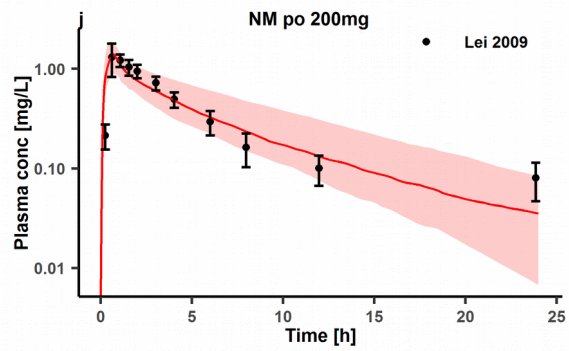
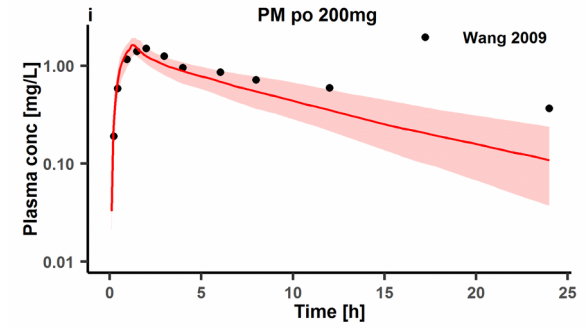
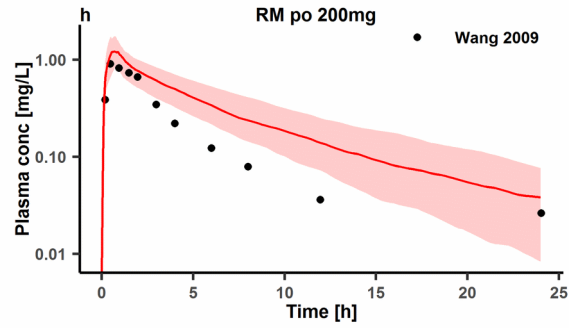
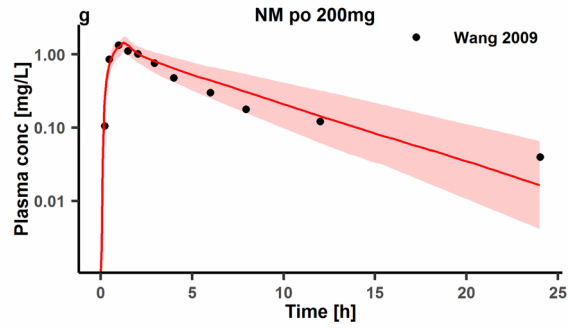
Observed individual data reported in the literature are shown as dots [34–37]. Population simulation medians are shown as lines; the shaded areas illustrate the 95% population prediction intervals. Details of dosing regimens, study populations, predicted versus observed PK parameters are summarized in **Table 2**. iv, intravenously, po; Plasma conc: plasma concentration; RM: rapid metabolizers, NM: normal metabolizers, IM: intermediate metabolizers, PM: poor metabolizers; Rengel: Rengelshausen.

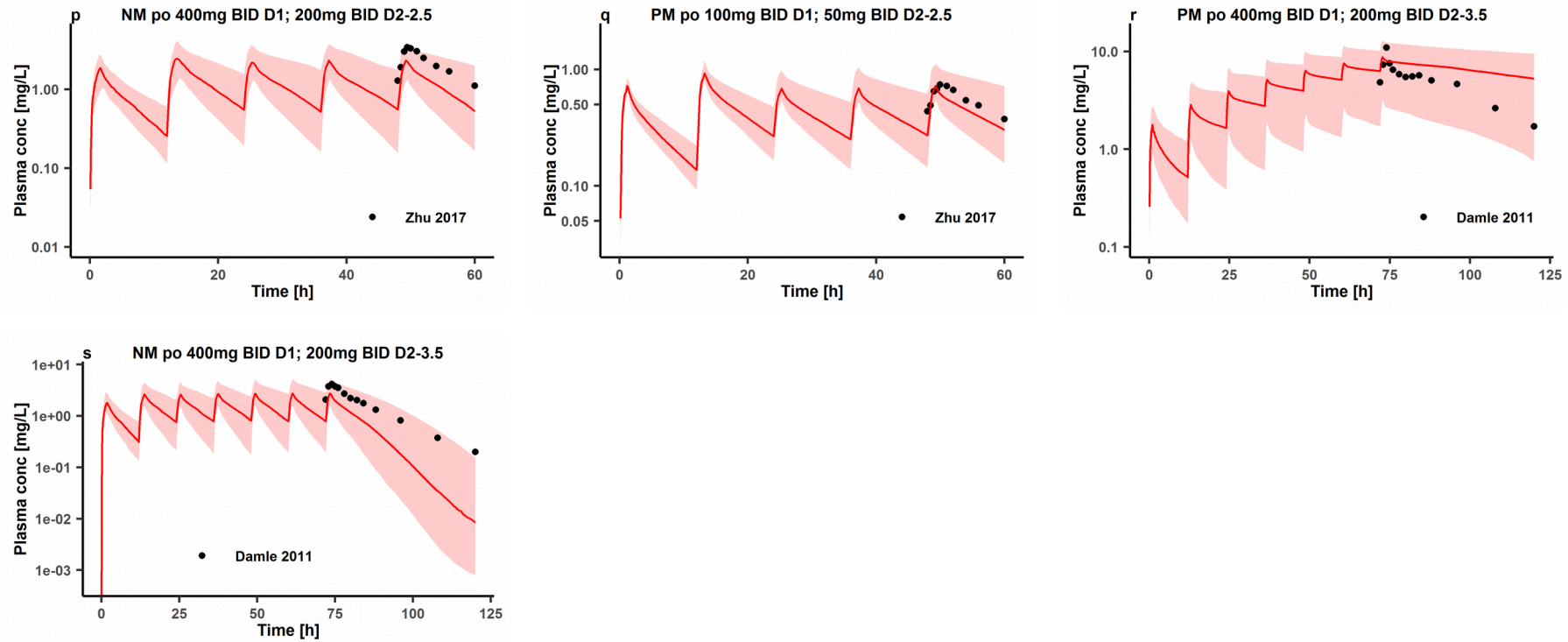
**Figure S6 Prediction performance of voriconazole PBPK model on aggregate plasma concentrations for a single intravenous dose (semi-logarithmic scale)**

Observed aggregate data reported in the literature are shown as dots [18,19]. Population simulation medians are shown as lines; the shaded areas illustrate the 68% population prediction intervals. Details of dosing regimens, study populations, predicted versus observed PK parameters are summarized in **Table 1**. iv: intravenously; Plasma conc: plasma concentration.

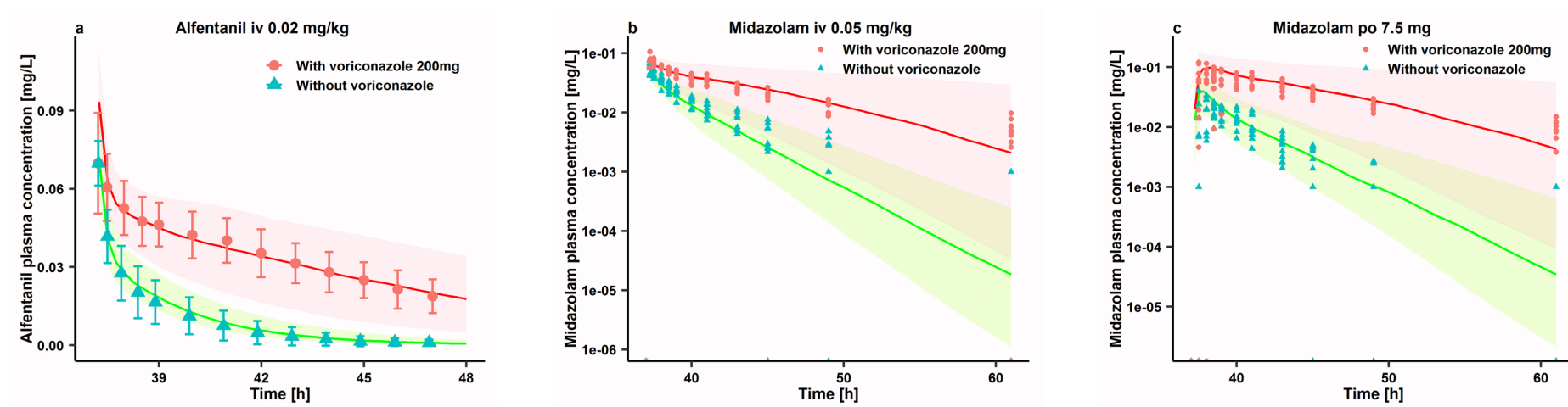
**Figure S7 Prediction performance of voriconazole PBPK model on aggregate plasma concentrations in different CYP2C19 genotype groups (semi-logarithmic scale)**







Observed aggregate data reported in the literature are shown as dots or dots  $\pm$  SD [16,17,20–23]. Population simulation medians are shown as lines; the shaded areas illustrate the 68% population prediction intervals. Details of dosing regimens, study populations, predicted versus observed PK parameters are summarized in **Table 2**. D: day of treatment according to the numbering in the reference; QD: once daily, BID: twice daily; iv: intravenously, po: oral; Plasma conc: plasma concentration; RM: rapid metabolizers, NM: normal metabolizers, IM: intermediate metabolizers, PM: poor metabolizers.

**Figure S8 Prediction performance of voriconazole PBPK model in DDIs with CYP3A4 probe substrates (semi-logarithmic scale)**

Voriconazole model integrated with models of CYP3A4 probe substrates predicted the inhibitory effects of voriconazole on CYP3A4 *in vivo*. Population predictions of a) alfentanil or b, c) midazolam plasma concentration-time datasets, with and without voriconazole treatment were compared to observed data shown as green triangles (control) or red dots (treatment) or symbols  $\pm$  SD [24,38]. Population simulation median are shown as green lines (control) or red lines (treatment); the shaded areas illustrate the respective a) 68% and b, c) 95% population prediction intervals. iv: intravenous; po: oral. Details of dosing regimens, study populations, predicted versus observed DDI AUC ratios and  $C_{max}$  ratios are summarized in **Table 3**.

**REFERENCES**

1. Walsky RL, Obach RS. Validated assays for human cytochrome P450 activities. *Drug Metab Dispos.* 2004;32:647–60.
2. Obach RS, Walsky RL, Venkatakrishnan K. Mechanism-based inactivation of human cytochrome P450 enzymes and the prediction of drug-drug interactions. *Drug Metab Dispos.* 2006;35:246–55.
3. European Medicines Agency. Guideline on bioanalytical method validation 21 July 2011 EMEA/CHMP/EWP/192217/2009 Rev. 1 Corr. 2\*\*.
4. GraphPad Software. GraphPad curve fitting guide. 1995.
5. Perloff ES, Mason AK, Dehal SS, Blanchard AP, Morgan L, Ho T, et al. Validation of cytochrome P450 time-dependent inhibition assays: a two-time point IC<sub>50</sub> shift approach facilitates  $k_{inact}$  assay design. *Xenobiotica.* 2009;39:99–112.
6. Purkins L, Wood N, Greenhalgh K, Eve MD, Oliver SD, Nichols D. The pharmacokinetics and safety of intravenous voriconazole—a novel wide-spectrum antifungal agent. *Br J Clin Pharmacol.* 2003;56:2–9.
7. Purkins L, Wood N, Ghahramani P, Greenhalgh K, Allen MJ, Kleinermans D. Pharmacokinetics and safety of voriconazole following intravenous- to oral-dose escalation regimens. *Antimicrob Agents Chemother.* 2002;46:2546–53.
8. Purkins L, Wood N, Greenhalgh K, Allen MJ, Oliver SD. Voriconazole, a novel wide-spectrum triazole: oral pharmacokinetics and safety. *Br J Clin Pharmacol.* 2003;56 Suppl 1:10–6.
9. Purkins L, Wood N, Kleinermans D, Greenhalgh K, Nichols D. Effect of food on the pharmacokinetics of multiple-dose oral voriconazole. *Br J Clin Pharmacol.* 2003;56:17–23.
10. Purkins L, Wood N, Ghahramani P, Kleinermans D, Layton G, Nichols D. No clinically significant effect of erythromycin or azithromycin on the pharmacokinetics of voriconazole in healthy male volunteers. *Br J Clin Pharmacol.* 2003;56:30–6.
11. Purkins L, Wood N, Kleinermans D, Nichols D. Histamine H<sub>2</sub>-receptor antagonists have no clinically significant effect on the steady-state pharmacokinetics of voriconazole. *Br J Clin Pharmacol.* 2003;56 Suppl 1:51–5.
12. Wood N, Tan K, Purkins L, Layton G, Hamlin J, Kleinermans D, et al. Effect of omeprazole on the steady-state pharmacokinetics of voriconazole. *Br J Clin Pharmacol.* 2003;56 Suppl 1:56–61.
13. Dowell JA, Schranz J, Baruch A, Foster G. Safety and pharmacokinetics of coadministered voriconazole and anidulafungin. *J Clin Pharmacol.* 2005;45:1373–82.
14. Kakuda TN, Van Solingen-Ristea R, Aharchi F, Smedt G De, Witek J, Nijs S, et al. Pharmacokinetics and short-term safety of etravirine in combination with fluconazole or voriconazole in HIV-negative volunteers. *J Clin Pharmacol.* 2013;53:41–50.
15. Zhu L, Brüggemann RJ, Uy J, Colbers A, Hruska MW, Chung E, et al. CYP2C19 genotype-dependent pharmacokinetic drug interaction between voriconazole and ritonavir-boosted atazanavir in healthy subjects. *J Clin Pharmacol.* 2017;57:235–46.
16. Lee S, Kim B-H, Nam W-S, Yoon SH, Cho J-Y, Shin S-G, et al. Effect of CYP2C19 polymorphism on the pharmacokinetics of voriconazole after single and multiple doses in healthy volunteers. *J Clin Pharmacol.* 2012;52:195–203.
17. Damle B, Varma M V, Wood N. Pharmacokinetics of voriconazole administered concomitantly with fluconazole and population-based simulation for sequential use. *Antimicrob Agents Chemother.* 2011;55:5172–7.
18. Hohmann N, Kreuter R, Blank A, Weiss J, Burhenne J, Haefeli WE, et al. Autoinhibitory properties of the parent but not of the N-oxide metabolite contribute to infusion rate-dependent voriconazole pharmacokinetics. *Br J Clin Pharmacol.* 2017;83:1954–65.

19. Chung H, Lee H, Han H, An H, Lim KS, Lee Y, et al. A pharmacokinetic comparison of two voriconazole formulations and the effect of CYP2C19 polymorphism on their pharmacokinetic profiles. *Drug Des Devel Ther.* 2015;9:2609–16.
20. Weiss J, ten Hoevel MM, Burhenne J, Walter-Sack I, Hoffmann MM, Rengelshausen J, et al. CYP2C19 genotype is a major factor contributing to the highly variable pharmacokinetics of voriconazole. *J Clin Pharmacol.* 2009;49:196–204.
21. Lei H-P, Wang G, Wang L-S, Ou-yang D, Chen H, Li Q, et al. Lack of effect of ginkgo biloba on voriconazole pharmacokinetics in Chinese volunteers identified as CYP2C19 poor and extensive metabolizers. *Ann Pharmacother.* 2009;43:726–31.
22. Miao Q, Wang Z, Zhang Y, Miao P, Zhao Y, Zhang Y, et al. *In vitro* potential modulation of baicalin and baicalein on P-glycoprotein activity and expression in Caco-2 cells and rat gut sacs. *Pharm Biol.* 2016;54:1548–56.
23. Wang G, Lei H, Li Z, Tan Z, Guo D, Fan L, et al. The CYP2C19 ultra-rapid metabolizer genotype influences the pharmacokinetics of voriconazole in healthy male volunteers. *Eur J Clin Pharmacol.* 2009;65:281–5.
24. Saari TI, Laine K, Leino K, Valtonen M, Neuvonen PJ, Olkkola KT. Effect of voriconazole on the pharmacokinetics and pharmacodynamics of intravenous and oral midazolam. *Clin Pharmacol Ther.* 2006;79:362–70.
25. Purkins L, Wood N, Ghahramani P, Love ER, Eve MD, Fielding A. Coadministration of voriconazole and phenytoin: pharmacokinetic interaction, safety, and toleration. *Br J Clin Pharmacol.* 2003;56 Suppl 1:37–44.
26. Marshall WL, McCrea JB, Macha S, Menzel K, Liu F, van Schanke A, et al. Pharmacokinetics and tolerability of letermovir coadministered with azole antifungals (posaconazole or voriconazole) in healthy subjects. *J Clin Pharmacol.* 2018;58:897–904.
27. Liu P, Foster G, LaBadie RR, Gutierrez MJ, Sharma A. Pharmacokinetic interaction between voriconazole and efavirenz at steady state in healthy male subjects. *J Clin Pharmacol.* 2008;48:73–84.
28. Andrews E, Damle BD, Fang A, Foster G, Crownover P, LaBadie R, et al. Pharmacokinetics and tolerability of voriconazole and a combination oral contraceptive co-administered in healthy female subjects. *Br J Clin Pharmacol.* 2008;65:531–9.
29. Damle B, LaBadie R, Crownover P, Glue P. Pharmacokinetic interactions of efavirenz and voriconazole in healthy volunteers. *Br J Clin Pharmacol.* 2008;65:523–30.
30. Dodds Ashley ES, Zaas AK, Fang AF, Damle B, Perfect JR. Comparative pharmacokinetics of voriconazole administered orally as either crushed or whole tablets. *Antimicrob Agents Chemother.* 2007;51:877–80.
31. Keirns J, Sawamoto T, Holum M, Buell D, Wisemandle W, Alak A. Steady-state pharmacokinetics of micafungin and voriconazole after separate and concomitant dosing in healthy adults. *Antimicrob Agents Chemother.* 2007;51:787–90.
32. Liu P, Foster G, Gandelman K, LaBadie RR, Allison MJ, Gutierrez MJ, et al. Steady-state pharmacokinetic and safety profiles of voriconazole and ritonavir in healthy male subjects. *Antimicrob Agents Chemother.* 2007;51:3617–26.
33. Purkins L, Wood N, Kleinermans D, Love ER. No clinically significant pharmacokinetic interactions between voriconazole and indinavir in healthy volunteers. *Br J Clin Pharmacol.* 2003;56 Suppl 1:62–8.
34. Scholz I, Oberwittler H, Riedel K-D, Burhenne J, Weiss J, Haefeli WE, et al. Pharmacokinetics, metabolism and bioavailability of the triazole antifungal agent voriconazole in relation to CYP2C19 genotype. *Br J Clin Pharmacol.* 2009;68:906–15.
35. Hohmann N, Kocheise F, Carls A, Burhenne J, Weiss J, Haefeli WE, et al. Dose-dependent bioavailability and CYP3A inhibition contribute to non-linear pharmacokinetics of voriconazole. *Clin Pharmacokinet.* 2016;55:1535–45.
36. Mikus G, Schöwel V, Drzewinska M, Rengelshausen J, Ding R, Riedel KD, et al. Potent cytochrome P450 2C19 genotype-related interaction between voriconazole and the cytochrome P450 3A4 inhibitor ritonavir. *Clin*

Pharmacol Ther. 2006;80:126–35.

37. Rengelshausen J, Banfield M, Riedel K, Burhenne J, Weiss J, Thomsen T, et al. Opposite effects of short-term and long-term St John's wort intake on voriconazole pharmacokinetics. *Clin Pharmacol Ther.* 2005;78:25–33.

38. Saari TI, Laine K, Leino K, Valtonen M, Neuvonen PJ, Olkkola KT. Voriconazole, but not terbinafine, markedly reduces alfentanil clearance and prolongs its half-life. *Clin Pharmacol Ther.* 2006;80:502–8.

# A Novel Study Design Using Continuous Intravenous and Intraduodenal Infusions of Midazolam and Voriconazole for Mechanistic Quantitative Assessment of Hepatic and Intestinal CYP3A Inhibition

The Journal of Clinical Pharmacology  
2020, 00(0) 1–17  
© 2020 The Authors. The *Journal of Clinical Pharmacology* published by Wiley Periodicals LLC on behalf of American College of Clinical Pharmacology  
DOI: 10.1002/jcph.1619

Xia Li, MSc<sup>1</sup>, Lisa Junge, PhD<sup>1</sup>, Max Taubert, MD<sup>1</sup>, Anabelle von Georg, PhD<sup>1</sup>, Dominik Dahlinger, PhD<sup>1</sup>, Chris Starke, PhD<sup>1</sup>, Sebastian Frechen, MD<sup>1</sup>, Christoph Stelzer, PharmD<sup>2</sup>, Martina Kinzig, PhD<sup>2</sup>, Fritz Sörgel, PhD<sup>2,3</sup>, Ulrich Jaehde, PhD<sup>4</sup>, Ulrich Töx, MD<sup>5</sup>, Tobias Goeser, MD<sup>5</sup>, and Uwe Fuhr, MD<sup>1</sup>

## Abstract

The extent of a drug-drug interaction (DDI) mediated by cytochrome P450 (CYP) 3A inhibitors is highly variable during a dosing interval, as it depends on the temporal course of victim and perpetrator drug concentrations at intestinal and hepatic CYP3A expression sites. Capturing the time course of inhibition is therefore difficult using standard DDI studies assessing changes in area under the curve; thus, a novel design was developed. In a 4-period changeover pilot study, 6 healthy men received intraduodenal or intravenous infusions of the CYP3A substrate midazolam (MDZ) at a rate of 0.26 mg/h for 24 hours. This was combined with intraduodenal or intravenous infusion of the CYP3A inhibitor voriconazole (VRZ), administered at rates of 7.5 mg/h from 8 to 16 hours and of 15 mg/h from 16 to 24 hours, after starting midazolam administration. Plasma and urine concentrations of VRZ, MDZ, and its major metabolites were quantified by liquid chromatography-tandem mass spectrometry and analyzed by semiphysiological population pharmacokinetic nonlinear mixed-effects modeling. A model including mechanism-based inactivation of the metabolizing enzymes (maximum inactivation rate constant  $k_{\text{inact}}$ , 2.83 h<sup>-1</sup>; dissociation rate constant  $K_i$ , 9.33 μM) described the pharmacokinetics of VRZ well. By introducing competitive inhibition by VRZ on primary and secondary MDZ metabolism, concentration-time profiles, MDZ and its metabolites were captured appropriately. The model provides estimates of local concentrations of substrate and inhibitor at the major CYP3A expression sites and thus of the respective dynamic extent of inhibition. A combination of intravenous and intraduodenal infusions of inhibitors and substrates has the potential to provide a more accurate assessment of DDIs occurring in both gut wall and liver.

## Keywords

voriconazole, midazolam, CYP3A, drug-drug interaction, semiphysiological population pharmacokinetic modeling

The cytochrome P450 enzymes of the subfamily CYP3A (mainly CYP3A4 and CYP3A5) are the principal enzymes mediating rate-limiting steps in the metabolism of around 30% of therapeutic drugs.<sup>1</sup> At

the same time, their activity is inhibited by many medicines,<sup>2</sup> and CYP3A inhibition is a major mechanism to cause drug-drug interactions (DDIs) with clinically relevant consequences.<sup>3</sup> Thus, it is important

<sup>1</sup>University of Cologne, Faculty of Medicine and University Hospital Cologne, Center for Pharmacology, Department I of Pharmacology, Cologne, Germany

<sup>2</sup>IMBP-Institute for Biomedical and Pharmaceutical Research, Nurnberg-Heroldsberg, Germany

<sup>3</sup>Institute of Pharmacology, West German Heart and Vascular Centre, University of Duisburg-Essen, Essen, Germany

<sup>4</sup>Institute of Pharmacy, Clinical Pharmacy, University of Bonn, Bonn, Germany

<sup>5</sup>Department of Gastroenterology and Hepatology, University Hospital of Cologne, Cologne, Germany

This is an open access article under the terms of the Creative Commons Attribution-NonCommercial-NoDerivs License, which permits use and distribution in any medium, provided the original work is properly cited, the use is non-commercial and no modifications or adaptations are made.

Submitted for publication 31 January 2020; accepted 24 March 2020.

## Corresponding Author:

Uwe Fuhr, MD, University of Cologne, Faculty of Medicine and University Hospital Cologne, Center for Pharmacology, Department I of Pharmacology; Gleueler Straße 24, 50931 Cologne, Germany  
Email: uwe.fuhr@uk-koeln.de

to quantitatively assess the time course and extent of CYP3A inhibition to minimize the risk of adverse drug reactions from such DDIs.

The currently available information on DDIs caused by inhibition of CYP3A is typically limited to *in vitro* interaction studies<sup>4</sup> and to experimental clinical studies in which the maximal extent interaction is tested, usually using a high-dose steady state of an inhibitor and concomitant single doses of the respective substrate.<sup>5-8</sup> Substrates in such studies are either therapeutically relevant drugs with a high likelihood of coadministration or probe drugs selectively metabolized by CYP3A. This approach, however, only provides an average of the extent of inhibition, assuming the perpetrator concentration is constant during the dosing interval, whereas indeed it is fluctuating considerably.<sup>9,10</sup> For the usual design of DDI studies, the observed extent of interaction, especially for substrates with rapid absorption and extensive first-pass metabolism, depends critically on the time course of local inhibitor and substrate concentration. Because these drug concentrations in the local tissue cannot be measured directly, a dynamic modeling approach is required for their description and thus the time course inhibition.<sup>11-13</sup>

Because CYP3A is mainly expressed in gut wall and liver, DDIs attributable to CYP3A inhibition also occur at both sites.<sup>14</sup> The respective contributions to DDIs vary with time according to the concentrations of perpetrator and substrate drugs in the gut wall and liver. To dissect the relative contribution of both sites, oral and intravenous administrations are required, using either separate administration,<sup>15,16</sup> concomitant administration of mass-labeled substances,<sup>8,17</sup> or semisimultaneous administration along with evaluation by a semiphysiological model.<sup>18,19</sup> However, after oral administration, the drug absorption process including the first-pass metabolism often cannot be modeled well because the observation in plasma is the combined result of drug release, intrainestinal transport, absorption, secretion, and intestinal and hepatic first-pass metabolism, which all vary considerably along the gut.<sup>20,21</sup>

Thus, a novel study design was developed to investigate the time course of hepatic and intestinal CYP3A activity in the presence of a CYP3A inhibitor. In this study, substrate and inhibitor were infused continuously and simultaneously at constant infusion rates via intravenous catheters or duodenal tubes to avoid variability attributable to drug release and to the effective site of intestinal drug absorption.

In the present pilot study, midazolam (MDZ) was used as a probe substrate for the *in vivo* assessment of CYP3A activity as recommended by the US Food and Drug Administration and European Medicines Agency.<sup>22,23</sup> MDZ undergoes exten-

sive first-pass metabolism mediated by CYP3A in the gut wall and liver.<sup>24,25</sup> The primary metabolism of MDZ occurs mainly (60%-80%) via CYP3A4-mediated 1'-hydroxylation<sup>26</sup> and, to a lesser extent (5%), by 4-hydroxylation.<sup>27</sup> Most of the hydroxylated metabolites are subsequently metabolized by UDP-glucuronosyltransferases (UGT1A4, 2B4, 2B7).<sup>28</sup> Direct N-glucuronidation of MDZ via UGT1A4 accounts for less than 2% of a dose.<sup>29</sup> Voriconazole (VRZ) was administered as a CYP3A inhibitor.<sup>30</sup> VRZ is extensively metabolized by CYP3A4 and CYP2C19 and meanwhile also inhibits both enzymes.<sup>31</sup> VRZ acts as a strong inhibitor for CYP3A with the inhibition constant  $K_i$  of 0.15 to 0.66  $\mu\text{M}$  for the metabolism of MDZ *in vitro*,<sup>31,32</sup> and also a strong inhibitor *in vivo* at therapeutic doses.<sup>6,33</sup> Also, VRZ is reported to exhibit "autoinhibition" on CYP3A4 *in vivo*.<sup>33,34</sup> Our previous *in vitro* study showed time-dependent inactivation of CYP3A4 by VRZ, with a dissociation rate constant  $K_I$  of 9.33  $\mu\text{M}$ .<sup>35</sup>

Based on the data set from this study, we developed a semiphysiological model to describe local concentrations of the substrate and the inhibitor at the gut wall and liver expression sites of CYP3A and the time course of respective enzyme activity.

## Methods

After approval by the Ethics Committee of the Faculty of Medicine, University of Cologne, Germany (application number 12-051; date of approval: June 6, 2012), the study was carried out in accordance with the standards of Good Clinical Practice, the applicable regulations, and the ethical principles described in the Declaration of Helsinki. All subjects provided the completed informed consent form.

### Study Population

Six healthy white men were enrolled in the study. The volunteers were examined and determined to be healthy by medical history, physical examination, vital signs, electrocardiogram, and clinical laboratory tests including hematology, blood chemistry, and urine screening for illicit drugs. Main exclusion criteria included smoking; consumption of alcohol, grapefruit products, methylxanthine-containing beverages and foods; taking any medication 2 weeks or chronic treatment 8 weeks prior to the study; participating in a trial with a novel investigational medications within 8 weeks or a registered compound within 4 weeks before the study; and having a special diet or lifestyle.

### Study Design

The pilot study was designed as an open-label, changeover, randomized, 3-period clinical trial to characterize the alteration of MDZ pharmacokinetics by



intravenous or intestinal coadministration of VRZ. Both drugs were administered either intravenously or via a duodenal tube directly into the intestinal lumen. Intended periods included the combinations of periods: MDZ (intravenously) and VRZ (intestinal lumen); MDZ (intestinal lumen) and VRZ (intravenously); and MDZ (intestinal lumen) and VRZ (intestinal lumen). In periods during which intraduodenal administration was not feasible for technical reasons, this was switched to intravenous administration, resulting in an additional period with intravenous coadministration of MDZ and VRZ in 3 individuals (subject 2, 3, and 4).

### Study Conduct

Ten milliliters of MDZ solution (MDZ Ratiopharm V 5 mg/5 mL Injektionslösung, Ratiopharm GmbH, Ulm, Germany) were transferred into a 50-mL perfusor syringe containing 40 mL of 5% glucose solution (final concentration of 0.2 mg/mL).

Two hundred milligrams of VRZ (Vfend 200 mg Pulver zur Herstellung einer Infusionslösung, Pfizer Pharma GmbH, Berlin, Germany) was dissolved by the addition of 19 mL of water to obtain a VRZ solution with a concentration of 10 mg/mL. Twenty milliliters of this solution was transferred into a 50-mL perfusor syringe containing 30 mL of 5% glucose solution (final concentration of 4 mg/mL).

We used separate catheters or duodenal tubes to administer each individual drug. Thus, prior to the infusion, up to 3 indwelling venous catheters were placed at the forearms of subjects. For periods including intravenous administration, these were placed at both forearms, with one arm for the infusion(s) and the other side for blood sampling. For intestinal administration, 1 or 2 duodenal tubes (Freka Endo Tube CH/FR 8, 250 cm, LL, Fresenius Kabi AG, Hessen, Germany) were placed under anesthesia with propofol (Propofol 1% [10 mg/1 mL] MCT Fresenius, Fresenius Kabi, Bad Homburg, Germany) by a gastroenterologist. Venous catheters and duodenal tubes were connected to the infusion syringe by a perfusor line (Original Perfusor-Leitung PE, 200 cm, 1\*2 mm, B.Braun, Hessen, Germany). The infusion rate was controlled by the infusion pump (Perfusor Space, B.Braun, Hessen, Germany).

The infusions of MDZ and VRZ were continuous and simultaneous via 2 perfusors. The same size of syringe (50 mL) was used for both drugs, and the placement of both syringe pumps was fixed to the level of the heart. Because the duodenal tube had a dead volume of 7.0 mL, a 7.0-mL bolus of the respective infusion solutions was given to start the infusion. MDZ was infused at a scheduled constant rate of 1.3 mL/h for 24 hours (equal to 0.26 mg/h), whereas VRZ was started 8 hours after the start of the MDZ infusion, and its dose

rate was double after another 8 hours with scheduled infusion rates of 1.6 and 3.2 mL/h (equal to 6.4 and 12.8 mg/h). Both infusions were stopped 24 hours after starting the MDZ infusion. If infusion pumps gave the alarm to indicate that tubes were blocked, the position of volunteers was changed and/or tubes were flushed with tiny volumes of the solution used for the administration to reestablish patency of the tubes. In those cases in which the maneuvers were not immediately successful, a small bolus dose was administered to compensate for the delay in administration.

To standardize any effect caused by the gastrointestinal passage of fluids and food, the subjects drank 200 mL of water at the following times: -1, 1, 3, 7:45, 11, 13, 15, 17, 19, 21, and 24 hours and received standardized snacks at 3, 11, 15, and 19 hours relative to the start of the MDZ infusion. After the end of the infusion, food was offered 24, 27, and 35 hours postdose. A washout phase was at least 7 days between periods.

### Blood and Urine Sampling

For determination of MDZ and its metabolites, that is, 1'-hydroxy-midazolam (1'-OH-MDZ) and 4-hydroxy-midazolam (4-OH-MDZ), as well as VRZ and its main metabolite VRZ N-oxide plasma concentration, blood samples were taken predose and 0.5, 1, 2, 3, 4, 5, 6, 7, 8, 8.5, 9, 10, 11, 12, 13, 14, 15, 16, 16.5, 17, 18, 19, 20, 21, 22, 23, 24, 24.5, 25, 26, 27, 28, 32, and 36 hours after onset of the MDZ infusion. For each sample, 2.7 mL of blood was withdrawn when MDZ was administered alone, and 4.5 mL of blood was withdrawn during coadministration of VRZ. After centrifugation at 4°C, plasma samples were stored at -80°C until quantified.

Urine was collected within intervals of 0-8, 8-16, 16-24, and 24-36 hours after starting the infusion of MDZ to determine recovery of MDZ and its metabolites in urine.

### Analytical Assays

The concentrations of MDZ, 1'-OH-MDZ, 4-OH-MDZ, VRZ, and VRZ N-oxide in plasma, as well as of MDZ, MDZ-N-glucuronide, 1'-OH-MDZ, 1'-OH-MDZ-glucuronide, 4-OH-MDZ, and 4-OH-MDZ-glucuronide in urine were determined using high-performance liquid chromatography coupled to mass spectrometry. The methods are presented in detail in the Supplementary Methods and Table S1. The lower limit of quantification (LLOQ) was 0.05 ng/mL for MDZ/1'-OH-MDZ/4-OH-MDZ in plasma, 10 ng/mL for VRZ/VRZ N-oxide in plasma, 0.5 ng/mL for MDZ/4-OH-MDZ in urine, and 1 ng/mL for 1'-OH-MDZ in urine.

**Table 1.** Physiological and Drug Parameters Used for the Semiphysiological Population Pharmacokinetic Model of Midazolam and Voriconazole and Their Metabolites

Parameter	Definition of Parameter	Value	Reference
<b>Midazolam (MDZ)</b>			
$f_{uB,MDZ}$	Unbound fraction of MDZ in blood	0.033	63
$f_{uG,MDZ}$	Unbound fraction of MDZ in gut wall	1	43
B/P ratio <sub>MDZ</sub>	Blood-to-plasma ratio of MDZ	0.66	8,63
CL <sub>PERMEABILITY, MDZ</sub> (L/h)	Permeability of MDZ	10.6	43
<b>1'-OH-midazolam (1'-OH-MDZ)</b>			
$f_{uB,1'-OH-MDZ}$	Unbound fraction of 1'-OH-MDZ in blood	1	
$f_{uG,1'-OH-MDZ}$	Unbound fraction of 1'-OH-MDZ in gut wall	1	43
B/P ratio <sub>1'-OH-MDZ</sub>	Blood-to-plasma ratio of 1'-OH-MDZ	1	
<b>4-OH-midazolam (4-OH-MDZ)</b>			
$f_{uB,4-OH-MDZ}$	Unbound fraction of 4-OH-MDZ in blood	1	
$f_{uG,4-OH-MDZ}$	Unbound fraction of 4-OH-MDZ in gut wall	1	43
B/P ratio <sub>4-OH-MDZ</sub>	Blood-to-plasma ratio of 4-OH-MDZ	1	
<b>Voriconazole (VRZ)</b>			
$f_{uB,VRZ}$	Unbound fraction of VRZ in blood	0.42	30,64-66
$f_{uG,VRZ}$	Unbound fraction of VRZ in gut wall	1	43
B/P ratio <sub>VRZ</sub>	Blood-to-plasma ratio of VRZ	1	
CL <sub>PERMEABILITY,VRZ</sub> (L/h)	Permeability of VRZ	6.5	35,43
<b>Voriconazole N-oxide (VRZ N-oxide)</b>			
$f_{uB,VRZ-N-oxide}$	Unbound fraction of VRZ N-oxide in blood	1	
$f_{uG,VRZ-N-oxide}$	Unbound fraction of VRZ N-oxide in gut wall	1	43
B/P ratio <sub>VRZ-N-oxide</sub>	Blood-to-plasma ratio of VRZ N-oxide	1	
<b>Physiological parameter</b>			
Q <sub>H</sub> (L/h)	Blood flow of liver	$3.75 \times \text{body weight}^{0.75}$	67
Q <sub>PV</sub> (L/h)	Blood flow of portal vein	$0.75 \times Q_H$	68
Q <sub>HA</sub> (L/h)	Blood flow of hepatic artery	$0.25 \times Q_H$	68
Q <sub>INTEST</sub> (L/h)	Blood flow of small intestine	$0.4 \times Q_H$	68
Q <sub>MUCOSA</sub> (L/h)	Blood flow of gut mucosa	$0.8 \times Q_{INTEST}$	43
Q <sub>villi</sub> (L/h)	Blood flow of villous blood flow	$0.6 \times Q_{MUCOSA}$	43
V <sub>H</sub> (L)	Volume of liver	1	
V <sub>PV</sub> (L)	Volume of portal vein	1	
V <sub>G</sub> (L)	Volume of gut wall	1	

### Model Development

A population pharmacokinetic nonlinear mixed-effects model was built with NONMEM 7.4.1 (Icon Development Solutions, Ellicott City, Maryland). Model diagnostics were conducted using XPOSE 4.5.0.<sup>36</sup> Perl-speaks-NONMEM<sup>37</sup> served as an application programming interface. Data visualization was performed using R 3.5.1 (R Foundation for Statistical Computing, Vienna, Austria).

To quantitatively assess the contribution of intestinal and hepatic MDZ metabolism, a semiphysiological model was developed including a conventional distributional compartmental PK model with additional physiological compartments for gut lumen, gut wall, portal vein, liver, and urine. Physiological parameters entered into the model were taken from the literature (Table 1). A basic version of this model was originally proposed by Frechen et al.<sup>13</sup> In this project, we introduced an enzyme compartment and also extended the model to integrate metabolites, that is, VRZ N-oxide as well as several metabolites of MDZ, that is, 1'-OH-MDZ

and 4-OH-MDZ in the plasma and MDZ-glucuronide, 1'-OH-MDZ, and 1'-OH-MDZ-glucuronide in the urine.

In addition, the case deletion diagnostics (CCD) approach was used for sensitivity analysis with regard to individual subjects and to explore the sources of the high observed variability.<sup>38</sup>

In the current project, quasi-steady-state approximation was applied to calculate the amounts in the respective compartment with the assumption that all compounds reach an equilibrium in compartments, which means the output and input rates are equal in the gut wall, portal vein, and liver compartments.<sup>39</sup> This method was used to reduce the run time of the software.

### Model Evaluation

Model selection was based on the biological plausibility, metabolic pathways, objective function value (OFV, a drop of 6.63 being considered statistically significant with  $P < .01$ ), and results of goodness-of-fit plots (GOF). In addition, eta shrinkage was assessed to

confirm the informatory content of individual predictions (eta shrinkage < 20%).

Because of the small number of subjects (6 subjects), bootstrap analysis was not performed. Being a highly complex model, first-order conditional estimation with interaction (FOCE-I) could provide parameter estimates but would not provide reasonable estimates of parameter variability. Therefore, following FOCE-I, Monte Carlo importance sampling expectation maximization was used to generate information about the uncertainty of parameters.<sup>40</sup>

Model trend and variability were finally assessed by visual predictive checks (VPCs) performed by simulating 1000 replicates of the original study design.<sup>41</sup>

### Simulations

Simulations based on the estimates of the fixed-effect parameters from the final model were conducted in 1000 virtual subjects with NONMEM. First, the simulation of the original study design was performed to describe the substrate, inhibitor, and metabolite concentrations versus time in liver and intestine, as well as the full-time course of relative enzyme activity at both sides. Second, the simulation was carried out according to the study design of Saari et al<sup>6</sup> (ie, subjects were administered VRZ orally 400 mg twice a day on the first day and 200 mg twice daily on the second day, with MDZ administered 0.05 mg/kg intravenously or 7.5 mg orally 1 hour after the last dose of VRZ and during a control period). Then, the 90% confidence interval of predicted exposure of MDZ, 1'-OH-MDZ and VRZ were compared with the observed drug plasma concentrations.

## Results

### Clinical Trial and Study Population

The present DDI study between MDZ and VRZ was carried out in 6 healthy men (age range of 27-44 years; body mass index of 22.2-33.0 kg/m<sup>2</sup>). Because of intermittent problems occurring during administration of the drugs (in most cases clogged tubes), actual doses and thus infusion rates varied slightly from the originally planned overall doses (6.24 mg for MDZ, 153.6 mg for VRZ). By weighting the syringe before and after the end of the infusion, the actual infusion amounts were recorded in Table S2. A bolus dose was given in the case of blocked tubes (see in Table S2). Also, the period of combined MDZ (intestinal lumen) and VRZ (intestinal lumen) was repeated for subject 5 because of a leakage of the duodenal tube at the connector between the perfusion tube and the perfusion line.

MDZ and VRZ doses were well tolerated. Four subjects felt mild tiredness several hours after administration of MDZ. One subject experienced moderate

diarrhea unrelated to study drug intake. He also had a vasovagal reaction and vomiting on venipuncture in 1 period, which was suspended and repeated on a separate occasion. Subject 4 prematurely discontinued the study after 2 periods for reasons unrelated to the study.

A total number of 2721 drug plasma samples ( $n_{\text{MDZ}} = 638$ ,  $n_{\text{VRZ}} = 404$ ,  $n_{\text{VRZ N-oxide}} = 455$ ,  $n_{1\text{'-OH-MDZ}} = 633$ , and  $n_{4\text{-OH-MDZ}} = 591$ ) and 170 urine samples ( $n_{\text{MDZ-glucuronide}} = 45$ ,  $n_{1\text{'-OH-MDZ-glucuronide}} = 75$ , and  $n_{1\text{'-OH-MDZ}} = 50$ ) were quantified. The percentages for plasma samples below LLOQ were  $P_{\text{MDZ}} = 0.932\%$ ,  $P_{\text{VRZ}} = 13.3\%$ ,  $P_{\text{VRZ N-oxide}} = 2.57\%$ ,  $P_{1\text{'-OH-MDZ}} = 1.71\%$ , and  $P_{4\text{-OH-MDZ}} = 8.23\%$ ; and for urine samples below LLOQ were  $P_{1\text{'-OH-MDZ-glucuronide}} = 1.32\%$ ,  $P_{1\text{'-OH-MDZ}} = 34.2\%$ , and  $P_{\text{MDZ-glucuronide}} = 39.5\%$ . Within the entire 36-hour collection interval the median (90%CI) intravenous dose of MDZ recovered in the urine as the metabolites 1'-OH-MDZ and 1'-OH-MDZ-glucuronide was 85.3% (70.6%-102%), and for intraduodenal administration of doses of MDZ, it was 59.7% (44.8%-65.3%) identified in the urine as the formation of 1'-OH-MDZ and 1'-OH-MDZ-glucuronide. Only 0.250% (0.0204%-0.413%) of the administered dose was recovered as MDZ-glucuronide. The urinary excretion of 1'-OH-MDZ, 1'-OH-MDZ-glucuronide, and MDZ-glucuronide was further used in the model development to estimate the ratio of each metabolic pathway of MDZ (Figure 1). The amounts of unchanged MDZ, 4-OH-MDZ, and 4-OH-MDZ-glucuronide in urine were too low to be quantified and were neglected for model development. The observations of each substance below the limit of quantification (BLQ) were integrated into the model with the M3 method to maximize the likelihood for BLQ observations with respect to the model parameters, and the likelihood for an observation was taken as the likelihood that it was indeed BLQ.<sup>42</sup> Based on this data set, the semiphysiological population pharmacokinetic model was developed for the 2 parent drugs as well as 5 of the metabolites.

### Model Development

The structure of the model is presented in Figure 2. Physiological compartments were incorporated in the model using the respective organ blood flows (Table 1). The "well-stirred" model was applied in the hepatic and intestinal compartments to estimate the intestinal and hepatic extraction of the drug at both sites, assuming that the drug in both the gut wall and liver compartment reaches equilibrium (equations 1 and 2); each subspace (ie, vascular, interstitial, and intracellular space) is considered homogenous; the transfer of free drug is perfusion-limited, neglect of conventional tissue to blood partitioning constants. Physiological parameters

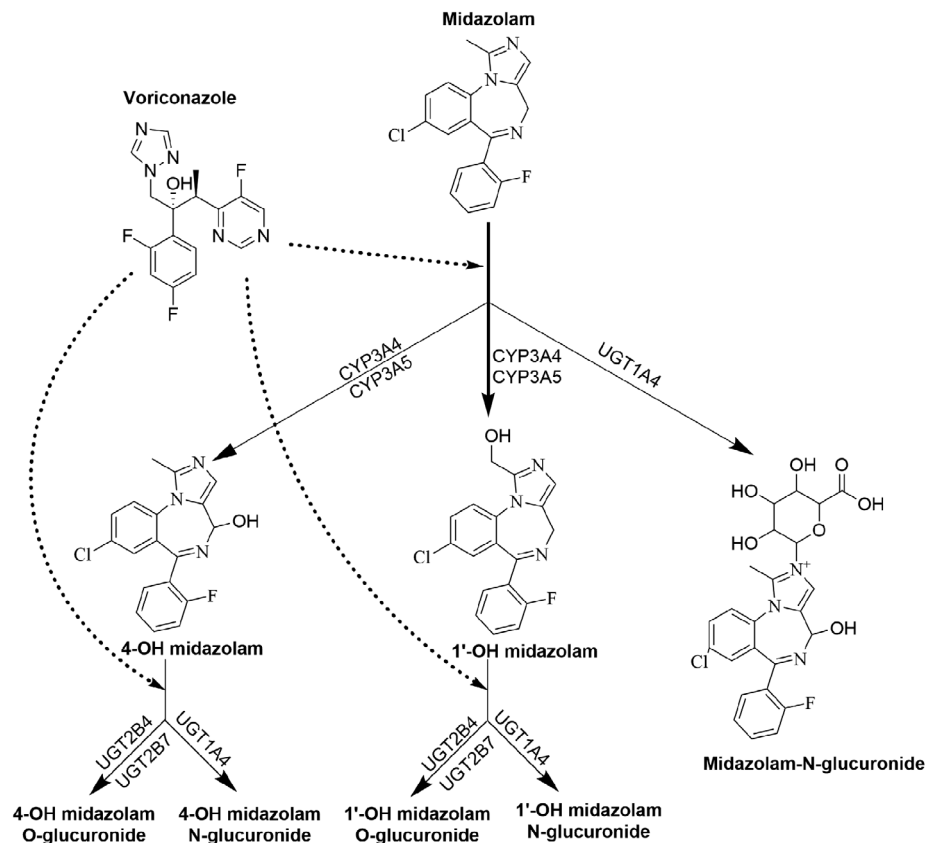


**Figure 1.** Drug-drug interaction between voriconazole and midazolam and its metabolite network. Schematic illustration of the inhibition of voriconazole on the midazolam pathway considered in the present evaluation. Dashed lines indicate inhibition.

and drug physicochemical properties used for model development are summarized in Table 1.

$$E_H = \frac{CL_{Int,H} \times fu_B}{Q_H + CL_{Int,H} \times fu_B} \quad (1)$$

$$E_G = \frac{CL_{Int,G} \times fu_G}{Q_G + CL_{Int,G} \times fu_G} \quad (2)$$

where  $E_H$ , is hepatic extraction and  $E_G$  is intestinal extraction;  $fu_B$ ,  $fu_G$  is the ratio of unbound drug concentration in plasma versus total drug concentration in blood ( $fu_B = \frac{fu}{Cb/Cp}$ );  $CL_{Int,H}$  is intrinsic hepatic clearance and  $CL_{Int,G}$  is gut wall clearance;  $Q_H$  is the hepatic blood flow set to an allometric expression of body weight; and  $Q_G$  is the relevant villous blood flow calculated by equation 3.<sup>43</sup>

$$Q_G = \frac{Q_{villi} CL_{perm}}{Q_{villi} + CL_{perm}} \quad (3)$$

where  $Q_{villi}$  is villous blood flow, and  $CL_{perm}$  is the permeability of the drug.

**MDZ Model.** A model consisting of a central and a peripheral systemic compartment plus 3 “physio-

logical” compartments (representing gut wall, portal vein, and liver) with linear elimination and a combined residual error model appropriately described the concentrations of MDZ (Figure 2).

**1'-OH-MDZ and 1'-OH-MDZ-Glucuronide Model.** The 1'-hydroxylation pathway accounted for most of the primary metabolism of MDZ. The input to the gut wall and liver compartments of 1'-OH-MDZ was modeled by the “well-stirred” model and reflected the respective partial extraction of MDZ in these compartments. The partial metabolic fraction  $F_{1'-OH-MDZ}$  in both the gut wall and liver was finally estimated to be 75.4% (see in Table 2).

Subsequently 1'-OH-MDZ was conjugated to form 1'-OH-MDZ-glucuronide at both the gut wall and liver sites, which was finally excreted into the urine. Glucuronidation into 1'-OH-MDZ-glucuronide was also modeled by the “well-stirred” model as the extraction of 1'-OH-MDZ from the gut wall and liver compartments. Because of nonspecific  $\beta$ -glucuronidase treatment, 1'-OH-MDZ-glucuronide was the total amount of 1'-OH-MDZ-O-glucuronide and 1'-OH-MDZ-N-glucuronide (see Supplementary Methods). The fraction of 1'-OH-MDZ metabolized to the glucuronides

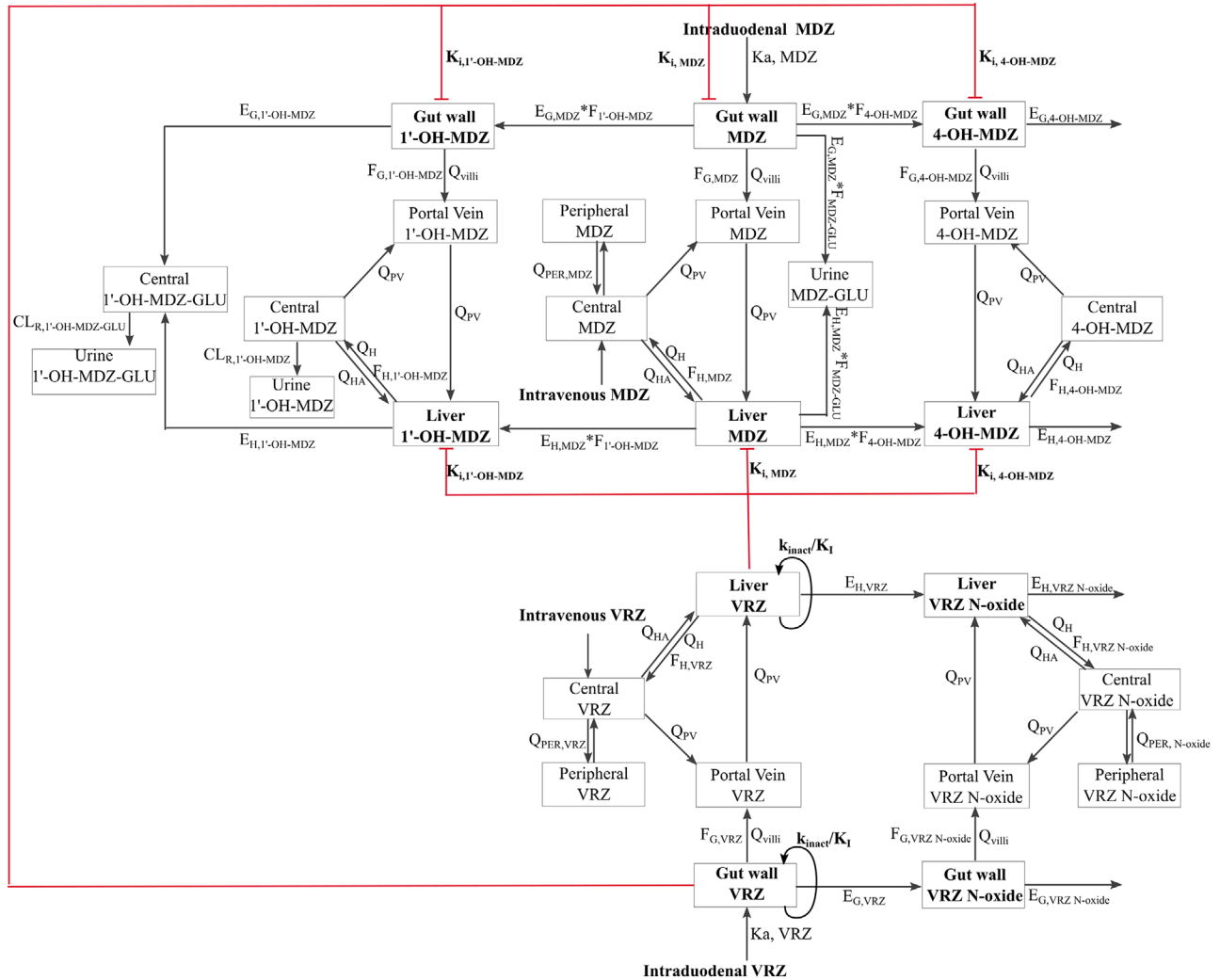


**Figure 2.** Scheme of semiphysiological population pharmacokinetic model of midazolam, 1'-hydroxy-midazolam, 4-hydroxy-midazolam, voriconazole, and voriconazole N-oxide.  $k_{inact}/K_i$  represents autoinhibition of VRZ on its own enzyme. Dashed arrows describe the inhibitory effect of VRZ at the enzyme site on liver and gut wall clearances of MDZ, 1'-OH-MDZ, and 4-OH-MDZ. The definitions of abbreviations refer to Tables 1 and 2.

was assumed to be unity because the other known pathway (CYP3A-mediated hydroxylation) accounts for less than 1% and also no data of its respective metabolite (1,4-di-OH-MDZ) were available.<sup>44</sup> Renal clearance of 1'-OH-MDZ-glucuronide was then estimated based on the amounts of 1'-OH-MDZ-glucuronide excreted in urine.

Unconjugated 1'-OH-MDZ excreted into the urine from the central compartment was also integrated into the model to estimate renal clearance of 1'-OH-MDZ.

**4-OH-MDZ Model.** Although the metabolic pathway from MDZ to 4-OH-MDZ is less important, we still successfully quantified the plasma concentrations of 4-OH-MDZ in this project. This metabolite was also incorporated into the model by the respective partial extraction of MDZ in the gut wall and liver com-

partments. However, the amount of 4-OH-MDZ and its subsequent conjugate (4-OH-MDZ glucuronide) in urine was too low to be quantified, and also the metabolite from another subsequent pathway (1,4-di-OH-MDZ) was not measured.<sup>44</sup> Thus, the partial metabolic fraction  $F_{4-OH-MDZ}$  could not be estimated and was fixed to 5% according to the literature.<sup>27</sup>

**MDZ Glucuronide Model.** MDZ can also be directly conjugated to form MDZ-glucuronide and then be excreted into the urine. This pathway was introduced into the model assuming that the input of MDZ-glucuronide was the partial extraction fraction ( $F_{MDZ-glucuronide}$ ) of MDZ into the gut wall and liver compartments. This value was estimated to be 0.218% based on the amount of MDZ glucuronide excreted in the urine (see in Table 2).

**Table 2.** Pharmacokinetic Parameters of the Final Model

Parameter (Unit)	Definition of Parameter	All Subjects		Without Subject 3 (as Sensitivity Analysis)	
		Estimate	RSE (%)	Estimate	RSE (%)
<i>θ</i> – Estimates					
CL <sub>Int,H,MDZ</sub> (L)	Unbound intrinsic hepatic clearance of MDZ	1060	13.6	1160	7.50
CL <sub>Int,G,MDZ</sub> (L)	Unbound intrinsic intestinal clearance of MDZ	15.8	21.7	17.1	10.6
Q <sub>PER,MDZ</sub> (L/h)	Distributional clearance to peripheral compartment of MDZ	19.9	15.9	21.7	18.7
V <sub>CEN,MDZ</sub> (L)	Volume of distribution in central compartment of MDZ	71.7	6.60	68.4	7.70
V <sub>PER,MDZ</sub> (L)	Volume of distribution in peripheral compartment of MDZ	65.9	7.80	62.1	9.10
K <sub>a,MDZ</sub> (h <sup>-1</sup> )	First-order absorption rate constant of MDZ	1.57	19.2	1.43	19.1
CL <sub>Int,H,1'-OH-MDZ</sub> (L/h)	Unbound intrinsic hepatic clearance of 1'-OH-MDZ	175	7.80	181	12.7
CL <sub>Int,G,1'-OH-MDZ</sub> (L/h)	Unbound intrinsic intestinal clearance of 1'-OH-MDZ	65.6	19.8	61.3	19.7
V <sub>CEN,1'-OH-MDZ</sub> (L)	Volume of distribution in central compartment of 1'-OH-MDZ	63.6	12.2	64.1	13.2
F <sub>1'-OH-MDZ</sub>	Fraction of the metabolic pathway from MDZ to 1'-OH-MDZ	0.754	35.4	0.715	30.1
CL <sub>R,1'-OH-MDZ</sub> (L/h)	Clearance from central compartment to urine of 1'-OH-MDZ	1.29	29.1	2.11	15.5
CL <sub>R,1'-OH-MDZ-GLU</sub> (L/h)	Clearance from central compartment to urine of 1'-OH-MDZ-GLU	2.43	72.0	1.79	81
CL <sub>Int,H,4-OH-MDZ</sub> (L/h)	Unbound intrinsic hepatic clearance of 4-OH-MDZ	54.6	12.9	59.2	14.7
CL <sub>Int,G,4-OH-MDZ</sub> (L/h)	Unbound intrinsic intestinal clearance of 4-OH-MDZ	53.5	7.30	53.7	8.10
V <sub>CEN,4-OH-MDZ</sub> (L)	Volume of distribution in central compartment of 4-OH-MDZ	50.4	7.10	51.1	8.50
F <sub>4-OH-MDZ</sub>	Fraction of the metabolic pathway from MDZ to 4-OH-MDZ	0.05(FIX)	-	0.05(FIX)	-
F <sub>MDZ-GLU</sub> (L/h)	Fraction of the metabolic pathway from MDZ to MDZ-GLU	0.218	15.2	0.174	21.8
CL <sub>Int,H,VRZ</sub> (L/h)	Unbound intrinsic hepatic clearance of VRZ	171	29.6	145	33.7
CL <sub>Int,G,VRZ</sub> (L/h)	Unbound intrinsic intestinal clearance of VRZ	35.7	52.7	36.3	33.3
Q <sub>PER,VRZ</sub> (L/h)	Distributional clearance to peripheral compartment of VRZ	27.5	7.10	21.9	9.30
V <sub>CEN,VRZ</sub> (L)	Volume of distribution in central compartment of VRZ	127	4.70	150	4.50
V <sub>PER,VRZ</sub> (L)	Volume of distribution in peripheral compartment of VRZ	381	14.6	431	18.6
K <sub>a,VRZ</sub> (h <sup>-1</sup> )	First-order absorption/transit rate constant of VRZ	1.86	15.3	3.20	24.7
k <sub>inact</sub> (h <sup>-1</sup> )	Maximum inactivation rate constant of VRZ	2.83	28.9	2.97	22.4
K <sub>i</sub> (μM)	Dissociation rate constant of VRZ	9.33(FIX)	-	9.33(FIX)	-
CL <sub>Int,H,VRZ N-oxide</sub> (L/h)	Unbound intrinsic hepatic clearance of VRZ-N-oxide	6.70	17.8	6.56	18.0
CL <sub>Int,G,VRZ N-oxide</sub> (L/h)	Unbound intrinsic intestinal clearance of VRZ-N-oxide	41.0	33.9	49.2	25.6
Q <sub>PER,VRZ N-oxide</sub> (L/h)	Distributional clearance to peripheral compartment of VRZ-N-oxide	39.5	68.4	255	233
V <sub>CEN,VRZ N-oxide</sub> (l)	Volume of distribution in central compartment of VRZ-N-oxide	19.0	37.4	14.6	21.0
V <sub>PER,VRZ N-oxide</sub> (L)	Volume of distribution in peripheral compartment of VRZ-N-oxide	19.0	37.5	23.9	129
K <sub>i,MDZ</sub> (μM)	Inhibition constant of VRZ for inhibition of MDZ	0.586	27.8	0.363	19.6
K <sub>i,1'-OH-MDZ</sub> (μM)	Inhibition constant of VRZ for inhibition of 1'-OH-MDZ	1.13	50.4	0.690	34.2
K <sub>i,4-OH-MDZ</sub> (μM)	Inhibition constant of VRZ for inhibition of 4-OH-MDZ	0.356	16.7	0.322	16.2
<i>ω</i> <sup>2</sup> – Estimates					
IIV CL <sub>Int,H,MDZ</sub> (CV%)	Interindividual variability on hepatic clearance of MDZ	30.8	9.10	29.3	4.50
IIV CL <sub>Int,G,MDZ</sub> (CV%)	Interindividual variability on intestinal clearance of MDZ	42.0	10.8	43.8	9.80
IIV CL <sub>Int,H,VRZ</sub> (CV%)	Interindividual variability on hepatic clearance of VRZ	70.1	5.00	63.8	7.30
IIV CL <sub>Int,G,VRZ</sub> (CV%)	Interindividual variability on intestinal clearance of VRZ	74.0	4.10	80.4	7.10
IIV CL <sub>Int,H,1'-OH-MDZ</sub> (CV%)	Interindividual variability on hepatic clearance of 1'-OH-MDZ	28.1	13.2	18.7	19.0
IIV CL <sub>Int,G,1'-OH-MDZ</sub> (CV%)	Interindividual variability on intestinal clearance of 1'-OH-MDZ	39.5	20.7	48.4	17.4
IIV CL <sub>Int,H,4-OH-MDZ</sub> (CV%)	Interindividual variability on hepatic clearance of 4-OH-MDZ	25.8	7.40	22.3	2.60
IIV CL <sub>Int,H,VRZ N-oxide</sub> (CV%)	Interindividual variability on hepatic clearance of VRZ N-oxide	28.3	3.60	31.2	5.00
IIV CL <sub>Int,G,VRZ N-oxide</sub> (CV%)	Interindividual variability on intestinal clearance of VRZ N-oxide	48.5	2.40	56.7	2.10
IIV K <sub>i,MDZ</sub> (CV%)	Interindividual variability on inhibition of MDZ	116	1.50	51.6	6.20
IIV K <sub>i,1'-OH-MDZ</sub> (CV%)	Interindividual variability on inhibition of 1'-OH-MDZ	122	7.80	63.6	11.8
IIV K <sub>i,4-OH-MDZ</sub> (CV%)	Interindividual variability on inhibition of 4-OH-MDZ	36.2	5.10	30.7	5.40
IIV k <sub>inact,VRZ</sub> (CV%)	Interindividual variability on maximum inactivation rate of VRZ	20.8	35.6	21.1	29.9
<i>σ</i> <sup>2</sup> – Estimates					
RV <sub>MDZ</sub> (CV%)	Proportional residual variability of MDZ	11.6	9.10	12.0	9.90
RV <sub>MDZ</sub> (SD, nmol/L)	Additive residual variability of MDZ	1.75	7.10	1.64	8.40
RV <sub>1'-OH-MDZ</sub> (CV%)	Proportional variability of 1'-OH-MDZ	11.3	10.8	0.0981	472
RV <sub>1'-OH-MDZ</sub> (SD, nmol/L)	Additive variability of 1'-OH-MDZ	0.328	5.90	0.38	3.60
RV <sub>4-OH-MDZ</sub> (CV%)	Proportional variability of 4-OH-MDZ	5.50	33.3	1.32	256
RV <sub>4-OH-MDZ</sub> (SD, nmol/L)	Additive variability of 4-OH-MDZ	0.0994	4.90	0.106	3.7
RV <sub>VRZ</sub> (CV%)	Proportional variability of VRZ	18.5	5.20	17.8	5.80
RV <sub>VRZ</sub> (SD, nmol/L)	Additive variability of VRZ	15.9	10.1	16.3	11.7

(Continued)



Table 2. Continued

Parameter (Unit)	Definition of Parameter	All Subjects		Without Subject 3 (as Sensitivity Analysis)	
		Estimate	RSE (%)	Estimate	RSE (%)
$RV_{VRZ\ N\text{-oxide}}$ (CV%)	Proportional variability of VRZ N-oxide	11.5	7.20	13.0	5.70
$RV_{VRZ\ N\text{-oxide}}$ (SD, nmol/L)	Additive variability of VRZ N-oxide	76.5	11.2	44.6	13.7
$RV_{MDZ\text{-GLU}}$ (SD, nmol)	Additive variability of MDZ-GLU in urine	9.45	11.3	9.44	13.5
$RV_{1'\text{-OH-MDZ-GLU}}$ (CV%)	Proportional residual variability of 1'-OH-MDZ-GLU in urine	41.0	12.8	42.6	12.2
$RV_{1'\text{-OH-MDZ\ urine}}$ (CV%)	Proportional residual variability of 1'-OH-MDZ in urine	178	34.7	77.4	33.9
$RV_{1'\text{-OH-MDZ\ urine}}$ (SD, nmol)	Additive residual variability of 1'-OH-MDZ in urine	23.5	36.3	23.1	35.3

MDZ, midazolam; 1'-OH-MDZ, 1'-OH-midazolam; 4-OH-MDZ, 4-OH-midazolam; MDZ-GLU, midazolam-glucuronide; 1'-OH-MDZ-GLU, 1'-OH midazolam-glucuronide; VRZ, voriconazole; VRZ N-oxide, voriconazole N-oxide; CV, coefficient variation; SD, standard deviation. CV% for IIV computed as  $\sqrt{\omega^2}$ ; CV% for RV computed as  $\sqrt{\sigma^2}$ .

**VRZ and VRZ N-Oxide Models.** The structure of the semiphysiological model for VRZ was identical to that of MDZ, and gut wall and liver extractions of VRZ were introduced with a “well-stirred” model. VRZ was metabolized into VRZ N-oxide in the gut wall and liver. The input of VRZ N-oxide was modeled as the extraction of VRZ in both the gut wall and liver compartments. Because of a lack of urine data, the formation ratio of the primary metabolite VRZ N-oxide could not be estimated. Also, no data of other metabolites, for example, 4-hydroxyvoriconazole, were available. Therefore, the metabolic ratio to VRZ N-oxide was assumed to be unity.

**Mechanistic Inhibition by VRZ.** Because our previous research showed that VRZ exerts time-dependent inhibition on its metabolic enzymes, mechanism-based inactivation was integrated into the model to describe the autoinhibition of VRZ metabolism, considering the synthesis and natural degradation of enzymes in the gut wall and liver. The incorporation of the mechanistic inhibition model in the gut wall and liver compartments significantly improved the model of VRZ ( $\Delta\text{OFV} = -162$ ). It was not identifiable to separately attribute the metabolic pathways to CYP3A or CYP2C19 in this project. Therefore, mechanistic inhibition was introduced (equation 4) on total metabolic enzymes of VRZ in both the gut wall and liver.

$$\frac{dE_{(t)}}{dt} = K_{deg} \times E_0 - K_{deg} \times E_{(t)} - \frac{k_{inact} \times [I]}{K_I + [I]} \times E_{(t)} \quad (4)$$

where  $E_{(t)}$  is the amount of active enzyme present at time  $t$ ;  $E_0$  is the amount of original active enzyme, fixed to be 1;  $K_{deg}$  is the first-order degradation rate of the enzyme in the absence of VRZ;  $K_I$  is the dissociation rate constant, obtained from in vitro experiments<sup>35</sup>;  $[I]$ : unbound concentration of VRZ at the enzyme sites; and  $k_{inact}$  is the maximum inactivation rate constant.

The degradation  $K_{deg}$  was fixed to 0.023 hour<sup>-1</sup> in liver and 0.03 hour<sup>-1</sup> in the gut wall, which were the mean values of  $K_{deg}$  for CYP3A (0.019 and 0.03 hour<sup>-1</sup> in the liver and gut wall) and CYP2C19 (0.026 and 0.03 hour<sup>-1</sup> in the liver and gut wall), according to the values provided by PK-SIM (version 7.3.0, part of the Open Systems Pharmacology suite).

**Inhibition of MDZ Metabolism by VRC.** In vivo the metabolism of MDZ includes reversible as well as irreversible inhibition.<sup>35</sup> However, in the data set of the present study, it was not possible to obtain identifiable estimates describing both reversible and irreversible inhibition of VRZ on the metabolism of MDZ at the same time. If both inhibitory mechanisms were introduced on the condition that the reversible inhibition constant  $K_{i,MDZ}$  was fixed to be 0.47  $\mu\text{M}$  (according to the in vitro assay<sup>35</sup>), the OFV decreased by 371. If mechanistic inhibition of VRZ was introduced alone in the metabolism of MDZ, the OFV dropped by 334. When only a direct reversible inhibitory effect of VRZ was integrated into the metabolism of MDZ with equation 5, it resulted in a better fit ( $\Delta\text{OFV} = -433$ ). Thus, the reversible inhibition model was finally selected.

$$CL_{Int} = \frac{CL_{Int0}}{1 + \frac{[I]}{K_{i,MDZ}}} \quad (5)$$

where  $CL_{Int}$  is intrinsic clearance;  $CL_{Int0}$  is intrinsic baseline clearance in the absence of VRZ in the gut wall and liver;  $K_{i,MDZ}$  is the inhibition constant of VRZ for inhibition of MDZ metabolism.

Furthermore, VRZ also exhibited competitive inhibition of UGT2B4 and 2B7 in in vitro assays,<sup>45</sup> suggesting the integration of a competitive model into the metabolism of 1'-OH-MDZ and 4-OH-MDZ. Analogous to the inhibition of CYP3A, the inhibition of VRZ on UGT was described with the inhibition constant of  $K_{i,1'\text{-OH-MDZ}}$  and  $K_{i,4\text{-OH-MDZ}}$  at the

**Table 3.** Summary of Individual Pharmacokinetic Parameters Based on Post Hoc Estimates (Median With 90% Confidence Intervals)

Drug	Bioavailability (%)	Hepatic Extraction $E_H$ (%)	Intestinal Extraction $E_G$ (%)	Total Hepatic Clearance $CL_H$ (L/h)	Total Intestinal Clearance $CL_G$ (L/h)
Midazolam	30.8 (16.0-60.0)	18.3 (13.1-28.7)	62.5 (21.7-79.2)	19.8 (12.7-29.9)	4.30 (1.42-5.57)
Voriconazole	18.7 (2.24-62.0)	37.9 (9.93-61.7)	74.6 (26.8-95.6)	128 (25.9-392)	15.0 (1.79-108)

enzyme sites in the liver and gut wall, resulting in further improvement of the model ( $\Delta OFV = -234.5$  and  $-402$ ). The final model structure is depicted in Figure 2.

**Parameter Estimates.** Parameter estimates and their relative standard error of the final model are presented in Table 2. The estimated inhibition constant of VRZ on the metabolism of MDZ  $K_{i,MDZ}$  was  $0.586 \mu M$ , which was similar to the inhibition of 4-OH-MDZ metabolism with a  $K_{i,4-OH-MDZ}$  of  $0.356 \mu M$ , whereas VRZ exhibited a weaker inhibitory effect on glucuronide conjugation of 1'-OH-MDZ with a  $K_{i,1'-OH-MDZ}$  of  $1.13 \mu M$ .

The gut wall and liver extraction ratios of the 2 parent drugs as well as 3 metabolites could be calculated with equations 1 and 2 based on the parameter estimates of intrinsic clearance. Furthermore, the bioavailability of each substance was calculated with equation 6. All these parameters, along with the total hepatic and intestinal clearance values, are reported in Table 3.

$$\text{Bioavailability} = (1 - E_H) \times (1 - E_G) \times 100\% \quad (6)$$

Interindividual variability (IIV) of hepatic and intestinal clearance for MDZ was independently estimated to quantify the variability of CYP3A activity at both enzyme sites, with values of 30.8% for hepatic clearance and 42.0% for intestinal clearance. The IIV of hepatic and intestinal clearance for VRZ was high ( $CV > 70\%$ ). When integrating IIV of  $K_i$  values to explore the variability in the extent of inhibition, the IIV of  $K_{i,MDZ}$  and  $K_{i,1'-OH-MDZ}$  were high, with values of 116% and 122%.

The CCD results pointed out that subject 3 exhibited a great difference in the inhibition constant. Comparing the parameter estimates based on the data sets with and without subject 3 (in Table 2), we observed that  $K_{i,1'-OH-MDZ}$  dropped from  $1.13$  to  $0.690 \mu M$ , and especially, the IIV for  $K_{i,1'-OH-MDZ}$  decreased from 122% to 63.6%; meanwhile,  $K_{i,MDZ}$  was also reduced from  $0.586$  to  $0.363 \mu M$ , and the IIV for  $K_{i,MDZ}$  declined more than half when ignoring the data set of subject 3. This indicated that the DDI for subject 3 might be different. Furthermore, we plotted the individual

predicted concentrations of the inhibitor VRZ and substrates MDZ and 1'-OH-MDZ for all the subjects and found that inhibition of VRZ on the metabolism of MDZ and 1'-OH-MDZ was not obvious for subject 3 because of the weaker inhibitory activity. The effect of omission of subject 3 on the other pharmacokinetic parameters, however, was minor. Therefore, subject 3 was finally retained in the model development and evaluation.

#### Model Evaluation

The GOF of the semiphysiological pharmacokinetic model for MDZ, 1'-OH-MDZ, 4-OH-MDZ, VRZ and VRZ N-oxide (in Figure 3) indicated that the final model fits the observed plasma concentration-time profile of both parent drugs and metabolites for each treatment well. The conditional weighted residuals were homogeneously scattered around the null ordinates with no obvious trend, except for a slight misspecification for 1'-OH-MDZ in the first 10 hours. Individual predictions were informative for model evaluation with a low extent of eta shrinkage. Plots from the observed versus population prediction of VRZ plasma concentration showed high IIV for pharmacokinetics of VRZ. Urine data were not described as well as the plasma data by the model, as shown in the GOF plots, but results were acceptable and could not be improved further (Figure S1).

The VPC of the final pharmacokinetic model for 4 treatments (in Figure 4) confirmed a good predictive performance of the model. The 90% confidence intervals for medians and 5th and 95th percentiles of the simulated predictions were in good agreement with the observed data and covered the variability sufficiently. A slight underprediction in the period of combined MDZ intestinal lumen, VRZ intravenous treatment for the 90% confidence intervals for medians of MDZ and VRZ was considered tolerable (Figure 4). Because only 3 individuals participated in the combined intravenous MDZ, intravenous VRZ treatment, the confidence intervals for median and 5th and 95th percentiles in this period overlapped.

#### Simulation

Figure 5 depicts the concentration-time profiles of parents and metabolites in liver and intestine, as well



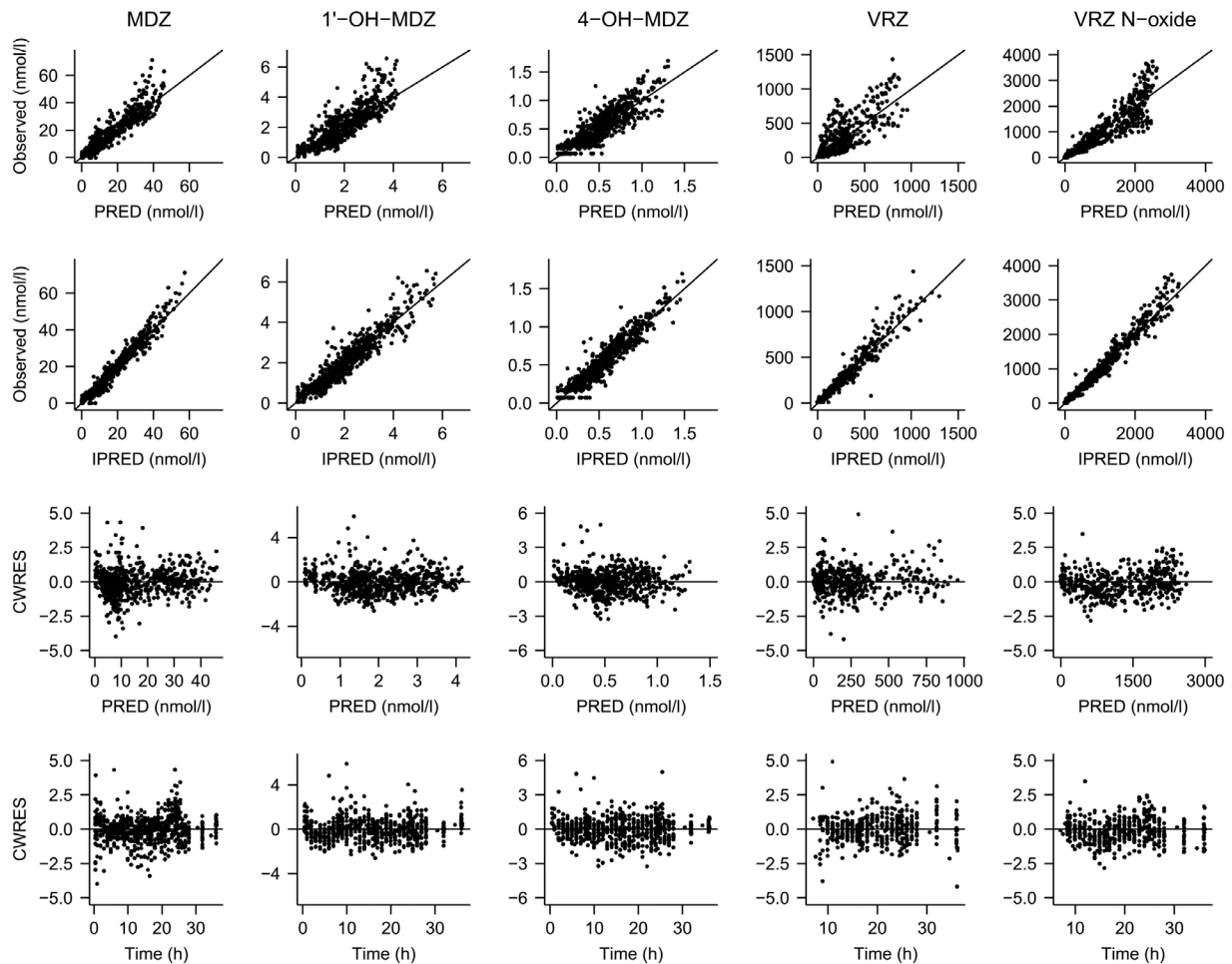


**Figure 3.** Goodness-of-fit plots of the final model for midazolam, 1'-OH-midazolam, 4-OH-midazolam, voriconazole, and voriconazole N-oxide concentration in plasma (all study periods). MDZ, midazolam; 1'-OH-MDZ, 1'-hydroxy-midazolam; 4-OH-MDZ, 4-hydroxy-midazolam; VRZ, voriconazole; VRZ N-oxide, voriconazole N-oxide. Observed plasma drug concentrations (observed) versus population predictions (PRED) and individual predictions (IPRED) obtained from the final population semiphysiological model. Conditional weighted residuals (CWRES) versus PRED and time after the start of MDZ infusion.

as the full-time course of relative enzyme activity. Maximum inhibition of enzyme was reached in liver directly at the end of voriconazole infusion independent of administration route. However, the enzyme activity in the intestine was inhibited only after intraduodenal infusion of voriconazole, and the maximum inhibition appeared at the end of voriconazole infusion. because of the equilibrium of inhibition rate and enzyme synthesis rate, the enzyme activity in liver reached steady state after the end of infusion of voriconazole. In the gut wall, the concentration of voriconazole dropped down to nearly zero when stopping the infusion of voriconazole, in which case, enzyme activity recovered gradually.

By simulating the study by Saari et al,<sup>6</sup> the model-predicted exposure of MDZ and 1'-OH-MDZ after intravenous administration of MDZ were consistent with the observations (Figure S2, period 1), whereas

the slight underprediction were detected for oral administration (Figure S2, period 3). During VRZ treatment, predicted MDZ concentrations were lower than the observed plasma concentrations (Figure S2, periods 2 and 4), but the predicted/observed area under the curve (AUC) and  $C_{max}$  ratios were within a 2-fold range, which was finally considered tolerable. For 1'-OH-MDZ, the predictions gave a better reflection of the observations.

## Discussion

In the present study, both MDZ and VRZ were administered by intestinal or intravenous infusions during different periods to provide the data required to separately assess the DDI at the intestinal and hepatic sites. The pharmacokinetics of VRZ was appropriately described by integrating mechanism-based inactivation

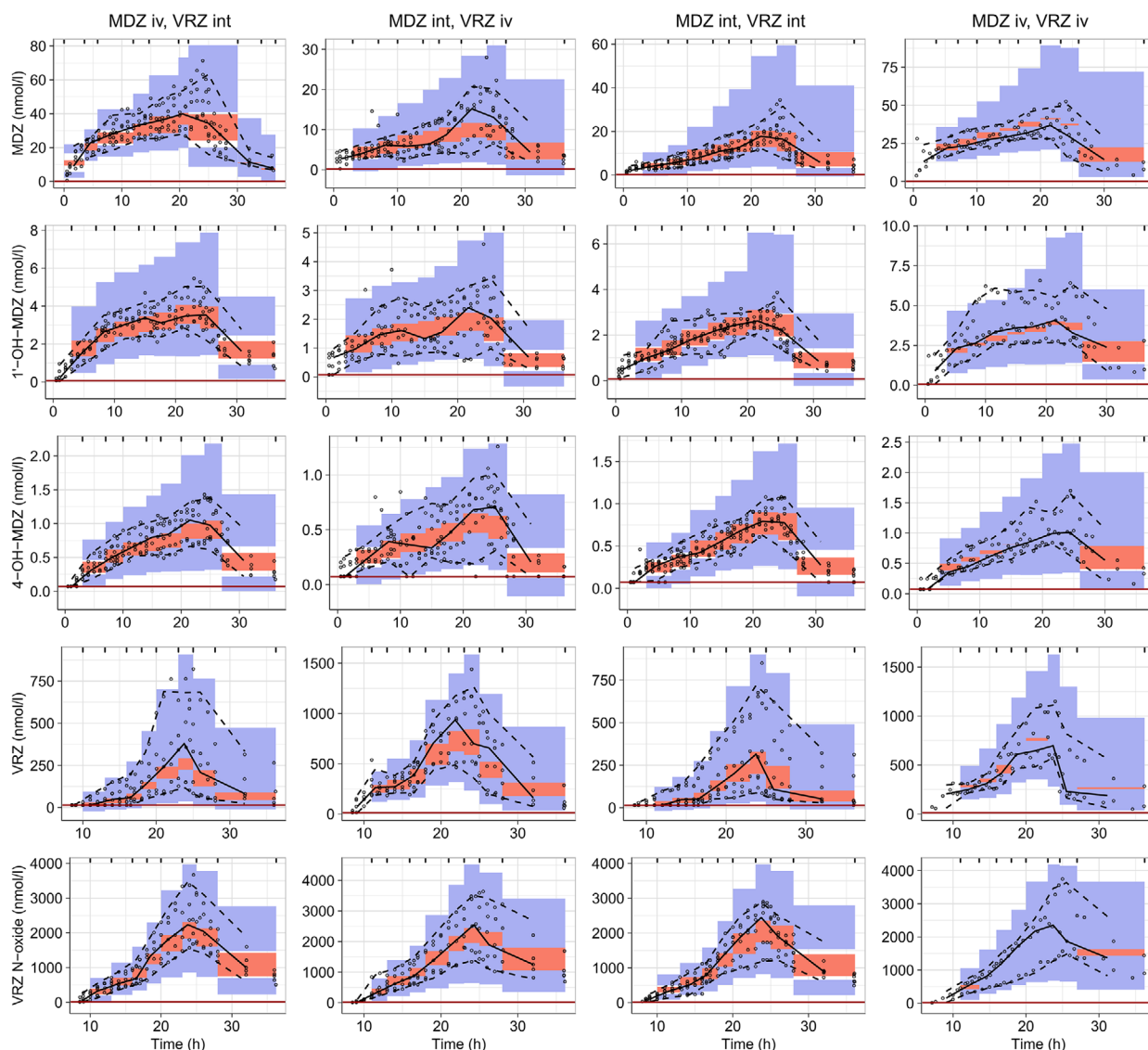


**Figure 4.** Visual predictive checks of the final model for midazolam, 1'-OH-midazolam, 4-OH-midazolam, voriconazole, and voriconazole N-oxide under 4 treatments. MDZ, midazolam; 1'-OH-MDZ, 1'-hydroxy-midazolam; 4-OH-MDZ, 4-hydroxy-midazolam; VRZ, voriconazole; VRZ N-oxide, voriconazole N-oxide; Time, time after the start of MDZ infusion; iv, intravenous administration; int, intraduodenal administration. Black circles represent observed concentrations. The solid line represents the median of observed plasma concentrations, whereas 5th and 95th percentiles of the observations are described by the dashed line. The red shaded areas represent simulation-based 90% confidence intervals for the median. The 90% confidence intervals for the corresponding percentiles of the predictions are shown as blue-shaded areas. The red lines show the lower limit of quantification for each substance.

of its own metabolic enzymes in the model. Also, the concentration-time profiles of the victim drugs (MDZ and its metabolites) were captured well by the model. Thus, the time course of hepatic and intestinal CYP3A activity could be described appropriately.

Compared with fully empirical models, semiphysiological modeling enables the prediction of local drug concentrations in the gut wall and liver. Therefore, the inhibition process could be described directly at the enzyme expression sites, taking the dynamic inhibition by actual concentrations of the perpetrator as well

as synthesis and natural degradation of the enzymes into account.<sup>11,12</sup> We found a VRZ inhibition constant,  $K_{i, MDZ}$ , of  $0.586 \mu\text{M}$  for the effect on the metabolism of MDZ, which was in good agreement with those from our previous in vitro assay ( $0.47 \mu\text{M}$ ; 95%CI,  $0.344\text{--}0.636 \mu\text{M}$ ),<sup>35</sup> and similar to the values obtained in another clinical study ( $0.34 \mu\text{M}$ ).<sup>13</sup> Furthermore, VRZ was identified to inhibit MDZ phase 2 metabolism, resulting in inhibition constant  $K_{i, 1'-OH-MDZ}$  of  $1.13 \mu\text{M}$  for the effect on the glucuronidation of 1'-OH-MDZ. The estimated value was in line with the result from

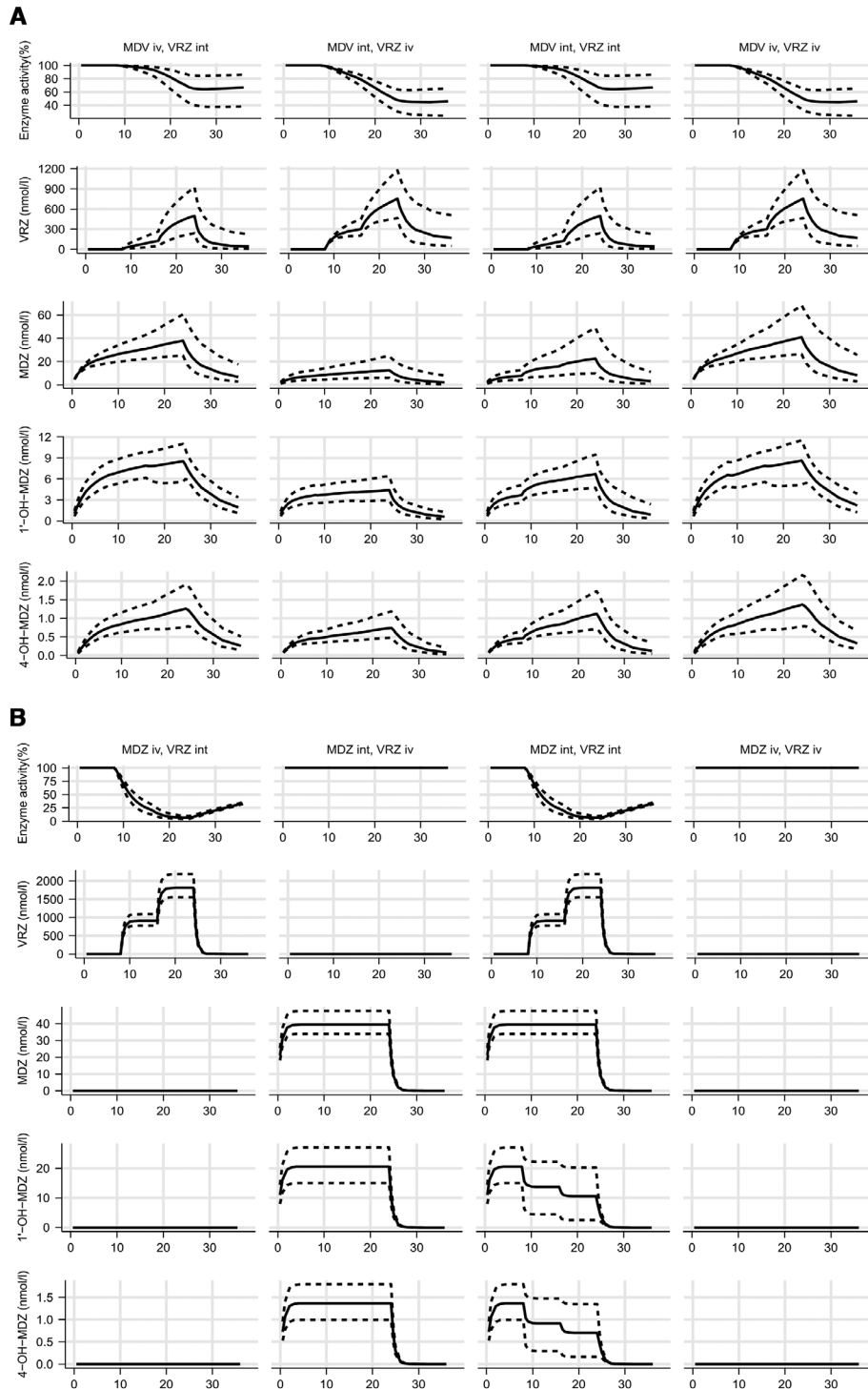


**Figure 5.** Predicted full-time course of relative CYP3A activity as well as predicted concentration-time profiles of voriconazole, midazolam, 1'-OH-midazolam, and 4-OH-midazolam in the liver (A) and intestine (B). The solid line represents the median of prediction, whereas the 5th and 95th percentiles of the predictions are described by the dashed line.

another clinical trial with an inhibition constant of  $1.4 \mu\text{M}$ .<sup>13</sup> This finding is also supported by in vitro data, showing that VRZ inhibits UGT2B4 (a major enzyme mediating this step) with a  $K_{i,UGT2B4}$  of  $1.09\text{--}7.80 \mu\text{M}$ .<sup>45</sup> Although UGT2B7 and 1A4 also mediate

glucuronidation of 1'-OH-MDZ,<sup>29</sup> our model was not able to separately describe the contribution to this metabolic pathway mediated by each enzyme. Therefore, inhibition of glucuronidation in the model was described by a global inhibition constant. All the above

showed that this semiphysiological modeling approach could depict a more precise and mechanistic picture of the inhibition process for DDI, providing a useful tool for in vitro to in vivo extrapolations. However, it is unclear to which extent the empirical component of the model would limit the correctness of such extrapolations, which therefore need to be further validated.

PBPK modeling might be a useful tool to overcome this limitation in exploring DDIs. However, PBPK could only provide total IIV for the observed PK data, which are actually the combined results from IIV for each underlying pharmacokinetic process or parameter. The PBPK approach to quantify variability is knowledge driven rather than data driven. The present semiphysiological population model is set out to identify the key parameters that contribute to IIV and meanwhile, quantify the IIV of these parameters. This approach showed that both intrinsic intestinal and hepatic clearances, as well as inhibition constants, contributed significantly to overall IIV (shown in Table 2). The IIV of hepatic clearance of MDZ (30.8%) representing the variability of active CYP3A abundance in the liver was independent of the IIV in intestinal clearance (42.0%), confirming that the activity of CYP3A at the 2 sites has low correlation and needs to be considered separately.<sup>8,46,47</sup> High variability in VRZ hepatic and intestinal clearance (>70%) was consistent with the published literature,<sup>48,49</sup> which might reflect the presence of CYP2C19 variants (which have not been tested in the study population). The high variability for  $K_{i,MDZ}$  and  $K_{i,1'-OH-MDZ}$  estimates (>100%) may be attributable to several root causes. It might be a consequence of CYP3A polymorphisms because azole antifungals have a higher affinity for CYP3A4 compared with CYP3A5<sup>32,50</sup> and individuals carrying a CYP3A5\*1 allele were less susceptible to inhibition.<sup>51</sup> This may explain the observations in subject 3. Part of the remaining unexplained variability in inhibition constants may be the propagation of the IIV in other processes that could not be described by the present model. In addition, the unstable drug delivery rate or the exact location of duodenal probes placed endoscopically might have contributed to this IIV.

Independent of the modeling method, the combination of intravenous and intestinal administration is a useful approach to assess systemic and presystemic CYP3A metabolism and inhibition.<sup>16</sup> We did not expect that the peculiar way of MDZ administration with regard to input rate and localization would have an impact on MDZ pharmacokinetic processes because pharmacokinetic data of oral and intravenous MDZ showed dose linearity for the single dose range of 0.075-7.5 mg.<sup>6-8,14,52</sup> Our results confirmed this assumption and also indicated that no saturation of MDZ metabolism by

CYP3A occurred. In our evaluation, MDZ total hepatic clearance of 19.8 L/h (Table 3) was similar to the published values (19.4-31.4 L/h) after intravenous administration.<sup>26,53-55</sup> The sum of estimated MDZ hepatic and intestinal clearance of 24.1 L/h is consistent with the reported total clearance of 22.8-39.8 L/h after oral administration.<sup>53,56,57</sup> The bioavailability of MDZ (30.8%) was also in good agreement with the reported value (30%-50%).<sup>14</sup> Urinary excretion of MDZ metabolites (Figure 1) was also essentially consistent with published data.<sup>29</sup> The contribution of the 1'-OH-MDZ pathway was estimated to be 75.4%, which is consistent with the previously reported range that 60%-80% of MDZ dose was recovered as 1'-OH-MDZ-GLU in the urine.<sup>26</sup> Urinary excretion of the direct N-glucuronide of MDZ, which is formed by UGT1A4, accounted for about 0.2% of the MDZ dose in our study, which is lower than the published fraction of 1%-2%.<sup>29</sup>

In contrast, in the case of VRZ, the peculiar way of administration was relevant for its pharmacokinetic behavior. The bioavailability of VRZ in the present study (18.7%) was much lower than the value reported for therapeutic doses (82.6%).<sup>58</sup> One possible reason is that the enzymes mediating VRZ metabolism were saturated at therapeutic doses but not at the low dose/dose rate used in the present study, which is supported by reports on dose-dependent bioavailability of VRZ.<sup>33</sup> Autoinhibition of VRZ metabolism at high doses might also contribute to the discrepancy in bioavailability. Daily chronic VRZ doses used in DDI studies were typically in the range of 200 to 800 mg.<sup>6,59</sup> In the present study, dose and input rate of VRZ were low because we aimed at investigating a gradual response rather than maximal inhibition. In addition, we used 2 input rates to achieve 2 intestinal/hepatic concentrations of VRZ, which is the minimum to assess the concentration dependence of the extent of inhibition.

A constant rate intestinal or intravenous infusion was used to provide constant exposure of both MDZ and VRZ at the respective sites of metabolism for a certain period and thus to facilitate the identifiability of pharmacokinetic parameters. We avoided known sources to cause untoward variability in infusion rates, such as using a single catheter for delivery of more than 1 drug,<sup>60</sup> using different syringe sizes<sup>61</sup> or ignorance of the placement of syringe pumps.<sup>62</sup> Still, during the conduction of the study, some unexpected problems occurred with regard to the infusions, as the infusion pumps occasionally indicated that the tubes were blocked. Our maneuvers to compensate for such problems (see the Methods section) certainly increased the variability in delivery rate while safeguarding the total dose. These obvious problems also indicate the fluctuations in delivery rates may have occurred that



did not result in stopping of the infusion and thus went unnoticed.

Therefore, several limitations of this study need to be considered. The small number of subjects participating in this pilot project limits a precise and accurate estimation of IIV. The unexpected variability in infusion rates is another limitation. Third, the metabolism of VRZ is complex, and we could not separate the metabolic pathways of VRZ mediated by CYP3A and 2C19 in our model. The fourth limitation is our inability to fully describe the complicated mechanisms of enzyme inhibition by VRZ and to separate the reversible and irreversible inhibition of VRZ. Fifth, the development of the physiological components of the model required fixing certain parameters (Table 1), which may result in a scaling effect on other parameters or in a bias in the distribution of these parameters as mentioned above for the variability of  $K_{i,MDZ}$  and  $K_{i,1'-OH-MDZ}$ . Finally, our results obtained at low doses of VRZ predicted well the exposure of VRZ at high doses because we were obviously not able to fully capture the nonlinear pharmacokinetics of VRZ. Thus, we suggest refining and improving this DDI study design with additional information, in this case, for example, provided by (1) using a larger sample size, (2) determining CYP3A5/CYP2C19 genotypes, (3) safeguarding a more steady infusion rate (to this end some investigations in the sources of the respective variability are required), (4) using a single inhibitor infusion rate in one period and assessing dose dependence in separate periods, and (5) selecting a perpetrator with less complicated mechanisms of interaction (eg, without mechanism-based inhibition). Obviously, choices for this combined intravenous and intraduodenal administration are limited to drugs for which both oral and intravenous formulations are available.

## Conclusions

The combination of intravenous and intraduodenal infusions of inhibitors and substrates has the potential to provide a more accurate assessment of DDIs occurring in both gut wall and liver. Using this approach, a detailed description of the inhibitory effects of VRZ on MDZ metabolism at the hepatic and intestinal CYP3A expression sites was possible, including the time course of inhibition and respective sources of interindividual variability. The model may be helpful to assess the potential of VRZ to cause DDIs with other CYP3A substrates. Further studies with lower complexity (inhibitors without mechanism-based inhibition, single inhibitor infusion rate per study period) and larger sample sizes are required to further evaluate this approach.

## Acknowledgments

We appreciate the support from our colleagues during the conduct of the study at the Center for Pharmacology of the University of Cologne, Faculty of Medicine and University Hospital Cologne, Germany, including Paola Di Gion, Christian Queckenberg, Ali Sigaroudi, Benedict Steffens, Carsten Müller, Martin Wiesen, Dennis Rokitta, Daria Kraus, Johanna Krüger, Dirk Kroll, and Ingrid Fehrenz. We also appreciate the excellent suggestions to evaluate the uncertainty of parameters from Sebastian Ueckert and Shijun Wang at Uppsala University, Sweden. We also thank the volunteers for their participation in this study.

## Conflicts of Interest

Sebastian Frechen is now an employee and potential shareholder of Bayer AG, Leverkusen, Germany. Contributions to this article are from the time of employment at the University of Cologne, Faculty of Medicine and University Hospital Cologne, Center for Pharmacology. Authors declare no conflicts of interest.

## Funding

X.L. obtained financial support provided by the China Scholarship Council during the study and during article preparation (no. 201406920024).

## Author Contributions

U.F. and U.J. designed the research. U.F. supervised the clinical trial. L.J., A.G., D.D., C.S., S.F., and C.S. performed the clinical trial. M.K. and F.S. quantified the sample of midazolam and its metabolites. L.J. quantified the sample of voriconazole and voriconazole N-oxide. Gastroenterologists U.T. and T.G. placed duodenal tubes in subjects. X.L. evaluated the data sets, developed models, and wrote the article. M.T. provided technique support during model development. U.F. reviewed and edited the article.

## Data Sharing

Clinical trial data in the project cannot be shared because of the confidentiality of the data.

## References

1. Zanger UM, Schwab M. Cytochrome P450 enzymes in drug metabolism: regulation of gene expression, enzyme activities, and impact of genetic variation. *Pharmacol Ther.* 2013;138(1):103-141.
2. Liu YT, Hao HP, Liu CX, Wang GJ, Xie HG. Drugs as CYP3A probes, inducers, and inhibitors. *Drug Metab Rev.* 2007;39(4):699-721.
3. Dresser GK, Spence JD, Bailey DG. Pharmacokinetic-pharmacodynamic consequences and clinical relevance of cytochrome P450 3A4 inhibition. *Clin Pharmacokinet.* 2000;38(1):41-57.
4. Obach RS, Walsky RL, Venkatakrishnan K. Mechanism-based inactivation of human cytochrome P450 enzymes and

- the prediction of drug-drug interactions. *Drug Metab Dispos.* 2006;35(2):246-255.
5. Halama B, Hohmann N, Burhenne J, Weiss J, Mikus G, Haefeli WE. A nanogram dose of the CYP3A probe substrate midazolam to evaluate drug interactions. *Clin Pharmacol Ther.* 2013;93(6):564-571.
  6. Saari TI, Laine K, Leino K, Valtonen M, Neuvonen PJ, Olkkola KT. Effect of voriconazole on the pharmacokinetics and pharmacodynamics of intravenous and oral midazolam. *Clin Pharmacol Ther.* 2006;79(4):362-370.
  7. Eap C, Buclin T, Cucchia G, et al. Oral administration of a low dose of midazolam (75microg) as an in vivo probe for CYP3A activity. *Eur J Clin Pharmacol.* 2004;60(4):237-246.
  8. Gorski JC, Jones DR, Haehner-Daniels BD, Hamman MA, O'Mara EM, Hall SD. The contribution of intestinal and hepatic CYP3A to the interaction between midazolam and clarithromycin. *Clin Pharmacol Ther.* 1998;64(2):133-143.
  9. Einolf HJ. Comparison of different approaches to predict metabolic drug-drug interactions. *Xenobiotica.* 2007;37(10):1257-1294.
  10. Einolf HJ, Chen L, Fahmi OA, et al. Evaluation of various static and dynamic modeling methods to predict clinical CYP3A induction using in vitro CYP3A4 mRNA induction data. *Clin Pharmacol Ther.* 2014;95(2):179-188.
  11. Quinney SK, Zhang X, Lucksiri A, Gorski JC, Li L, Hall SD. Physiologically based pharmacokinetic model of mechanism-based inhibition of CYP3A by clarithromycin. *Drug Metab Dispos.* 2010;38(2):241-248.
  12. Zhang X, Quinney SK, Gorski JC, Jones DR, Hall SD. Semi-physiologically based pharmacokinetic models for the inhibition of midazolam clearance by diltiazem and its major metabolite. *Drug Metab Dispos.* 2009;37(8):1587-1597.
  13. Frechen S, Junge L, Saari TI, et al. A semiphysiological population pharmacokinetic model for dynamic inhibition of liver and gut wall cytochrome P450 3A by voriconazole. *Clin Pharmacokinet.* 2013;52(9):763-781.
  14. Fuhr U, Hsin C, Li X, Jabrane W, Sörgel F. Assessment of pharmacokinetic drug-drug interactions in humans: in vivo probe substrates for drug metabolism and drug transport revisited. *Annu Rev Pharmacol Toxicol.* 2019;59(1):507-536.
  15. Tsunoda SM, Velez RL, Vov Moltke LL, Greenblatt DJ. Differentiation of intestinal and hepatic cytochrome P450 3A activity with use of midazolam as an in vivo probe: Effect of ketoconazole. *Clin Pharmacol Ther.* 1999;66(5):461-471.
  16. Hohmann N, Kocheise F, Carls A, Burhenne J, Haefeli WE, Mikus G. Midazolam microdose to determine systemic and pre-systemic metabolic CYP3A activity in humans. *Br J Clin Pharmacol.* 2015;79(2):278-285.
  17. Quinney SK, Haehner BD, Rhoades MB, Lin Z, Gorski JC, Hall SD. Interaction between midazolam and clarithromycin in the elderly. *Br J Clin Pharmacol.* 2008;65(1):98-109.
  18. Gazzaz M, Kinzig M, Schaeffeler E, et al. Drinking ethanol has few acute effects on CYP2C9, CYP2C19, NAT2, and P-glycoprotein activities but somewhat inhibits CYP1A2, CYP2D6, and intestinal CYP3A: so what? *Clin Pharmacol Ther.* 2018;104(6):1249-1259.
  19. Lee J, Chaves-Gnecco D, Amico JA, Kroboth PD, Wilson JW, Frye RF. Application of semisimultaneous midazolam administration for hepatic and intestinal cytochrome P450 3A phenotyping. *Clin Pharmacol Ther.* 2002;72(6):718-728.
  20. Kimura T, Higaki K. Gastrointestinal transit and drug absorption. *Biol Pharm Bull.* 2002;25(2):149-164.
  21. Rouge N, Buri P, Doelker E. Drug absorption sites in the gastrointestinal tract and dosage forms for site-specific delivery. *Int J Pharm.* 1996;136(1-2):117-139.
  22. U.S. Food and Drug Administration. Clinical drug interaction studies-study design, data analysis, and clinical implications guidance for industry. October 2017.
  23. European Medicines Agency. Guideline on the investigation of drug interactions. June 2012.
  24. Thummel KE, O'Shea D, Paine MF, et al. Oral first-pass elimination of midazolam involves both gastrointestinal and hepatic CYP3A-mediated metabolism. *Clin Pharmacol Ther.* 1996;59(5):491-502.
  25. Paine MF, Shen DD, Kunze KL, et al. First-pass metabolism of midazolam by the human intestine. *Clin Pharmacol Ther.* 1996;60(1):14-24.
  26. Heizmann P, Eckert M, Ziegler WH. Pharmacokinetics and bioavailability of midazolam in man. *Br J Clin Pharmacol.* 1983;16(suppl 1): 43S-49S.
  27. Kabi F. Midazolam injection, USP Rx only. [https://www.accessdata.fda.gov/drugsatfda\\_docs/label/2017/208878Orig1s0001bl.pdf](https://www.accessdata.fda.gov/drugsatfda_docs/label/2017/208878Orig1s0001bl.pdf). Accessed September 2019. Issued March 2017.
  28. Nguyen HQ, Kimoto E, Callegari E, Obach RS. Mechanistic modeling to predict midazolam metabolite exposure from in vitro data. *Drug Metab Dispos.* 2016;44(5):781-791.
  29. Hyland R, Osborne T, Payne A, et al. In vitro and in vivo glucuronidation of midazolam in humans. *Br J Clin Pharmacol.* 2009;67(4):445-454.
  30. Pfizer. VFEND® I.V. (voriconazole) for Injection VFEND® Tablets VFEND® for Oral Suspension. [https://www.accessdata.fda.gov/drugsatfda\\_docs/label/2010/021266s025s027s029s030,021267s025s029s032s033,021630s014s018s020s0211bl.pdf](https://www.accessdata.fda.gov/drugsatfda_docs/label/2010/021266s025s027s029s030,021267s025s029s032s033,021630s014s018s020s0211bl.pdf). Accessed August 2019. Revised June 2010.
  31. Jeong S, Nguyen PD, Desta Z. Comprehensive in vitro analysis of voriconazole inhibition of eight cytochrome P450 (CYP) enzymes: major effect on CYPs 2B6, 2C9, 2C19, and 3A. *Antimicrob Agents Chemother.* 2009;53(2):541-551.
  32. Yamazaki H, Nakamoto M, Shimizu M, Murayama N, Niwa T. Potential impact of cytochrome P450 3A5 in human liver on drug interactions with triazoles. *Br J Clin Pharmacol.* 2010;69(6):593-597.
  33. Hohmann N, Kocheise F, Carls A, et al. Dose-dependent bioavailability and CYP3A Inhibition contribute to non-linear pharmacokinetics of voriconazole. *Clin Pharmacokinet.* 2016;55(12):1535-1545.
  34. Hohmann N, Kreuter R, Blank A, et al. Autoinhibitory properties of the parent but not of the N-oxide metabolite contribute to infusion rate-dependent voriconazole pharmacokinetics. *Br J Clin Pharmacol.* 2017;83(9):1954-1965.
  35. Li X, Frechen S, Moj D, et al. A physiologically-based pharmacokinetic model of voriconazole integrating time-dependent inhibition of CYP3A4, genetic polymorphisms of CYP2C19 and Predictions Of Drug-Drug Interactions. *Clin Pharmacokinet.* 2019; 10.1007/s40262-019-00856-z.
  36. Jonsson EN, Karlsson MO. Xpose—an S-PLUS based population pharmacokinetic/pharmacodynamic model building aid for NONMEM. *Comput Methods Programs Biomed.* 1998;58(1):51-64.
  37. Lindbom L, Ribbing J, Jonsson EN. Perl-speaks-NONMEM (PsN)—a Perl module for NONMEM related programming. *Comput Methods Programs Biomed.* 2004;75(2):85-94.
  38. Keizer RJ, Karlsson MO, Hooker A. Modeling and simulation workbench for NONMEM: tutorial on Pirana, PsN, and Xpose. *CPT pharmacometrics Syst Pharmacol.* 2013;2(6):e50.
  39. Brill MJE, Väitalo PAJ, Darwich AS, et al. Semiphysiologically based pharmacokinetic model for midazolam and CYP3A mediated metabolite 1-OH-midazolam in morbidly obese and weight loss surgery patients. *CPT pharmacometrics Syst Pharmacol.* 2016;5(1):20-30.

40. Bauer RJ. NONMEM tutorial part II: estimation methods and advanced examples. *CPT Pharmacometrics Syst Pharmacol*. 2019;8(8):538-556.
41. Post TM, Freijer JI, Ploeger BA, Danhof M. Extensions to the visual predictive check to facilitate model performance evaluation. *J Pharmacokinet Pharmacodyn*. 2008;35(2):185-202.
42. Beal SL. Ways to fit a PK model with some data below the quantification limit. *J Pharmacokinet Pharmacodyn*. 2001;28(5):481-504.
43. Yang J, Jamei M, Yeo KR, Tucker GT, Rostami-Hodjegan A. Prediction of intestinal first-pass drug metabolism. *Curr Drug Metab*. 2007;8(7):676-684.
44. Vossen M, Sevestre M, Niederalt C, Jang I-J, Willmann S, Edginton AN. Dynamically simulating the interaction of midazolam and the CYP3A4 inhibitor itraconazole using individual coupled whole-body physiologically-based pharmacokinetic (WB-PBPK) models. *Theor Biol Med Model*. 2007;4(13):1-15.
45. Junge L. In silico, in vitro und in vivo Charakterisierung der Hemmung ausgewählter Fremdstoff-metabolisierender Enzyme des Menschen durch Voriconazol. <http://hss.ulb.uni-bonn.de/2016/4308/4308.htm>. 2016.
46. Paine MF, Hart HL, Ludington SS, Haining RL, Rettie AE, Zeldin DC. The human intestinal cytochrome P450 "pie." *Drug Metab Dispos*. 2006;34(5):880-886.
47. von Richter O, Burk O, Fromm MP, Thon K, Eichelbaum M, Kivistö K. Cytochrome P450 3A4 and P-glycoprotein expression in human small intestinal enterocytes and hepatocytes: a comparative analysis in paired tissue specimens. *Clin Pharmacol Ther*. 2004;75(3):172-183.
48. Theuretzbacher U, Ihle F, Derendorf H. Pharmacokinetic/pharmacodynamic profile of voriconazole. *Clin Pharmacokinet*. 2006;45(7):649-663.
49. Purkins L, Wood N, Ghahramani P, Greenhalgh K, Allen MJ, Kleinermans D. Pharmacokinetics and safety of voriconazole following intravenous- to oral-dose escalation regimens. *Antimicrob Agents Chemother*. 2002;46(8):2546-2553.
50. Gibbs MA, Thummel KE, Shen DD, Kunze KL. Inhibition of cytochrome P-450 3A (CYP3A) in human intestinal and liver microsomes: comparison of  $K_i$  values and impact of CYP3A5 expression. *Drug Metab Dispos*. 1999;27(2):180-187.
51. YU K, Cho J-Y, Jang I-J, et al. Effect of the CYP3A5 genotype on the pharmacokinetics of intravenous midazolam during inhibited and induced metabolic states\*1. *Clin Pharmacol Ther*. 2004;76(2):104-112.
52. Lappin G, Kuhnz W, Jochimsen R, et al. Use of microdosing to predict pharmacokinetics at the therapeutic dose: Experience with 5 drugs. *Clin Pharmacol Ther*. 2006;80(3):203-215.
53. Mandona JW, Tuk B, van Steveninck AL, Breimer DD, Cohen AF, Danhof M. Pharmacokinetic-pharmacodynamic modeling of the central nervous system effects of midazolam and its main metabolite  $\alpha$ -hydroxymidazolam in healthy volunteers. *Clin Pharmacol Ther*. 1992;51(6):715-728.
54. Clausen T, Wolff J, Hansen P, et al. Pharmacokinetics of midazolam and alpha-hydroxy-midazolam following rectal and intravenous administration. *Br J Clin Pharmacol*. 1988;25(4):457-463.
55. Pentikainen PJ, Valisalmi L, Himberg JJ, Crevoisier C. Pharmacokinetics of midazolam following intravenous and oral administration in patients with chronic liver disease and in healthy subjects. *J Clin Pharmacol*. 1989;29(3):272-277.
56. van Rongen A, Kervezee L, Brill M, et al. Population pharmacokinetic model characterizing 24-hour variation in the pharmacokinetics of oral and intravenous midazolam in healthy volunteers. *CPT pharmacometrics Syst Pharmacol*. 2015;4(8):454-464.
57. Anderson BJ, Larsson P. A maturation model for midazolam clearance. *Pediatr Anesth*. 2011;21(3):302-308.
58. Scholz I, Oberwittler H, Riedel K-D, et al. Pharmacokinetics, metabolism and bioavailability of the triazole antifungal agent voriconazole in relation to CYP2C19 genotype. *Br J Clin Pharmacol*. 2009;68(6):906-915.
59. Shi H-Y, Yan J, Zhu W-H, et al. Effects of erythromycin on voriconazole pharmacokinetics and association with CYP2C19 polymorphism. *Eur J Clin Pharmacol*. 2010;66(11):1131-1136.
60. Snijder RA, Konings MK, Lucas P, Egberts TC, Timmerman AD. Flow variability and its physical causes in infusion technology: A systematic review of in vitro measurement and modeling studies. *Biomed Tech*. 2015;60(4):277-300.
61. Schmidt N, Saez C, Seri I, Maturana A. Impact of syringe size on the performance of infusion pumps at low flow rates. *Pediatr Crit Carefile*. 2010;11(2):282-286.
62. Neff TA, Fischer JE, Schulz G, Baenziger O, Weiss M. Infusion pump performance with vertical displacement: Effect of syringe pump and assembly type. *Intensive Care Med*. 2001;27(1):287-291.
63. Ito K, Ogihara K, Kanamitsu S, Itoh T. Prediction of the in vivo interaction between midazolam and macrolides based on in vitro studies using human liver microsomes. *Drug Metab Dispos*. 2003;31(7):945-954.
64. Zane NR, Thakker DR. A Physiologically Based Pharmacokinetic Model for Voriconazole Disposition Predicts Intestinal First-pass Metabolism in Children. *Clin Pharmacokinetic*. 2014;53(12):1171-1182.
65. Damle B, Varma MV, Wood N. Pharmacokinetics of Voriconazole Administered Concomitantly with Fluconazole and Population-Based Simulation for Sequential Use. *Antimicrob Agents Chemother*. 2011;55(11):5172-5177.
66. Qi F, Zhu L, Li N, Ge T, Xu G, Liao. Influence of different proton pump inhibitors on the pharmacokinetics of voriconazole. *Int J Antimicrob Agents*. 2017;49(4):403-409.
67. Brown RP, Delp MD, Lindstedt SL, Rhomberg LR, Beliles RP. Physiological Parameter Values for Physiologically Based Pharmacokinetic Models. *Toxicol Ind Health*. 1997;13(4):407-484.
68. Williams LR, Leggett RW. Reference values for resting blood flow to organs of man. *Clin Phys Physiol Meas*. 1989;10(3):187-217.

## Supplemental Information

Additional supplemental information can be found by clicking the Supplements link in the PDF toolbar or the Supplemental Information section at the end of web-based version of this article.

**A novel study design using continuous intravenous and intraduodenal infusions of midazolam and voriconazole for mechanistic quantitative assessment of hepatic and intestinal CYP3A inhibition  
(Supplementary document)**

**Xia Li<sup>1</sup>, Lisa Junge<sup>1</sup>, Max Taubert<sup>1</sup>, Anabelle von Georg<sup>1</sup>, Dominik Dahlinger<sup>1</sup>, Chris Starke<sup>1</sup>, Sebastian Frechen<sup>1</sup>, Christoph Stelzer<sup>2</sup>, Martina Kinzig<sup>2</sup>, Fritz Sörgel<sup>2,3</sup>, Ulrich Jaehde<sup>4</sup>, Ulrich Töx<sup>5</sup>, Tobias Goeser<sup>5</sup>, Uwe Fuhr<sup>1</sup>**

1 University of Cologne, Faculty of Medicine and University Hospital Cologne, Center for Pharmacology, Department I of Pharmacology, Cologne, Germany;

2 IMBP-Institute for Biomedical and Pharmaceutical Research, Nurnberg-Heroldsberg, Germany;

3 Institute of Pharmacology, West German Heart and Vascular Centre, University of Duisburg-Essen, Essen, Germany;

4 Institute of Pharmacy, Clinical Pharmacy, University of Bonn, Germany;

5 Department of Gastroenterology and Hepatology, University Hospital of Cologne, Cologne, Germany.

Corresponding author:

Univ.-Prof. Dr. med. Uwe Fuhr

University of Cologne, Faculty of Medicine and University Hospital Cologne, Center for Pharmacology, Department I of Pharmacology; Gleueler Straße 24, 50931 Cologne, Germany

Email: [uwe.fuhr@uk-koeln.de](mailto:uwe.fuhr@uk-koeln.de)

Tel: +49-(0)-221-478-6672 (office), -5230 (direct line)

Fax +49-(0)-221-478-7011



## Table of contents

### METHODS

Chemicals	3
Quantification of VRZ and VRZ N-oxide in plasma, MDZ, MDZ-N-glucuronide, 1'-OH-MDZ, 1'-OH-MDZ-glucuronide, and 4-OH-MDZ, and 4-OH-MDZ-glucuronide in urine	3
Quantification of MDZ, 1'-OH-MDZ and 4'-OH-MDZ in plasma	4

### TABLES

Table S1 LC/MS conditions	5
Table S2 Actual infusion doses and rates of voriconazole and midazolam	6

### FIGURES

Figure S1 Goodness-of-fit plots of the final model for midazolam-N-glucuronide, 1'-OH-midazolam-glucuronide, and 1'-OH-midazolam in urine (all study periods).	7
Figure S2 Observed plasma concentrations of MDZ, 1'-OH-MDZ, VRZ as reported by Saari et al. 2006 compared to the model predicted simulation <sup>8</sup>	
Figure S3 The comparison of observed and predicted plasma concentration-time profiles of parent drugs as well as the metabolites in each subject	10

Reference	13
-----------	----

NONMEM CODE	14
-------------	----

## **METHODS**

### **Chemicals**

Midazolam (MDZ), 1'-hydroxymidazolam (1'-OH-MDZ), voriconazole (VRZ), ketoconazole (KET), diazepam, and  $\beta$ -glucuronidase from *Helix pomatia* were purchased from Sigma-Aldrich (St Louis, MO, USA). Voriconazole N-oxide (VRZ N-oxide) and 4-hydroxymidazolam (4-OH-MDZ) were obtained from Santa Cruz Biotechnology (Heidelberg, Germany). Methanol (Gradient grade for MS), acetonitrile (Gradient grade for LC), formic acid (98-100% p.a.), and sodium chloride were bought from Merck (Darmstadt, Germany). Ammonium acetate (>99.0%) was purchased from Fluka Chemie AG (Switzerland).

### **Quantification of VRZ and VRZ N-oxide in plasma, MDZ, MDZ-N-glucuronide, 1'-OH-MDZ, 1'-OH-MDZ-glucuronide, 4-OH-MDZ, and 4-OH-MDZ-glucuronide in urine**

Concentrations of VRZ and VRZ N-oxide were quantified in plasma by LC/MS/MS methods using a TSQ Quantum, Surveyor MS Pump and Autosampler (Thermo Finnigan, CA, USA). In brief, 200  $\mu$ L of plasma samples were mixed with 400  $\mu$ L acetonitrile (ACN), and then spiked with 20  $\mu$ L of the internal standard working solution (ISTD, 5000 ng/ml KET), while the calibration standards (EP) and quality control (QC) samples were prepared by adding 20  $\mu$ L of the appropriate combined working solution to 200  $\mu$ L of blank human plasma, then adding 380  $\mu$ L of acetonitrile and 20  $\mu$ L of ISTD (KET).

For urine samples, 50  $\mu$ L of the urine sample were mixed with 250  $\mu$ L of 0.2 M ammonium acetate buffer (pH 4.75) with the addition of 600  $\mu$ L MeOH and 100  $\mu$ L of the ISTD (5000 ng/ml diazepam). To prepare the EP and QC samples, 3  $\mu$ L of 1'-OH-MDZ and 3  $\mu$ L of the combination of MDZ and 4'-OH-MDZ working solution in urine were mixed with 44  $\mu$ L blank urine. Then, the EP and QC samples were processed in the same way as unknown urine samples.

To determine the glucuronidated fraction of MDZ, 1'-OH-MDZ, and 4-OH-MDZ, the samples were measured two times, once without  $\beta$ -glucuronidase treatment as described above and another after glucuronide cleavage. For glucuronide cleavage, 50  $\mu$ L of urine sample mixed with 125  $\mu$ L of 0.2 M ammonium acetate buffer (pH 4.75) and 125  $\mu$ L  $\beta$ -glucuronidase suspension (3,200 U/ml) were incubated at 37 °C for 24 h. Then, 600  $\mu$ L of MeOH with 100  $\mu$ L of ISTD (diazepam) was added, vortexed and kept on ice for a few minutes to stop the enzymatic reaction.

After vortexing for 10 seconds and centrifuging with 20.800x g (14.000 rpm) for 10 min, 200  $\mu$ L of the supernatant were transferred to screw-capped glass vials for LC-MS/MS analysis. 20  $\mu$ L of the sample was injected into a Hypersil Gold column (50  $\times$  2.1 mm, 5  $\mu$ m, Thermo Electron, Runcorn, U.K.) with a Security Guard precolumn (4x2.0mm, Phenomenex, Torrance, CA, USA) and eluted at a flow rate of 300  $\mu$ L/min. The column temperature was maintained at 30°C. Mass spectra were acquired using in the positive ion mode at a scan rate of 0.15 s/scan. LC/MS parameters, solvent gradient, standard curve ranges, and precision and accuracy are listed in **Table S1**.

### **Quantification of MDZ, 1'-OH-MDZ and 4'-OH-MDZ in plasma**

Quantification of MDZ, 1'-OH-MDZ and 4'-OH-MDZ in plasma was performed using an AB SCIEX API 5000 triple quadrupole mass spectrometer (AB SCIEX, Concord, Ontario, Canada) and a binary Agilent 1200 pump (Agilent Technologies Inc., Waldbronn, Germany) with the Analyst software version 1.6.2 (AB SCIEX, Concord, Ontario, Canada). 50  $\mu$ L of each plasma sample were placed in a polypropylene-tube. Samples were de-proteinized with 100  $\mu$ L acetonitrile containing the ISTD (MDZ-d4 and 1'-OH-MDZ-d4), subsequently vortex-shaked and centrifuged. The supernatant was further diluted with 200  $\mu$ L Milli-Q®-water and 20  $\mu$ L were injected into a Synergie Polar RP 100 Å column (50x4.6 mm, 2.5 Mm, Sigma-Aldrich Chemie GmbH, Germany). The compounds were detected with MRM (Multiple

Reaction Monitoring) and mass spectrometry conditions are described in **Table 1**. The high concentration working solution for calibration standards (WCS1) and quality control sample (WQC1) were separately prepared, by adding 90  $\mu$ L stock solution containing each analyte to 1.91 mL of blank human plasma. Then, 10-fold dilutions of WCS1 and WQC1 with the blank human plasma produced WCS2 and WQC2, respectively. Next, the highest concentrated calibration standard (CS1) and quality control sample (QC1) were obtained by diluting WCS2 and WQC2 with blank human plasma. The following calibration standards (CS2-8) and quality control samples (QC2-4) were prepared by adding the appropriate volume of CS<sub>n</sub>-1 and QC<sub>n</sub>-1 and to blank human plasma, respectively. Organic solvent (methanol) concentration in CS1-8 and QC1-4 was less than 0.03 % (v/v). Finally, the calibration standards and quality control samples were processed in the same way as unknown plasma samples.

**TABLES**

**Table S1 LC/MS conditions**

Analyte	Mass transition	Standard curve range	LC gradient	retention time	Precision Intra-day	Accuracy Intra-day	Precision Inter-day	Accuracy Inter-day
	<i>m/z</i>	ng/mL		min	%	%	%	%
VRZ (p)	350.1→281.2	10-1000		0.8	<10.8	<7.9	<12.1	<7.5
VRZ N-oxide (p)	366.1→224.1	10-1000	%B (min)	0.61	<13.9	<8.9	<9.46	<6.9
Ketoconazole (p). IS	531.2→489.3	-	0(0)→0(2.5)→100(5)→0(6) <sup>a</sup>	0.66				
MDZ (u)	326.0→291.0	0.5-100		3.44	<14.8	<9.43	<7.62	<9.00
1'-OH-MDZ (u)	342.0→324.1	1-1000	%B (min)	3.58	<6.9	<17.2	<12.6	<13.0
4-OH-MDZ (u)	342.0→325.2	0.5-100	20(0)→20(1)→90(3)→90(4.5)→20(6) <sup>b</sup>	3.34	<12.5	<14.4	<6.7	<15.2
Diazepam (u), IS	285.0→193.1	-		4.12				
MDZ (p)	326.2→291.3	0.05-74.5	Isocratic	2.6	0.7-6.0	99.0-102.0	4.6-7.1	97.3- 101.2
MDZ-d4(p)	329.9→295.0	-	elution with	2.6	-	-	-	-
1'-OH-MDZ (p)	342.3→203.1	0.051-75.5	0.5% formic acid and	2.7	1.6-3.2	99.3-101.9	3.3-6.7	99.6- 102.0
1'-OH-MDZ-d4(p)	346.3→203.1	-	methanol	2.7	-	-	-	-
4-OH-MDZ (p)	342.3→325.2	0.05-74.6		2.2	2.1-5.4	98.6-100.6	5.6-7.9	97.9- 101.2

<sup>a</sup> mobile phase A was 0.1% formic acid in 10 mM ammonium formate/0.1% formic acid in acetonitrile 50/50 (v/v), and solvent B was 0.1% formic acid in acetonitrile;

<sup>b</sup> mobile phase A was 0.1% formic acid in water, and solvent B was MeOH.

**MDZ**, midazolam; **1'-OH-MDZ**, 1'-OH-midazolam; **4-OH-MDZ**, 4-OH-midazolam; **VRZ**, voriconazole; **VRZ N-oxide**, voriconazole N-oxide; u, urine; p, plasma.

**Table S2 Actual infusion doses and rates of voriconazole and midazolam\***

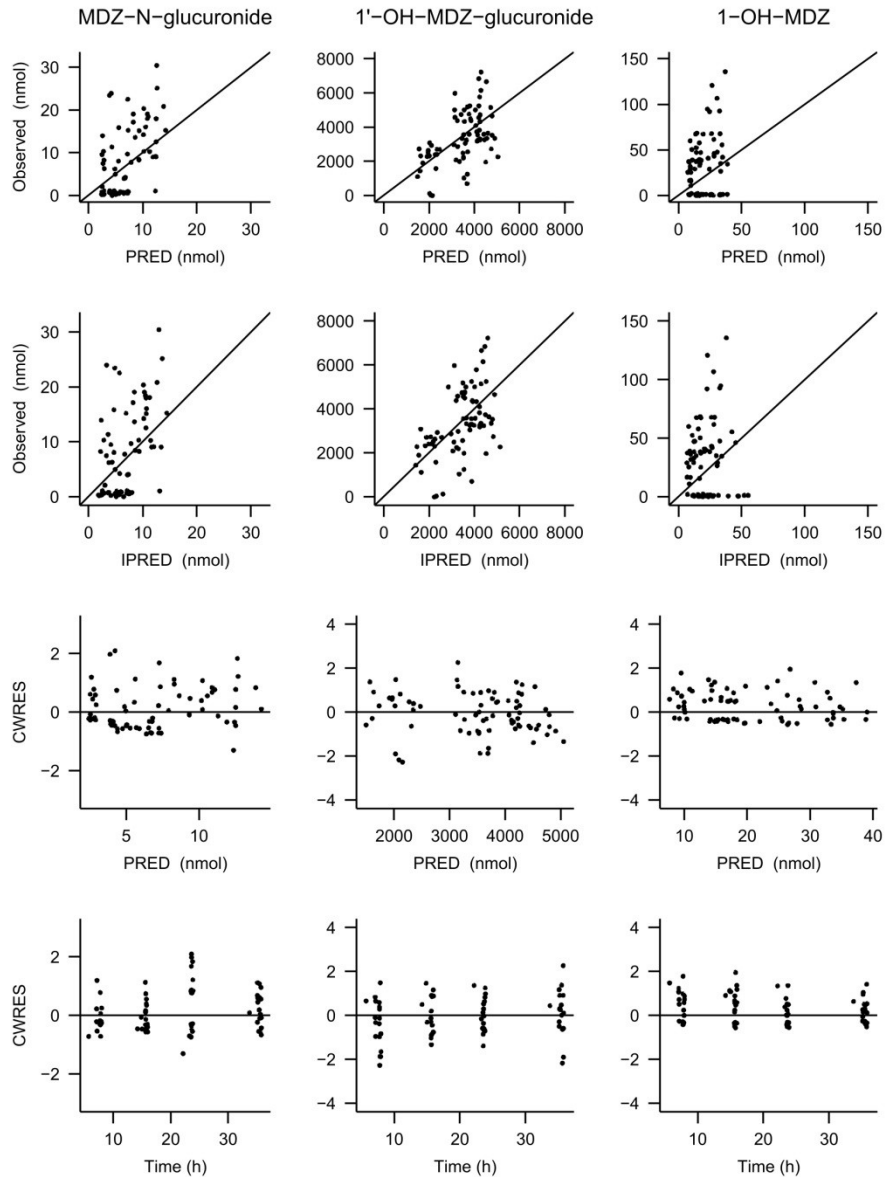
Subject	Period	Midazolam		Voriconazole			
		Dose* [mg]	Infusion rate [mg/h]	Low dose* [mg]	Infusion rate [mg/h]	High dose* [mg]	Infusion rate [mg/h]
1	MDZ iv, VRZ int	6.59	0.274	48.9	6.11	96.7	12.2
	MDZ int, VRZ iv	6.25	0.260	56.3	7.05	113	14.1
	MDZ int, VRZ int	6.39	0.266	43.2	5.4	86.3	10.8
2	MDZ iv, VRZ int	6.00	0.250	53.9	6.74	108	13.5
	MDZ int, VRZ iv	6.71	0.280	55.1	6.91	109	13.8
	MDZ int, VRZ int	6.59	0.274	56.7	7.10	114	14.2
	MDZ iv, VRZ iv	6.11	0.254	45.5	7.38	118	14.8
3				11.6	Bolus(9.75h)*		
	MDZ iv, VRZ int	6.00	0.250	54.0	6.80	109	13.6
	MDZ int, VRZ iv	6.44	0.268	47.4	7.90	121	15.8
	MDZ int, VRZ iv			12.8	Bolus(11.0h)*		
	MDZ int, VRZ int	6.34	0.264	53.3	6.66	107	13.3
	MDZ iv, VRZ iv	7.11	0.296	49.3	7.34	117	14.7
4	MDZ iv, VRZ iv			8.00	Bolus(9.20h)*		
	MDZ int, VRZ int	6.24	0.260	56.9	7.13	113	14.2
	MDZ iv, VRZ iv	6.56	0.290	56.7	7.08	112	14.2
5	MDZ iv, VRZ iv	0.400	Bolus(2.13h)*				
	MDZ iv, VRZ int	6.47	0.270	56.8	7.11	114	14.2
	MDZ int, VRZ iv	6.24	0.260	45.5	5.69	88.0	11.4
	MDZ int, VRZ int	6.60	0.275	55.4	6.92	110	13.8
6	MDZ int, VRZ int	6.46	0.269	55.4	6.94	111	13.9
	MDZ iv, VRZ int	7.39	0.308	52.2	6.53	99.3	13.1
	MDZ int, VRZ iv	6.32	0.263	52.3	6.54	105	13.1
	MDZ int, VRZ int	5.51	0.230	47.0	6.71	107	13.4

\*as determined by weight control of the infusion system.

\* A bolus dose was given in the case of blocked tubes and the recorded time for a bolus dose is the time after the start of MDZ infusion.

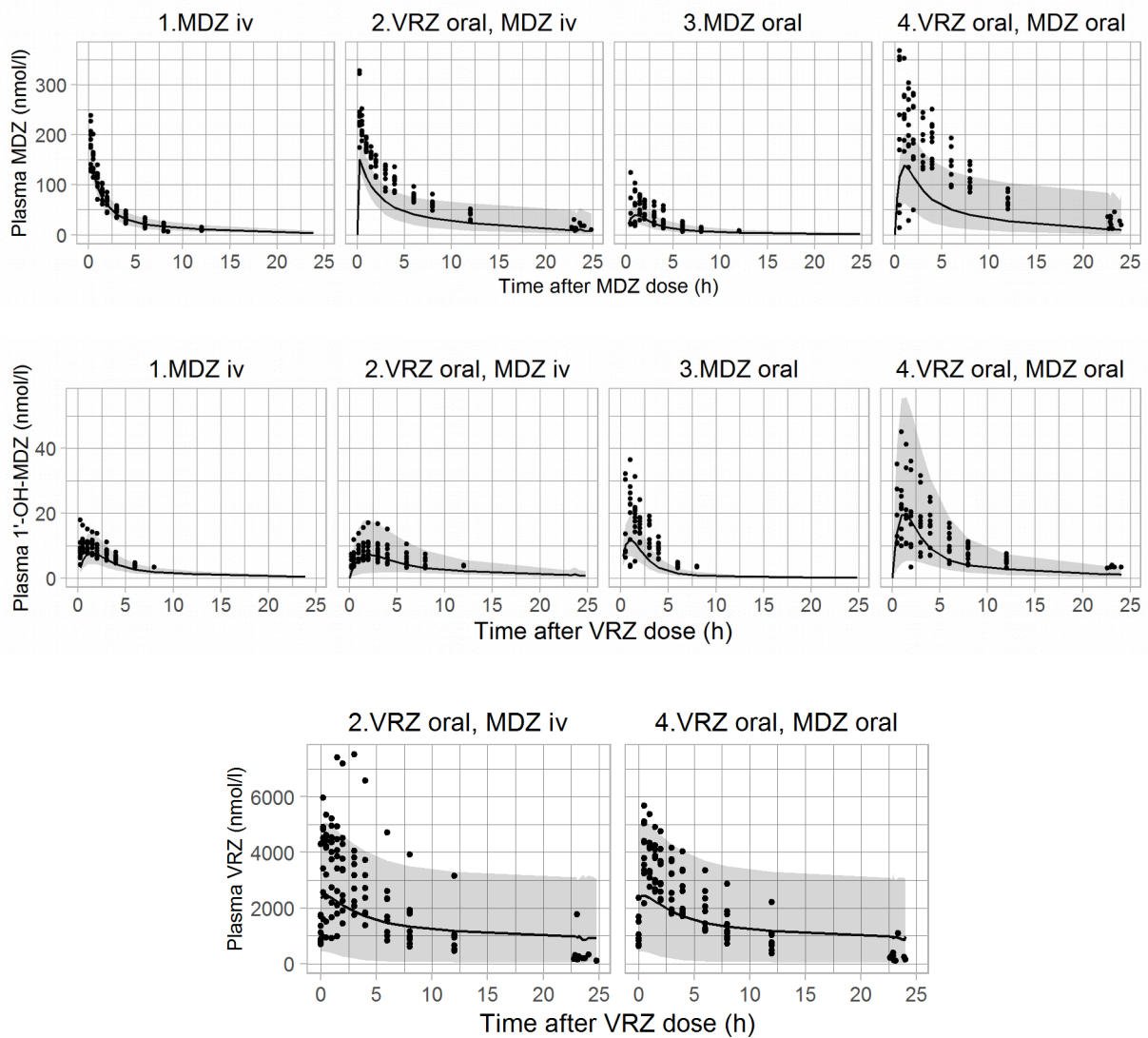
## FIGURES

**Figure S1 Goodness-of-fit plots of the final model for midazolam-N-glucuronide, 1'-OH-midazolam-glucuronide, and 1-OH-midazolam in urine (all study periods).**



MDZ-N-glucuronide, midazolam-N-glucuronide; 1'-OH-MDZ-glucuronide, 1'-hydroxy-midazolam-glucuronide; 1'-OH-MDZ, 1'-hydroxy-midazolam. Observed drug amounts in urine (Observed) versus population predictions (PRED) and individual predictions (IPRED) obtained from the final population semi-physiological model. Conditional weighted residuals (CWRES) versus PRED and time after the start of MDZ infusion. The observations below the limit of quantification were also shown in the plots.

**Figure S2 Observed plasma concentrations of MDZ, 1'-OH-MDZ, VRZ as reported by Saari et al. 2006 compared to the model predicted simulation**

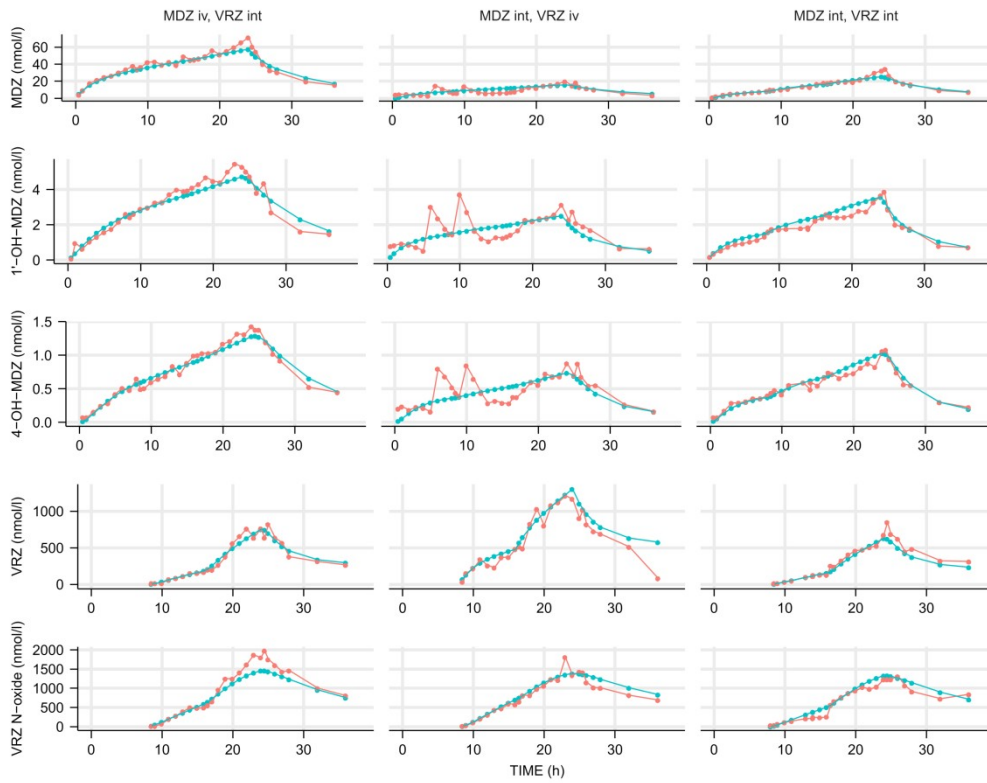


MDZ, midazolam; 1'-OH-MDZ, 1'-hydroxy-midazolam; VRZ, voriconazole, iv, intravenous. Model prediction were obtained by simulating the Saari <sup>1</sup> study design for 1000 virtual subjects. The shaded areas represent simulation-based 90% confidence intervals and the line represents the median of predicted plasma concentrations, while observed concentrations are described by the black dots. Administration of VRZ was done orally on the first day with 400 mg twice daily, the dose was 200mg twice daily on the second day. MDZ was administered at a dose of 0.05 mg/kg intravenously, or 7.5 mg orally, at 1 h after the last dose of VRZ (periods 2 and 4) and during the control (periods 1 and 3).

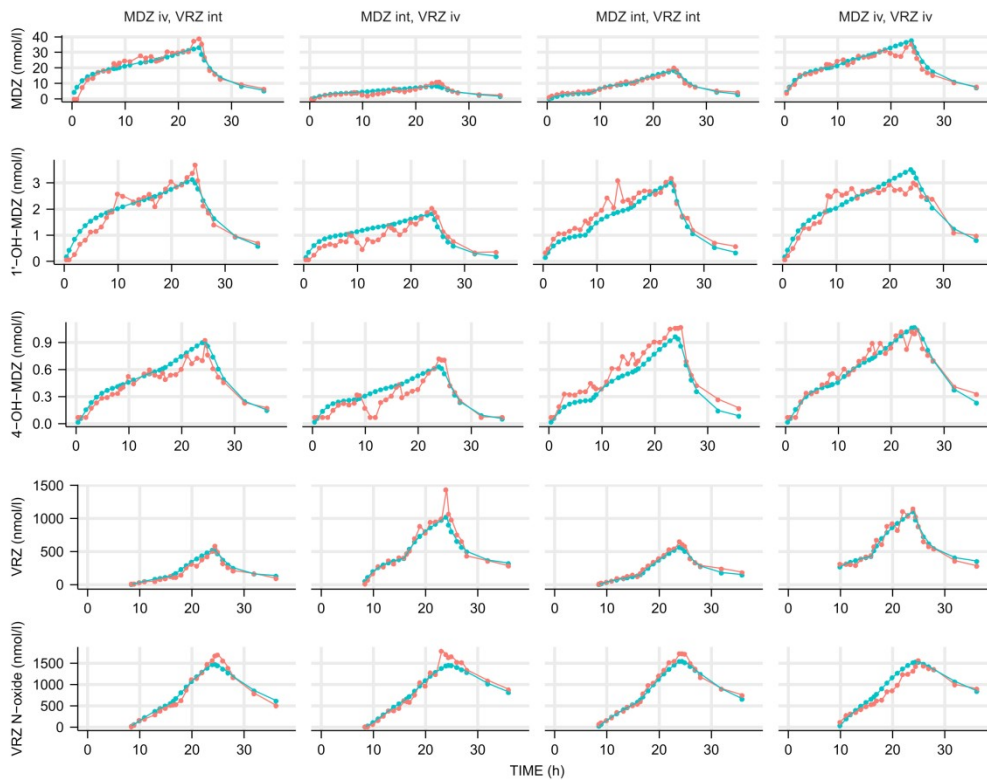


**Figure S3 The comparison of observed and predicted plasma concentration-time profiles of parent drugs as well as the metabolites in each subject**

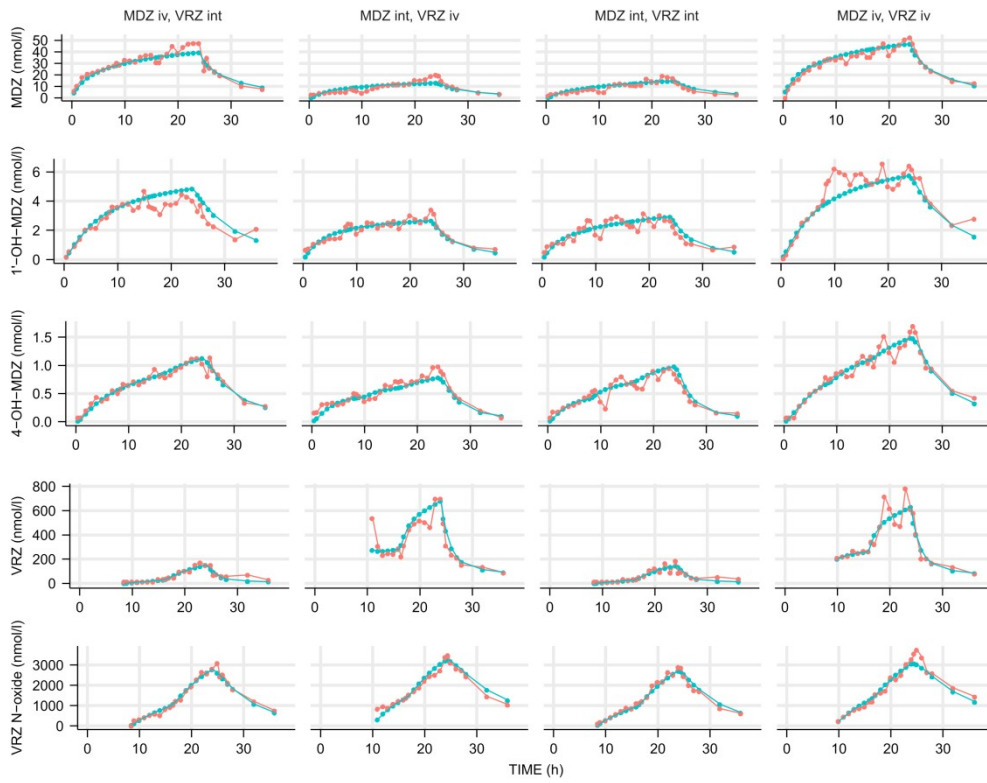
a) ID 1



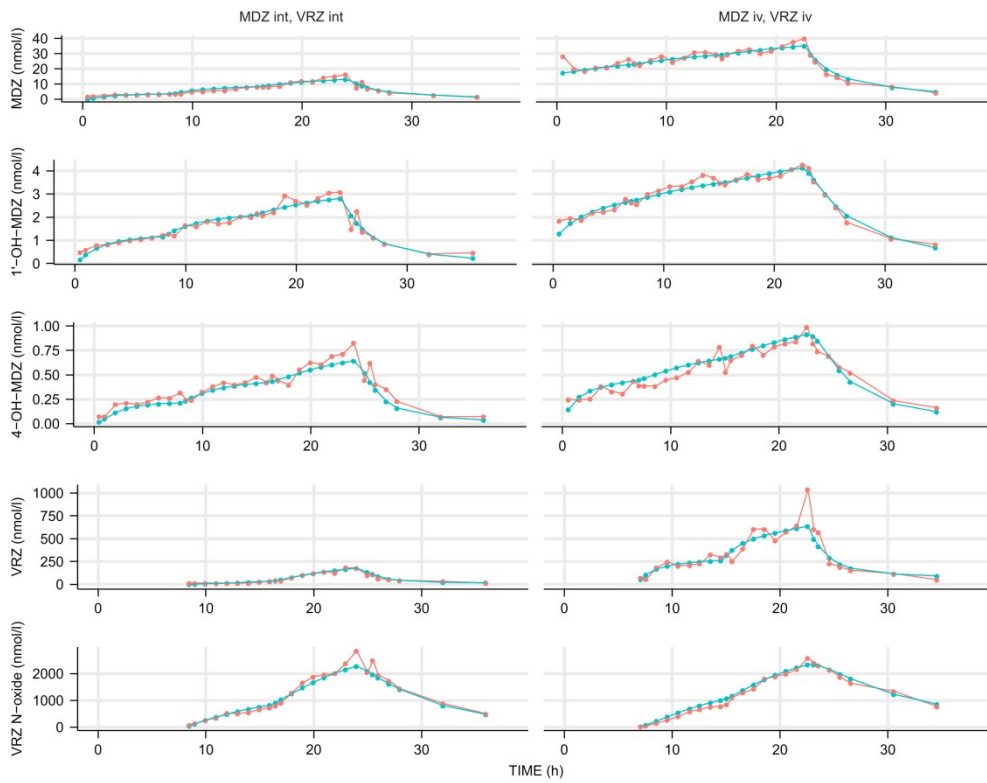
b) ID 2



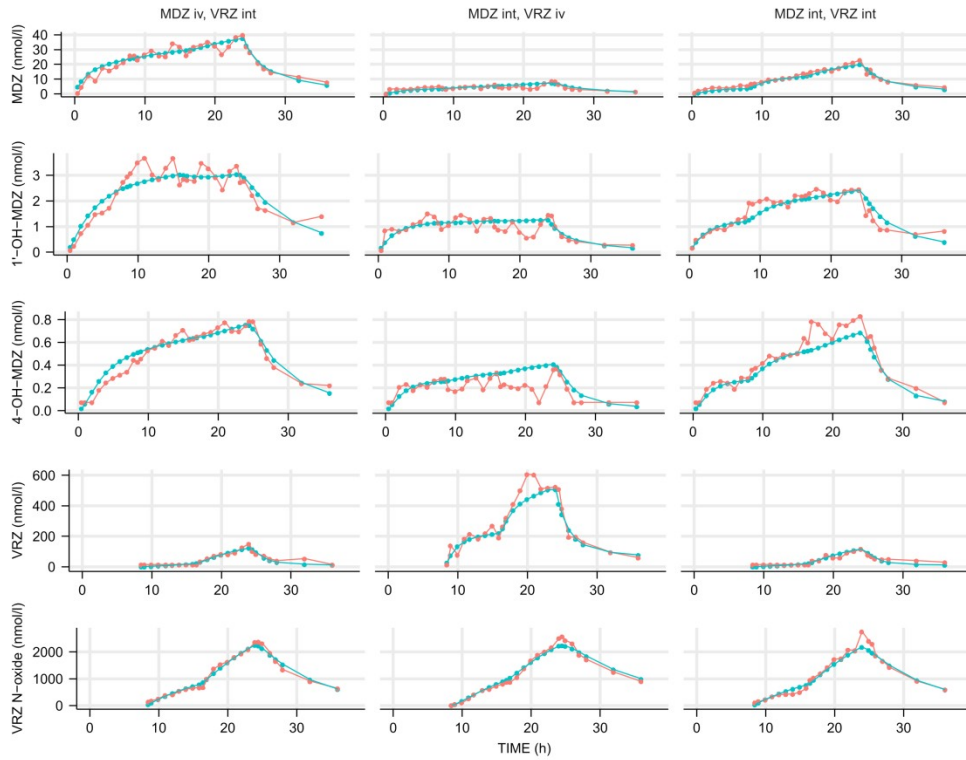
c) ID 3



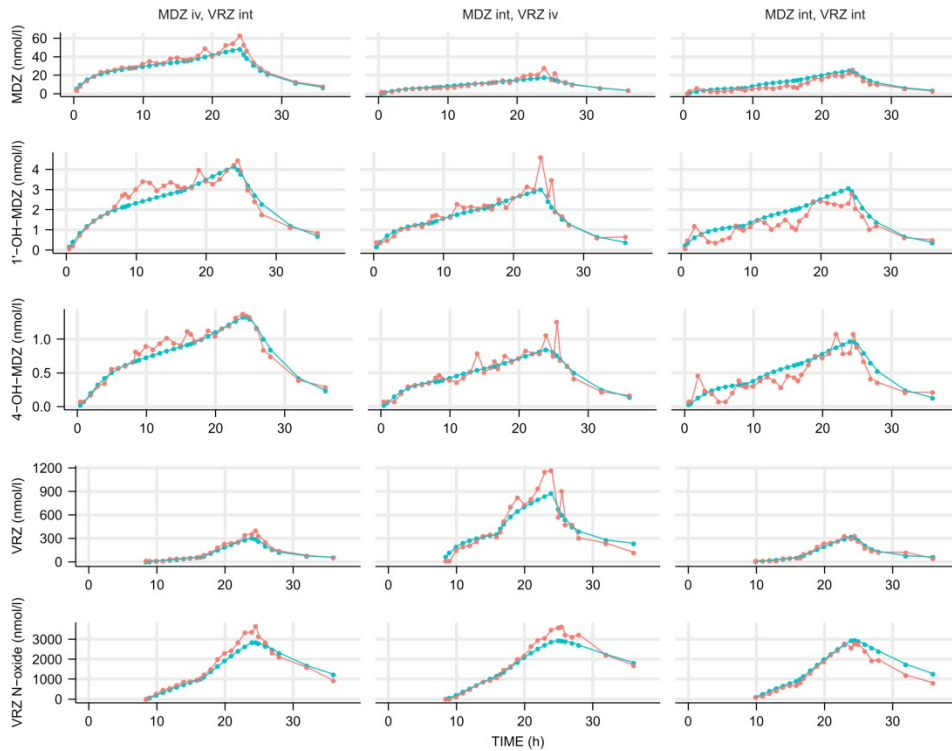
d) ID 4



e) ID 5



f) ID 6



Comparison between observed plasma drug concentrations (red) and individual predictions (green) obtained from the final population semi-physiological model versus time after the start of MDZ infusion.

## Reference

1. Saari TI, Laine K, Leino K, Valtonen M, Neuvonen PJ, Olkkola KT. Effect of voriconazole on the pharmacokinetics and pharmacodynamics of intravenous and oral midazolam. *Clin Pharmacol Ther.* 2006;79(4):362-370. doi:10.1016/j.clpt.2005.12.305

\$\$SIZES MAXFCN=100000000 LNP4=80000 LVR=60 DIMNEW=2000

\$PROBLEM DDI of MDZ and VRZ

\$INPUT

ID PER NMTIME=DROP TIME TAFE=DROP EVID AMTNG=DROP RATENG=DROP AMT RATE ;AMT in nmol, RATE in nmol/h

CMT DVNGL=DROP DV ; DV in nmol/l (plasma), nmol (urine)

DVLGNOMOLL=DROP BQL FLAG MDV WEIGHT HEIGHT AGE

UVOL ; Urine volume

STRAT ; vpc stratification

\$DATA MOL\_vrz\_mdz\_xl\_urine\_uM.csv IGNORE=@ WIDE

IGNORE=(DV.EQ.-99,EXTRAPER.EQ.1,DT.EQ.1)

\$\$SUBROUTINE ADVAN13 TOL=9 ; Set up differential equation mode

\$MODEL

COMP(MDZDEP) ;1 MDZ deposit

COMP(MDZCEN) ;2 MDZ central

COMP(VRZDEP) ;3 VRZ deposit

COMP(VRZCEN) ;4 VRZ central

COMP(1OHMDZCEN) ;5 1-OH-MDZ central

COMP(4OHMDZCEN) ;6 4-OH-MDZ central

COMP(1OHMDZUR) ;7 1-OH-MDZ urine

COMP(NOXIDECEN) ;8 VRZ NOXIDE central

COMP(MDZGLUUR) ;9 MDZ-GLU urine

COMP(1OHMDZGLUUR) ;10 1-OH-MDZ GLU urine

COMP(MDZPER) ;11 MDZ peripheral

COMP(VRZPER) ;12 VRZ peripheral

COMP(1OHMDPER) ;13 VRZ NOXIDE peripheral

COMP(1OHMDPER) ;14 1-OH-MDZ GLU central

COMP(CYPLIV) ;15 Enzyme site liver

COMP(CYPGUT) ;16 Enzyme site gut

\$PK

VWGT=WEIGHT/70

; Basic physiological Parameters

QH = 3.75\*WEIGHT\*\*0.75 ; Hepatic blood flow (Chien et al . 2006, Brown et al. 1997)

QPV = 0.75\*QH ; Portal vein blood flow (75% from liver blood flow) (Williams et al. 1989)

QHA = 0.25\*QH ; Hepatic artery blood flow (25% from liver blood flow) (Williams et al. 1989)

VH = 1 ; Hepatic compartment volumn fixed to 1 L.

VPV = 1 ; Portal vein compartment volumn fixed to 1 L.

QIN = 0.4\*QH ; Small intestinal blood flow (Williams et Leggett, Clin Phys Physiol Meas. 1989)

QMU = 0.8\*QIN ; Mucosa blood flow (Yang et al., Curr Drug Metab 2007)

QVI = 0.6\*QMU ; Villous blood flow(Yang et al., Curr Drug Metab 2007)

VGW = 1 ; Volume of Gut wall fixed to 1 L.

; Midazolam PK parameters

KA = THETA(1) ; Absorption rate constant of MDZ

VCEN = THETA(2) ; Central distribution volume of MDZ

VPER = THETA(3)\*VWGT ; Peripheral distribution volume of MDZ

Q = THETA(4) ; Inter-compartmental clearance between central and peripheral compartment of MDZ

K23=Q/VCEN ; Rate constant from central to peripheral compartment of MDZ

K32=Q/VPER ; Rate constant from peripheral to central compartment of MDZ

CLH0=THETA(5)\*EXP(ETA(1)) ; Unbound intrinsic hepatic clearance of MDZ

KI=THETA(6)\*EXP(ETA(2)) ; Inhibition constant of voriconazole on the metabolism of MDZ

CLG0 = THETA(7)\*EXP(ETA(3)) ; Unbound intrinsic intestinal clearance of MDZ

; Physicochemical characteristics of midazolam

FU = 0.02 ; Unbound fraction of MDZ in plasma in healthy human (Ito et al. 2003, Lown et al. 1995: 0.022, Thummel et al. 1996: 0.02, Trouvin et al. 1988: 0.019)

RATIO = 0.66 ; Blood to plasma partitioning ratio of MDZ in human (Ito et al. 2003, Gorski et al. 1996)

FUB = FU/RATIO ; Unbound fraction of MDZ in Blood is 0.033

FUG = 1 ; Unbound fraction of MDZ in gut (assumed to be 1, Yang et al., Curr Drug Metab 2007)

CLP = 10.6 ; Permeability of MDZ 10.6 L/h = 0.1766 L/min (Yang et al. 2007)

; Voriconazole PK parameters

VKA = THETA(8) ; Absorption rate constant of VRZ  
VVCEN = THETA(9) ; Central distribution volume of VRZ  
VVPER = THETA(10) ; Peripheral distribution volume of VRZ  
VQ = THETA(11) ; Inter-compartmental clearance between central and peripheral compartment of VRZ  
KV23 = VQ/VVCEN ; Rate constant from central to peripheral compartment of VRZ  
KV32 = VQ/VVPER ; Rate constant from peripheral to central compartment of VRZ  
VCLH0 = THETA(12)\*EXP(ETA(4)) ; Unbound intrinsic hepatic clearance of VRZ  
VCLG0 = THETA(13)\*EXP(ETA(5)) ; Unbound intrinsic intestinal clearance of VRZ

; Physicochemical characteristics of voriconazole

VFU = 0.42 ; Unbound fraction of VRZ in plasma (Damle et al. Antimicrob Agents Chemother. 2011)  
VRATIO = 1 ; Blood to plasma partitioning ratio of VRZ in human, assumed to be 1  
VFUB= VFU/VRATIO ; Unbound fraction of VRZ in blood  
VFUG= 1 ; Unbound fraction of VRZ in gut (assumed to be 1, Yang et al., Curr Drug Metab 2007)  
VCLP= 6.5 ; Permeability of VRZ  $2.71 * 10.6 / 4.4 = 6.504$  (Yang et al. 2007, Li et al. Clinical Pharmacokinetics 2019)

; Time dependent inhibition parameters

KDEGL=0.023 ; First-order degradation rate of the enzyme in the absence of inhibitor in the liver(PK-Sim default,  $\ln 2 / t_{1/2}$  h<sup>-1</sup>)  
KDEGG=0.03 ; First-order degradation rate of the enzyme in the absence of inhibitor in the gut(PK-Sim default,  $\ln 2 / t_{1/2}$  h<sup>-1</sup>)  
E0L=1 ; Amount of original active enzyme in liver, fixed to be 1  
E0G=1 ; Amount of original active enzyme in gut, fixed to be 1  
KINACT = THETA(14)\*EXP(ETA(6)) ; Maximum inactivation rate constant of VRZ  
KTDI = 9330 ; Dissociation rate constant of VRZ  
A\_0(15)= E0L ; Amount of original active enzyme in liver  
A\_0(16)= E0G ; Amount of original active enzyme in gut

; 1-OH-MDZ PK parameters

MVMET=THETA(15) ; Central distribution volume of 1-OH-MDZ  
CLHM0=THETA(16)\*EXP(ETA(7)); Unbound intrinsic hepatic clearance of 1-OH-MDZ  
KI1OH=THETA(17)\*EXP(ETA(8)); Inhibition constant of voriconazole on the metabolism of 1-OH-MDZ  
CLGM0=THETA(18)\*EXP(ETA(9)); Unbound intrinsic intestinal clearance of 1-OH-MDZ

$R1 = \text{EXP}(\text{THETA}(19)) / (1 + \text{EXP}(\text{THETA}(19)))$  ; Ratio of metabolism pathway to produce 1-OH-MDZ

$FUBM=1$  ; Unbound fraction of 1-OH-MDZ in blood

$FUGM=1$  ; Unbound fraction of 1-OH-MDZ in gut

; 1-OH-MDZ-GLU PK parameters

$KR1 = \text{THETA}(20)$  ; Renal clearance of 1-OH-MDZ-GLU

; 1-OH-MDZ-URINE PK parameters

$KR2 = \text{THETA}(21)$  ; Renal clearance of 1-OH-MDZ-URINE

; 4-OH-MDZ PK parameters

$MVMET4 = \text{THETA}(22)$  ; Central distribution volume of 4-OH-MDZ

$CLHM40 = \text{THETA}(23) * \text{EXP}(\text{ETA}(10))$  ; Unbound intrinsic hepatic clearance of 4-OH-MDZ

$KI4OH = \text{THETA}(24) * \text{EXP}(\text{ETA}(11))$  ; Inhibition constant of voriconazole on the metabolism of 4-OH-MDZ

$CLGM40 = \text{THETA}(25)$  ; Unbound intrinsic intestinal clearance of 4-OH-MDZ

$R2 = \text{THETA}(26)$  ; Ratio of metabolism pathway to produce 4-OH-MDZ

$FUBM4=1$  ; Unbound fraction of 4-OH-MDZ in blood

$FUGM4=1$  ; Unbound fraction of 4-OH-MDZ in gut

; VRZ noxide PK parameters

$VVMET = \text{THETA}(27) * \text{VWGT}$  ; Central distribution volume of VRZ noxide

$VVPERM = \text{THETA}(28) * \text{VWGT}$  ; Peripheral distribution volume of VRZ noxide

$VQM = \text{THETA}(29)$  ; Inter-compartmental clearance between central and peripheral compartment of VRZ noxide

$KV23M = VQM / VVMET$  ; Rate constant from central to peripheral compartment of VRZ noxide

$KV32M = VQM / VVPERM$  ; Rate constant from peripheral to central compartment of VRZ noxide

$VCLHM = \text{THETA}(30) * \text{EXP}(\text{ETA}(12))$  ; Unbound intrinsic hepatic clearance of VRZ noxide

$VCLGM = \text{THETA}(31) * \text{EXP}(\text{ETA}(13))$  ; Unbound intrinsic intestinal clearance of VRZ noxide

$VFUBM=1$  ; Unbound fraction of VRZ noxide in blood

$VFUGM=1$  ; Unbound fraction of VRZ noxide in gut

; MDZ-GLU PK parameters

$R3 = \text{THETA}(32)$  ; Ratio of metabolism pathway to produce MDZ-GLU



\$DES

$$VCLH = VCLH0 * A(15) / E0L$$

$$VCLG = VCLG0 * A(16) / E0G$$

; VRZ well-stirred hepatic extraction

$$VEH = (VCLH * VFUB) / (QH + (VCLH * VFUB))$$

$$VCLHepatic = QH * VEH$$

$$VFH = 1 - VEH$$

; VRZ well-stirred gut extraction

$$VQGUT = (QVI * VCLP) / (QVI + VCLP)$$

$$VEG = (VCLG * VFUG) / (VQGUT + (VCLG * VFUG))$$

$$VCLGut = VQGUT * VEG$$

$$VFG = 1 - VEG$$

$$VAGUTW = (VKA * A(3)) / ((QVI) / VGW) \quad ; \text{Amount of VRZ in gut compartment}$$

$$VAPV = ((QVI / VGW) * VAGUTW * VFG + QPV / VVCEN * A(4)) / (QPV / VPV) \quad ; \text{Amount of VRZ in portal vein compartment}$$

$$VAH = (QHA / VVCEN * A(4) + QPV / VPV * VAPV) / ((QH) / VH) \quad ; \text{Amount of VRZ in liver compartment}$$

$$CONVOLIV = VFUB * VAH / VH \quad ; \text{Concentration of unbound VRZ in liver compartment}$$

$$CONVOGUT = VAGUTW / VGW \quad ; \text{Concentration of unbound VRZ in gut compartment}$$

; MDZ: competitive model in liver

$$CLH = CLH0 / (1 + CONVOLIV / KI)$$

; MDZ: competitive model in gut

$$CLG = CLG0 / (1 + CONVOGUT / KI)$$

; MDZ well-stirred hepatic extraction

$$EH = (CLH * FUB) / (QH + (CLH * FUB))$$

$$CL_{Hepatic} = QH * EH$$

$$FH = 1 - EH$$

; MDZ well-stirred gut extraction

$$QGUT = (QVI * CLP) / (QVI + CLP)$$

$$EG = (CLG * FUG) / (QGUT + (CLG * FUG))$$

$$CL_{Gut} = QGUT * EG$$

$$FG = 1 - EG$$

$$AGUTW = KA * A(1) / (QVI / VGW) \quad ; \text{Amount of MDZ in gut compartment}$$

$$APV = ((QVI / VGW) * AGUTW * FG + QPV / VCEN * A(2)) / (QPV / VPV) \quad ; \text{Amount of MDZ in portal vein compartment}$$

$$AH = (QHA / VCEN * A(2) + QPV / VPV * APV) / (QH / VH) \quad ; \text{Amount of MDZ in liver compartment}$$

; 1-OH-MDZ: competitive model in liver

$$CL_{HM} = CL_{HM0} / (1 + CONVOLIV / KI_{1OH})$$

; 1-OH-MDZ: competitive model in gut

$$CL_{GM} = CL_{GM0} / (1 + CONVOGUT / KI_{1OH})$$

; 1-OH-MDZ well-stirred hepatic extraction

$$E_{HM} = (CL_{HM} * FUBM) / (QH + (CL_{HM} * FUBM))$$

$$CL_{Hepatic1OH} = QH * E_{HM}$$

$$F_{HM} = 1 - E_{HM}$$

; 1-OH-MDZ well-stirred gut extraction, QGUT = Qvilli (QVI) in this case

$$E_{GM} = (CL_{GM} * FUGM) / (QVI + (CL_{GM} * FUGM))$$

$$CL_{Gut1OH} = QGUT * E_{GM}$$

$$F_{GM} = 1 - E_{GM}$$

; 1-OH-MDZ

$AGUTWM=(1-FG)*AGUTW*R1$  ; Amount of 1-OH-MDZ in gut compartment

$APVM=((QVI/VGW)*AGUTWM*FGM+ QPV/MVMET*A(5))/(QPV/VPV)$  ; Amount of 1-OH-MDZ in portal vein compartment

$AHM=(QHA/MVMET*A(5)+QPV/VPV*APVM+QH/VH*AH*EH*R1)/(QH/VH)$  ; Amount of 1-OH-MDZ in liver compartment

;4-OH-MDZ: competitive model in liver

$CLHM4 = CLHM40 / (1+CONVOLIV/KI4OH)$

;4-OH-MDZ: competitive model in gut

$CLGM4 = CLGM40 / (1+CONVOGUT/KI4OH)$

;4-OH-MDZ well stirred hepatic extraction

$EHM4= (CLHM4*FUBM4)/(QH+(CLHM4*FUBM4))$

$CLHepaticM4 = QH*EHM4$

$FHM4= 1-EHM4$

;4-OH-MDZ well stirred gut extraction,  $QGUT = Qvilli (QVI)$  in this case

$EGM4= (CLGM4*FUGM4)/(QVI+(CLGM4*FUGM4))$

$CLGutM4=QGUT*EGM4$

$FGM4= 1-EGM4$

;4-OH-MDZ

$AGUTWM4=(1-FG)*AGUTW*R2$  ; Amount of 4-OH-MDZ in gut compartment

$APVM4=((QVI/VGW)*AGUTWM4*FGM4+ QPV/MVMET4*A(6))/(QPV/VPV)$  ; Amount of 4-OH-MDZ in portal vein compartment

$AHM4=(QHA/MVMET4*A(6)+QPV/VPV*APVM4+QH/VH*AH*EH*R2)/(QH/VH)$  ; Amount of 4-OH-MDZ in liver compartment

;VRZ noxide well stirred hepatic extraction

$VEHM= (VCLHM*VFUBM)/(QH+(VCLHM*VFUBM))$

$CLHepaticMN = QH*VEHM$

$VFHM= 1-VEHM$

;VRZ noxide well stirred gut extraction, QGUT = Qvilli (QVI) in this case

$$\text{VEGM} = (\text{VCLGM} * \text{VFUGM}) / (\text{QVI} + (\text{VCLGM} * \text{VFUGM}))$$

$$\text{CLGutMN} = \text{QGUT} * \text{VEGM}$$

$$\text{VFGM} = 1 - \text{VEGM}$$

$$\text{VAGUTWM} = (1 - \text{VFG}) * \text{VAGUTW} \quad ; \text{ Amount of VRZ noxide in gut compartment}$$

$$\text{VAPVM} = ((\text{QVI} / \text{VGW}) * \text{VAGUTWM} * \text{VFGM} + \text{QPV} / \text{VVMET} * \text{A}(8)) / (\text{QPV} / \text{VPV}) \quad ; \text{ Amount of VRZ noxide in portal vein compartment}$$

$$\text{VAHM} = (\text{QHA} / \text{VVMET} * \text{A}(8) + \text{QPV} / \text{VPV} * \text{VAPVM} + \text{QH} / \text{VH} * \text{VAH} * \text{VEH}) / (\text{QH} / \text{VH}) \quad ; \text{ Amount of VRZ noxide in liver compartment}$$

;MDZ

$$\text{DADT}(1) = -\text{KA} * \text{A}(1); \text{ MDZ deposit}$$

$$\text{DADT}(2) = \text{FH} * (\text{QH} / \text{VH}) * \text{AH} - (\text{QHA} / \text{VCEN}) * \text{A}(2) - (\text{QPV} / \text{VCEN}) * \text{A}(2) - \text{K23} * \text{A}(2) + \text{K32} * \text{A}(11); \text{ MDZ central compartment}$$

$$\text{DADT}(11) = \text{K23} * \text{A}(2) - \text{K32} * \text{A}(11); \text{ MDZ peripheral compartment}$$

;VRZ

$$\text{DADT}(3) = -\text{VKA} * \text{A}(3); \text{ VRZ deposit}$$

$$\text{DADT}(4) = \text{VFH} * (\text{QH} / \text{VH}) * \text{VAH} - (\text{QHA} / \text{VVCEN}) * \text{A}(4) - (\text{QPV} / \text{VVCEN}) * \text{A}(4) - \text{KV23} * \text{A}(4) + \text{KV32} * \text{A}(12); \text{ VRZ central compartment}$$

$$\text{DADT}(12) = \text{KV23} * \text{A}(4) - \text{KV32} * \text{A}(12); \text{ VRZ peripheral compartment}$$

;Enzyme

$$\text{DADT}(15) = \text{KDEGL} * \text{E0L} - \text{KDEGL} * \text{A}(15) - \text{KINACT} * \text{CONVOLIV} * \text{A}(15) / (\text{KTDI} + \text{CONVOLIV}); \text{ Enzyme compartment in liver}$$

$$\text{DADT}(16) = \text{KDEGG} * \text{E0G} - \text{KDEGG} * \text{A}(16) - \text{KINACT} * \text{CONVOGUT} * \text{A}(16) / (\text{KTDI} + \text{CONVOGUT}); \text{ Enzyme compartment in gut}$$

;1-OH-MDZ

$$\text{DADT}(5) = \text{FHM} * (\text{QH} / \text{VH}) * \text{AHM} - (\text{QHA} / \text{MVMET}) * \text{A}(5) - (\text{QPV} / \text{MVMET}) * \text{A}(5) - \text{KR2} / \text{MVMET} * \text{A}(5); \text{ 1-OH-MDZ central compartment}$$

;1-OH-MDZ-GLU

$$\text{DADT}(14) = \text{EHM} * (\text{QH} / \text{VH}) * \text{AHM} + \text{EGM} * (\text{QVI} / \text{VGW}) * \text{AGUTWM} - \text{KR1} * \text{A}(14); \text{ 1-OH-MDZ-GLU central compartment}$$

DADT(10)=KR1\*A(14); 1-OH-MDZ-GLU urine compartment

;1-OH-MDZ URINE

DADT(7)=KR2/MVMET\*A(5); 1-OH-MDZ urine compartment

;4-OH-MDZ

DADT(6)=FHM4\*(QH/VH)\*AHM4-(QHA/MVMET4)\*A(6)-(QPV/MVMET4)\*A(6); 4-OH-MDZ central compartment

;MDZ GLU

DADT(9)=EH\*(QH/VH)\*AH\*R3+EG\*(QVI/VGW)\*AGUTW\*R3; MDZ-GLU urine compartment

;noxide

DADT(8)=VFHM\*(QH/VH)\*VAHM-(QHA/VVMET)\*A(8)-(QPV/VVMET)\*A(8)-KV23M\*A(8)+KV32M\*A(13); VRZ noxide central compartment

DADT(13)=KV23M\*A(8)-KV32M\*A(13); VRZ noxide peripheral compartment

CMDZ\_GUT=AGUTW/VGW

CMDZ\_APV=APV/VPV

CMDZ\_AH=AH/VH

CVRZ\_GUT=VAGUTW/VGW

CVRZ\_APV=VAPV/VPV

CVRZ\_AH=VAH/VH

C1OH\_GUT=AGUTWM/VGW

C1OH\_APV=APVM/VPV

C1OH\_AH=AHM/VH

C4OH\_GUT=AGUTWM4/VGW

C4OH\_APV=APVM4/VPV

C4OH\_AH=AHM4/VH

CNOXIDE\_GUT=VAGUTWM/VGW

CNOXIDE\_APV=VAPVM/VPV

CNOXIDE\_AH=VAHM/VH

\$ERROR

;MDZ

IPRED=0

CON2=A(2)/VCEN

IF(CON2.GT.0.AND.FLAG.EQ.1) THEN

IPRED = CON2

LLOQ =0.1534

RUVCV=THETA(33)

RUVSD=THETA(34)

ENDIF

;VRZ

CON4=A(4)/VVCEN

IF(CON4.GT.0.AND.FLAG.EQ.4) THEN

IPRED = CON4

LLOQ =14.3

RUVCV=THETA(35)

RUVSD=THETA(36)

ENDIF

;1-OH-MDZ

CON5=A(5)/MVMET

IF(CON5.GT.0.AND.FLAG.EQ.2) THEN

IPRED = CON5

LLOQ =0.0731

RUVCV=THETA(37)

RUVSD=THETA(38)

ENDIF

;1-OH-MDZ-GLU in urine

CON10=A(10)

IF(CON10.GT.0.AND.FLAG.EQ.10) THEN

IPRED = CON10

LLOQ =1.462

RUVCV=THETA(39)

RUVSD=0

ENDIF

;1-OH-MDZ in urine

CON7=A(7)

IF(CON7.GT.0.AND.FLAG.EQ.7) THEN

IPRED = CON7

LLOQ =1.462

RUVCV=THETA(40)

RUVSD=THETA(41)

ENDIF

;4-OH-MDZ

CON6=A(6)/MVMET4

IF(CON6.GT.0.AND.FLAG.EQ.3) THEN

IPRED = CON6

LLOQ =0.0731

RUVCV=THETA(42)

RUVSD=THETA(43)

ENDIF

;MDZ-GLU in urine

CON9=A(9)

IF(CON9.GT.0.AND.FLAG.EQ.9) THEN

IPRED = CON9

LLOQ =1.534

RUVCV=0

RUVSD=THETA(44)

ENDIF

;VRZ noxide

CON8=A(8)/VVMET

IF(CON8.GT.0.AND.FLAG.EQ.5) THEN

IPRED = CON8

LLOQ =13.7

RUVCV=THETA(45)

RUVSD=THETA(46)

ENDIF

PROP=IPRED\*RUVCV

ADD=RUVSD

SD=SQRT(PROP\*PROP+ADD\*ADD)

IRES = DV-IPRED

IWRES = IRES/SD ; Individual weighted residual

;MDZ

IF(CON2.GT.0.AND.FLAG.EQ.1.AND.BQL.EQ.0) THEN ;DV>LOQ

F\_FLAG=0

Y=IPRED+SD\*EPS(1)

ENDIF

;VRZ

IF(CON4.GT.0.AND.FLAG.EQ.4.AND.BQL.EQ.0) THEN ;DV>LOQ

F\_FLAG=0

Y=IPRED+SD\*EPS(1)

ENDIF

;1-OH-MDZ

IF(CON5.GT.0.AND.FLAG.EQ.2.AND.BQL.EQ.0) THEN ;DV>LOQ

F\_FLAG=0



Y=IPRED+SD\*EPS(1)

ENDIF

;1-OH-MDZ-GLU in urine

IF(CON10.GT.0.AND.FLAG.EQ.10.AND.BQL.EQ.0) THEN ;DV>LOQ

F\_FLAG=0

Y=IPRED+SD\*EPS(1)

ENDIF

;1-OH-MDZ in urine

IF(CON7.GT.0.AND.FLAG.EQ.7.AND.BQL.EQ.0) THEN ;DV>LOQ

F\_FLAG=0

Y=IPRED+SD\*EPS(1)

ENDIF

;4-OH-MDZ

IF(CON6.GT.0.AND.FLAG.EQ.3.AND.BQL.EQ.0) THEN ;DV>LOQ

F\_FLAG=0

Y=IPRED+SD\*EPS(1)

ENDIF

;MDZ-GLU in urine

IF(CON9.GT.0.AND.FLAG.EQ.9.AND.BQL.EQ.0) THEN ;DV>LOQ

F\_FLAG=0

Y=IPRED+SD\*EPS(1)

ENDIF

;VRZ noxide

IF(CON8.GT.0.AND.FLAG.EQ.5.AND.BQL.EQ.0) THEN ;DV>LOQ

F\_FLAG=0

Y=IPRED+SD\*EPS(1)

ENDIF

IF(BQL.EQ.1) THEN ;DV<LOQ

DUM = (LLOQ-IPRED)/SD

DUM2= PHI(DUM)

F\_FLAG=1

Y=DUM2

ENDIF

CMDZ=A(2)/VCEN

CVRZ=A(4)/VVCEN

C1OH=A(5)/MVMET

C4OH=A(6)/MVMET4

C1OHU=A(7)

CNOXIDE=A(8)/VVMET

CMDZG=A(9)

C1OHG=A(10)

C\_EN\_H=A(15)

C\_EN\_G=A(16)

\$THETA

(0,1.56595) ; 1 KA of MDZ

(0,71.6554) ; 2 Central volume of MDZ

(0,65.924) ; 3 Peripheral volume of MDZ

(0,19.864) ; 4 Inter-compartmental clearance of MDZ

(0,1056.97) ; 5 Unbound intrinsic hepatic clearance of MDZ CLH0

(0,585.556) ; 6 Inhibition constant of voriconazole on the metabolism of MDZ KI

(0,15.76) ; 7 Unbound intrinsic intestinal clearance of MDZ

(0,1.85737) ; 8 KA of VRZ

(0,126.887) ; 9 Central distribution volume of VRZ

(0,381.27) ; 10 Peripheral distribution volume of VRZ

(0,27.5397) ; 11 Inter-compartmental clearance of VRZ

(0,170.714) ; 12 Unbound intrinsic hepatic clearance of VRZ

(0,35.7479) ; 13 Unbound intrinsic intestinal clearance of VRZ

(0,2.83486) ; 14 Maximum inactivation rate constant KINACT of VRZ

- (0,63.5859) ; 15 Central volume of 1-OH-MDZ
- (0,174.756) ; 16 Unbound intrinsic hepatic clearance of 1-OH-MDZ
- (0,1129.38) ; 17 Inhibition constant of voriconazole on the metabolism of 1-OH-MDZ
- (0,65.5993) ; 18 Unbound intrinsic intestinal clearance of 1-OH-MDZ
- (0,1.11964) ; 19 Ratio of metabolism pathway to produce 1-OH-MDZ
- (0,2.43463) ; 20 Renal clearance of 1-OH-MDZ-GLU
- (0,1.28698) ; 21 Renal clearance of 1-OH-MDZ
- (0,50.4056) ; 22 Central volume of 4-OH-MDZ
- (0,54.5577) ; 23 Unbound intrinsic hepatic clearance of 4-OH-MDZ
- (0,356.364) ; 24 Inhibition constant of VRZ on the metabolism of 4-OH-MDZ
- (0,53.4795) ; 25 Unbound intrinsic intestinal clearance of 4-OH-MDZ
- 0.05 FIX ; 26 R2\_Ratio of metabolism pathway to produce 4-OH-MDZ
- (0,19.0283) ; 27 Central volume of VRZ noxide
- (0,18.9937) ; 28 Peripheral volume of VRZ noxide
- (0,39.4553) ; 29 Inter-compartmental clearance between central and peripheral compartment of VRZ noxide
- (0,6.70374) ; 30 Unbound intrinsic hepatic clearance of VRZ noxide
- (0,41.0461) ; 31 Unbound intrinsic intestinal clearance of VRZ noxide
- (0,0.00218237) ; 32 Ratio of metabolism pathway to produce MDZ-GLU
- 
- (0,0.116066) ; 33 MDZ proportional residual variability
- (0,1.75202) ; 34 MDZ additive residual variability
- (0,0.184852) ; 35 VRZ proportional residual variability
- (0,15.8977) ; 36 VRZ additive residual variability
- (0,0.112954) ; 37 1'-OH-MDZ proportional residual variability
- (0,0.327841) ; 38 1'-OH-MDZ additive residual variability
- (0,0.410081) ; 39 1'-OH-MDZ-GLU proportional residual variability in urine
- (0,1.77595) ; 40 1'-OH-MDZ proportional residual variability in urine
- (0,23.4544) ; 41 1'-OH-MDZ additive residual variability in urine
- (0,0.0549721) ; 42 4-OH-MDZ proportional residual variability
- (0,0.0993569) ; 43 4-OH-MDZ additive residual variability
- (0,9.44845) ; 44 MDZ GLU additive residual variability
- (0,0.11486) ; 45 VRZ noxide proportional residual variability
- (0,76.4859) ; 46 VRZ noxide additive residual variability

\$OMEGA BLOCK(1)

0.0949754 ; 1 CLH\_MDZ\_IIV

\$OMEGA BLOCK(1)

1.33553 ; 2 KI\_MDZ\_IIV

\$OMEGA BLOCK(1)

0.175965 ; 3 CLG\_MDZ\_IIV

\$OMEGA BLOCK(1)

0.492487 ; 4 CLH\_VRZ\_IIV

\$OMEGA BLOCK(1)

0.546855 ; 5 CLG\_VRZ\_IIV

\$OMEGA BLOCK(1)

0.0431021 ; 6 KINACT\_IIV

\$OMEGA BLOCK(2)

0.0789412 ; 7 CLH\_1OHMDZ\_IIV

-0.294826 1.4798 ; 8 KI1OH\_IIV

\$OMEGA BLOCK(1)

0.156088 ; 9 CLG\_1OHMDZ\_IIV

\$OMEGA BLOCK(1)

0.0666667 ; 10 CLH\_4OH

\$OMEGA BLOCK(1)

0.130909 ; 11 KI\_4OH\_IIV

\$OMEGA BLOCK(1)

0.0801889 ; 12 CLH\_NOXIDE

\$OMEGA BLOCK(1)

0.235021 ; 13 CLG\_NOXIDE

\$\$SIGMA 1 FIX

\$ESTIMATION METHOD=1 INTERACTION NOABORT LAPLACIAN MAX=9999 NSIG=2 SIGL=9  
PRINT=1 MSFO=msf052

\$ESTIMATION METHOD=IMP AUTO=1 EONLY=1 ISAMPLE=2000 NITER=30

\$COVARIANCE MATRIX=R SIGL=8 TOL=9 UNCONDITIONAL PRINT=E ; PARAFIELD=ON

\$TABLE ID TIME PER IPRED CMT FLAG MDV EVID BQL EXTRAPER DT CWRES

IWRES NOPRINT ; Don't include in the output file (i.e., "OUTPUT")

ONEHEADER ; Don't add a new header after 900 lines

FILE=sdtab052 ; Name of the output file

\$TABLE ID TIME PER CMT FLAG KA VCEN VPER Q CLH0 CLG0 CLH CLG

CLHepatic CLGut VKA VVCEN VVPER VQ VCLH0 VCLG0 VCLH VCLG

VCLHepatic VCLGut MVMET CLHM0 CLGM0 CLHM CLGM CLHepatic1OH

CLGut1OH MVMET4 CLHM40 CLGM40 CLHM4 CLGM4 CLHepaticM4

CLGutM4 VVMET VCLHM VCLGM VVPERM VQM CLHepaticMN CLGutMN

VEH VEG EH EG EHM EGM EHM4 EGM4 VEHM VEGM KI KI1OH KI4OH

KINACT KR1 KR2 R1 R2 NOPRINT ONEHEADER FILE=patab052

\$TABLE ID PER TIME MDV BQL EXTRAPER DT EVID FLAG CMT CMDZ CVRZ

C1OH C4OH C1OHU CNOXIDE CMDZG C1OHG C\_EN\_H C\_EN\_G CMDZ\_GUT

CMDZ\_APV CMDZ\_AH CVRZ\_GUT CVRZ\_APV CVRZ\_AH C1OH\_GUT

C1OH\_APV C1OH\_AH C4OH\_GUT C4OH\_APV C4OH\_AH CNOXIDE\_GUT

CNOXIDE\_APV CNOXIDE\_AH CONVOLIV CONVOGUT NOPRINT ONEHEADER

FILE=mytab052



# A Single Dose of Baicalin Has No Clinically Significant Effect on the Pharmacokinetics of Cyclosporine A in Healthy Chinese Volunteers

Ruijuan Liu<sup>1,2†</sup>, Xia Li<sup>3†</sup>, Jingyao Wei<sup>1,2</sup>, Shuaibing Liu<sup>1,2</sup>, Yuanyuan Chang<sup>1,2</sup>, Jiali Zhang<sup>1,2</sup>, Ji Zhang<sup>1,2</sup>, Xiaojian Zhang<sup>1,2</sup>, Uwe Fuhr<sup>3</sup>, Max Taubert<sup>3</sup> and Xin Tian<sup>1,2\*</sup>

<sup>1</sup>Department of Pharmacy, The First Affiliated Hospital of Zhengzhou University, Zhengzhou, China, <sup>2</sup>Henan Key Laboratory of Precision Clinical Pharmacy, Zhengzhou, China, <sup>3</sup>Department I of Pharmacology, Faculty of Medicine and University Hospital Cologne, Center for Pharmacology, University of Cologne, Cologne, Germany

## OPEN ACCESS

### Edited by:

Thomas Dorlo,  
The Netherlands Cancer Institute  
(NKI), Netherlands

### Reviewed by:

Constantin Mircioiu,  
Carol Davila University of  
Medicine and Pharmacy, Romania  
Maria Adriana Neag,  
Iuliu Hațieganu University of  
Medicine and Pharmacy, Romania

### \*Correspondence:

Xin Tian  
tianx@zzu.edu.cn

<sup>†</sup>These authors have contributed  
equally to this work

### Specialty section:

This article was submitted to  
Drug Metabolism and Transport,  
a section of the journal  
Frontiers in Pharmacology

Received: 18 January 2019

Accepted: 24 April 2019

Published: 14 May 2019

### Citation:

Liu R, Li X, Wei J, Liu S, Chang Y,  
Zhang J, Zhang J, Zhang X, Fuhr U,  
Taubert M and Tian X (2019) A Single  
Dose of Baicalin Has No Clinically  
Significant Effect on the  
Pharmacokinetics of Cyclosporine A  
in Healthy Chinese Volunteers.  
*Front. Pharmacol.* 10:518.  
doi: 10.3389/fphar.2019.00518

Despite its narrow therapeutic window and large interindividual variability, cyclosporine A (CsA) is the first-line therapy following organ transplantation. Metabolized mainly by CYP3A and being a substrate of P-glycoprotein (P-gp), CsA is susceptible to drug–drug interactions. Baicalin (BG) is a drug used for adjuvant therapy of hepatitis in traditional Chinese medicine. Since its aglycone baicalein (B) inhibits CYP3A and P-gP, co-administration might affect CsA pharmacokinetics. This study investigated the effect of BG on CsA pharmacokinetics. In a two-period study, 16 healthy volunteers received a single 200 mg oral CsA dose alone (reference period) or in combination with 500 mg BG (test period). Pharmacokinetic evaluation of CsA was carried out using non-compartmental analysis (NCA) and population pharmacokinetics (popPK). Treatments were compared using the standard bioequivalence method. Based on NCA, 90% CIs of AUC and  $C_{max}$  test-to-reference ratios were within bioequivalence boundaries. In the popPK analysis, a two-compartment model (clearance/F 62.8 L/h, central and peripheral volume of distribution/F 254 L and 388 L) with transit compartments for absorption appropriately described CsA concentrations. No clinically relevant effect of 500 mg BG co-administration on CsA pharmacokinetics was identified and both treatments were well tolerated.

**Keywords:** cyclosporine A, baicalin, pharmacokinetics, non-compartmental analysis, population pharmacokinetics, healthy volunteers

## INTRODUCTION

As an immunosuppressant drug, cyclosporine A (CsA) has been widely used in transplantation since the early 1980s (Colombo and Ammirati, 2011). From then on, CsA remained a first-line therapy for patients with solid organ transplantation. However, CsA has a narrow therapeutic range and large interindividual pharmacokinetic variability. While underexposure might cause graft versus host disease (Rogosheske et al., 2014) and acute rejection episodes, overexposure might result in toxicity (Bardazzi et al., 2018). CsA is categorized as a biopharmaceutical classification system (BSC) class II drug due to low solubility and high permeability (Onoue et al., 2010).

After oral administration, CsA is absorbed from the gastrointestinal tract with a bioavailability of approximately 30% (Drewe et al., 1992). As a lipophilic molecule, CsA has a high volume of distribution (3–5 L/kg); in blood, cyclosporine is extensively bound to erythrocytes. In plasma, approximately 90% is bound to proteins, primarily lipoproteins (U.S. Food and Drug Administration, 2015). The disposition of cyclosporine is generally biphasic, with a terminal half-life of approximately 8.4 h (range 5–18 h) (U.S. Food and Drug Administration, 2015). Cyclosporine is extensively metabolized by CYP3A4 and CYP3A5 and subject to efflux from renal tubular cells and other cells via P-glycoprotein (P-gp) (Hebert, 1997). Therefore, co-administration of CYP3A or P-gp inhibitors may alter the pharmacokinetics of CsA. For example, concomitant administration of ketoconazole has been reported to elevate CsA concentrations several-fold (Albengres and Tillement, 1992; Keogh et al., 1995). Imatinib, a potent inhibitor of CYP3A4 and P-gp, approximately doubled CsA exposure (Atiq et al., 2016).

Baicalin (baicalein 7-O-glucuronide, BG), the major bioactive compound from *Scutellaria baicalensis* (Shi et al., 2016), is widely applied in traditional Chinese medicine for the treatment of inflammation, hepatitis, various infections, and tumors (Xi et al., 2015; Zhao et al., 2016; Gong et al., 2017; Ming et al., 2018). In 2005, baicalin capsules (250 mg per capsule, approval no. H20158009) were approved by the state food and drug administration of China for the adjuvant therapy of hepatitis (2 capsules 3 times a day). After oral administration, BG is rapidly hydrolyzed to baicalein (B) by  $\beta$ -glucuronidase derived from intestinal bacteria (Huang et al., 2019). Both BG and its aglycone baicalein (B) have a low hydrophilicity (solubility of BG is 0.057 mg/ml in water) (Wu et al., 2011) and a relatively low permeability as determined in the Caco2 cell system [for BG,  $P_{app} = (0.275 \pm 1.14) \times 10^{-6}$  cm/s (Zhu et al., 2013); for B,  $P_{app} = 9.0 \times 10^{-6}$  cm/s (Cai et al., 2016)], resulting in a very low oral bioavailability for both baicalin (2.2%) and baicalein (Wu et al., 2014). Compared to BG, B could be better absorbed in the gastrointestinal tract and then conjugated to BG in the gut wall and liver (Liu et al., 2009; Zhang et al., 2011). BG is extensively bound to proteins (86–92%) in human plasma (Tang et al., 2006), has a short elimination half-life ( $6.36 \pm 5.85$  h), and undergoes extensive metabolism (Noh et al., 2016).

Inflammation is a significant problem in organ transplant patients. With the anti-inflammatory and antioxidant properties of BG and its aglycone B, co-administration of BG might benefit the organ transplant patients treated with CsA (Shieh et al., 2000; Dinda et al., 2017). However, several lines of evidence suggest that BG may cause drug–drug interactions in humans. B is an inhibitor of CYP3A and P-gp in rats (Morisaki et al., 2013; Miao et al., 2016). For example, intravenous administration of high BG doses (0.23–0.90 g/kg) to rats decreased the clearance of midazolam by up to 43% (Xin et al., 2013). In human liver microsomes, B was reported to potently inhibit CYP3A4 (Ki for mixed-type inhibition of bufalin 5'-hydroxylation 2.3  $\mu$ M; IC<sub>50</sub> for inhibition of midazolam and nifedipine at their Km concentrations 13 and 15  $\mu$ M, respectively) (Li et al., 2018). On the other hand, it has been

reported that B (but not BG) may activate the human pregnane X receptors and the human constitutive androstane receptor (CAR) (Morisaki et al., 2013; Cheng et al., 2014; Miao et al., 2016), which could mediate CYP3A and P-gp induction. A recent study in rats indeed showed that single intravenous dose and multiple doses of BG had no effect on the pharmacokinetics of CsA, while oral administration significantly decreased  $C_{max}$  and  $AUC_{0-\infty}$  of CsA. This indicates that BG might affect intestinal absorption and/or secretion of CsA. Further study revealed that after multiple oral doses of BG treatment, the expression of P-gp of rats increased in the intestine, but was not changed in the liver (Tian et al., 2019). Beyond affecting CYP3A and P-gp, co-administration of BG also changed plasma protein binding and apparent volumes of distribution of nifedipine, another CYP3A probe, in rats (Cheng et al., 2014). An early study in rats which directly investigated the effects of *Scutellaria radix* decoction, BG, or B on CsA pharmacokinetics provided mixed findings: the decoction reduced exposure to oral but not to intravenous CsA, while BG and even more so B increased exposure to oral CsA (Lai et al., 2004).

These results indicate that indeed co-medication with BG might alter the pharmacokinetics of CsA in humans and also indicate that any respective DDIs may be mediated by several mechanisms. So far, no clinical studies have been reported on drug–drug interactions between BG and CsA. The aim of the current study, therefore, was to explore a potential effect of BG on CsA exposure in healthy volunteers and to assess possible effects on individual pharmacokinetic processes in detail.

## MATERIALS AND METHODS

### Chemicals and Reagents

Cyclosporine soft capsules (25 mg, trade name: Sandimmun Neoral) were obtained from Novartis Pharma (Basle, Switzerland); this preparation is an immediate release microemulsion. BG capsules (250 mg, trade name: Jinmeiji) were purchased from Dongguan Jinmeiji pharmaceutical company (Dongguan, China). The reference standards of cyclosporine A and cyclosporine D were purchased from Toronto Research Chemicals (Toronto, Canada). All chemicals and solvents were of HPLC grade.

### Study Population

After approval by the Ethics Committee of the first affiliated hospital of Zhengzhou University (Henan, China; approval no. SR201509), the clinical trial was performed at this hospital in accordance with the standards of Good Clinical Practice, all applicable regulations, specific legal requirements, and ethical principles as described in the Declaration of Helsinki. Subjects provided written informed consent after a comprehensive explanation of the study protocol and before any procedure was performed.

Sixteen healthy Chinese participants (8 males and 8 females, age range 19–34 years, body mass index 19.4–25.6 kg/m<sup>2</sup>) were enrolled in the study. Based on an intraindividual coefficient

of variation of not more than 19% for CsA AUC and  $C_{\max}$  (Avramoff et al., 2007), this sample's size would be appropriate to assess absence of an interaction with  $\alpha = 0.05$  and a power of 90% if the true ratios for the test over reference were in the 0.95–1.05 range. Participants were ascertained to be mentally and physically healthy by medical history, clinical examination, electrocardiography, and routine laboratory analyses consisting of hematology, blood chemistry, urine screening for illicit drugs, and a quantitative pregnancy test in women to exclude pregnancy. Main exclusion criteria included: excessive smoking (more than five cigarettes per day); alcohol intake exceeding 25 g per week; a history of clinically significant cardiovascular, renal, hepatic, pulmonary, gastrointestinal, or psychiatric diseases; a history of known allergy or intolerance to any drugs; a history of drug abuse; abnormalities in clinical laboratory parameters; donating of blood or losing blood within 3 months; and suffering from any organ damage within the previous 3 months. Subjects were required to abstain from using medications, alcohol, cigarettes, and from food and beverages containing grapefruit within 2 weeks before the first dose of study medications and during the study.

## Study Design

The study was a single center, open-labeled, two-period, fixed-sequence clinical trial. All eligible subjects were admitted to the clinical trial institution and were offered a standard dinner 1 day before the trial. After overnight fasting, the participants were administered 200 mg CsA orally (eight soft capsules) together with 240 ml of water in the morning on day 1 during the first period. Water intake was allowed 2 h after administration of the drug. All participants were given a standardized meal 4 h after dosing. In the second period, after a washout period of 2 weeks, the same procedure was repeated with CsA in combination with 500 mg BG (two capsules).

## Blood Sampling

Blood samples (4 ml each) were collected at multiple time points pre-dose, 0.5, 1.0, 1.5, 2, 2.5, 3, 4, 6, 8, 10, 12, 16, 24, 36, and 48 h after dosing on days 1 and 15, respectively. Blood samples were withdrawn using vacuum tubes containing EDTA- $K_2$  and immediately transferred to labeled tubes. The samples were stored at  $-80^{\circ}\text{C}$  for subsequent analysis.

## Quantification of Cyclosporine A in Blood

The analytical method for quantification of CsA in blood samples was validated according to the pertinent U.S. FDA guideline (U.S. Food and Drug Administration, 2018). Processing of the whole blood samples involved a two-step protein precipitation. Fifty microliters of zinc sulfate (10 mM) were added to 50  $\mu\text{l}$  of a sample. After vortexing, internal standard (IS) cyclosporine D and 800  $\mu\text{l}$  of methanol-acetonitrile (v:v = 1:1) were added and vortexed. After centrifugation, an aliquot (2  $\mu\text{l}$ ) of the supernatant was then injected onto an ultra high-performance liquid chromatography coupled with tandem mass spectrometry (UHPLC–MS/MS) device for analysis.

UHPLC–MS/MS was performed using an ExionLC™ analytical UHPLC system (AB Sciex, MA, USA), coupled with a Qtrap 4,500 mass spectrometer (AB Sciex, Framingham, MA, USA), equipped with the Turbo IonSpray interface. Chromatographic separation was performed on a Waters (Dublin, Ireland) BEH  $C_{18}$  2.1 mm  $\times$  100 mm, 1.6  $\mu\text{m}$  column, eluted with a mobile phase consisting of mobile phase A (water with 0.1% formic acid and 2 mM ammonium acetate) and B (methanol with 0.1% formic acid) at a flow rate of 400  $\mu\text{l}/\text{min}$ . The gradient elution was 0–0.8 min 65% B; 0.81–3.9 min 100% B; 4.0–5.0 min 65% B. Retention times for CsA and IS were 2.49 and 2.54 min, respectively. The protonated analyte ions were detected in positive ionization and multiple reaction monitoring modes. The mass transition pairs of  $m/z$  1220.0  $\rightarrow$  1202.8 and 1234.0  $\rightarrow$  1216.8 were used to detect CsA and IS. The declustering potentials of CsA and IS were both 60 eV; the entrance potentials were 3 and 6 eV; the collision cell exit potentials were both 30 eV; and the collision energy was 23 and 22 eV, respectively. Calibration curves were linear over the concentration range of 10–3,000 ng/ml. Intra-day and inter-day coefficients of variation were lower than 7.43% in terms of relative standard deviation for the lower limit of quantification (LLOQ) and for low, medium, and high concentration quality control samples of CsA. The mean accuracy was within  $\pm 7.0\%$  in terms of relative error for CsA. The LLOQ was 10 ng/ml.

## Safety and Tolerability Assessments

For enrolled volunteers, safety and tolerability of CsA when given alone or in combination with BG were assessed throughout the study by monitoring adverse events (AEs), standard clinical laboratory tests (clinical biochemistry, urinalysis, hematology), physical examinations, vital signs, and 12-lead electrocardiograms (ECGs). A follow-up visit was conducted about 10 days following the last dose of study medication.

## Non-compartmental Analysis

To directly assess the quantitative effect of BG on CsA exposure, standard non-compartmental analysis by use of the WinNonlin 7.0 software (Pharsight, St Louis, MO, USA) was applied to determine pharmacokinetic parameters of CsA in the periods with and without BG co-administration. Statistical analyses were performed by use of SPSS software version 11.5 (SPSS, Inc., Chicago, IL, USA). Exploratory statistical comparisons of pharmacokinetic parameters between male and female subjects were performed by the *t*-test for independent data. A nonparametric test was used to compare  $T_{\max}$  between male and female subjects, and between the reference and BG treatment.  $p < 0.05$  was considered a significant difference. To compare exposure between treatments, point estimates and 90% confidence intervals (CIs) of the geometric mean ratios of AUC and  $C_{\max}$  of treatment over reference were used. No relevant effect of BG on CsA exposure was assumed if 90% CIs of the geometric mean of test-to-reference ratios for these parameters were within the range of 0.80–1.25. Respective descriptive comparisons were also made for further pharmacokinetic parameters where appropriate.



## Population Pharmacokinetic Analysis

### Basic Population Pharmacokinetic Analysis

To assess potential effects of BG co-administration on individual pharmacokinetic processes in detail, a population pharmacokinetic nonlinear mixed-effects model was developed with NONMEM 7.4.1 (Icon Development Solutions, Ellicott City, MD, USA). Data preparation and graphical data visualization were conducted using R 3.4.2 (R Foundation for Statistical Computing, Vienna, Austria). Model diagnostics were performed with XPOSE 4.5.0.9. The toolkit Perl-speaks-NONMEM (PsN) (Lindbom et al., 2004) served as an application programming interface to NONMEM to aid model development and evaluation. The structural pharmacokinetic model was built step by step, beginning with a one-compartment model with linear elimination kinetics and expanded up to a three-compartment model. Interindividual (IIV) and inter-occasion variability were tested, and additive, proportional, and combined error models were evaluated. Model selection was based on a change of 3.84 points in the objective function value (OFV) being considered as statistically significant with  $p < 0.05$ . The Akaike Information Criteria (AIC) were compared to select non-nested models.

### Absorption Model Selection

The absorption process of CsA is complicated and influenced by many physiological factors. It seemed that the previously published conventional absorption models (first- or zero-order, with or without lag time) were not appropriate to optimally describe the absorption profiles in the present study. Thus, other additional absorption models were tested, including Weibull-type function models, Gaussian density function models, erlang-type absorption, and transit compartment models. The model selection was based on both visual (goodness of fit plots) and numerical (OFV and AIC) procedures.

### Covariate Selection

Based on previous knowledge on CsA pharmacokinetics, demographic and clinical variables such as age, weight, sex, hematocrit, alanine aminotransferase (ALT), aspartate aminotransferase (AST), total bilirubin, and albumin were tested for covariates analysis on PK parameters. Visual (parameter vs. covariate scatter plots) covariate screening procedures were first performed before adding each covariate to the basic model. The Stepwise Covariate Model with both forward and backward selection was further used to analyze covariates. The criteria for integration of covariates were a decrease in OFV  $> 3.84$  ( $p < 0.05$ ) in the forward selection and an increase in OFV  $> 6.64$  ( $p < 0.01$ ) in the backward selection (approximate to  $\chi^2$  distribution,  $\chi_{0.05,1}^2 = 3.84$ ;  $\chi_{0.01,1}^2 = 6.64$ ).

### Effect of Baicalin on the Pharmacokinetics of Cyclosporine A

An effect of BG was introduced on the following pharmacokinetic parameters of the final model of CsA with Eq. 1: number of transit compartments (N), mean transit time (MTT), absorption rate constant (Ka), apparent clearance (CL/F), Vc/F (apparent central volume of distribution), Vp/F (apparent peripheral

volume of distribution), and Q/F (apparent intercompartmental clearance). A bootstrap analysis was conducted for each model. For an effect of a covariate as a factor on an individual parameter of CsA to be considered as potentially clinically relevant, both the 95% CIs for BG effects from the 1,000 bootstrap results must not include unity (Ravva et al., 2009), and the 95% would need to be at least partially outside a 0.80–1.25 range.

$$PAR = TVPAR \times \theta_{PAR}^{test} \quad (1)$$

Eq. 1 PAR population pharmacokinetic parameter, representing N, MTT, Ka, CL/F, Vc/F, Vp/F, Q/F, respectively; TVPAR population median of each parameter; test (test, 0 = CsA alone, 1 = co-administration with BG),  $\theta^{test}$  the effect of co-administration with BG on each parameter.

## Model Evaluation

Reliability and precision of model parameter estimates were confirmed by comparison to nonparametric medians and 95% CIs obtained from bootstrap statistics with 1,000 samples generated by resampling individuals with replacement (Ette, 1997; Parke et al., 1999; Lindbom et al., 2005). The model trend and variability were confirmed by visual predictive checks (VPC) performed by simulating 1,000 replicates of the original study design (Post et al., 2008).

## RESULTS

### Non-compartmental Analysis

Mean blood concentration-time profiles of CsA are presented in **Figure 1**. These were nearly identical in the reference and treatment periods. Non-compartmental pharmacokinetic parameters of CsA for both periods are summarized in **Table 1**.

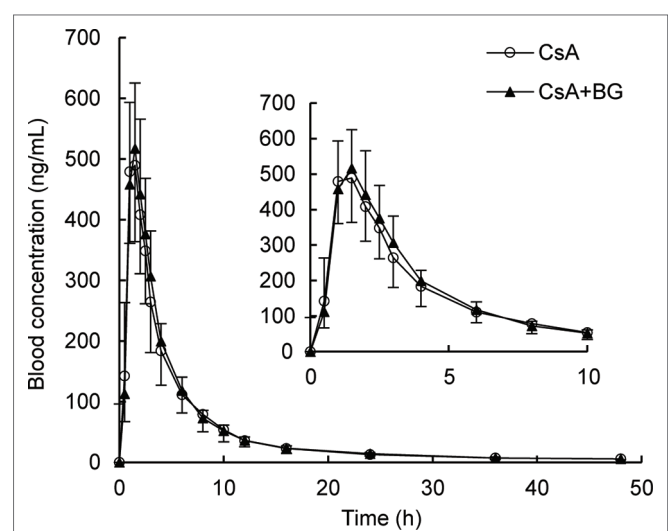


**FIGURE 1** | Geometric mean blood concentration-time profile of CsA in 16 healthy volunteers after single oral administration of 200 mg CsA alone or co-administration with 500 mg BG.

**TABLE 1 |** Pharmacokinetic parameters of CsA after single oral administration of 200 mg CsA alone or co-administration with 500 mg BG in 16 healthy individuals (non-compartmental analysis).

Parameters	CsA alone (R)	CsA + BG (T)	T/R ratio: point estimate (90% CI)
$AUC_{0-48}$ ( $h \cdot \mu g/ml$ )	2.19 (19.7%)	2.22 (24.8%)	101% (88.4–116%)
$AUC_{0-\infty}$ ( $h \cdot \mu g/ml$ )	2.33 (18.9%)	2.38 (24.4%)	102% (89.1–116%)
$C_{max}$ (ng/ml)	541 (15.7%)	558 (17.5%)	103% (93.1–114%)
$T_{max}$ (h)	1.5 (1.0–2.5)	1.5 (1.0–2.5)	–
$t_{1/2}$ (h)	7.44 (23.7%)	7.60 (37.4%)	102% (83.0–126%)
$MRT_{0-48}$ (h)	5.42 (22.5%)	5.24 (14.2%)	96.6% (86.7–108%)
$CL/F$ (L/h)	85.7 (19.5%)	84.2 (26.4%)	98.2% (86.0–112%)
$Vz/F$ (L)	920 (24.4%)	924 (29.7%)	100% (83.8–120%)

Data are presented as geometric mean with coefficient of variation (CV) and  $T_{max}$  as median (range). Abbreviations are as follows: CI, confidence interval;  $AUC_{0-48}$ , AUC from time 0 to 48 h after administration;  $AUC_{0-\infty}$ , AUC extrapolated to infinity;  $C_{max}$ , maximum observed blood concentration; F, (unknown) bioavailability;  $T_{max}$ , time to reach  $C_{max}$ ;  $t_{1/2}$ , apparent terminal elimination half-life;  $MRT_{0-48}$ , mean residence time from 0 to 48 h;  $CL/F$ , apparent clearance;  $Vz/F$ , apparent volume of distribution during terminal phase; T/R ratio, geometric mean of parameter values CsA + BG to CsA alone.

Parameters were similar for test and reference periods, with point estimates for geometric mean test/reference ratios for  $AUC_{0-48}$ ,  $AUC_{0-\infty}$ ,  $C_{max}$ ,  $t_{1/2}$ ,  $MRT_{0-48}$ ,  $CL/F$ , and  $Vz/F$  ranging from 0.97 to 1.03. The 90% CIs of geometric mean ratios of treatment to reference for  $AUC_{0-48}$ ,  $AUC_{0-\infty}$ , and  $C_{max}$  as the key parameters describing CsA exposure were within the standard bioequivalence interval of 80–125%, indicating that CsA exposure was not affected by co-administration with BG in this study. In addition, no significant differences ( $p > 0.05$ ) were observed in  $C_{max}$ ,  $AUC_{0-48}$ ,  $AUC_{0-\infty}$ ,  $T_{max}$ ,  $t_{1/2}$ ,  $MRT_{0-48}$ ,  $CL/F$ , and  $Vz/F$  of CsA between male and female subjects.

## Population Pharmacokinetic Analysis Model Development

A two-compartment model with linear elimination with a proportional error model was selected as the structural model. Compared to other absorption models, the transit compartment model provided a statistically significant improvement in the fit (lowest OFV and AIC) and the best performance in the visual exploration of diagnostic plots (Figure 2).

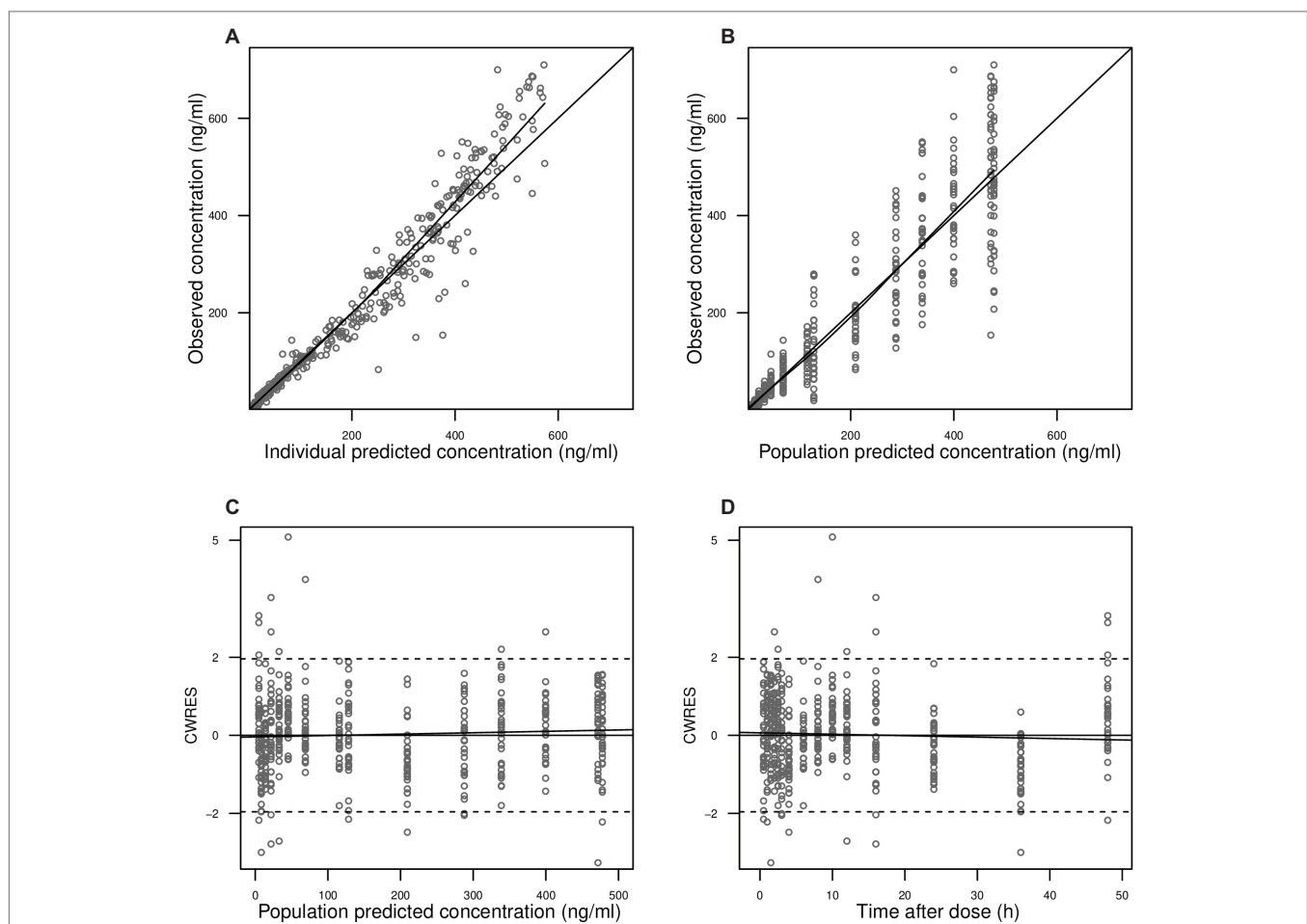


**FIGURE 2 |** Goodness-of-fit plots. Observed blood CsA concentrations versus individual predictions (A) and population predictions (B) as obtained from the pharmacokinetic model. Conditional weighted residuals (CWRES) versus population predicted blood CsA concentrations (C) and versus time after the first dose (D).

Although zero-order absorption with a lag time including IIV on lag time also described the absorption phase well, the bootstrap analysis indicated this absorption model was not stable, as 729 of 1,000 runs were unsuccessful. In contrast, the bootstrap analysis confirmed that the transit model with IIV or interoccasional variability (IOV) for MTT and N is stable. In comparison to an abrupt switch of the absorption rate at a certain point of time for the lag time model, the transit model more closely reflects physiological conditions with a gradually increasing absorption rate over time. Introduction of IOV for MTT and N improved the model significantly (OFV reduced by 35.03 points and 74.30 points, respectively). IIV was estimated on CL, Ka, Q, and N, leading to a significant drop in OFV by 141.0, 47.9, 35.2, and 4.4 points, respectively. Pharmacokinetic parameter estimates of the final model are presented in **Table 2**. Although several demographic and clinical parameters (age, weight, sex, hematocrit, ALT, AST, total bilirubin, and albumin) were tested as potential covariates on PK parameters, no significant covariate was identified with both visual and numerical covariate screening procedures (e.g., Stepwise Covariate Model).

### Model Evaluation

In **Figure 2A**, observed blood CsA concentrations versus individual predicted CsA concentrations exhibited a slight underestimation for high concentrations, while the weighted residual plot (**Figures 2C,D**) indicated that this misspecification would be acceptable because most of the residuals fell within +2 and -2 units of the null ordinate. The conditional weighted residuals (CWRES) plots (**Figure 2D**) appeared to show misspecification, but individual CWRES revealed that this was due to the high variability of the pharmacokinetics of CsA. While it appears that the introduction of additional compartments might attenuate the apparent misspecification, this was not supported by the respective statistical criteria. In addition, the goodness-of-fit plots of the population pharmacokinetic model for CsA in each treatment further indicated that the final model fit well the observed concentration-time profile of CsA for both treatments. In the VPC of the final population PK model with the transit compartments, medians and 2.5th and 97.5th percentiles of the simulated data were in good agreement with the observed data, verifying

**TABLE 2** | Comparison of the tested absorption models for the pharmacokinetics of CsA in the population pharmacokinetic analysis.

Model	Model tested	OFV	AIC
M1	First-order absorption	3555.31	3577.31
M2	First-order absorption with lag time	3361.25	3387.25
M3	Zero-order absorption	3446.47	3468.47
M4	Zero-order absorption with lag time	3359.28	3386.37
M5	Weibull function	3358.69	3384.69
M6	Gaussian function	3365.05	3391.04
M7	Erlang frequency (five sequential compartments)	3364.35	3388.35
M8	Transit compartment	3331.80	3357.80

the good performance of this model (**Figure 3**). The median parameter estimates and 95% CI obtained from bootstrap are summarized in **Table 3**.

### Effect of Baicalin Co-administration on the Pharmacokinetics of Cyclosporine A

With the exceptions of Ka and Q, the 95% CIs of the factor “BG co-treatment” on the parameters included 1.0 and were inside the 0.8–1.25 range, suggesting that BG did not affect the respective pharmacokinetic parameters of CsA to a clinically relevant extent (**Figure 4**). For Ka and Q, the CIs also included unity but were wide and exceeded the range, reflecting pronounced interindividual variability.

### Safety and Tolerability

No severe or serious adverse events were observed and all subjects were in good health. All participants completed the study with adequate compliance and no subject dropped out of the study.

Forty-three adverse events occurred in 13 subjects after administration of CsA (**Table 4**). In the first reference period, 11 subjects suffered 20 events, especially abdominal discomfort, which was the most frequently reported drug-related AE. In the second treatment period, 13 subjects reported 23 events where heartburn, accounting for 21.7% of events in this period, was most frequently reported. All but one AE in the two periods were considered as related to the study medication. No notable change was recorded in the vital signs or clinical laboratory variables when comparing baseline and end of study evaluations. Besides, there were no clinically relevant changes in ECG in individuals during the study. All the AEs reported were mild and resolved without dose interruption, treatment, or sequelae.

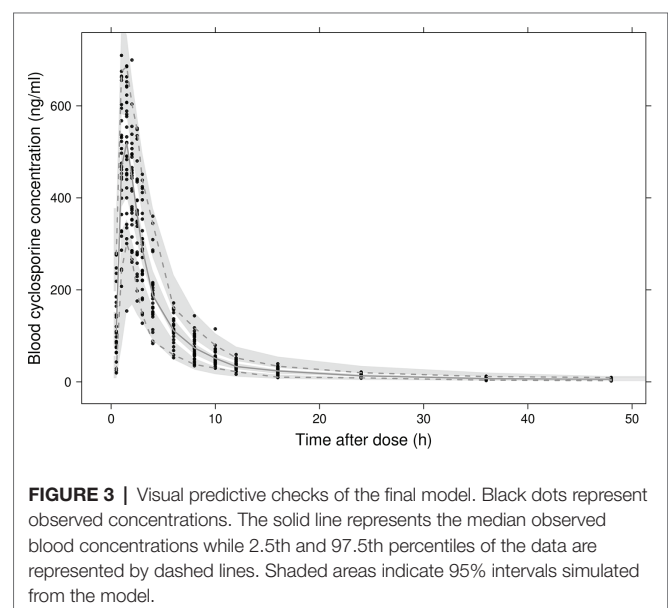


**FIGURE 3** | Visual predictive checks of the final model. Black dots represent observed concentrations. The solid line represents the median observed blood concentrations while 2.5th and 97.5th percentiles of the data are represented by dashed lines. Shaded areas indicate 95% intervals simulated from the model.

**TABLE 3** | Pharmacokinetic parameter estimates of the final population pharmacokinetic model of CsA.

Parameter (unit)	Definition of parameter	Bootstrap	
		Median	95% CI <sup>a</sup>
<b><math>\theta</math>-Estimates</b>			
CL / F (l/h)	Apparent clearance	62.8	(54.4–71.2)
V <sub>c</sub> / F (l)	Apparent central volume of distribution	254	(226–281)
V <sub>p</sub> / F (l)	Apparent peripheral volume of distribution	388	(344–456)
Q (l/h)	Intercompartmental clearance between central and peripheral compartment	23.6	(19.3–29.5)
K <sub>a</sub> (h <sup>-1</sup> )	Absorption rate constant	12.4	(6.57–33.9)
MTT (h)	Mean transit time	0.812	(0.797–0.831)
N	Number of transit compartment	20.2	(16.6–25.6)
<b><math>\omega^2</math>-Estimates</b>			
IIV CL (CV%)	Interindividual variability on clearance	12.6	(3.69–20.4)
IIV K <sub>a</sub> (CV%)	Interindividual variability on absorption rate	155	(55.9–628)
IIV Q (CV%)	Interindividual variability on distributional clearance	25.7	(7.74–42.0)
IIV N (CV%)	Interindividual variability on number of transit compartments	20.2	(7.57–38.2)
IOV MTT (CV%)	Inter-occasional variability on mean transit time	4.39	(2.31–6.18)
IOV N (CV%)	Inter-occasional variability on number of transit compartments	17.6	(9.32–25.2)
<b><math>\sigma^2</math>-Estimates</b>			
PRV (CV%)	Proportional residual variability	19.4	(16.0–22.9)

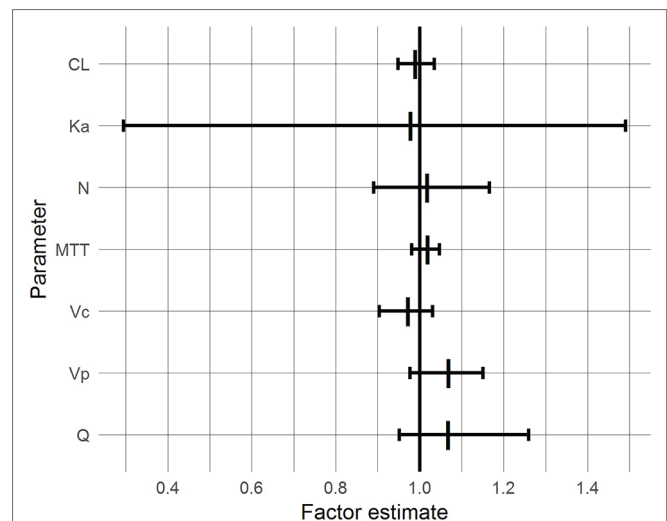
<sup>a</sup>CI, confidence interval (nonparametric) based on 2.5 and 97.5% percentiles obtained by the bootstrap analysis based on the final model applied to the original dataset; F, bioavailability.

CV% for IIV and IOV computed as  $\sqrt{\exp(\omega^2)-1}$ ; CV% for PRV computed as  $\sqrt{\exp(\sigma^2)-1}$ .

## DISCUSSION

In this study, non-compartmental analysis of the blood concentration vs. time profiles of CsA indicated that co-administration of a single 500 mg BG dose has no clinically relevant effect on the exposure of CsA in healthy volunteers. The compartmental population pharmacokinetic analysis further confirmed this result for underlying pharmacokinetic processes.

After oral administration, BG, due to low lipophilicity, may either be directly absorbed by the action of uptake transporters, or undergo hydrolysis by intestinal glucuronidase or intestinal microflora to release its aglycone B (Akao et al., 2010; Kang et al., 2014; Noh et al., 2016; Kalapos-Kovács et al., 2018). B is probably better absorbed and then efficiently conjugated to BG in the gut wall and the liver and thus restored to its original form BG (baicalein 7-O-glucuronide) as well as to baicalein 6-O-glucuronide (Liu et al., 2009; Zhang et al., 2011).

**FIGURE 4** | 95% confidence intervals (bars) and medians (vertical lines) of BG effects based on a bootstrap with 1,000 samples.**TABLE 4** | Summary of adverse events in the clinic trial.

Adverse events	Number of events (CsA alone)	Number of events (CsA + BG)
Headache	–	1
Nausea	3	3
Dizziness	1	–
Altered taste	1	–
Abdominal discomfort	4	2
Heartburn	3	5
Mouth ulcer <sup>a</sup>	–	1
Feeling hot	3	4
Oesophagitis	1	1
Pharyngitis	3	3
Palpitation	1	–
Chest congestion	–	3

<sup>a</sup>Which was considered unlikely to be related to the study drug.

Thus, both BG and B would be present at the various locations of CYP3A4 and P-gp in the gut wall and the liver, with the potential to modify their activity and/or expression (Morisaki et al., 2013; Miao et al., 2016), if sufficient concentrations were reached.

However, an effect of BG on the pharmacokinetics of CsA was not observed in this study based on all but two of the assessments. The observation in the population pharmacokinetic analysis that 95% CIs for Ka and Q exceeded the “no relevant effect” range probably just reflects that the study was not powered to quantify an effect on these parameters. There are three potential explanations for the finding that BG did not cause a drug–drug interaction (DDI). First, formation of B, the much more active moiety to cause DDIs (Morisaki et al., 2013; Xin et al., 2013; Tian et al., 2019), from BG may be very limited in humans *in vivo*. Second, even if B would be generated extensively, it is subject to (re-)glucuronidation in the gut, the gut wall, and/or the liver (Akao et al., 2010), thus losing (most of the) effects on CYP3A4 and P-gp. Indeed, when B single



doses were administered directly to healthy volunteers, exposure to BG exceeded that to B more than 10-fold (Li et al., 2014), indicating that glucuronidation of B in humans is rapid and extensive. Third, it cannot be excluded that competing mechanisms of inhibition would cancel each other out, but the different time courses of inhibition of drug metabolizing enzymes, transporter, or protein binding vs. induction by increased protein synthesis make this explanation unlikely. In summary, independent of the underlying mechanism, it appears that the systemic exposure of B produced after a single oral administration of BG in this study was too low to affect the activities of CYP3A and P-gp.

The present study is the first to study any DDI of BG in humans. One study in rats reported that single dose of BG (136.6 mg/kg) markedly elevated the  $C_{max}$  and AUC of CsA to about 4 times and 6 times, respectively, compared with CsA administered alone (Lai et al., 2004). However, our recent study in rats showed that multiple intravenous doses of BG did not affect the exposure of CsA but multiple oral administrations of BG (80 mg/kg) could decrease the  $C_{max}$  and  $AUC_{0-\infty}$  of CsA by 38 and 25%, respectively (Tian et al., 2019). Further study resulted in that after multiple oral doses of BG treatment, the expression of P-gp of rats increased in the intestine, but was not changed in the liver (Tian et al., 2019). The different results of the two studies in rats might be related to the dosage, and the different results between rats and humans might be caused by the species differences, particularly in the formation and re-glucuronidation of B.

The additional use of population pharmacokinetic analysis might serve as a powerful tool to improve the understanding of potential DDI. First, the non-compartmental analysis might result in poorly estimated parameters such as clearance and volume(s) of distribution and confound sources of variability such as interindividual, intraindividual, and inter-occasion variability based on the actual observation instead of basic pharmacokinetic parameters as the dependent variable. Secondly, the population pharmacokinetic approach enables to assess PK processes underlying drug exposure separately. This way, it was possible to show that neither clearance nor volumes of distribution of CsA, which are the most important PK parameters to describe exposure, were affected by BG. As a limitation, it was not possible to separately describe intestinal and hepatic metabolism of CsA and thus to assess interaction at these two sites separately; to this end, both oral and intravenous administration of CsA would have been required (Gazzaz et al., 2018).

Pharmacokinetic data of BG in humans are sparse. Published data include the pharmacokinetics of BG after oral administration of BG to healthy subjects in a bioequivalence study (Wu et al., 2005), and pharmacokinetics of BG and B after single and multiple oral doses of B administered to healthy volunteers (Li et al., 2014; Pang et al., 2016). The AUC of BG after oral administration of 750 mg BG ( $613 \text{ ng h ml}^{-1}$ ) (Wu et al., 2005) was similar to that after oral administration of only 100 mg B ( $580 \text{ ng h ml}^{-1}$ ) (Li et al., 2014), which would be compatible with poor bioavailability of BG; unfortunately, in the study with BG administration, B concentrations were not quantified. Furthermore, BG was absorbed very slowly,

with a  $T_{max}$  of 7.4 h (Wu et al., 2005), while B was absorbed much faster with a  $T_{max}$  of about 1 h for both BG and B (Li et al., 2014). These data suggest that both extent and temporal course of systemic concentrations of BG and probably its metabolite B in the present study were not sufficient to mediate an effect on CsA pharmacokinetics.

Although the current study would not suggest that dose adjustment might be warranted when BG and CsA are co-administered, because of the limited information on BG pharmacokinetics, a mechanistic extrapolation to other settings such as chronic BG dosing, higher BG doses, different timing of BG doses, or administration of B instead of BG would not be possible. Thus, in additional studies, BG and B plasma and/or blood concentrations should be quantified. Secondly, multiple dosages of BG should be used to treat the subjects before the administration of CsA to achieve maximal BG/B exposure as the single treatment of BG might not have been enough to modify CYP3A4 and/or P-gp. Furthermore, while in this study, the pharmacokinetic parameters of CsA were consistent with other healthy volunteer studies of CsA (Garg et al., 2011), clearance of CsA in healthy volunteers was two times higher than that of kidney or liver transplant patients (Bo et al., 2010), suggesting that DDI results from healthy volunteers might not be directly extrapolated to organ transplant patients. Thus, future investigations to evaluate the effect of chronic BG administration on CsA pharmacokinetics in patients would also be of interest. Finally, CYP3A5 genotype affects the clearance of CsA (Song et al., 2012). Thus, subjects with different CYP3A5 genotypes would be preferable to be recruited for subsequent studies.

Both the pharmacokinetic data and the limited safety data of the present study do not provide evidence that BG co-administration with CsA would cause an additional risk. The possibility of co-treatment with these drugs for transplant patients might be beneficial, because BG could exert antiviral, anti-inflammatory, anti-oxidation, and anti-proliferation effects (Lee et al., 2015; Ming et al., 2018). Indeed, in an observational study, it was reported that when BG was given with the antiviral drug telbivudine for the treatment of hepatitis in the clinic, the liver function (ALT) normalization rate, HBV DNA and hepatitis B virus markers (HBeAg) negative conversion rate, and anti-HBe serum conversion rate in the treatment group (BG and telbivudine,  $n = 64$ ) were significantly higher compared to the reference group (telbivudine alone,  $n = 62$ ) (Fang et al., 2011). Thus, these first results on a potential DDI between BG/B and CsA are encouraging and should be expanded by further studies as described above.

## CONCLUSION

In summary, this is the first clinical study to investigate the effect of BG on CsA pharmacokinetics in humans. The current dosage of BG (500 mg single dose) and CsA (200 mg single dose) was generally safe and well tolerated in the adult subjects without serious adverse events observed. Both non-compartmental analysis and the population pharmacokinetic approach did not

provide any evidence that the exposure to CsA and/or underlying pharmacokinetic processes of CsA were changed to a clinically relevant extent by BG. These results need to be confirmed in studies with maximal chronic exposure to BG and quantification of BG and B.

## ETHICS STATEMENT

This study was carried out in accordance with the standards of Good Clinical Practice, all applicable regulations, specific legal requirements, and ethical principles as described in the Declaration of Helsinki with written informed consent from all subjects. All subjects gave written informed consent in accordance with the Declaration of Helsinki. The protocol was approved by the Ethics Committee of at the first affiliated hospital of Zhengzhou University (Henan, China; approval no. SR201509).

## REFERENCES

- Akao, T., Kawabata, K., Yanagisawa, E., Ishihara, K., Mizuhara, Y., Wakui, Y., et al. (2010). Baicalin, the predominant flavone glucuronide of *Scutellariae radix*, is absorbed from the rat gastrointestinal tract as the aglycone and restored to its original form. *J. Pharm. Pharmacol.* 52, 1563–1568. doi: 10.1211/0022357001777621
- Albengres, E., and Tillement, J. P. (1992). Cyclosporin and ketoconazole, drug interaction or therapeutic association? *Int. J. Clin. Pharmacol. Ther. Toxicol.* 30, 555–570.
- Atiq, F., Broers, A. E., Andrews, L. M., Doorduyn, J. K., Koch, B. C., Van Gelder, T., et al. (2016). A clinically relevant pharmacokinetic interaction between cyclosporine and imatinib. *Eur. J. Clin. Pharmacol.* 72, 719–723. doi: 10.1007/s00228-016-2038-9
- Avramoff, A., Laor, A., Kitzes-Cohen, R., Farin, D., and Domb, A. J. (2007). Comparative in vivo bioequivalence and in vitro dissolution of two cyclosporin A soft gelatin capsule formulations. *Int. J. Clin. Pharmacol. Ther.* 45, 126–132. doi: 10.5414/CP45126
- Bardazzi, F., Odorici, G., Magnano, M., Patrizi, A., and Tengattini, V. (2018). Cyclosporine in clinical practice: a retrospective study comparing fixed dose and body weight-based dose regimens in psoriatic patients. *G. Ital. Dermatol. Venereol.* doi: 10.23736/S0392-0488.18.05651-1
- Bo, S., Xiao-Yu, L., Jun-Wei, G., Jian-Zhong, R., Yan-Kun, G., Zhi-Hai, P., et al. (2010). Population pharmacokinetic study of cyclosporine based on NONMEM in Chinese liver transplant recipients. *Ther. Drug Monit.* 32, 715–722. doi: 10.1097/FTD.0b013e3181fb6ce3
- Cai, Y., Li, S., Li, T., Zhou, R., Wai, T. S., and Yan, R. (2016). Oral pharmacokinetics of baicalin, wogonoside, oroxylin A 7-O- $\beta$ -D-glucuronide and their aglycones from an aqueous extract of *Scutellariae Radix* in the rat. *J. Chromatogr. B* 1026, 124–133. doi: 10.1016/j.jchromb.2015.11.049
- Cheng, Z. Y., Tian, X., Gao, J., Li, H. M., Jia, L. J., and Qiao, H. L. (2014). Contribution of baicalin on the plasma protein binding displacement and CYP3A activity inhibition to the pharmacokinetic changes of nifedipine in rats in vivo and in vitro. *PLoS One* 9:e87234. doi: 10.1371/journal.pone.0087234
- Colombo, D., and Ammirati, E. (2011). Cyclosporine in transplantation—a history of converging timelines. *J. Biol. Regul. Homeost. Agents* 25, 493–504. doi: 10.1186/1471-2172-12-56
- Dinda, B., Dinda, S., DasSharma, S., Banik, R., Chakraborty, A., and Dinda, M. (2017). Therapeutic potentials of baicalin and its aglycone, baicalein against inflammatory disorders. *Eur. J. Med. Chem.* 131, 68–80. doi: 10.1016/j.ejmech.2017.03.004
- Drewe, J., Beglinger, C., and Kissel, T. (1992). The absorption site of cyclosporin in the human gastrointestinal tract. *Br. J. Clin. Pharmacol.* 33, 39–43.

## AUTHOR CONTRIBUTIONS

XT and XZ designed and supervised the clinical trial. RL, JW, SL, YC, JiZ, and JiaZ carried out the clinical trial. RL, JW, and XL performed the non-compartmental analysis. XL conducted the population pharmacokinetic analysis. XL, RL, UF, and JW wrote the manuscript. UF, MT, and XT edited the manuscript.

## FUNDING

This work was financially supported by National Natural Science Foundation of China (No. U1504831 and 81603287), China Scholarship Council (No. 201406920024 XL), Scientific and Technological Project of Henan Province (No. 172102310145) and the Youth Innovation Fund of the First Affiliated Hospital of Zhengzhou University (No. YNQN2017202 and YNQN2017134).

- Ette, E. I. (1997). Stability and performance of a population pharmacokinetic model. *J. Clin. Pharmacol.* 37, 486–495. doi: 10.1002/j.1552-4604.1997.tb04326.x
- Fang, L. I., Mei, H. E., and Ru-Gui, L. I. (2011). Influence of baicalin and telbivudine on chronic hepatitis B cirrhosis and early serum indexes of liver fibrosis. *Med. J. West China* 23, 2112–2116. doi: 10.3969/j.issn.1672-3511.2011.11.016
- Garg, V., Heeswijk, R. V., Lee, J. E., Alves, K., Nadkarni, P., and Luo, X. (2011). Effect of telaprevir on the pharmacokinetics of cyclosporine and tacrolimus. *Hepatology* 54, 20–27. doi: 10.1002/hep.24443
- Gazzaz, M., Kinzig, M., Schaeffeler, E., Jübner, M., Hsin, C. H., Li, X., et al. (2018). Drinking ethanol has little acute effects on CYP2C9, CYP2C19, NAT2 and P-glycoprotein activities but somewhat inhibits CYP1A2, CYP2D6 and intestinal CYP3A – so what? *Clin. Pharmacol. Ther.* 104, 1249–1259. doi: 10.1002/cpt.1083
- Gong, W. Y., Zhao, Z. X., Liu, B. J., Lu, L. W., and Dong, J. C. (2017). Exploring the chemopreventive properties and perspectives of baicalin and its aglycone baicalein in solid tumors. *Eur. J. Med. Chem.* 126, 844–852. doi: 10.1016/j.ejmech.2016.11.058
- Hebert, M. F. (1997). Contributions of hepatic and intestinal metabolism and P-glycoprotein to cyclosporine and tacrolimus oral drug delivery. *Adv. Drug Deliv. Rev.* 27, 201–214. doi: 10.1016/S0169-409X(97)00043-4
- Huang, T., Liu, Y., and Zhang, C. (2019). Pharmacokinetics and bioavailability enhancement of baicalin: a review. *Eur. J. Drug Metab. Pharmacokinet.* 44, 159–168. doi: 10.1007/s13318-018-0509-3
- Kalapos-Kovács, B., Juhász, V., Temesszentandrás-Ambrus, C., Magda, B., Szabó, P. T., Antal, L., et al. (2018). Baicalin is a substrate of OATP2B1 and OATP1B3. *Phytother. Res.* 32, 1647–1650. doi: 10.1002/ptr.6095
- Kang, M. J., Ko, G. S., Oh, D. G., Kim, J. S., Noh, K., Kang, W., et al. (2014). Role of metabolism by intestinal microbiota in pharmacokinetics of oral baicalin. *Arch. Pharm. Res.* 37, 371–378. doi: 10.1007/s12272-013-0179-2
- Keogh, A., Spratt, P., McCosker, C., Macdonald, P., Mundy, J., and Kaan, A. (1995). Ketoconazole to reduce the need for cyclosporine after cardiac transplantation. *N. Engl. J. Med.* 333, 628–633. doi: 10.1056/NEJM199509073331004
- Lai, M. Y., Hsiu, S. L., Hou, Y. C., Tsai, S. Y., and Chao, P. D. (2004). Significant decrease of cyclosporine bioavailability in rats caused by a decoction of the roots of *Scutellaria baicalensis*. *Planta Med.* 70, 132–137. doi: 10.1055/s-2004-815489
- Lee, W., Ku, S. K., and Bae, J. S. (2015). Anti-inflammatory effects of baicalin, baicalein, and wogonin in vitro and in vivo. *Inflammation* 38, 110–125. doi: 10.1007/s10753-014-0013-0
- Li, Y., Ning, J., Wang, Y., Wang, C., Sun, C., Huo, X., et al. (2018). Drug interaction study of flavonoids toward CYP3A4 and their quantitative structure activity relationship (QSAR) analysis for predicting potential effects. *Toxicol. Lett.* 294, 27–36. doi: 10.1016/j.toxlet.2018.05.008

- Li, M., Shi, A., Pang, H., Xue, W., Li, Y., Cao, G., et al. (2014). Safety, tolerability, and pharmacokinetics of a single ascending dose of baicalein chewable tablets in healthy subjects. *J. Ethnopharmacol.* 156, 210–215. doi: 10.1016/j.jep.2014.08.031
- Lindbom, L., Pihlgren, P., Jonsson, E. N., and Jonsson, N. (2005). PsN-Toolkit - A collection of computer intensive statistical methods for non-linear mixed effect modeling using NONMEM. *Comput. Methods Prog. Biomed.* 79, 241–257. doi: 10.1016/j.cmpb.2005.04.005
- Lindbom, L., Ribbing, J., and Jonsson, E. N. (2004). Perl-speaks-NONMEM (PsN)—a Perl module for NONMEM related programming. *Comput. Methods Prog. Biomed.* 75, 85–94. doi: 10.1016/j.cmpb.2003.11.003
- Liu, W. Y., Xu, W. L., Li, P., Feng, F., and Li, D. (2009). Tissue distribution and excretion of baicalein and its main metabolite in rats by LC-MS/MS. *Chin. J. Pharm. Anal.* 40, 348–352.
- Miao, Q., Wang, Z., Zhang, Y., Miao, P., Zhao, Y., Zhang, Y., et al. (2016). In vitro potential modulation of baicalin and baicalein on P-glycoprotein activity and expression in Caco-2 cells and rat gut sacs. *Pharm. Biol.* 54, 1548–1556. doi: 10.3109/13880209.2015.1107744
- Ming, J., Li, Z., and Zhu, G. (2018). Protective role of flavonoid baicalin from *Scutellaria baicalensis* in periodontal disease pathogenesis: a literature review. *Complement. Ther. Med.* 38, 11–18. doi: 10.1016/j.ctim.2018.03.010
- Morisaki, T., Hou, X. L., Takahashi, K., and Takahashi, K. (2013). Baicalin pharmacokinetic profile of absorption process using novel in-vitro model: cytochrome P450 3A4-induced Caco-2 cell monolayers combined with rat intestinal rinse fluids. *J. Pharm. Pharmacol.* 65, 1526–1535. doi: 10.1111/jphp.12127
- Noh, K., Kang, Y., Nepal, M. R., Jeong, K. S., Oh, D. G., Kang, M. J., et al. (2016). Role of intestinal microbiota in baicalin-induced drug interaction and its pharmacokinetics. *Molecules* 21:337. doi: 10.3390/molecules21030337
- Onoue, S., Sato, H., Ogawa, K., Kawabata, Y., Mizumoto, T., Yuminoki, K., et al. (2010). Improved dissolution and pharmacokinetic behavior of cyclosporine A using high-energy amorphous solid dispersion approach. *Int. J. Pharm.* 399, 94–101. doi: 10.1016/j.ijpharm.2010.08.007
- Pang, H., Xue, W., Shi, A., Li, M., Li, Y., Cao, G., et al. (2016). Multiple-ascending-dose pharmacokinetics and safety evaluation of baicalein chewable tablets in healthy Chinese volunteers. *Clin. Drug Investig.* 36, 713–724. doi: 10.1007/s40261-016-0418-7
- Parke, J., Holford, N. H., and Charles, B. G. (1999). A procedure for generating bootstrap samples for the validation of nonlinear mixed-effects population models. *Comput. Methods Prog. Biomed.* 59, 19–29. doi: 10.1016/s0169-2607(98)00098-4
- Post, T. M., Freijer, J. I., Ploeger, B. A., and Danhof, M. (2008). Extensions to the visual predictive check to facilitate model performance evaluation. *J. Pharmacokinetic. Pharmacodyn.* 35, 185–202. doi: 10.1007/s10928-007-9081-1
- Ravva, P., Gastonguay, M. R., Tensfeldt, T. G., and Faessel, H. M. (2009). Population pharmacokinetic analysis of varenicline in adult smokers. *Br. J. Clin. Pharmacol.* 68, 669–681. doi: 10.1111/j.1365-2125.2009.03520.x
- Rogosheske, J. R., Fargen, A. D., DeFor, T. E., Warlick, E., Arora, M., Blazar, B. R., et al. (2014). Higher therapeutic CsA levels early post transplantation reduce risk of acute GVHD and improves survival. *Bone Marrow Transplant.* 49, 122–125. doi: 10.1038/bmt.2013.139
- Shi, H., Ren, K., Lv, B., Zhang, W., Zhao, Y., Tan, R. X., et al. (2016). Baicalin from *Scutellaria baicalensis* blocks respiratory syncytial virus (RSV) infection and reduces inflammatory cell infiltration and lung injury in mice. *Sci. Rep.* 6:35851. doi: 10.1038/srep35851
- Shieh, D. E., Liu, L. T., and Lin, C. C. (2000). Antioxidant and free radical scavenging effects of baicalein, baicalin and wogonin. *Anticancer Res.* 20, 2861–2865. doi: 10.1097/00001813-200009000-00012
- Song, J., Kim, M. G., Choi, B., Han, N. Y., Yun, H. Y., Yoon, J. H., et al. (2012). CYP3A5 polymorphism effect on cyclosporine pharmacokinetics in living donor renal transplant recipients: analysis by population pharmacokinetics. *Ann. Pharmacother.* 46, 1141–1151. doi: 10.1345/aph.1R004
- Tang, Y., Zhu, H., Zhang, Y., and Huang, C. (2006). Determination of human plasma protein binding of baicalin by ultrafiltration and high-performance liquid chromatography. *Biomed. Chromatogr.* 20, 1116–1119. doi: 10.1002/bmc.655
- Tian, X., Chang, Y., Wei, J., Liu, R., Wang, L., Zhang, J., et al. (2019). Baicalin reduces cyclosporin bioavailability by inducing intestinal p-glycoprotein in rats. *J. Pharm. Pharmacol.* 71, 788–796. doi: 10.1111/jphp.13067
- U.S. Food and Drug Administration (2015). *Novartis Label: Neoral soft gelatin capsules (cyclosporine capsules, USP) modified*. Available at: [https://www.accessdata.fda.gov/drugsatfda\\_docs/label/2019/050715s035,050716s038lbl.pdf](https://www.accessdata.fda.gov/drugsatfda_docs/label/2019/050715s035,050716s038lbl.pdf) (Accessed March 31, 2015).
- U.S. Food and Drug Administration (2018). *Guidance for Industry, bioanalytical method validation*. Available at: <http://www.fda.gov/downloads/Drugs/GuidanceComplianceRegulatoryInformation/Guidances/ucm070107.pdf> (Accessed May 24, 2018).
- Wu, H., Liu, Z., Peng, J., Li, L., Li, N., Li, J., et al. (2011). Design and evaluation of baicalin-containing in situ pH-triggered gelling system for sustained ophthalmic drug delivery. *Int. J. Pharm.* 410, 31–40. doi: 10.1016/j.ijpharm.2011.03.007
- Wu, H., Long, X., Yuan, F., Chen, L., Pan, S., Liu, Y., et al. (2014). Combined use of phospholipid complexes and self-emulsifying microemulsions for improving the oral absorption of a BCS class IV compound, baicalin. *Acta Pharm. Sin. B* 4, 217–226. doi: 10.1016/j.apsb.2014.03.002
- Wu, L., Zhang, Z. J., guo, X. F., Tian, Y., and Chen, Y. (2005). Bioequivalence study of baicalin capsules in healthy volunteers. *Chin. J. New Drugs Clin. Rem.* 24, 60074–60072. doi: 10.1016/S1872-2040(08)
- Xi, Y., Wu, M., Li, H., Dong, S., Luo, E., Gu, M., et al. (2015). Baicalin attenuates high fat diet-induced obesity and liver dysfunction: dose-response and potential role of CaMKKbeta/AMPK/ACC pathway. *Cell. Physiol. Biochem.* 35, 2349–2359. doi: 10.1159/000374037
- Xin, T., Zhen-Yu, C., Han, J., Jie, G., and Hai-Ling, Q. (2013). Inhibitory effects of baicalin on the expression and activity of CYP3A induce the pharmacokinetic changes of midazolam in rats. *Evid. Based Complement. Alternat. Med.* 2013:179643. doi: 10.1155/2013/179643
- Zhang, L., Li, C., Lin, G., Krajcsi, P., and Zuo, Z. (2011). Hepatic metabolism and disposition of baicalein via the coupling of conjugation enzymes and transporters—In vitro and In vivo evidences. *AAPS J.* 13, 378–389. doi: 10.1208/s12248-011-9277-6
- Zhao, W., Liu, L., Wang, Y., Mao, T., and Li, J. (2016). Effects of a combination of puerarin, baicalin and berberine on the expression of proliferator-activated receptor-gamma and insulin receptor in a rat model of nonalcoholic fatty liver disease. *Exp. Ther. Med.* 11, 183–190. doi: 10.3892/etm.2015.2846
- Zhu, M. L., Liang, X. L., Zhao, L. J., Liao, Z. G., Zhao, G. W., Cao, Y. C., et al. (2013). Elucidation of the transport mechanism of baicalin and the influence of a *Radix Angelicae Dahuricae* extract on the absorption of baicalin in a Caco-2 cell monolayer model. *J. Ethnopharmacol.* 150, 553–559. doi: 10.1016/j.jep.2013.09.011

**Conflict of Interest Statement:** The authors declare that the research was conducted in the absence of any commercial or financial relationships that could be construed as a potential conflict of interest.

Copyright © 2019 Liu, Li, Wei, Liu, Chang, Zhang, Zhang, Zhang, Fuhr, Taubert and Tian. This is an open-access article distributed under the terms of the Creative Commons Attribution License (CC BY). The use, distribution or reproduction in other forums is permitted, provided the original author(s) and the copyright owner(s) are credited and that the original publication in this journal is cited, in accordance with accepted academic practice. No use, distribution or reproduction is permitted which does not comply with these terms.

# Drinking Ethanol Has Few Acute Effects on CYP2C9, CYP2C19, NAT2, and P-Glycoprotein Activities but Somewhat Inhibits CYP1A2, CYP2D6, and Intestinal CYP3A: So What?

Malaz Gazzaz<sup>1,2</sup>, Martina Kinzig<sup>3</sup>, Elke Schaeffeler<sup>4,5</sup>, Martin Jübner<sup>6</sup>, Chih-hsuan Hsin<sup>1</sup>, Xia Li<sup>1</sup>, Max Taubert<sup>1</sup>, Christina Trueck<sup>1</sup>, Juliane Iltgen-Breburda<sup>7</sup>, Daria Kraus<sup>1,8</sup>, Christian Queckenberg<sup>1,8</sup>, Marc Stoffel<sup>1</sup>, Matthias Schwab<sup>4,9,10</sup>, Fritz Sörgel<sup>3,11</sup> and Uwe Fuhr<sup>1</sup>

We quantified the effect of acute ethanol exposure (initial blood concentrations 0.7 g/L) on major drug metabolizing enzymes and p-glycoprotein. Sixteen healthy Caucasians participated in a randomized crossover study with repeated administration of either vodka or water. Enzyme/transporter activity was assessed by a cocktail of probe substrates, including caffeine (CYP1A2/NAT2), tolbutamide (CYP2C9), omeprazole (CYP2C19), dextromethorphan (CYP2D6), midazolam (CYP3A), and digoxin (P-glycoprotein). The ratio of AUC<sub>0-t</sub> of dextromethorphan for ethanol/water coadministration was 1.95 (90% confidence interval (CI) 1.48–2.58). The effect was strongest in individuals with a CYP2D6 genotype predicting high activity ( $n = 7$ , ratio 2.66, 90% CI 1.65–4.27). Ethanol increased caffeine AUC<sub>0-t</sub> 1.38-fold (90% CI 1.25–1.52) and reduced intestinal midazolam extraction 0.77-fold (90% CI 0.69–0.86). The other probe drugs were not affected by ethanol. The results suggest that acute ethanol intake typically has no clinically important effect on the enzymes/transporters tested.

## Study Highlights

### WHAT IS THE CURRENT KNOWLEDGE ON THE TOPIC?

High ethanol concentrations have pronounced but equivocal effects on the activity of several cytochrome P450 enzymes *in vitro*. *In vivo* data on ethanol–drug interactions are sparse.

### WHAT QUESTION DID THIS STUDY ADDRESS?

The study aimed at quantifying the effect of high acute ethanol intake on the activity of CYP1A2, CYP2C9, CYP2C19, CYP2D6, CYP3A, NAT2, and P-glycoprotein in people.

### WHAT DOES THIS STUDY ADD TO OUR KNOWLEDGE?

Ethanol intake achieving concentrations of about 0.7 g/L had little or no effect on the pharmacokinetics of probe drugs

for the respective enzymes/transporters, with limited inhibition of CYP1A2, CYP2D6, and intestinal CYP3A. Any ethanol effects were smallish compared to interindividual pharmacokinetic variability.

### HOW MIGHT THIS CHANGE CLINICAL PHARMACOLOGY OR TRANSLATIONAL SCIENCE?

The results provide reassurance that ethanol intake typically does not cause clinically relevant pharmacokinetic interactions with drugs, depending on the enzymes/transporters tested. For extremely high ethanol intake, occasionally concentrations of sensitive drugs with pronounced first-pass metabolism by CYP1A2, CYP2D6, or CYP3A may increase to a relevant extent.

Beverages containing ethanol are easily available and socially accepted in many geographic areas. According to WHO estimates, worldwide almost 40% of the population aged 15 years or older consume alcoholic beverages,<sup>1</sup> suggesting a high probability of occasional consumption during drug therapy. This may cause various pharmacokinetic and/or pharmacodynamic interactions

between ethanol and medications.<sup>2,3</sup> One of the possible sources of alcohol–drug interactions seems to be an effect of ethanol on the activity of drug-metabolizing enzymes, including cytochrome P450 enzymes (CYPs), and/or on drug transporters. Mixed, albeit generally small, effects of acute ethanol exposure on the pharmacokinetics of benzodiazepines and amitriptyline in early

<sup>1</sup>Department I of Pharmacology, University Hospital Cologne, Germany; <sup>2</sup>Department of Clinical Pharmacy, College of Pharmacy, Umm Al-Qura University, Makkah, Saudi Arabia; <sup>3</sup>Institute for Biomedical and Pharmaceutical Research, Nürnberg-Heroldsberg, Germany; <sup>4</sup>Dr. Margarete-Fischer-Bosch Institute of Clinical Pharmacology, Stuttgart, Germany; <sup>5</sup>University of Tuebingen, Tuebingen, Germany; <sup>6</sup>Institute of Legal Medicine, Faculty of Medicine, University of Cologne, Germany; <sup>7</sup>Pharmacy, University Hospital Cologne, Germany; <sup>8</sup>Clinical Trials Centre, University Hospital Cologne, Germany; <sup>9</sup>Department of Clinical Pharmacology, University Hospital Tuebingen, Germany; <sup>10</sup>Department of Pharmacy and Biochemistry, University of Tuebingen, Tuebingen, Germany; <sup>11</sup>Institute of Pharmacology, Faculty of Medicine, University Duisburg-Essen, Essen, Germany. Correspondence: Uwe Fuhr (uwe.fuhr@uk-koeln.de)



**Table 1** Distribution of genotypes for enzymes and transporters

Enzyme/transporter	Functional genotype groups according to predicted activity (where available) and genotypes (absolute frequency)			
CYP1A2	(i) normal/normal (16) *1A/*1A (1), *1A/*1F (8), *1F/*1F (7)			
CYP2C9	(i) normal/normal or normal/reduced (12) *1/*1 (8), *1/*2 (3), *1/*12 (1)		(ii) normal/very low or reduced/reduced (4) *1/*3 (3), *2/*2 (1)	
CYP2C19	(i) Increased/increased or normal/increased (3) “ultrarapid metabolizer” *17/*17 (2), *17/*1 (1)	(ii) normal/normal (7), “extensive metabolizer” *1/*1 (7)	(iii) normal/none (6), “intermediate metabolizer” *1/*2A (4), *1/*2B (2)	
CYP2D6	(i) normal/normal or normal/reduced (7) *1/*1 (2), *1/*2 (2), *2/*2 (2), *1/*10 (1)	(ii) normal/very low or normal/none (6) *1/*41 (2), *1/*3 (1), *1/*4 (2), *2/*4 (1)	(iii) very low/none or none/none (3) *41/*4 (2), *4/*4 (1)	
CYP3A4	(i) normal/normal (16) *1/*1 (16)			
CYP3A5	(i) normal/none (3), “intermediate metabolizer” *1A/*3C (3)		(ii) none/none (13), “poor metabolizer” *3C/*3C (13)	
NAT2	(i) rapid/rapid (1) *4/*4 (1)	(ii) rapid/slow (10) *4/*5 (6), *4/*6 (4)	(iii) rapid/slow or slow/slow (2) *4/*5E or *5/*6 (2)	(iv) slow/slow (3) *5/*5 (1), *6/*6 (2)
P-gp	(i) 1236C/1236C, 2677G/2677G, 3435C/3435C (3)	(ii) 1236C/1236C, 2677G/2677G, 3435C/3435T (2)	(iii) 1236C/1236T, 2677G/2677T, 3435C/3435T (8)	(iv) 1236T/1236T, 2677T/2677T, 3435T/3435T (3)

For nomenclature, see <http://www.cypalleles.ki.se/>; [http://nat.mbg.duth.gr/Human%20NAT2%20alleles\\_2013.htm](http://nat.mbg.duth.gr/Human%20NAT2%20alleles_2013.htm); <https://www.ncbi.nlm.nih.gov/pubmed/20216335>.

clinical studies were later attributed to respective changes of CYP activities.<sup>4–6</sup> Specific research on the effect of chronic and acute consumption of ethanol on human CYP activity *in vivo* was mainly carried out for CYP2E1. In a clinical study, a dramatic decrease in CYP2E1 activity by (mean) 93.2% (95% confidence interval (CI) 89.7–96.7) was reported in seven volunteers after acute ethanol consumption.<sup>7</sup> In contrast, chronic ethanol consumption significantly induced CYP2E1 activity about 2-fold,<sup>8,9</sup> probably related to a decelerated CYP2E1 degradation.<sup>10</sup>

*In vitro* studies on the effect of ethanol on CYPs were mainly conducted to identify appropriate solvents for substrates and inhibitors for these experiments and gave conflicting results. In a systematic study, adding ethanol to the incubation medium inhibited activities of some cDNA-expressed human CYPs in a concentration-dependent way (inhibition at 1% ethanol: CYP1A1 by 69%, CYP2B6 by 80%, CYP2C19 by 72%, and CYP2D6 by 59%), while effects on CYP1A2, CYP2A6, CYP2C8, CYP2C9, and CYP3A4 were minor.<sup>11</sup> The inhibitory effect of 1% ethanol on CYP2C9, however, was about 80% in another study, where again no relevant effect on CYP3A4 was seen.<sup>12</sup> Surprisingly, in enzyme kinetic analyses, 1% ethanol increased CYP1A2 and CYP3A4 intrinsic clearance about 2-fold.<sup>13</sup> These data suggest that ethanol may change drug metabolism *in vitro* by several mechanisms, including enzyme inhibition, enzyme degradation, and a direct effect on the chemical interaction of individual enzyme–substrate pairs.<sup>13</sup>

Given the potential relevance of ethanol-related drug interactions, the complexity of *in vitro* interactions, and the paucity of information, the main objective of the present investigation was to systematically assess the effect of acute ethanol consumption

on the activity of the major cytochrome P450 enzymes, on *N*-acetyltransferase type 2 (NAT2) and on P-glycoprotein (P-gp). To this end, a cocktail phenotyping study was conducted in healthy volunteers, using selective substrates to quantify activities of the respective enzymes/transporters in the presence or absence of ethanol.

## RESULTS

Eight women and eight men took part in the study. All individuals judged as eligible for participation in the clinical study were included and completed the study. Mean age ( $\pm$ standard deviation (SD)) was  $33.8 \pm 10.3$  years, body height was  $1.75 \pm 0.11$  M, and body weight was  $73.4 \pm 17.1$  kg (body mass index (BMI)  $23.8 \pm 3.34$  kg/m<sup>2</sup>).

## Tolerability

Ethanol administration was related to the typical adverse effects, which included dizziness in eight volunteers, nausea in four, and headache in three. Because of nausea, one of the subjects had to stop ethanol intake after the second dose. Overall, volunteers described ethanol effects as increasingly unpleasant during the respective period, indicating that higher doses would not have been tolerated. Cocktail drugs were generally well tolerated, except for tiredness and sleepiness immediately after injecting midazolam.

## Enzyme and transporter genotypes

Genotyping results and functional genotype groups are summarized in **Table 1**. No activity (“null”) or very low activity alleles were present for CYP2C19 (10 extensive metabolizers (EMs), six

**Table 2 Ethanol population pharmacokinetics parameters**

Parameter	Model, mean (95% CI) <sup>a</sup>	Bootstrap, medians (95% CI) <sup>b</sup>
$V_{max}$ (g/h)	6.99 (6.58–7.40)	6.98 (6.49–7.57)
Effect of SEX on $K_a$	0.402 (0.27–0.54)	0.40 (0.26–0.54)
$K_m$ (g/l)	0.0821 FIX <sup>5</sup>	0.0821
$V$ (l)	31.6 (29.7–33.5)	31.8 (29.7–34.1)
Effect of WEIGHT on $V$	1.35 (1.09–1.61)	1.34 (1.05–1.66)
$K_a$ (h <sup>-1</sup> )	1.40 (1.18–1.62)	1.40 (1.22–1.65)
$M$ (factor)	1860 (1787–1932)	1856 (1776–1948)
$IIV V_{max}$ (CV%)	10.1% (7.32%–12.9%)	9.41% (5.83%–12.19%)
$IIV K_a$ (CV%)	18.6% (11.7%–25.5%)	17.7% (8.80%–24.8%)
Additive error (CV%)	8.00 (6.37–9.63)	7.86 (6.29–9.58)

$V_{max}$ , maximum reaction velocity;  $K_m$ , the substrate concentration at which the reaction rate is half of  $V_{max}$ ;  $V$ , volume of distribution;  $K_a$ , first-order absorption rate constant;  $M$ , ratio of blood ethanol concentration and breath ethanol concentration;  $IIV$ , interindividual variability.

<sup>a</sup>Confidence interval based on standard errors obtained by NONMEM (assuming normal distribution in the log domain of respective parameter, computed as  $\theta \pm z_{1-\alpha/2} \times SE$  where  $SE$  is the standard error provided by NONMEM and  $z_{1-\alpha/2}$  is the 0.975 percentile of the standard normal distribution). <sup>b</sup>Nonparametric confidence interval based on 2.5% and 97.5% percentiles obtained by the bootstrap analysis (1000 replicates). CV% for  $IIV$ , computed as  $\sqrt{\exp(\omega^2)} - 1$ .

intermediate metabolizers (IMs)), CYP2D6 (predicted overall activity was high in seven, moderate in six, and very low/absent in three individuals), and CYP3A5 (3 IMs, 13 poor metabolizers (PMs)).

### Ethanol exposure

Ethanol pharmacokinetics was best described by an empirical simple one-compartment model with saturable elimination, with body weight having a significant (exponential) relationship to the volume of distribution, and male sex being related to reduced (4%) maximal ethanol elimination capacity (for details of model development, see **Supplementary Document**). The respective pharmacokinetic parameters obtained for the model are presented in **Table 2**. Typical ethanol exposure in the study was simulated based on this model (**Figure 1**). A mean concentration of about 0.7 g/L blood was maintained until 4 hours after oral cocktail administration; thereafter, concentrations fluctuated at lower levels and often dropped to the lower limit of quantification between maintenance ethanol administrations.

### Midazolam model to assess CYP3A activity

To separately assess the contribution of both intestinal and hepatic CYP3A expression sites to midazolam metabolism, a published semiphysiological compartmental model<sup>14</sup> was developed further (for a scheme of the actual model, see **Figure 2**), taking concentrations of midazolam and 1'-hydroxymidazolam into account. The second metabolite, 4-hydroxymidazolam, was not incorporated into the model to limit complexity. A detailed description of model development and validation is given in the **Supplementary Document**. The estimates of population pharmacokinetic parameters obtained from the model are shown in **Table 3**.

### Pharmacokinetic parameters of probe drugs and their variability

The results for main pharmacokinetic parameters of the probe drugs are shown in **Table 4** and in **Table S3** of the **Supplementary**

**Document** (for a detailed list of primary and additional pharmacokinetic parameters according to the study protocol, see Section 1 of the **Supplementary Document**). Intersubject variability in plasma concentration vs. time profiles (**Figure 3**) and in derived pharmacokinetic parameters was considerable, as reflected by coefficients of variation exceeding 1,000% for CYP2D6-dependent dextromethorphan and ranging from about 20–100% for other substances (**Table 4**). As expected, enzyme/transporter activity in part depended on functional genotype groups (**Figure 3**) (see also **Table S4, Supplementary Document**); the genotype effect was most pronounced for CYP2D6 variant groups. Intrasubject variability was as expected

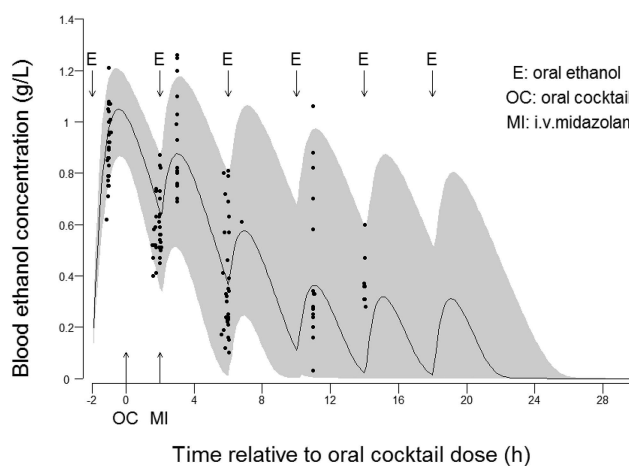


**Figure 1** Ethanol blood concentration reached in the study. Ethanol was administered as a loading dose and subsequent maintenance doses (“E,” see section “Study design, ethanol, and drug administration”). Black dots indicate observed blood ethanol concentrations (or breath ethanol concentrations transformed to blood ethanol concentrations) in the study (values below the lower limit of quantification are not shown). The line and the shaded area represent a simulation of mean value and the 95% confidence interval, respectively, based on the final population pharmacokinetic model.

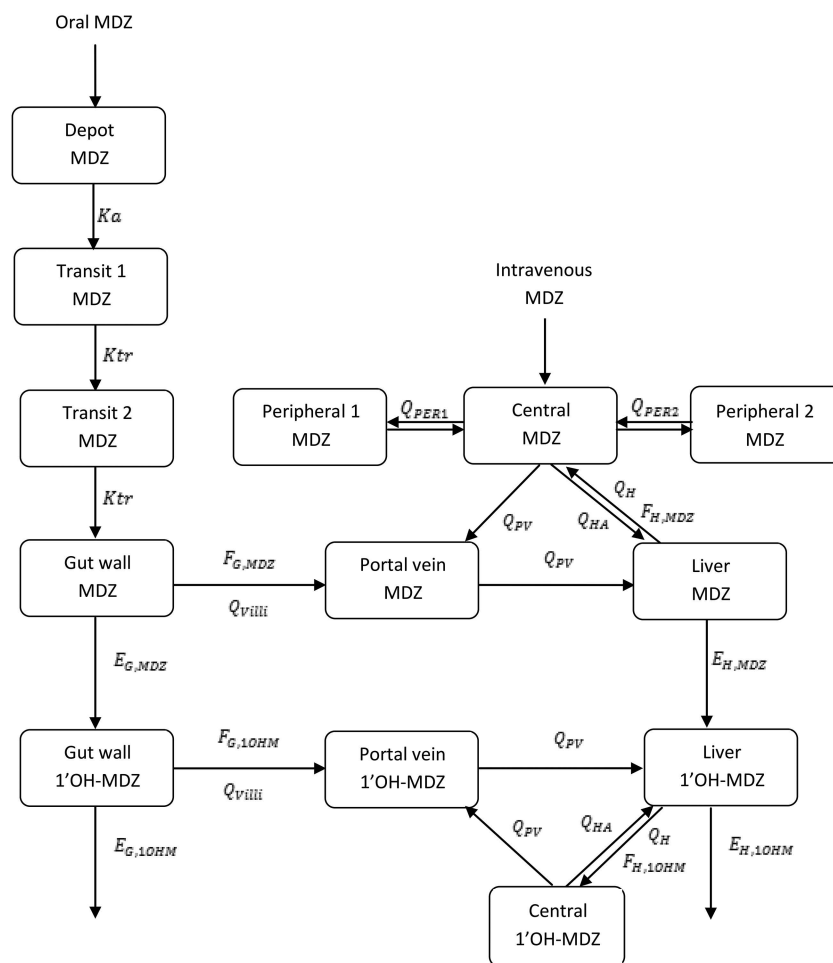


**Figure 2** Scheme of semiphysiological population pharmacokinetic model of midazolam (top) and 1'-OH-midazolam (bottom). MDZ, midazolam; 1'-OH-MDZ or 1OHM 1-OH-midazolam;  $K_a$ , absorption rate constant of MDZ;  $K_{tr}$  transit rate constant (equal to  $K_a$ );  $Q_{viii}$ , villous blood flow in gut;  $Q_H$ , blood flow in liver;  $Q_{HA}$ , blood flow in hepatic artery;  $Q_{PV}$ , blood flow in portal vein;  $Q_{PER1}$ , rate constant from central to peripheral compartment 1;  $Q_{PER2}$ , rate constant from central to peripheral compartment 2;  $E_{H,MDZ}$ , hepatic extraction of MDZ;  $F_{H,MDZ}$ , hepatic availability of MDZ;  $E_{H,1OHM}$ , hepatic extraction of 1'-OH-MDZ;  $F_{H,1OHM}$ , hepatic availability of 1'-OH-MDZ;  $E_{G,MDZ}$ , intestinal extraction of MDZ;  $F_{G,MDZ}$ , intestinal availability of MDZ;  $E_{G,1OHM}$ , intestinal extraction of 1'-OH-MDZ;  $F_{G,1OHM}$ , intestinal availability of 1'-OH-MDZ.

(<25%) in most cases but exceeded this threshold for dextromethorphan-derived pharmacokinetic parameters and for renal secretion of digoxin (Table 4), but this did not preclude achieving the respective objectives of the trial.

#### Ethanol effects on enzyme and transporter activity

The largest effect of ethanol was seen on the pharmacokinetics of dextromethorphan, where exposure to the parent substance in the entire group of participants was almost doubled ( $AUC_{0-t}$  ratio ethanol/water 1.95, 90% CI 1.48–2.58), clearly indicating an inhibitory effect on CYP2D6 (Tables 4, S3). The effect was most pronounced for CYP2D6 EMs ( $n = 7$ , ratio 2.66, 90% CI 1.65–4.27), smaller in IMs ( $n = 6$ , 1.81, 90% CI 1.20–2.75), and essentially absent for individuals predicted to have low or lacking CYP2D6 activity ( $n = 3$ , 1.17, 90% CI 0.83–1.65). With this exception, the level of ethanol exposure achieved in the present study had little or no effects on the pharmacokinetics of the other probe drugs (Table 4, and Supplementary Document). Some reduction was seen for intestinal extraction of midazolam

(ratio ethanol/water 0.77 (90% CI 0.69–0.86)), demonstrating a weak inhibitory effect on intestinal CYP3A activity. Furthermore, ethanol increased caffeine exposure with an  $AUC_{0-t}$  ratio ethanol/water of 1.38 (90% CI 1.25–1.52), indicating an unequivocal but limited inhibitory effect on CYP1A2 activity. Although the null hypotheses “relevant interaction present” could not be formally rejected in all other cases, any potential further changes in respective enzyme/transporter activity were considered to be clearly negligible (Tables 4, S3, Figure 3).

#### DISCUSSION

We found that acute ethanol intake achieving concentrations of about 0.7 g/L maintained for several hours has no (CYP2C9, CYP2C19, hepatic CYP3A, intestinal P-gp, and renal P-gp) or minor (CYP1A2, intestinal CYP3A) effect on pharmacokinetic parameters of probe drugs reflecting the activity of the respective enzymes/transporters. In contrast, exposure to the CYP2D6 substrate dextromethorphan was doubled, which, however, should not be overestimated (see below). Any ethanol effects were

**Table 3 Population pharmacokinetic parameters of the final midazolam model**

Parameter (unit)	Definition of parameter	NONMEM <sup>a</sup>		Bootstrap	
		Estimate	90% CI <sup>b</sup>	Median	90% CI <sup>c</sup>
<b><math>\theta</math> – Estimates</b>					
$CL_{int,H}(l/h)$	Unbound intrinsic hepatic clearance of MDZ	2310	(1968 – 2652)	2282	(1976–2612)
$CL_{int,G}(l/h)$	Unbound intrinsic intestinal clearance of MDZ	8.37	(6.86 – 9.88)	8.5	(6.9–10.2)
$Q_{PER1}(l/h)$	Distributional clearance to peripheral compartment 1 of MDZ	249	(229 – 268)	249	(233 –280)
$Q_{PER2}(l/h)$	Distributional clearance to peripheral compartment 2 of MDZ	19.4	(18.4 – 20.4)	19.3	(17.9–20.9)
$V_{MDZ}(l)$	Volume of distribution in central compartment of MDZ	12.9	(9.7 – 16.1)	12.8	(9.9 – 16.3)
$V_{PER1}(l)$	Volume of distribution in peripheral compartment 1 of MDZ	41.6	(39.5 – 43.7)	41.6	(39.2– 43.9)
$V_{PER2}(l)$	Volume of distribution in peripheral compartment 2 of MDZ	86.5	(79.4 – 93.6)	86.8	(80.1–93.1)
$CL_{int,H,1OHM}(l/h)$	Unbound intrinsic hepatic clearance of 1'-OH-MDZ	189	(164 – 214)	187	(162–215)
$CL_{int,GW,1OHM}(l/h)$	Unbound intrinsic intestinal clearance of 1'-OH-MDZ	20.5	(14.4 –26.6)	20.3	(14.8–27.6)
$V_{1OHM}(l)$	Volume of distribution in central compartment of 1'-OH-MDZ	51.0	(44.3 – 57.7)	51.3	(46.6–59.2)
$Ka(h^{-1})$	First-order absorption /transit rate constant of MDZ	6.38	(5.33 – 7.43)	6.35	(5.42–7.43)
$CL_{PERM}(l)$	Permeability of MDZ	10.6	(FIXED) <sup>11</sup>	10.6	
$Ethanol_{Ka}$	Effect of alcohol on absorption rate constant of MDZ	–0.286	(–0.347 – –0.225)	–0.272	(–0.344 – –0.165)
$Ethanol_{CL_{int,c}}$	Effect of alcohol on intrinsic intestinal clearance of MDZ	–0.278	(–0.374 – –0.182)	–0.277	(–0.390 – –0.145)
<b><math>\omega^2</math> – Estimates</b>					
$IIV CL_{int,H}(CV\%)$	Interindividual variability on hepatic clearance of MDZ	32.8	(17.7 – 47.9)	31.5	(14.4–45.8)
$IIV CL_{int,G}(CV\%)$	Interindividual variability on intestinal clearance of MDZ	52.3	(37.7 – 66.9)	50.9	(31.5–67.6)
$IIV V_{MDZ}(CV\%)$	Interindividual variability on central volume of MDZ	58.9	(43.4 – 74.4)	55.9	(35.0–75.9)
$IIV V_{PER2}(CV\%)$	Interindividual variability on peripheral volume 2 of MDZ	16.2	(4.70 – 27.7)	16.0	(5.0–26.9)
$IIV CL_{int,H,1OHM}(CV\%)$	Interindividual variability on hepatic clearance of 1'-OH-MDZ	30.7	(20.6 – 40.8)	29.3	(17.1–39.0)
$IIV V_{1OHM}(CV\%)$	Interindividual variability on central volume of 1'-OH-MDZ	19.8	(8.7 – 30.9)	19.7	(4.3–28.4)
$IIV Ka(CV\%)$	Interindividual variability on absorption rate of MDZ	39.1	(28.8 – 49.4)	36.5	(25.6–47.0)
$IOV Ka(CV\%)$	Interoccasional variability on absorption rate of MDZ	21.7	(14.2 – 29.2)	20.7	(12.6–29.9)

Table 3 Continued on next page

Table 3 Continued

Parameter (unit)	Definition of parameter	NONMEM <sup>a</sup>		Bootstrap	
		Estimate	90% CI <sup>b</sup>	Median	90% CI <sup>c</sup>
IOV CL <sub>Int,H</sub> (CV%)	Interoccasional variability on hepatic clearance of MDZ	19.0	(13.4–24.6)	18.1	(12.9–23.8)
IOV CL <sub>Int,G</sub> (CV%)	Interoccasional variability on intestinal clearance of MDZ	31.6	(17.6–45.6)	29.5	(19.9–47.2)
IOV CL <sub>Int,H,10HM</sub> (CV%)	Interoccasional variability on hepatic clearance of 1'-OH-MDZ	22.1	(15.9–28.3)	22.0	(15.4–27.6)
$\sigma^2$ – Estimates					
RV MDZ(CV%)	Proportional residual variability of MDZ	15.7	(14.3–17.1)	15.8	(14.3–17.5)
RV MDZ(CV%)	Additive residual variability of MDZ	29.9	(19.4–40.4)	28.9	(10.7–39.9)
RV1OHM(CV%)	Proportional variability of 1'-OH-MDZ	19.5	(17.0–22.0)	19.4	(17.1–21.9)
RV1OHM(CV%)	Additive variability of 1'-OH-MDZ	12.7	(8.64–16.8)	12.6	(8.96–17.8)

<sup>a</sup>Values estimated by the final model applied to the original dataset. <sup>b</sup>Confidence interval based on standard errors obtained by NONMEM (assuming normal distribution in log domain of respective parameter, computed as  $\theta \pm z_{1-\alpha/2} \times SE$  where SE is the standard error provided by NONMEM and  $z_{1-\alpha/2}$  is the 0.95 percentile of the standard normal distribution). <sup>c</sup>Confidence interval (nonparametric) based on 5% and 95% percentiles obtained by the bootstrap analysis. CV% for IIV and IOV computed as  $\sqrt{\exp(\omega^2)-1}$ ; CV% for RV computed as  $\sqrt{\sigma^2}$ ; MDZ midazolam; 1'-OH-MDZ or 10HM 1'-OH-midazolam.

smallish compared to interindividual pharmacokinetic variability from unknown sources or—mainly for CYP2D6—from known genetic polymorphisms.

As a side note, it is interesting to emphasize that the two individuals with a CYP2D6\*4/CYP2D6\*41 genotype clearly had a poor metabolizer phenotype (Figure 3), indicating the CYP2D6 activity related to the \*41 allele is very low. This is in accordance with our previous results<sup>15</sup> but questions the allocation of a value of 0.5 of the CYP2D6 activity score to this allele.<sup>16</sup>

The selection of phenotyping agents as well as simultaneous assessment of enzyme and transporter activity by a cocktail approach is generally accepted from both a scientific and a regulatory perspective, despite some limitations for some of them.<sup>17–20</sup> Although not all individual doses and all combinations of the drugs used in the present cocktail have been directly validated *in vivo*, there is extensive evidence that doses, metrics used to assess enzyme or transporter activities, and the combination in a cocktail were essentially suitable (for a detailed discussion, see Section 8.2 of Supplementary Document). For the period with coadministration of water, the pharmacokinetics were similar to published values for all probe drugs.<sup>21–28</sup>

Ethanol pharmacokinetics is in accordance with published data,<sup>29</sup> while ethanol exposure did not fully reach the intended level, partially reflecting the safety margin used. We used a staggered administration of ethanol and the probe drugs to avoid immediate effects of ethanol that would not be mediated by changes in enzyme or transporter activity, e.g., regarding drug solubility, local perfusion, or gastrointestinal motility. Furthermore, the maximum ethanol dose that can be given to healthy volunteers may be exceeded by far for recreational or addictive use. Thus, maximum ethanol effects, in particular when taking drugs

directly with ethanol-containing beverages, may be larger than those observed here.

Still, it is generally reassuring that major pharmacokinetic players are not subject to meaningful effects of ethanol at the achieved level of ethanol exposure. In order to assess the possible clinical consequences of the limited effects observed, characteristics of individual probe drugs need to be considered. In particular, both probe drugs and therapeutic drugs with extensive first-pass metabolism are more prone to be drug–drug interaction victims (“sensitive probe substrates”<sup>17</sup>), because small relative changes in the respective extraction ratio (ER) cause much larger relative changes in the bioavailable fraction (F) of the drug, as  $F = 1 - ER$  (assuming complete absorption).

Indeed, dextromethorphan undergoes an exceptionally pronounced first-pass metabolism by CYP2D6, with an estimated oral bioavailability of 1–2% for EMs (but 80% for PMs).<sup>30</sup> Our observation that inhibitory effects of ethanol on dextromethorphan metabolism depend on CYP2D6 genotype and related CYP2D6 expression thus supports the specificity of the effect. In general, inhibition of CYP2D6 may be relevant, because about a quarter of marketed drugs are metabolized by CYP2D6.<sup>31</sup> The magnitude of the ethanol effect on other drugs depending on CYP2D6 metabolism will, however, be clearly less than 2-fold and in most cases without clinical relevance, as illustrated by the following comparison: Another recommended CYP2D6 probe drug is desipramine,<sup>17</sup> which had a higher average absolute bioavailability in individuals with unspecified CYP2D6 genotype (i.e., >90% IMs and EMs) of about 40%.<sup>32</sup> In CYP2D6 EMs, multiple 90-mg doses of cinacalcet, a potent CYP2D6 inhibitor, increased desipramine AUC about 3.6-fold,<sup>33</sup> while multiple 50-mg doses increased dextromethorphan AUC 11-fold.<sup>34</sup>



**Table 4** Probe drugs, metrics used for quantification of enzyme or transporter activity, and main results

Probe drug	Enzyme/ transporter	Metrics	Ethanol (E) period: geometric mean (CV)	Water (W) period: geometric mean (CV)	E/W ratio (%): point estimate, (90% CI)	Intrasubject CV
Caffeine 150 mg, tablets	CYP1A2	Caffeine AUC <sub>0–24h</sub> (h * μM)	218 (48.9%)	158 (59.0%)	138% (125–152%)	15.7
	NAT2	Urinary molar ratio (AFMU + AAMU)/ (AFMU + AAMU + 1X + 1U) 6–10 hours postdose (MR <sub>NAT2</sub> )	28.5 (62.2%)	29.9 (55.0%)	95.3% (90.5–100%)	8.3
Tolbutamide 125 mg, tablet	CYP2C9	Tolbutamide AUC <sub>0–24h</sub> (h * μM)	495 (22.0%)	520 (24.3%)	95.2% (92.0–98.6%)	5.6
Omeprazole 20 mg, enteric coated tablet	CYP2C19	Molar omeprazole AUC <sub>0–24h</sub> / 5-OH- omeprazole AUC <sub>0–24h</sub> ratio (MR <sub>CYP2C19</sub> )	1.61 (58.5%)	1.65 (69.6%)	97.4% (88.1–108%)	16.3
		omeprazole AUC <sub>0–24h</sub> (h * nM)	1.83 (90.4%)	1.65 (109%)	111% (99.2–124%)	17.9
Dextromethorphan- HBr 30 mg, capsules	CYP2D6	Molar dextromethorphan AUC <sub>0–24h</sub> / dextrophan AUC <sub>0–24h</sub> ratio (MR <sub>CYP2D6</sub> )	0.362 (684%)	0.250 (1329%)	145% (90.3–233%)	89.0
		dextromethorphan AUC <sub>0–24h</sub> (h * nM)	31.3 (384%)	16.0 (869%)	195% (148–258%)	46.7
Midazolam 2 mg, oral solution + midazolam 1 mg, i.v. solution 2 hours later	Hepatic CYP3A	hepatic clearance of midazolam(L/h)	40.2 (20.9%)	38.3 (19.3%)	105% (98.9–111%)	9.66
	Intestinal CYP3A	intestinal extraction of midazolam(fraction)	0.428 (30.0%)	0.555 (20.9%)	77.2% (69.1–86.2%)	18.0
Digoxin 0.5 mg, tablets	Intestinal P-gp Renal P-gp	C <sub>max</sub> of digoxin (nM)	3.22 (32.5%)	3.06 (31.5%)	105% (90.6–122%)	24.3
		digoxin clearance by renal secretion (L/h) (arithmetic mean and CV)	3.22 (72.9%)	2.87 (72.4%)	112% (87.3–137%)	40.0

CV, coefficient of variation; AUC<sub>0–24h</sub>, area under the concentration vs. time curve up to 24 hours; AFMU, 5-acetylamino-6-formylamino-3-methyluracil; AAMU, 5-acetylamino-6-amino-3-methyluracil; 1X, 1-methylxanthine; 1U, 1-methyluric acid; MR, metabolic ratio; C<sub>max</sub>, maximal concentration after dosing; shaded values indicate that 90% CI of the E/W ratios crossed the predefined “no relevant interaction” borders of 0.70–1.43-fold.

In contrast, the effects of ethanol on the exposure of CYP1A2-dependent drugs may be larger than the observed 1.38-fold AUC increase of caffeine. Oral bioavailability of caffeine is 100%, while that of tizanidine, another recommended CYP1A2 probe drug,<sup>35</sup> is reduced by first-pass metabolism to 20–40%.<sup>36</sup> Ciprofloxacin (500 mg b.i.d.), a moderate CYP1A2 inhibitor, increased caffeine exposure 2.1-fold, but tizanidine exposure 9.8-fold.<sup>36</sup>

These two examples reflect a dilemma of the current probe drug approach in drug interaction assessment. Even if an accepted probe drug is used,<sup>35</sup> which was selected exclusively based on its ability to reflect the activity of the respective enzyme or transporter,<sup>37</sup> its metrics may not have a simple linear relationship to this activity. Thus, reliable quantitative prediction of changes in the pharmacokinetics of therapeutic drugs depending on the same enzyme/transporter would not only require detailed knowledge on the pharmacokinetic properties of the probe drug and the therapeutic drugs, but rather a quantitative description of all their relevant pharmacokinetic processes. Generating physiologically based pharmacokinetic

(PBPK) models of all involved drugs would be the method of choice to this end,<sup>38</sup> but the general use of this laborious method is still limited by capacity problems.

In conclusion, acute effects of moderate ethanol exposure on the activity of major players in the pharmacokinetics of many drugs appear to be negligible. This information is relevant in drug therapy, but also in court cases on driving under the influence or on work-related accidents. Still, in particular the combination of high ethanol exposure with sensitive drugs (i.e., those with extensive first-pass metabolism by CYP2D6, CYP1A2, or CYP3A) may occasionally cause a relevant increase in drug exposure.

## METHODS

The study was approved by the Ethics Committee of the Faculty of Medicine, University of Cologne, Germany, and conducted in accordance with applicable regulations and the ethical principles described in the Declaration of Helsinki. It is registered at clinicaltrials.gov with the ID NCT02515526.

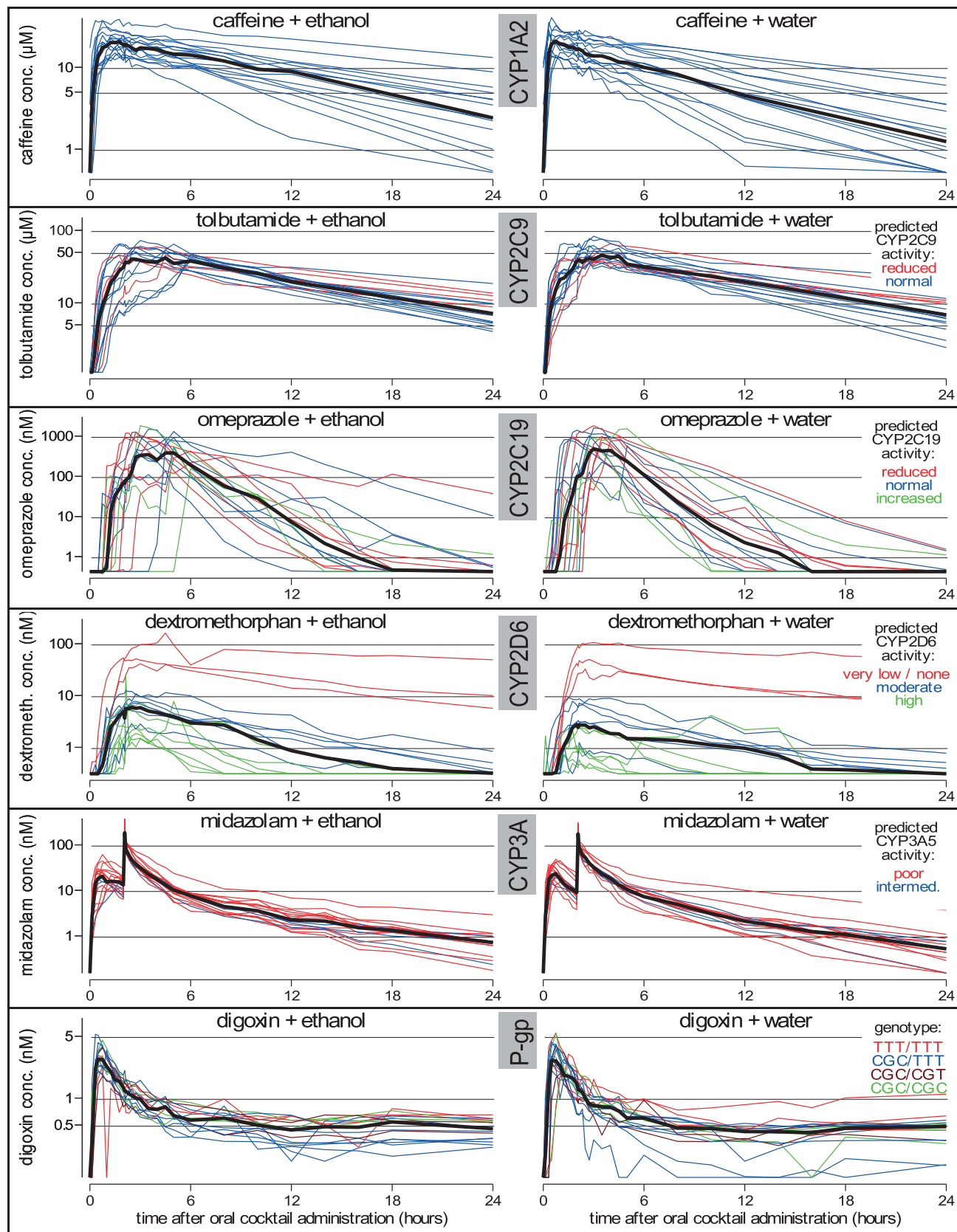


**Figure 3** Log concentration vs. time profiles of probe drugs for genotypes grouped according to predicted activity where applicable. Black line: overall median; colored lines reflect individual volunteers. For groups, see **Table 4**. For the purpose of the graphical display only, concentrations below the lower limit of quantification (LLOQ, equal to lower end of the respective y-axes) were set to LLOQ.

## Study population

Sixteen healthy volunteers were recruited and gave written informed consent for participation in the study. The volunteers were considered healthy on the basis of medical history, physical examination, vital signs, electrocardiogram, and clinical laboratory tests. Requirements of the volunteers were: Caucasian, nonsmokers, aged between 18 and 55 years, having a BMI between 18.5 and 30 kg/m<sup>2</sup>, and for females not being pregnant. Main exclusion criteria were: taking any medication within 1 week prior to the study or receiving chronic treatment (more than 3 days) within the previous 8 weeks; regularly consuming more than 30 g of alcohol daily; or not abstaining from alcohol (other than that given during the study), from methylxanthine-containing beverages and foods, and from grapefruit products starting 72 hours before admission to the study ward.

## Study design, ethanol, and drug administration

The study had an open-label, single-center, two-period, crossover design with randomly allocated sequences, evaluating pharmacokinetic parameters of probe substrates of major drug metabolizing cytochrome P450 enzymes by a cocktail of probe substrates, including oral caffeine (CYP1A2/*N*-acetyltransferase type 2 (NAT2)), oral tolbutamide (CYP2C9), oral omeprazole (CYP2C19), oral dextromethorphan (CYP2D6), oral and intravenous midazolam (intestinal CYP3A and hepatic CYP3A), and oral digoxin (intestinal and renal P-glycoprotein). In the test period, six doses of an ethanol-containing beverage (Wodka Gorbatschow 50% (v/v, equal to 395 g ethanol per L), Henkell & Co. Sektkellerei, Wiesbaden, Germany) were given. The doses were estimated using Widmark's equation<sup>39</sup> with the aim of reaching and maintaining a blood ethanol concentration (BEC) approaching 1 g per L. A loading dose (males, 0.76 g ethanol per kg of body weight; females, 0.65 g/kg) was given 2 hours before administration of oral probe drugs; subsequently, five maintenance ethanol doses (males, 0.30 g/kg; females, 0.26 g/kg body weight) were given every 4 hours (Figure 1). In the reference period, water was given instead of ethanol at the same timepoints.

In both periods, the cocktail of oral probe drugs was then administered 2 hours after the first ethanol dose, and 1 mg of midazolam was injected intravenously another 2 hours thereafter (for drug preparations used, see Section 1 of **Supplementary Document**). Volunteers were hospitalized during active study periods. Food intake was restricted from 10 hours before until 4 hours after cocktail administration, with subsequent administration of standardized nutrition until discharge. The washout between study periods was 14 days. In each active period, blood sampling for quantification of probe drugs (and their metabolites, where applicable) was done (h:min) predose and at 0:08, 0:20, 0:30, 0:45, 1:00, 1:15, 1:30, 1:45, 2:00 (just prior to midazolam i.v. dose), 2:05, 2:08, 2:20, 2:30, 2:45, 3:00, 3:30, 4:00, 4:30, 5:00, 6:00, 8:00, 10:00, 12:00, 14:00, 16:00, 18:00, and 24:00 hours postdose (times relative to oral administration of the probe cocktail). Caffeine, paraxanthine, and tolbutamide and were not quantified in the samples taken 14:00, 16:00, and 18:00 postdose because these were considered essentially noninformative. In parallel, urine was scheduled to be collected for the following periods (h:min): predose to 6:00, 6:00–10:00, 10:00–14:00, 14:00–18:00, and 18:00–24:00 hours postdose. In the study, urine collection periods were completed just prior to scheduled times to avoid interference with blood sampling times. Urine volumes were measured by weight control, assuming a density of 1 g per mL, and two aliquots were kept for analysis. All samples were stored at –65°C or lower until analysis. To determine BEC during the test period, blood samples were taken at (h:min) –2:00, –1:00, 2:00, 3:00, 6:00, 11:00, 14:00, 24:00, 28:00 (prior to dismissal) hours relative to oral administration of the probe cocktail. Six alcohol breath tests (at –2:00, –1:00, 2:00, 6:00, 14:00, 28:00 hours) with immediate availability of results were carried out additionally for safety reasons but were also used for assessment of ethanol pharmacokinetics (for more details, see **Supplementary Document**).

## Genotyping

Allelic variants related to impaired enzyme activity may compromise the assessment of ethanol effects. Therefore, a blood sample was taken at the start of the first period to genotype for major variants in enzymes and transporters (Table 4), using the DMET Plus microarray (Affymetrix, Santa Clara, CA).

## Quantification of ethanol

Concentrations of ethanol in blood samples were quantified by gas chromatography with flame ionization detection (see **Supplementary Document**). The lower limit of quantification (LLOQ) for ethanol was 0.1 g/L. Ethanol breath quantification was done by the Alcotest 7401 plus device (Drägerwerk, Lübeck, Germany).

## Quantification of probe drugs

Probe drugs and their metabolites (where applicable) were quantified by liquid chromatography / tandem mass spectrometry (AB SCIEX API 5000 triple quadrupole devices with the Analyst software v. 1.6.2; AB SCIEX, Concord, Ontario, Canada) using mass-labeled internal standards. Samples were processed by protein precipitation with acetonitrile and/or dilution for all substances except digoxin,<sup>40</sup> where solid phase extraction was used (Strata-X SPE Cartridges, Phenomenex, Torrance, CA).<sup>41</sup>

All assays fulfilled current standard validation criteria as described in respective European Medicines Agency (EMA) and US Food and Drug Administration (FDA) guidelines, with accuracy and precision meeting the requirements—and in most cases exceeding them significantly. The sensitivity of all assays was sufficient to allow for a proper assessment of pharmacokinetic parameters (see **Supplementary Document**).

## Pharmacokinetic evaluation

For ethanol and midazolam, compartmental population pharmacokinetic models were developed (NONMEM v. 7.2.0, Development Solutions, Ellicott, MD). This approach was used for ethanol to describe the exposure to ethanol and to incorporate both blood and breath concentrations, and for midazolam to separately assess hepatic and intestinal CYP3A activity. Plasma pharmacokinetics of all other probe drugs was evaluated by the standard noncompartmental approach (Phoenix WinNonlin 7.0, Certara, Princeton, NJ). Renal clearance  $CL_r$  of digoxin was calculated as amount excreted in urine divided by the area under the concentration vs. time curve in plasma ( $Ae_{0-24h}/AUC_{0-24h}$ ), and renal secretion of digoxin was calculated as  $CL_r - f_u$  (fraction unbound = 0.7)<sup>27,42</sup> \* GFR (glomerular filtration rate), where GFR was estimated from the creatinine plasma concentration obtained in the screening examination using the Cockcroft–Gault equation.<sup>43</sup> Suitable primary and additional pharmacokinetic parameters selected as phenotyping metrics to estimate enzyme or transporter activity<sup>18,40,44,45</sup> are shown in Table 3 and in the **Supplementary Document**.

## Statistical analysis

Data were analyzed by the authors. Summary statistics were calculated using Microsoft Excel 2007 (Seattle, WA) or Phoenix WinNonlin. Individual pharmacokinetic parameters (midazolam: individual *post-hoc* estimates derived from the population pharmacokinetic model) were compared between the test (ethanol) and the reference (water) period by the average bioequivalence method,<sup>46</sup> calculating point estimates and 90% CI for test/reference ratios. To this end, a general linear analysis of variance (ANOVA) model with effects for sequence, subject within sequence, period, and intervention (ethanol or water) as implemented in Phoenix WinNonlin was applied on log transformed values (renal secretion: untransformed values). The sample size was based on the assumption that intraindividual coefficients of variation would not exceed 25% for any phenotyping metric.<sup>18,40,44</sup> Formally, a sample size of  $n = 14$  would allow rejection of each separate null hypothesis “relevant effect of ethanol present” with  $\alpha = 0.05$  (two-sided) and a power of at least 90%, using 0.7–1.43 as “no relevant interaction” margins for test/reference ratios. Two additional subjects were included to account for



eventual dropouts. Exploratory analysis for genotype subgroups was done to account for the role of low or null activity alleles on ethanol effects.

Additional Supporting Information may be found in the online version of this article.

#### ACKNOWLEDGMENTS

We thank our colleagues at the Department I of Pharmacology, Clinical Pharmacology Unit, University Hospital Cologne, Germany, for their support during the conduct of the study, including Amir Alihodzic, Samira Boussettaoui, Dominik Dahlinger, Ingrid Fehrenz, Dirk Kroll, Kathi Krüsemann, Ahmed Suleiman, and Yingying Tian. We also appreciate the technical support by Stefan Winter and Andrea Jamuth at the Dr. Margarete-Fischer-Bosch Institute of Clinical Pharmacology, Stuttgart, Germany. Also, we thank the volunteers for their participation in this challenging study.

#### FUNDING

M.G. was supported by a grant of the Government of Saudi-Arabia. X.L. was supported by a PhD grant provided by China Scholarship Council. Mat.S. and E.S. were supported by the European Commission Horizon 2020 UPGx grant 668353 and by the Robert Bosch Stiftung (Stuttgart, Germany).

#### CONFLICT OF INTEREST

The authors declare no competing interests for this work.

#### AUTHOR CONTRIBUTIONS

M.G., M.K., E.S., M.J., C-h.H., X.L., Mat.S., F.S., and U.F. wrote the article; M.G., J. I.-B., D.K., C.Q., Mat.S., and U.F. designed the research; M.G., M.K., E.S., M.J., C-h.H., X.L., M.T., J.I.-B., Mar.S., Mat.S., and U.F. performed the research; M.G., C-h.H., X.L., M.T., C.T., and U.F. analyzed the data.

© 2018 American Society for Clinical Pharmacology and Therapeutics

- WHO. Global status report on alcohol and health 2014. WHO. <[http://www.who.int/substance\\_abuse/publications/global\\_alcohol\\_report/en/](http://www.who.int/substance_abuse/publications/global_alcohol_report/en/)> (2016).
- Chan, L.-N. & Anderson, G.D. Pharmacokinetic and pharmacodynamic drug interactions with ethanol (alcohol). *Clin. Pharmacokinet.* **53**, 1115–1136 (2014).
- Johnson, B.A. & Seneviratne, C. Alcohol-medical drug interactions. *Handb. Clin. Neurol.* **125**, 543–559 (2014).
- Tanaka, E. & Misawa, S. Pharmacokinetic interactions between acute alcohol ingestion and single doses of benzodiazepines, and tricyclic and tetracyclic antidepressants — an update. *J. Clin. Pharm. Ther.* **23**, 331–336 (1998).
- Dorian, P. et al. Amitriptyline and ethanol: pharmacokinetic and pharmacodynamic interaction. *Eur. J. Clin. Pharmacol.* **25**, 325–331 (1983).
- Sellers, E.M., Naranjo, C.A., Giles, H.G., Frecker, R.C. & Beeching, M. Intravenous diazepam and oral ethanol interaction. *Clin. Pharmacol. Ther.* **28**, 638–645 (1980).
- Loizou, G.D. & Cocker, J. The effects of alcohol and diallyl sulphide on CYP2E1 activity in humans: a phenotyping study using chlorzoxazone. *Hum. Exp. Toxicol.* **20**, 321–327 (2001).
- Oneta, C.M. et al. Dynamics of cytochrome P4502E1 activity in man: induction by ethanol and disappearance during withdrawal phase. *J. Hepatol.* **36**, 47–52 (2002).
- Girre, C. et al. Assessment of cytochrome P4502E1 induction in alcoholic patients by chlorzoxazone pharmacokinetics. *Biochem. Pharmacol.* **47**, 1503–1508 (1994).
- Zhukov, A. & Ingelman-Sundberg, M. Relationship between cytochrome P450 catalytic cycling and stability: fast degradation of ethanol-inducible cytochrome P450 2E1 (CYP2E1) in hepatoma cells is abolished by inactivation of its electron donor NADPH-cytochrome P450 reductase. *Biochem. J.* 453–458 (1999).
- Busby, W.F., Ackermann, J.M. & Crespi, C.L. Effect of methanol, ethanol, dimethyl sulfoxide, and acetonitrile on in vitro activities of cDNA-expressed human cytochromes P-450. *Drug Metab. Dispos.* **27** (1999).
- González-Pérez, V., Connolly, E.A., Bridges, A.S., Wienkers, L.C. & Paine, M.F. Impact of organic solvents on cytochrome P450 probe reactions: filling the gap with (S)-Warfarin and midazolam hydroxylation. *Drug Metab. Dispos.* **40**, 2136–2142 (2012).
- Rokitta, D., Pfeiffer, K., Streich, C., Gerwin, H. & Fuhr, U. The effect of organic solvents on enzyme kinetic parameters of human CYP3A4 and CYP1A2 in vitro. *Toxicol. Mech. Methods* **23**, 576–583 (2013).
- Frechen, S. et al. A semiphysiological population pharmacokinetic model for dynamic inhibition of liver and gut wall cytochrome P450 3A by voriconazole. *Clin. Pharmacokinet.* **52**, 763–781 (2013).
- Abduljalil, K. et al. Assessment of activity levels for CYP2D6\*1, CYP2D6\*2, and CYP2D6\*41 genes by population pharmacokinetics of dextromethorphan. *Clin. Pharmacol. Ther.* **88**, 643–651 (2010).
- Gaedigk, A., Sangkuhl, K., Whirl-Carrillo, M., Klein, T. & Leeder, J.S. Prediction of CYP2D6 phenotype from genotype across world populations. *Genet. Med.* **19**, 69–76 (2017).
- European Medicines Agency. Guideline on the investigation of drug interactions 21 June 2012 CPMP/EWP/560/95/Rev. 1 Corr. 2\*\*. <[http://www.ema.europa.eu/docs/en\\_GB/document\\_library/Scientific\\_guideline/2012/07/WC500129606.pdf](http://www.ema.europa.eu/docs/en_GB/document_library/Scientific_guideline/2012/07/WC500129606.pdf)> (2012).
- Fuhr, U., Jetter, A. & Kirchheiner, J. Appropriate phenotyping procedures for drug metabolizing enzymes and transporters in humans and their simultaneous use in the 'cocktail' approach. *Clin. Pharmacol. Ther.* **81**, 270–283 (2007).
- Andrés, F. de & Llerena, A. Simultaneous determination of cytochrome p450 oxidation capacity in humans: a review on the phenotyping cocktail approach. *Curr. Pharm. Biotechnol.* **17**, 1159–1180 (2016).
- Scotcher, D., Jones, C.R., Galetin, A. & Rostami-Hodjegan, A. Delineating the role of various factors in renal disposition of digoxin through application of physiologically based kidney model to renal impairment populations. *J. Pharmacol. Exp. Ther.* **360**, 484–495 (2017).
- Streetman, D.S. et al. Combined phenotypic assessment of CYP1A2, CYP2C19, CYP2D6, CYP3A, N-acetyltransferase-2, and xanthine oxidase with the 'Cooperstown cocktail.' *Clin. Pharmacol. Ther.* **68**, 375–383 (2000).
- Blakey, G.E. et al. Pharmacokinetic and pharmacodynamic assessment of a five-probe metabolic cocktail for CYPs 1A2, 3A4, 2C9, 2D6 and 2E1. *Br. J. Clin. Pharmacol.* **57**, 162–169 (2004).
- Kirby, B. et al. Simultaneous measurement of in vivo P-glycoprotein and cytochrome P450 3A activities. *J. Clin. Pharmacol.* **46**, 1313–1319 (2006).
- Ryu, J.Y. et al. Development of the 'Inje cocktail' for high-throughput evaluation of five human cytochrome P450 isoforms in vivo. *Clin. Pharmacol. Ther.* **82**, 531–540 (2007).
- Turpault, S. et al. Pharmacokinetic assessment of a five-probe cocktail for CYPs 1A2, 2C9, 2C19, 2D6 and 3A. *Br. J. Clin. Pharmacol.* **68**, 928–935 (2009).
- Donzelli, M. et al. The Basel cocktail for simultaneous phenotyping of human cytochrome P450 isoforms in plasma, saliva and dried blood spots. *Clin. Pharmacokinet.* **53**, 271–282 (2014).
- Rengelshausen, J. et al. Contribution of increased oral bioavailability and reduced nonglomerular renal clearance of digoxin to the digoxin-clarithromycin interaction. *Br. J. Clin. Pharmacol.* **56**, 32–38 (2003).
- Zhang, X.-Y., Tian, Y., Zhang, Z.-J., Rui, J.-Z. & Cao, X.-M. Pharmacokinetics and bioequivalence study of two digoxin formulations after single-dose administration in healthy Chinese male volunteers. *Arzneimittelforschung* **61**, 601–604 (2012).
- Wilkinson, P.K. et al. Blood ethanol concentrations during and following constant-rate intravenous infusion of alcohol. *Clin. Pharmacol. Ther.* **19**, 213–223 (1976).
- Capon, D.A. et al. The influence of CYP2D6 polymorphism and quinidine on the disposition and antitussive effect of dextromethorphan in humans. *Clin. Pharmacol. Ther.* **60**, 295–307 (1996).
- Ingelman-Sundberg, M. Genetic polymorphisms of cytochrome P450 2D6 (CYP2D6): clinical consequences, evolutionary aspects and functional diversity. *Pharmacogenomics J.* **5**, 6–13 (2005).

32. Ciraulo, D.A., Barnhill, J.G. & Jaffe, J.H. Clinical pharmacokinetics of imipramine and desipramine in alcoholics and normal volunteers. *Clin. Pharmacol. Ther.* **43**, 509–518 (1988).
33. Harris, R.Z., Salfi, M., Posvar, E., Hoelscher, D. & Padhi, D. Pharmacokinetics of desipramine HCl when administered with cinacalcet HCl. *Eur. J. Clin. Pharmacol.* **63**, 159–163 (2007).
34. Nakashima, D. *et al.* Effect of cinacalcet hydrochloride, a new calcimimetic agent, on the pharmacokinetics of dextromethorphan: in vitro and clinical studies. *J. Clin. Pharmacol.* **47**, 1311–1319 (2007).
35. U.S. Food and Drug Administration. Clinical Drug Interaction Studies — Study Design, Data Analysis, and Clinical Implications Guidance for Industry. *Draft Guidance as of October 2017*. <<https://go.usa.gov/xngDH>> (2017).
36. Granfors, M., Backman, J., Neuvonen, M. & Neuvonen, P. Ciprofloxacin greatly increases concentrations and hypotensive effect of tizanidine by inhibiting its cytochrome P450 1A2-mediated presystemic metabolism. *Clin. Pharmacol. Ther.* **76**, 598–606 (2004).
37. Fuhr, U. Pharmacokinetic phenotyping to predict drug-drug interactions: time to divorce the hybrid concept of simultaneous mechanistic-based and exposure-based assessment. *Clin. Pharmacol. Ther.* **103**, 42–42 (2018).
38. Moj, D. *et al.* Clarithromycin, midazolam, and digoxin: Application of PBPK modeling to gain new insights into drug–drug interactions and co-medication regimens. *AAPS J.* **19**, 298–312 (2017).
39. Seidl, S., Jensen, U. & Alt, A. The calculation of blood ethanol concentrations in males and females. *Int. J. Legal Med.* **114**, 71–77 (2000).
40. Zadayan, G. *et al.* Effect of Ginkgo biloba special extract EGb 761® on human cytochrome P450 activity: a cocktail interaction study in healthy volunteers. *Eur. J. Clin. Pharmacol.* **68**, 553–560 (2012).
41. Trass, M., Layne, J. & Koerner, P. Rapid LC/MS/MS analysis of digoxin and digitoxin in plasma using Strata-X SPE cartridges and Kinetex® 2.6 µm C8 Core-Shell HPLC/UHPLC Columns. (TN-1099). Torrance, CA: Phenomenex Inc. <<https://az621941.vo.msecnd.net/documents/bac42b4d-2aa2-4957-bfc4-9bc36c39c436.pdf>>.
42. Actavis UK Ltd SPC Digoxin Tablets BP 250 micrograms. <<https://www.medicines.org.uk/emc/medicine/23944>> (2013).
43. Cockcroft, D.W. & Gault, H. Prediction of creatinine clearance from serum creatinine. *Nephron* **16**, 31–41 (1976).
44. Doroshenko, O. *et al.* Drug cocktail interaction study on the effect of the orally administered lavender oil preparation silexan on cytochrome P450 enzymes in healthy volunteers. *Drug Metab. Dispos.* **41**, 987–993 (2013).
45. Jetter, A. *et al.* Phenotyping of N-acetyltransferase type 2 and xanthine oxidase with caffeine: when should urine samples be collected? *Eur. J. Clin. Pharmacol.* **65**, 411–417 (2009).
46. Steinijans, V.W., Hartmann, M., Huber, R. & Radtke, H.W. Lack of pharmacokinetic interaction as an equivalence problem. *Int. J. Clin. Pharmacol. Ther.* **34**, S25–30 (1996).

## **Drinking ethanol has little acute effects on CYP2C9, CYP2C19, NAT2 and P-glycoprotein activities but somewhat inhibits CYP1A2, CYP2D6 and intestinal CYP3A – so what?**

### **Supplementary document**

Malaz Gazzaz (1,2), Martina Kinzig(3), Elke Schaeffeler (4,5), Martin Jübner (6), Chih-hsuan Hsin (1), Xia Li (1), Max Taubert (1), Christina Trueck (1), Juliane Iltgen-Breburda (7), Daria Kraus (1,8), Christian Queckenberg (1,8), Marc Stoffel (1), Matthias Schwab (4,9,10), Fritz Sörgel (3), Uwe Fuhr (1)

(1) Department I of Pharmacology, University Hospital Cologne, Germany

(2) Department of Clinical Pharmacy, College of Pharmacy, Umm Al-Qura University, Makkah, Saudi Arabia

(3) Institute for Biomedical and Pharmaceutical Research, Nürnberg-Heroldsberg, Germany

(4) Dr. Margarete-Fischer-Bosch Institute of Clinical Pharmacology, Auerbachstrasse 112, Stuttgart, Germany

(5) University of Tuebingen, Tuebingen, Germany

(6) Institute of Legal Medicine, Faculty of Medicine, University of Cologne, Germany

(7) Pharmacy, University Hospital Cologne, Germany

(8) Clinical Trials Centre, University Hospital Cologne, Germany.

(9) Department of Clinical Pharmacology, University Hospital Tuebingen, Germany

(10) Department of Pharmacy and Biochemistry, University of Tuebingen, Tuebingen, Germany

### **Corresponding author contact information:**

Univ.-Prof. Dr. med. Uwe Fuhr

Department I of Pharmacology, Center for Pharmacology, Clinical Pharmacology Unit

University Hospital Cologne (AÖR)

Gleueler Straße 24, 50931 Köln, Germany

email [uwe.fuhr@uk-koeln.de](mailto:uwe.fuhr@uk-koeln.de)

phone +49-(0)-221-478-6672 (office), -5230 (direct line); fax +49-(0)-221-478-7011

## 1. Identity and manufacturers of probe drugs

The oral cocktail consisted of the following probe substances:

- a) *Test product*                      *Percoffedrinol N Aristo® 50 Tabletten*  
Manufacturer:                      Aristo Pharma GmbH, Berlin, Germany  
Dosage form:                      tablets  
Drug substance:                      caffeine (CYP1A2, NAT2)  
Strength:                              50 mg caffeine  
Dose to be administered:        150 mg (three tablets)
- b) *Test product*                      *Tolbutamide 500 PCH Tabletten*  
Manufacturer:                      Pharmachemie B.V., Haarlem, The Netherlands  
Dosage form:                      tablets  
Drug substance:                      tolbutamide (CYP2C9)  
Strength:                              500 mg tolbutamide  
Dose to be administered:        125 mg (1/4 of a tablet, assessed by weight control)
- c) *Test product*                      *Omeprazol Ratiopharm® NT 20 mg magensaftres.Hartkap.*  
Manufacturer:                      ratiopharm GmbH, Ulm, Germany  
Dosage form:                      capsule  
Drug substance:                      omeprazole (CYP2C19)  
Strength:                              20 mg omeprazole  
Dose to be administered:        20 mg (one capsule)
- d) *Test product*                      *Hustenstiller Ratiopharm®*  
Manufacturer:                      ratiopharm GmbH, Ulm, Germany  
Dosage form:                      capsule  
Drug substance:                      dextromethorphan-HBr (CYP2D6)  
Strength:                              30 mg dextromethorphan-HBr  
Dose to be administered:        30 mg (one capsule)
- e) *Test product*                      *Digacin® 0.25 mg*  
Manufacturer:                      Mibe GmbH Arzneimittel, Brehna, Germany  
Dosage form:                      tablets  
Drug substance:                      digoxin (intestinal & renal P-glycoprotein)  
Strength:                              0.25 mg digoxin  
Dose to be administered:        0.5 mg (two tablets)
- f) *Test product*                      *Midazolam-ratiopharm 5 mg/5 ml Injektionslösung*  
Manufacturer:                      ratiopharm GmbH, Ulm, Germany

Dosage form: solution (given orally)  
Drug substance: midazolam (intestinal + hepatic CYP3A4)  
Strength: 5 mg midazolam  
Dose to be administered: 2 mg (2 ml, assessed by weight control)

Additionally, 1mg of midazolam for assessment of hepatic CYP3A4 were given i.v.2 hours after cocktail administration.

*g) Test product* Midazolam-ratiopharm 5 mg/5 ml Injektionslösung  
Manufacturer: ratiopharm GmbH, Ulm, Germany  
Dosage form: solution (given intravenously)  
Drug substance: midazolam (hepatic CYP3A4)  
Strength: 5 mg midazolam  
Dose to be administered: 1 mg (1 ml, assessed by weight control)

## 2. Pharmacokinetic parameters to be assessed

Primary pharmacokinetic characteristics for probe drugs (“metrics”) according to the study protocol were:

CYP1A2:  $AUC_{0-t}$  of caffeine in plasma

NAT2 activity:  $(AFMU + AAMU) / (AFMU + AAMU + 1X + 1U)$  ratio in urine

CYP2C9:  $AUC_{0-t}$  of tolbutamide in plasma

CYP2C19: Molar omeprazole / 5-OH-omepazole  $AUC_{0-t}$  ratio in plasma

CYP2D6: Molar dextromethorphan / dextrorphan  $AUC_{0-t}$  ratio in plasma

Hepatic CYP3A4: hepatic clearance of midazolam

Intestinal CYP3A4: intestinal extraction of midazolam

Intestinal p-glycoprotein: absolute bioavailability of digoxin (calculated as  $A_e$ ) (because  $A_e$  could not be extrapolated to infinity,  $A_e$  could not be used to provide an estimate of absolute bioavailability)

Renal p-glycoprotein: renal secretion of digoxin

According to the study protocol, the following phenotyping metrics were considered as complimentary (further pharmacokinetic parameters of the phenotyping substances and safety parameters would also be reported):

CYP1A2: Molar paraxanthine / caffeine  $AUC_{0-t}$  ratio; molar paraxanthine / caffeine plasma concentration ratio 6 h post-dose

CYP2C9: Tolbutamide plasma concentration 24 h post-dose

CYP2C19:  $AUC_{0-t}$  of omeprazole in plasma

CYP2C19: Molar omeprazole / 5-OH-omeprazole plasma concentration ratio 3 h post-dose

CYP2D6:  $AUC_{0-t}$  of dextromethorphan in plasma

CYP2D6: Molar dextromethorphan / dextrorphan plasma concentration ratio 3 h post-dose

Intestinal p-glycoprotein: digoxin  $C_{max}$

### 3. Quantification of ethanol

Blood ethanol concentrations (BEC) were quantified by headspace gas chromatography with a capillary column, using a method established and routinely used for legal purposes<sup>1</sup>.

#### 3.1. Instrumentation

A PerkinElmer® TurboMatrix Headspace (HS) autosampler connected to a PerkinElmer Clarus 500 Gas Chromatograph (GC) with flame ionization detector (FID) was used in these experiments (PerkinElmer, Rodgau, Germany), equipped with a PerkinElmer® Elite-BAC2 capillary column with dimensions 30 m x 0.32 mm x 1.2  $\mu$ m (film thickness).

#### 3.2. Experimental Conditions

All samples were stored at 4°C until preparation. The samples were centrifuged at 3,500 rpm for 10 minutes (Megafuge 10, Heraeus, Hanau, Germany) to separate serum. 50  $\mu$ L serum were added to 500  $\mu$ L tertiary butanol (0.04 %, internal standard). A zero check (Medidrug® Basis line S, Medichem, Steinenbronn, Germany) and a stock standard (Medidrug® Ethanol S-plus, Medichem) were used as quality control for the experiments. All experiments were carried out as repeat determination in 20 mL headspace vials, capped with PTFE silicone septa. After measurement, ethanol concentration in whole blood was calculated using a divisor of 1.236 (average water content of blood x relative density of serum).

The headspace and GC-FID operating conditions were as follows: Headspace conditions: Oven temperature 65 °C, needle temperature 95 °C, transfer line temperature 130 °C carrier gas nitrogen 130 kPa, heating time 16 min, injection time 0.05 min, holding time 0.2 min

cycle time 2.6 min; GC conditions: Carrier gas hydrogen at 110 kPa , split mode 5 mL/min, 2.55 min isothermal at 60 °C, FID at 260 °C with constant flow of 45 mL/min hydrogen and 450 mL/min air.

### **3.3. Validation procedure**

The method was validated according to the guidelines of the Society of Toxicological and Forensic Chemistry (GTFCh) in Germany<sup>2</sup> and fulfills requirements for legal (court) purposes. All statistical evaluations were done by using Valistat software version 2.04 from Arvecon (Walldorf, Germany). Therefore, the following experiments were performed:

#### 3.3.1. Calibration

A seven-point calibration curve was created establishing method linearity and calibration range. Seven headspace vials were prepared with 500 µL of 0.04 % t-butanol used as internal standard. 50 µL of standard solution (0.1 g/L; 0.2 g/L; 0.5 g/L; 1 g/L; 2 g/L; 3 g/L, 4 g/L) were added into the vials.

#### 3.3.2. Accuracy and Precision

Accuracy (bias) and precision were determined using commercially available control samples (Medichem GmbH, Steinenbronn, Germany, treated as “unknowns”) at three different concentrations (0.194 g/L, 1.064 g/L, 2.959 g/L) with two replicates for each concentration (intra-day precision). The procedure was repeated on nine different occasions to give inter-day precision data. Bias was calculated by the deviation of the mean result from the true value determined by calibration expressed as a percentage.

#### 3.3.3. Limit of detection / quantification

The limit of detection (LOD) was determined as the response that was at least three times the response compared to the blank response (signal-to-noise). Lower limit of quantification (LLOQ) was determined at a concentration of 0.1 g/L with five replicates by accuracy and precision data. In this regard, permissible deviation is  $\leq 20\%$  relative standard deviation (RSD) and  $\pm 20\%$  bias.

#### 3.3.4 Results of Validation

Calibration showed excellent linearity in the range from 0.1 to 4.0 mg/L by linear regression with a coefficient of correlation of 0.9999. Accuracy was determined with a bias of +3.3% at a concentration of 0.194 g/L, a bias of +2.5% at a concentration of 1.064 g/L and a bias of +1.6% at a concentration of 2.959 g/L. For the three concentrations inter-day coefficients of variation % for the method over nine days was 1.0, 1.1 and 0.7%, respectively, as well as intra-day precision was 0.5, 0.6 and 0.3%, respectively.

The LOD was found to be 0.05 mg/L (signal to noise ratio of 8), the LLOQ was found to be 0.1 mg/L, the latter with a relative standard deviation of 4% and a bias of 18%. All validation data fulfilled the requirements of GTFCh guideline used. Thus, HS-GC method applied is suitable for the quantification of ethanol in the samples of the study.

## **4. Quantification of probe drugs and their metabolites**

### **4.1. CYP2D6, CYP3A, CYP2C19 and NAT2 probes**

For quantification of probe drugs three different liquid chromatography systems (assay 1: midazolam and metabolites in plasma; assay 2: omeprazole, 5-hydroxyomeprazole, dextropropranolol and dextromethorphan in plasma; assay 3: caffeine metabolites in urine) consisted of a binary LC-pump (Agilent 1200 Series, Agilent Technologies, Waldbronn, Germany) and two analytical columns (assay 1 and 2: Synergie 2.5u Polar RP 100A, 50x4.6 mm, assay 3: Aqua 3u C18 125A, 50 x 4.6 mm, Phenomenex, Aschaffenburg, Germany). For assay 1 isocratic elution was performed with 0.5% formic acid and methanol as well as for assay 3 isocratic elution was performed with 0.5% formic acid and methanol/THF (v/v, 1/1). For assay 2 a gradient elution was performed with 0.1% formic acid and methanol. Determination was performed using an AB SCIEX API 5000 triple quadrupole mass spectrometer (AB SCIEX, Concord, Ontario, Canada) and Analyst software version 1.6.2 (AB SCIEX, Concord, Ontario, Canada). In brief, 50 µL of each plasma sample (assay 2 and 3) was placed in a polypropylene-tube. Samples were deproteinized with 100 µL (assay 1) or 300 µL (assay 2) acetonitrile containing the internal standard (assay 2: midazolam-d<sub>3</sub> and 1'-hydroxymidazolam-d<sub>4</sub>; assay 3: omeprazole-d<sub>3</sub>, 5-hydroxyomeprazole-d<sub>3</sub>, dextromethorphan-d<sub>3</sub>), subsequently vortex-shaken and centrifuged. The supernatant was further diluted with water and 20 µL were injected into the LC-MS/MS system. 20 µL of the urine samples (assay



3) were mixed with 0.1% formic acid containing the internal standards (1U-d<sub>3</sub>, 1X-d<sub>3</sub>, AFMU-d<sub>3</sub>), vortex-shaken and 20 µL were injected into the LC-MS/MS system. The compounds were detected with MRM (Multiple Reaction Monitoring); mass spectrometry conditions are described in Table S1.

Calibration standards and spiked quality controls samples (SQC) were prepared by adding a defined amount of the corresponding analyte-solution to human drug free plasma or for urine to 0.1 % formic acid. Calibration was performed by weighted (1/concentration<sup>2</sup>) linear regression. Linearity for each compound could be demonstrated over the respective ranges. These were: dextrorphan 0.0757 - 20.4 ng/mL; dextromethorphan 0.0837 - 22.6 ng/mL; midazolam 0.0492 - 73.7 ng/mL; 1'-hydroxymidazolam 0.0449 - 67.3 ng/mL; 4-hydroxymidazolam 0.0474 - 71.1 ng/mL; omeprazole 0.1474 - 358.2 ng/mL; 5-hydroxyomeprazole 0.2292 - 371.4 ng/mL; 1U 0.226 - 19.5 µg/mL; 1X 0.115 - 19.9 µg/mL; AAMU 0.454 - 19.6 µg/mL; and AFMU 0.228 - 19.7 µg/mL.

Precision and accuracy for each compound at high, medium and low concentrations within the calibration range was determined in human plasma or 0.1 % formic acid (as a surrogate for urine). The assays for all substances were accurate (bias within -4.0% to 8.0%) and precise (within-run and between-run coefficients of variation below 10% in all cases except for AAMU at the medium concentration (14.5 %)). In addition, the incurred samples reanalyses of assay 1 and 2 showed reliability of these assays (mean absolute bias between 1.4% and 5.9%).

## 4.2. CYP1A2 and CYP2C9 probes

Plasma sample preparation for the caffeine (CAF), paraxanthine (PAX) and tolbutamide (TOL) assay was followed by the previously described protein precipitation method<sup>3</sup>. 200µl plasma samples were precipitated with 400µl acetonitrile. For this method, two internal standards, 20µl Caffeine-d<sub>3</sub> (300ng/ml) and 20µl Tolbutamide-d<sub>9</sub> (300ng/ml) were added. After vortex mixing for 10 seconds samples were centrifuged for 10 minutes at room temperature at 16100 g, 200µl of supernatant were transferred into HPLC-vials and 20µL were injected into the liquid chromatography / tandem mass spectrometry device.

Concentration of plasma samples for CAF, PAX and TOL assay were determined on an API 5000 device with QJET™ Ion Guide (Applied Biosystems, Foster City, CA, USA), linked to a binary Agilent 1200 pump and an Agilent 1260 Infinity standard autosampler (Agilent 1260, Agilent Technologies

Inc., Santa Clara, CA, USA) by using a previously described LC-MS/MS method with minor modifications<sup>3</sup>. The effluent of LC system was delivered through a reversed-phase column (125x2mm, 3µm; Nucleodur C18 Isis, Macherey-Nagel, Düren, Germany) with a precolumn (4x2.0mm) (SecurityGuard Guard Cartridge, Phenomenex, Torrance, CA, USA). The column temperature was maintained at 30°C and the samples were stored at 4°C until injection. Chromatography was performed using a gradient solvent system composed of 0.1% formic acid (A) and acetonitrile (B) (0 -> 0.5min A:B 80:20, 0.5-> 2min A:B 80:20-> A:B 30:70, 2-> 4min A:B 30:70-> A:B 65:35, 4 -> 5.5min A:B 65:35, 5.5-> 6min A:B 65:35-> A:B 80:20, 6 -> 7min A:B 80:20). CAF, PAX, CAF-d3, TOL and Tol-d9 were detected with positive electrospray ionization (ESI+) in the positive multiple reaction monitoring mode (MRM+) with the following ion transitions [m/z]:195.0-> 138.1 for CAF, 181.0->124.0 for PAX, 198.1->138.1 for CAF-d3, 271.1->91.1 for TOL, and 280.2->91.0 for TOL-d9. CAF, CAF-d3 and PAX were eluted after 1.22 min and retention time of TOL and its isotope-labeled internal standard was 4.95 min. The lower limits of quantification (LLOQ) for CAF and PAX were 100ng/mL and for TOL 300ng/mL. Instrument control and data acquisition were performed with the analyst 1.6.2 software (Applied Biosystems). Peak area ratios (analyte /internal standard) were used for quantification and calibration functions were calculated via weighted (1/x) least squares linear regression. Linearity for each analyte could be demonstrated over the respective calibration ranges, which were: caffeine and paraxanthine 100-5000 ng/mL, tolbutamide 300-15000 ng/mL.

Precision and accuracy for each compound at high, medium and low concentrations and at the lower limit of quantification was determined in human plasma. The assays for all substances were accurate (absolute bias below 7.3 %) and precise (within-run and between-run coefficients of variation below 10 % and below 15 %, respectively, in all cases except for paraxanthine at LLOQ (16.5 %)).

### **4.3. P-gp probe**

Plasma and urine samples for the digoxin assay were cleaned up and concentrated via solid phase extraction (Strata-X SPE Cartridges, Phenomenex, USA) according to an application note from Phenomenex (TN-1099) and digoxin-d3 was used as the internal standard. Briefly, 0.5 mL of a plasma sample or 0.3 mL of a urine sample were diluted with 2.5mL or 2.7mL ultrapure water, respectively, and samples were spiked with 20µl of digoxin-d3 solution. SPE columns were conditioned by adding 2mL methanol and equilibrated with 2mL 10mM amino acetate in water (pH=6.7). The prepared samples were loaded on the equilibrated columns and allowed to drain. Each column was then washed with 2mL 10mM amino acetate in water: 100% methanol (50:50) and dried under maximum

vacuum for 2 min. Digoxin and digoxin-d3 were eluted with 2mL 100% methanol. The solvent was evaporated to dryness at 50°C under a stream of nitrogen. The dried residues were reconstituted with 150µL 10mM amino acetate in water: 10mM amino acetate in methanol (50: 50) and vortexed for 10 seconds in order to increase the recovery. After vortexing, samples were centrifuged for 10 minutes at room temperature at 16100 g. Then, 40µL of the final solution was injected into the LC-MS/MS system.

Concentration of plasma samples for CAF, PAX and TOL assay were determined on an API 5000 device with QJET™ Ion Guide (Applied Biosystems, Foster City, CA, USA), linked to a binary Agilent 1200 pump and an Agilent 1260 Infinity standard autosampler (Agilent 1260, Agilent Technologies Inc., Santa Clara, CA, USA). Digoxin concentrations in plasma and urine were analyzed by reverse phase chromatography (Kinetex C8 column, particle size 2.6µm, pore size 100Å, 50x2.1 mm, Phenomenex, Torrance, CA, USA) with a precolumn (4x2.1mm) (SecurityGuard ULTR, Phenomenex, Torrance, CA, USA). The gradient solvent system consisted of 10mM amino acetate in water (pH=6.7) (A) and 10mM amino acetate in methanol (B) (0 -> 2.5min A:B 50:50 -> A:B 0:100, 2.5-> 4.5min A:B 0:100 -> A:B 50:50, 4.5-> 4.51min A:B 0:100 -> A:B 50:50, 4.51 -> 7min A:B 50:50). The column temperature was maintained at 40°C and the samples were stored at 4°C until injection. Digoxin and digoxin-d3 were detected with positive electrospray ionization (ESI+) in the positive multiple reaction monitoring mode (MRM+) with the following ion transitions [m/z]: 798.3 -> 651.4 for digoxin and 802.62-> 96.90 for digoxin-d3. The lower limits of quantification (LLOQ) for digoxin in plasma were 0.1g/mL and for digoxin in urine were 1ng/mL. Instrument control and data acquisition were performed with the analyst 1.6.2 software (Applied Biosystems). Peak area ratios (analyte /internal standard) were used for quantification and calibration functions were calculated via a weighted (1/x) least squares linear regression. The calibration range for digoxin in plasma was 0.1-24.3 ng/mL and in urine 1-300 ng/mL

Precision and accuracy was determined in plasma and urine at high, medium and low concentrations and at the lower limit of quantification. The assay was accurate (absolute bias below 7.4 % in plasma and below 11.3 % in urine) and precise (within-run and between-run coefficients of variation below 10 % and below 15 %, respectively, in all cases).

## 5. Population pharmacokinetic model for ethanol

Stepwise model development was carried out using standard methods<sup>4</sup>. A one-compartment model with first-order absorption and Michaelis-Menten type elimination pathway was suitable as the basic

model and was clearly better than linear or exponential concentration decline ( $\Delta$ OFV [objective function value], -9.291). The value of  $Km$  could not be estimated and thus was fixed as 0.0821 g/L according to the literature<sup>5</sup>.

Because data were obtained from both blood and breath ethanol concentrations, breath ethanol concentrations ( $C_{\text{breath}}$ ) were assumed to have a linear relationship<sup>6</sup> to blood ethanol concentrations (BEC) as described by Eq. S5.1:

$$\text{Eq. S5.1} \quad \text{BEC} = M \times C_{\text{breath}}$$

The Stepwise Covariate Model (SCM) was used to analyze covariates. Volume of distribution  $V$  had a significant relationship with body weight ( $\Delta$ OFV, -152.53), and sex had a small albeit significant effect on maximal elimination capacity  $V_{\text{max}}$  ( $\Delta$ OFV, -19.285). These two covariates were described using the following equations, respectively:

$$\text{Eq. S5.2} \quad V_{\text{max}} = \theta_{V_{\text{max}}} \times \left( 1 + \text{SEX} \times \theta_{\text{Effect of SEX on } K_a} \right); (0 = \text{Female}; 1 = \text{Male})$$

$$\text{Eq. S5.3} \quad V = \theta_V \times \left( \frac{\text{WEIGHT}}{70} \right)^{\theta_{\text{Effect of WEIGHT on } V}}$$

Where  $V_{\text{max}}$  is maximum reaction velocity,  $\theta_{V_{\text{max}}}$  is the typical value of the maximum reaction velocity,  $\theta_{\text{Effect of SEX on } K_a}$  is the effect of sex on the first-order absorption rate constant  $K_a$ ,  $V$  is the volume of distribution,  $\theta_V$  is the typical value of the volume of distribution,  $\theta_{\text{Effect of WEIGHT on } V}$  is the effect of weight on volume of distribution.

According to published data<sup>7</sup>, fat-free body mass (FFM) was also examined as covariate, but in this case did not improve the model further, probably because the subjects in our clinic trial all had normal body weight within a narrow range. All of the model parameters were well estimated (Table 1 of main document) as reflected by narrow 95% confidence intervals (95%CI).

The diagnostic plots are presented in Fig. S1, parts A to E. In Fig. S1 B, observed blood ethanol concentrations (BEC) versus population predicted BEC showed a slight overestimation for low concentrations; however, the weighted residual plots (Fig. S1 C, D) indicate that this misspecification is considered acceptable because most of the residuals fell within +2 and -2 units of the null ordinate. To evaluate the final model obtained from the full data set, a visual predictive check was performed. A set of simulated data sets was generated from the final model and the real data compared with the distribution of the simulated data (Fig. S1 E). A plot of the time course of median prediction along with the 5th–95th percentiles for the simulated value is presented. This graph shows that the data fit well within the 5th–95th percentiles and were distributed symmetrically around the

median. The observed median was very similar to the simulated median. Based on this final model, we simulated the mean value of BEC versus time with 95% confidence interval to demonstrate ethanol exposure in the study population (see Fig.1 of main document)

## 6. Population pharmacokinetic model for midazolam

### 6.1. Midazolam model

The model for midazolam (MDZ) was developed stepwise starting with the MDZ data set without ethanol treatment. Initially, standard simple models (one-, two- or three-compartment models) were tested. A three-compartment model with two parallel peripheral compartments was then favored as an initial model due to a better fit than a two-compartment model ( $\Delta OFV$ , -365.723).

However, with this empirical model, only total systemic clearance of MDZ can be obtained directly. Since MDZ is mainly cleared metabolically by cytochrome P450 3A (CYP3A4, and, if expressed, CYP3A5) in the gut and liver, the contribution of gut CYP3A is important when administered orally. To assess the contribution of both sites of expression to midazolam metabolism, obviously an empirical model is not optimal, and more complex semi-physiological models are more suitable.

Therefore, based on the initial model, a semi-physiological model was further developed, which includes compartments standing for the gut wall, the portal vein and the liver as well as empirical central, peripheral compartment 1 and peripheral compartment 2, respectively. This model was originally proposed by Frechen et al.<sup>8</sup>. Physiological and drug parameters used for the development of this semi-physiological population pharmacokinetic model of midazolam are summarized in Table S2.

After testing from 1 to 20 intestinal transit compartments, absorption of MDZ was best described as a first-order absorption model with two transit compartments, in which the transit compartment rate ( $KTR$ ) was set equal to the oral absorption rate ( $Ka$ ).

Metabolism of MDZ by CYP3A in liver and gut wall forms the major metabolite (60%-80%) 1'-OH-midazolam (1'-OH-MDZ)<sup>9</sup>. During metabolite formation, MDZ in both liver and gut wall compartment reaches equilibrium, indicating that the well-stirred model could describe the metabolism of MDZ in both compartments (eq. S6.1.1 and S6.1.2).

$$\text{Eq. S6.1.1 } E_{H,MDZ} = \frac{CL_{f,H} \times fu_{B,MDZ}}{Q_H + CL_{f,H} \times fu_{B,MDZ}}$$

$$\text{Eq. S6.1.2 } E_{G,MDZ} = \frac{CL_{f,G} \times fu_{G,MDZ}}{Q_G + CL_{f,G} \times fu_{G,MDZ}}$$

where  $E_{H,MDZ}$ ,  $E_{G,MDZ}$  is hepatic and gut wall extraction, respectively;  $fu_{B,MDZ}$ ,  $fu_{G,MDZ}$  is the unbound fraction of MDZ in blood and gut wall;  $CL_{f,H}$ ,  $CL_{f,G}$  is intrinsic hepatic and gut wall clearance;  $Q_H$  is the hepatic blood flow; and  $Q_G$  is the relevant villous blood flow calculated by eq. S6.1.3<sup>10</sup>.

$$\text{Eq. S6.1.3 } Q_G = \frac{Q_{villi} CL_{perm}}{Q_{villi} + CL_{perm}}$$

where  $Q_{villi}$  is villous blood flow,  $CL_{perm}$  is midazolam permeability.

## 6.2. 1'-OH-midazolam model

Since 1'-OH-MDZ accounts for the majority of MDZ metabolites, formation of the second (minor) metabolite, 4-OH-midazolam, was ignored for the model to reduce complexity<sup>8</sup>. Thus, the input of 1'-OH-MDZ was modeled as the extraction of its parent drug in the representative compartments. Like for the parent, the metabolism of 1'-OH-MDZ can also be described by the well-stirred modeled in both liver and gut wall compartment. The structural model for MDZ and 1'-OH-MDZ is given in Fig. 2 of the main document.

## 6.3. Model reduction by quasi-steady state approximation

Quasi-steady-state approximation (QSSA) is a mathematical way of simplifying the differential equations with the assumption that the drug reaches an equilibrium in the compartments, which means the output and input rates are equal in the respective compartments. In our case, MDZ and 1'-OH-MDZ were assumed to reach equilibrium in gut wall, portal vein and liver compartments. According to Brill et al.<sup>11</sup>, this method was applied here to calculate the amounts in each compartment and to reduce run time of the software to a manageable level.

## 6.4. Model covariates

At first, sex was tested as covariate on clearance (according to published data, see<sup>12</sup>) but this did not improve the model. Then body weight was successfully introduced as covariate on all volumes of distribution, assuming a linear relationship which was better than an exponential relationship (eq. S6.4.1-S6.4.4).

$$\text{Eq. S6.4.1 } V_{MDZ} = \theta_{V_{MDZ}} \times (WEIGHT/70)$$

$$\text{Eq. S6.4.2 } V_{PER1} = \theta_{V_{PER1}} \times (WEIGHT/70)$$

$$\text{Eq. S6.4.3 } V_{PER2} = \theta_{V_{PER2}} \times (WEIGHT/70)$$

$$\text{Eq. S6.4.4 } V_{1OHM} = \theta_{V_{1OHM}} \times (WEIGHT/70)$$

where  $V_{MDZ}$  is volume of distribution in the central compartment of MDZ,  $V_{PER1}$  is volume of distribution in peripheral compartment 1 of MDZ,  $V_{PER2}$  is volume of distribution in peripheral compartment 2 of MDZ,  $V_{1OHM}$  is volume of distribution in central compartment of 1-OH-MDZ.

## 6.5. Effect of ethanol

After establishment of the above semi-physiological MDZ model, the other period data set with ethanol treatment (test period) was introduced into the model. At first, assuming that the treatment of ethanol does not affect MDZ metabolism, the test period was introduced as inter-occasion variability (IOV) on four key and physiologically meaningful parameters, including intrinsic hepatic clearance of MDZ ( $CL_{f,H}$ ), intrinsic intestinal clearance of MDZ ( $CL_{f,G}$ ), first-order absorption rate constant of MDZ ( $Ka$ ) and intrinsic hepatic clearance of 1-OH-MDZ ( $CL_{f,H,1OHM}$ ). Plotting the ETA ( $\eta$ : the discrepancy of an individual parameter from the typical population value) of absorption and metabolism in test and reference period, it was obvious that exposure to ethanol had effects on  $Ka$  as well as  $CL_{f,G}$  while it had nearly no effects on  $CL_{f,H}$ , and  $CL_{f,H,1OHM}$ . Subsequently, these two periods were separated into two models, and with the plots of the individual predicted parameters of absorption and metabolism in test and reference period for these separated models (Fig. S6.2), the ethanol effect on  $Ka$  and  $CL_{f,G}$  became more obvious. Furthermore, after introducing an effect of ethanol on  $Ka$  and  $CL_{f,G}$  with eqs. S6.5.1 and S6.5.2 in the model including both periods, the objective function value (OFV) decreased by 17.085. Meanwhile, the  $IOV Ka$  decreased from 0.103 to 0.0461; and the  $IOV CL_{f,G}$  dropped from 0.173 to 0.0954. All above analyses confirmed that ethanol would decrease both absorption / transit rate constant and intestinal clearance of MDZ, and has no effect on hepatic clearance of MDZ and 1-OH-MDZ.

$$\text{Eq. S6.5.1 } Ka = \theta_{Ka} \times (1 + ethanol \times \theta_{effect\ of\ ethanol\ on\ Ka}); (ethanol : 0 = reference ; 1 = test)$$

$$\text{Eq. S6.5.2 } CL_{f,G} = \theta_{CL_{f,G}} \times (1 + ethanol \times \theta_{effect\ of\ ethanol\ on\ CL_{f,G}}); (ethanol : 0 = reference ; 1 = test)$$

## 6.6. Model evaluation

Model selection criteria were biological plausibility and results of standard goodness-of-fit plots (Fig. S2). To assess accuracy and precision of the final model parameters, a bootstrap analysis was carried out. Through re-sampling individuals with replacement from the original data set, 1000 bootstrap data sets were created and evaluated. Median of respective parameter estimates and 90% CIs are presented in Table 2 of the main document, along with the point estimates of the final model and CIs obtained by NONMEM from the original data set.

## 7. Additional results

Pharmacokinetic parameters of probe drugs not reported in the main document including their comparison between treatments are shown in Table S3. Major pharmacokinetic parameters presented separately for genotype groups according to their predicted activity (for the period without ethanol co-administration only) are displayed in Table S4.

## 8. Appropriateness of phenotyping drug cocktail

The selection of individual phenotyping agents is in accordance with scientific publications and regulatory guidance documents based thereon<sup>13,14</sup>.

### 8.1. Appropriateness of individual dosages

All individual drugs have dose-linear and/or concentration-linear pharmacokinetics in the small dose range which is relevant here, i.e. for the dose range including doses in the present study and doses in other studies used for validation of the application of the respective drug for phenotyping. This is supported by trials comparing different doses, by pharmacokinetic characteristics reported for the respective substances showing that first pass metabolism and/or elimination is not saturated at higher doses / concentrations, and by enzyme kinetic considerations: For all CYP phenotyping drugs used here, the enzyme to be assessed mediates the major fraction of overall metabolism and reflects the high affinity site of metabolism. For digoxin, P-gp is a major transporter mediating intestinal and renal secretion. Linear pharmacokinetics in vivo demonstrates that according to the Michaelis-



Menten equation,  $v = V_{max} * [S] / (K_m + [S])$ , substrate concentrations are well below  $K_m$  for the respective high affinity enzyme or transporter. Changing the dose in any direction would have a linear effect on turnover rates by this enzyme / transporter – and also by other enzymes or transporters with a lower affinity (which can be found for any phenotyping drug). Thus, for the limited dose ranges being relevant here, no shift of phenotyping specificity is to be expected. Furthermore, the doses used in the present cocktail have been evaluated previously in a large number of investigations, both when administered alone or as part of a cocktail (see below).

**Caffeine (CYP1A2; NAT2):** The definite proof that caffeine at doses in the range between 100 and 165 mg would closely reflect hepatic CYP1A2 expression and activity was provided in a study conducted in 1996<sup>15</sup>. Almost any later studies, also those using lower caffeine doses (with the disadvantage that results are more prone to be confounded by dietary caffeine intake) directly or indirectly refer to this study. Strictly spoken, doses lower than 100 mg which have been used in some cocktail studies would need justification (if any is needed at all), rather than the use of 150 mg doses. The use of the 150 mg dose for NAT2 phenotyping has been validated by comparison to NAT2 genotype<sup>16</sup>.

**Tolbutamide (CYP2C9):** Tolbutamide has been validated by comparison to CYP2C9 genotype and by co-administration of selective inhibitors for the 500 mg dose<sup>13</sup>; the 125 mg dose has been further validated by comparison to genotype<sup>17</sup>.

**Omeprazole (CYP2C19):** Validation of omeprazole as a CYP2C19 phenotyping drug is limited although it is recommended<sup>14</sup> and used in almost any phenotyping cocktail because of the lack of suitable alternatives. Doses used to this end range from 10 to 40 mg (see below).

**Dextromethorphan (CYP2D6):** While urinary metabolic ratios have been used for decades, more recent evidence supports the use of plasma pharmacokinetics following a 30 mg oral dose for phenotyping<sup>18,19</sup> but lower doses were also used.

**Midazolam (CYP3A):** Midazolam is the standard CYP3A phenotyping agent for DDI assessment<sup>14</sup> and has been validated at a tremendous dose range from 0.001 mg intravenous / 0.003 mg oral) to 1 mg intravenous / 3 mg oral or even higher<sup>20,21</sup>

**Digoxin (P-gp):** Digoxin is considered as an appropriate probe drug for intestinal and renal P-gp activity<sup>14</sup>, although effects of genetic variants on respective pharmacokinetic parameters

have not been found consistently<sup>22</sup>. P-gp induction and inhibitions studies however strongly support the use of digoxin as a P-gp probe drug, while indeed selectivity issues remain, specifically with regard to the role of OATP4C1 in renal secretion of digoxin<sup>23</sup>. Because of tolerability concerns, previous studies in healthy volunteers used the lowest doses achieving quantifiable concentrations, typically in the 0.25 mg to 1 mg range<sup>24-26</sup>.

## 8.2. Potential mutual interactions of individual probes

The current EMA “Guideline on the investigation of drug interactions”<sup>14</sup> stipulates for phenotyping cocktails: “It should have been demonstrated in vivo that the probe drugs combined in the “cocktail” do not interact with each other. The doses used should preferably be the doses used in this validation. Deviations from this should be justified.”. Taking the incomplete validation of some of the probe drugs into account (see above), the relative importance of a complete lack of mutual interaction will probably be limited especially when using intra-individual comparisons; also, there is no agreement on how exactly this should be tested. In some studies, it has been examined whether AUCs of parent drugs were the same when given alone or when given together with the other cocktail components<sup>27</sup>. This approach however does not exclude that two of the cocktail components may have opposite effects on a third component which cancel each other under the conditions of the validation experiment. In other studies, a stepwise patchwork approach has been used<sup>28,29</sup>. Separate pair-wise investigations of all possible combinations would generally not easily be feasible and have never been done. On the other hand, otherwise in vivo DDI studies are required only to address enzymes known to contribute to at least 25 % to overall metabolism of a given drug<sup>14</sup>. This way, for the selective CYP or transporter substrates used here, almost no mutual *in vivo* DDI studies would be required between cocktail components because the anticipated effect of even strong inhibitors (or inducers) not affecting the main pathway of the probe drugs would be negligible.

For the cocktail used here, there is no specific validation study “demonstrating *in vivo* that the probe drugs combined in the “cocktail” do not interact with each other” preferably at the doses used. The detailed justification for omitting respective studies is described below:

a) **Induction** of other drug metabolizing enzymes is not relevant here because for none of the drugs used here, *in vivo* induction of any drug metabolizing enzyme or transporter by

any of the few known mechanisms is known at the dose range studied, especially not for single doses. (Omeprazole is a CYP1A2 inducer in vitro and is used as such but exposure in the present study is not sufficient to mediate a respective DDI with caffeine<sup>30</sup>). Because any induction of remotely possible relevance in this setting would be by a mechanism increasing the activity of several enzymes and transporters, such a mechanism would certainly not have been missed for these drugs which are marketed since decades. Inhibition of other drugs metabolizing enzymes is therefore the only mechanism of major relevance for the present combination.

b) It should be understood that if there is no **inhibition** of a metabolic pathway by other cocktail components (i.e., not more than an increase of AUC of a potential victim drug to 125 % of control as a worst case scenario), than e.g. doubling the dose of one of the components which is a perpetrator would increase the AUC of the victim drug to not more than 150 % of control (assuming competitive inhibition). While this would formally be outside the “no interaction” range, it would not be a tremendous increase and would not invalidate the intraindividual comparison done in cocktail-based DDI studies. Furthermore, typically there were close to zero effects of various cocktails on the activity of individual pathways (see below), suggesting that a higher dose of potential perpetrators would remain irrelevant.

c) There are **specific in vivo studies** for some cocktails addressing the problem of mutual interactions by various study designs, which have in part used the same phenotyping drugs as used in the present study, covering a dose range which often includes the doses used in the present study. The most important of these studies, all using oral administration, are:

- Streetman et al. 2000<sup>31</sup>: caffeine about 150 mg, omeprazole 40 mg, dextromethorphan 30 mg, midazolam about 2 mg, overall result: no mutual interaction, but null hypotheses were “no DDI” and sometimes metabolic ratios were used instead of AUC
- Blakey et al. 2004<sup>32</sup>: caffeine 100 mg, tolbutamide 250 mg, debrisoquine 5 mg, chlorzoxazone 250 mg, midazolam about 2 mg; overall result: no mutual interaction, but except for midazolam, no full AUCs were used.
- Kirby et al. 2006<sup>25</sup> digoxin 0.5 mg, midazolam 2 mg (digoxin 1 hour after midazolam); overall result: no mutual interaction.
- Ryu JY et al. 2007<sup>33</sup>: caffeine 93 mg, losartan 30-50 mg, omeprazole 20 mg, dextromethorphan 30 mg, midazolam 2 mg, overall result: no mutual interaction.

- Turpault et al. 2009<sup>27</sup>: caffeine 100 mg, warfarin 10 mg, omeprazole 20 mg, metoprolol 100 mg, midazolam about 2 mg; overall result: no mutual interaction
- Donzelli et al. 2014<sup>34</sup>: caffeine 100 mg, losartan 12.5 mg, omeprazole 10 mg, metoprolol 12.5 mg, midazolam 2 mg; overall result: no mutual interaction
- Bosilkovska et al. 2016<sup>29</sup>: caffeine 50 mg, bupropion 20 mg, flurbiprofen 10 mg, omeprazole 10 mg, dextromethorphan 10 mg, midazolam 1 mg, fexofenadine 25 mg; overall result: no mutual interaction

The available information from these studies is briefly summarized in Table S5. In summary, there is sufficient immediate evidence that there is no mutual interaction between caffeine, omeprazole, dextromethorphan, and midazolam also at the doses used in the present study. As correctly pointed out in a commentary by Ma et al (2012)<sup>35</sup>, inclusion of tolbutamide into the cocktail needs further consideration, while we disagree with these authors that conducting an additional *in vivo* study would be the only way to assess the possibility that tolbutamide might interact with the other cocktail components. In an own study, these authors indeed incorporated warfarin instead of tolbutamide as a CYP2C9 substrate by an additional *in vivo* study, but used “lack of interaction” instead of the standard “presence of interaction”<sup>14</sup> as the null hypothesis for their main evaluation of a possible interaction<sup>36</sup>.

As a **potential perpetrator, tolbutamide** (250 mg) had no effect on caffeine or midazolam. It had also no effect on debrisoquine, another fully validated CYP2D6 substrate, and thus at least no major effect on dextromethorphan would be expected (see table S5). With regard to a potential effect of tolbutamide on CYP2C19 and thus on omeprazole pharmacokinetics, it has been shown that tolbutamide binds to CYP2C19 and is metabolized there to a small extent, but the low abundance of CYP2C19 compared to CYP2C9 suggests that CYP2C19 mediated metabolism is irrelevant for tolbutamide pharmacokinetics *in vivo*<sup>37,38</sup>. The affinity of tolbutamide to CYP2C19 however is slightly lower than to CYP2C9<sup>38</sup>. As tolbutamide pharmacokinetics *in vivo* does not provide evidence for saturation at doses of 500 mg or even more, there is no evidence that tolbutamide would occupy a major fraction of CYP2C9 binding sites. Because of the lower affinity to CYP2C19, thus there is also no evidence for relevant occupancy of CYP2C19 binding sites by tolbutamide and thus for inhibition of CYP2C19 *in vivo*. These considerations are supported by a number of *in vitro* cocktails where high concentrations of tolbutamide had no relevant inhibitory effect on the metabolism of

CYP2C19 substrates including omeprazole<sup>39-41</sup>. In summary, the available evidence suggests that a dose of 125 mg tolbutamide as used in the present study has no effect on the pharmacokinetics of the other cocktail components.

As a **potential victim**, **tolbutamide** kinetics was not affected by caffeine or midazolam. Furthermore, dextromethorphan as well as omeprazole had no effect on a number of CYP2C9 substrates other than tolbutamide (see above). Because tolbutamide elimination depends essentially exclusively on CYP2C9<sup>17</sup>, no effect of dextromethorphan or omeprazole on tolbutamide elimination is to be expected. In addition, omeprazole at very high concentrations did not inhibit tolbutamide metabolism in vitro<sup>42</sup>, and in vitro cocktails also did not provide evidence for a relevant effect on tolbutamide metabolism or on the metabolism of other CYP2C9 substrates by dextromethorphan or omeprazole<sup>39-41</sup>. In summary, the available evidence suggests that the pharmacokinetics of a dose of 125 mg tolbutamide as used in the present study is not affected by the other cocktail components.

Likewise, there is only limited assessment of incorporating digoxin into a phenotyping cocktail used to quantify enzyme activity.

As a **potential perpetrator**, according to the respective Pharmacogenomics Knowledgebase (PharmGKB) entry accessed October 22, 2017, **digoxin** is not known to be an inducer or inhibitor of human cytochrome P-450 enzymes<sup>43</sup>, while this information is probably more based on decades of experience rather than on an up-to-date battery of preclinical and clinical studies. With regard to respective clinical assessments, **digoxin** (0.5 mg) had no effect on midazolam pharmacokinetics (see table S5); the lack of an effect of digoxin on human CYP3A is confirmed by in vitro data<sup>44</sup>. There were also no obvious effects of digoxin co-administration on tolbutamide concentrations in diabetic patients<sup>45</sup>. In summary, the available evidence does not suggest that a dose of 0.5 mg digoxin as used in the present study would alter the pharmacokinetics of the other cocktail components to a major extent.

As a **potential victim**, **digoxin** does not undergo primary metabolism by human cytochrome P450 enzymes to a relevant extent<sup>46</sup>, and its secretion across the apical membranes of intestinal and renal tubular cells appears to be relative selectively mediated by P-gp in vitro and in vivo<sup>43,22</sup>. Further transporters located at the basolateral membranes appear to mediate digoxin uptake into the cells as the prerequisite for subsequent secretion, including OATP4C1 and OATP1B3<sup>43,47</sup>. Typically, P-gp activity appears to be the rate-limiting process of

digoxin intestinal secretion<sup>22</sup>, while for renal secretion of digoxin OATP4C1 may be even more important<sup>23</sup>. In general, in vitro screening suggests that only a small fraction of drugs would be able to change OATP4C1 activity in vivo, and specifically tolbutamide had no effect in vitro<sup>48</sup>. A caveat can be derived from an unexpected interaction with bupropion with increased renal elimination of digoxin<sup>49</sup>, probably indeed mediated by activation of OATP4C1 by bupropion and/or its metabolites<sup>47</sup>. Potential mechanisms beyond P-gp modulation by which digoxin pharmacokinetics may be affected are thus limited. In vivo, kinetics of digoxin was not affected by midazolam<sup>25</sup>. Furthermore, caffeine, dextromethorphan and omeprazole had no effect on fexofenadine<sup>29</sup>, another P-gp substrate. While proton pump inhibitors including omeprazole are P-gp inhibitors in vitro<sup>50</sup>, omeprazole increased digoxin absorption in clinical DDI studies by 10 % only<sup>51</sup>. Digoxin pharmacokinetics in our study was similar to studies with administration of single doses of digoxin only in healthy volunteers<sup>24,52</sup>. In summary, the available evidence suggests that the pharmacokinetics of a dose of 0.5 mg digoxin as used in the present study would not considerably be affected by the other cocktail components.

## 9. References for supplementary document

1. Macchia, T. *et al.* Ethanol in biological fluids: Headspace gc measurement. *J. Anal. Toxicol.* **19**, 241–246 (1995).
2. Aderjan, R. *et al.* Richtlinien zur bestimmung der blutalkoholkonzentration (BAK) für forensische zwecke - BAK-richtlinien. *Blutalkohol* **48**, 137–143 (2011).
3. Zadoyan, G. *et al.* Effect of Ginkgo biloba special extract EGb 761® on human cytochrome P450 activity: a cocktail interaction study in healthy volunteers. *Eur. J. Clin. Pharmacol.* **68**, 553–560 (2012).
4. Mould, D. R. & Upton, R. N. Basic concepts in population modeling, simulation, and model-based drug development-part 2: introduction to pharmacokinetic modeling methods. *CPT Pharmacometrics Syst Pharmacol* **2**, e38 (2013).
5. Wilkinson, P. K. *et al.* Blood ethanol concentrations during and following constant-rate intravenous infusion of alcohol. *Clin Pharmacol Ther* **19**, 213–223 (1976).
6. Lindberg, L. *et al.* Breath alcohol concentration determined with a new analyzer using free exhalation predicts almost precisely the arterial blood alcohol concentration. *Forensic Sci Int* **168**, 200–207 (2007).
7. Holford N, Jiang Y, Murry DJ, Brown TL, M. G. The Influence of Body Composition on Ethanol Pharmacokinetics using a Rate Dependent Extraction Model. In *PAGE. Abstr. Annu. Meet. Popul. Approach Gr. Eur. ISSN 1871-6032* **24**, ISSN 1871-6032 (2015).

8. Frechen, S. *et al.* A semiphysiological population pharmacokinetic model for dynamic inhibition of liver and gut wall cytochrome P450 3A by voriconazole. *Clin. Pharmacokinet.* **52**, 763–81 (2013).
9. Vossen, M. *et al.* Dynamically simulating the interaction of midazolam and the CYP3A4 inhibitor itraconazole using individual coupled whole-body physiologically-based pharmacokinetic (WB-PBPK) models. *Theor Biol Med Model* **4**, 13 (2007).
10. Yang, J., Jamei, M., Yeo, K. R., Tucker, G. T. & Rostami-Hodjegan, A. Prediction of intestinal first-pass drug metabolism. *Curr Drug Metab* **8**, 676–684 (2007).
11. Brill, M. J. *et al.* Semiphysiologically based pharmacokinetic model for midazolam and CYP3A mediated metabolite 1-OH-midazolam in morbidly obese and weight loss surgery patients. *CPT Pharmacometrics Syst Pharmacol* **5**, 20–30 (2016).
12. Kashuba, A. D. *et al.* Quantification of 3-month intraindividual variability and the influence of sex and menstrual cycle phase on CYP3A activity as measured by phenotyping with intravenous midazolam. *Clin Pharmacol Ther* **64**, 269–277 (1998).
13. Fuhr, U., Jetter, A. & Kirchheiner, J. Appropriate Phenotyping Procedures for Drug Metabolizing Enzymes and Transporters in Humans and Their Simultaneous Use in the ‘Cocktail’ Approach. *Clin. Pharmacol. Ther.* **81**, 270–283 (2007).
14. European Medicines Agency *Guideline on the investigation of drug interactions 21 June 2012 CPMP/EWP/560/95/Rev. 1 Corr. 2\*\**. (2012).at <[http://www.ema.europa.eu/docs/en\\_GB/document\\_library/Scientific\\_guideline/2012/07/WC500129606.pdf](http://www.ema.europa.eu/docs/en_GB/document_library/Scientific_guideline/2012/07/WC500129606.pdf)>
15. Fuhr, U. *et al.* Evaluation of caffeine as a test drug for CYP1A2, NAT2 and CYP2E1 phenotyping in man by in vivo versus in vitro correlations. *Pharmacogenetics* **6**, 159–76 (1996).
16. Jetter, A. *et al.* Phenotyping of N-acetyltransferase type 2 and xanthine oxidase with caffeine: when should urine samples be collected? *Eur. J. Clin. Pharmacol.* **65**, 411–417 (2009).
17. Jetter, A. *et al.* Cytochrome P450 2C9 phenotyping using low-dose tolbutamide. *Eur. J. Clin. Pharmacol.* **60**, 165–171 (2004).
18. Frank, D., Jaehde, U. & Fuhr, U. Evaluation of probe drugs and pharmacokinetic metrics for CYP2D6 phenotyping. *Eur. J. Clin. Pharmacol.* **63**, 321–333 (2007).
19. Abduljalil, K. *et al.* Assessment of Activity Levels for CYP2D6\*1, CYP2D6\*2, and CYP2D6\*41 Genes by Population Pharmacokinetics of Dextromethorphan. *Clin. Pharmacol. Ther.* **88**, 643–651 (2010).
20. Eap, C. B. *et al.* Oral administration of a low dose of midazolam (75 microg) as an in vivo probe for CYP3A activity. *Eur. J. Clin. Pharmacol.* **60**, 237–246 (2004).
21. Hohmann, N. *et al.* Midazolam microdose to determine systemic and pre-systemic metabolic CYP3A activity in humans. *Br. J. Clin. Pharmacol.* **79**, 278–285 (2015).
22. Oswald, S., Terhaag, B. & Siegmund, W. In Vivo Probes of Drug Transport: Commonly Used Probe Drugs to Assess Function of Intestinal P-glycoprotein (ABCB1) in Humans. In *Handb. Exp. Pharmacol.* 403–447 (2011).doi:10.1007/978-3-642-14541-4\_11
23. Scotcher, D., Jones, C. R., Galetin, A. & Rostami-Hodjegan, A. Delineating the Role of

- Various Factors in Renal Disposition of Digoxin through Application of Physiologically Based Kidney Model to Renal Impairment Populations. *J. Pharmacol. Exp. Ther.* **360**, 484–495 (2017).
24. Rengelshausen, J. *et al.* Contribution of increased oral bioavailability and reduced nonglomerular renal clearance of digoxin to the digoxin-clarithromycin interaction. *Br. J. Clin. Pharmacol.* **56**, 32–8 (2003).
  25. Kirby, B. *et al.* Simultaneous Measurement of In Vivo P-glycoprotein and Cytochrome P450 3A Activities. *J. Clin. Pharmacol.* **46**, 1313–1319 (2006).
  26. Jetter, A. *et al.* Do activities of cytochrome P450 (CYP)3A, CYP2D6 and P-glycoprotein differ between healthy volunteers and HIV-infected patients? *Antivir. Ther.* **15**, 975–983 (2010).
  27. Turpault, S. *et al.* Pharmacokinetic assessment of a five-probe cocktail for CYPs 1A2, 2C9, 2C19, 2D6 and 3A. *Br. J. Clin. Pharmacol.* **68**, 928–935 (2009).
  28. Bosilkovska, M., Clément, M., Dayer, P., Desmeules, J. & Daali, Y. Incorporation of Flurbiprofen in a 4-Drug Cytochrome P450 Phenotyping Cocktail. *Basic Clin. Pharmacol. Toxicol.* **115**, 465–466 (2014).
  29. Bosilkovska, M. *et al.* Evaluation of Mutual Drug–Drug Interaction within Geneva Cocktail for Cytochrome P450 Phenotyping using Innovative Dried Blood Sampling Method. *Basic Clin. Pharmacol. Toxicol.* **119**, 284–290 (2016).
  30. Rost, K. L. *et al.* Omeprazole weakly inhibits CYP1A2 activity in man. *Int. J. Clin. Pharmacol. Ther.* **37**, 567–74 (1999).
  31. Streetman, D. S. *et al.* Combined phenotypic assessment of CYP1A2, CYP2C19, CYP2D6, CYP3A, N-acetyltransferase-2, and xanthine oxidase with the ‘Cooperstown cocktail’. *Clin. Pharmacol. Ther.* **68**, 375–383 (2000).
  32. Blakey, G. E. *et al.* Pharmacokinetic and pharmacodynamic assessment of a five-probe metabolic cocktail for CYPs 1A2, 3A4, 2C9, 2D6 and 2E1. *Br. J. Clin. Pharmacol.* **57**, 162–169 (2004).
  33. Ryu, J. Y. *et al.* Development of the ‘Inje cocktail’ for high-throughput evaluation of five human cytochrome P450 isoforms in vivo. *Clin Pharmacol Ther* **82**, 531–540 (2007).
  34. Donzelli, M. *et al.* The Basel cocktail for simultaneous phenotyping of human cytochrome P450 isoforms in plasma, saliva and dried blood spots. *Clin. Pharmacokinet.* **53**, 271–282 (2014).
  35. Ma, J. D., Nafziger, A. N. & Bertino, J. S. Validating phenotyping cocktails: more work needs to be done. *J. Clin. Pharmacol.* **52**, 1772–3 (2012).
  36. Chainuvati, S. *et al.* Combined phenotypic assessment of cytochrome P450 1A2, 2C9, 2C19, 2D6, and 3A, N-acetyltransferase-2, and xanthine oxidase activities with the ‘Cooperstown 5+1 cocktail’. *Clin. Pharmacol. Ther.* **74**, 437–447 (2003).
  37. Horsmans, Y., Kanyinda, J. M. & Desager, J. P. Relationship between mephenytoin, phenytoin and tolbutamide hydroxylations in healthy African subjects. *Pharmacol. Ther.* **78**, 86–88 (1996).
  38. Lasker, J. M., Wester, M. R., Aramsombatdee, E. & Raucy, J. L. Characterization of



- CYP2C19 and CYP2C9 from human liver: respective roles in microsomal tolbutamide, S-mephenytoin, and omeprazole hydroxylations. *Arch. Biochem. Biophys.* **353**, 16–28 (1998).
39. Lee, K. S. & Kim, S. K. Direct and metabolism-dependent cytochrome P450 inhibition assays for evaluating drug-drug interactions. *J. Appl. Toxicol.* **33**, 100–108 (2013).
  40. Otten, J. N., Hingorani, G. P., Hartley, D. P., Kragerud, S. D. & Franklin, R. B. An in vitro, high throughput, seven CYP cocktail inhibition assay for the evaluation of new chemical entities using LC-MS/MS. *Drug Metab. Lett.* **5**, 17–24 (2011).
  41. Dahlinger, D. *et al.* Development and validation of an in vitro, seven-in-one human cytochrome P450 assay for evaluation of both direct and time-dependent inhibition. *J. Pharmacol. Toxicol. Methods* **77**, 66–75 (2016).
  42. Furuta, S. *et al.* Inhibition of drug metabolism in human liver microsomes by nizatidine, cimetidine and omeprazole. *Xenobiotica* **31**, 1–10 (2001).
  43. Whirl-Carrillo, M. *et al.* Pharmacogenomics Knowledge for Personalized Medicine. *Clin. Pharmacol. Ther.* **92**, 414–417 (2012).
  44. Cook, C. S., Berry, L. M. & Burton, E. Prediction of *in vivo* drug interactions with eplerenone in man from *in vitro* metabolic inhibition data. *Xenobiotica* **34**, 215–228 (2004).
  45. Kolenda, K. D., Grille, W. & Johnsen, K. Arzneimittelwechselwirkungen bei der Therapie mit Tolbutamid: Beeinflussung von Serumspiegel und Halbwertszeit durch einige gebräuchliche Pharmaka bei Altersdiabetikern. *Med. Klin.* **74**, 1914–22 (1979).
  46. Lacarelle, B. *et al.* Metabolism of digoxin, digoxigenin digitoxosides and digoxigenin in human hepatocytes and liver microsomes. *Fundam. Clin. Pharmacol.* **5**, 567–82 (1991).
  47. He, J., Yu, Y., Prasad, B., Chen, X. & Unadkat, J. D. Mechanism of an unusual, but clinically significant, digoxin-bupropion drug interaction. *Biopharm. Drug Dispos.* **35**, 253–263 (2014).
  48. Sato, T., Mishima, E., Mano, N., Abe, T. & Yamaguchi, H. Potential Drug Interactions Mediated by Renal Organic Anion Transporter OATP4C1. *J. Pharmacol. Exp. Ther.* **362**, 271–277 (2017).
  49. Kirby, B. J. *et al.* Complex Drug Interactions of the HIV Protease Inhibitors 3: Effect of Simultaneous or Staggered Dosing of Digoxin and Ritonavir, Nelfinavir, Rifampin, or Bupropion. *Drug Metab. Dispos.* **40**, 610–616 (2012).
  50. Pauli-Magnus, C., Rekersbrink, S., Klotz, U. & Fromm, M. F. Interaction of omeprazole, lansoprazole and pantoprazole with P-glycoprotein. *Naunyn. Schmiedeberg's Arch. Pharmacol.* **364**, 551–7 (2001).
  51. Andersson, T. Omeprazole Drug Interaction Studies. *Clin. Pharmacokinet.* **21**, 195–212 (1991).
  52. Zhang, X.-Y., Tian, Y., Zhang, Z.-J., Rui, J.-Z. & Cao, X.-M. Pharmacokinetics and bioequivalence study of two digoxin formulations after single-dose administration in healthy Chinese male volunteers. *Arzneimittelforschung* **61**, 601–604 (2012).

**Table S1: Conditions for MS/MS analysis of CYP2D6, CYP3A, CYP2C19 and NAT2 probes**

Assay #	Analyte	Precursor	Product	Mode	Retention time	Internal standard
2	Dextropropranolol	258.20	157.10	Positive	1.1	Omeprazole-d <sub>3</sub>
2	Dextromethorphan	275.20	171.40	Positive	1.6	Dextromethorphan-d <sub>3</sub>
2	Dextromethorphan-d <sub>3</sub>	272.20	171.40	Positive	1.6	-
1	Midazolam	326.20	291.30	Positive	2.4	Midazolam-d <sub>4</sub>
1	Midazolam-d <sub>4</sub>	329.20	291.30	Positive	2.4	-
1	1'-Hydroxymidazolam	342.30	203.10	Positive	2.5	1'-Hydroxymidazolam-d <sub>4</sub>
1	1'-Hydroxymidazolam-d <sub>4</sub>	346.30	203.10	Positive	2.5	-
1	4-Hydroxymidazolam	342.20	325.2	Positive	2.0	1'-Hydroxymidazolam-d <sub>4</sub>
2	Omeprazole	346.10	198.30	Positive	1.2	Omeprazole-d <sub>3</sub>
2	Omeprazole-d <sub>3</sub>	349.10	198.30	Positive	1.2	-
2	5-Hydroxyomeprazole	362.30	214.10	Positive	0.9	5-Hydroxyomeprazole-d <sub>3</sub>
2	5-Hydroxyomeprazole-d <sub>3</sub>	365.30	214.10	Positive	0.9	-
3	1U	183.30	155.10	Positive	1.8	1U-d <sub>3</sub>
3	1U-d <sub>3</sub>	186.30	158.10	Positive	1.8	-
3	1X	167.10	110.30	Positive	1.9	1X-d <sub>3</sub>
3	1X-d <sub>3</sub>	170.10	110.30	Positive	1.9	-
3	AAMU	199.30	181.00	Positive	1.2	AFMU-d <sub>3</sub>
3	AFMU	227.20	185.20	Positive	1.3	AFMU-d <sub>3</sub>
3	AFMU-d <sub>3</sub>	230.20	188.20	Positive	1.3	-

**Table S2. Physiological and drug parameters used for the semi-physiological population pharmacokinetic model of midazolam**

Parameter	Value	Reference
<b>Midazolam (MDZ)</b>		
$f_{u_{B,MDZ}}$	0.033	8
$f_{u_{GW,MDZ}}$	1	8
$B/P\ ratio_{MDZ}$	0.66	8
$CL_{PERMEABILITY}$ (l/h)	10.6	11
<b>1'-OH-Midazolam (MET)</b>		
$f_{u_{B,MET}}$	1	
$f_{u_{GW,MET}}$	1	8
$B/P\ ratio_{MET}$	1	
<b>Physiological Parameter</b>		
$Q_H$ (l/h)	$3.75 \times \text{Body Weight}^{0.75}$	8
$Q_{PV}$ (l/h)	$0.75 \times Q_H (=72)$	8
$Q_{HA}$ (l/h)	$0.25 \times Q_H (=24)$	8
$Q_{INTEST}$ (l/h)	$0.4 \times Q_H (=38)$	8
$Q_{MUCOSA}$ (l/h)	$0.8 \times Q_{INTEST} (=31)$	8
$Q_{villi}$ (l/h)	$0.6 \times Q_{MUCOSA} (=18)$	8
$V_H$ (l)	1	
$V_{PV}$ (l)	1	
$V_G$ (l)	1	

$f_{u_B}$  unbound fraction in blood;  $f_{u_G}$  unbound fraction in gut wall;  $B/P\ ratio$  blood/plasma-ratio;  $Q$  respective blood flow of liver ( $Q_H$ ), portal vein ( $Q_{PV}$ ), hepatic artery ( $Q_{HA}$ ), small intestine ( $Q_{INTEST}$ ), gut mucosa ( $Q_{MUCOSA}$ ), and villous blood flow ( $Q_{villi}$ );  $V$  respective volume of liver ( $V_H$ ), portal vein ( $V_{PV}$ ), gut wall ( $V_G$ ). Values of  $Q$  for a subject of 75 kg in round parentheses. For references, see text of supplementary document

**Table S3: Pharmacokinetic parameters of probe drugs for test and reference periods and the effect of ethanol on pharmacokinetic parameters**

Probe drug & period	Pharmacokinetic parameters given as geometric mean (95% CI) except for $t_{max}$ where median (range) is presented							
<b>caffeine</b>	$C_{max}$ ( $\mu\text{M}$ )	$t_{max}$ (h)	$AUC_{0-24h}$ (h * $\mu\text{M}$ )	$AUC_{0-\infty}$ (h * $\mu\text{M}$ )	$t_{1/2}$ (h)	PX/CAF $AUC_{0-t}$ ratio <sup>a</sup>	PX/CAF $C_{6h}$ ratio <sup>b</sup>	urinary NAT2 ratio <sup>c</sup>
Ethanol (E)	22.0 (11.5-42.1)	1.50 (0.750-2.13)	218 (81.3-585)	256 (75.6-867)	7.64 (3.03-19.3)	0.416 (0.160-1.08)	0.296 (0.108-0.809)	0.285 (0.084-0.966)
Water (W)	22.1 (10.9-45.1)	0.625(0.333-2.00)	158 (49.4-508)	174 (46.0-657)	6.02 (2.54-14.3)	0.642 (0.253-1.63)	0.563 (0.160-1.98)	0.299 (0.100-0.896)
<b>E/W ratio (90 % CI)</b>	<b>0.99 (0.93-1.06)</b>		<b>1.38 (1.25-1.52)</b>	<b>1.47 (1.33-1.64)</b>	<b>1.27 (1.16-1.39)</b>	<b>0.65 (0.58-0.72)</b>	<b>0.53 (0.46-0.60)</b>	<b>0.95 (0.91-1.00)</b>
<b>tolbutamide</b>	$C_{max}$ ( $\mu\text{M}$ )	$t_{max}$ (h)	$AUC_{0-24h}$ (h * $\mu\text{M}$ )	$AUC_{0-\infty}$ (h * $\mu\text{M}$ )	$t_{1/2}$ (h)	$C_{24h}$ ( $\mu\text{M}$ )		
Ethanol (E)	51.3 (33.6-78.5)	2.88 (1.75-6.00)	495 (311-787)	610 (329-1128)	8.89 (4.39-18.0)	7.63 (2.96-19.6)		
Water (W)	51.7 (29.5-90.4)	2.88 (1.25-5.00)	520 (312-866)	633 (312-1282)	8.70 (4.22-17.9)	7.27 (2.13-24.9)		
<b>E/W ratio (90 % CI)</b>	<b>0.99 (0.93-1.06)</b>		<b>0.95 (0.92-0.99)</b>	<b>0.96 (0.92-1.01)</b>	<b>1.02 (0.97-1.08)</b>	<b>1.05 (0.93-1.18)</b>		
<b>omeprazole</b>	$C_{max}$ (nM)	$t_{max}$ (h)	$AUC_{0-24h}$ (h * $\mu\text{M}$ )	$AUC_{0-\infty}$ (h * $\mu\text{M}$ )	$t_{1/2}$ (h)	OM/OH-OM $AUC_{0-t}$ ratio <sup>d</sup>	OM/OH-OM $C_{3h}$ ratio <sup>e</sup>	
Ethanol (E)	750 (183-3077)	4.00 (2.33-8.00)	1.83 (0.352-9.50)	1.84 (0.349-9.72)	2.07 (0.448-9.60)	1.61 (0.336-7.69)	2.47 (0.481-12.7)	
Water (W)	762 (149-3909)	3.00 (1.50-5.03)	1.65 (0.250-10.9)	1.65 (0.251-10.9)	1.56 (0.448-5.42)	1.65 (0.300-9.07)	1.96 (0.338-11.4)	
<b>E/W ratio (90 % CI)</b>	<b>0.98 (0.80-1.21)</b>		<b>1.11 (0.99-1.24)</b>	<b>1.11 (1.00-1.24)</b>	<b>1.33 (1.01-1.75)</b>	<b>0.97 (0.88-1.08)</b>	<b>1.08 (0.94-1.24)</b>	
<b>dextromethorphan</b>	$C_{max}$ (nM)	$t_{max}$ (h)	$AUC_{0-24h}$ (h * nM)	$AUC_{0-\infty}$ (h * nM)	$t_{1/2}$ (h)	DM/DOR $AUC_{0-t}$ ratio <sup>f</sup>	DM/DOR $C_{3h}$ ratio <sup>g</sup>	
Ethanol (E)	6.42 (0.42-98.6)	2.63 (1.25-4.50)	31.3 (0.909-1080)	37.58 (0.863-1637)	5.25 (0.808-34.1)	0.362 (0.0055-23.9)	0.311 (0.0066-14.7)	
Water (W)	3.13 (0.115-85.2)	2.13 (1.25-10.0)	16.0 (0.189-1359)	24.62 (0.304-1997)	6.51 (1.21-34.9)	0.250 (0.020-31.9)	0.234 (0.0035-15.8)	
<b>E/W ratio (90 % CI)</b>	<b>2.05 (1.64-2.55)</b>		<b>1.95 (1.48-2.58)</b>	<b>1.52 (1.16-2.01)</b>	<b>0.81 (0.57-1.16)</b>	<b>1.45 (0.90-2.32)</b>	<b>1.33 (0.89-1.98)</b>	
<b>midazolam</b>	$C_{max,oral,midazolam}$ (nM)	$t_{max,oral,midazolam}$ (h)	$Ka_{oral,midazolam}$ (h <sup>-1</sup> )	$CL_{midazolam}$ (L/h)	$t_{1/2,midazolam}$ (h)	$E_{intest.,midazolam}$ (fraction)	$CL_{1'-OH-midazolam}$ (L/h)	$E_{intest.,1'-OH-midaz.}$ (fraction)
Ethanol (E)	24.4(9.80-60.5)	0.75(0.5-1.75)	4.40(1.43-13.6)	32.7(21.6-49.7)	1.24(0.86-2.05)	0.428(0.210-0.860)	61.6(41.5-91.4)	0.823(0.800-0.840)
Water (W)	26.6(11.7-60.4)	0.63(0.33-1.00)	6.67(3.17-14.1)	31.4(20.7-47.7)	1.22(0.88-2.71)	0.555(0.340-0.910)	61.3(38.3-98.0)	0.734(0.710-0.760)
<b>E/W ratio (90 % CI)</b>	<b>0.92 (0.84-1.00)</b>		<b>0.66 (0.56-0.78)</b>	<b>1.04 (0.99-1.09)</b>	<b>0.93 (0.82-1.04)</b>	<b>0.77 (0.69-0.86)</b>	<b>1.00 (0.95-1.06)</b>	<b>1.12 (1.12-1.12)</b>
<b>digoxin</b>	$C_{max}$ (nM)	$t_{max}$ (h)	$AUC_{0-24h}$ (h * nM)	$Ae_{0-24h}$ (% of dose)	$CL_{renal}$ (L/h)	$CL_{renal,secretion}$ (L/h)		
Ethanol (E)	3.22 (1.64-6.33)	0.75 (0.50-1.75)	14.2 (7.15-28.4)	17.5(8.28-26.8)	7.64 (4.24-13.8)	3.22 (-1.78-8.23)		
Water (W)	3.06 (1.59-5.89)	0.75 (0.33-1.00)	15.6 (10.1-24.0)	18.6(6.80-30.4)	7.32 (4.06-13.2)	2.87 (-1.56-7.30)		
<b>E/W ratio (90 % CI)</b>	<b>1.05 (0.91-1.22)</b>		<b>0.91 (0.80-1.04)</b>	<b>0.94(0.80-1.09)</b>	<b>1.04 (0.95-1.15)</b>	<b>1.12 (0.873-1.37)</b>		

(legend overleaf)

Ae, amount excreted in urine;  $AUC_{0-t}$ , area under the plasma concentration-time curve between 0 and time of last quantifiable concentration;  $AUC_{0-\infty}$ , area under the plasma concentration-time curve extrapolated to infinity; C, plasma concentration;  $C_{max}$ , maximal plasma concentration; CL, clearance;  $CL_{renal\ secretion}$ , fraction of renal clearance attributable to tubular secretion;  $E_{intest}$ , intestinal extraction;  $K_a$ , absorption constant (equal to  $K_{tr}$  = transfer rate for the two transit compartments);  $t_{1/2}$ , apparent terminal elimination half-life; shaded values indicate that 90 % CI of the E/W ratios crossed the predefined “no relevant interaction” borders of 0.70- to 1.43-fold.

<sup>a</sup>Molar paraxanthine / caffeine  $AUC_{0-t}$  ratio;

<sup>b</sup>Molar paraxanthine / caffeine plasma concentration ratio 6 h post-dose;

<sup>c</sup>Molar ratio of caffeine metabolites in urine (5-acetylamino-6-formylamino-3-methyluracil [AFMU] + 5-acetylamino-6-amino-3-methyluracil [AAMU]) / (AFMU + AAMU + 1-methylxanthine + 1-methyluric acid);

<sup>d</sup>Molar omeprazole / 5-OH-omepazole  $AUC_{0-t}$  ratio;

<sup>e</sup>Molar omeprazole / 5-OH-omepazole plasma concentration ratio 3 h post-dose;

<sup>f</sup>Molar dextromethorphan / dextrorphan  $AUC_{0-t}$  ratio

<sup>g</sup>Molar dextromethorphan / dextrorphan plasma concentration ratio 3 h post-dose

**Table S4: Descriptive analysis of phenotyping metrics in the reference (water) period according to respective genotype groups**

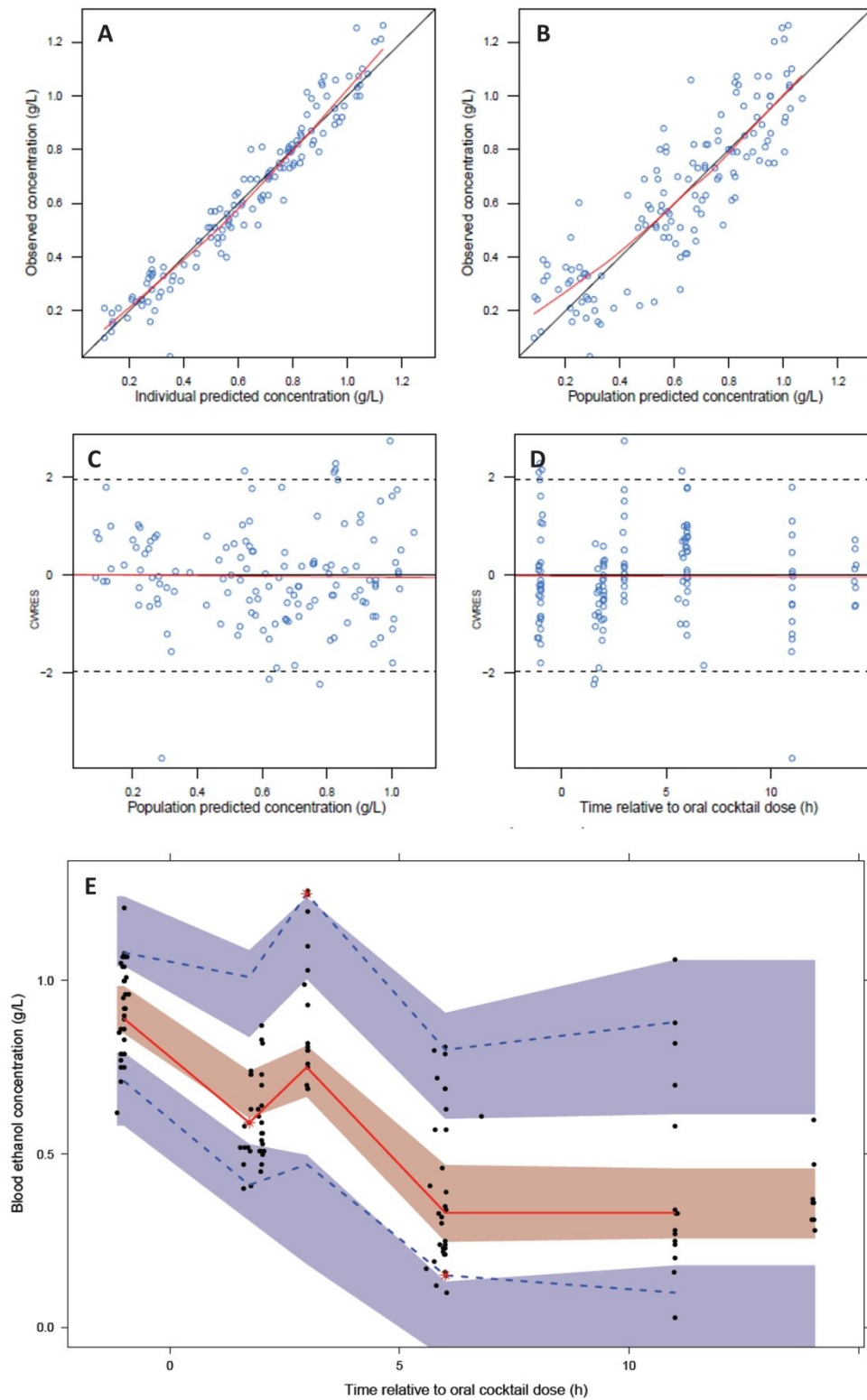
enzyme / transporter	metric	geom. mean (CV%) for genotype group:			
		i	ii	iii	iv
CYP2C9	Tolbutamide AUC <sub>0-24h</sub> (h * μM)	504 (24.8 %)	568 (23.7 %)		
CYP2C19	Molar omeprazole AUC <sub>0-24h</sub> / 5-OH-omepazole AUC <sub>0-24h</sub> ratio (MR <sub>CYP2C19</sub> );	0.969 (163 %)	1.73 (97.9 %)	2.04 (66.4 %)	
CYP2C19	omepazole AUC <sub>0-24h</sub> (h * μM)	0.884 (361 %)	1.79 (81.2 %)	2.04 (68.7 %)	
CYP2D6	Molar dextromethorphan AUC <sub>0-24h</sub> / dextrorphan AUC <sub>0-24h</sub> ratio (MR <sub>CYP2D6</sub> );	0.0500 (203 %)	0.258 (85.7 %)	10.1 (424 %)	
CYP2D6	dextromethorphan AUC <sub>0-24h</sub> (h * nM)	3.26 (172 %)	19.8 (128 %)	43.2 (102 %)	
CYP3A5	hepatic clearance of midazolam (L/h)	40.9 (5.17 %)	37.7 (25.0 %)		
CYP3A5	intestinal extraction of midazolam (fraction)	0.656 (8.73 %)	0.534 (24.3 %)		
NAT2	Urinary molar ratio (AFMU+AAMU)/ (AFMU+AAMU+1X+1U) 6 -10 hours postdose (MR <sub>NAT2</sub> )	0.519 (---)	0.402 (10.5 %)	0.139 (29.2 %)	0.155 (27.3 %)
P-gp	C <sub>max</sub> of digoxin (nM)	3.33 (27.5 %)	2.55 (55.5 %)	3.14 (34.5 %)	2.97 (25.0 %)
P-gp	digoxin clearance by renal secretion* (L/h)	3.43 (47.5 %)	4.67 (58.7 %)	2.22 (93.0 %)	2.85 (83.5 %)

i...iv genotype groups refer to essentially decreasing predicted activity, for identification of groups see Table 4 of main document; CV, coefficient of variation; AUC<sub>0-24h</sub>, area under the concentration vs. time curve up to 24 hours; AFMU, 5-acetylamino-6-formylamino-3-methyluracil; AAMU, 5-acetylamino-6-amino-3-methyluracil; 1X, 1-methylxantine; 1U, 1-methyluric acid); MR, metabolic ratio; C<sub>max</sub>, maximal concentration after dosing; \*for renal secretion, an additive model was used, thus arithmetic means and CVs are presented

**Table S5: Mutual interactions between probe drugs tested in specific cocktail studies.**

	<b>Perpe- trator</b>	<b>Caffeine (C) 150 mg</b>	<b>Tolbutamide (T) 125 mg</b>	<b>Omeprazole (O) 20 mg</b>	<b>Dextromethor- phan HBr (D) 30 mg</b>	<b>Midazolam (M) 2 mg</b>	<b>Digoxin (Dig) 0.5 mg</b>
<b>Victim</b>							
<b>Caffeine 150 mg</b>	-		T 250 mg no effect on C 100 mg	O up to 40 mg no effect on C 50-150 mg	D up to 30 mg no effect on C 50-150 mg	M up to 2 mg no effect on C 50-150 mg	(see text)
<b>Tolbutamide 125 mg</b>	C up to 100 mg no effect on T 250 mg and no effect on any other CYP2C9 probe	-		O up to 20 mg no effect on any other CYP2C9 probe	D up to 30 mg no effect on any other CYP2C9 probe	M up to 2 mg no effect on T 250 mg and no effect on any other CYP2C9 probe	(see text)
<b>Omeprazole 20 mg</b>	C up to 150 mg no effect on O 10 - 40 mg	(see text)		-	D up to 30 mg no effect on O 10 - 40 mg	M up to 2 mg no effect on O 10 - 40 mg	(see text)
<b>Dextro- methorphan HBr 30 mg</b>	C up to 150 mg no effect on D 10 - 30 mg	T 250 mg no effect on another CYP2D6 probe		O up to 40 mg no effect on D 10 - 30 mg	-	M up to 2 mg no effect on on D 10 - 30 mg	(see text)
<b>Midazolam 2 mg</b>	C up to 150 mg no effect on M 1 - 2 mg	T 250 mg no effect on M 2 mg		O up to 40 mg no effect on M 1 - 2 mg	D up to 30 mg no effect on M 1 - 2 mg	-	Dig 0.5 mg no effect on M 2 mg
<b>Digoxin 0.5 mg</b>	C 50 mg no effect on another P-gp probe	(see text)		O 10 mg no effect on another P-gp probe	D 50 mg no effect on another P-gp probe	M up to 2 mg no effect on Dig and no effect on another P-gp probe	-

Bold text indicates drugs and doses used in the present study (for references and explanations, see supplementary text document).

**Figure S1: Evaluation of final ethanol model.**

Goodness-of-fit plots A,B,C,D (CWRES, conditional weighted residuals) and visual predictive check (E). In the VPC, points indicate observed concentrations. Dashed blue lines represent the 2.5th and 97.5th percentiles of the observed data and the red solid line represents the median of the observed data. The shaded areas cover the 95% confidence intervals of the corresponding 2.5th, 50th and 97.5th percentiles of the simulated data.



**Figure S2** Goodness-of-fit plots of the final model for midazolam and 1'-hydroxymidazolam